Phosphorylation of the M1 muscarinic acetylcholine receptor provides neuroprotection in mouse prion disease.

Miriam Scarpa

BSc (Hons)

Submitted in fulfilment of the requirements for the Degree of

Doctor of Philosophy

Institute of Molecular, Cell and Systems Biology

College of Medical, Veterinary & Life Sciences

University of Glasgow

March 2022

Abstract

The M1 muscarinic acetylcholine receptor (mAChR) plays a crucial role in learning and memory and is a validated drug target for the treatment of Alzheimer's disease (AD). Pharmacological activation of the M1 mAChR can not only improve cognitive symptoms in AD patients but has also been proven to slow down disease progression in preclinical mouse models of neurodegeneration. Thus, the M1 mAChR has a promising potential as drug target for disease-modifying therapies of AD (Scarpa et al., 2020). However, development of clinically effective M1 mAChR-targeted ligands has been challenging due to associated adverse effects, highlighting the need to dissect clinically relevant M1 mAChR-mediated pathways from those leading to undesirable outcomes. By employing a novel transgenic mouse model expressing a phosphorylation-deficient mutant of the M1 mAChR (M1-PD) (Butcher et al., 2016), our group previously found that adverse effects can be minimised through pathways favouring receptor phosphorylation (Bradley et al., 2020). This thesis aimed to extend this study and explore the role of M1 mAChR phosphorylation/arrestin-dependent pathways in the disease modification potential of the M1 mAChR. I combined M1-PD transgenic mice with prion neurodegenerative disease, a model of terminal neurodegeneration, leading to the discovery that disease is accelerated in M1-PD mice, thereby revealing an inherent neuroprotective property of the M1 mAChR that is dependent on receptor phosphorylation.

To provide insight into the potential signalling mechanisms of the M1-PD, *in vitro* functional assays were performed on cell lines expressing the M1-PD version or wild-type of the M1 mAChR. Lack of receptor phosphorylation significantly impaired agonist-induced receptor internalisation, which is an important process in the desensitisation of G protein-dependent signalling. However, removal of M1 mAChR receptor phosphorylation was shown to have little impact on phosphoinositide accumulation, which is indicative of $G\alpha_q$ protein activation.

The mouse prion disease model was then investigated through behavioural observations and histological and biochemical studies to characterise neurodegenerative disease progression through the detection of markers of disease. Mouse prion disease is caused by neurotoxic aggregates of misfolded prion proteins, and shares key hallmarks with human neurodegenerative diseases

such as AD. These include memory and hippocampal function decline, disease markers such as APO-E, clusterin and serpinA3N, and widespread neuroinflammation, as indicated by the upregulation of astrocytic and microglial markers GFAP, Vimentin, Iba1 and CD86. Importantly, the appearance of misfolded, neurotoxic prion was shown to occur prior to the start of dosing studies of M1 mAChR-selective ligands (Bradley et al., 2017, Dwomoh et al., 2021), establishing that the therapeutic effects exerted by the M1 mAChR are not due to prevention of disease, but disease-modification. In this thesis, mouse prion disease model was also demonstrated to feature the significant upregulation of pro-inflammatory cytokines TNF-α, IL-1β and IL-6, similar to other neurodegenerative disorders characterised by chronic neuroinflammation.

Removal of M1 mAChR phosphorylation in mice caused a significant acceleration of prion neurodegenerative disease progression. This was evident from behavioural changes such as faster hippocampal decline and symptom onset and shorter lifespan compared to wild-type animals, but also significantly elevated accumulation of misfolded prion and upregulation of markers of disease and neuroinflammation. Particularly, the pro-inflammatory cytokine TNF-α was significantly upregulated in prion-infected M1-PD mice with compared to wild-type mice, suggesting the M1 mAChR might be involved in the regulation of TNF-α. These findings unravelled an important neuroprotective property that is inherent to the M1 mAChR and depends on the receptor's phosphorylation/arrestin-dependent signalling. In addition, these data have important implications for development of new drug treatments for neurodegenerative diseases, especially, M1 mAChR ligands that maintain receptor phosphorylation will more likely deliver neuroprotection that could not only improve memory symptoms but slow disease progression. Given the parallels between mouse prion disease and human proteinopathies, the neuroprotective mechanism observed here mediated by the M1 mAChR, is likely to be relevant to other human neurodegenerative conditions such as AD.

Table of Contents

List of Tables

List of Figures

List of Publications

Scarpa, M., Molloy, C., Jenkins, L., Strellis, B., Budgett, R.F., Hesse, S., Dwomoh L., Marsango S., Tejeda G.S., Rossi M., Ahmed Z., Milligan G., Hudson B.D., Tobin A.B., Bradley S.J. (2021) Biased M1 muscarinic receptor mutant mice show accelerated progression of prion neurodegenerative disease. *Proc Natl Acad Sci U S A;118(50): e2107389118. doi: 0.1073/pnas.2107389118.*

Dwomoh, L., Rossi, M., **Scarpa, M.**, Khajehali, E., Molloy, C., Herzyk, P., Mistry, S. N., Bottrill, A. R., Sexton, P. M., Christopoulos, A., Conn, P. J., Lindsley, C. W., Bradley, S. J. & Tobin, A. B. 2021. Activation of M1 muscarinic receptors reduce pathology and slow progression of neurodegenerative disease. *bioRxiv*, 2021.07.30.454298. (Under review in Science Signaling)

Scarpa, M., Hesse, S., Bradley, S.J. (2020). M1 muscarinic acetylcholine receptors: A therapeutic strategy for symptomatic and disease-modifying effects in Alzheimer's disease? *Advances in Pharmacology*, APHA Volume 88: 277-310.

Bradley, S.J., Molloy, C., Valuskova, P., Dwomoh, L., **Scarpa, M.**, Rossi, M., Finlayson, L., Svensson, K.A., Chernet, E., Barth, V.N., Gherbi, K., Sykes, D.A, Wilson, C.A., Mistry, R., Sexton, P.M., Christopoulos, A., Mogg, A.J., Rosethorne, E.M., Sakata, S., Challiss, RAJ, Broad L.B., and Tobin A.B. (2020*). Nature Chemical Biology* 16: 240–249

Acknowledgements

First and foremost, I would like to express my gratitude to my supervisors Sophie and Andrew. This PhD programme has been a fantastic learning process to me, by experiencing ups and downs it has been a great growth not only as a scientist, but also for my personal development. Your support allowed me to be creative and pursue my ideas, as well as extend my network. A special thank goes to Sophie – as your first PhD student, I could not have asked for a better support and example as an independent woman in science. I would also like to thank Shan, for his supervision at Eli Lilly and co., who has been very supportive throughout my placement in industry, despite the unprecedented circumstances.

The warmest thank you goes to my parents and family. Mamma e Papá, senza di voi non sarei mai arrivata fino a qui. Grazie per il vostro amore e supporto incondizionato. Il vostro esempio mi ha sempre guidata e mi guiderá sempre nel mio percorso come scienziata e come donna. Grazie per tutti i vostri sacrifici e amore che mi hanno consentita di arrivare cosí in alto. Ringrazio di cuore anche il resto della mia famiglia – Andrea, nonna Nella, nonna Dina, nonno Vittorio, zia Ale e Piero, zia Mara e zio Berto – il vostro supporto e incoraggiamento mi hanno sempre sostenuta in questa lunga e faticosa avventura!

I am also extremely grateful to all my friends, especially my friends from Lab241 that have lived this adventure with me first-hand. Thank you especially Eloise, Jose, Nini, Becca and Louis for being my biggest fans always, even when I felt at my lowest. A huge thank you goes to Kerry, who's been my partner in crime since the second lockdown, probably the hardest phase of my PhD process. Thank you for being so supportive and listening to my practice talks a million times. I would also like to thank my friends from home – Sebastiano, Chiara, Giulia, Diana – who have always been there and believed in me despite the physical distance. A huge thank you goes to Fergus, who has been the biggest cheerleader – thank you for always believing in me and being so encouraging.

A special thank you goes to Sansa and Shadow – even if you will never be able to read this, I am very grateful to have you as my wee companions that always cheer me up!

Author's Declaration

December 2021

"I declare that, except where explicit reference is made to the contribution of others, this thesis is the result of my own work and has not been submitted for any other degree at the University of Glasgow or any other institution."

Miriam Scarpa

Definitions/Abbreviations

5-HT	5- hydroxy tryptamine
Aß	Amyloid ß
ac	Anterior commissure
AC	Adenylyl cyclase
ACh	Acetylcholine
AChE	Acetylcholinesterase
AD	Alzheimer's disease
ADAM	A disintegrin and metalloproteinase
AHL	Amphetamine-induced hyper-locomotion
AICD	Amyloid precursor protein intracellular domain
AKT	Protein kinase B
AP2	Adaptor protein 2
APO-E	Apolipoprotein E
APP	Amyloid precursor protein
AR	Adrenergic receptor
ATR	Angiotensin receptor
ATP	Adenosine triphosphate
BACE	Beta secretase 1
BDNF	Brain-derived neurotrophic factor
BQCA	Benzyl quinolone carboxylic acid
BRET	Bioluminescence Resonance Energy Transfer
BSE	Bovine spongiform encephalopathy
cAMP	Cyclic adenosine monophosphate
cc	Corpus callosum
CCL	C-C motif chemokine ligand
CCR	Chemokine receptor
CD86	Cluster of Differentiation 86
ChAT	Choline acetyltransferase
CHO	Chinese hamster ovary
CHRM	Cholinergic Receptor Muscarinic 1
CJD	Creutzfeldt-Jakob disease
CK	Casein kinase
CLU	Clusterin

CNO	Clozapine-N-oxide
CNS	Central nervous system
COPD	Chronic obstructive pulmonary disease
CPu	Caudate putamen
CSF	Cerebrospinal fluid
CT	Cycle threshold
ctx	Cortex
CWD	Chronic Wasting Disease
DR	Dopamine receptor
DAG	Diacylglycerol
DMSO	Dimethyl sulfoxide
DREADD	Designer Receptors Exclusively Activated by Designer Drugs
DS	Dentate gyrus
ECL	Extracellular loop
EEA1	Early endosomal antigen 1
EM	Electron microscopy
EOAD	Early-onset Alzheimer's disease
ERK	Extracellular signal-regulated kinase
f	fornix
FDA	Food and Drug Administration
FRET	Fluorescence resonance energy transfer
FZD	Frizzled
GAIN	GPCR autoproteolysis inducing
GDP	Guanosine diphosphate
GEF	Guanine nucleotide-exchange factor
GFAP	Glial fibrillary acidic protein
GI	Gastrointestinal
GIP	Glucose-dependent insulinotropic polypeptide
GLP	Glucagon-like peptide
GPCR	G protein-coupled receptor
GPS	G protein-coupled receptor proteolysis site
GRK	G protein-coupled receptor kinase
GTP	Guanosine triphosphate
GWAS	Genome-wide association studies
HA	Hemagglutinin

HD	Huntington's disease
HH	Hedgehog
hpc	Hippocampus
HTh	Hypothalamus
HTRF	Homogeneous Time Resolved Fluorescence
Iba1	Ionized calcium binding adaptor molecule 1
ICC	Immunocytochemistry
ICL	Intracellular loop
IFN	Interferon
IHC	Immunohistochemistry
IL	Interleukin
IP	Inositol monophosphate
IP3	inositol triphosphate
IUPHAR	International Union of Basic and Clinical Pharmacology
JNK	c-Jun N-terminal Kinase
KO	knockout
LOAD	Late-onset Alzheimer's disease
mAChR	Muscarinic acetylcholine receptor
MAP2	Microtubule-associated protein 2
MAPK	Mitogen-activated protein kinase
mb	Midbrain
md	Medulla
MS	Mass spectroscopy
NAM	Negative allosteric modulator
NBH	Normal brain homogenate
NE	Norepinephrine
NeuN	Neuronal nucleus
NFT	Neurofibrillary tangle
NMDA	N-methyl-D-aspartate
NMR	Nuclear resonance microscopy
NOR	Novel object recognition
NTSR	Neurotensin receptor
OR	Opioid receptor
PAM	Positive allosteric modulator
PD	Parkinson's disease

PD	Phosphorylation-deficient
PI3K	Phosphoinositide 3-kinases
PK	cAMP-dependent protein kinase
PKC	Protein Kinase C
PLC	Phospholipase C
Pn	Pons
PNS	Peripheral nervous system
PrP	Prion Protein
PSD95	Postsynaptic density protein 95
PSEN	Presenilin
PTHR	Parathyroid hormone receptor
RML	Rocky Mountain Laboratory
RT	Reverse transcriptase
SAPK	Stress-activated protein kinase
SMO	Smoothened
SNR	Substantia nigra
Th	Thalamus
TM	Transmembrane
TNF	Tumour necrosis factor
TOR	Target of rapamycin
TREM2	Triggering Receptor Expressed On Myeloid Cells 2
UPR	Unfolded protein response
V	Vasopressin
Ve	Vestibule
VFD	Venus fly-trap domain
VIP	Vasoactive intestinal peptide
WB	Western blot
Wnt	Wingless/Int-1
WT	Wild type

Chapter 1 Introduction

1.1 G protein-coupled receptors

1.1.1 Overview of GPCRs

G protein-coupled receptors (GPCRs) are the largest superfamily of human membrane receptors, accounting for over 800 members, including around 400 sensory receptors (Hauser et al., 2017, Mombaerts, 2004). They are expressed in every organ and they mediate intracellular signalling in response to various stimuli including light, odorants, hormones, and neurotransmitters (Fredriksson et al., 2003). Given their functional diversity, GPCRs are involved in a plethora of functions in health and pathology, representing the most attractive therapeutic targets. In fact, GPCRs are the target for over 30% of all prescription drugs (Santos et al., 2017).

All GPCRs share a similar transmembrane (TM) domain with a common structural architecture that is crucial to transduce signalling from the ligand-binding pocket and across the membrane to the G protein-coupling interface (Venkatakrishnan et al., 2013). The TM domain consists of 7 α-helices embedded in the cell membrane connected by three intracellular (ICL) and extracellular (ECL) loops (Rosenbaum et al., 2009) (Figure 1-1). Receptor stability is largely maintained by disulphide bridges in the extracellular regions between ECL2 and a cysteine residue in the TM3 that is highly conserved in most GPCRs (except for Sphingosine 1-phosphate receptors) (Venkatakrishnan et al., 2013). The N-terminus and, in some cases, the ECLs, show high structural diversity as they are often involved in receptor functionality and ligand binding, especially as for some GPCR classes it is the main ligand binding site. In particular, the ECL2 has been suggested to play a role in ligand recognition and selectivity (Kruse et al., 2012, Dror et al., 2011, González et al., 2011, Manglik et al., 2012). While the ECL2 is usually found to contain α-helices, ß-sheets or other super-secondary structures, ECL1 and ECL3 normally lack structural elements and are relatively short in length (Unal and Karnik, 2012). Most GPCR subfamilies include an extracellular domain attached to the N-terminus that plays a role in ligand binding (Fredriksson et al., 2003, Lagerström and Schiöth, 2008), whereas rhodopsin-like (class A) GPCRs feature only the TM domain with N- and C-termini of variable length and the endogenous ligand binding site lies within the TM core (Baldwin, 1993) (Figure 1-1).

1.1.2 GPCR subfamilies

Based on sequence and evolutionary conservation, GPCRs have been divided into a classification of subfamilies that has been revised over the years (Kolakowski, 1994, Fredriksson et al., 2003). In particular, the sequencing of the human genome in 2001 allowed for a more comprehensive analysis of the repertoire of vertebrate GPCRs. This resulted in the now commonly accepted classification system termed GRAFS (Schiöth and Fredriksson, 2005), which was also adopted by the International Union of Basic and Clinical Pharmacology (IUPHAR) (Foord et al., 2005). GRAFS classes consist of Glutamate family (class C), Rhodopsin family (class A), Adhesion (class B2), Frizzled (class F) and Secretin-like (class B1) receptor families (Figure 1-1) (Alexander et al., 2021).

Receptors of the **glutamate family (class C)** share a distinguishing dimeric quaternary structure that binds ligands by employing a Venus flytrap domain (VTD) in their large N-terminal lobes (Kunishima et al., 2000, Kaupmann et al., 1998). The **rhodopsin family (class A)** is the largest and most diverse subfamily of GPCRs with 719 members, including almost all (435) recognised sensory receptors (Fredriksson et al., 2003, Davenport et al., 2013). In addition, this subfamily includes receptors that respond to a wide variety of ligands ranging from small molecules, neurotransmitters, peptides and hormones, and contribute to the largest number of therapeutic targets (Wess, 1993, Gershengorn et al., 1998, Milligan et al., 2017, Vu et al., 1991). **Adhesion receptors (class B2)** are phylogenetically related to class B1 receptors with which they share similarities in the TM domain. However, they feature a distinctive, large extracellular N-terminal domain that is autoproteolytically cleaved at a conserved GPCR proteolysis site (GPS) embedded in a GPCR autoproteolysis inducing (GAIN) domain (Prömel et al., 2013). The **frizzled family (class F)** includes frizzled (FZD) and smoothened (SMO) receptors (Foord et al., 2005, Schulte, 2010) that are respectively activated by secreted Wingless/Int-1 (Wnt) glycoproteins and Hedgehog (HH) proteins (Chen and Struhl, 1996, Vinson and Adler, 1987, Vinson et al., 1989). FZD and SMO receptors share a characteristic N-terminal signal sequence followed by a highly conserved cysteine-rich domain (CRD) that is important for ligand recognition (Vinson et al., 1989, Dann et al., 2001). The **secretin family (class B)** comprises only 15 genes in humans, 9 of which respond to structurally related ligands such

as secretin, glucagon and glucagon-like peptides (GLP-1, GLP-2)(Harmar, 2001). Secretin receptors share an extracellular peptide hormone-binding domain that is the most diverse region within the family (Bazarsuren et al., 2002).

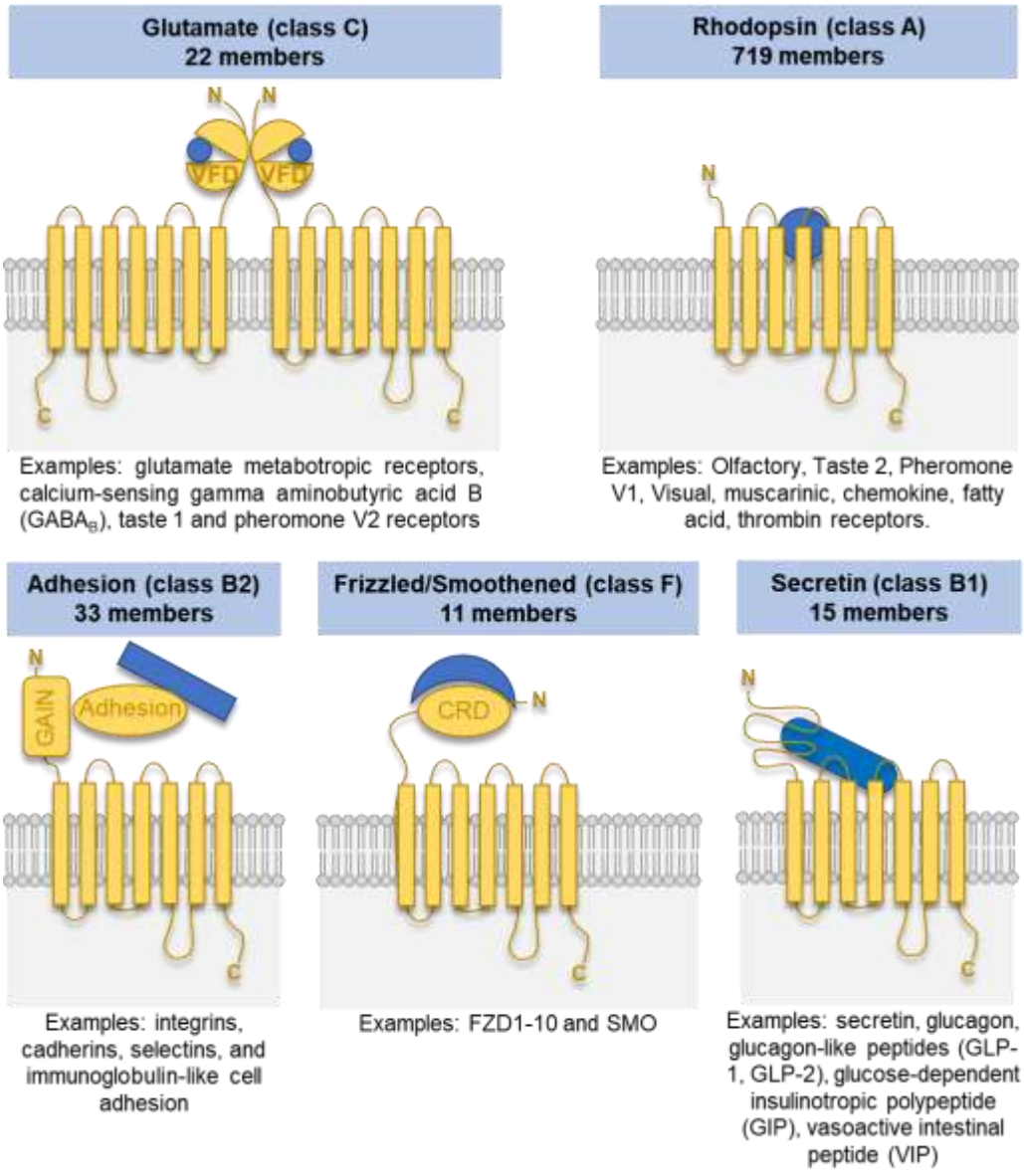

Figure 1-1 Structural features of GPCR subfamilies and examples. GPCRs share a TM domain comprising 7 α-helices, an extracellular N-terminus, and an intracellular C-terminus. Whilst the intracellular regions are relatively conserved, the extracellular region is highly diverse across the different subfamilies. Blue shapes represent the different modes of ligand interaction with respective GPCR families. Most glutamate receptors exist in dimeric form and employ a VFD for ligand binding. Rhodopsin-like receptors have relatively short N-terminus, and their orthosteric ligand binding pocket lies deep into the TM domain. Adhesion GPCRs feature a GAIN domain that catalyses the cleavage of the N-terminus such that the adhesion domains are non-covalently associated with the receptor. Frizzled/smoothened family receptors contain an N-terminal cysteine-rich domain (CRD). Examples for each GPCR subfamily (in humans) are included, as well as the number of currently recognised members as reported by Alexander et al. (2021).

1.1.3 Canonical GPCR signalling

GPCRs transduce signalling when ligand binding induces an active receptor conformation, permitting coupling to intracellular transducers such as heterotrimeric guanine nucleotide-binding proteins (G proteins) that consist of Gα, Gß and Gγ subunits (Lambright et al., 1996). The mammalian genome encodes for 16 Gα subunits (Hermans, 2003), six different Gß-subunits and 12 Gγ-subunits (Gautam et al., 1998). G subunits can combine to form different heterotrimeric G protein complexes providing a diverse source of signalling mediators. Whilst Gα subunits can signal independently, Gß and Gγ subunits function as an individual subunit as obligate heterodimers (Gßγ).

Upon stimulus or ligand binding, receptors undergo conformational changes that induce guanine exchange factor activity catalysing the exchange of guanosine diphosphate (GDP) for guanosine triphosphate (GTP) on the Gα subunit. This causes a structural rearrangement of the G protein complex and disassociation of the GTP-bound Gα and Gßγ subunits (Oldham and Hamm, 2008, Neer and Clapham, 1988, Janetopoulos et al., 2001). Disassociated G protein subunits transduce the signal to produce a range of intracellular second messengers such as cyclic adenosine monophosphate (cAMP), inositol triphosphate (IP3) and diacylglycerol (DAG) (Neves et al., 2002). This signalling is terminated by hydrolysis of GTP to GDP that is mediated by the Ras-like GTPase domain of Gα. This mechanism is promoted by the binding of regulators of G protein signalling that encourages the re-association of G protein subunits (Mann et al., 2016).

Whilst Gßγ subunits are considered functionally interchangeable, Gα subunits activate distinct nonredundant signalling effectors (Smrcka, 2008, Wettschureck and Offermanns, 2005). Based on preferential downstream signalling and sequence conservation, the 16 Gα subunits are classified into four functional families: **$G\alpha_s$** ($G\alpha_{s(S)}$, $G\alpha_{s(XL)}$ and $G\alpha_{s(olf)}$), **$G\alpha_{i/o}$** ($G\alpha_o$, $G\alpha_{i\ (1\text{-}3)}$, $G\alpha_t$, $G\alpha_z$ and $G\alpha_{gust}$), **$G\alpha_{q/11}$** ($G\alpha_q$, $G\alpha_{11}$, $G\alpha_{14}$ and $G\alpha_{15/16}$), and **$G\alpha_{12/13}$** ($G\alpha_{12}$ and $G\alpha_{13}$). $G\alpha_s$, $G\alpha_{i/o}$, $G\alpha_{q/11}$ and $G\alpha_{12/13}$ respectively induce stimulation of adenylyl cyclase (AC), inactivation of AC, activation of phospholipase C (PLC) and Rho-family of guanine nucleotide-exchange factors (GEFs), each of which affect distinct signalling pathways (Neer, 1995, Luttrell, 2008) (Figure 1-2). In addition, Gßγ heterodimers can also contribute to signal transduction, for example by activating several downstream

effectors, modulating ion channels, and acting as scaffolds for kinases (Khan et al., 2016).

It is now well established that individual GPCRs can couple to different Gα protein families, and that distinct receptors can activate the same families of Gα proteins (Wootten et al., 2018). Ligand-stabilised receptor conformations can select the coupling of G protein subunit families resulting in differential signalling outcomes. This has been largely observed with agonists for μ-opioid receptors (μORs) (Saidak et al., 2006), parathyroid hormone receptors (PTHRs) (Appleton et al., 2013) and dopamine receptors (DRs) (Möller et al., 2017).

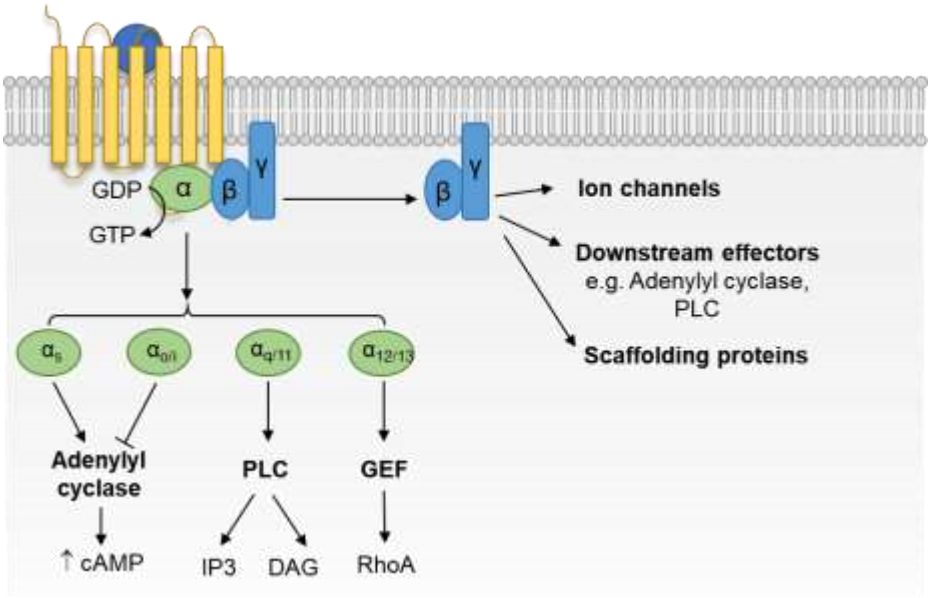

Figure 1-2 G protein-dependent signalling. Activation of GPCRs upon ligand binding induces conformational changes in the receptors. Conformational changes facilitate guanosine nucleotide exchange in Gα subunits, which causes disassociation of Gα and Gβγ subunits. Gα subunits belonging to different functional classes interact with distinct effectors i.e., adenylyl cyclase, phospholipase C (PLC) or guanine exchange factors (GEF) to engage a range of different downstream signalling pathways. Activated, disassociated Gβγ subunits also engage with signalling effectors such as ion channels.

1.1.4 GPCR desensitisation and internalisation

GPCR signalling is normally terminated by receptor phosphorylation at multiple serine and threonine residues in the C-terminal tail and/or ICLs by the action of kinases such as GPCR kinases (GRKs) (Tobin, 2008). Intracellular phosphorylation increases receptor affinity for other interacting partners such as arrestins (Carman and Benovic, 1998). Receptor interaction with arrestins induces G protein displacement by steric hindrance and termination of G protein-dependent signalling (signalling desensitisation) (Arshavsky et al., 1985, Sibley et

al., 1986, Benovic et al., 1987, Shukla et al., 2013, Staus et al., 2020). Arrestins also function as scaffolds by interacting with clathrin and adaptor protein 2 (AP2) to induce receptor endocytosis (Zhang et al., 1996, Goodman et al., 1996), or with additional signalling partners to facilitate G protein-independent signalling such as by activation of mitogen-activated protein kinase (MAPK) (Wei et al., 2003, Shenoy et al., 2006). See Chapter 3 for a detailed review on GPCR phosphorylation, arrestin interactions and phosphorylation/arrestin-dependent signalling.

1.1.5 Pharmacology of GPCR ligands

The action of a ligand at a receptor is defined by inherent pharmacological parameters such as affinity and efficacy. Affinity represents the strength of the interaction between such ligand and its binding site and can be experimentally determined by measuring ligand binding using fluorescent or radiolabelled ligands. The efficacy of a ligand reflects its ability to induce a receptor response, for example, at activating specific downstream effectors. When a suitable labelled ligand is not available, the affinity of a compound can be estimated by defining its potency in functional assays (Rosenkilde and Schwartz, 2000). Both potency and efficacy values are normally determined by functional assays and therefore care must be taken as these values might vary depending on the assay system employed and receptor reserve present (Kenakin, 2001, Kenakin, 2002).

Depending on their interaction with GPCRs, ligands can be broadly divided into three categories: orthosteric, allosteric and bitopic. Orthosteric ligands bind to the same site as the endogenous ligand, whereas allosteric ligands bind to regions of the receptor that are topologically distinct from the orthosteric binding site. Bitopic ligands are compounds with the ability of concomitantly interacting with both orthosteric and allosteric sites on a single receptor (Valant et al., 2012). Depending on affinity, potency, and efficacy parameters, orthosteric ligands can be broadly classified as full, partial, or inverse agonists and neutral antagonists (Figure 1-3). The pharmacology of allosteric ligands is considerably complicated to define, due to the wide range of distinct active states that a GPCR can adopt depending on interactions with both bound ligand(s) and intracellular effectors e.g. G proteins (Stallaert et al., 2011).

However, allosteric ligands can be broadly categorised into allosteric agonists, neutral allosteric antagonists, and positive or negative allosteric modulators (PAMs and NAMs) (Christopoulos et al., 2014). Furthermore, the types of ligands described above may also display 'signalling bias', which is the ability to preferentially activate a signalling pathway over another. (Luttrell and Kenakin, 2011).

Allosteric modulators display 'cooperativity' with the bound orthosteric ligand, which is the ability to induce such molecular changes in the receptor that modulate the receptor affinity and/or efficacy for the bound ligands. PAMs can exist as pure PAMs or agonist (ago)-PAMs. Pure PAMs can modulate receptor activity only in the presence of a receptor-bound orthosteric ligand (Bridges and Lindsley, 2008). Whereas, ago-PAMs are able to enhance the activity mediated by the orthosteric ligand similarly to pure PAMs, but in addition they can facilitate receptor activation in their own right (Langmead et al., 2006). Therefore, pure PAMs often represent an attractive targeting approach for the modulation of GPCRs in disease since they can maintain the physiological temporal and spatial signalling and their effect can be saturated (Foster et al., 2014). In addition, allosteric modulators, including ago-PAMs that display modest cooperativity, will less likely exert intrinsic activity, suggesting they represent potentially safer drugs if administered in larger doses, compared to orthosteric compounds (Gregory et al., 2007). Since allosteric compounds are targeted to binding sites that are distinct from the orthosteric site, they also offer improved selectivity when targeting conserved receptor subclasses such as muscarinic receptor subtypes (Bradley et al., 2017), or peptide receptors such as chemokine receptors, to allow targeting with small-molecule drugs (Dragic et al., 2000).

Bitopic ligands are attractive compounds as they can offer "the best of both worlds" (Valant et al., 2012): the benefits of targeting the orthosteric site (i.e., efficacy and affinity) with added affinity and selectivity by interaction with distinct, allosteric sites. Most bitopic ligands were initially designed or identified as only orthosteric or allosteric, and only extensive pharmacological assessments revealed the bitopic mode of binding (Valant et al., 2008, Lane et al., 2013, Bradley et al., 2018).

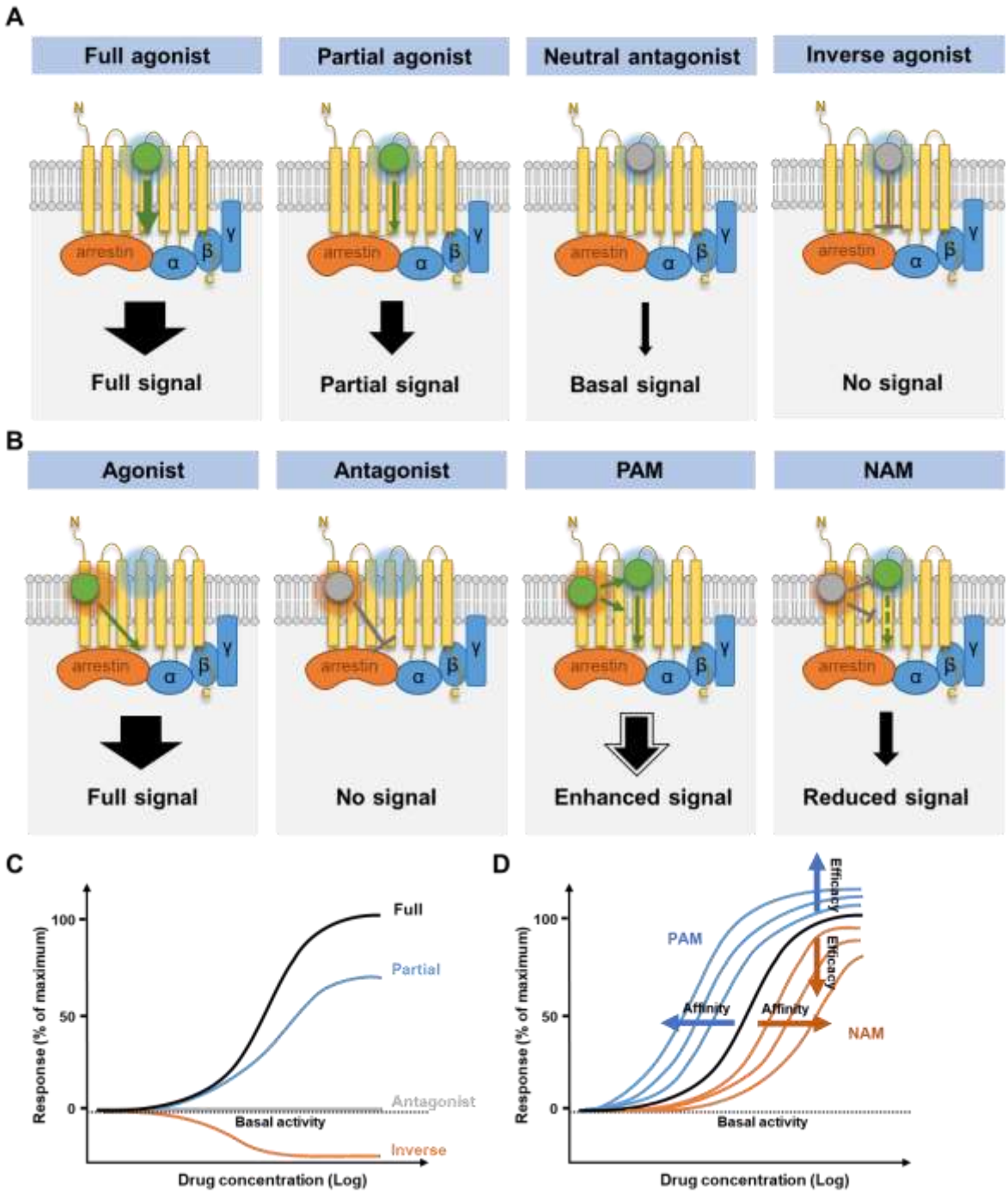

Figure 1-3 Pharmacology of GPCR ligands. (A-B) Simplified representation of the pharmacological properties of orthosteric **(A)** and allosteric **(B)** ligands. **(A)** Orthosteric ligands interact with the receptor by binding to the orthosteric site (blue shading), and they can be full or partial agonists (green) when they activate the receptor up to maximal or partial stimulation, respectively. Orthosteric ligands can also be neutral antagonists (grey), when they compete with agonists but do not affect the receptor's basal activity, or inverse agonists (grey) when they can inhibit basal or constitutive activity of the receptor. **(B)** Allosteric agonists directly facilitate receptor activation by interacting with allosteric sites (orange shading). Allosteric neutral antagonists (grey) bind to allosteric sites but display no cooperativity with orthosteric ligands. PAMs (green) potentiate the effect of the bound orthosteric compound whereas NAMs (grey) attenuate the effects. Adding to the diversity and complexity of orthosteric and allosteric ligands, bitopic ligands combine the properties of both orthosteric and allosteric, and all these types of ligands might display signalling bias by promoting preferred downstream signalling pathways over others. **(C-D)** Theoretical concentration-response curves illustrating the response of different orthosteric (C) and allosteric (D) ligands. **(C)** A full agonist (black) induces a maximal response at its receptor whereas a partial agonist (blue) induces a response that is significantly lower than the maximal response possible at the receptor. Neutral antagonists (grey) produce no response at a receptor, and inverse agonists (orange) decrease the baseline activity of the receptor. **(D)** The concentration-response curve of an

orthosteric agonist in the absence of allosteric ligands is illustrated in black. The addition of PAMs (blue) increases the affinity and/or efficacy of an orthosteric agonist, whereas NAMs (orange) cause a decrease in affinity and/or efficacy. Allosteric agonist and antagonists (in the absence of orthosteric ligands) behave similarly to orthosteric agonists and antagonists.

1.2 GPCRs as drug targets

1.2.1 Therapeutic potential of GPCRs

Given the broad range of physiological end points modulated by GPCRs, it is unsurprising that one third of approved drugs target members of this receptor superfamily (Sriram and Insel, 2018, Santos et al., 2017, Hauser et al., 2017). GPCRs possess an invaluable druggability, which has been proven in both historical and ongoing successes of targeting GPCRs for the pharmacological treatment of diseases. Numerous factors contribute to the attractiveness of GPCRs for drug targeting including the easy accessibility to ligands due to expression on the plasma membrane, and the possibility of targeting these receptors with small, low molecular weight molecules.

Many of the approved drugs are physiological agonists (Sriram and Insel, 2018). For example, epinephrine, the endogenous agonist of adrenergic receptors, is the active ingredient of EpiPen auto-injectors for the emergency treatment of allergic reactions such as anaphylaxis (Sicherer and Simons, 2017). Dopamine, estradiol, vasopressin, acetylcholine, and glucagon are also natural agonists that are used for therapeutic targeting of GPCRs (Sriram and Insel, 2018). GPCR signalling can also be manipulated in the desired manner by designing synthetic molecules with different pharmacological properties. For instance, maraviroc is a small-molecule antagonist that is selective for the chemokine receptor 5 (CCR5) and was approved for the treatment of HIV-1 infection. Maraviroc prevents the virus to enter the cell *via* interaction with CCR5 (Lieberman-Blum et al., 2008). In addition, numerous drugs target proteins that are upstream or downstream of GPCRs to regulate agonist availability or the concentrations of second messengers, thereby contributing to the modulation of receptor signalling (Sriram and Insel, 2018). For example, serotonin (5-HT) or norepinephrine (NE) reuptake inhibitors are commonly therapeutically used for their antidepressant activity by enhancing the availability of these neurotransmitters *via* interactions with 5-HT and NE transporters (Shelton, 2019).

Despite GPCRs being widely recognised as useful drug targets, a large proportion of the GPCR superfamily remains unexploited, with only approximately 15% of the over 800 human GPCRs currently being targeted by medications (Insel et al., 2015, Sriram and Insel, 2018). This implies that new opportunities for novel drug targets still exist in the vast repertoire of GPCRs. In addition, despite significant efforts, there are over 100 non-olfactory GPCRs, termed ‘orphans’, that currently lack a recognised endogenous ligand, resulting in challenges in the characterisation of their physiological functions (Milligan, 2018, Alexander et al., 2021). Apart from SMO and ADGRG3, no orphan receptors are currently targeted by medicines, therefore, such receptors represent a potentially prolific collection of novel drug targets (Milligan, 2018, Sriram and Insel, 2018). For instance, the de-orphanisation of OX1 and OX2 receptors, which respond to neuropeptides orexin A and orexin B, led to the development of suvorexant that is a dual orexin receptor antagonist now approved for the treatment of insomnia (Norman and Anderson, 2016).

1.2.2 Muscarinic receptors as drug targets

Muscarinic receptors (mAChRs) are a family of GPCRs that are broadly expressed in the cholinergic system both in the peripheral nervous system (PNS) and in the central nervous system (CNS) (Levey et al., 1991, Levey, 1993). Muscarinic receptors play key roles in a wide range of physiological processes such as motor control, cardiovascular, renal and gastrointestinal (GI) functions, learning and memory, nociception and sleep-wake cycle (Bonner et al., 1988, Bonner et al., 1987, Felder et al., 2000, Briand et al., 2007, Wess et al., 2007, Bymaster et al., 2003a, Bymaster et al., 2003b). It is therefore unsurprising that muscarinic receptors represent promising drug targets for the treatment of important conditions including diabetes, obesity, pain, asthma, Alzheimer's disease (AD) and schizophrenia (see Wess et al. (2007) for a comprehensive review on the therapeutic potential of mAChR subtypes). The multiple functions mediated by cholinergic receptors were established in humans through the administration of clinically available anticholinergic - medications that antagonise muscarinic receptors. However, the specific physiological role of individual mAChR subtypes was established by the generation of transgenic mice lacking individual muscarinic subtypes (Bymaster et al., 2003b). Individual mAChR subtypes are found uniquely expressed or might be found co-expressed throughout the

nervous system and, accordingly, they might play unique or overlapping roles (Bymaster et al., 2003b) (Table 1-1).

In the PNS, the cholinergic system plays a predominant role in the airways (Kolahian and Gosens, 2012). Specifically, the M1, M2 and M3 muscarinic subtypes were shown to induce bronchoconstriction by triggering smooth muscle contraction and mucus secretion, and to be involved in the pathophysiology of asthma and chronic obstructive pulmonary disease (COPD) (Gosens et al., 2006, Kistemaker and Gosens, 2015, Buels and Fryer, 2012). Anticholinergics have been clinically used for many years for the treatment of COPD, and more recently for treating asthma (Hamelmann, 2018, Gosens and Gross, 2018).

In the CNS, cholinergic neurotransmission was demonstrated in preclinical and clinical studies to operate in a dynamic balance with the dopaminergic system, and disruption of this balance might cause neurological and psychiatric disorders (Di Chiara et al., 1994, Lester et al., 2010). Thus, muscarinic receptors, particularly the M1, M4 and M5 subtypes, have been proposed as possible targets for the treatment of neurological conditions such as schizophrenia, Parkinson's disease (PD), drug and alcohol abuse, and AD (Wess et al., 2007, Langmead et al., 2008). For instance, the M1 and M4 subtypes were reported to be specifically reduced in the striatum, hippocampus, and prefrontal cortex of patients with schizophrenia. Therefore, pharmacological activation of M1 and M4 mAChRs has been viewed as a promising therapeutic approach for the treatment of this psychiatric condition (Dean et al., 1996, Crook et al., 2000, Dean et al., 2002). This was supported by clinical trials for the M1/M4-preferring agonist xanomeline that displayed robust effects against cognitive impairments as well as psychosis-like behaviour in AD and schizophrenic patients (Bodick et al., 1997b, Shekhar et al., 2008). However, recent studies using M1 and M4 mAChR knockout mice indicated that the M4 subtype primarily drives the antipsychotic effects of xanomeline, suggesting that M4-selective allosteric agonists or PAMs would likely be beneficial for the treatment of schizophrenia (Thomsen et al., 2012, Woolley et al., 2009). Instead, the negative modulation of M4 mAChR might be beneficial for the treatment of PD-associated motor symptoms as it was shown that transgenic mice lacking M4 mAChRs display attenuated motor-side, cataleptic response in a model of antipsychotic-induced parkinsonism (Karasawa et al., 2003, Fink-Jensen et al., 2011). Further, M5 mAChR-targeted antagonists have

been proposed as a potential therapeutic avenue for the treatment of drug abuse (Raffa, 2009). This concept was prompted by the discovery that addiction (withdrawal effects) induced by the prototypical opioid drug morphine, but not the associated beneficial analgesic effects, were attenuated in M5 mAChR-knockout mice (Basile et al., 2002, Yamada et al., 2003). In addition, inhibition of M5 mAChR signalling has also been proposed for the pharmacological treatment of alcohol dependence. M5 mAChR transcripts were found up-regulated in the brain of In Indiana alcohol-preferring rats following long-term alcohol consumption, and a M5-selective NAM could significantly reduce alcohol self-administration in rats (Berizzi et al., 2018, Walker et al., 2021).

The focus of this thesis however will be the M1 mAChR as a putative target for disease modification in neurodegenerative disease. Given its role in cognitive processes, the M1 subtype has long been viewed as a promising target for the treatment of cognitive impairments of AD (Fisher, 2008a, Ladner and Lee, 1998). Importantly, emerging evidence in preclinical animal studies has demonstrated the disease-modifying potential of targeting the M1 mAChR for the treatment of AD and likely other neurodegenerative diseases (Scarpa et al., 2020, Dwomoh et al., 2021, Lebois et al., 2017, Bradley et al., 2017, Jones et al., 2008).

SUBTYPE	PERIPHERAL FUNCTIONS	CENTRAL FUNCTIONS	TISSUE	DISEASE RELEVANCE
M1	– Salivation (Bymaster et al., 2003a)	– Learning and memory (Anagnostaras et al., 2003) – Hippocampal PI hydrolysis (Bymaster et al., 2003a) – MAPK stimulation (Hamilton and Nathanson, 2001) – Locomotor activity (Bradley et al., 2020)	Cerebral cortex, hippocampus, striatum, thalamus, sympathetic ganglia, glandular tissue	– Cognitive dysfunction and AD (Scarpa et al., 2020) – Schizophrenia (Shekhar et al., 2008)
M2	– Temperature regulation (Bymaster et al., 2003a) – Smooth muscle contraction (Stengel et al., 2000)	– Auto-inhibition (Zhang et al., 2002) – Analgesia (Gomeza et al., 2001)	Hindbrain, thalamus, cerebral cortex, hippocampus, striatum, smooth muscle of heart, lung, gastrointestinal tract, and bladder	– Cognitive dysfunction and AD (Seeger et al., 2004) – Pain
M3	– Temperature regulation (Bymaster et al., 2003a) – Smooth muscle contraction (Matsui et al., 2000) – Salivation (Bymaster et al., 2003a)	– Weight control (Yamada et al., 2001b)	Cerebral cortex, hippocampus, smooth muscle of heart, lung, gastrointestinal tract and bladder, glandular tissues	– COPD – Asthma – Urinary incontinence – Irritable bowel syndrome
M4	– Salivation (Bymaster et al., 2003a)	– Blockade of dopamine release – Auto-inhibition (Zhang et al., 2002) – Analgesia (Gomeza et al., 2001) – Dopamine-mediated locomotor activity (Gomeza et al., 1999)	Striatum, cerebral cortex, hippocampus	– Parkinson's disease – Schizophrenia – Neuropathic pain
M5		– Cerebral vasculature tone (Yamada et al., 2001a) – Dopamine-mediated addiction (Yamada et al., 2001a)	Substantia nigra	– Drug and alcohol dependence – Parkinson's disease – Schizophrenia

Table 1-1 Role of the M1-M5 subtypes of the mAChR family in the PNS and CNS. The physiological roles of each of the muscarinic subtypes in the PNS and CNS are included alongside their expression profile and disease relevance. Most physiological roles were assessed using receptor subtype knockout mice (Bymaster et al., 2003b) and this table was generated by combining information from Bymaster et al. (2003b) and Langmead et al. (2008). See Wess et al. (2007) for a comprehensive review on the disease relevance of mAChR subtypes.

1.3 The M1 muscarinic acetylcholine receptor (mAChR)

1.3.1 Overview of the mAChR family

Muscarinic acetylcholine receptors are a family of GPCRs activated by the neurotransmitter acetylcholine (ACh), alongside nicotinic receptors, and they comprise five subtypes (M1–M5) encoded by distinct CHRM genes (Hulme et al., 1990). The mAChR family are members of class A (rhodopsin-like) GPCRs (Fredriksson et al., 2003). Members of this family differ in their G protein-selectivity, with M1, M3, and M5 mAChRs preferentially coupling to the $G\alpha_{q/11}$ family of G proteins, while the M2 and M4 subtypes preferentially couple to the $G\alpha_{i/o}$ family (Caulfield and Birdsall, 1998, Nathanson, 1987, Wess, 1993, Felder, 1995).

The amino acid sequences of the mAChR subtypes are highly conserved, with 50-60% sequence homology (Figure 1-4). Particularly, the mAChR family share a highly conserved orthosteric binding pocket deep in the TM domain and some residues in the extracellular region. In particular, they share an aspartate residue in TM3 (D105 in position 3.32 according to Ballesteros-Weinstein numbering) that is critical for ligand binding(Wess, 1993, Hulme et al., 2003).

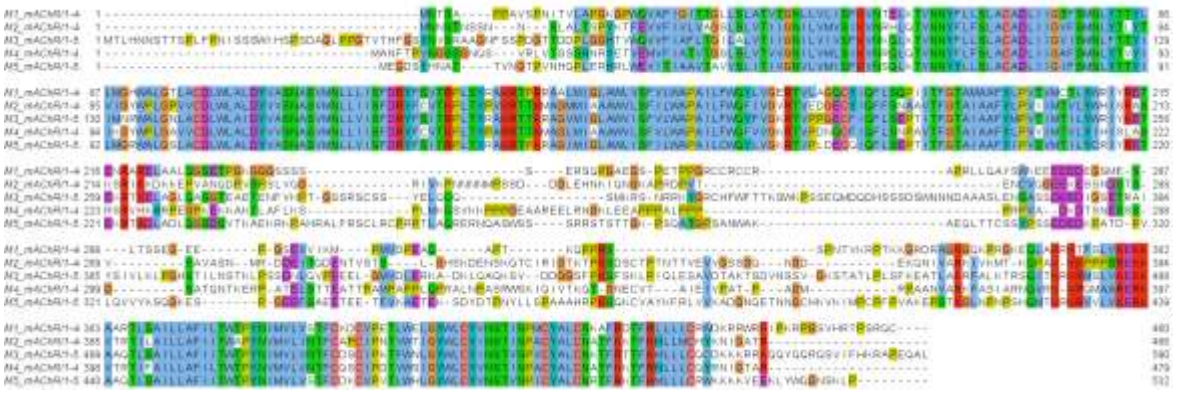

Figure 1-4 Sequence alignment of M1-M5 mAChR. Amino acid sequences of the human M1-M5 mAChR were retrieved using UniProtKB and multiple sequence alignment was conducted using Clustal Omega. The colour code indicates the amino acid type that is matched to the residue at that position according to a Clustal threshold criteria: Blue for hydrophobic (A, I, L, M, F, W,V and C), red for positively charged (K and R), magenta for negatively charged (E and D), green for polar (N, Q, S and T), pink for cysteines (C), orange for glycines (G), yellow for prolines (P), cyan for aromatic (H and Y) and white for unconserved/unmatched and gaps.

1.1.1 M1 mAChR expression and structure

The M1 mAChR constitutes around 50% of the total expression among the muscarinic family (Levey, 1993). It is not widely expressed in the periphery, but it can be found significantly expressed in the salivary glands and sympathetic ganglia (Levey, 1993, Caulfield and Birdsall, 1998). Importantly, M1 mAChRs are highly expressed in all the major areas of the forebrain, including the cerebral cortex and hippocampus (Levey, 1993, Volpicelli and Levey, 2004) where they play crucial roles in cognition, particularly short-term memory (Fisher, 2008a, Ladner and Lee, 1998).

The M1 mAChR, similar to the other muscarinic subtypes, share the same structural signatures of other class A GPCRs (Vuckovic et al., 2019, Kruse et al., 2012, Haga et al., 2012, Thal et al., 2016, Venkatakrishnan et al., 2013) with the orthosteric ligand-binding pocket lying deep in the TM core, specifically involving amino acid residues within TM3, TM5 and TM7 (Wess, 1993, Heitz et al., 1999, Hulme et al., 2003). High-resolution X-ray crystallisation revealed a high degree of conservation in the orthosteric binding pocket across the muscarinic subtypes (Vuckovic et al., 2019, Thal et al., 2016). There are subtle differences in the extracellular and intracellular sites of the M1 mAChR compared to the other members of the family, but a striking difference between subtypes can be observed in the large extracellular vestibule, which is a dynamic structure in muscarinic receptors. The extracellular vestibule contains residues involved in allosteric binding of muscarinic receptors that form the “roof” of the orthosteric site and the “floor” of the allosteric site. In fact, the extracellular interface with TM7 and between ECL2 and ECL3 have been proven to participate in the binding of allosteric ligands and they were demonstrated to contain residues that are less conserved than other regions within the TM core (Birdsall and Lazareno, 2005, Gregory et al., 2007). In addition to non-conserved residues between the muscarinic subtypes, the vestibule also includes a “common” allosteric pocket which comprises of shared residues among the subtypes (Figure 1-5).

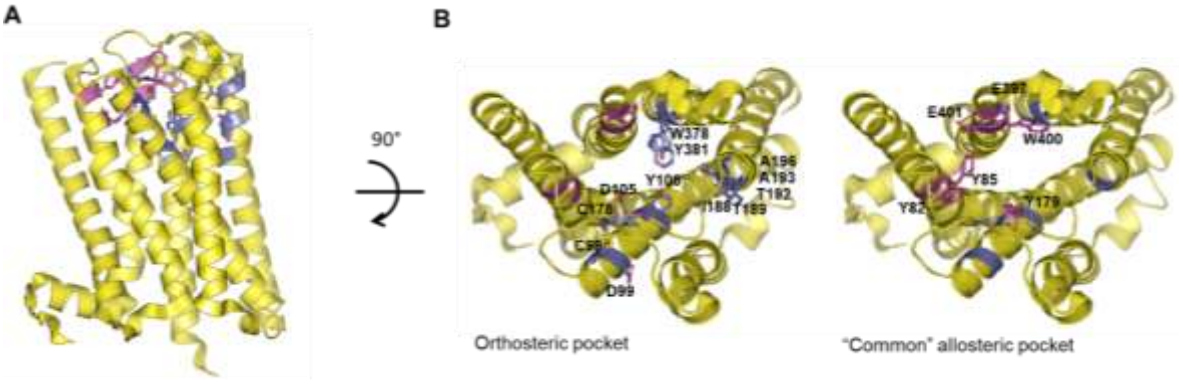

Figure 1-5 Structure of the M1 mAChR depicting the orthosteric and allosteric binding pockets. The M1 mAChR crystal structure is viewed from the **(A)** membrane or **(B)** the extracellular side. Crystallisation of the M1 mAChR revealed a high degree of sequence conservation in the orthosteric binding pocket across M1-M4 mAChRs (Thal et al., 2016). The conserved residues in the orthosteric pocket (blue) include C98 (3.25), D99 (3.26), D105 (3.32), Y106 (3.33), C178 (45.50), I188 (5.39), T189 (5.40), T192 (5.43), A193 (5.44), A196 (5.46), W378 (6.48), Y381 (6.51). The "common" allosteric binding pocket is comprised of residues (magenta) within a large extracellular vestibule of the receptors and include Y82 (2.60), Y85 (2.63), Y179 (45.51), E397 (7.31), W400 (7.34) and E401 (7.35). Images reproduced using the PyMOL Molecular Graphics System, Version 2.0 Schrödinger, LLC.

Most recent studies using single-particle cryo-EM enabled to obtain a structure of the M1 mAChR bound to a potent agonist, iperoxo, and engaged with heterotrimeric $G\alpha_{11}$ protein (Maeda et al., 2019). The comparison of the $G\alpha_{11}$-bound M1 mAChR with the previously obtained structure of the inactive receptor bound to the inverse agonist tiotropium (Thal et al., 2016), unravelled the activation mechanism of the M1 mAChR. In its active state, the M1 mAChR shows an outward displacement of the TM6, accompanied by a small rotation of the helix as well as a tilt of TM5 toward TM6. In addition, the TM6 moves closer to the ECL2 (Tyr179-Ser388) causing a contraction in the extracellular vestibule. Key residues for receptor activation as well as the TM5, TM6 and ECL2 re-arrangement were similar in the M1 and M2 subtypes, indicating the mechanism of activation might be shared among the members of the mAChR family. These conformational changes allow the C-terminal helix of the Gα subunit to interact with the receptor core (Maeda et al., 2019).

1.3.2 Examples of M1 mAChR ligands

Given the therapeutic potential of targeting M1 mAChR, a diverse repertoire of M1 mAChR is currently available (see Birdsall et al., (2021) for a comprehensive list of M1 mAChR ligands). The highly conserved orthosteric binding pocket has represented a limitation for the development of ligands with receptor subtype selectivity, however the use of non-selective orthosteric muscarinic ligands have

been an advantageous tool to explore the signalling and physiological role of this receptor family. For instance, non-selective mAChR antagonists, such as scopolamine, were demonstrated to induce cognitive impairments in animals and healthy individuals (Bartus et al., 1982, Flicker et al., 1990, Rusted and Warburton, 1988). In contrast, muscarinic orthosteric agonists such as physostigmine and the M1/M4-preferring xanomeline, were shown to improve cognitive symptoms in AD or dementia patients, and in animals treated with mAChR-antagonists or cholinergic impairments (Bodick et al., 1997a, Rupniak et al., 1991, Aigner and Mishkin, 1986). This reinforced the potential of targeting mAChRs for the treatment of cognitive decline.

The muscarinic subtypes each possess allosteric binding sites that are non-conserved across the family of mAChRs, providing the opportunity for the design of ligands with high subtype-selectivity (Wess, 2005, Presland, 2005, Conn et al., 2009). AC42 was the first M1 mAChR-selective allosteric agonist that was identified in 2002, however, this compound and respective analogues were found to be unsuitable for *in vivo* studies due to limited potency and pharmacokinetic properties (Spalding et al., 2002, Spalding et al., 2006). Later, TBPB was characterised as a novel allosteric agonist with high selectivity for the M1 mAChR and displayed robust anti-psychotic effects in rats (Jones et al., 2008). The first prototypical M1 mAChR PAM, the highly selective benzyl quinolone carboxylic acid (BQCA), was originally developed by Merck (Ma et al., 2009). BQCA was found to enhance the functional responses mediated by the M1 mAChR without activating the receptor directly (Shirey et al., 2009). In addition BQCA was found to exert significative pro-cognitive activity in a mouse model with scopolamine-induced memory deficits (Ma et al., 2009), and slow down prion disease in mice (Bradley et al., 2017), indicating for the first time that this allosteric compound could afford similar beneficial therapeutic effects to orthosteric muscarinic ligands. Further PAMs that are structurally related to BQCA were generated by Merck, including PQCA and MK-7622, but it should be noted that there now exists a diverse collection of structurally distinct M1 PAM chemotypes, arising from Merck, Pfizer, Vanderbilt Centre for Neuroscience Drug Discovery (VCNDD) and Monash Institute for Pharmaceutical Sciences (MIPS) that possess distinct pharmacological properties.

The first M1 mAChR –selective bitopic ligand to be discovered, McN-A-342 (Roszkowski, 1961) was initially identified as a selective agonist. Later in the 1980's, McN-A-342 was further characterised as described as an allosteric ligand due to the high subtype-selectivity (Birdsall et al., 1983), and subsequently demonstrated to be a bitopic ligand (Valant et al., 2008). The bitopic mode of action was unravelled by sequential truncation of this compound and extensive pharmacological characterisation that resulted in the identification of orthosteric and allosteric fragments (Valant et al., 2008). The discovery of McN-A-342 as a bitopic ligand subsequentially prompted the identification or re-evaluation of compounds displaying similar pharmacology profiles (Lebois et al., 2010, Lebois et al., 2011, Digby et al., 2012, Watt et al., 2011). Among these, GSK1034702, that was previously described as a potent allosteric agonist at the M1 mAChR with pro-cognitive effects in rodents (Budzik et al., 2010), was later re-characterised as a bitopic agonist (Bradley et al., 2018).

1.4 M1 mAChR as therapeutic target for AD

1.4.1 Alzheimer's disease (AD)

The M1 mAChR has been an established target for the symptomatic treatment of AD for years (Fisher, 2008a, Scarpa et al., 2020). AD is the most common form of neurodegeneration as well as the most frequent cause of dementia. Despite remarkable effort, no treatments are available to prevent, slow or stop neurodegenerative conditions, and the prevalence of these diseases is increasing due to the growing lifespan of the human population (Hou et al., 2019). Whilst the familial, early-onset form of AD (EOAD) is caused by rare genetic autosomal mutations accounting for only 5% of cases, the majority of cases are sporadic, late-onset AD (LOAD), which is a multifactorial condition driven by multiple genetic and environmental factors (Bateman et al., 2011). Genome-wide association studies (GWAS) have identified over 20 genetic risk factors of LOAD including genes implicated in inflammation, lipid metabolism and endocytosis (Karch and Goate, 2015). For instance, the APO-E gene, that encodes for a lipoprotein complex regulating transport delivery and distribution of lipids from one tissue to another (Mahley and Rall, 2000), is the single greatest risk for LOAD (Verghese et al., 2011). Epidemiological studies suggest that among the environmental risk factors, hypertension and diabetes confer higher AD risk,

whereas education and physical exercise might be protective against disease (Xu et al., 2015).

AD was described for the first time over a century ago (Alzheimer, 1907) but its pathophysiology is still to be elucidated. The major neuropathological hallmarks of AD are amyloid ß (Aß) plaques and neurofibrillary tangles (NFTs) (Serrano-Pozo et al., 2011). Aß plaques are extracellular deposits formed by abnormally folded Aß isoforms 1-40 and 1-42 (Aß40 and Aß42) as a result of aberrant cleavage and processing of amyloid precursor protein (APP) (Seeman and Seeman, 2011) (Figure 1-6). APP is a transmembrane glycoprotein type I with functions in intracellular signalling in response to environmental conditions as well as in neuronal development (van der Kant and Goldstein, 2015). Most cases of EOAD are associated with mutations in genes that cause an imbalance in the synthesis and processing of APP leading to the accumulation of pathogenic Aß-42 peptides (Figure 1-6). These are mutations in three main genes; the APP gene and two homologous genes that encode the catalytic subunit of γ-secretase, prenisilin 1 (PSEN1) and prenisilin 2 (PSEN2) (Price and Sisodia, 1998).

NFTs consist of paired helical filaments made of hyperphosphorylated tau, a microtubule-associated protein involved in axonal transport and neuronal growth. Tau normally localises in the axons of adult neurons but in AD it becomes hyperphosphorylated and 'mis-sorted' into the somatodendritic compartment leading to the formation of NFTs (Zempel and Mandelkow, 2014). NFT pathology is better correlated with neuronal and synaptic loss as well as clinical features compared to Aß plaque deposits (Serrano-Pozo et al., 2011), which reach a plateau level in the early symptomatic stage of disease (Ingelsson et al., 2004). However, Aß plaques and NFT pathology have been demonstrated to have a synergistic relationship as their convergence (but not tau and Aß plaques individually) was found to be associated with brain atrophy and cognitive decline in animal models of disease and AD patients, (Sperling et al., 2019, Timmers et al., 2019, Hanseeuw et al., 2017, Wang et al., 2016, Busche and Hyman, 2020).

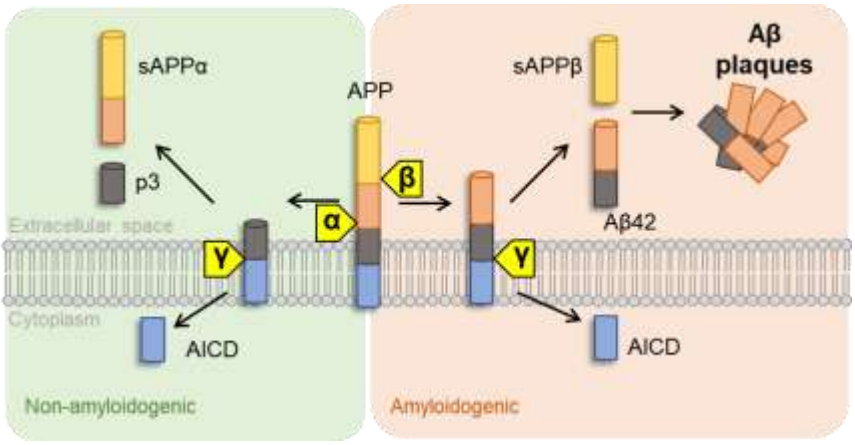

Figure 1-6 Amyloidogenic and non-amyloidogenic processing of APP. In the non-amyloidogenic pathway, initial cleavage of APP occurs by α-secretases such as A Disintegrin And Metalloproteinase (ADAMs) 10 and 17, in the Trans-Golgi Network or at the plasma membrane (Lammich et al., 1999). This results in the formation of non-pathogenic, soluble APPα peptides (sAPPα), p3 fragments and APP intracellular domain (AICD). In contrast, the amyloidogenic processing of APP occurs through the cleavage of APP by β-secretase at the cell surface and in early endosomes (Kinoshita et al., 2003), followed by the cleavage by γ-secretase. This yields to AICD, soluble APPβ peptides (sAPPβ) and pathogenic Aβ42 peptides which are secreted and lead to the formation of Aβ plaques.

Cholinergic transmission (Figure 1-7) is also found impaired in the brain of AD patients, whereby cholinergic signalling is decreased ('cholinergic hypofunction') due to the selective loss of pre-synaptic cholinergic neurons particularly in the hippocampus and neocortex (Whitehouse et al., 1981, Whitehouse et al., 1982, Levey, 1996, Svensson et al., 1992). It was reported that patients with advanced AD have less than 100,000 cholinergic neurons compared to the about 500,000 in healthy adults (Schliebs and Arendt, 2006). In addition, transcription of choline acetyltransferase (ChAT), an enzyme expressed in pre-synaptic cholinergic neurons, is found significantly decreased in AD patients, resulting in further disruption of cholinergic transmission amongst the already few cholinergic neurons (Strada et al., 1992, Wilcock et al., 1982). These observations have since driven the efforts to pharmacologically enhance the cholinergic signalling as therapeutic avenue for AD, starting from the current frontline treatment available.

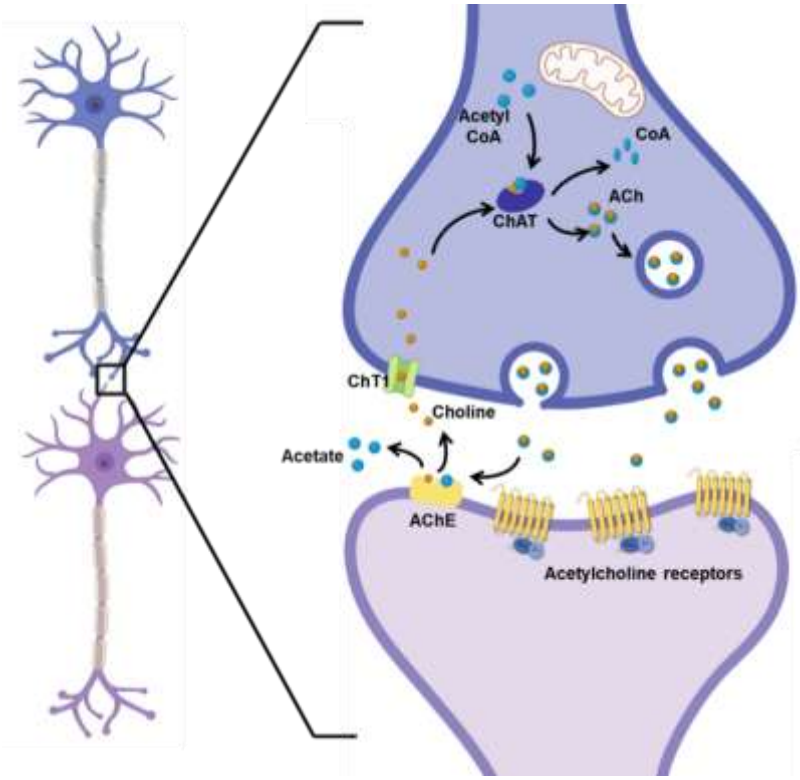

Figure 1-7 Cholinergic neurotransmission. Cholinergic neurotransmission relies on a system that involves synthesis, storage, transport, and degradation of ACh. Synthesis of ACh occurs at pre-synaptic cholinergic neurons (blue), and it is catalysed by the enzyme ChAT. ChAT can synthesise the neurotransmitter from acetyl coenzyme A (CoA) (produced by glycolysis in mitochondria), and choline (recycled and taken up from the synaptic cleft by the presynaptic neurons) (Nachmansohn and Machado, 1943). Newly synthesised ACh is transported by vesicular ACh transporters from the cytosol to into synaptic vesicles and released in the synaptic cleft. In the synaptic cleft, ACh can bind to and activate acetylcholine receptors such as muscarinic and nicotinic receptors expressed on post-synaptic neurons (purple). In the synaptic cleft, ACh is rapidly hydrolysed by the enzyme acetylcholinesterase (AChE), releasing acetate and choline, which is re-uptaken into the presynaptic cholinergic neuron by the high-affinity choline transporter (ChT1)(Birks and MacIntosh, 1961).

1.4.2 Current therapies and clinical trials for AD treatment

The current frontline treatment options for AD aim to restore cholinergic transmission in the brain, by inhibiting the enzyme acetylcholinesterase (AChE) that is responsible for the breakdown of ACh at the post-synaptic terminal (see Figure 1-7). AChE inhibitors can temporarily ameliorate some of the symptoms of AD however they have a limited therapeutic potential, and they are only efficacious for mild to moderate AD (Neugroschl and Wang, 2011). In addition, their non-specific nature represents a major drawback, causing GI and cardiovascular side effects induced by potentiation of cholinergic signalling in the PNS, including exocrine secretions, bradycardia and GI distress due to contraction of cardiac and smooth muscle (Courtney et al., 2004, Inglis, 2002). This results in modest overall efficacy of AChE inhibitors, and dose limitations, highlighting the need for receptor subtype- and tissue-specific agonists.

Furthermore, long-term treatment with donepezil offers no disease-modifying effects (Courtney et al., 2004). Therefore, there remains a significant unmet clinical need to develop novel therapies for AD with improved adverse effect profiles that can treat symptoms associated with AD and positively modify the underlying pathophysiology.

Most recently, aducanumab, a human IgG1 monoclonal antibody developed by Biogen, was approved by the US Food and Drug Administration (FDA) using the accelerated approval pathway, which is dedicated to drugs for serious or life-threatening illnesses (Food and Drug Administration, 2021). Aducanumab is specific against a conformational epitope found on Aß peptides that was originally derived from healthy, aged, cognitively normal donors with the rationale that these donors' immune systems had successfully resisted AD and therefore their antibodies could be therapeutically beneficial (Sevigny et al., 2016). Aducanumab was demonstrated to be able to reduce Aß burden in AD patients however many argue that there is not (yet) robust evidence for aducanumab's efficacy on cognitive or disease-modifying endpoint (Sevigny et al., 2016, Mullard, 2021). Other antibody-based immunotherapies directed against Aß peptides have been advanced to clinical trials, such as solanezumab (Eli Lilly and co.), gantenerumab (Roche), crenezumab (Roche), however solanezumab has been terminated due to lack of efficacy (Huang et al., 2020a). Two trials (AN-1792 and CAD106) using active immunotherapy strategies that consisted of diverse Aß peptides with the aim of boosting the immune response against disease-associated Aß isomers also were terminated due to adverse responses and no treatment effects (Gilman et al., 2005, Wiessner et al., 2011). Other potential drug therapies have been developed to lower Aß pathology in AD, such as beta secretase-1 (BACE-1) inhibitors. These are designed to inhibit amyloidogenic processing of APP (Vassar, 2002). However, since 2016, numerous trials on AD patients at different disease stages (prodromal, pre-clinical, early, mild to moderate) for BACE1 inhibitors have failed in phase 3 mostly due to lack of efficacy, with some compound causing further decline in cognition (Huang et al., 2020a).

Numerous compounds have also been developed to antagonise tau aggregation and formation of NFT. For example, TRx0237 (LMTX) is a tau aggregation inhibitor designed by TauRx Therapeutics Ltd that was shown to decrease the

level of aggregated tau proteins and ameliorate tau-related neuronal damage. TRx0237 was shown to significantly decrease the rate of disease progression in a Phase III trial for the treatment of early and mild-moderate AD (Wilcock et al., 2018). Other anti-tau therapies for AD include AADvac, which is a vaccine against pathological forms of tau, and an anti-tau antibody designed to capture and neutralise tau aggregates, zagotenemab (LY3303560) (Congdon and Sigurdsson, 2018, Huang et al., 2020a). Trials for AADvac and zagotenemab are still ongoing.

Several anti-inflammatory therapies have also been proposed in clinical trials. Amongst these, azeliragon is an antagonist of the receptor for advanced glycation end products (RAGE), which regulates multiple physiological processes in the CNS such as transport of plasma Aß, inflammatory process, oxidation stress, and blood flow (Burstein et al., 2018). Azeliragon reached phase III clinical trial for patients with mild AD however it recently failed due to lack of efficacy. In addition, therapies for the symptomatic treatment of AD are currently in trial, including both cognitive enhancers and therapies for the behavioural psychological symptoms of dementia. These include for example AXS-05, which is a combination of a N-methyl-D-aspartate (NMDA) receptor antagonist, a glutamate receptor modulator, a sigma-1 receptor agonist, and an inhibitor of the serotonin and NE transporters, that is being trialled in phase III for the treatment of agitation in AD patients (Wang and Reddy, 2017, Huang et al., 2020a).

1.4.3 The M1 mAChR as a target for the treatment of AD

Based on the cholinergic hypofunction in AD, many drug discovery programmes over the years have focussed their efforts on the development of compounds that are able to improve cholinergic transmission in pathology. In particular, the selective pharmacological activation of the M1 mAChR has been viewed as a promising approach for the symptomatic and disease-modifying treatment of AD and other forms of dementia (Fisher, 2008a, Scarpa et al., 2020).

Especially, the selective targeting of the M1 subtype represents a safer therapeutic strategy for improving cognitive function in AD as it would avoid off-target adverse responses that are associated with the non-selective mode of

action of AChE inhibitors (Inglis, 2002, Courtney et al., 2004) or other non-selective muscarinic compounds (Bodick et al., 1997b). M1 mAChRs are abundant in the regions of the forebrain, including the cerebral cortex and hippocampus (Levey, 1993, Volpicelli and Levey, 2004), where they are the predominant muscarinic receptor subtype (Bradley et al., 2017). These are the regions that are the most affected in AD, as human post-mortem AD brains display a substantial reduction in basal forebrain neurons, including a significant reduction in the cholinergic innervation of the neocortex and hippocampus (Whitehouse et al., 1981, Whitehouse et al., 1982). Importantly, the M1 mAChR plays a crucial role in cognition, particularly short-term memory which is impaired in AD (Fisher, 2008a, Ladner and Lee, 1998). Genetic deletion of M1 mAChRs in mice leads to deficits in working memory and memory consolidation (Anagnostaras et al., 2003). In addition to pro-cognitive activity, emerging evidence has been demonstrating that the M1 mAChR plays a neuroprotective role in neurodegenerative disease (Scarpa et al., 2021) as well as its pharmacological activation can exert disease modifying effects in a diverse range of models of AD and neurodegeneration (Scarpa et al., 2020, Dwomoh et al., 2021). See Chapter 5 for a detailed review.

Importantly, the M1 mAChR provides an important advantage as a drug target for the treatment of AD because it is expressed in post-synaptic neurons and remains relatively unchanged over disease progression since AD is characterised by loss of mainly pre-synaptic neurons (Levey, 1996, Svensson et al., 1992, Bradley et al., 2017, Mulugeta et al., 2003, Mash et al., 1985, Overk et al., 2010). Therefore, drugs directly targeting the M1 mAChR would likely remain efficacious in late-stage AD, unlike AChE inhibitors.

1.4.1 Types of M1 mAChR ligands for the treatment of AD

AChE inhibitors only provide therapeutic benefit to mild to moderate AD patients, and they lose efficacy as neurodegeneration progresses, likely due the fact that ACh release from cholinergic neurons is significantly diminished at later stages of disease (Neugroschl and Wang, 2011, Anand et al., 2014). Therefore, there is an unmet need for therapeutics for advanced to severe AD (Jack et al., 2012), and the diverse repertoire of M1 mAChR ligands might offer a promising prospective for patient stratification accordingly to disease stages.

For instance, pure M1 PAMs that lack intrinsic activity would be most beneficial at preclinical stages of disease, where neuronal loss is at early stages (Jack et al., 2012). In fact, pure M1 PAMs would likely restore cholinergic signalling by increasing the affinity and/or efficacy of the endogenous ligand ACh, maintaining the physiological spatiotemporal signalling characteristics and reducing the likelihood of over-stimulation of the receptor that could lead to adverse responses (Moran et al., 2018b). However, given that pure PAMs are probe-dependent, they may lose their therapeutic efficacy as disease progresses, when cholinergic neurons are being depleted and levels of endogenous ACh lower (Davies and Maloney, 1976, Perry et al., 1977). Thus, at later stages, ago-PAMs could be an alternative approach to pure PAMs since they would still be able to promote receptor signalling in the absence of ACh while still conferring high receptor subtype selectivity.

For later, severe stages of disease, when neurodegeneration is advanced and presynaptic cholinergic neurons are depleted, M1 mAChR-selective orthosteric or bitopic agonists may have improved therapeutic value compared to allosteric modulators. In fact, this type of ligand would still be able to bind M1 mAChRs with high affinity and efficaciously modulate receptor activity independently of endogenous ACh levels.

1.4.2 M1 mAChR-selective biased ligands for the treatment AD

In addition to displaying distinct modes of interaction (orthosteric, allosteric or bitopic) and different affinity/potency and efficacy properties, M1 ligands can also induce biased signalling. For example, some M1 mAChR ligands can preferentially activate G protein-dependent signalling over phosphorylation/arrestin-dependent pathways, leading to different physiological outcomes (Bradley et al., 2020). Development of M1 mAChR biased ligands may offer an approach to direct receptor signalling toward clinically beneficial outcomes, whilst avoiding pathways that lead to toxic/adverse responses. Previously, we developed a G protein-biased M1 mAChR mouse model, whereby removing receptor phosphorylation sites uncoupled the receptor from phosphorylation/arrestin-dependent signalling pathways (Bradley et al., 2020). This study emphasised the importance of the M1 mAChR phosphorylation in driving clinically relevant responses, such as improvements in learning and

memory and anxiolytic behaviour and protecting against peripheral and central cholinergic adverse responses.

The clinical use of ligands with signalling bias for the treatment of disease has been proposed for several GPCR-targeted therapeutics. For instance, it was encouraged for antipsychotic drugs targeting dopaminergic receptors (Lawler et al., 1999), for angiotensin analogues for the treatment of heart failure was the produced by Trevena, TRV027 (Felker et al., 2015), and for opioid medications for analgesia targeting μOR (Che et al., 2021). The promise of GPCR-targeted biased ligands is reviewed in detail in Chapter 3.

1.5 General aims of the thesis

Despite significant efforts, there is an unmet clinical need for disease-modifying treatments that are able to prevent, slow or stop neurodegenerative conditions such as AD (Hou et al., 2019). Given that GPCRs are involved in virtually any physiological process in both the PNS and CNS, it is unsurprising that members of this receptor superfamily are proposed as promising targets for the treatment of AD and other neurodegenerative disorders. Particular focus has been placed on the M1 subtype of the muscarinic family, as it has long been a validated target for the treatment of cognitive dysfunction, given its pivotal role in memory and learning and promising efficacy in clinical trials for the treatment of AD (Levey, 1996, Foster et al., 2014). Most importantly, emerging evidence has been pointing towards the disease-modifying potential of pharmacologically targeting the M1 mAChR for the treatment of neurodegeneration (Scarpa et al., 2020). This demonstrated there is still hope for potential new treatments for AD that are not only going to treat symptoms but can also modify the underlying pathophysiology.

Drug discovery programmes have invested significantly in the development of novel M1 mAChR ligands for the treatment of neurodegenerative disease, significantly improving the receptor-subtype selectivity to minimise off-target adverse effects associated to the activation of peripheral muscarinic subtypes (Scarpa et al., 2020, Gregory et al., 2007, Davoren et al., 2016). However, it has emerged that even highly selective M1 ligands might induce unwanted adverse responses by activating unwanted downstream signalling pathways (Rook et al.,

2017, Moran et al., 2018b). To tackle this issue, we propose the use of M1 mAChR- ligands for therapeutic application that are designed to drive GPCR signalling pathways that lead to clinically beneficial outcomes in preference to ones that are likely to result in adverse responses. It is therefore important to define the subtle pharmacological properties of M1 mAChR ligands that drive adverse toxic effects (seizures) opposed to those that drive the beneficial therapeutic outcomes (pro-cognitive activity and disease-modification). By employing a novel transgenic mouse model expressing a phosphorylation-deficient mutant M1 mAChR (M1-PD), our group found that adverse effects can be minimised by ensuring receptor phosphorylation (Bradley et al., 2020). My thesis aims to extend this study and explore the role of phosphorylation/arrestin-dependent signalling pathways in the context of neurodegenerative disease, as this will be crucial to understand the role of this receptor in pathology and provide further insights in the disease-modifying therapeutic potential of the M1 mAChR. I will therefore combine the M1-PD mice with mouse prion disease, an animal model for terminal neurodegeneration. To this end, the work presented in this thesis is based on three general aims:

1. Investigate the M1-PD signalling in comparison to the wild-type, *in vitro* (Chapter 3)

2. Characterise disease progression and markers of neurodegeneration and neuroinflammation in the mouse prion disease model (Chapter 4)

3. Assess the impact of removing the phosphorylation/arrestin-dependent signalling pathway on prion neurodegenerative disease progression (Chapter 5)

Chapter 2 Materials and Methods

2.1 Materials

Listed are key materials used in this project and the corresponding suppliers, with the product number (P/N) also detailed where possible.

2.1.1 Pharmacological compounds

Acetylcholine chloride ≥99% (TLC) (Sigma, P/N: A6625)

Atropine Sulphate Salt (Sigma, P/N: A-0257)

Carbachol (Sigma, P/N: PHR1511)

CNO – Clozapine N-Oxide (Tocris, P/N: 4636/50)

GSK1034702 – synthetised by Eli Lilly (Windlesham, Surrey, UK)

[^{3}H]-NMS – Scopolamine methyl chloride, [N-methyl- ^{3}H]-Scopolamine (PerkinElmer, P/N:NET636001MC)

Pilocarpine hydrochloride (Tocris, P/N: 0694)

2.1.2 General Materials and Reagents

Acrylamide Bis-Acrylamide Stock Solution, 30% Acrylamide (w/v) Ratio 37.5:1 (Severn Biotech Ltd, P/N: 20-2100-10)

Brilliant III Ultra-Fast SYBR Green (Agilent, P/N: 600882)

Calcium chloride solution (Sigma, P/N: 21115)

cOmplete™, Mini, EDTA-free Protease Inhibitor Cocktail (Sigma-Aldrich, P/N: 11836170001)

Dulbecco's Phosphate Buffered Saline (PBS) (Thermo Fisher Scientific, P/N: 14190094)

EDTA 0.5M, pH 8.0 (Invitrogen, P/N: 15575-038)

Foetal Bovine Serum (FBS) (Thermo Fisher Scientific, P/N: 10500064)

Goat serum (Sigma, P/N: G9023)

HBSS - Hank's Balanced Salt Solution (Thermo Fisher Scientific, P/N: 14025-050)

HBSS (10X) [+] $CaCl_2$, [+] $MgCl_2$ - Hank's Balanced Salt Solution (Thermo Fisher Scientific, P/N: 14025-049)

HEPES (1M) (Gibco, P/N: 15630-080)

Hygromycin B Solution (Santa Cruz Biotechnologies, P/N: sc-29067)

Nutrient Mixture F-12 Ham with L-glutamine and sodium bicarbonate (Sigma, P/N: N6658)

Penicillin-Streptomycin (Pen-Strep) (10,000U/mL) (Thermo Fisher Scientific, P/N: 15140122)

Phosphatase Inhibitor Cocktail tablets, 20 tablets (PhosSTO EASTpack) (Sigma-Aldrich, P/N: 04906837001)

Poly-D-lysine (Thermo Fisher Scientific, P/N: A3890401)

Precision Plus Protein All Blue Prestained Protein Standards (Bio-Rad, P/N: 1610373)

Proteinase K from *Engyodontium album* (Sigma, P/N: P2308)

Triton X-100 (Sigma, P/N: T9284)

Trypan Blue Solution (0.4%) (Sigma-Aldrich, P/N: T8154)

Tween-20 (Sigma, P/N: P7949)

Ultima Gold Liquid Scintillation Counting Cocktail (Perkin Elmer, P/N: 6013326)

VECTASHIELD® Hardset™ Antifade Mounting Medium with DAPI (Vector

Laboratories, P/N: H-1500).

SuperSignal™ West Pico PLUS Chemiluminescent substrate (Thermo Fisher Scientific, P/N:34578)

Zeocin (solution) 1 g (10 x 1 mL) (InvivoGen, P/N: ant-zn-1)

2.1.3 Kits

High-Capacity cDNA Reverse Transcription Kit (Applied Biosystems™, P/N: 4368813).

RNeasy Plus Mini Kit (Qiagen, P/N: 74134).

Pierce™ BCA Protein Assay Kit (Thermo Fisher Scientific, P/N: 23227)

IP-One – $G\alpha_q$ kit HTRF® assay (CisBio; P/N: 62IPAPEC)

Lysis & Detection Buffer (IP-One assay; CisBio; P/N: 62CL6FDF)

2.1.4 Histology materials (used at Eli Lilly and Co.)

a Reagents

Automation Haematoxylin (DAKO, P/N: S3301)

Cresyl 'Fast' Violet (acetate; 0.1% working solution; Merck, P/N: 2381-85-3)

ImmPACT DAB kit – 3,3'diaminobenzidine (Vector Labs, P/N: SK-4105)

Iron Alum (10% working solution; Merck, P/N: 7783-83-7)

Normal Goat serum (Vector Labs, P/N: S-1000)

Shandon ClearVue Mountant XYL (Thermo Scientific)

Solochrome cyanine (0.2% working solution; Merck, P/N: 3564-18-9)

Vectastain Elite RTU ABC Kit – Avidin-biotin complex (Vector Labs, P/N: PK-7100)

b Specialised equipment

Autostainer 720 (Thermo Scientific)

ClearVue coverslipper (Thermo Scientific)

Imagescope software (version 12.2.1.5005; Aperio)

Scanscope AT slide scanner (Aperio)

2.1.5 RNAScope materials (used at Eli Lilly and Co.)

a Probes

Peptidylpropyl isomerase B (PPIB; housekeeping reference) – mm-ppib (ACDBio, P/N: 313918)

Mouse Tumour Necrosis Factor α (TNFα) – mm-TNFα (ACDBio, P/N: 311088)

Mouse Interleukin 1ß (IL-1ß) – mm-il1b (ACDBio, P/N: 316898)

b Reagents

Hydrogen peroxide (ACDBio, P/N: 322335)

Protease III (ACDBio, P/N: 322337)

Signal amplification and BROWN detection reagents (ACDBio, P/N: 322310)

Washing buffer (ACDBio, P/N: 310091)

50% Gill's hematoxylin I (American Master Tech Scientific, P/N: HXGHE1LT)

2.1.6 Recipes for Buffers and Solutions

Binding assay buffer – 110 mM NaCl, 5.4 mM KCl, 1.8 mM $CaCl_2$, 1 mM $MgSO_4$, 25 mM glucose, 20 mM HEPES, 58 mM sucrose.

Blocking buffer for immunocytochemistry (CHO cells) - 2% (w/v) bovine serum albumin (BSA), 0.1% (v/v) Triton X-100 in TBS

Fixing solution – 4% (w/v) Paraformaldehyde (PFA) in PBS

IP1 Stimulation buffer – HBSS, 20mM HEPES, 1.2mM $CaCl_2$, 30mM $LiCl_2$; pH 7.4.

Krebs-Henseleit buffer (KHB) – 118 mM NaCl, 4.7 mM KCl, 4 mM $NaHCO_3$, 1.3 mM $CaCl_2$, 1.2 mM $MgSO_4$, 1.2 mM KH_2PO_4, 11.7 mM glucose, 8.5 mM HEPES.

Laemmli sample buffer (4x) – 250 mM Tris-base, pH 6.8, 4% (w/v) SDS, 40% (v/v) glycerol, 10% ß-mercaptoethanol and 0.04% (w/v) bromophenol blue.

Lysis Buffer – 1 M Tris-HCl pH 7.5, 0.5 M EDTA pH 8.0, EGTA pH 8.0, 10% (v/v) Triton X-100, 0.1% ß-mercapto-ethanol.

Radioimmunoprecipitation assay (RIPA) buffer – 50 mM Tris-HCl pH 8, 150 mM NaCl, 0.5% (w/v) sodium-deoxycholate, 1% (v/v) IGEPAL CA-630, 0.1% (v/v) SDS.

T/E buffer - 10 mM Tris, 1 mM EDTA, pH 8.0

TBS-Tween – TBS and 0.1% (v/v) Tween-20.

Transfer buffer – 25 mM Tris-base, 192 mM glycine, and 20% ethanol.

Tris Buffered Saline (TBS) - 20 mM Tris-HCl, pH 7.6, 137 mM NaCl.

Tris-Glycine SDS Running buffer – 5 mM Tris-Cl, 250 mM glycine, 0.1% SDS.

2.1.7 List of Primary antibodies

Antigen	Species	Working dilution	Source and P/N
Akt (pan)	mouse	1:1000 (WB)	Cell Signaling (2920)
α-tubulin	mouse	1:10,000 (WB)	Abcam (ab7291)
Apolipoprotein E (APO-E)	rabbit	1:1000 (WB)	Abcam (ab183596)
ß-actin	mouse	1:1000 (WB)	Abcam (ab6276)
Choline Acetyltransferase (ChAT)	rabbit	1:1000 (WB), 1:500 (IHC)	Abcam (ab178850)
Clusterin	goat	1:1000 (WB)	R&D Systems (AF2747)
Early endosomal antigen 1 (EEA1)	rabbit	1:1000 (ICC)	Thermo Fisher (PA1-063A)
Galectin 1	mouse	1:1000 (WB)	Abcam (ab138513)
Glial Fibrillary Acidic Protein (GFAP)	mouse	1:5000 (WB), 1:1000 (IHC)	Sigma-Aldrich (G3893)
GFAP *(for avidin-biotin complex IHC only)*	rabbit	1:4000 (IHC)	Biogenex (AR020-5R)
Human influenza hemagglutinin (HA)	rat	1:1000 (WB), 1:500 (IHC), 1:1000 (ICC)	Roche (12158167001)
Ionized calcium binding adaptor molecule 1 (Iba1)	rabbit	1:1000 (WB), 1:500 (IHC)	Thermo Fisher (PA5-27436)
Iba1 *(for avidin-biotin complex IHC only)*	rabbit	1:4000 (IHC)	Abcam (ab178846)
Microtubule-associated protein 2 (MAP2)	chicken	1:5000 (WB), 1:1000 (IHC)	BioLegend (822501)
Neuronal Nucleus (NeuN)	mouse	1:1000 (WB), 1:1000 (IHC)	Millipore (2159655

Prion protease resistant protein 27-30 *(for avidin-biotin complex IHC only)*	rabbit	1:400 (IHC)	Abcam (ab187555)
p38 MAPK	rabbit	1:1000 (WB)	Cell Signaling (9212)
p44/42 MAPK (Erk1/2)	rabbit	1:1000 (WB)	Cell Signaling (9102)
Phospho-Akt (S473)	rabbit	1:1000 (WB)	Cell Signaling (9271)
Phospho-p38 MAPK (T180/Y182)	mouse	1:1000 (WB)	Cell Signaling (9216)
Phospho-p44/42 MAPK (Erk1 (Y204)/Erk2 (Y187))	mouse	1:1000 (WB)	Cell Signaling (5726)
Phospho-SAPK/JNK (T183/Y185)	mouse	1:1000 (WB)	Cell Signaling (9255)
Postsynaptic density protein 95 (PSD95)	rabbit	1:2000 (WB)	Abcam (ab18258)
Prion protein (PrP)	mouse	1:1000 (WB)	Abcam (ab61409)
SAPK/JNK	rabbit	1:1000 (WB)	Cell Signaling (9252)
SerpinA3N	goat	1:1000 (WB)	R&D Systems (AF4709)
SynapsinI	rabbit	1:2000 (WB)	Abcam (ab64581)
Sodium Potassium ATPase	rabbit	1:10,000(WB)	Abcam (ab76020)
Vimentin	mouse	1:2000 (WB), 1:2000 (IHC)	R&D Systems (MAB21052)

Table 2-1 List and description of primary antibodies. Primary antibodies are listed according to their antigen, and details include species they are made in, working dilutions for western blot (WB), immunohistochemistry (IHC) or immunocytochemistry (ICC), and purchase details.

2.1.8 List of Secondary antibodies (western blot)

Antibody	Working Dilution	Source and P/N
IRDye 800CW Donkey anti-Chicken igG (H+L)	1:10,000	LI-COR Biotechnology (926-32218)
IRDye 680LT Donkey anti-Mouse IgG (H+L)	1:10,000	LI-COR Biotechnology (926-68022)
IRDye® 800CW Donkey anti-Mouse IgG (H + L)	1:10,000	LI-COR Biotechnology (926-32212)
Goat Anti-mouse IgG (H+L)-HRP Conjugate	1:4000	Bio-Rad (1721011)

IRDye 800CW Donkey anti-Rabbit IgG (H+L)	1:10,000	LI-COR Biotechnology (926-32213)
IRDye® 800CW Goat anti-Rat IgG (H + L)	1:10,000	LI-COR Biotechnology (926-32219)
Anti-Rat IgG (H+L)-HRP Conjugate	1:4000	Bio-Rad (5204-2504)

Table 2-2 List and description of secondary antibodies for western blots. The working solutions were made in 5% milk in TBS-T.

2.1.9 List of Secondary antibodies (Immunohistochemistry and Immunocytochemistry)

Antibody	Working dilution	Source and P/N
AlexaFluor™ 488 goat anti-rat IgG (H+L)	1:400	Invitrogen (A11006)
AlexaFluor™ 594 goat anti-mouse IgG (H+L)	1:400	Invitrogen (A11005)
AlexaFluor™ 488 goat anti-mouse IgG (H+L)	1:400	Invitrogen (A11001)
AlexaFluor™ 488 goat anti-rabbit IgG (H+L)	1:400	Invitrogen (A11008)
AlexaFluor™ 594 goat anti-chicken IgY (H+L)	1:400	Invitrogen (A11042)
AlexaFluor™ 594 goat anti-rabbit IgG (H+L)	1:400	Invitrogen (A11012)
Biotinylated goat anti-mouse IgG	1:200	Vector Labs (BA-9200)
Biotinylated goat anti-rabbit IgG1	1:200	Vector Labs (BA-1000)

Table 2-3 List and description of secondary antibodies for immunohistochemistry and immunocytochemistry

2.1.10 List of Primers

Primer Template	Primer assay name	Source and P/N
CD86 (mouse)	Mm_Cd86_1_SG	Qiagen (QT01055250)
Chrm1 (mouse)	Mm_Chrm1_1_SG	Qiagen (QT00282527)
Gfap (mouse)	Mm_Gfap_1_SG	Qiagen (QT00101143)
IL-1ß (mouse)	Mm_Il1b_2_SG	Qiagen (QT01048355)
IL-4 (mouse)	Mm_Il4_1_SG	Qiagen (QT00160678)
IL-6 (mouse)	Mm_Il6_1_SG	Qiagen (QT00098875)
IL-10 (mouse)	Mm_Il10_1_SG	Qiagen (QT00106169)
IL-11 (mouse)	Mm_Il11_1_SG	Qiagen (QT00122122)

IL-13 (mouse)	Mm_Il13_1_SG	Qiagen (QT00099554)
Prion protein (mouse)	Mm_Prnp_1_SG	Qiagen (QT00101080)
TNF-α (mouse)	Mm_Tnf_1_SG	Qiagen (QT00104006)
α-tubulin (mouse)	Mm_Tuba1b_1_SG	Qiagen (QT00198877)

Table 2-4 List and description of primer assays for quantitative PCR.

2.1.11 Specialised equipment

Immunoblotting apparatus - power supplies, gel casting apparatus, electrophoresis chamber etc. from the Bio-Rad Mini-PROTEAN range (Bio-Rad Laboratories Ltd.)

FLUOstar OPTIMA Microplate Reader (BMG Labtech)

LI-COR Odyssey Sa Infrared Imaging System (LI-COR Biosciences)

Liquid Scintillation Counter (Beckman Coulter, UK LS6500)

QuantStudio™ 5 Real-Time PCR System (Thermo Fisher Scientific)

2.2 Cell culture

2.2.1 Generation of CHO Flp-In™ cell lines

Chinese Hamster Ovary (CHO) cells were previously generated using the Flp-In™ system to stably and constitutively express HA-tagged versions of the following receptors:

1) **M1-WT**: mouse wild type M1 mAChR
2) **M1-PD**: phosphorylation-deficient (PD) mutant of the mouse M1 mAChR
3) **M1-DR**: designer receptor exclusively activated by designer drugs (DREADD) of the human M1 mAChR
4) **M1-PD DR**: PD, DREADD of the human M1 mAChR

CHO Flp-In cells were co-transfected with pcDNA5FRT containing the M1 mAChR and pOG44, and transfected cells were selected with hygromycin B (Butcher et al., 2016). To facilitate detection of the receptors, an haemagglutinin (HA) epitope tag was fused to the C-terminus of the receptors.

2.2.2 CHO cell line maintenance

CHO cells were cultured at 37°C and 5% CO_2 in a humidified atmosphere and grown to confluence in Nutrient Mixture F12 Ham containing 10% foetal bovine serum (FBS), and penicillin/streptomycin (100 U/mL). For non-transfected CHO cells expressing flippase (Flp-In), the media was supplemented with 1µg/mL Zeocin (InvivoGen), and for stably transfected Flp-In CHO cell lines 0.4µg/mL hygromycin (Santa Cruz Biotechnologies) was added.

To passage cell lines, the respective culture medium was aspirated, and cells were washed with sterile Dulbecco's PBS (Thermo Fisher Scientific), followed by incubation with PBS-EDTA for approximately 5 min at 37°C. Upon detachment of cells from the culture vessel, culture medium was added, and the cell suspension was transferred to a centrifuge tube to spin for 2 min at 1000 x *g*. After discarding the supernatant, the cell pellet was resuspended in a volume of fresh media required to achieve 10x the desired dilution for cell passaging. The cell suspension was then transferred into a sterile culture vessel with an appropriate volume of fresh culture medium added to achieve the desired dilution.

2.2.3 Determination of cell viability

Live cell counts were performed through trypan blue staining and manual haemocytometer counting. Cell suspensions were gently mixed and combined with 0.4% trypan blue (1:1). This dye penetrates and bypasses the plasma membrane of severely damaged and dead cells and stains them blue thereby allowing the determination of cell viability by observation using a light microscope. Through manual counting with a haemocytometer, an estimation of total number of living cells per mL suspension was obtained. Typically, >90% of cells were deemed viable.

2.2.4 Cryopreservation

Cell lines were cryopreserved for long-term storage in liquid nitrogen or in -80°C freezers. Confluent cells were detached by incubating with PBD-EDTA and subjected to centrifugation at 1000 x *g* for 5 min. The pellet was resuspended in FBS + 10% (v/v) DMSO (1 mL per T75 flask) and 1 mL aliquots frozen at − 80°C

before transferring to liquid nitrogen storage. Cryopreserved cells were revived by thawing rapidly in a 37°C water bath and transferring to 10 mL pre-warmed culture medium in a flask. Cells were split after 16-24h.

2.3 Pharmacological and functional assays

2.3.1 [^{3}H]-NMS Saturation Binding Assay

Cells were plated at 50,000 cells/well on clear 24-well plates and grown to confluence over 48 hours. After two washes with warm binding assay buffer, cell monolayers were incubated for two hours at 37°C with binding assay buffer containing increasing concentrations of the tritiated radioligand [^{3}H] N-methyl scopolamine ([^{3}H]-NMS). After two washes with 0.9% NaCl to remove unbound ligand, cells were solubilised with 0.1 M NaOH, and transferred to scintillation vials. Bound radioactivity was determined by liquid scintillation (Ultima Gold; PerkinElmer, Boston, MA) counting. Nonspecific binding (N.S.B.) was determined in the presence of 10 μM atropine. Data were analysed using GraphPad Prism 7 to obtain non-linear regression curves.

2.3.2 Receptor Internalisation Assay

Cells were plated at 50,000 cells/mL on clear 24-well plates and grown to confluence. Cell monolayers were washed twice with warmed PBS and incubated with serum-free F12 medium at 37°C in a humidified atmosphere of 5% CO_2 in air. Two versions of this assay were performed to generate a time-course or a concentration-response curve for receptor internalisation in response to ligands. For the time-course receptor internalisation assay, the ligands were added at consistent concentration of 100 μM but stimulated for increasing amount of time periods in a reverse time-course manner (4 hours, one hour, 30 min, 15 min, 5 min, 0 min). For the concentration-response curve internalisation assay, ligands were added for one hour but with increasing concentrations. Following incubation with the test compounds at 37°, cells were transferred to an ice bath and washed twice with ice-cold Krebs-Henseleit buffer (KHB). Cells were then incubated overnight (16 hours) at 4°C with a saturating concentration of [^{3}H]-NMS (3 nM) to label cell-surface receptors. After radiolabelling, cells were washed twice with ice-cold KHB to remove unbound radioligand, solubilised with 0.1 M NaOH, and transferred to scintillation vials. Bound radioactivity was

determined by liquid scintillation (Ultima Gold; PerkinElmer, Boston, MA) counting. N.S.B. was determined in the presence of 10 µM atropine. Data are shown as a percentage of [^{3}H]-NMS specific binding normalised to the basal.

2.3.3 IP1 Accumulation Assay (CHO cells)

$G\alpha_q$ protein signalling was determined by measuring inositide signalling pathway through the detection of the by-product inositol-1-phosphate (IP1) accumulation using the IP1 HTRF® assay kit (CisBio). Cells were plated on 96-well plates at 40,000 cells/well of seeding density and grown for 24 hours prior to the assay. Cells were washed and incubated (90 µL) in IP1 stimulation buffer (Hank's Balanced Salt Solution (HBSS) w/o phenol red containing 20 mM HEPES, 1.2 mM $CaCl_2$; 30 mM LiCl; pH7.4) for one hour at 37˚C prior drug treatments. 10X concentrated test compounds were added (10 µL/well) to the 96-well plates and incubated at 37˚C for one hour. Following the treatment, the stimulation buffer was removed, and lysis buffer (IP-One assay kit, CisBio) was added (40 µL/well). Following 10 min-incubation on a shaker at 600 rpm, cell suspensions (7µL/well) were added to 384-well white proxiplates (PerkinElmer). The IP1-d2 conjugate and the anti-IP1 cryptate Tb conjugate (IP-One Tb™ assay kit, CisBio) were diluted together 1:40 in lysis buffer and 3 µL of the antibody mix were added to each well. The plate was incubated at 37˚C for 1-24 hours and FRET between d2-conjugated IP1 (emission at 665 nm) and Lumi4™-Tb cryptate conjugated anti-IP1 antibody (emission at 620 nm) was detected using a CLARIOstar plate reader (BMG Labtech). Results were calculated from absorbance ratio at 665/620 nm and normalised to the maximal response stimulated at the reference receptor (M1-WT or M1-DR), or compound (ACh or CNO), as stated.

2.3.4 Immunocytochemistry for receptor internalisation

CHO cells were grown for 24 hours to achieve 60-80% confluence on 13 mm glass coverslips coated with 0.01% poly-D-lysine. Cells were stimulated with 100 µM carbachol (M1-WT and M1-PD) or CNO (M1-DR or M1-PD DR) for one hour, briefly transferred on ice to prevent further receptor trafficking and fixed using 4% PFA. After fixation, cells were blocked and permeabilised using 2% BSA in TBS-Triton X-100 (0.1%). Incubation with primary antibodies was carried out at 4˚C overnight or at room temperature for two hours. Following three washes with

TBS buffer, AlexaFluor secondary antibody incubation (1:400 dilution in TBS) was conducted in the dark for two hours at room temperature. Following three quick washes with TBS to remove any residual antibodies, coverslips were mounted on glass slides using VECTASHIELD HardSet Antifade Mounting Medium with DAPI, let dry overnight at 4°C and sealed using nail varnish. Slides were stored at 4°C in the dark until imaging. Imaging was conducted using a Zeiss confocal microscope (63x objective) using the same settings for each separate experiment. Co-localisation coefficients were obtained through Zeiss Black software, where they are calculated using Manders' formula (see 2.9.3).

2.4 Immunoblotting

2.4.1 Sample preparation for immunoblotting

a Preparation of lysates from cultured cells

Cells were cultured to confluence on 6-well tissue culture plates and, following two washes with ice-cold PBS, cells are lysed in 500 µL per well of lysis buffer. Samples were collected by scraping on ice and centrifuged at 15,000 rpm for 15 min at 4°C. Resulting supernatant was extracted and protein concentration was measured using BCA assay (see d). Following preparation, cell lysates were added to 4X Laemmli sample buffer to give 1X final concentration. Samples were heated at 37°C for 30 min and briefly centrifuged before loading on a gel.

b Homogenate preparation

Frozen tissue was homogenised in ice-cold RIPA buffer with one tablet of each protease inhibitor cocktail and phosphatase inhibitor cocktail using a sonicator at amplitude 3-5 Hz. The homogenate was mixed for 30 min at 4°C and centrifuged at 21000 x *g* for 15 min. Resulting supernatant was collected, and following BCA assay to measure protein concentration, the sample was diluted in RIPA buffer (containing protease and phosphatase inhibitor cocktails) to a concentration of 4 µg/µL and stored at -80°C until use.

c Membrane extract preparation

Frozen hippocampi and cortices were homogenised by sonication at 3-5 µg amplitude in 500 µL of T/E buffer containing proteinase and phosphatase

inhibitors. Samples were then centrifuged at 10,000 x *g* for 10 min at 4 °C. Supernatants were mixed with additional 500 µL T/E buffer and centrifuged at 15,000 x *g* for 1 hour at 4 °C. The pellets were then solubilised in 400 µL of RIPA buffer including phosphatase and proteinase inhibitors and incubated for at least 2 hours at 4°C with end-over-end rotation. After centrifugation of samples at 14,000 x *g* for 10 min at 4°C, the supernatants (membrane extracts) were transferred to fresh microcentrifuge tubes and stored at -80°C until use. Protein concentrations were determined by using the Micro BCA protein assay reagent kit according to the manufacturer's instructions.

d BCA protein assay

When appropriate, a BCA protein assay was employed to measure protein concentrations. 10 µL of each unknown protein sample (tissue samples were diluted 1:10 in RIPA buffer) and a range of BSA protein standards (0-10 mg/mL) in duplicate were combined with the manufacturer's BCA assay mix, and incubated at 37°C for 30 min. The absorbance at 562 nm was recorded using a microplate reader.

2.4.2 SDS-PAGE

Polyacrylamide resolving gels were cast using the Bio-rad mini-Protean III equipment. The final percentage of acrylamide was determined by the size of the protein of interest, typically 8% for proteins >60 kDa and 12% for proteins <60 kDa. Other components were 375 mM Tris (pH 8.8), 0.1% SDS (w/v), 0.1% APS (w/v), and 200 nM TEMED, diluted in distilled water. Typical gel thickness was 1.5 mm. The stacking gel was cast on top of the resolving gel once it had set. The reagents required to make this gel were the same as the resolving gel, but at a final concentration of 5% acrylamide, 125 mM Tris (pH 6.8), 0.1% SDS (v/v), 0.1% APS(v/v), and 200 nM TEMED. Samples were usually electrophoresed in Tris-glycine SDS running buffer starting at 60 V, and at 150 V once the samples reached the end of the stacking gel (~30 min).

2.4.3 Probing and detection

Following SDS-PAGE, nitrocellulose membranes and gels were equilibrated in transfer buffer for 5 min, the gel was placed in direct contact with a membrane

within a tight sandwich of transfer sponges and 1 mm Whatman chromatography paper in a transfer cassette. This in turn was placed within a transfer tank that was filled with transfer buffer, and transfer was allowed for 2 hours at constant voltage of 60 V. Then, membranes were incubated in 5% (w/v) non-fat milk powder in TBS-T for 30-45 min at room temperature to block nonspecific binding sites. Blocked membranes were incubated with primary antibody at 4°C overnight or room temperature for 2 hours, and blots were subsequently washed with TBS-T and incubated for one hour at room temperature with the relevant secondary antibody. Following TBS-T washes, proteins were visualised using LICOR Odyssey SA scanner using the appropriate lasers, or with the ECL detection system.

2.4.4 Proteinase K Digestion

For assessing levels of scrapie prion protein (PrP_{Sc}), brain tissues were homogenised in RIPA buffer (as described above) and digested with proteinase K prior western blotting. Homogenates (40 µg) were incubated with 0.01 mg/mL of proteinase K for 10 min at 37°C, then re-suspended into Laemmli sample buffer (containing 20% ß-mercaptoethanol) to achieve a concentration of 0.3 µg/µL. Normally (unless otherwise stated) 30 µL of samples were loaded onto a 12% acrylamide gel, and western blotting was conducted as described above.

2.5 Gene expression analysis

2.5.1 RNA extraction from brain tissue

RNA extraction was performed from frozen brain tissue using the Qiagen RNeasy Plus Mini kit as per manufacturer instructions. Briefly, following homogenisation in RLT Buffer containing 10% ß-mercaptoethanol, the homogenate was centrifuged at 10,000 x *g* for 30 sec in a gDNA eliminator column. The aqueous phase containing RNA was collected and mixed with 70% ethanol, then applied to a RNeasy Mini spin column and subjected to centrifugation at 8000 x *g* for 15 sec at room temperature. The flow-through was discarded and the column was washed with guanidine containing stringent wash buffer, then washed with mild wash buffer, centrifuging for 2 min after the final wash to remove residual ethanol. RNA was eluted in 30-40 µL nuclease-free water.

a Determination of RNA concentration

RNA concentration was determined by measuring absorbance at 260 nm using a Nanodrop spectrophotometer. RNA purity was assessed accordingly the absorbance ratios at 230/260 nm and 260/280 nm, with ratios of 1.8–2.2 considered pure. RNA was stored at –80°C until use.

2.5.2 Reverse transcription (RT)

For cDNA synthesis, extracted RNA was reverse transcribed using a High-Capacity cDNA Reverse Transcription Kit with RNase Inhibitor (Applied Biosystems™, P/N: 4368813). 20 µL reactions were set up in PCR tubes as follows; 10 µL of total RNA template (1 µg) was mixed with 10 µL of reaction mix containing the following components:

- 1x RT buffer,
- 50 units MultiScribe Reverse Transcriptase
- 4 mM dNTP Mix
- 1x RT random primers
- RNAse-free water

Reaction mixtures were incubated in a thermal cycler using the following conditions:

1.	Annealing	10 min	25°C
2.	Extension	120 min	37°C
3.	Inactivation	5 min	85°C
4.	End	∞	4°C

Each reaction was performed in the presence and absence of RT enzyme (-RT control). cDNA samples were stored at -20°C until quantitative real-time (qRT)-PCR was performed.

2.5.3 Quantitative Real-Time PCR (qRT-PCR)

qRT-PCR was conducted using Brilliant III Ultra-Fast SYBR® Green QPCR Master Mix (Agilent). The primer assays used are detailed in Table 2-4. Each reaction was set up in a total volume of 14 µL in duplicate or triplicate in 384-well

MicroAmp® Optical PCR plates (Life Technologies) using the following components:

- 7 µL SYBR Green Master Mix
- 1.4 µL primers (10 µM stock)
- 1.4 µL RT product (or –RT control sample)
- RNAse-free water

Plates were read on a QuantStudio™ 5 Real-Time PCR System (Thermo Fisher Scientific) using the fluorescence channel for SYBR Green. The amplification cycles were set up using the following conditions:

1.	Preheating	3 min	95°C
2.	Denaturing	5 sec	95°C
3.	Annealing	12 sec	60°C
4.	Repeat steps 2–3 (x40)		

Followed by the following conditions to produce a melt curve:

1.	Heating	1 sec	95°C
2.	Annealing	20 sec	60°C
3.	Heating	1 sec	95°C

Comparative cycle threshold (C_T) values were obtained using QuantStudio™ Design and Analysis software (Thermo Fisher Scientific).

2.6 Histology

2.6.1 Tissue harvest and preparation for histology

Mice were anaesthetised with 3% isoflurane (2L/min O_2) and transcardial perfused with 20 mL of ice-cold PBS followed by 20 mL of freshly prepared 4% PFA (unless otherwise stated). Following perfusions, brains were immediately removed and further fixed in 4% PFA at room temperature for 24-72h and stored in PBS with 0.02% sodium azide at 4°C until tissue processing.

2.6.2 Tissue processing

All the brains were processed by the University of Glasgow Histology Research service (Veterinary Diagnostic services) using the following overnight (17 hours) protocol:

1. Ethanol 1 hour (4x)
2. Ethanol 1.5 hour
3. Ethanol 2 hour
4. Xylene 1 hour (2x)
5. Xylene 1.5 hour
6. Paraffin wax 2 hours (3x)

At the University of Glasgow, paraffin-embedded brains were sagittally cut in 3 µm sections using a Thermo Shando HM340 rotary microtome by the University of Glasgow Histology Research service and baked in a 37ºC oven overnight.

At Eli Lilly and co., paraffin-embedded brains were sagittally cut by me in 6 µm sections using a rotatory microtome and air-dried at 45 ºC on a heated platform for at least 24 hours. Dry sections could then be stored at room temperature until required.

2.6.3 Deparaffinisation and rehydration of brain sections

For experiments conducted at the University of Glasgow, deparaffinisation and rehydration were performed by the University of Glasgow Histology Research service using the following conditions:

1. Histoclear (a Xylene substitute) to de-wax 5 min
2. 100% Ethanol 5 min (2x)
3. 70% Ethanol 5 min
4. Water 5 min

For experiments conducted at Eli Lilly and co., deparaffinisation and rehydration were conducted by me using the following protocol:

1. Xylene 5 min (3x)
2. Industrial Methylated Spirit (IMS) 5 min (2x)

3. 70% IMS 5 min
4. Water 5 min

Following deparaffinisation and rehydration, sections were subjected to either antigen retrieval for immunohistochemistry, or solochrome cyanine or haematoxylin and eosin staining (H&E) staining.

2.6.4 Heat-induced epitope retrieval

At the University of Glasgow, antigen retrieval was performed by the University of Glasgow Histology Research service using a Menarini Access Retrieval Unit with Sodium Citrate buffer (pH 6.0) for 1 min 40 sec at 125ºC full pressure.

At Eli Lilly and co., antigen retrieval was performed by heat-induced epitope retrieval at 100°C for 20 min – unless stated otherwise – using Lab Vision PT Module (Thermo Fisher Scientific) in Citrate Buffer. For immunohistochemical staining of PrP_{Sc}, antigen retrieval was performed at approximately 100°C in deionised water for 30 min using a vegetable steamer (Russel Hobs).

2.6.5 Solochrome staining

Rehydrated sections were stained using the following conditions:

1. Solochrome cyanine (0.2% in distilled water) 12-15 min
2. Running tap water 5 min
3. 10% Iron Alum (Ferric Ammonium Sulphate) 2 min *max* (3x)
4. Running tap water 5 min
5. Cresyl 'Fast' Violet (acetate) Time depends on desired staining intensity

Following solochrome cyanine staining, section dehydration was carried out by short incubations (incubation times varied depending on the stain retention) through an alcohol gradient as follows:

1. Water 1 min
2. 70% IMS 10 sec
3. 100% IMS 20-30 sec (3x)
4. Xylene 1-2 min (3x)

Slides were coverslipped using Shandon ClearVue Mountant XYL and ClearVue coverslipper (Thermo Scientific). Stained slides were scanned and digitized using a Scanscope AT slide scanner (Aperio) at 20x magnification and viewed using Imagescope software (version 12.2.1.5005; Aperio).

2.6.6 Selection of levels for histological analysis

PFA (4%)-perfused and fixed brains from Tg37 control or prion mice were paraffin wax-embedded and the left hemisphere was sagittally sectioned using a rotary microtome. From the middle segment, 6 µm serial sections were cut from bregma 0 to approximately lateral 3 mm and mounted on glass slides (three sections per slide). One slide with sections every 15 consecutive slides (every 250-270 µm approximately, taking sectioning errors and waste into account) were stained using solochrome cyanine to enable the observation of relevant brain structures (Figure 2-1). Solochrome cyanine (also called eriochrome cyanine R, chromoxane cyanin R and chromoxane B) is a polycyclic aromatic sulfonic acid which has been employed as a histological stain to demonstrate a number of tissue elements such as osteoid in bone and myelin in neural tissues (Kiernan, 1984, Kiernan, 2007).

Solochrome cyanine staining informed the choice of the appropriate sagittal anatomical levels that would allow the view of many regions of interest for further histopathological analyses (Figure 2-1B). Two levels were picked for two main reasons: 1) to determine whether the spread of pathology differs laterally across the brain; 2) many of the regions are viewed better in separate planes, for example the fornix (f) is visible in bregma lateral 0.72mm whereas the caudate putamen (CPu; the mouse equivalent of the human striatum) is best viewed in bregma lateral 1.68mm. The brain structures that can be identified at these levels include anterior commissure (ac), caudate putamen (CPu), cortex (ctx), corpus callosum (cc), dorsal subiculum (DS), fornix (f), hippocampus (hpc), hypothalamus (HTh), midbrain (mb), medulla (md), pons (Pn), substantia nigra (SNR), thalamus (Th), and vestibule (Ve).

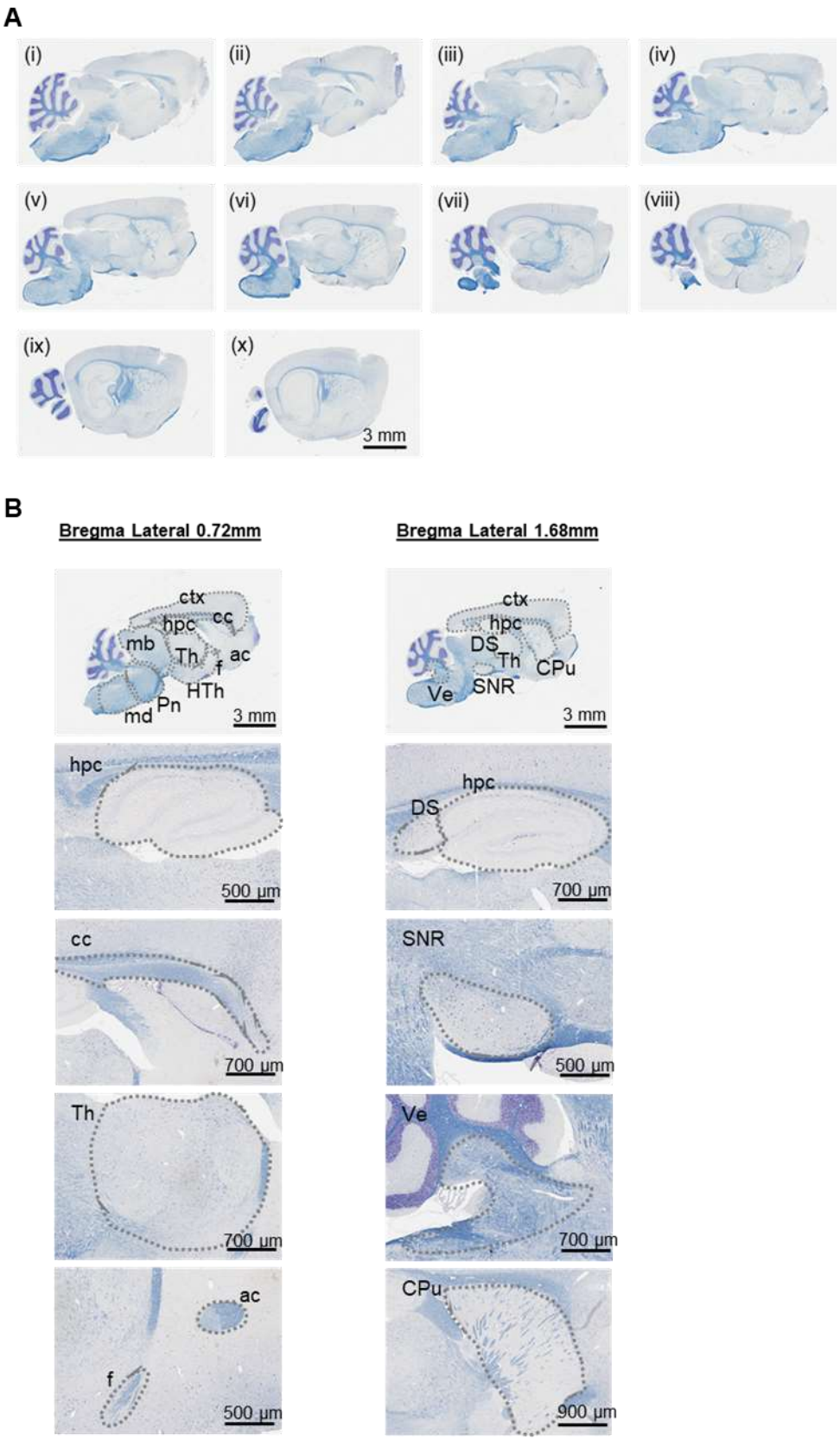

Figure 2-1 Anatomical brain structures of hemizygous Tg37 mice visualised by solochrome cyanine staining. (A) Representative examples of solochrome cyanine staining of sagittal sections every 250-270 µm approximately (accounting for sectioning errors and waste) enabled the staining of myelin sheaths and the visualisation of anatomical structures. **(B)** Representative images of sagittal anatomical levels at bregma lateral 0.72 mm and 1.68mm. The brain structures that can be identified at these levels include anterior commissure (ac), caudate putamen (CPu), cortex (ctx), corpus callosum (cc), dorsal subiculum (DS), fornix (f), hippocampus (hpc), hypothalamus (HTh), midbrain (mb), medulla (md), pons (Pn), substantia nigra (SNR), thalamus (Th), and vestibule (Ve).

2.6.7 Haematoxylin and eosin staining (H&E)

Following sample rehydration (sections to water), H&E staining was performed by the University of Glasgow Histology Research service using the following protocol:

1. Haematoxylin (Gill) for 5 mins
2. Wash in water
3. Differentiate in 1% acid alcohol
4. Wash in water
5. Wash in Blue in Scotts tap water substitute (STWS) (regional)
6. Eosin (Putts) for 5 mins
7. Wash in water
8. Dehydrate, clear and mount in synthetic resin mounting media

Images showing the whole brain were taken with a x4, and the hippocampus using x20 or 40x objectives on a Zeiss EVOS FL Auto 2.

2.6.8 Immunohistochemistry (Avidin-biotin complex method)

Immunohistochemistry using the avidin-biotin complex detection method was conducted at Eli Lilly and co. using an autostainer (720, Thermo Scientific) following steps below:

1. 0.3% H2O2	10 min
2. Normal goat serum (Vector Labs)	30 min
3. Primary antibody (see Table 2-1 for details)	60 min
4. Secondary antibody (see Table 2-3 for details)	30 min
5. Avidin-biotin complex solution (Vectastain Elite RTU ABC kit)	30 min
6. 3,3'-diaminobenzidine (ImmPACT DAB kit)	5 min
7. Haematoxylin (for counterstaining)	5 min

Dehydration was carried out by incubations through an alcohol gradient as follows:

1. Warm water	5 min
2. 70% IMS	5 min
3. 100% IMS	5 min (2x)

4. Xylene 5 min (3x)

Following cover slipping of slides as described above (2.6.5), slides were scanned, and images were digitised with Scanscope AT slide scanner (Aperio) at 20x magnification. Visualization of the digitized tissue sections and delineation of the regions of interest were achieved using Imagescope software (version 12.2.1.5005; Aperio). Positivity was quantified automatically using a positive pixel algorithm calibrated to ignore non-specific staining.

2.6.9 Immunohistochemistry (fluorescence)

Following antigen retrieval, sections were washed in TBS with 0.1% triton x-100, and blocked overnight at 4˚C in TBS, 0.1% triton X-100, 10% goat serum and 1% BSA. Incubation with primary antibodies was conducted in blocking buffer overnight at 4˚C or for two hours at room temperature. Following three washes, slides were incubated with Alexa Fluor fluorescent secondary antibodies (see Table 2-3) for 2 hours at room temperature in blocking buffer. Following three washes, slices were mounted on glass slides using VECTASHIELD HardSet Antifade Mounting Medium with DAPI, let dry overnight at 4˚C and sealed using nail varnish. All images were taken using a LSM 880 confocal laser scanning microscope (Zeiss).

2.6.10 RNAScope

RNAScope experiment were conducted at Eli Lilly and co. using a BOND RX Fully Automated Research Stainer (Leica) set up with the following steps:

Deparaffination

1. Bake at 60˚C for 30 min
2. BOND dewaxing solution at 72˚C for 30 seconds

Antigen retrieval

3. ER2 (EDTA buffer pH 9.0) at 95˚C for 15 min
4. BOND wash solution 4x, rapid washes no incubation
5. BOND wash solution 1x, 3 min incubation

Protease and hydrogen peroxide treatment

6. ACD enzyme (protease) 40˚C for 15 min
7. BOND wash solution 3x, rapid washes no incubation

8. Hydrogen peroxide for 10 min
9. BOND wash solution 3x, rapid washes no incubation

Probe application

10. Probe application 42C for 120 min

Amplification using signal amplification and detection reagents (ACDBio, P/N: 322310). Before adding each AMP reagent, samples were washed twice with washing buffer (ACDBio, P/N: 310091)

11. AMP 1 for 30 min
12. AMP 2 for 15 min
13. AMP 3 for 30 min
14. AMP 4 for 15 min
15. AMP 5 for 30 min
16. AMP6 for 15 min

Chromogen reaction and hematoxylin staining

17. BOND wash solution 4X, 1 min each wash
18. RNAscope 2.5 LSx Rinse 2X, 5 min each
19. Mixed red refine-LSx for 1 min
20. Mixed red refine-LSx for 10 min
21. BOND wash solution 4X, rapid washes no incubation
22. RNAscope 2.5 LSx hematoxylin for 5 min
23. Deionized water 6X, rapid washes no incubation
24. RNAscope 2.5LSx bluing solution for 5 min
25. Deionized water 6X, rapid washes no incubation

Slides were then coverslipped using Shandon ClearVue Mountant XYL and ClearVue coverslipper (Thermo Scientific). The stained slides were scanned and digitized using the Scanscope AT slide scanner (Aperio) at 20x magnification and viewed using Imagescope software (version 12.2.1.5005; Aperio).

2.7 Experimental animals

2.7.1 Ethics statement

All procedures were conducted in accordance with the Animals (Scientific Procedures) Act 1986 under personal licence IFC7EAB62, held by the

undersigned, and project licence 70/8473 or PP7704105, held by Prof Andrew B. Tobin (University of Glasgow).

2.7.2 Mouse maintenance and diet

Mice were fed ad libitum with a standard mouse chow. The mAChR knockout mice were backcrossed for at least 10 generations onto the black C57BL6/NTAC background. The Tg37 mouse line that overexpresses mouse PrPn has been described previously (Mallucci et al., 2003).

2.7.3 Generation of knock-in animals

For the generation of knock-in mice was carried out by Genoway using a Cre/lox system. Briefly, constructs containing the loxP-Stop-loxP cassette upstream of a sequence encoding for the HA-tagged (C-terminus) version of the M1-WT and M1-PD receptors, were generated and inserted within the encoding exon (exon 3) of the M1 mAChR gene (Chmr1) of C57BL/6 mice. The M1-PD is the coding sequence of the mouse M1 mAChR with mutations in the third intracellular loop and C-terminal tail that replace 20 serine/threonine residues with alanine (Butcher et al., 2016, Bradley et al., 2020) (Figure 3-2). Targeted constructs were transfected in embryonic stem cells which were injected into blastocysts for the generation of chimeric mice. Breeding of chimeras with C57BL/6 and Cre-recombinase expressing mice allowed the generation of heterozygous mice, which were in turn bred for the generation of homozygous lines.

2.7.4 Prion infection of mice

Mice aged 3 to 4 weeks were inoculated by intracerebral injection into the left parietal lobe with 1% brain homogenate (20 µl) infected with Rocky Mountain Laboratory (RML) prion as described previously (Mallucci et al., 2003). Inoculum of RML prion-infected brain homogenate were derived from RML mouse-passaged scrapie prions that were originally derived from the “drowsy goat” line (Kimberlin and Walker, 1978, Chandler, 1961). Inoculations were conducted using a free-hand injection method by the animal technician to maximise consistency. Control mice received 1% normal brain homogenate (NBH) (20 µl).

2.7.5 Tissue harvest

Cerebral tissues (cortex, hippocampus, and striatum) were harvested at sacrifice by cervical dislocation. Harvested tissues were snap frozen in dry ice and stored at − 80°C until use.

2.8 Behavioural observations

2.8.1 Symptom scoring and survival studies

Prion-infected mice were scored according to the appearance of recognised early indicator and confirmatory signs of prion disease. Early indicator signs included piloerection, sustained erect ears, erect penis, clasping of hind legs when lifted by tail, rigid tail, unsustained hunched posture, mild loss of coordination, and being subdued. Confirmatory signs of prion disease included ataxia, impairment of righting reflex, dragging of limbs, sustained hunched posture, and significant abnormal breathing. Symptom onset was established with the appearance of at least two of the early indicator signs of disease, whereas mice were culled when they developed clinical disease which was determined by the appearance of two early indicator signs plus one confirmatory sign or of two confirmatory signs alone.

2.8.2 Burrowing

Assessment of burrowing on control and prion infected M1-WT and M1-PD mice was conducted from 9 weeks post inoculation (w.p.i.). The burrowing test involved mice being placed into individual cages with a plastic cylinder filled with 140 g of food pellets. Food remaining in the cylinders after 2 hours was weighed and the amount displaced (“burrowed”) was calculated. Prior to the burrowing test, mice were placed in the burrowing cage for a 2-hour period. The test was then repeated on a weekly basis.

2.8.3 Fear conditioning

For behavioural testing of control and prion infected Tg37 mice, 9 w.p.i. male mice were used. For control or prion infected M1-WT and M1-PD mice, behavioural experiments were performed on 16 w.p.i. male and female mice.

The above was to ensure that the testing was conducted prior to the appearance of clinical symptoms (listed 2.7.5). Mice were acclimatized to the behavioural room overnight prior to the day of the test. For fear conditioning, mice were placed in the conditioning chamber (Stoelting ANY-maze Fear Conditioning System) and, after a 2-min adaptation period, received 3 tone-foot shock pairings where the foot shock (unconditioned stimulus [US]; 2 seconds; 0.4 mA) always co-terminated with a tone (conditioned stimulus [CS]; 2.8 kH; 85 dB; 30 seconds). The CS-US pairings were separated by 1-min intervals. After completion of training, the mice remained in the conditioning chamber for 1 min and were then returned to their home cages. The next day, mice were placed back in the conditioning chamber, and time spent immobile was recorded for 3 min to assess context-dependent learning. The following day (day 3), mice were placed back in the conditioning chamber, and following a 2-min adaptation period, the tone was played for 2 min, and time spent immobile was recorded to assess cue-specific (tone) learning. Data were analysed using ANY-maze software.

2.8.4 Y-Maze (Spontaneous alternation)

For control or prion infected M1-WT and M1-PD mice, behavioural experiments were performed on 16 w.p.i. male and female mice, as for fear-conditioning (2.8.3). Mice were habituated to the behavioural testing suite overnight prior to the test. Mice were placed for 8 min into the centre of a Y maze (grey, non-reflective base plate) with three identical arms (A, B, C; lane width: 5 cm; arm length: 35 cm; arm height: 10cm). Activity was recorded using ANY-maze software. Spontaneous alternation behaviour was calculated manually by counting the number of “ABC” sequences (in any order) as a proportion of the total triplet sequences made during the 8-min test.

2.9 Data Analysis

2.9.1 Statistical analysis

Statistical analyses were carried out using GraphPad Prism 9 software. For statistical analysis of differences between groups of measures, data were assumed to be normally distributed and were therefore compared using parametric tests. Generally, either two-tailed unpaired student’s t test (for two

groups) or two-way ANalysis Of Variance (ANOVA) (for three or more groups). In Figure 5-18, mixed-effects model (for analysis of repeated measures) was used instead of two-way ANOVA whenever the numbers of data-points differed between groups. Multiple-comparisons post hoc corrections were used following two-way ANOVA when several statistical tests were performed simultaneously (Figure 2-2). Tukey's multiple comparisons, or Fisher's Least significant differences (LSD) were used when comparing the mean of every group of data with every other mean (e.g., control vs disease at time point A, control vs disease at time-point B, and across time-points). Sidak's multiple comparisons was used when comparing selected sets of means (e.g., control vs disease and wild-type vs mutant independently). Dunnett's multiple comparisons was performed when comparing the mean of every group to one reference mean (e.g., vehicle vs drug A and vehicle vs drug B).

For statistical analysis of relationships of covariation between variables (correlations), Pearson Correlation test was used assuming Gaussian distribution of data. For analysis of survival curves, Gehan-Breslow-Wilcoxon test was applied. This test provides more weight to events (i.e., death) at earlier time points.

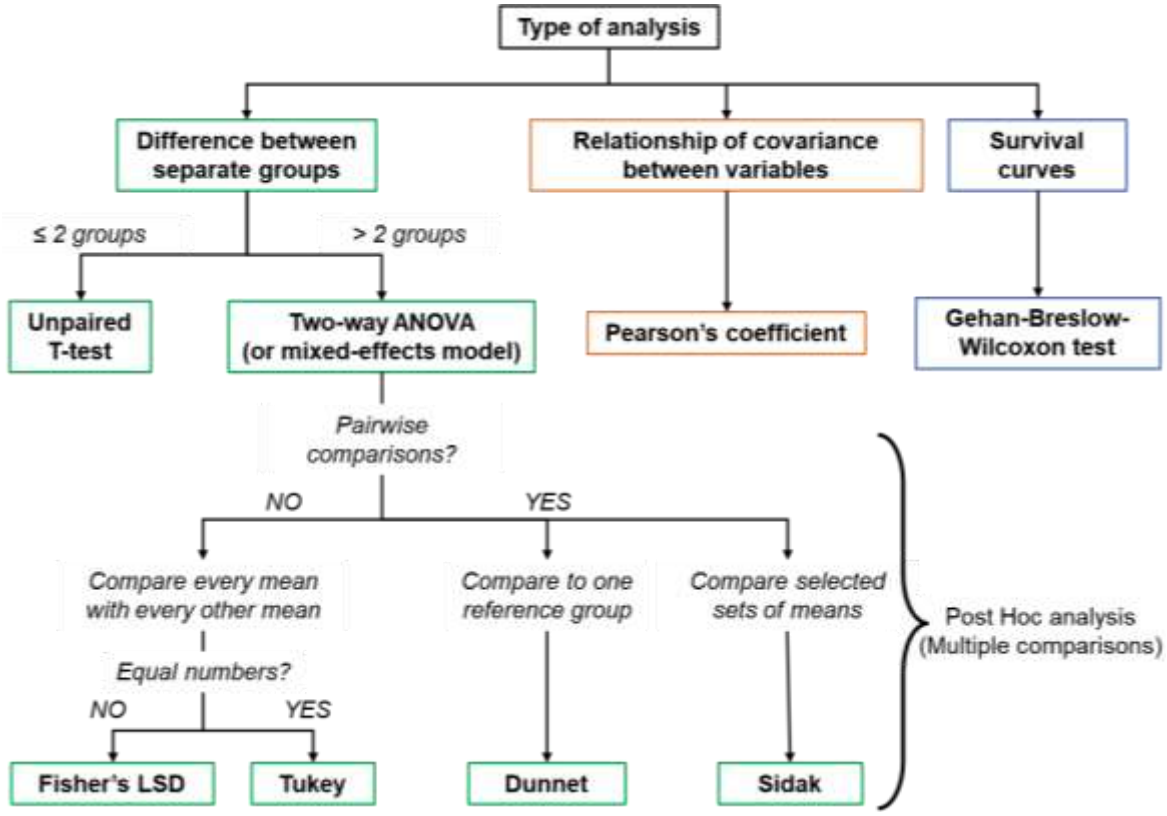

Figure 2-2. Decision tree for the selection of appropriate statistical test. In this thesis, data was statistically analysed to test for differences between separate groups (or unpaired measurements), relationships of covariance between variables (or correlations) and differences between survival curves. Pearson Correlation test was used to analyse correlations assuming Gaussian distribution of data. For analysis of survival curves, Gehan-Breslow-Wilcoxon test was performed, that provides more weight to events (i.e., death) at earlier time points. When analysing differences between groups, unpaired T-test (for 2 or less groups of measures) or two-way ANOVA (for 3 or more groups) were performed. Mixed-effects model was conducted instead of two-way ANOVA for repeated measures whenever the number of samples differed between groups. Following two-way ANOVA, post hoc analyses were performed to correct for multiple comparisons, and these included Fisher's LSD, Tukey's, Dunnett's or Sidak's multiple comparisons.

2.9.2 Analysis of binding parameters

Binding studies help estimate important pharmacological parameters that are indicative of ligand affinity. In this thesis, membrane impermeable, radiolabelled muscarinic antagonist [^{3}H]-NMS was employed to assess probe surface muscarinic receptors in saturation binding assays.

The **saturation binding** assay determines the specific binding of the radiolabelled ligand [^{3}H]-NMS at increasing ligand concentration and allows to calculate the maximum specific binding in terms of B_{max} that corresponds to receptor expression. In addition, the equilibrium binding constant Kd is calculated and corresponds to the concentration of ligand required to occupy half of all the receptor sites and indicates ligand affinity. B_{max} and Kd

parameters were established by GraphPad Prism using the following model for one-site specific binding, where X is the radioligand concentration or probe:

$$Specific\ binding\ (Y) = Bmax \times \frac{Bmax \times X}{Kd + X}$$

The [^{3}H]-NMS internalisation assay was a modified version of the saturation binding assay to generate a concentration-response curve for receptor internalisation with increasing stimulation periods or agonist concentrations (2.3.2). In particular, [^{3}H]-NMS specific binding with increasing agonist concentrations was used to fit an inhibition non-linear regression curve in GraphPad Prism (as radiolabelled surface receptors are expected to decrease with increased agonist-induced receptor internalisation) to calculate EC_{50} and E_{max}. The EC_{50} corresponds to the effective concentration of agonist where 50% of the maximal effect is observed and is indicative of ligand potency; E_{max} corresponds to the maximal response produced by a ligand and represents its efficacy.

Similarly, the IP1 accumulation assay was analysed in GraphPad Prism using a stimulation non-linear regression curve model to estimate the potency (EC_{50}) and efficacy (E_{max}) of the tested ligands.

2.9.3 Co-localisation analysis

Immunocytochemistry images were analysed using Zeiss ZEN 3.2 software to determine co-localisation of HA (receptor tag) with Early Endosomal antigen 1 (EEA1) in double-stained CHO cells. Co-localised pixels were examined between the two channels of the respective bound secondary antibodies. Data was collected from 10 separate fields of view and from three separate experiments (N=3). Co-localisation coefficients were obtained by Zeiss ZEN 3.2 using the Manders' equation (Manders et al., 1993).

2.9.4 Calculation of signalling bias

Concentration–response curves obtained from functional assays were fitted according to a four-parameter logistic equation in GraphPad Prism 9 to determine minimum and maximum asymptotes, EC_{50} and slope. To assess agonist bias, the same concentration–response curves were analysed according to a

modified form of the operational model of agonism, recast to directly yield a transduction ratio ($\log(\tau/K_A)$) (van der Westhuizen et al., 2018), where basal represents the response in the absence of agonist, E_{max} represents the maximal response of the assay system, K_A represents the equilibrium dissociation constant of the agonist, [A] represents the concentration of agonist, τ is an index of the coupling efficiency (or efficacy) of the agonist, and n is the slope of the transducer function linking agonist occupancy to response. For the analysis, all agonist curves at each pathway were globally fitted to the model with the parameters, basal, E_{max} and n shared between all agonists. For full agonists, $\log K_A$ was constrained to a value of zero, whereas for partial agonists this was directly estimated by the curve fitting procedure; the $\log(\tau/K_A)$ parameter was estimated as a unique measure of activity for each agonist. Agonist bias factors ($\Delta\Delta\log10(\tau/KA)$) were calculated as previously described (van der Westhuizen et al., 2018).

2.9.5 Spongiosis scoring

Spongiosis is characterised by the presence of 'spongiotic vesicles' and is one of the main hallmarks of prion disease (Mallucci et al., 2003). A 4-point scoring system was established to determine the extent of spongiosis across samples in a more objective manner:

Score 0 – No observable vesicles
Score 1 – Vesicles are present <5 in a given 200 μm^2 area
Score 2 – Vesicles are present >5 in a given 200 μm^2 area
Score 3 – Vesicles are large and spread across the area

2.9.6 Densitometry for immunoblotting

Quantification of intensity of western blot bands was achieved by measuring the median pixel intensity (arbitrary units) using Image Studio Lite (Version 5.2), a LICOR-recommended software for blot analysis. The background signal was automatically corrected by this software. Band intensity corresponding to the protein of interest was always normalised to housekeeper protein, typically α-tubulin.

2.9.7 qRT-PCR data analysis

C_T values were compared with a suitable internal control (housekeeper gene), typically α-tubulin or 18S (run in parallel) for normalisation and to calculate ΔC_T values (ΔC_T = C_T of housekeeper − C_T of test gene). ΔC_T values were then compared with the reference conditions, typically the M1-WT controls, to calculate the $\Delta\Delta C_T$. All the data is finally expressed as $2^{-\Delta\Delta CT}$ to get the expression fold change.

Chapter 3 *In vitro* characterisation of a phosphorylation-deficient mutant of the M1 muscarinic acetylcholine receptor

3.1 Introduction

GPCRs are some of the most attractive drug targets for the treatment of many diseases because of their involvement in virtually all physiological functions in health and pathology (Santos et al., 2017). In addition to beneficial therapeutic effects however, pharmacological modulation of GPCRs might also be associated to unwanted adverse responses. To tackle this issue, many have set out to determine the optimal pharmacological properties of GPCR-targeted ligands that will deliver clinical efficacy whilst minimising associated adverse responses. Specifically, biased ligands might offer a great advantage to this end. Signalling bias is based on the bimodal signalling mode of GPCRs that operate by coupling to two major branches of signalling: G protein-dependent signalling and phosphorylation/arrestin-dependent pathways. Biased ligands could be designed to drive GPCR signalling pathways that lead to clinically relevant responses in preference to ones that could lead to adverse responses, thus representing a more efficient and safer therapeutic options.

3.1.1 Biased signalling

Traditionally, GPCRs were envisioned to exist in a spontaneous equilibrium between inactive and active states, that are stabilised by binding of antagonists or agonists respectively (De Lean et al., 1980). According to this concept, where activated GPCRs would mediate signalling pathways by coupling to downstream effectors in a uniform manner, the resulting biological outcome at a cellular level is determined by the stability of receptor conformations and tissue- or cell-specific expression of effectors. However, over the past three decades, a great deal of research has demonstrated that GPCRs can adopt multiple distinct active states. In fact, GPCRs are pleiotropic and can couple to and signal via both G protein and non-G protein effectors (Galandrin et al., 2007, Roth and Chuang, 1987). Different receptor active states exhibit different affinities for multiple effectors leading to the ‘unbalanced’ activation between different downstream signalling pathways, resulting in *signalling bias*. Whilst the physiological response is still determined by tissue-specific receptor expression, the overall cellular signalling outcome is determined by the proportion of receptor population that exist in the potential active states (Luttrell et al., 2018).

In this context, ligand structure plays a vital role in determining signalling bias, since it stabilises the receptor into distinct conformational states and influences the efficiency with which the receptor engages different downstream effectors. For example, a study employing 19F-NMR spectroscopy, a method that allows detection of changes in line shapes and chemical shifts of intracellularly located ^{19}F-labels in a receptor, showed that ß-arrestin biased ligands and unbiased full and partial agonists at the $ß_2$ adrenergic receptor ($ß_2$AR) induce distinct structural rearrangements in the cytoplasmic regions of the receptor (Liu et al., 2012). Importantly, ligands do not cause the receptor to change signalling partners (Saulière et al., 2012). Ligand binding induces a conformational change in the receptor in a way that allows **G protein coupling** and/or the unmasking of intracellular domains that can be modified - for example by **phosphorylation** – and interact with **arrestins** (Kobilka, 2002, Nygaard et al., 2013, Shukla et al., 2013, Dror et al., 2015, Palczewski et al., 1991, Chen et al., 1993).

Ligand-stabilised receptor conformations can select the coupling of G protein subunit families resulting in differential signalling outcomes. This has been largely observed with agonists for μOR (Saidak et al., 2006), PTHR (Appleton et al., 2013) and DR (Möller et al., 2017). For instance, different D_2R ligands were shown to preferentially activate Gα subunits i2, i3, oA or oB with important implications for the development of antipsychotic drugs (Möller et al., 2017). Also, four opioid ligands (DAMGO, endomorphins 1 and 2, and morphine) were found to produce significant differences in potencies for $G\alpha_{i1}$ *versus* $G\alpha_{oA}$ activation, highlighting the potential for greater selectivity of clinically relevant signalling pathways opposed to the ones leading to undesirable outcomes (Saidak et al., 2006).

Different ligands can stabilise the receptor to induce distinct receptor-arrestin interactions, and receptor phosphorylation plays an important role in defining receptor interactions with other binding and/or signalling partners (Tobin, 2008, Reiter et al., 2012). Distinct ligand-receptor conformations define the so-called *phosphorylation barcode* of the receptor (discussed in detail in 3.1.2), ultimately influencing the interaction with signalling partners such as arrestins, and signalling outcome (Tobin et al., 2008, Butcher et al., 2011, Nobles et al., 2011, Zhou et al., 2017). Biased ligands can also stabilise the receptor to

promote differential internalisation outcomes such as rapid recycling or receptor degradation. For example, synthetic agonists exendin-4 and liraglutide induce slower recycling of glucagon-like peptide 1 (GLP-1) receptors compared to endogenous GLP-1, resulting in prolonged receptor-mediated cAMP signalling (Roed et al., 2014).

3.1.2 Phosphorylation of GPCRs

Receptor activation was first reported to induce phosphorylation of rhodopsin in the 1970s, before the GPCR superfamily was even named (Kühn and Dreyer, 1972, Kühn, 1974). Upon stimulation, GPCRs become phosphorylated at intracellular residues by a family of protein kinases called GPCR kinases (GRKs) (Benovic et al., 1989). There are seven known GRK isoforms (GRK1-7) that can be categorised into three groups; GRK1/7, GRK2/3, and GRK4/5/6. GRK1/7 are GRKs that target visual GPCRs. GRK2/3 exclusively phosphorylate activated GPCRs as they feature a pleckstrin homology (PH) domain that binds to Gβγ only when disassociated from the Gα subunit, leading to signalling termination (Touhara et al., 1994, Lodowski et al., 2003, Haga and Haga, 1992, Li et al., 2003, Pitcher et al., 1992). GRK4/5/6 do not possess a PH domain and instead they are associated to the plasma membrane through palmitoylation of their C-terminal cysteines and/or *via* interactions with membrane phospholipids (Gurevich et al., 2012, Stoffel et al., 1994, Premont et al., 1996, Thiyagarajan et al., 2004). GRK4/5/6 were shown to phosphorylate inactive GPCRs (Rankin et al., 2006, Baameur et al., 2010, Li et al., 2015).

Whilst GPCRs display a significant functional diversity, only a handful of arrestins and GRKs are known to regulate the signalling of hundreds of GPCRs. To explain this phenomenon, the *phosphorylation barcode* was hypothesised. According to this concept, receptors are phosphorylated by different GRKs at different sets of intracellular sites establishing a phosphorylation barcode that instructs or determines the way the receptor interact with arrestins (Tobin et al., 2008, Butcher et al., 2011). For instance, a mass spectrometry (MS)-based quantitative phosphoproteomic analysis had mapped phosphorylation sites on the β_2AR and established that GRK2 and GRK6 phosphorylate the receptor at distinct phosphorylation sites at its C-terminal tail, inducing different arrestin conformations associated with distinct signalling outcomes (Nobles et al., 2011).

GRK2 was shown to phosphorylate sites that were mostly responsible for $ß_2$AR internalisation, whereas GRK6-mediated phosphorylation contributed to ß-arrestin–mediated activation of extracellular signal-regulated kinase (ERK). Both GRK2 and GRK6 contributed to receptor desensitisation. Furthermore, Nobles et al. (2011) demonstrated that two different $ß_2$AR ligands, ß-arrestin–biased carvedilol and the unbiased full agonist isoproterenol, induced distinct phosphorylation barcodes leading to different signalling outcomes in HEK293 cells expressing $ß_2$ARs. Other examples are endogenous ligands CCL19 and CCL21 of the CCR7 chemokine receptor. Both CCL19 and CCL21 could promote G protein-dependent signalling, calcium mobilization and ERK activation with equal potency but only CCL19 promotes robust desensitization (Kohout et al., 2004). In accordance with the barcode hypothesis, it was demonstrated that CCL19 leads to robust CCR7 phosphorylation and ß-arrestin2 recruitment catalysed by both GRK3 and GRK6, whereas CCL21 activates GRK6 alone resulting in weaker interaction with ß-arrestin2 (Zidar et al., 2009). Agonist-specific phosphorylation barcodes have been reported for other GPCRs including opioid receptors (Just et al., 2013) and serotonin 5-HT_{2A} receptors (González-Maeso et al., 2007).

A recent study employed a panel of combinatorial GRK knockout HEK293 cell lines to investigate individual contributions of GRK2, 3, 5, and 6 in the arrestin-dependent regulation of GPCR signalling, internalisation, and trafficking for 12 different GPCRs (Drube et al., 2022). They established that GRKs do not select for specific C-terminal and ICL3 sequences, but instead for the overall receptor conformation based on the availability of phosphor-acceptor sites and binding domains. Furthermore, they found that GRKs might have the overlapping or distinct functions depending on individual GPCRs, and that different receptors have different intrinsic affinities for GRKs, regardless of their phosphorylation status. For example, while $ß_2$AR requires higher levels of GRK expression to induce ß-arrestin2 recruitment, PTH1R and M5 mAChR were shown to induce robust ß-arrestin2 recruitment with endogenous levels of GRK2 expression to induce ß-arrestin2 recruitment. This does not exclude the phosphorylation barcode hypothesis, since different phosphorylation patterns might still be able to induce different arrestin-receptor interactions resulting in the engagement of distinct signalling outcomes. However, this study highlighted that in addition to

tissue specific GRK expression levels, the affinity of individual GPCRs for GRK subtypes plays a key regulatory role in the receptor signalling outcome, uncovering another layer of complexity to GPCR signalling regulation.

Importantly, in addition to GRKs, GPCRs were previously reported to be phosphorylated by alternative kinases. For example, the M1 and M3 mAChRs were demonstrated to be phosphorylated by casein kinase 1α and casein kinase 2, respectively (Torrecilla et al., 2007, Mou et al., 2006), and protein kinase Cß (PKCß) was shown to contribute to the phosphorylation of C5aR1 (Pollok-Kopp et al., 2007).

3.1.3 Arrestin interactions

Although receptor phosphorylation can reduce G protein-dependent signalling, G protein displacement and signalling termination requires receptor interaction with arrestins (Arshavsky et al., 1985, Sibley et al., 1986, Benovic et al., 1987). Arrestins are a family of four proteins (i.e., arrestin1-4) comprising the so-called visual arrestins (arrestin1/4) that are expressed exclusively in the retina, and non-visual or ß-arrestins (arrestin2/3 a.k.a. ß-arrestin1/2), which regulate a wide array of GPCRs and are responsible for the desensitisation of most non-visual GPCRs (Luttrell and Lefkowitz, 2002, Gurevich and Gurevich, 2006, Lohse et al., 1990, Lohse et al., 1992). ß-arrestins share 78% sequence similarity and are ubiquitously expressed in tissues, but their expression levels vary in different cell types (Sterne-Marr et al., 1993, Attramadal et al., 1992). Binding of arrestins to active and phosphorylated GPCRs was first described for visual arrestin-1 (Siderovski et al., 1996) and non-visual arrestin-2 (Krasel et al., 2005).

All arrestins share a similar structure in their inactive state, consisting of ß-sheets arranged in two lobe-like domains (N- and C-domain) connected through a 12- residue linker region, and with four loops exposed in the central binding site for receptor interactions (Hirsch et al., 1999, Han et al., 2001, Zhan et al., 2011, Sutton et al., 2005). One of these, the so-called finger loop, interacts with the transmembrane core of active GPCRs competing with Gα subunits and determines the binding preferences of arrestins to receptors (Vishnivetskiy et al., 2004, Vishnivetskiy et al., 2011, Chen et al., 2017). GPCRs are categorised into two classes according to arrestin binding; Class A and B receptors (Oakley et

al., 1999, Oakley et al., 2000, Luttrell and Lefkowitz, 2002). Class A receptors (β_2AR, μOR, endothelin type A receptor, D_{1A}R, and α_{1b} adrenergic receptor) interact with β-arrestins forming transient and rapidly disassociating complexes and have higher affinity for β-arrestin2 than β-arrestin1. Class B receptors (angiotensin II type 1A receptor, neurotensin receptor 1 (NTSR1), vasopressin V_2 receptor (V_2R), thyrotropin-releasing hormone receptor, and substance P receptor) form long-lived, stable complexes with arrestins, and have similar high affinities for both β-arrestins. A serine/threonine cluster in the C-terminal tail of GPCRs determines the stability of receptor-arrestin complexes, as shown by the β_2V_2R chimera. The β_2V_2R is a class A receptor (β_2AR) that harbours the C-terminus from a class B receptor (V_2R) that exhibits a class B-like interaction with arrestins (Oakley et al., 1999).

Biochemical and biophysical studies have identified two distinct structural domains in receptors that are crucial for their interaction with arrestins (Gurevich and Gurevich, 2004, Park et al., 2016, Sommer et al., 2015). These are the receptor *tail* that is the phosphorylated C-terminus, and the receptor *core* that comprises the cytoplasmatic surface of receptors. Structural studies using single-particle electron microscopy (EM) of an antibody-stabilised complex of β-arrestin1 with the β_2V_2R chimera allowed the visualisation of the interactions between GPCRs and arrestins. This study unravelled a biphasic mode of interaction whereby receptor-arrestin complexes are found as *partially engaged* and/or *fully engaged* complexes (Shukla et al., 2014, Ghosh et al., 2015). The partially engaged complex consists of the arrestin being bound to the receptor only through the tail, whereas in the fully engaged complex, arrestins bind to the receptor by interacting with both the receptor tail and core (Figure 3-1). Receptor-arrestin complexes may comprise of a mixture of partially and fully engaged depending on the receptor phosphorylation status and conformation.

Most recent cryo-EM structures of β-arrestin1 in complex with NTSR1 (Huang et al., 2020b) and the M2 mAChR (Staus et al., 2020) have provided an even more detailed insight into the interaction between GPCRs and arrestins. These structures demonstrated that in the core interaction, the finger loop of β-arrestin1 interacts with the receptor core in a way that is very similar to the interaction between the α5 helix of the Gα subunits with the receptor, further

explaining the steric hindrance mechanism of G protein-signalling desensitisation (Chaturvedi et al., 2020). Further, these structures reveal the apparent contact between the C-terminal loops of ß-arrestin1 with the detergent micelle or lipid nanodisc, suggesting that ß-arrestin1 anchors to the membrane bilayer, likely regulating receptor desensitisation and internalisation (Staus et al., 2020). This feature was also previously reported in a double electron resonance spectroscopy study of visual arrestins in complex with rhodopsin (Zhuo et al., 2014)

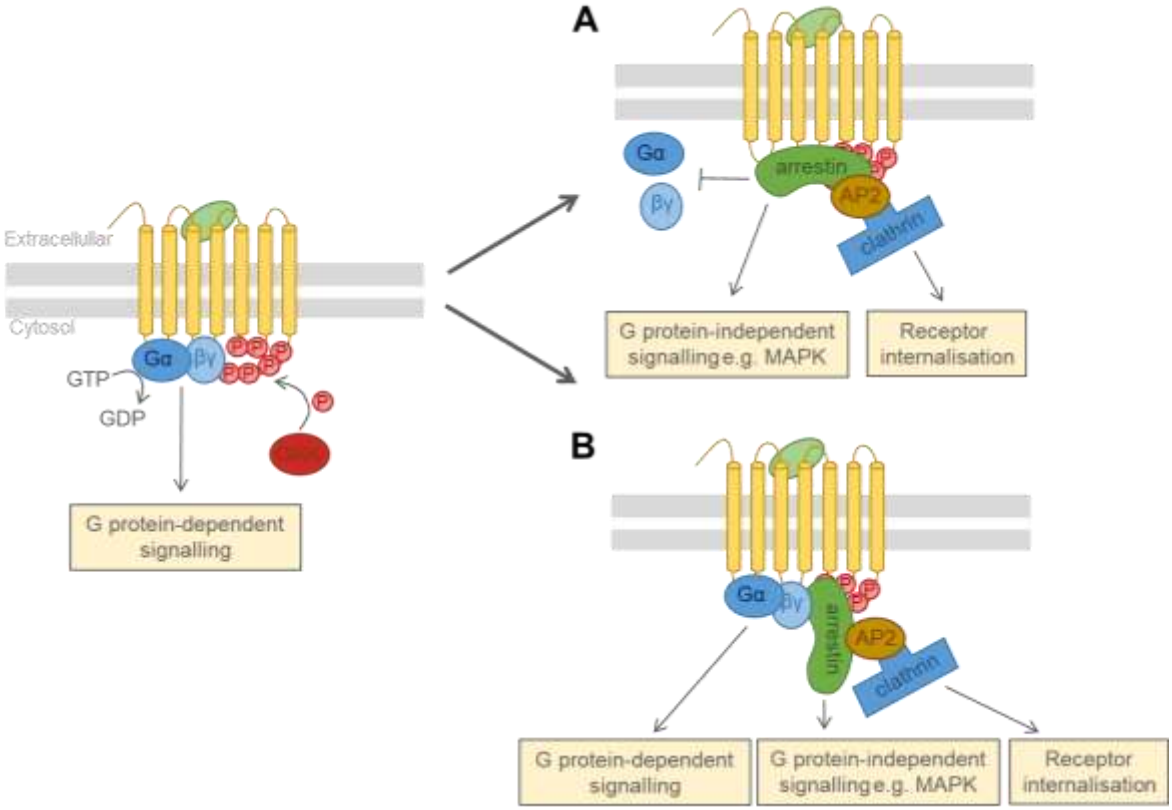

Figure 3-1 Representation of GPCR signalling complexes. GPCRs are normally coupled to heterotrimeric G proteins made of Gα and Gβγ subunits. Upon agonist binding, guanine exchanging factor domains of G proteins facilitate the exchange of GDP bound to the Gα subunit of inactive heterotrimer to GTP. Then Gα and Gβγ subunits dissociate from the GPCR and mediate various signalling pathways (G protein-dependent signalling). GRKs also bind and phosphorylate agonist activated GPCRs. This induces recruitment of arrestins to the receptor. **(A)** arrestin hinders G protein-dependent signalling by displacing G protein from the receptor and induces clathrin-mediated internalisation by interaction with AP2 and clathrin and G protein-independent signalling by interaction with signalling effectors such as MAPK. **(B)** Agonist-activated GPCRs can also form super-complexes with partially engaged arrestins and G proteins and are able to mediate signalling *via* G protein-dependent and G protein-independent pathways simultaneously, from the cell membrane and from endosomes.

3.1.4 Receptor desensitisation and internalisation

Arrestins have long been considered crucial mediators in 'arresting' G protein-dependent signalling (Wilden et al., 1986, Benovic et al., 1987), and the most recent structural studies have revealed the molecular basis of this mechanism. Following receptor activation, agonist-induced changes in receptor conformation and phosphorylation allow for interactions with arrestin. The binding sites for Gα proteins and arrestins overlap and, consequently, arrestin binding causes G protein uncoupling by steric hindrance (Rasmussen et al., 2011, Kang et al., 2015, Carpenter et al., 2016, Liang et al., 2017, Zhang et al., 2017, Szczepek et al., 2014, Chaturvedi et al., 2020). Arrestins bind with high affinity to phosphate groups, which interacts with the positively charged regions on the arrestin molecule, strengthening the interaction with the receptor (Zhou et al., 2017). Altogether, receptor phosphorylation and interaction with arrestin result in the termination of G protein-dependent signalling (*desensitisation*) by blocking receptor coupling to G proteins (Benovic et al., 1987, Lohse, 1993).

Multiple GPCRs have been shown to induce robust G protein-dependent signalling in endosomes after initial agonist stimulation, rather than being desensitised, contradicting the traditional model of GPCR desensitisation (Calebiro et al., 2009, Ferrandon et al., 2009, Feinstein et al., 2013, Irannejad et al., 2013, Mullershausen et al., 2009). However, the partially engaged receptor-arrestin complex reported in the structural studies on the chimeric $ß_2V_2R$ (Shukla et al., 2014) suggests that it might be possible for a GPCR to engage with both arrestins and G proteins simultaneously. It was demonstrated *in vitro* that GPCRs can form megaplexes; $ß_2V_2R$ chimera and V_2R were shown to form super-complexes with $Gα_s$ subunits and ß-arrestins when internalised (Thomsen et al., 2016). A purified, agonist-stimulated antibody-stabilised $ß_2V_2R$ -ß-arrestin1 could strongly interact with heterotrimeric $Gα_s$ proteins through its membrane core while coupling to ß-arrestin1 simultaneously through the receptor C-tail (Figure 3-1). Importantly, this super-complex could drive receptor internalisation without displacing G protein-dependent signalling (Thomsen et al., 2016).

ß-arrestins also facilitate clathrin-mediated internalisation of many GPCRs (Zhang et al., 1996, Goodman et al., 1996). Clathrin-mediated internalisation or endocytosis consists of invaginations of the plasma membrane called clathrin-

coated pits, which are enveloped with clathrin and AP2 complexes. Clathrin-coated pits pinch off from the plasma membrane helped by the GTPase dynamin, to form vesicles containing the internalised receptors. Both ß-arrestins are able to effectively bind clathrin (Goodman et al., 1996) and AP2 (Laporte et al., 1999). In addition, knockout or silencing of ß-arrestins was demonstrated to compromise receptor internalisation (Kohout et al., 2001, Ahn et al., 2003) whereas overexpression of ß-arrestins was shown to enhance receptor internalisation and rescue endocytosis of internalisation-defective mutant GPCRs (Ferguson et al., 1996). ß-arrestins bind to clathrin and AP2 *via* their C-terminal tail (Kim and Benovic, 2002) and upon GPCR binding to ß-arrestins, the latter undergo conformational changes causing the release of their C-tail which becomes accessible for interactions with clathrin and AP2 (Zhuo et al., 2014).

Interestingly, the interaction of ß-arrestin2 with E3 ubiquitin ligase Mdm2 was demonstrated to be essential for mediating receptor internalisation. Mdm2 was shown to specifically ubiquitinate ß-arrestin2 upon agonist stimulation, and removal of Mdm2 activity resulted in the ablation of $ß_2$AR internalisation (Shenoy et al., 2001, Shenoy et al., 2009). In addition, ubiquitination of ß-arrestin was demonstrated to be important for clathrin binding, receptor interactions and scaffolding of signalling partners e.g., MAPK. Thus, suggesting that ubiquitination acts as an efficient mediator for multiple interactions of ß-arrestin (Shenoy et al., 2006). Further, SUMOylation of ß-arrestin2 was shown to be important for interaction with AP2 and clathrin-mediated receptor internalisation (Wyatt et al., 2011).

The fate of internalised receptors is determined by the stability of the receptor-arrestin complex (Oakley et al., 1999). Class A receptors, as discussed above, typically interact with ß-arrestin in a transient manner, displaying a fast disassociation rate and recycling back to the plasma membrane. Instead, class B receptors form stable complexes with ß-arrestins, and they are internalised together into endosomes (Luttrell and Lefkowitz, 2002, Oakley et al., 2000, Shenoy and Lefkowitz, 2011).

3.1.5 Arrestin-mediated signalling

In the past couple of decades, arrestins have been proposed not only to desensitise GPCR signalling but also to transduce signalling through G protein-independent pathways (Rajagopal et al., 2011, Luttrell et al., 1999). As discussed above, arrestins can bind to GPCRs and act as scaffolds for cytoplasmic signalling proteins to mediate arrestin/phosphorylation-dependent signalling (Figure 3-1)(Wei et al., 2003, Shenoy et al., 2006). Receptor-bound arrestins have been shown to bind and activate members of several important pathways including the Src-family kinases, ERK, MAPK kinase MEK, and c-jun N-terminal kinase (JNK) and phosphodiesterases (Luttrell et al., 1999, McDonald et al., 2000, Houslay and Baillie, 2005, Shenoy et al., 2006, DeWire et al., 2007, Song et al., 2009, Perry et al., 2002, Nelson et al., 2007).

Conflicting evidence has emerged about whether ERK1/2 activation is arrestin-dependent and G protein-independent (Shenoy et al., 2006), or instead requires GPCR activation (Alvarez-Curto et al., 2016, Grundmann et al., 2018). For instance, β_2AR-mediated ERK signalling was demonstrated to not require the presence of arrestins (O'Hayre et al., 2017), and ERK signalling mediated by the M1 mAChR in HEK293 cells was shown to be $G\alpha_q$ protein-dependent (Scarpa et al., 2021). However, these findings do not necessarily exclude that arrestin-mediated signalling exists. A possible explanation to the contradicting evidence is that arrestins, by acting as scaffolds, bring together signalling effectors e.g. MAPKs to facilitate signal transduction but still require the upstream effectors to be activated (Gurevich and Gurevich, 2019). In this way, before arrestin-mediated signalling is initiated, the most upstream signalling effectors of the pathway need to be activated in an arrestin-independent manner.

3.1.6 The promise of biased ligands

Signalling bias can be exploited therapeutically with the aim of developing more selective and effective drugs. Biased ligands could be selected or designed to promote the activation of clinically relevant signalling pathways while avoiding those leading to undesirable side-effects. An early biased ligand that was taken to clinical trials for heart failure was the angiotensin analogue produced by Trevena, TRV027 (Felker et al., 2015). This ligand was developed as an

improvement on existing angiotensin receptor (ATR) blockers and was demonstrated to be a ß-arrestin-biased agonist of AT_1R that does not activate $G\alpha_q$ proteins, therefore acting as an antagonist at AT_1R-mediated $G\alpha_q$ protein signalling. Specifically, while the inhibition of AT_1R-mediated $G\alpha_q$ signalling is beneficial against heart failure, the activation of arrestin-mediated pathways holds cardioprotective properties (Monasky et al., 2013, Violin et al., 2010). Despite TRV027 failing at Phase 2b clinical trials in acute heart failure for unmet primary or secondary endpoints, it has recently been entered into a National Institutes of Health (NIH)-funded Accelerating Covid-19 Therapeutic Intervention and Vaccines clinical trial in patients infected with SARS-CoV-2. TRV027 in fact, hinders the signalling that causes acute lung damage and abnormal blood clotting ($G\alpha_q$ signalling) whilst stimulating reparative mechanisms that enhance lung function and boost anti-inflammatory effects (arrestin-mediated signalling) properties (Monasky et al., 2013, Violin et al., 2010).

Another example of therapeutic advantage of biased ligands is represented by opioid medications for analgesia. Based on studies showing that analgesic effects are mediated by $G\alpha_i$-dependent pathways while adverse effects (e.g. tolerance, addiction and respiratory depression) are mediated by ß-arrestin pathways at the μOR, drug development programmes have focussed on G protein-biased agonists at opioid receptors (Che et al., 2021). Oliceridine (TRV130) is a G protein-biased agonist at the μOR, and it was clinically approved in 2020 for the treatment of moderate to acute pain. Oliceridine displayed potent analgesic effects that were superior to those observed with placebo and reduced respiratory and GI side effects compared to morphine (Soergel et al., 2014).

Having established that biased ligands hold promising therapeutic potential for the treatment of many diseases, the rationale design of novel biased ligands requires the translation of biased signalling observed *in vitro* into *in vivo* systems to truly understand the physiological relevance (Kenakin, 2019).

3.1.7 Strategies for investigation of biased signalling

One of the main strategies to investigate biased signalling is through the generation of genetic knockouts of GPCR signalling partners; arrestins and G proteins. Deletion of both ß-arrestin isoforms is lethal, therefore only single

isoform knockouts are possible. ß-arrestin2 knockout mice (but not ß-arrestin1) have been generated, and displayed remarkable potentiation and prolongation of analgesic effects following treatment with morphine (Bohn et al., 1999), whereas adverse effects such as respiratory suppression and constipation were attenuated in the same mice compared to wild-type animals treated with morphine (Raehal et al., 2005). These studies led to the discovery that G protein-biased opioids have the potential of inducing robust analgesia whilst minimising typical opioid adverse effects, prompting the development of the now clinically approved oliceridine (Soergel et al., 2014). ß-arrestin2 knockout mice were also employed to probe the efficacy and side effect liability of D_2R-targeting antipsychotic drugs (Allen et al., 2011). Allen et al (2011) demonstrated that the antipsychotic effects of D_2R biased ligands were attenuated in ß-arrestin2 knockout mice compared to wild-type, and that these D_2R ligands reduced locomotory activity in wild-type mice but not in ß-arrestin2 knockouts. This indicated that ß-arrestin signalling can be a significant contributor to both antipsychotic efficacy and protection against typical antipsychotic adverse effects such as catalepsy. The use of ß-arrestin2 knockout mice also provided evidence that κOR-mediated G protein-dependent signalling drives analgesic-like effects and aversion, while κOR-mediated ß-arrestin-2 signalling induces motor incoordination. Thus, G protein–biased κOR agonists represent novel potential analgesics with reduced abuse potential and fewer deleterious side effects compared with unbiased agonists (White et al., 2015).

Targeted disruption of all the 16 GNAS genes encoding the different Gα subunits has been performed in mice as single or combinatorial mutations (Wettschureck and Offermanns, 2005). However, since Gα subunits are ubiquitously expressed, many of these transgenic mouse lines have detrimental phenotypes (Minetti Giulia et al., 2014, Okae and Iwakura, 2010, Zhang et al., 2011). In addition, GPCRs interact with members spanning within and across the four Gα functional groupings ($G\alpha_{i/o}$, $G\alpha_{q/11}$, $G\alpha_{s}$, $G\alpha_{12/13}$) and systemic knockouts of Gα subunits might not be helpful to determine signalling bias of an individual GPCR. Some cell- and tissue-specific knockout mice for Gα subunits have however proven useful. For example, chondrocyte-specific knockout of $G\alpha_s$ was employed to study PTHR-mediated signalling in regulating chondrocyte differentiation (Sakamoto et al., 2005). In another study, genetic deletion of a hematopoietic-

specific gene coding for $G\alpha_{11}$ in mice was useful to determine the role of this G protein in C5aR-mediated macrophage chemotaxis (van den Bos et al., 2020).

An alternative approach to explore the role of biased signalling of GPCRs in natural physiology is by the generation of knock-in animals whereby the endogenous *GPCR* gene is replaced with a gene encoding for a phosphorylation-deficient (PD) mutant of the receptor. Removal of a receptor's intracellular phosphorylation sites supposedly results in uncoupling from phosphorylation/arrestin-dependent signalling and the receptor becomes a G protein-biased mutant. This approach has been successfully employed to dissect M3 mAChR signalling. MS-identified intracellular phosphorylation sites of the M3 mAChR (Butcher et al., 2011) were removed, thereby uncoupling the receptor from arrestin as well as arrestin-dependent mechanisms such as receptor internalisation (Poulin et al., 2010, Kong et al., 2010, Bradley et al., 2016). Mouse strains expressing the PD mutant of the M3 mAChR were demonstrated to have hippocampal-based learning and memory deficits (Poulin et al., 2010) and impairment in glucose tolerance and insulin secretion (Kong et al., 2010). These studies led therefore to the discovery that the M3 mAChR regulates cognition, glucose tolerance and insulin release *via* phosphorylation/arrestin-dependent signalling pathways. In addition, the M3 mAChR mediates airway smooth muscle contraction and is a therapeutic target for asthma and COPD where airway smooth muscle contraction is found upregulated (Gosens et al., 2006). By employing M3-PD mice, Bradley et al. (2016) demonstrated that this receptor regulates bronchoconstriction *via* a phosphorylation/arrestin-dependent mechanism. The authors therefore proposed that M3 mAChR ligands showing stimulus bias toward receptor phosphorylation/arrestin signalling would preferentially regulate bronchoconstriction whilst being devoid of potential adverse outcomes such salivary secretion, weight gain, and mechanisms associated with cell survival (Bradley et al., 2016).

Although the G protein-biased opioid ligand TRV130 was approved for the treatment of moderate to acute pain, some typical opioid agonist side effects are still present (Viscusi et al., 2016). Kliewer et al. (2019) generated knock-in mice expressing a PD mutant of the μOR that fails to recruit ß-arrestin to validate the role of phosphorylation/arrestin-dependent signalling in inducing opioid-related adverse responses. Analgesia was previously shown to be

mediated by G protein-dependent signalling, while adverse effects by arrestin-mediated pathways. Compared to wild-type animals, μOR-PD knock-in mice were demonstrated to have significantly enhanced analgesic response to opioids fentanyl and morphine. However, interestingly, both fentanyl and morphine still induced some side-effects including respiratory depression, constipation and hyperlocomotion in mice expressing the μOR-PD mutant, while tolerance was abolished. Later, Kliewer et al. (2020) confirmed that respiratory depression in indeed *not* driven by ß-arrestin2-dependent pathways, by conducting a study on ß-arrestin2 knockout mice.

The Designer Receptor Exclusively Activated by a Designer Drug (DREADD) technology has also been proven very successful in selectively probing the physiological role of signalling mediated by GPCRs subtypes. DREADD receptors are normally generated by mutations within the orthosteric binding pocket that render the receptor incapable of binding to its endogenous ligand. Instead, most DREADD receptors respond to a compound that would otherwise be biologically inert, such as clozapine-N-oxide (CNO) (Armbruster et al., 2007). In particular, the combination of DREADD and mutations conferring signalling bias has been very beneficial to explore biased signalling of GPCRs subtypes that are activated by the same endogenous ligand such as for the family of muscarinic receptors. For instance, a G protein-biased DREADD mutant of the M3 mAChR that lacks the ability to interact with ß-arrestins was generated as a tool to study the physiological relevance of $G\alpha_{q/11}$-dependent signalling pathways mediated by this receptor (Hu et al., 2016). In addition, mice expressing a DREADD-PD version of the M1 mAChR were successfully employed to establish that the M1 mAChR drives cholinergic adverse responses such as epileptic-like seizures in response to agonists in the absence of phosphorylation. Thus, maintaining receptor phosphorylation when therapeutically targeting the M1 mAChR for the treatment of neurodegenerative diseases would minimise possible associated side-effects (Bradley et al., 2020).

3.1.8 The M1-PD mouse model

The M1 mAChR has caught intense interest as one of the most promising targets for the symptomatic treatment of cognitive impairment in neurodegenerative and neuropsychiatric conditions such as AD (Sarter et al., 2012). This is because

M1 mAChRs are abundant in key cognitive brain regions including the cerebral cortex and hippocampus (Levey, 1993, Volpicelli and Levey, 2004), where they are the predominant muscarinic receptor subtype (Bradley et al., 2017) and play a crucial role in cognition (Fisher, 2008b, Ladner and Lee, 1998). Over the past four decades, many pharmaceutical companies have put a lot of effort in the development of selective M1 mAChR ligands for the treatment of AD. However, despite overwhelming preclinical evidence suggesting that M1 mAChR-activating ligands show significant potential not only for cognitive enhancement, but also for disease-modification (Scarpa et al., 2020), translating these findings to successful clinical outcomes has so far been proven challenging. This is largely due to cholinergic side effects associated with the on-target activity at the M1 mAChR (Rook et al., 2017, Engers et al., 2018, Moran et al., 2018b) as well as off-target activation of peripheral M2 and M3 mAChRs (Bymaster et al., 2003a, Melancon et al., 2013).

To tackle this issue, it is important to define the optimal pharmacological properties of orthosteric and allosteric M1 mAChR ligands that will deliver clinical efficacy whilst minimising cholinergic adverse responses (van der Westhuizen et al., 2020). To do this, we explored the physiological importance of signalling bias of the M1 mAChR by the generation of a genetically engineered mouse strain that expresses a PD mutant of the M1 mAChR (M1-PD) (Bradley et al., 2020). The mutated residues of the M1-PD receptor included MS-identified phosphorylation sites (Butcher et al., 2016) and other putative serine phosphorylation sites in ICL3 and C-terminal tail (Figure 3-2). The M1-PD receptor was shown to be uncoupled from receptor phosphorylation/arrestin-dependent signalling but elicit near normal coupling to $G\alpha_{q/11}$-dependent pathways (Bradley et al., 2020).

By using M1-PD knock-in mice, the importance of M1 mAChR phosphorylation/arrestin-dependent signalling in the regulation of anxiety-like behaviours and learning and memory has been elucidated, suggesting that maintenance of receptor phosphorylation is important to deliver clinical efficacy while minimising adverse responses (Bradley et al., 2020). In addition, our studies showed that ligands displaying a bias towards phosphorylation-dependent signalling are less likely to induce cholinergic adverse effects and seizures (Bradley et al., 2020). It was demonstrated that pilocarpine, a well-

characterised muscarinic partial agonist that drives robust seizures despite acting as a partial agonist of muscarinic receptors (Hedlund and Bartfai, 1981), showed bias towards G protein-dependent versus phosphorylation-dependent signalling *in vitro*, whereas the bitopic ligand GSK1034702 displayed no bias across these pathways (Bradley et al., 2020).

This thesis aims to further explore the role of the M1 mAChR phosphorylation/arrestin-dependent signalling in the disease-modifying potential of activating the M1 mAChR for the treatment of neurodegenerative conditions. To do this, it was first important to define the *in vitro* behaviour of the M1-PD receptor compared with the wild-type M1 mAChR to understand the possible molecular mechanisms underpinning the differences observed *in vivo*.

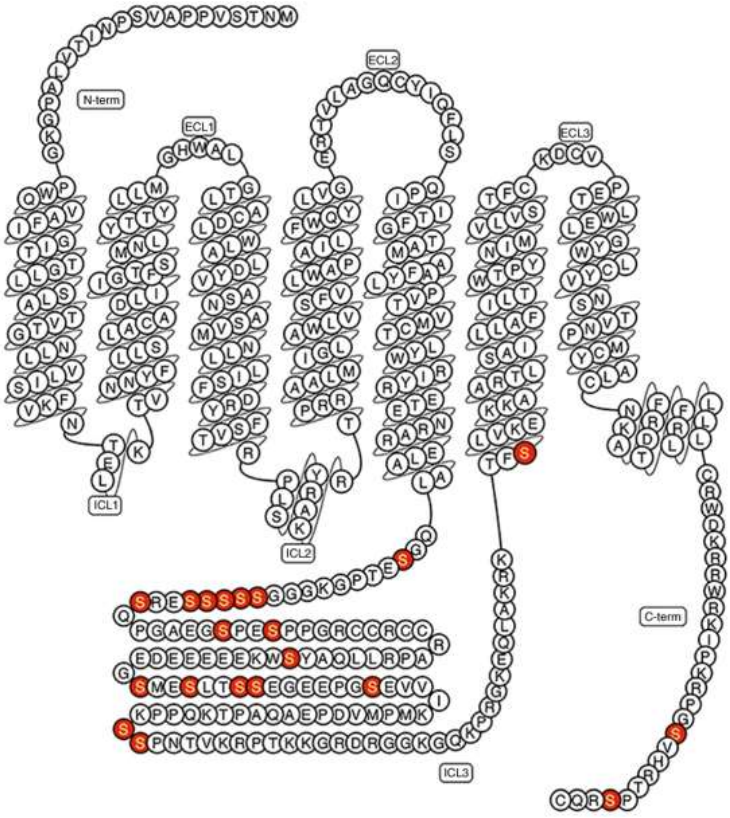

Figure 3-2 The phosphorylation-deficient version of the M1 mAChR (M1-PD). Snake plot of the M1 mAChR identifying the mutations introduced to generate the M1-PD receptor. Adapted from (Bradley et al., 2020).

3.1.9 Aims

The aims for this chapter were to determine the impact of removing phosphorylation sites of the M1 mAChR *in vitro* to assess the receptor signalling bias and establish whether the DREADD version of the receptor display similar

properties. Finally, this chapter aimed to assess the signalling profile of putative biased ligands (GSK1034702 and pilocarpine) at the M1 mAChR.

3.2 Results

3.2.1 Expression and function of wild-type and phosphorylation-deficient mutant M1 mAChR in CHO Flp-In cells

A phosphorylation-deficient version of the murine M1 mAChR (M1-PD) was generated whereby all MS-identified and putative intracellular phosphorylation sites were removed (Bradley et al., 2020, Butcher et al., 2016). The M1-PD as well as the wild-type M1 mAChR (M1-WT) were stably and constitutively expressed in Chinese hamster ovary (CHO) cells using the Flp-In™ system, which allows high-level expression of a protein of interest from a Flp-In expression vector. The M1-WT- and M1-PD-expressing CHO cell lines allowed the *in vitro* analysis of localisation and pharmacological profile of these receptors.

To facilitate detection of the receptors, a haemagglutinin (HA) epitope tag was fused to the C-terminus of both the M1-WT and M1-PD receptors. Protein expression was biochemically tested by western blot using an anti-HA antibody (Figure 3-3A-B). This confirmed that the M1-WT and M1-PD receptors are equally expressed (P=0.3, unpaired T test) in the Flp-In™ CHO cell lines. The expression of M1-WT was confirmed by the presence of a 75 kDa band whilst the M1-PD showed a slightly lower molecular weight band, which is expected due to the nature of its mutations. In fact, the replacement of serine residues with alanine residues is expected to lower the molecular weight due to the smaller size of their sidechains.

Protein expression was further assessed by conducting a saturation binding assay using tritiated N-methyl-scopolamine ([^{3}H]-NMS). The M1-WT and M1-PD receptors showed similar B_{max} (total concentration of receptors) values (M1-WT = 2131 fmol/mg; M1-PD= 2052 fmol/mg), indicating that they are expressed similarly in the CHO cell lines (Figure 3-3C-D). The K_D (equilibrium disassociation constant) of [^{3}H]-NMS for the M1-WT (0.8±0.1 nM) is consistent with data previously reported in the lab (unpublished).

The K_D value of [^{3}H]-NMS for the M1-PD (0.6 nM) is slightly (by around 0.2 nM) but significantly lower than the M1-WT (Figure 3-3, Table 3-1), suggesting [^{3}H]-NMS has higher affinity for the M1-PD compared to the M1-WT. Given that the mutations on the M1-PD are distant from the orthosteric binding site, it is unlikely that they would impact the binding property of the receptors. On the other hand, as demonstrated below, the M1-PD receptor shows impaired internalisation compared to the M1-WT (Figure 3-4), leading to a higher proportion of receptors being present at the cell surface. Considering that the NMS is not membrane-permeable, maximal receptor occupancy might be reached faster for the M1-PD compared to the M1-WT receptor, resulting in higher K_D.

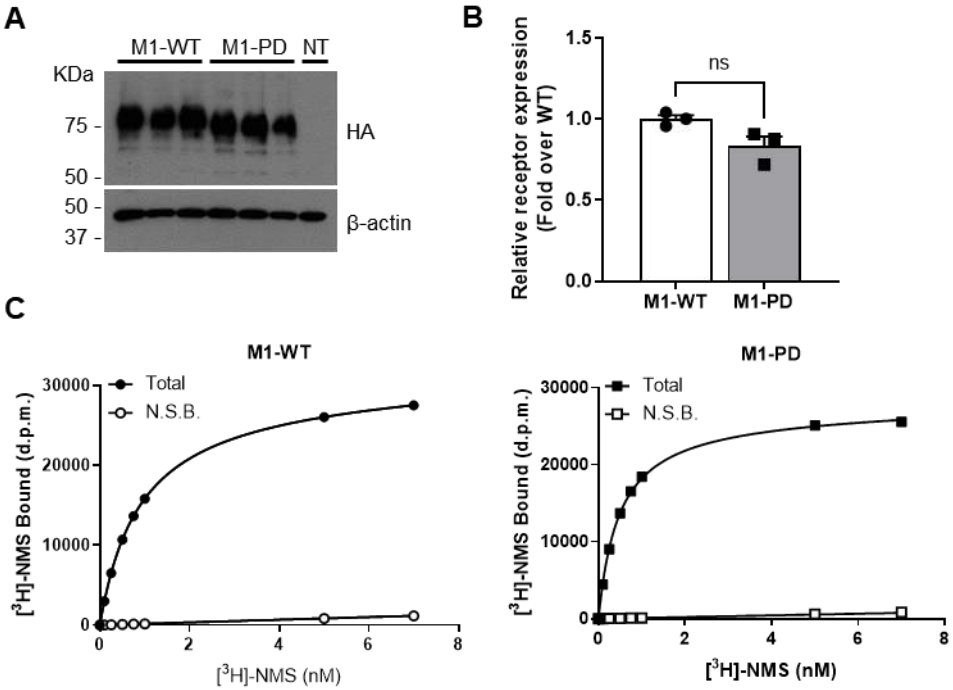

Figure 3-3 The M1-WT and M1-PD expression levels are equivalent in Flp-In CHO cells. (A) Western blot analysis of solubilised membranes (10µg) from Flp-In CHO cells expressing HA-tagged M1-WT and M1-PD using anti-HA antibody. β-actin was used as a loading control. NT, non-transfected. **(B)** Band intensity analysis (ImageJ) for receptor expression. Data is expressed as mean ± S.E.M. of fold over M1-WT and normalised to β-actin. Statistical analysis conducted was unpaired T test. **(C)** Non-linear regression curves of [^{3}H]-NMS saturation binding assay on M1-WT and M1-PD-expressing CHO cells, representative of three separate experiments. Total and non-specific binding (N.S.B.) of [^{3}H]-NMS are displayed as disintegrations per minute (d.p.m.). N.S.B. was conducted in the presence of atropine (10 µM) to control for non-specific binding of [^{3}H]-NMS.

	K_D (nM)		B_{max} (fmol/mg)		
	Mean ± S.E.M.	*P*	Mean ± S.E.M.	*P*	*N*
M1-WT	0.8 ± 0.1	0.02*	2131 ± 305	0.93	3
M1-PD	0.6 ± 0.01		2052 ± 674		3

Table 3-1 The M1-PD shows equivalent occupancy by [^{3}H]-NMS but higher affinity compared to the M1-WT when expressed in CHO Flp-In cells. B_{max} (fmol/mg) and K_D (nM) values obtained

from [^{3}H]-NMS saturation binding curves from three separate experiments conducted in duplicates (N=3). Data is displayed as mean ± S.E.M., and the statistical analysis used unpaired T-test (*P<0.05).

Receptor endocytosis was assessed by immunocytochemical co-staining of M1-WT and M1-PD-expressing cells following agonist stimulation (1 hour, 100 μM) using antibodies against the HA-tag attached to the receptor C-terminus, and the EEA1, which is a marker for early endosomes. It is evident that M1-WT receptors are found mainly localised at the cell membrane of CHO cells in basal conditions and undergo internalisation to the perinuclear region following treatment with the muscarinic agonist carbachol (Figure 3-4A). The M1-WT shows robust (P<0.01) co-localisation with EEA1 following carbachol stimulation, which could be quantified by estimating co-localisation coefficients using the Mender's equation (Figure 3-4B), indicating receptor internalisation. On the other hand, whilst most M1-PD receptors are also found localised at the cell membrane under basal conditions, these mutant receptors do not re-localise in response to agonist stimulation and are retained at the cell membrane (Figure 3-4A). The co-localisation coefficient of the M1-PD with EEA1 shows no change upon carbachol stimulation compared to the vehicle, and is significantly (P<0.05) lower than the one of the M1-WT with EEA1 (Figure 3-4B), suggesting that endocytosis of the M1-PD receptor is impaired compared to the M1-WT.

Receptor internalisation was also assessed using [^{3}H]-NMS labelling assay of M1-WT and M1-PD CHO cells. Since NMS is not membrane-permeable, [^{3}H]-NMS allows radiolabelling of the muscarinic receptors present on the cell membrane. Following carbachol treatment for increasing lengths of time, CHO cells were incubated at 4˚C to slow down intracellular trafficking and incubated overnight with [^{3}H]-NMS. M1-WT receptors showed a significant (P<0.05) decrease in cell surface expression from 30 min of agonist treatment (Figure 3-4C). Most receptor internalisation occurred within the first hour of treatment with about 30% of internalised receptors and reaching around 40% internalised receptors after 4 hours treatment. In contrast, M1-PD receptors showed no change in level of surface receptors at any of the time-points (Figure 3-4C).

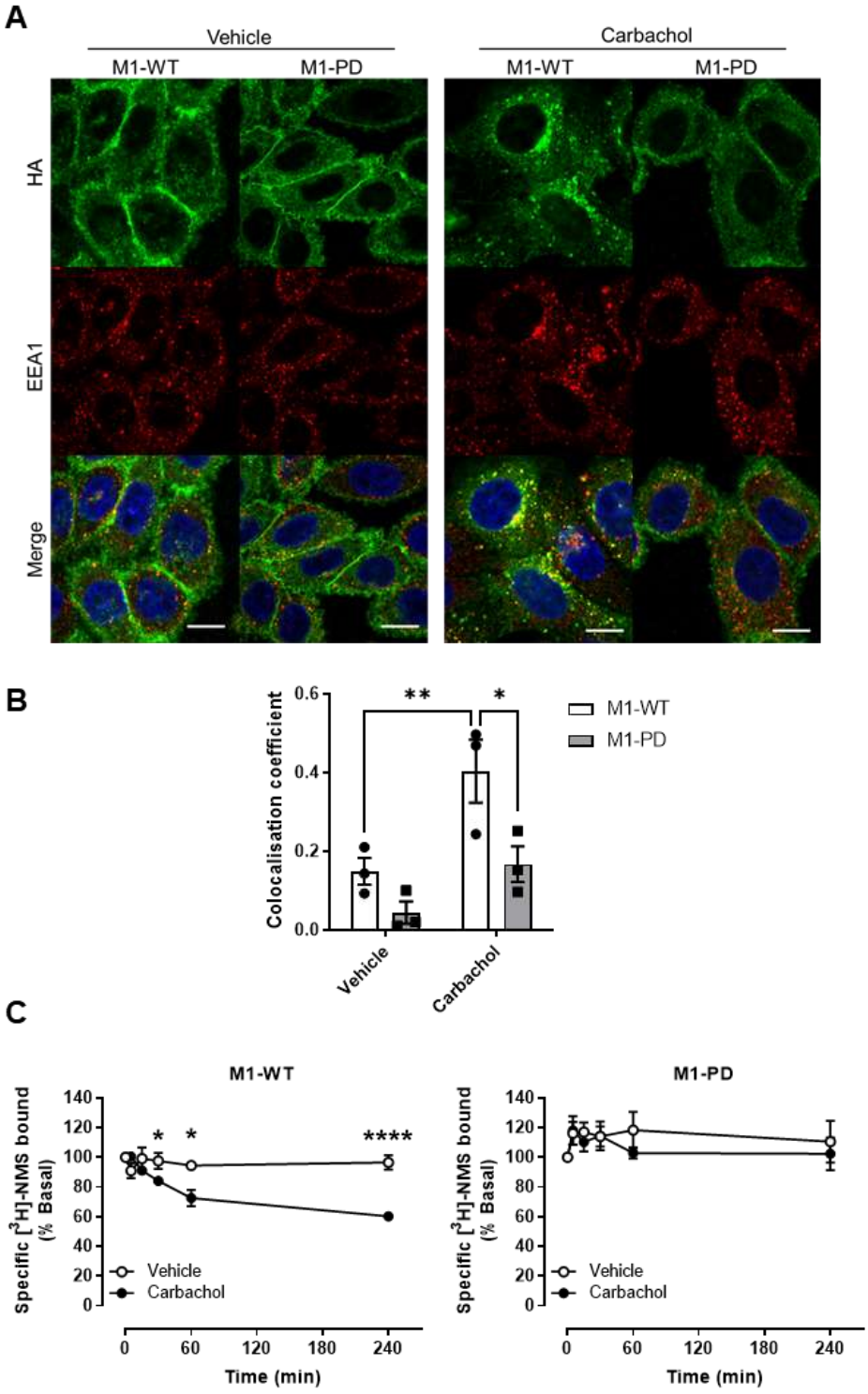

Figure 3-4 Agonist-induced internalisation of the M1-WT and M1-PD receptors in intact CHO cells. (A) Representative images of immunocytochemical staining using antibodies against HA and EEA1 to determine the subcellular localisation of M1-WT and M1-PD receptors in CHO cells in response to vehicle or carbachol (1 hour, 100 µM) treatment. Scale bar: 10 µm. **(B)** Co-localisationcoefficients (Manders' equation) of HA with EEA1 in M1-WT and M1-PD cells treated with carbachol (100 µM) or vehicle for 1 hour. Data is expressed as an average from 10 fields of view from three separate experiments (N=3). *P value<0.05, two-way ANOVA (Tukey multiple

comparison). **(C)** Time-course of agonist-induced internalisation of the M1-WT and M1-PD receptors in response to vehicle or carbachol (100 μM). After agonist or vehicle treatment for the indicated time-points, receptor internalisation was measured by radiolabelling surface receptors with [^{3}H]-NMS overnight at 4°C. Data are expressed as mean ± S.E.M. of percentage of bound [^{3}H]-NMS relative to basal from four separate experiments (N=4) implemented in triplicates. *P<0.01, ***P=0.0002, ****P<0.0001, Two-way ANOVA (Fisher's Least Significant Difference (LSD) test).

The M1 mAChR preferentially couples with $G\alpha_{q/11}$ proteins that activate the inositide signalling pathway. One way to assess $G\alpha_{q/11}$ protein-dependent signalling is by detecting the accumulation of inositol phosphate (IP1), a by-product of the inositide signalling pathway. A concentration-response curve for IP1 accumulation in response to carbachol allowed to assess the potency (EC_{50}) and efficacy (E_{max}) of this compound at the M1-PD compared to the M1-WT (Figure 3-5). Treatment of M1-WT CHO cells with the muscarinic orthosteric agonist, carbachol induced robust IP1 accumulation with an EC_{50} (effective concentration of the agonist where 50% of its maximal effect is observed) at a micromolar concentration (pEC_{50}=6.8). Carbachol showed the same potency at eliciting IP1 accumulation in the M1-PD CHO cell as in the M1-WT. However, M1-PD CHO cells showed higher maximal response, or E_{max}, compared to the M1-WT by approximately 30%. This might be due to the reduction in receptor-ß-arrestin interaction that would result in a lesser displacement of G protein signalling. To control for the response specificity to the muscarinic receptor, IP1 accumulation was also assayed in response to the maximal concentration of carbachol (100 μM) in the presence of the competitive muscarinic antagonist, atropine (Figure 3-5). In the presence of atropine, IP1 accumulation was reduced to the same level as the baseline in M1-WT cells. However, in M1-PD cells, IP1 accumulation in the presence of atropine was reduced to a level that was around 50% lower than the baseline level. It can be hypothesised that IP1 accumulation response is mostly mediates by M1 mAChRs at the cell membrane (rather than internalised receptors), therefore the response will be higher for internalisation-deficient M1-PD receptors compared to M1-WT. Therefore, antagonist treatment would

result in a more robust suppression of response in M1-PD cells compared to M1-WT.

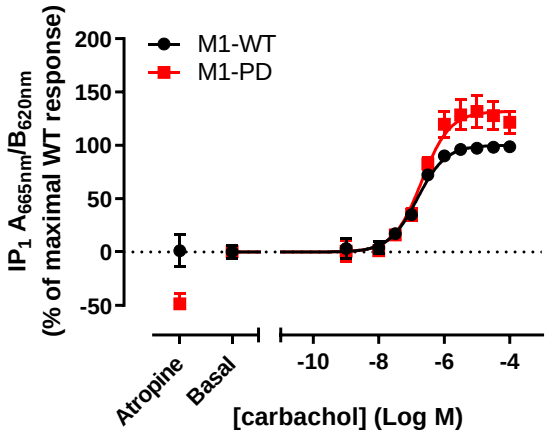

Figure 3-5 IP1 accumulation assay in M1-WT and M1-PD-expressing CHO cells. IP accumulation was measured as representative of G protein-dependent signalling. Non-linear regression curve of IP1 accumulation elicited by the muscarinic agonist carbachol *via* the murine M1-WT and M1-PD receptors expressed in CHO Flp-In cells (N=4). Atropine (10 µM) was added to a maximal concentration of carbachol (100 µM) to control for muscarinic receptor-specific response.

	pEC_{50}		E_{max}		
	Mean ± S.E.M.	*P*	Mean ± S.E.M.	*P*	*n*
M1-WT	6.8 ± 0.05	0.05	100.0 ± 0.0	0.06	*4*
M1-PD	6.7 ± 0.02		131.8 ± 13.4		*4*

Table 3-2 The M1-PD receptor shows equivalent G protein response in CHO Flp-In cells compared to the M1-WT. pEC_{50} and E_{max} values for IP1 accumulation in M1-WT and M1-PD, calculated from (Figure 3-5). Data are expressed as the means ± S.E.M. of 4 independent experiments implemented in duplicates (N=4). Statistical analysis performed is unpaired T test.

3.2.2 Expression and function of M1-DR and M1-PD DR receptors in Flp-In CHO cell lines

Our group had generated a DREADD version of the M1 mAChR (M1-DR) that is unable to bind to ACh and instead can be stimulated using CNO (Butcher et al., 2016). In addition, similar to the M1-WT, a phosphorylation-deficient version of the M1-DR receptor (M1-PD DR) was generated in order to dissect the bimodal signalling of the M1 mAChR (Bradley et al., 2020). It is important to verify that the M1-DR and M1-PD DR receptors possess the same signalling properties (bias) as the wild-type counterparts to ensure that the comparison is appropriate.

Similar to the M1-WT and M1-PD receptors, the humanised M1-DR and M1-PD DR receptors were previously stably and constitutively expressed in CHO cells using the Flp-In™ expression system. HA tags were also added to the C-termini of M1-

DR and M1-PD DR to facilitate receptor expression analysis. Western blots using an anti-HA antibody confirmed that M1-DR and M1-PD DR are expressed equally in the CHO cell lines (Figure 3-6).

Due to the impact of the DREADD mutations on the orthosteric binding capacity, [^{3}H]-NMS saturation binding assays were not possible to perform and therefore the expressed protein amount of the receptors in the cells could not be quantified.

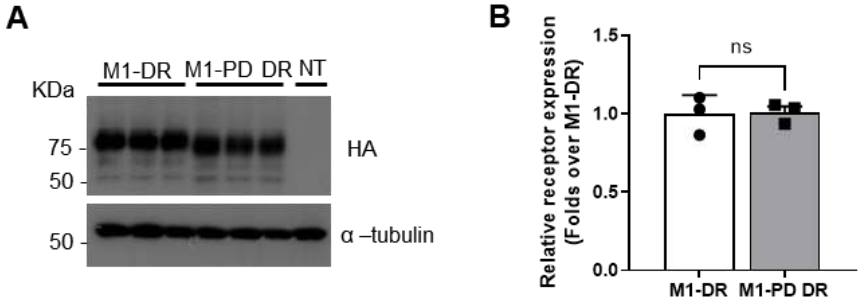

Figure 3-6 Expression of M1-DR and M1-PD DR receptors in Flp-In CHO cells. (A) Western blot analysis (using anti-HA antibody) of solubilised membranes (10µg) from Flp-In CHO cells stably transfected with HA-tagged M1-DR and M1-PD DR mutant receptors. α-tubulin was used as a loading control. NT, non-transfected. Band analysis (ImageJ) of (A) are expressed as mean ±S.D. in folds over M1-DR, normalised to the loading control.

IP1 accumulation was assessed in M1-DR and M1-PD DR CHO cells in response to treatment with CNO (Figure 3-7A). In addition, IP1 accumulation was assayed in response to Compound 21 (Figure 3-7B), a potent agonist for muscarinic DREADD receptors (Thompson et al., 2018). CNO and Compound 21 elicited IP1 accumulation response with a similar potency and efficacy, as indicated by the EC_{50} and E_{max} values derived from the concentration-response curves (Figure 3-7C). Interestingly, both CNO and Compound-21 have higher potency for the M1-PD DR receptor compared to the M1-DR, with a left-ward shift of its concentration-response curve, but only Compound-21 was significantly different (Table 3-3). Furthermore, the E_{max} of both CNO and Compound-21 is significantly lower for M1-PD DR cells compared to the M1-DR cells, which is the opposite of what was observed with their wild-type counterparts, the M1-WT and M1-PD.

M1-DR and M1-PD DR cells were also stimulated with CNO or Compound-21 in the presence of the antagonist atropine. As expected, atropine did not affect the IP1 response in M1-DR and M1-PD DR; in fact, because of the changes in the orthosteric pocket, the DREADD receptors should have lost the affinity for

atropine and consequently atropine should not be competitive for neither CNO nor Compound-21.

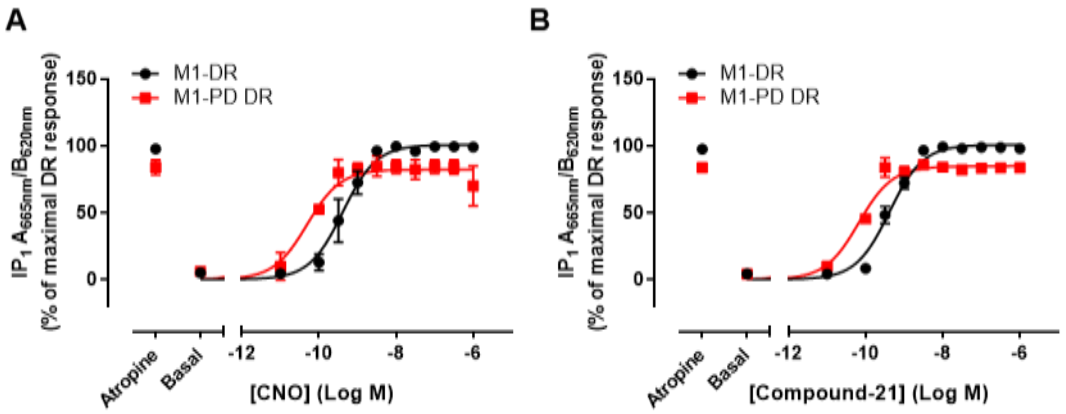

Figure 3-7 IP1 accumulation in M1-DR and M1-PD DR CHO Flp-In cells. IP1 accumulation elicited by one hour-treatment with CNO **(A)** and Compound-21 **(B)** *via* the DREADD and PD DREADD mutants of the human mAChR (M1-DR and M1-PD DR) expressed in CHO Flp-In cells. Atropine (10 µM) was added to show the lack of effect on the receptor with DREADD mutations. Data are expressed as the means ± S.E.M. of at least 4 independent experiments implemented in duplicates (N=4-5).

		pEC_{50}		E_{max}		
		Mean ± S.E.M.	***P***	**Mean ± S.E.M.**	***P***	***n***
CNO	**M1-DR**	9.7 ± 0.3	0.1	100.0 ± 0.0	0.02*	*5*
	M1-PD DR	10.8 ± 0.6		84.6 ± 5.7		*4*
Compound-21	**M1-DR**	9.5 ± 0.1	0.001***	100.0 ± 0.0	0.001***	*5*
	M1-PD DR	10.2 ± 0.1		84.4 ± 12.9		*4*

Table 3-3 IP1 response in M1-DR and M1-PD DR CHO Flp-In cells. Potency (pEC_{50}) and efficacy (E_{max}) indicators for CNO and Compound-21 at the M1-DR and M1-PD DR receptors in CHO Flp-In cells, derived from (Figure 3-7). Statistical analysis was multiple unpaired T test, *P=0.02, ****P<0.0001.

Immunocytochemical staining using anti-HA antibodies was conducted on CHO cells expressing the M1-DR and M1-PD DR following one hour treatment with vehicle or CNO (100 µM) at 37°C to detect receptor localisation. Co-staining with antibodies against EEA1 was included to assess receptor endocytosis. Most M1-DR receptors were found localised at the cell surface in the vehicle-treated cells and they show evident re-localisation to the perinuclear area upon stimulation with the agonist CNO (Figure 3-8A). Co-localisation of HA-tagged M1-DR with EEA1 is also evident and could be estimated using co-localisation coefficients,

indicating robust (P<0.05) internalisation of the M1-DR in response to CNO treatment (Figure 3-8B). In contrast, the M1-PD DR also localises at the cell membrane, but its localisation is not affected by agonist stimulation. No co-localisation occurs between M1-PD DR and the EEA1; the co-localisation coefficient shows no significant change with CNO treatment compared to the vehicle, and it is significantly lower than the CNO-treated M1-DR receptor (Figure 3-8B).

The above observations suggest that overall, the M1-DR and M1-PD DR behave similarly to their wild-type counterparts (the M1-WT and M1-PD receptors).

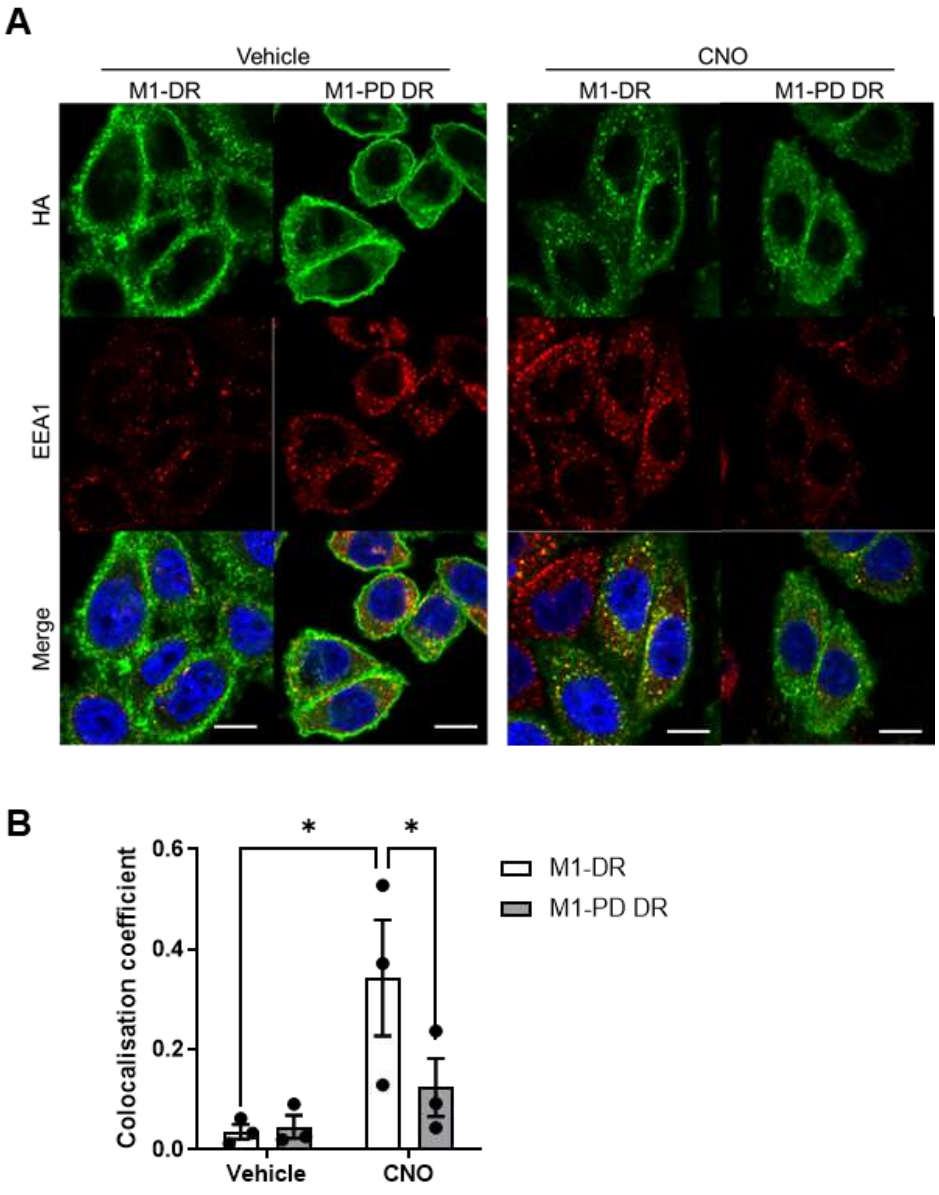

Figure 3-8 Agonist-induced receptor internalisation of M1-DR and M1-PD DR Flp-In CHO cell lines. (A) Representative images of immunocytochemical staining using antibodies against HA and EEA1 to determine the subcellular localisation of M1-DR and M1-PD DR receptors in CHO cells in response to vehicle or CNO (100 µM) one hour-treatment. Scale bar: 10 µm. **(B)** Co-

localisation coefficients (Manders' equation) of HA with EEA1 in M1-DR and M1-PD DR cells treated with CNO (100 μM) or vehicle for 1 hour. Data is expressed as means of co-localisation coefficients from 10 fields of view from three separate experiments (N=3). *P value<0.05, two-way ANOVA (Tukey multiple comparison).

3.2.3 Analysis of signalling response induced by M1 ligands ACh, GSK1034702 and pilocarpine

GSK1034702 and pilocarpine are muscarinic agonists that were previously reported to induce adverse responses in rodents, specifically epileptic-like seizures (Bradley et al., 2018). Epileptic-like seizures have been attributed to adverse effects in response to stimulation of the M1 mAChR (Cruickshank et al., 1994, Hamilton et al., 1997). Having determined receptor internalisation and G protein-dependent signalling in a G protein-biased version of the M1 mAChR (M1-PD) and compared to the wild-type receptor, I wished here to define the effects of GSK1034702 and pilocarpine on internalisation and G protein-dependent signalling (IP1 accumulation). By comparing GSK1034702 and pilocarpine with the endogenous agonist ACh, I was able to determine whether these ligands have signalling bias.

Agonist-induced internalisation of the M1 mAChR was measured using an [^{3}H]-NMS binding assay to quantify the receptors at the cell surface, as described above. ACh reduced surface receptors by 17% following 30 min agonist stimulation, which was significantly different ($P<0.05$) from both GSK1034702 and pilocarpine that instead induced no changes in surface receptors after 30 min-treatment (Figure 3-9A). In response to one hour- and four hour-treatment with ACh, surface receptors were decreased by around 24% and 56% respectively. Whilst GSK1034702 induced a reduction in surface receptors after 1 hour stimulation to levels like those induced by ACh ($P>0.05$), surface receptors remained unchanged after one hour of pilocarpine treatment (Figure 3-9A). The maximal length of treatment, four hours, led to around 56% of internalised receptors in response to ACh, which was significantly different ($P<0.01$) from the internalised receptors induced by GSK1034702 and pilocarpine (~19%).

A concentration-response curve for internalisation in response to ACh, GSK1034702 and pilocarpine was generated using a similar [^{3}H]-NMS binding assay, whereby M1-WT CHO cells were stimulated for one hour with varying agonist concentrations (Figure 3-9B). This assay allowed to derive potency

(pEC_{50}) and efficacy (E_{max}) values for agonist-induced internalisation in response to the tested M1 ligands (Table 3-5). Whilst the potency of GSK1034702 at inducing receptor internalisation seems higher than ACh and pilocarpine, it was not found statistically significant in an ordinary one-Way ANOVA test. GSK1034702 and pilocarpine were not significantly different at inducing receptor internalisation, the efficacy of GSK1034702 and pilocarpine was significantly lower compared to ACh (Figure 3-9B, Table 3-4). GSK1034702 gave variable results compared to the other M1 ligands, making the comparison less robust – this could be explained by the bitopic binding mode (Bradley et al., 2018) or the low solubility of the compound. Furthermore, ACh showed higher receptor internalisation at 100μM following one hour treatment in the concentration-response assay compared to the time-course (38% vs 24% internalised receptors).

Overall, these results indicate that the agonist-induced internalisation of the M1 mAChR in response to GSK1034702 and pilocarpine is significantly less in comparison with the receptor internalisation induced by the endogenous agonist ACh. Prolonged treatment with ACh results in a significant reduction in receptors at the cell surface by up to ~50%, whereas treatment with GSK1034702 and pilocarpine for the same length of time results in less receptor internalisation. However, it is important to consider that the apparent inability to induce receptor internalisation of GSK1034702 and pilocarpine to a similar extent as ACh, might be associated to their binding properties. Pilocarpine might only partially be able to displace [^{3}H]-NMS because of its partial agonism; whereas GSK1034702 might only partially able to displace [^{3}H]-NMS due to its bitopic binding mode that is subtly distinct from that of prototypical orthosteric ligands such as scopolamine (Bradley et al., 2018).

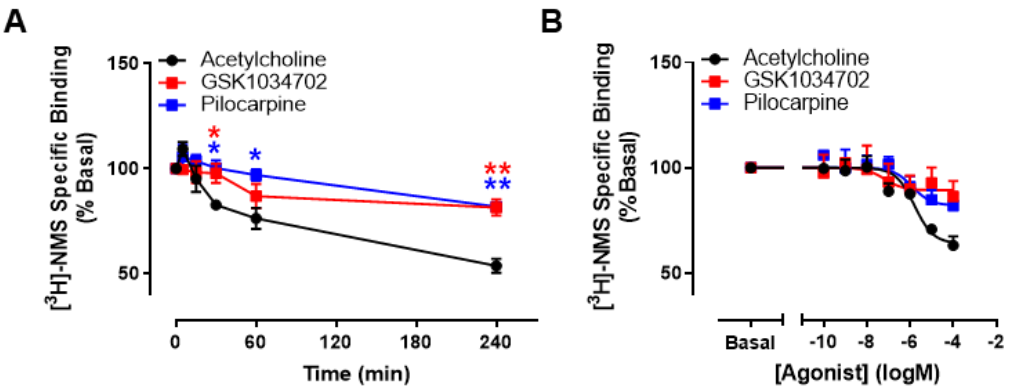

Figure 3-9 M1 mAChR internalisation induced by M1 ligands ACh, GSK1034702 and Pilocarpine in CHO Flp-In cells. Agonist-induced internalisation was measured using [^{3}H]-NMS to label surface receptors in Flp-In CHO cells expressing the murine M1-WT following treatment with the endogenous cholinergic ligand ACh, or GSK1034702 or Pilocarpine. Cells were either stimulated with constant concentration of M1 ligands (100 µM) in a time-course experiment **(A)** or treated with the M1 ligands at increasing concentration for one hour to generate a concentration-response curve **(B)**. Data are expressed as mean ± S.E.M. of percentage [^{3}H]-NMS bound relative to the time 0 or basal. *P<0.05, **P<0.002, two-way ANOVA (Fisher's LSD test), N=4-5.

	pEC_{50}		E_{max}		
	Mean±S.E.M.	***P***	**Mean±S.E.M.**	***P***	***n***
Acetylcholine	6.5 ± 0.9	-	62.3 ± 6.5	-	4
GSK1034702	7.5 ± 0.6	0.5	96.5 ± 10.9	0.0016**	5
Pilocarpine	5.7 ± 0.3	0.6	84.6 ± 4.1	0.028*	4

Table 3-4 Agonist-induced internalisation in response to M1 ligands ACh, GSK1034702 and pilocarpine in M1-WT CHO cells. Table of potency (pEC_{50}) and efficacy (E_{max}) indicators in agonist-induced internalisation measured using [^{3}H]-NMS radioligand-based internalisation assays (Figure 3-9). Statistical analysis performed is ordinary one-way ANOVA (Dunnett's multiple comparisons).

As discussed above, IP1 accumulation is indicative of $G\alpha_{q/11}$ protein-dependent signalling. IP1 accumulation was assayed is response to GSK1034702 and pilocarpine to assess whether they possess any bias towards G protein-dependent signalling compared to ACh (Figure 3-10). The three M1 ligands induced IP1 accumulation with equivalent efficacy (E_{max}), however their potency values (pEC_{50}) vary. GSK1034702 shows a minor but significant increase in potency (P<0.05) compared to ACh, whereas pilocarpine shows a significantly lower (P<0.0001) potency compared to ACh, with an evident right-ward shift of the concentration-response curve (Figure 3-10A, Table 3-5). Pilocarpine is a partial agonist at the M1 mAChR, which could explain the lower potency of this compound compared to the full agonist ACh. However, pilocarpine still induce an IP1 accumulation response with efficacy similar to a full agonist – this is

consistent with previous reports showing that pilocarpine is more efficacious in stimulating G protein-dependent signalling compared to GSK1034702 (Bradley et al., 2020). In addition, the presence of atropine to the 100 µM agonist treatment demonstrated that the IP1 response detected was specifically mediated by the muscarinic receptor.

IP1 accumulation in response to ACh, GSK1034702 and pilocarpine was also assessed in M1-PD CHO cells (Figure 3-10B). Similar to the carbachol-induced response (Figure 3-5), the three M1 ligands tested elicited an IP1 accumulation response with equivalent potency (pEC_{50}) an efficacy (E_{max}) at the M1-PD receptor as at the M1-WT (Table 3-5), which was tested using an unpaired T test ($P>0.06$). The addition of atropine to the top concentration used confirmed that it is a muscarinic-induced response.

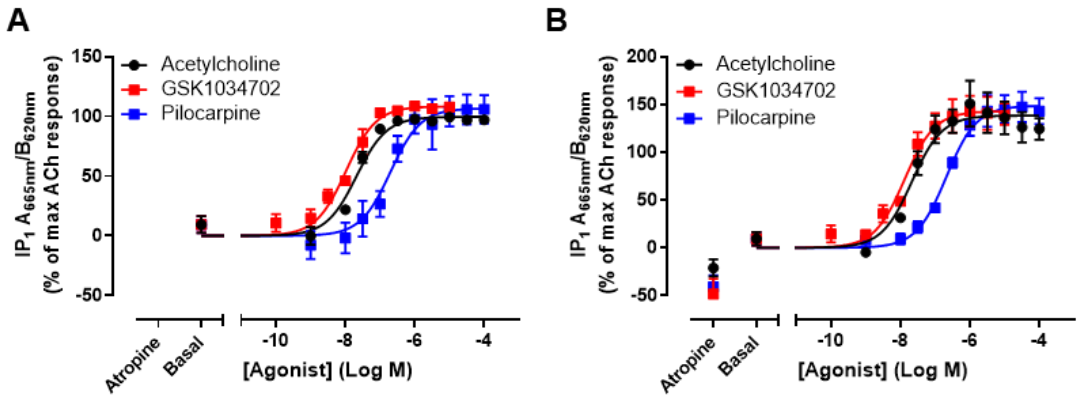

Figure 3-10 Concentration-response curves for Inositol phosphate (IP1) accumulation in M1-WT and M1-PD CHO cells in response to ACh, GSK1034702 and pilocarpine. IP_1 accumulation elicited by ACh, GSK1034702 or pilocarpine in M1-WT (A) and M1-PD (B) Flp-In CHO cells. Atropine (10 µM) was added to a maximal concentration of agonist to control for muscarinic receptor-specific response. Data are expressed as the means ± S.E.M., and the maximal response by ACh in M1-WT was used as reference for both curves (N=4).

		pEC_{50}		E_{max}		
		Mean±S.E.M.	*P*	Mean±S.E.M.	*P*	*n*
M1-WT	Acetylcholine	7.7 ± 0.1	-	100.0 ± 0.0	-	4
	GSK1034702	8.0 ± 0.0	0.05*	108.2 ± 1.5	0.7	4
	Pilocarpine	6.7 ± 0.1	<0.0001****	107.1 ± 12.1	0.8	4
M1-PD	Acetylcholine	7.7 ± 0.1	-	137.5 ± 16.5	-	4
	GSK1034702	7.9 ± 0.1	<0.0001****	142.6 ± 15.8	1	4
	Pilocarpine	6.7 ± 0.1	<0.0001****	148.7 ± 16.0	0.9	4

Table 3-5 IP1 accumulation response induced by M1 ligands ACh, GSK1034702 and pilocarpine in M1-WT and M1-PD CHO cells. Potency (pEC_{50}) and efficacy (E_{max}) for IP1

accumulation and agonist-induced internalisation in response to the M1 ligands were derived from (Figure 3-9, Figure 3-10). Statistical analysis performed is ordinary one-Way ANOVA (Dunnett's multiple comparisons) in relation to ACh response.

Signalling bias of GSK1034702 and pilocarpine at M1-WT was measured by fitting the concentration–response curves of IP1 accumulation and agonist-induced receptor internalisation to the operational model of agonism to derive a transduction coefficient (τ) for each of the responses. By comparing these with the transduction coefficient of the natural ligand ACh, we calculated the bias of the two ligands between G protein coupling (IP1 accumulation) and receptor phosphorylation (agonist-induced internalisation), expressed as a bias factor (Table 3-6). Unpaired T test between the Ligand Bias Factor of GSK1034702 and pilocarpine at the M1-WT and the one of acetylcholine showed no bias between G protein coupling and receptor phosphorylation pathways.

	$Log_{10}(\tau/KA)$		$\Delta Log_{10}(\tau/KA)$		Log Bias Factor $\Delta\Delta Log_{10}(\tau/K_A)$	
	IP1	Internalisation	IP1	Internalisation	IP1 - Internalisation	P
Acetylcholine	7.60 ± 0.07	4.01 ± 2.61	0 ± 0.10	0 ± 3.69	0 ± 3.69	
GSK1034702	7.97 ± 0.12	2.02 ± 3.12	0.37 ± 0.14	-1.99 ± 4.07	-2.36 ± 4.07	0.73
Pilocarpine	6.7 ± 0.11	2.46 ± 2.73	-0.90 ± 0.13	-1.55 ± 3.77	-0.65 ± 3.78	0.78

Table 3-6 Ligand bias calculations for acetylcholine, GSK1034702 and pilocarpine.
Transduction coefficients (Log10(τ/KA)) normalised to the reference ligand acetylcholine transduction coefficients (ΔLog10(τ/KA)), and Log Bias factor (ΔΔLog10(τ/KA)) for IP1 and agonist-induced internalisation at the M1 wild-type receptor expressed in CHO Flp-In cells. Statistical analysis was unpaired T test for GSK1034702 and pilocarpine vs acetylcholine (N=4-5).

3.3 Discussion

GPCRs are involved is a vast range of physiological functions in health and disease and for this reason they are the target of around a third of clinically approved drugs (Santos et al., 2017). However, in addition to beneficial therapeutic effects, pharmacological modulation of GPCRs might also induce adverse responses. This is due to the pleiotropic nature of GPCRs that can engage with multiple downstream effectors and signalling pathways (Costa-Neto et al., 2016). Biased ligands offer a promising therapeutic advantage by enabling the selective activation of clinically beneficial pathways against those leading to detrimental adverse responses (Kenakin, 2019). It is therefore fundamental to dissect the signalling pathways of a drug targeted GPCR to identify the appropriate response for a favourable physiological outcome with reduced undesirable adverse effects. Exploring a GPCR signalling bias would not only inform drug development programmes for the design of more efficacious and safer therapies, but also has the potential to provide further insights into the physiological role of bias signalling.

The M1 mAChR is a validated target for the treatment of neurodegenerative diseases such as AD (Felder et al., 2018, Foster et al., 2014). However, the generation of clinically effective M1 mAChR drugs has been challenging due to adverse effects associated with off-target activation of peripheral M2 and M3 mAChRs (Bymaster et al., 2003a, Melancon et al., 2013) as well as on-target activity at the M1 mAChR (Rook et al., 2017, Engers et al., 2018, Moran et al., 2018b). Our laboratory therefore set out to dissect the M1 mAChR-mediated signalling pathways to discern the clinically beneficial signalling from the ones leading to adverse responses, by generating genetically engineered mice expressing a phosphorylation deficient variant of the M1 mAChR (M1-PD) (Butcher et al., 2016, Bradley et al., 2020). PD variants of GPCRs have previously been proven successful in the investigation of biased signalling, leading to findings with important implications for drug development programmes. For instance, knock-in mice expressing a PD version of the M3 mAChR lacking MS-identified intracellular phosphorylation sites (Butcher et al., 2011) helped establish that the M3 mAChR regulates cognition, glucose tolerance and insulin release as well as bronchoconstriction *via* phosphorylation/arrestin-dependent signalling pathways (Poulin et al., 2010, Kong et al., 2010, Bradley et al., 2016).

In addition, knock-in mice expressing a PD mutant of the μOR that fails to recruit ß-arrestin were also generated to validate the analgesic potential of ß-arrestin-mediated signalling of opioids (Kliewer et al., 2019). In this chapter, the signalling properties of the M1-PD were assessed *in vitro* (in CHO Flp-In cell lines) and compared to the wild-type receptor (M1-WT) to provide insights into the molecular and signalling mechanisms underpinning the differences observed *in vivo*. After establishing the equivalent expression levels of the M1-WT and the M1-PD receptors in cell lines, the M1-PD receptor shows impaired agonist-induced internalisation while the $G\alpha_q$ protein signalling, measured in an IP1 accumulation assay, was retained. Implying that this mutant is a G protein-biased mutant of the M1 mAChR.

Phosphorylation of the M1 mAChR occurs at intracellular regions that include 14 phosphor-acceptor sites: nine serine and three threonine phosphorylation sites in the third intracellular loop and two serine phosphorylation sites in the C-terminal tail (Butcher et al., 2016). Like other GPCRs, phosphorylation of the M1 mAChR induces recruitment of ß-arrestin that causes receptor desensitisation by uncoupling the receptor from G proteins, and/or causing clathrin-mediated internalisation (Bradley et al., 2020, Thomas et al., 2009, Waugh et al., 1999). Previous studies from our group, using the same M1-PD mutant but in different *in vitro* transfection systems, showed that removal of M1 mAChR phosphorylation decreases receptor interaction with ß-arrestin by approximately 50% compared to wild-type receptors but does not completely abolish it (Scarpa et al., 2021, Bradley et al., 2020). Furthermore, though greatly reduced, receptor internalisation was still detected using a bystander BRET assay for receptor recruitment to early endosomes (Scarpa et al., 2021). Here, I confirmed previous findings, demonstrating that removal of all the phosphorylation sites of the M1 mAChR significantly reduces agonist induced receptor internalisation. Similarly, the PD version of the M1-DREADD receptor was found to be robustly decreased. Altogether, these data show that phosphorylation is important for ß-arrestin-receptor interactions and especially agonist-induced internalisation. However, the removal of phosphorylation sites does not completely disrupt these mechanisms. The observed residual binding of ß-arrestin to the M1-PD was still agonist-dependent (Scarpa et al., 2021, Bradley et al., 2020), suggesting that

there are regions of the receptors that contain arrestin-binding sites which are unmasked upon agonist activation, such as the ICL2 or ICL3.

Although phosphorylation is important to stabilise receptor-arrestin complexes (Zhou et al., 2017), β-arrestins can interact with GPCRs in a phosphorylation -dependent and -independent manner; respectively by binding to the phosphorylated C-terminal *tail* of the receptor *via* the arrestins' phosphor-sensor, and by interacting with the receptor cytoplasmic *core via* the arrestin's finger loop (Gurevich and Gurevich, 2006, Shukla et al., 2013, Zhou et al., 2017, Sommer et al., 2015). Single-particle EM studies of a ß-arrestin1-bound $ß_2V_2R$ chimera unravelled a biphasic mode of ß-arrestin binding whereby receptor-arrestin complexes are found as *partially engaged* (only bound through the receptor tail) and/or *fully engaged* complexes (bound through receptor core and tail) (Shukla et al., 2014, Ghosh et al., 2015). The phosphorylation-independent binding is suggested to rely on structural motifs that are exposed in active GPCR conformations. For instance, the ICL2 was shown to be involved in arrestin recruitment and endocytosis of 5-HT_{2C}, $ß_2$AR, $α_{2A}$AR and neuropeptide Y2 receptors (Marion et al., 2006). Specifically, the first 10 residues of ICL2 at the beginning of the DRY motif, which are important for interactions with both G proteins and arrestins (Barak et al., 1994), were shown to constitute a structural determinant for the phosphorylation-independent binding of ß-arrestins (Marion et al., 2006). Additionally, pull-down, and direct binding studies have demonstrated that several GPCRs are able to interact with arrestins in the absence of receptor phosphorylation, particularly *via* their ICL3. These include rhodopsin, $ß_2$AR, $α_{2A}$AR, vasopressin V1, HT_{2A}, δ opioid receptors and even the M2 and M3 muscarinic subtypes (Gurevich et al., 1995, Ferguson et al., 1996, Wu et al., 1997, Gelber et al., 1999, Cen et al., 2001, DeGraff et al., 2002, Wang and Limbird, 2002, Wu et al., 2006). Our data (Scarpa et al., 2021, Bradley et al., 2020) provides a strong indication that the M1 mAChR might interact with arrestins in a phosphorylation-independent manner. Given the relatively large size of the ICL3 (Figure 3-1), there is a possibility that the M1 mAChR ICL3 is involved in the interaction with arrestin, like the ICL3 of other subtypes of the muscarinic family (Wu et al., 1997, Gurevich et al., 1995). Additionally, recent nuclear magnetic resonance (NMR) spectroscopy studies have demonstrated that both C-tail and core-mediated interactions of GPCRs are required for the full

conformational change of ß-arrestin1 into its active state (Shiraishi et al., 2021). This further supports the concept that receptor phosphorylation is important, but not essential, for GPCR-arrestin interactions.

Following agonist activation, receptor phosphorylation and the subsequent interaction with ß-arrestin cause G protein uncoupling and signalling desensitisation by steric hindrance (Rasmussen et al., 2011, Kang et al., 2015, Carpenter et al., 2016, Liang et al., 2017, Zhang et al., 2017, Szczepek et al., 2014, Chaturvedi et al., 2020). Similar to the M3 and M5 subtypes, the M1 mAChR preferentially couples to $G\alpha_{q/11}$ class of G proteins (Wess, 1993, Felder, 1995), leading to phosphoinositide breakdown into inositol (1,4,5) trisphosphate and 1,2-diacylglycerol, that cause the increase of intracellular calcium (Nathanson, 2000). The M1 mAChR is able to undergo rapid agonist-induced phosphorylation and desensitisation (10-300s following agonist exposure), which was shown to eliminate the receptor reserve associated to G protein-induced IP3 signalling (Waugh et al., 1999). Removal of receptor phosphorylation in the M1-PD did not significantly affect IP3 signalling as measured by IP1 accumulation assay in response to the full agonist carbachol. This result was consistent with previous reports and suggests that lack of phosphorylation does not impact $G\alpha_q$ protein signalling; this could be due to the observed residual ß-arrestin recruitment to the M1-PD (Bradley et al., 2020, Scarpa et al., 2021).

Receptor phosphorylation and recruitment of ß-arrestin to activated GPCRs are known to be crucial for receptor internalisation (Ferguson et al., 1996). The M1 mAChR was confirmed here to require receptor phosphorylation for robust agonist-induced receptor internalisation as M1-PD receptors displayed a severely impaired internalisation (Bradley et al., 2020, Thomas et al., 2009, Waugh et al., 1999, Lee et al., 1998). In fact, the removal of intracellular phosphorylation sites robustly decreased the re-localisation of the M1 mAChR from the cell surface to the perinuclear area. Whereas the M1-WT receptor in CHO cells showed significant co-localisation with the early endosomal marker EEA1 following agonist treatment, the M1-PD receptor seems sequestered at the cell surface and does not co-colocalise with EEA1. This strongly indicates that the M1-PD receptor is impaired in phosphorylation/arrestin-dependent mechanisms, drawing to the conclusion that this variant is a G protein-biased receptor. However, though drastically reduced, receptor internalisation could still be

detected using a bystander BRET assay for receptor recruitment to early endosomes (Scarpa et al., 2021), indicating that immunocytochemistry might not be sufficiently sensitive to detect weak, residual receptor endocytosis.

Following receptor activation, the fate of internalised GPCRs, will be determined by both sorting signals in the receptor intracellular domain and the stability of the ß-arrestin interaction (Marchese and Trejo, 2013, Zenko and Hislop, 2017, Oakley et al., 1999). According to these results altogether with the observations by Scarpa et al. (2021) and Bradley et al. (2020), internalisation of M1-PD receptors was consistently severely impaired despite ß-arrestin recruitment is still detected around 50% compared to the wild-type receptors, suggesting that recruitment of ß-arrestins is not sufficient for efficient agonist-induced receptor internalisation. A similar observation was reported for a PD mutant of the $ß_2$AR (Krasel et al., 2008). Like for the M3 and M4 mAChR, agonist-induced internalisation of the M1 mAChR is dependent on clathrin and dynamin (Claing et al., 2000, Lee et al., 1998, Vögler et al., 1998, Yeatman et al., 2014). Binding of ß-arrestin to the receptor recruits AP2 and clathrin to the plasma membrane to initiate the formation of clathrin-coated pits (Goodman et al., 1996, Laporte et al., 1999). In addition, receptor interaction with E3 ubiquitin ligase Mdm2 was demonstrated to be important for agonist-induced receptor internalisation as well as for receptor interactions and scaffolding of signalling partners such as MAPK (Shenoy et al., 2006). The drastic impairment in agonist-induced internalisation despite the moderate ß-arrestin binding to the M1-PD might be explained by different conformational changes of ß-arrestin upon binding to the M1-PD compared to a fully phosphorylated receptor. Arrestins were demonstrated to undergo significant structural rearrangement upon binding to phosphorylated receptors (Zhuo et al., 2014, Kim et al., 2012) that might prepare the arrestin for interactions with binding partners such as AP2 or clathrin or ubiquitin ligases. For instance, ß-arrestins bind to clathrin and AP2 *via* their C-tail (Kim and Benovic, 2002) and upon GPCR binding to ß-arrestins, the latter undergo conformational changes causing the release of their C-tail which becomes accessible for interactions with clathrin and AP2 (Zhuo et al., 2014). Lack of receptor phosphorylation likely prevent the required conformational changes for arrestin to interact with its binding partners.

Different ligands can stabilise GPCRs in distinct conformations that preferentially interact with certain signalling partners e.g., G protein subtypes and arrestins resulting in differential signalling outcomes. For instance, distinct ligand-receptor conformations can promote phosphorylation by GRKs or other kinases at differential intracellular clusters, defining the so-called *phosphorylation barcode* (Tobin, 2008, Reiter et al., 2012). Different phosphorylation barcodes ultimately influence the interaction of signalling partners and downstream effectors determining the signalling outcome (Tobin et al., 2008, Butcher et al., 2011, Nobles et al., 2011, Zhou et al., 2017). For example, two different $ß_2$AR ligands, ß-arrestin–biased carvedilol and the unbiased full agonist isoproterenol, were demonstrated to cause distinct receptor phosphorylation patterns resulting in different signalling outcomes in HEK293 cells. Other examples are endogenous ligands CCL19 and CCL21 of the CCR7 chemokine receptor that could promote G protein-dependent signalling, calcium mobilization and ERK activation with equal potency, however only CCL19 promotes robust desensitization (Kohout et al., 2004). While CCL19 lead to robust CCR7 phosphorylation by both GRK3 and GRK6 and ß-arrestin2 recruitment, CCL21 activates GRK6 alone resulting in weaker interaction with ß-arrestin2 (Zidar et al., 2009). Agonist-specific phosphorylation barcodes have been reported for other GPCRs including ORs (Just et al., 2013) and serotonin 5-HT_{2A} receptors (González-Maeso et al., 2007).

Two M1 mAChR ligands, GSK1034702 and pilocarpine, were shown to induce seizures in rodents, and Bradley et al. (2020) tested whether they display signalling bias compared to the natural ligand ACh. Pilocarpine is a well-characterised muscarinic partial agonist that drives robust seizures despite acting as a partial agonist of muscarinic receptors (Hedlund and Bartfai, 1981), and GSK1034702 is a M1 mAChR bitopic ligand that also causes profound seizures in mice (Bradley et al., 2018). When administered *in vivo* to rats at equivalent occupancy levels, pilocarpine stimulated 6-fold increases in phosphoinositide turnover over basal in the cortex, compared to a ~2.5-fold increase stimulated by GSK1034702. This led to the conclusion that M1 agonists showing bias towards G protein-dependent signalling, in this case phosphoinositide responses, may result in adverse central and peripheral effects (Bradley et al., 2020). In this chapter, I aimed to analyse differences in IP1 accumulation response and

agonist-induced internalisation elicited by GSK1034702 and pilocarpine *in vitro* in comparison to the endogenous muscarinic agonist, ACh. In contrast to the findings on phosphoinositide accumulation in the cortex (Bradley et al., 2020), in the CHO FlP-In cell system, pilocarpine induced IP1 accumulation at the M1 mAChR with significantly lower potency and similar efficacy compared to ACh and GSK1034702, whereas GSK1034702 displayed similar IP1 accumulation response to ACh. Additionally, both GSK1034702 and pilocarpine induced significantly less receptor internalisation compared to ACh, and GSK1034702 induced virtually no receptor internalisation. In this study, ligand bias factors calculated for GSK1034702, or pilocarpine were not significantly different from ACh, indicating that they are not biased ligands (Table 3-6). While our observations for GSK1034702 agree with previous studies that showed no bias between G protein coupling and receptor phosphorylation pathways, pilocarpine was demonstrated to induce biased signalling toward G protein pathways (Bradley et al., 2020). The lack of statistical significance in this study could be however due to the high level of variance (S.E.M.) reported for the internalisation assay, and bystander BRET assays for receptor endocytosis in early endosomes as used in Scarpa et al. (2021) could help achieve a more robust comparison. In addition, GSK1034702 is a bitopic ligand and it was found to activate and phosphorylate both M1-WT and M1-DR receptors *in vitro* (Bradley et al., 2018). Therefore, the [^{3}H]-NMS-based internalisation assays might not be appropriate to assess internalisation induced by GSK1034702, since this ligand might not be pharmacologically structured to displace the orthosteric radioligand efficiently.

In conclusion, the data from my *in vitro* studies suggest that while removal of receptor phosphorylation has little impact on G protein-dependent signalling – phosphoinositide accumulation in this case – it significantly impairs agonist-induced receptor internalisation that is traditionally the main mechanism for receptor internalisation. However, as reported in other studies (Bradley et al., 2020, Scarpa et al., 2021), β-arrestin recruitment to the M1-PD variant is decreased by around 50%. GSK1034702 and pilocarpine, two muscarinic agonists that were shown to induce profound seizures in rodents, both induce similar levels of IP1 response *in vitro* but significantly less receptor internalisation compared to the natural agonist ACh. The lack of signalling bias of pilocarpine

calculated in this study however doesn't agree with previous studies (Bradley et al., 2020) but this might be due to the differences in the assays used. Altogether, the findings from this chapter suggest that *differences in physiological responses observed in the M1-PD mice are likely due to lack of phosphorylation/arrestin-dependent pathways and not to lack of G protein signalling desensitisation*. It would be important, however, to test signalling bias in primary cell systems as a valuable intermediate step between *in vitro* systems and *in vivo* studies, for example in primary hippocampal neurons, which are the most physiologically relevant for the M1 mAChR signalling (Levey, 1993). In fact, the stoichiometry of interacting partners e.g., GRKs, G proteins and arrestins, vary between different cell types and tissues, adding a layer of complexity to physiological signalling bias (Kenakin, 1997, Newman-Tancredi et al., 1997, Newman-Tancredi et al., 2000).

Chapter 4 Characterisation of mouse model of terminal neurodegeneration

4.1 Introduction

Worldwide, dementia affects around 55 million people, and AD is the most common form contributing to 60-70% of cases (Alzheimer's Association, 2021, World Health Organization, 2021). These figures are predicted to more than double by 2050 as the population ages, and the World Health Organization has recognised AD as a global health priority (Lane et al., 2018). Since this disease was first identified in 1907 when Alois Alzheimer reported the first case (Alzheimer, 1907), significant progress has been made in our understanding of AD. However, there are still no treatments that can halt or slow disease progression and the first treatment for AD to be approved since 2003 by the FDA was aducanumab in June 2021. Aducanumab, an Aß antibody that will be marketed by Biogen as Aduhelm, was approved using the accelerated approval pathway, which is dedicated to drugs for serious or life-threatening illnesses (Food and Drug Administration, 2021). Despite the initial excitement, many argue that there is not (yet) robust evidence for aducanumab's efficacy on cognition or disease-modifying endpoint (Sevigny et al., 2016, Mullard, 2021), despite its ability to lower Aß plaque pathology.

GPCRs are involved in almost all physiological processes and several GPCR families have been implicated in the pathogenesis of AD (Thathiah and De Strooper, 2011). Unsurprisingly, over recent years, a number of GPCR targets have been evaluated for clinical trials for AD (Hauser et al., 2017). Of these GPCRs, the M1 mAChR has caught intense interest as one of the most promising targets for the treatment of cognitive impairments of neurological diseases such as dementia and schizophrenia (Sarter et al., 2012). Many pharmaceutical companies have put a lot of effort into the development of selective M1 mAChR agonists for the symptomatic treatment of dementias and schizophrenia (Bodick et al., 1997b, Shekhar et al., 2008, Felder, 2019, Bakker et al., 2020). Importantly, more emerging evidence from preclinical animal models of neurodegenerative disease has demonstrated that selective activation of the M1 mAChR can not only reverse memory impairments but also exert disease-modifying effects that are able to significantly slow down disease progression (Scarpa et al., 2020, Bradley et al., 2017, Lebois et al., 2017, Ghoshal et al., 2016). However, translating these promising findings into successful clinical outcomes has so far been proven challenging. This is not only true for muscarinic

receptors, but also for other therapeutic approaches for the treatment of AD (Selkoe, 2011).

A major obstacle to the development of effective and safe therapeutics for AD arises from the challenge in translating the findings from animal model studies into clinical trials. As a consequence, significant effort has been invested into the development of animal models of AD that best recapitulate human disease, not only to investigate pathophysiology, but also to design and validate truly disease-modifying treatments (Selkoe, 2011, LaFerla and Green, 2012, Reardon, 2018).

4.1.1 Animal models of AD

a Natural animal models

Several animal species including polar bears, goats, sheep, cats, dogs and some non-human primates spontaneously develop AD-related pathology (Van Dam and De Deyn, 2011). These animals exhibit age-related deposition of Aß plaques, and some species also display tauopathies (i.e., baboons, rhesus monkey, spectacled bear, bison, guanaco, rabbits, reindeers, and Campbell's guenon (Härtig et al., 2000)). These pathologies also correlate with cognitive decline (Cummings et al., 1996, Voytko and Tinkler, 2004, Gunn-Moore et al., 2006, Rofina et al., 2006). Particularly, non-human primates represent an ideal animal model to investigate higher cognitive functions and neurodegeneration since they show the greatest similarity to humans, compared to other animals. However, even non-human primate models of disease suffer from several limitations, including that even aged animals lack NFT neuropathology, only a small proportion of the population will naturally develop disease, and the development of Aß pathology will develop in decades due to the long lifespans (Oikawa et al., 2010, Heuer et al., 2012). In addition, the use of these species for experimental research is not feasible for reasons including availability, the economic burden associated to their long lifespan, and/or ethical reasons.

A wide range of animal models have been developed to recapitulate the pathophysiology of AD followed by the correlation with cognitive decline, and these include induced/interventional models and transgenic models of disease.

b Induced models

In induced models of AD, pathology is produced by the injection of pharmacological and chemical agents, or by physical lesions. Most animal models within this category have been developed based on the cholinergic hypothesis of AD. For example, the most common pharmacological model is scopolamine-induced amnesia (Ebert and Kirch, 1998, Sunderland et al., 1986). Scopolamine is a muscarinic antagonist and is able to induce memory deficits by compromising information acquisition (Rush, 1988). Scopolamine-induced amnesia in animals has been extensively used to understand the role of the cholinergic system in learning and memory, as well as to evaluate cholinergic compounds for the treatment of cognitive deficits (Malviya et al., 2008, Ahmed and Gilani, 2009). Also mecamylamine, a nicotinic antagonist, can induce cognitive impairments and be used as an alternative model for cholinergic-associated amnesia (Moran, 1993). Other models of cognitive dysfunction can be induced by physical brain lesions, specifically, by lesioning the brain structures or systems that are essential for different processes of learning and memory, including the hippocampal, striatal and cortical regions (Gray and McNaughton, 1983, Glenn et al., 2003, Sloan et al., 2006). Lesion-induced amnesia provides useful insights into the neuronal mechanisms and networks underlying memory dysfunctions.

Another induced model of AD-associated pathology is the intracerebral or intracerebroventricular infusion of pathogenic Aß species in the brain of rodents. This can be achieved by acute administration using a single stereotactic injection (Harkany et al., 1998, Harkany et al., 2000), or repetitively through an implanted cannula in order to mimic the progressive nature of the disease (Yamada et al., 2005). Direct intracerebral infusion of Aß peptides causes cognitive deficits and other AD-like behavioural symptoms, disruption of cholinergic transmission (Yamada et al., 2005, Harkany et al., 1998, Sipos et al., 2007), and neuropathological changes including neuroinflammation and oxidative stress (Weldon et al., 1998).

c Transgenic models

Extraordinary advances in the understanding of the molecular basis of neurodegenerative conditions such as AD have been made using transgenic animal models. Multiple genetic mouse models and one genetic rat model (Cohen et al., 2013) have been generated to express AD-associated human genes to reproduce clinical disease. Transgenic non-mammalian species like zebrafish (*Danio rerio*), nematodes (*Caenorhabditis elegans*) and the fruit fly (*Drosophila melanogaster*) have also been extensively used to explore genetic interactions and molecular pathways in disease as well as for toxicological studies (particularly zebrafish) (Van Dam and De Deyn, 2011). These are particularly useful for their cost-effectiveness, availability, and ease of genetic manipulation. However, they are unable to provide insights into symptomatic or behavioural aspects, and despite genetic homologies, they are hardly comparable to the physiological and neurological complexity of mammalian models.

The first transgenic mouse model of AD came about in 1995 following the identification of mutations within the human APP gene carried by individuals with EOAD. These included the Indian familial AD mutation (V717F) (Murrell et al., 1991) and the Swedish mutations (K670N and M671L) (Haass et al., 1995). The PDAPP model, which carries the Indian mutation, was the first to be developed (Games et al., 1995), and was followed by the Tg2576 (Hsiao et al., 1996) and the APP23 mouse models (Sturchler-Pierrat et al., 1997) that carry the Swedish mutations. These mice display diffuse presence of plaques, neuroinflammation, hippocampal atrophy, synaptic and neurotransmitter dysfunction, as well as AD-like cognitive and behavioural impairments (Sasaguri et al., 2017). The discovery of familial AD mutations in the presenilin (PSEN) gene, which is also involved in APP processing, led to the development of single transgenic mouse models, PSEN1 and PSEN2. These mice do not display plaque pathology and have a few cognitive and behavioural impairments, and similarly to the APP-based model, they lack NFT pathology. However, double transgenic APP/PSEN mice, which display even higher levels of disease-associated Aß species Aß1–42 than single transgenic APP mice, show neuronal loss, neuroinflammation and cognitive and behavioural symptoms changes comparable to clinical AD (Van Dam and De Deyn, 2011).

One of the major drawbacks of APP/PSEN1 mouse models is the lack of NFT, and this was overcome with the generation of tau models, and double transgenic mice expressing mutant tau and APP. However, in these mice, Aß plaques and NFT do not co-localise in AD-relevant brain regions (Götz et al., 2004, Ribé et al., 2005). This prompted the development of triple transgenic mice, whereby two transgenic constructs carrying mutant APP and tau are microinjected into single-cell embryos from homozygous mutant PSEN1 mice, to prevent separating APP and tau expression. These triple transgenic mice, similar to AD, show deposition of Aß plaques prior to NFT pathology with a temporal and spatial profile equivalent to AD, in addition to inflammation, synaptic dysfunction and cognitive decline (Oddo et al., 2003a, Oddo et al., 2003b). Somatic transgenic models have also been developed, whereby AD-associated genes are selectively overexpressed in a cell- or tissue-specific manner by viral vector gene transfer technology (Hong et al., 2006, Lawlor et al., 2007).

4.1.2 Challenges with animal models

The various panel of animal models of disease have greatly contributed to our understanding of the molecular mechanisms underpinning neurodegenerative disease development and progression but have also been important for translational research for drug target discovery and validation as well as preclinical animal studies. Animal models offer the advantages of rapid development of symptoms and pathology, availability of large groups of subjects and accessibility to early stages of disease. However, the perfect animal model for human disease does not exist and different animal models suffer from limitations that researchers will need to consider during experimental design.

For example, even though induced models such as scopolamine-mediated amnesia or lesion models have been important to advance our understanding of the cholinergic or other neuronal systems, they lack AD-associated pathological hallmarks such as Aß plaques and NFT. Amyloid infusion displays localised neuropathology that is quite different from the diffuse distribution of Aß plaques in human AD. In addition, induced models do not develop progressive neurodegenerative disease, nor age-related disease progression.

Transgenic models of AD such as the ones discussed above (Alzforum, 2021) come with drawbacks that are mostly intrinsic to the genetic engineering system. For example, most transgenic mouse lines involve the over-expression of one or more AD-related genes, which might cause non-specific ER stress and other cellular artefacts that are not disease-associated (Saito et al., 2016). Crossbreeding with other mutants could also result in non-relevant disease phenotypes (Saito et al., 2014). In addition, whilst transgenic mouse lines can provide a representation of AD-relevant pathologies, they cannot reproduce the course of the disease in a natural fashion. In accordance, since mouse models do not progress to a severe or terminal stage of disease, they do not develop late stages of disease.

Another consideration is that APP, PSEN, and tau-based transgenic mouse models are representative of familial EOAD, which is the rarest (0.5%) form of AD (Lane et al., 2018). In the most recent years, great effort has been invested into the development of novel transgenic mouse models for AD that are based on genetic risk variants of LOAD such as APO-Ee4 and R47H-mutated Trem2 (Oblak et al., 2020). Examples are the APO-E4 knock-in mouse, alias JAX, that expresses a humanized APO-E4 allele from the endogenous ApoE locus, the Trem*R47H mouse carrying the disease-associated R47H allele of Trem2, and a mouse model expressing both human *APO-E4* and the *Trem2*R47H* mutation. Importantly, these mouse models show age-specific transcriptional changes that are comparable to the changes seen in clinical studies, representing useful models for LOAD (Pandey et al., 2020).

Since no perfect model of human AD exists, researchers need to ask themselves which animal model available is the most relevant to answer their research questions. Our group has employed the mouse prion disease model for translational pharmacology and target validation studies.

4.1.3 Prion disease

Neurodegenerative diseases such as AD, tauopathies, Huntington's disease (HD), PD and prion diseases are part of the same umbrella of diseases called proteinopathies. Proteinopathies are all caused by the formation of toxic protein aggregates in the brain, which ultimately lead to fatal neuronal loss. Each of

these disorders is caused by the misfolding of distinct proteins: APP and tau in AD, huntingtin in HD, α-synuclein in PD and prion protein (PrP) in prion disease. However, proteinopathies share general hallmarks of neurodegeneration, including synaptic and neuronal dysfunction, impaired protein recycling, mitochondrial dysfunction and potentially the unfolded protein response (UPR) response (Halliday and Mallucci, 2015).

Cellular prion protein (PrP_C) is responsible for the development of transmissible spongiform encephalopathies (TSE) such as Kuru and Creutzfeldt-Jakob disease (CJD) in humans, and bovine spongiform encephalopathy (BSE) or "mad cow". These are terminal neurodegenerative diseases characterised by motor and cognitive impairments, neuronal dysfunction and extensive brain damage that can affect a large variety of mammals including humans (Table 4-1) (Aguzzi and Haass, 2003). TSEs were first observed in sheep with scrapie disease, that were showing abnormal behaviour such as involuntary movements, ataxia and excessive scratching (Delez et al., 1957). TSEs are rare disorders in humans and the most common human TSE is CJD, which has a sporadic incidence rate of one new case per million people each year worldwide (Uttley et al., 2020). Another TSE observed in humans is Kuru, first reported in Papua New Guinea among members of Fore tribes. Kuru was once the most common cause of mortality in those communities (Gajdusek and Zigas, 1957), and the disease spread was associated with funerary cannibalism practices (Mead et al., 2003).

The term "prion" was coined by Stanley B. Prusiner who first defined the causing agent of TSE as "a small proteinaceous infection particle that is resistant to inactivation by most procedures that modify nucleic acids" (Prusiner, 1982). The first experimental infection of brain homogenates from scrapie-diseased goats was carried out in 1960 (Chandler, 1961) and led to the more convenient laboratory mouse model of prion disease. The murine prion model not only provided useful insights into prion pathologies, but also led to the development of a new disease model for terminal neurodegeneration.

DISEASE	HOST	AETIOLOGY
Bovine Spongiform Encephalopathy (BSE)	Bovine	Prion infection (*via* feed) (Nathanson et al., 1997)
Scrapie	Sheep and Goat	Scrapie prion infection by maternal and lateral transmission (Delez et al., 1957, Dickinson et al., 1974)
Chronic Wasting Disease (CWD)	Deer and elk	Indirect lateral transmission of CWD prion (Bartelt-Hunt and Bartz, 2013)
Iatrogenic Creutzfeldt-Jakob Disease (CJD)	Human	Infection from contaminated human tissue (e.g., medical procedure) (Duffy et al., 1974)
Sporadic CJD	Human	Spontaneous *PRNP* somatic mutation or a stochastic PrP structural change (Zerr and Parchi, 2018)
Variant CJD	Human	Infection by BSE-contaminated meat (Will et al., 1996, Ritchie et al., 2009)
Familial CJD	Human	Hereditary *PRNP* mutation (Jacob et al., 1950, Goldgaber et al., 1989, Owen et al., 1989)
Gerstmann-Sträussler-Scheinker Disease	Human	Hereditary *PRNP* mutation (Goldgaber et al., 1989, Gerstmann et al., 1935)
Fatal Familial Insomnia	Human	Hereditary *PRNP* mutation (Medori et al., 1992)
Kuru	Human	Transmission by cannibalism (Gajdusek and Zigas, 1957, Glasse, 1967, Mathews et al., 1968)

Table 4-1 Common prion diseases. List of prion diseases that occur in humans, bovines, sheep, goats, deer, and elks. Aetiology and references to key literature are also included.

a Structure of PrP

The normal cellular PrP_C is encoded by the highly conserved single-copy gene *PRNP* on chromosome 20 (Oesch et al., 1985) in humans and in a homologous region in mouse chromosome 2 (Sparkes et al., 1986). PrP_C is highly expressed and has so far been identified in all mammals and birds, as well as Xenopus laevis (Strumbo et al., 2001) and fish (Rivera-Milla et al., 2003).

PrP_C is single component membrane glycoprotein (Stahl et al., 1987) which is ubiquitously expressed at high levels, particularly in neurons (Kistner et al., 1996, Manson et al., 1992) where it mainly localises at synapses in cholesterol-rich microdomains (Vey et al., 1996, Naslavsky et al., 1997). PrP_C is at the cell membrane as an N-glycosylated, glycosylphosphatidylinositol (GPI) -anchored protein of 208-209 amino acids, which is exported to the cell surface following the cleavage of a 22-amino acid signal peptide (Figure 4-1). PrP_C has three glycosylation states (non-, mono-, or di-glycosylated) depending on the variable

glycosyl groups on two asparagine (Asn) residues on the N-terminal end; Asn-181 and Asn-197 in human and Asn-180 and Asn-196 in mice (Haraguchi et al., 1989).

The structure of PrP in its natively folded form was first revealed in 1996 through NMR spectroscopy (Riek et al., 1996), and its high-resolution three-dimensional crystal structure in 2001 (Knaus et al., 2001). However, the structure of the misfolded, disease-associated form of PrP, the scrapie PrP (PrP_{Sc}), remains elusive to date. This is due to unsurmountable challenges for X-ray crystallisation and NMR posed by the unique characteristics of PrP_{Sc} aggregates: 1) they contain PrP_{Sc} molecules with different sizes in dynamic equilibrium in solution and with different levels of glycosylation; 2) they typically have a high molecular weight; 3) they are mainly hydrophobic; 4) during purification, they tend to capture many contaminants due to their sticky nature; and 5) the yield of replication of PrP_{Sc} is too low for biophysical techniques (Diaz-Espinoza and Soto, 2012).

PrP_C has a high α-helix content (45%) and low ß-sheet (3%) (Riek et al., 1996). The C-terminal portion of the peptide feature a globular domain with three α-helices and interspersed with an antiparallel ß-pleated sheet as displayed in Figure 4-1 (Riek et al., 1996, Riek et al., 1997, Zahn et al., 2000). The N-terminal half of PrP is a flexible tail with a random-coil sequence (Shmerling et al., 1998), and containing a stretch of octapeptide repeats (OR), flanked by two positively charged clusters (CC). A single disulphide bond is present between two of the α-helices (Riek et al., 1996, Riek et al., 1997, Zahn et al., 2000). The globular domain of human PrP_C has a high sequence identity to many other mammals (Lysek et al., 2005), and the major structural features are also preserved in non-mammalian species (Calzolai et al., 2005).

In contrast to PrP_C, PrP_{Sc} has a high content of ß-sheets (around 40%) and lower α-helix content (30%) as measured by Fourier-transform infrared (Pan et al., 1993) and circular dichroism spectroscopy (Safar et al., 1993). The ß-sheets were shown to be located in the C-terminal side of the PrP molecule, as indicated by green-gold birefringence after staining with Congo red of amino-terminally truncated PrP_{Sc} (Prusiner et al., 1983).

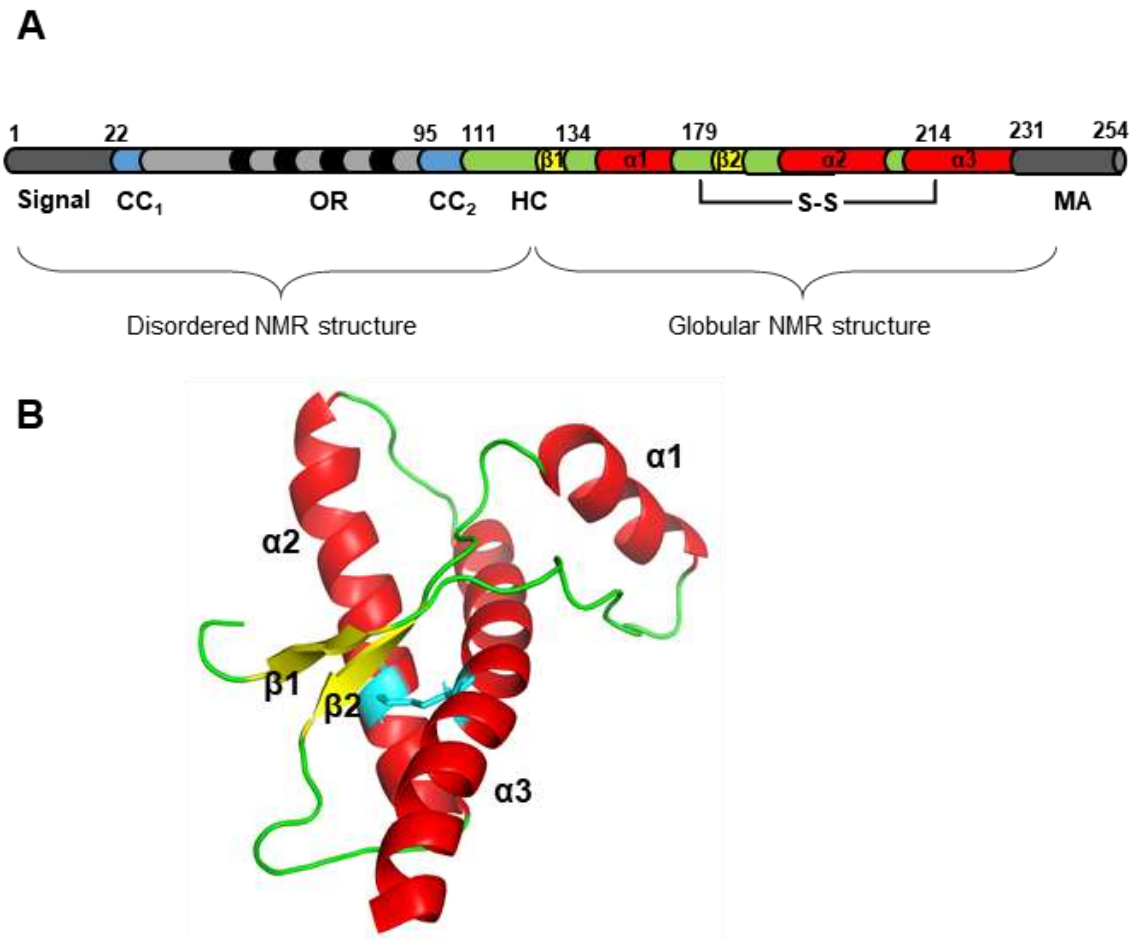

Figure 4-1 Structure of the human cellular prion protein.(A) Outline of the primary structure of PrP_C including posttranslational modifications. A secretory signal peptide residue at the extreme N-terminus. Charged clusters (CC), octapeptide repeat (OR), hydrophobic core (HC), membrane anchor region (MA), disulphide bridge (S-S). The secondary structures of the globular NMR structure are indicated as α1/2/3 and β1/2 for α-helices and β-sheets respectively. The numbers describe the position of the respective amino acids. **(B)** Ribbon diagram of the human PrP (121-230), corresponding to the C-terminal globular NMR structure (PDB code 1qlz). α-helices are displayed in red and the antiparallel two-stranded β-sheet in yellow. The connecting loops are displayed in green and the disulphide bond between cysteine 179 and 214 is shown in cyan. Image was reproduced using the PyMOL Molecular Graphics System, Version 2.0 Schrödinger, LLC.

b Function of PrP

Although PrP knockout mice were described almost three decades ago, the physiological function of PrP_C remains unclear. Two independent mouse lines were generated using homologous recombination in embryonic stem cells to cause the disruption of the PRNP gene; the Prnp0/0 (Zurich I) (Büeler et al., 1992) and Prnp-/- (Edinburgh) (Manson et al., 1994). No remarkable phenotypes were observed in terms of development and behaviour, although subtle abnormalities were revealed in neurophysiological and biochemical functions. For instance, hippocampal slices from PrP null mice were reported to have weakened gamma-aminobutyric acid type A ($GABA_A$) receptor-mediated fast inhibition (Collinge et al., 1994). PrP0/0 also displayed aberrant localisation of

neuronal nitric oxide synthase (nNOS) (Keshet et al., 1999) and neurons showed high susceptibility to oxidative stress in culture compared to wild-type (Brown et al., 1997).

The only significant discovery made on Prnp0/0 mice was that the ablation of PrP_C conferred resistance to prion neurodegeneration (Büeler et al., 1993).

c Mechanisms of prion toxicity

The infectivity of prions relies on the ability of the misfolded PrP_{Sc} to self-propagate by acting as a template for the conversion of natively folded PrP_C, hence initiating a misfolding-amplification cycle. The first seminal work to unravel the mechanism of self-propagation was the demonstration in a cell-free system that radioactive PrP_C incubated with unlabelled PrP_{Sc} led to the generation of radioactive PrP_{Sc} (Caughey et al., 1999). However, it was shown that the *in vitro* generation of PrP_{Sc} was less efficient using purified PrP_C instead of brain homogenate, suggesting that the conversion from PrP_C to its misfolded form might be facilitated by additional cofactors (Deleault et al., 2005). PrP_{Sc} formation *in vitro* was shown to require lipids and RNA for *in vitro* prion replication (Wang et al., 2010).

The severity and lethality of prion diseases are mostly associated with neuronal loss, synaptic damage and extensive spongiosis; however, the mechanism by which PrP_{Sc} can induce the disease is unclear. It has been established that the neurotoxicity is mainly mediated by small oligomers of misfolded PrP_{Sc}. This was first discovered with field-fractionation experiments, by which partially disaggregated PrP_{Sc} was fractioned by size, and each fraction was inoculated into the brain of hamsters. The peak infectivity was achieved by inoculation of 300-600 kDa aggregates, which would contain 14-28 PrP molecules (Silveira et al., 2005).

4.1.4 The mouse model of prion disease

In contrast to other animal models of neurodegenerative diseases such as AD, HD or PD, which are usually engineered to express human mutant proteins to reproduce the human disease phenotype, inoculation of prions in mice induces a true, natural model of murine prion neurodegenerative disease. Hence, studying

this mouse model of prion disease can give real insights into the development and progression of neurodegenerative proteinopathies, such as AD. Furthermore, in contrast to most animal models of neurodegeneration, prion infection of mice induces a progressive, terminal neurodegeneration that allows for survival studies and cost-effective assessment of the disease-modifying potential of novel compounds for the treatment of neurodegenerative disease.

The mouse model of prion disease that is used in our laboratory is based on the tg37 mouse, a transgenic M*lox*P mouse line that expresses PrP^C from M*lox*P transgenes at approximately 3 times wild-type levels (Mallucci et al., 2002). Prion disease is induced by manual intracerebral inoculation of 3-7 weeks old pups with Rocky Mountain Laboratory (RML) scrapie-infected brain homogenate (10% of the body weights) prepared from terminally sick prion diseased mice. The corresponding control mice are similarly inoculated except using normal brain homogenate (prepared from healthy animals). Prion diseased Tg37 mice show neuropathology at 8 weeks post inoculation (w.p.i.), including PrP^{Sc} deposition, reactive astrogliosis and spongiosis (formation of intraneuronal vacuoles in cells that have not yet degenerated), that is followed by symptoms onset at 10 w.p.i. and terminally ill animals normally succumb to scrapie around 12 w.p.i. (Mallucci et al., 2003).

Prion-diseased mice display progressive deficits in species-typical spontaneous behaviours, such as burrowing, nesting and novel object recognition (NOR) prior to the onset of motor impairments. These behavioural deficits strongly correlate with early stages prion pathology and loss of presynaptic terminals in the dorsal hippocampus (Mallucci, 2009). Similarly, loss of synapses, dendrites and spines is believed to be a central process to the development of the earliest symptoms common to several human neurodegenerative diseases, even prior to the deposit of Aß plaques and loss of neuronal cell bodies, which are irreversible and represent end-stage clinical disease. For example, loss of presynaptic terminals in AD is strongly correlated with cognitive impairments, independent from neuronal loss or deposition of amyloid-ß plaques (Näslund et al., 2000). Importantly, behavioural deficits in prion-diseased mice, as well as synaptic dysfunction, were demonstrated to be reversed with depletion of PrP^C, suggesting the potential for recovery of neuronal function (Mallucci et al., 2003, Mallucci et al., 2007). Impairments in burrowing, nesting or NOR behaviours can

be assessed through simple, non-invasive tests. Thus, mouse prion disease model could be useful for preclinical studies to assess modification of early stages of disease, before irreversible pathological changes occur.

4.1.5 Implications of prion disease biology for Alzheimer's disease therapeutics

Whilst prion disease and AD have distinct clinical signatures, incidence, symptom duration and pathophysiology, both neurodegenerations share fundamental pathological features. First, both AD and prion disease display an age requirement as, besides kuru and other rare cases, prion diseases also tend to manifest in middle age and older patients (Parchi et al., 1999). Consequently, prion diseases and AD show common age-related pathological responses such as oxidative stress, protein cross-links and adduct formation. In addition, similarly to AD, most prion disease cases occur sporadically (Castellani et al., 2004).

Emerging evidence has demonstrated that prion disease shares several signatures of disease with AD. Unbiased global proteomic and transcriptomic analysis of murine prion disease performed by our group established that murine prion disease is associated with neuroinflammation, markers of mitochondrial dysfunction and increased oxidative stress. Importantly, these pathology-associated mechanisms are also associated with AD and other forms of human neurodegenerative disease (Abolhassani et al., 2017, Gan et al., 2018, Richards et al., 2018, Wang et al., 2020). Moreover, we revealed that murine prion disease causes the upregulation of markers of AD and in particular proteins that are involved in misfolded protein clearance, further indicating that murine prion disease shares disease-adaptive changes with human neurodegeneration (Dwomoh et al., 2021).

Neuroinflammation, characterised by microgliosis and astrogliosis, is another common hallmark of neurodegenerative diseases (Amor et al., 2014, Ransohoff, 2016). Microglia were found in the brain of AD patients and in animal models of AD surrounding Aß plaques (Salter and Stevens, 2017). Similarly, in prion disease, it has been established that microglia activation occurs in the regions of PrP_{Sc} deposition and in response to PrP_{Sc} accumulation (Bate et al., 2002, Williams et al., 1997, Giese et al., 1998, Van Everbroeck et al., 2004, Kercher et

al., 2007, Sandberg et al., 2014, Vincenti et al., 2015, Gómez-Nicola et al., 2013). It was also shown that human and murine prion diseases share the robust upregulation of inducible, pro-inflammatory pathogenic miRNAs with AD such as miRNA-34a and/or miRNA-146a (Hill and Lukiw, 2016, Zhao et al., 2016, Basak et al., 2016, Boese et al., 2016, Lukiw et al., 2011).

Given that toxic misfolded proteins characteristic of proteinopathies i.e., Aß, tau, and α-synuclein all display prion-like mechanisms of seeding, propagation and transmission to other hosts (Duyckaerts et al., 2019), it is likely that these diseases share common cellular pathogenic mechanisms (Halliday and Mallucci, 2015, Shi et al., 2015, Condello et al., 2020). For instance, aggregates of Aß peptides behave as prions when injected into the brain of a mouse model of AD, with a pattern of deposition that depends on both the aggregates and the host (Meyer-Luehmann et al., 2006, Büeler et al., 1993). Defective protein recycling and/or degradation (Rubinsztein, 2006), mitochondrial dysfunction (Lin and Beal, 2006, Wong et al., 2001) and the UPR (Moreno et al., 2012) have been proposed to be some mechanisms at the basis of many neurodegenerative conditions. Particularly, the UPR reduces protein translation in response to cellular and ER stress and, as the name suggests, can be caused by the presence of unfolded proteins (Ron and Walter, 2007), which is a common feature for proteinopathies. The UPR and/or phosphorylation of the α-subunit of eukaryotic translation initiation factor (elF2α; that inhibits protein translation) were found upregulated in patients with AD, PD and prion disease (Hoozemans et al., 2009, Hoozemans et al., 2005, Unterberger et al., 2006, Moreno et al., 2012). This strongly suggest the UPR plays a central role in proteinopathies, however, how this causes neurodegeneration remains unclear.

In contrast to mouse models of AD in which neuronal loss is rare, the mouse prion disease model display presence of misfolded PrP accompanied by extensive neurodegeneration, allowing access to the mechanisms linking neuronal death and protein misfolding. Therefore, cellular and animal models of prion disease would contribute to our understanding of pathways underpinning prion-like pathologies such as AD. Uncovering the mechanism of prion spreading and toxicity will lead to the discovery of novel therapeutic avenues for neurodegenerative diseases such as AD that could potentially prevent disease progression (Condello et al., 2020).

4.1.6 Aims

The aims of this chapter were to identify AD-relevant markers of disease in the mouse prion disease and map their changes over the course of disease. This will not only be important to validate mouse prion disease as a useful model to assess the disease-modifying effects mediated by the M1 mAChR but will also provide details of prion disease markers that will be useful to efficiently track disease progression.

4.2 Results

4.2.1 Prion disease is characterised by the progressive accumulation of scrapie prion protein.

The misfolded, toxic form of prion, PrP_{Sc}, is partially resistant to digestion by protease (Prusiner, 1982). Previous studies conducted on RML prion infected Tg37 mice have focussed on the presence of PrP_{Sc} in the hippocampus (Mallucci et al., 2002, Mallucci et al., 2003, Bradley et al., 2017). This has been because the hippocampus is the most severely affected brain region, and the primary disease-associated behavioural phenotypes are hippocampal-based (burrowing task and fear-conditioned memory)(Bradley et al., 2017, Mallucci et al., 2002). Here, the presence of PrP_{Sc} was assessed in cortex, hippocampus and striatum and at weekly time-points of disease from 6 to 10 w.p.i. to see whether prion-infected Tg37 mice display misfolded PrP in other regions of the brain, and prior to 8 w.p.i. as it was previously demonstrated (Mallucci et al., 2003). PrP_{Sc} is detected by incubating tissue lysates with proteinase K in order to isolate the protease-resistant form of PrP. Then, PrP_{Sc} is detected *via* western blot using antibodies against PrP, which can recognise both cellular and scrapie forms (Figure 4-2 and Appendix Figure 1). The presence of PrP_{Sc} can be detected in all the tissues analysed – cortex, hippocampus, and striatum – from 6 w.p.i. Dosing studies for novel pharmacological compounds using Tg37 prion-infected mice usually start at 7 w.p.i., thus this data establishes that pathology has already developed at that stage. Whilst most animals display presence of PrP_{Sc} by 10 w.p.i., the amount of scrapie is variable within the same population. This might be reflected by differences in symptom onset as observed in Figure 4-26. Overall, striatum displays a trend of higher PrP_{Sc} compared to cortex and striatum. Since the propagation and accumulation of PrP_{Sc} depends on the levels of normal PrP_{C} (Mallucci et al., 2003), this is likely due to higher expression of PrP_{C} in the striatum, as indicated by the higher level of PrP_{Tot}, expressed as fold over α-tubulin (Figure 4-2B).

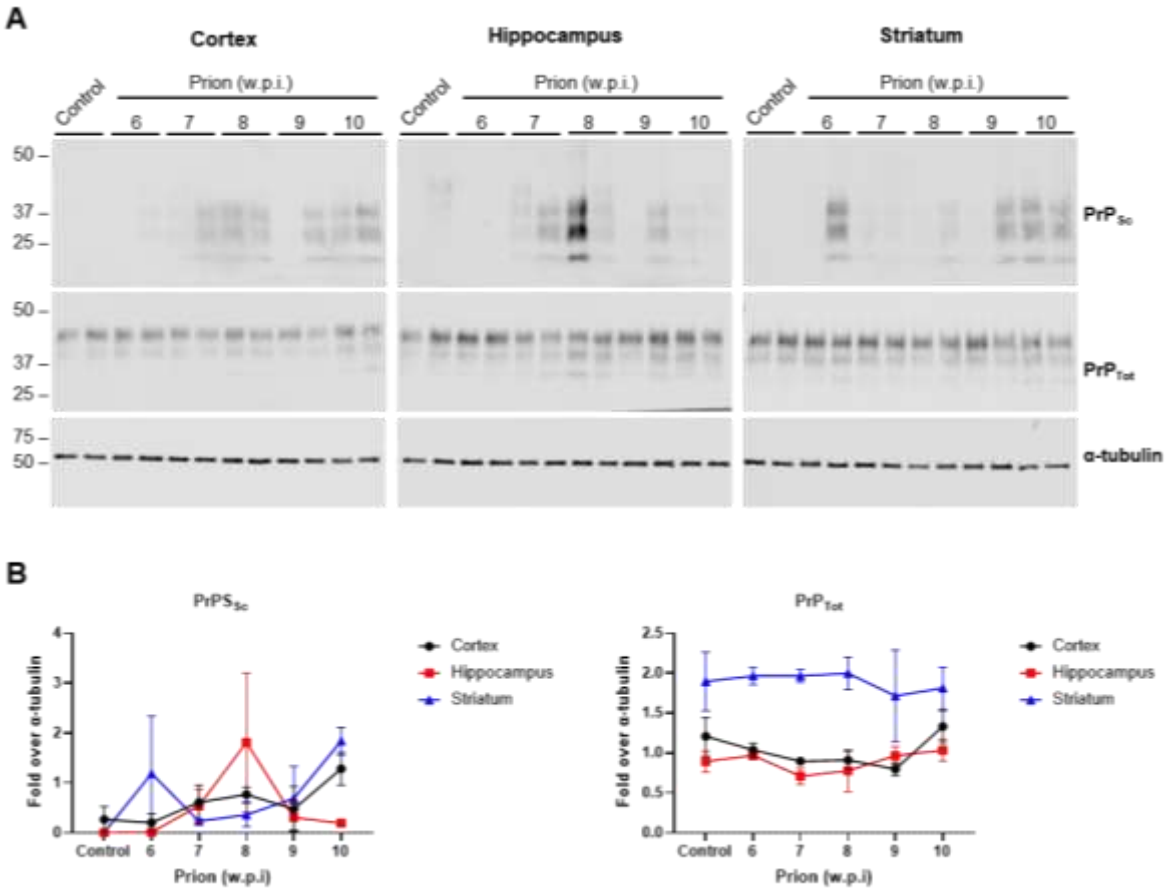

Figure 4-2 Prion-infected mice show the presence of protease-resistant scrapie prion protein (PrP_{Sc}) in cortex, hippocampus, and striatum from 6 w.p.i. Lysates of cortex, hippocampus, and striatum of 6, 7, 8, 9 and 10 w.p.i. control or prion-infected mice were incubated in the presence or absence of proteinase K (10 µg/mL, 37˚C for 10 minutes) prior to western blot to detect non-digested PrP_{Sc} and total prion of protein (PrP_{Tot}), respectively. **(A)** Western blot of two representative samples of cortex, hippocampus, and striatum from control (10 w.p.i.) and prion-infected mice at 6, 7, 8, 9 and 10 w.p.i. from Appendix Figure 1. **(B)** Band analysis of Appendix Figure 1 displaying PrP_{Sc} and PrP_{Tot} expression as a time course. Data shown as means ± S.E.M. of a ratio of α-tubulin expression (N=2).

The presence of PrP_{Sc} deposits was further characterised using histological techniques to have a greater anatomical resolution, at two distinct bregma lateral levels to analyse multiple brain regions (see 2.6.6). By using an antibody against protease-resistant prion protein 27-30 (abcam), that can recognise aggregates made of 27-30 PrP_{Sc} molecules, the precise site of PrP_{Sc} deposition in the mouse model of prion disease could be visualised (Figure 4-3). Then, immunoreactivity was quantified in prion-diseased mice using Imagescope, applying an algorithm that was tuned to recognise aggregates (Figure 4-4). Using this method, PrP_{Sc} deposits were only found in hippocampal regions and the neighbouring white matter tracks, cc and fimbria.

The strongest PrP_{Sc} staining was found in the CA2 region and the adjacent area within the cc at 8 and 10 w.p.i., particularly in the bregma lateral 0.68mm level. The fimbria displayed some dark stained aggregates, but not as prominently as they are observed in the CA2 and cc. The control brains did not display any aggregates characterised by dark staining, suggesting the antibody is sufficiently specific (Figure 4-3).

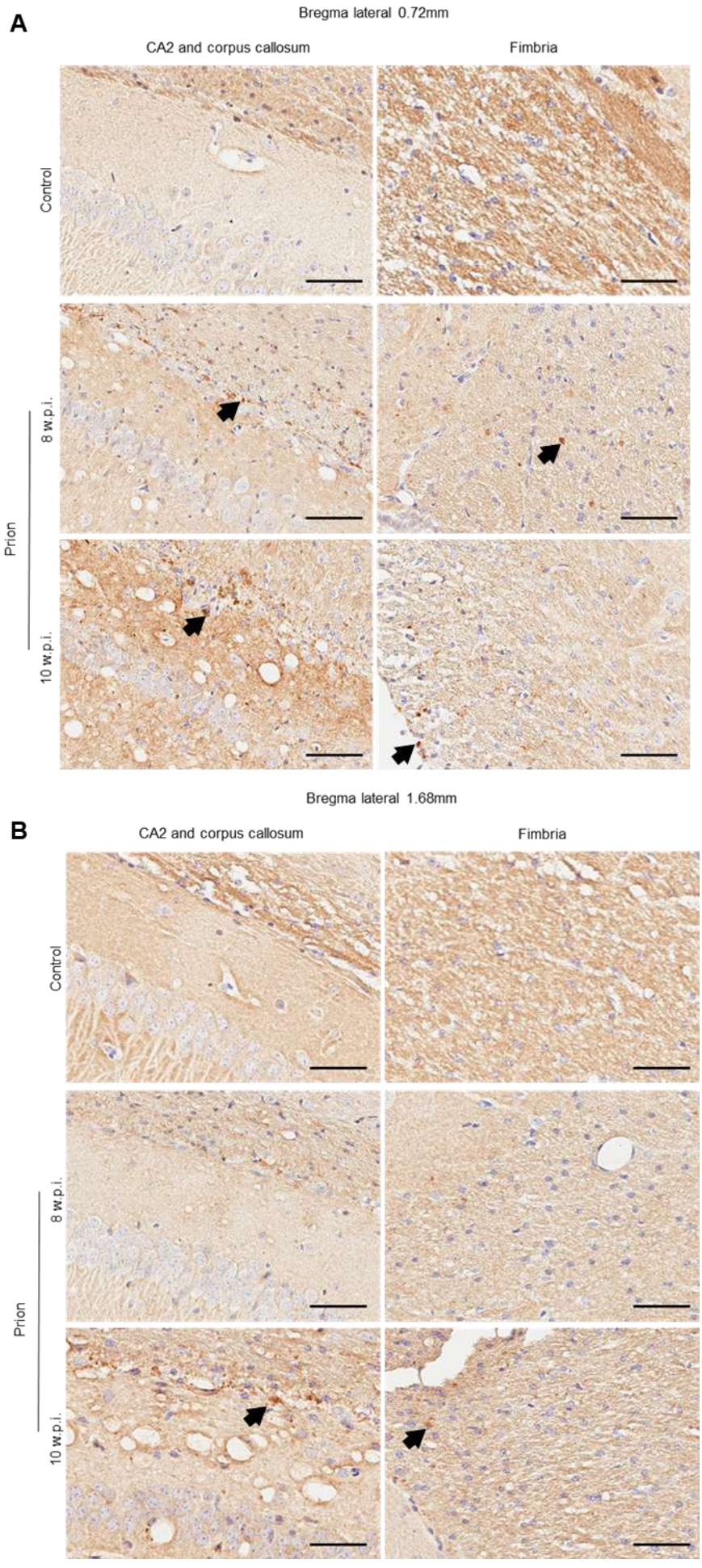
A
Bregma lateral 0.72mm
CA2 and corpus callosum
Fimbria
Control
Prion
8 w.p.i.
10 w.p.i.
B
Bregma lateral 1.68mm
CA2 and corpus callosum
Fimbria
Control
Prion
8 w.p.i.
10 w.p.i.

Figure 4-3 Immunohistochemical staining for visualisation of scrapie prion protein (PrP_{Sc}) in the brain of prion diseased mice. Left hand side hemisphere from 8- and 10- w.p.i. control and prion-infected mice were sectioned and processed for immunohistochemistry (avidin-biotin complex method) using antibodies against prion protease resistant protein 27-30 (abcam), that recognises macromolecules made of 27-30 PrP_{Sc}. Arrows indicate the signal of putative PrP_{Sc} aggregates that was accounted as positive immunoreactivity during the analysis in Figure 4-4 using Imagescope software. Representative images of 3-4 experiments (N=3-4) highlighting the sites of PrP_{Sc} deposition in bregma lateral level 0.72mm (A) and 1.68mm (B). Scale bar is 50µm.

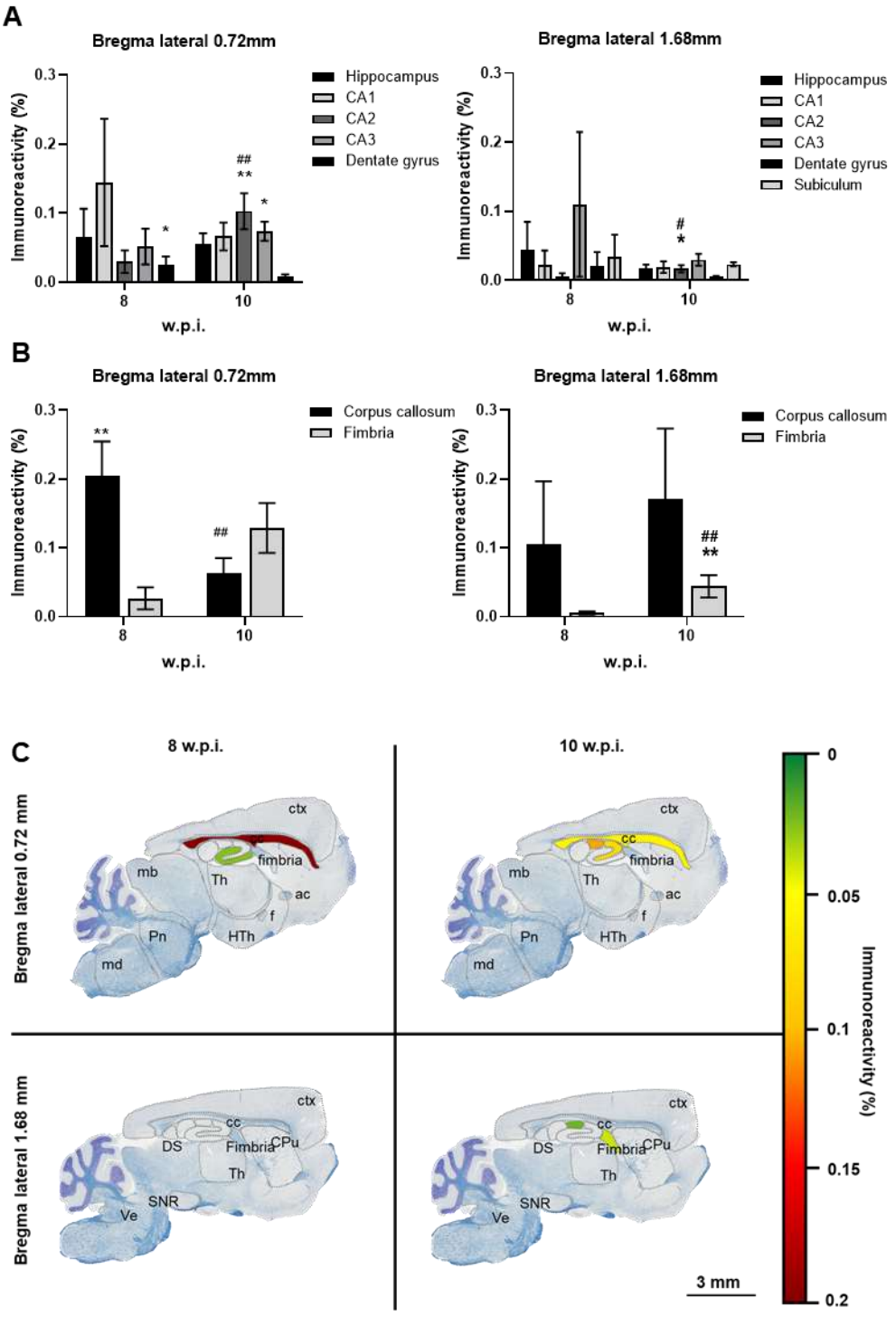

Figure 4-4 . Analysis of PrP_{Sc} in the brain of prion diseased mice. Brains from 8- and 10 w.p.i. control and prion-infected mice were sectioned and processed for immunohistochemistry (avidin-biotin complex method) using antibodies against prion protease resistant protein 27-30 (abcam), that recognises macromolecules made of 27-30 PrP_{Sc}. Dark stained aggregates in hippocampal **(A)** and other regions of interest **(B)** in sagittal sections at bregma lateral 0.72 mm and 1.68 mm were

quantified using Imagescope software (version 12.2.1.5005; Aperio). Data is displayed as mean ± S.E.M. *P<0.05, **P<0.01 for prion vs control; #P<0.05, ##P<0.01 for 10 w.p.i. vs 8 w.p.i.; Two-way ANOVA (Fisher's LSD test) (N=3-4). **(C)** Heatmap of significant changes in PrP_{Sc} aggregates detected across the bregma levels 0.72mm and 1.68mm, and brain regions including anterior commissure (ac), caudate putamen (CPu), cortex (ctx), corpus callosum (cc), dorsal subiculum (DS), fornix (f), hippocampus (hpc), hypothalamus (HTh), midbrain (mb), medulla (md), pons (Pn), substantia nigra (SNR), thalamus (Th), and vestibule (Ve).

4.2.2 Prion-infected mice show no significant neuronal loss at 10 w.p.i.

Neuronal loss was assessed with immunohistochemical staining using antibodies against neuronal nuclear protein (NeuN) (Figure 4-6). At bregma lateral 0.72mm, a decreasing trend in NeuN immunoreactivity is detected from 8 to 10 w.p.i. in hippocampal regions CA2, CA3, and dentate gyrus of prion-infected mice, suggesting neuronal loss might be occurring. However, no significant difference in NeuN was detected in any of the other brain regions analysed, at either of the bregma levels analysed. However, a thinning of the layer of pyramidal cell nuclei was observed in the CA1 and CA2 hippocampal regions of 10 w.p.i. prion-infected mice, as indicated by the arrows in the figure (Figure 4-5).

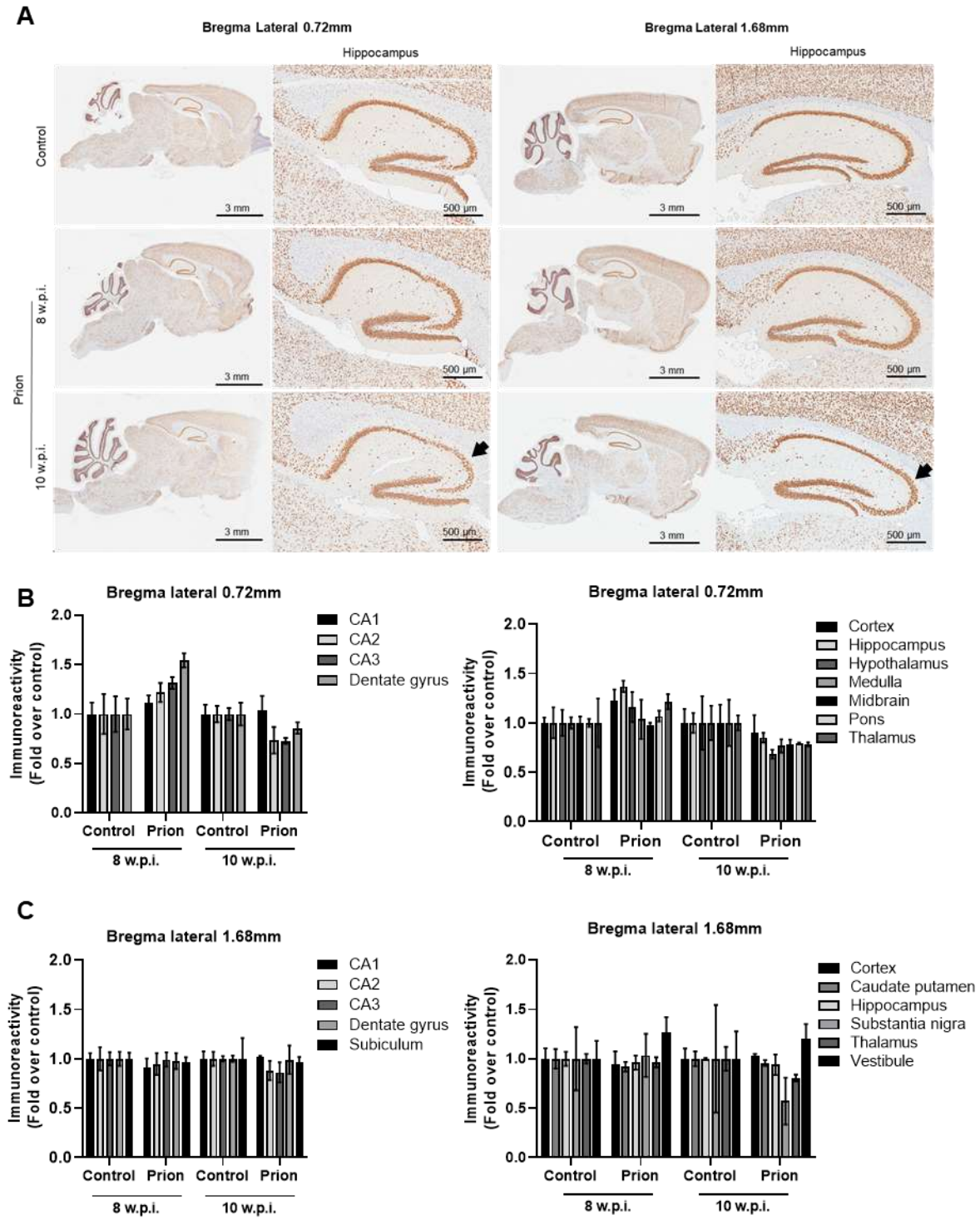

Figure 4-5 NeuN immunohistochemical staining of control or prion infected Tg37. Left hand side hemisphere from 8- and 10 w.p.i. control and prion-infected mice were sectioned and processed for immunohistochemistry (avidin-biotin complex method) using antibodies against the NeuN marker. **(A)** NeuN staining in the hippocampus of control or prion-infected mice, representative of 3-4 mice (N=3-4). Arrows indicate the regions of the layer of pyramidal cell nuclei. (B-C) NeuN staining in hippocampal and other regions of interest in sagittal sections at bregma lateral 0.72 mm **(B)** and 1.68 mm **(C)** were quantified using Imagescope software (version 12.2.1.5005; Aperio). Data is displayed as mean ± S.E.M. Statistical analysis conducted was two-way ANOVA Tukey Multiple comparisons (N=3-4).

Similar to AD, murine prion disease was shown to cause selective neuronal loss of presynaptic, cholinergic neurons (Cunningham et al., 2003, Bradley et al.,

2017). To analyse the presence of cholinergic, presynaptic, or post-synaptic neurons, cortex, hippocampus, and striatum from 10 w.p.i. prion-infected mice were assessed in western blots using antibodies against ChAT, Synapsin I and postsynaptic density protein 95 (PSD95) that are markers of cholinergic neurons, presynaptic and postsynaptic terminals, respectively (Figure 4-6). No significant difference was found between control- and prion-infected mice in the cortex, hippocampus, or striatum for any of the proteins analysed.

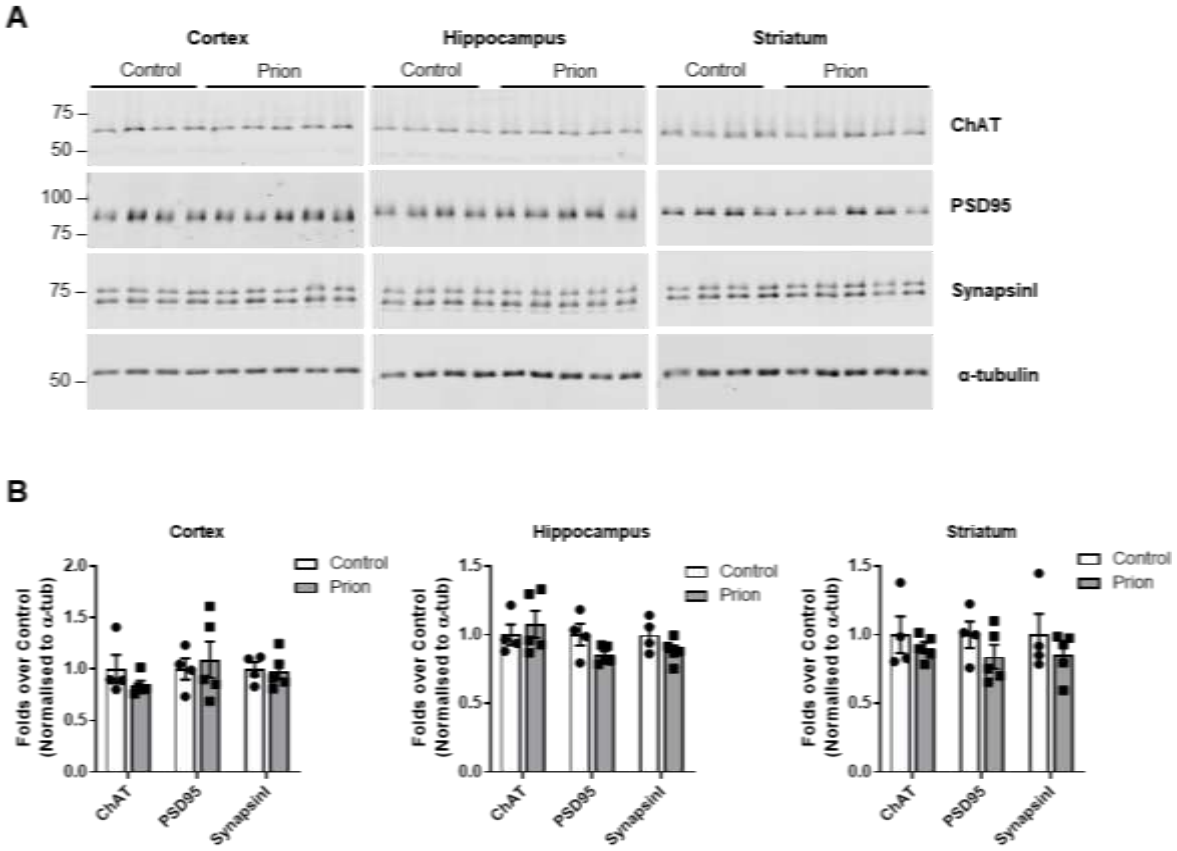

Figure 4-6 Prion-infected Tg37 mice show no changes in neuronal populations at 10 w.p.i. compared to control. (A) Western blot analysis of cortex, hippocampus, and striatum from 10 w.p.i. control or prion-infected using antibodies against ChAT, PSD95 and Synapsin I. **(B)** Band analysis for (A). Expression of ChAT, PSD95 and SynapsinI is shown as means ± S.E.M. of a ratio of α-tubulin expression. Statistical analysis conducted was multiple unpaired T tests of control vs. prion (N=4-5).

One of the early pathological changes that precedes the neuronal loss observed in mouse prion disease is the presence of spongiosis in the hippocampus (Mallucci et al., 2003). Solochrome cyanine staining facilitated the observation of the microanatomy of hippocampal sections and detection of spongiotic vesicles, and an arbitrary 4-point scoring system was designed to estimate spongiosis (Figure 4-7 and Table 4-2). Spongiotic vesicles could be detected in the hippocampus from 8 w.p.i. especially at bregma lateral 0.72mm. Spongiosis

was widespread in the hippocampus at 10 w.p.i. at both bregma levels, with an important presence of spongiotic vesicles particularly in CA1, CA2, CA3 and subiculum and to a lesser extent in the dentate gyrus. This suggests that spongiosis might peak in prion disease around 10 w.p.i. Since spongiosis was shown to precede neuronal loss (Mallucci et al., 2007), presence of extensive spongiosis but lack of neuronal loss in 10 w.p.i. prion-infected mice suggest that at this time-point neuronal death has yet to occur.

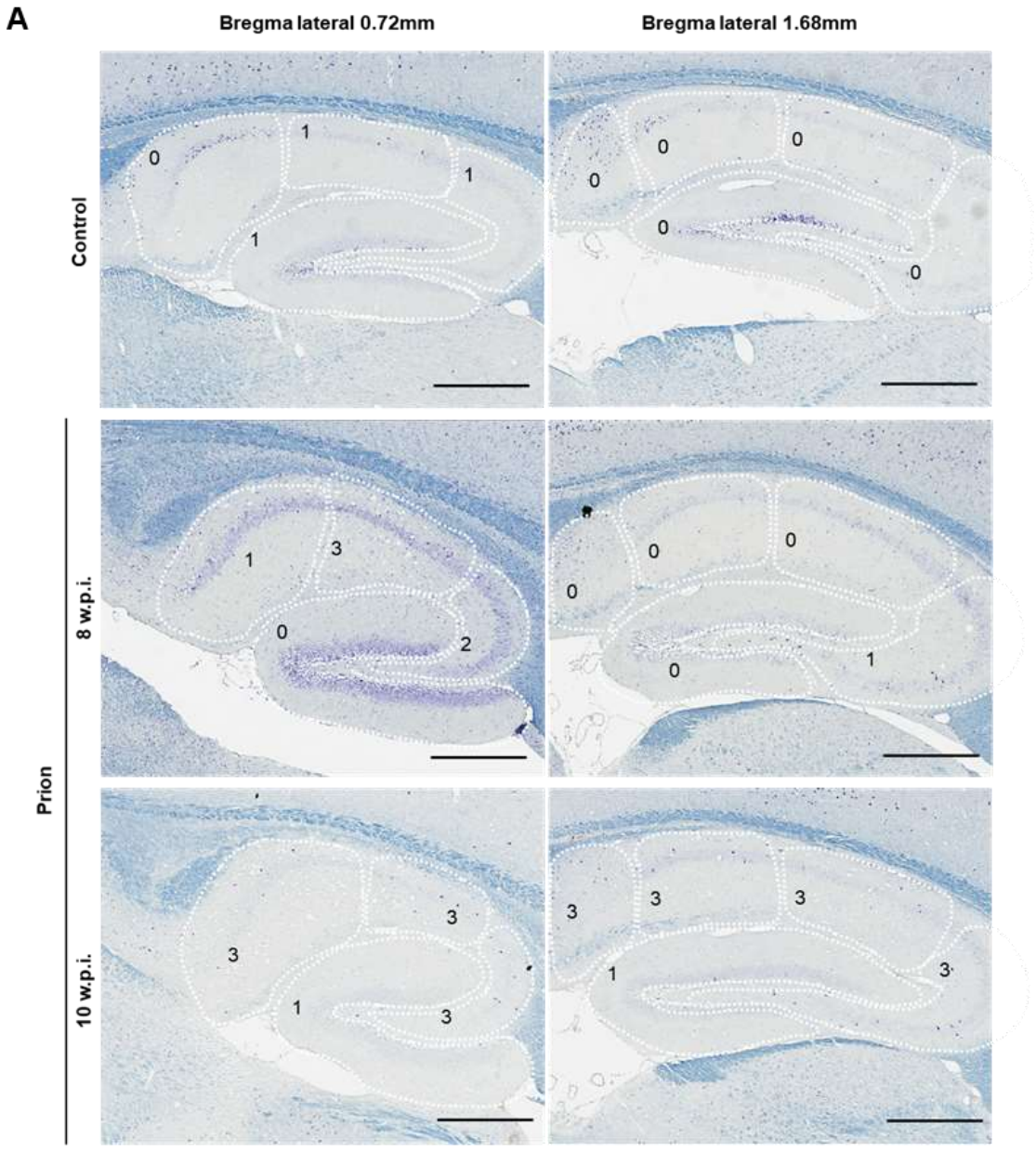

Spongiosis score	
0	No observable vesicles
1	Vesicles are present but <5 in a given 200 µm²
2	Vesicles are present in >5 in a given 200 µm²
3	Vesicles are large and spread across the area

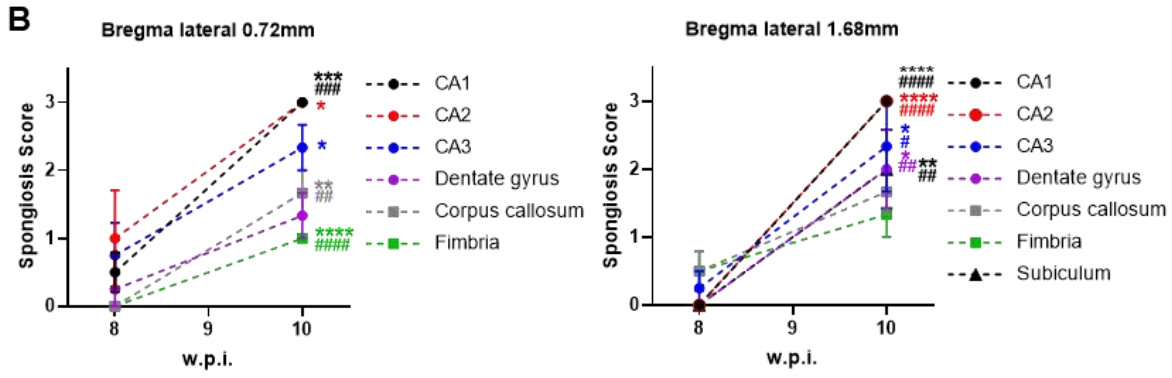

Figure 4-7 Spongiosis in the hippocampal regions of control and prion-infected mice at 8 and 10 w.p.i. (A) Representative images of 3-4 experiments (N=3-4) for solochrome cyanine

staining of sagittal sections at bregma lateral 0.72 mm and 1.68mm, with a map of the hippocampal regions and the scoring criteria (4-point scoring system). Scale bar is 500µm. **(B)** Time-course plot of spongiosis scores for hippocampal regions (CA1, CA2, CA3 and Dentate gyrus), Subiculum and white matter tracks Corpus callosum and Fimbria in bregma lateral 0.72mm and 1.68mm sections from 8 and 10 w.p.i. Data is plotted as mean ± S.E.M., and was analysed using two-way ANOVA Tukey's multiple comparisons where ****P<0.0001, ***P<0.001, **P<0.01, *P<0.05 for prion vs. control, and $^{\#\#\#\#}$P<0.0001, $^{\#\#\#}$P<0.001 $^{\#\#}$P<0.01 for 8 vs. 10 w.p.i. (N=3-4).

	Bregma Lateral 0.72mm				Bregma Lateral 1.68mm			
	8 w.p.i.		10 w.p.i.		8 w.p.i.		10 w.p.i.	
	Control	Prion	Control	Prion	Control	Prion	Control	Prion
CA1	0	0.5 ± 0.3	0.3 ± 0.3	3 ± 0	0	0	0	3 ± 0
CA2	0	1 ± 0.7	0.3 ± 0.3	3 ± 0	0.3 ± 0.3	0	0	3 ± 0
CA3	0	0.7 ± 0.5	0.3 ± 0.3	2.3 ± 0.3	0.3 ± 0.3	0.2 ± 0.2	0.3 ± 0.3	2.3 ± 0.7
Dentate gyrus	0	0.2 ± 0.2	0.3 ± 0.3	1.3 ± 0.3	0.3 ± 0.3	0	0.3 ± 0.3	2 ± 0.6
Corpus callosum	0	0	0.3 ± 0.3	1.7 ± 0.3	0.7 ± 0.3	0.5 ± 0.3	0.3 ± 0.5	1.7 ± 0.3
Fimbria	0	0	0	1 ± 0	0	0.5 ± 0.3	0.3 ± 0.4	1.3 ± 0.3
Subiculum	N/A	N/A	N/A	N/A	0	0	0	2 ± 0.6

Table 4-2 Spongiosis scores of the hippocampus of control and prion-infected mice at 8 and 10 w.p.i. Spongiosis was scored as shown in Figure 4-7A for hippocampal regions (CA1, CA2, CA3 and Dentate gyrus), subiculum, corpus callosum and fimbria in Bregma lateral 0.72mm and 1.68mm sections. Data was plotted as mean ± S.E.M. (N=3-4).

4.2.3 Murine prion disease shows an increase in key hallmarks of human neurodegeneration

Recently, our group have mapped the pathological changes in the hippocampus of prion diseased mice by conducting unbiased global transcriptomic and proteomic analyses. We have found several protein markers previously associated with human AD that are significantly upregulated in prion disease, which included APO-E, clusterin and the protease inhibitor serpinA3N (Dwomoh et al., 2021). Here, I assessed the expression level of APO-E, clusterin and serpinA3N in the cortex, hippocampus, and striatum over the course of disease (Figure 4-8 and Appendix Figure 2).

In murine prion disease, expression levels of APO-E, clusterin and serpinA3N show an increasing trend from 8 w.p.i., and they are found to be significantly upregulated at 9 w.p.i. in the cortex and striatum of prion-diseased mice compared to respective controls. Specifically, APO-E displayed a 2.2- and a 3.9-fold increase in the cortex (P<0.01) and striatum (P<0.0001) respectively; clusterin was found to be upregulated (P<0.01) in the cortex by 1.8-fold and in the striatum by 2.1-fold. Interestingly, serpinA3N showed the most consistent upregulation with prion disease in all the three tissues compared to the other disease markers, with a significant increase in 9 w.p.i. prion-infected mice by 2-

2.6-fold compared to the respective controls. At 10 w.p.i., there is an increasing trend in APO-E, clusterin and serpinA3N but only sepinA3N is significantly upregulated in the cortex and striatum compared to control mice. This data suggests *that serpinA3N might be the first disease marker to be upregulated in mouse prion disease compared to APO-E and clusterin.*

Another protein that was found to be upregulated with prion disease was galectin-1 (Dwomoh et al., 2021). Galectins modulate the activation of astrocytes and microglia, playing both pro- and anti-inflammatory role in neurodegenerative conditions (Dhirapong et al., 2009). In western blots, galectin-1 shows an increasing trend with prion disease from 8 to 9 w.p.i. however, no significant differences were detected in prion-infected mice compared to controls (Figure 4-9).

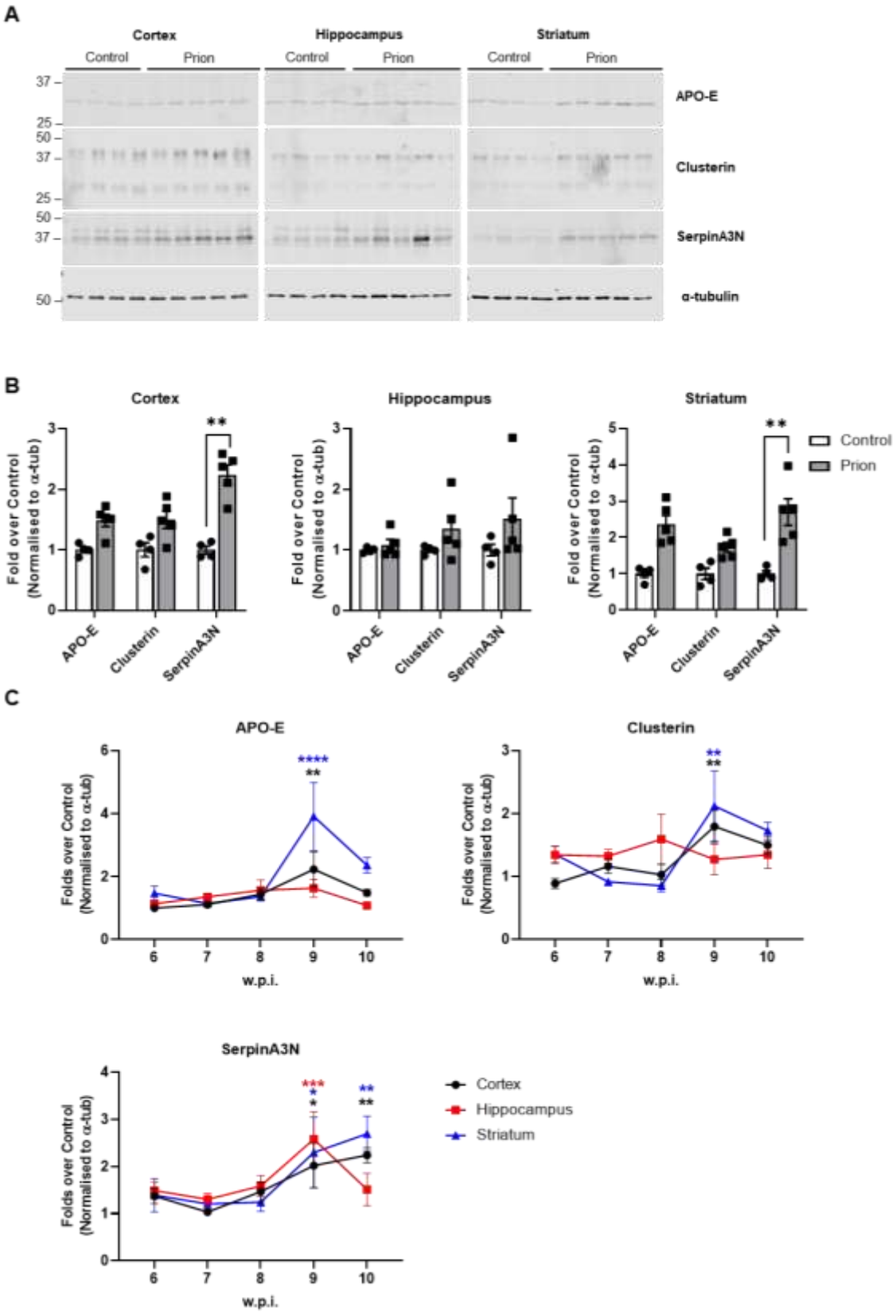

Figure 4-8 APO-E, SerpinA3N and clusterin expression levels are increased in prion-infected mice. APO-E, clusterin and serpinA3N were detected *via* western blot in the cortex, hippocampus, and striatum of control and prion-infected mice. Blots of samples from 10 w.p.i. mice are displayed in **(A)** and band analysis of 10 w.p.i. mice is shown in **(B)** as means ± S.E.M. of a ratio of α-tubulin expression relative to control-infected mice (N=4-5). **(C)** Time-course plots of band analysis of APO-E, clusterin and serpinA3N in control and prion-mice at 6, 7, 8, 9 and 10 w.p.i. (N=4-8) from Appendix Figure 2. Data were analysed using two-way ANOVA with Sidak's multiple comparisons test for prion vs. control, where ****P<0.0001, ***P<0.001, **P<0.01, *P<0.05.

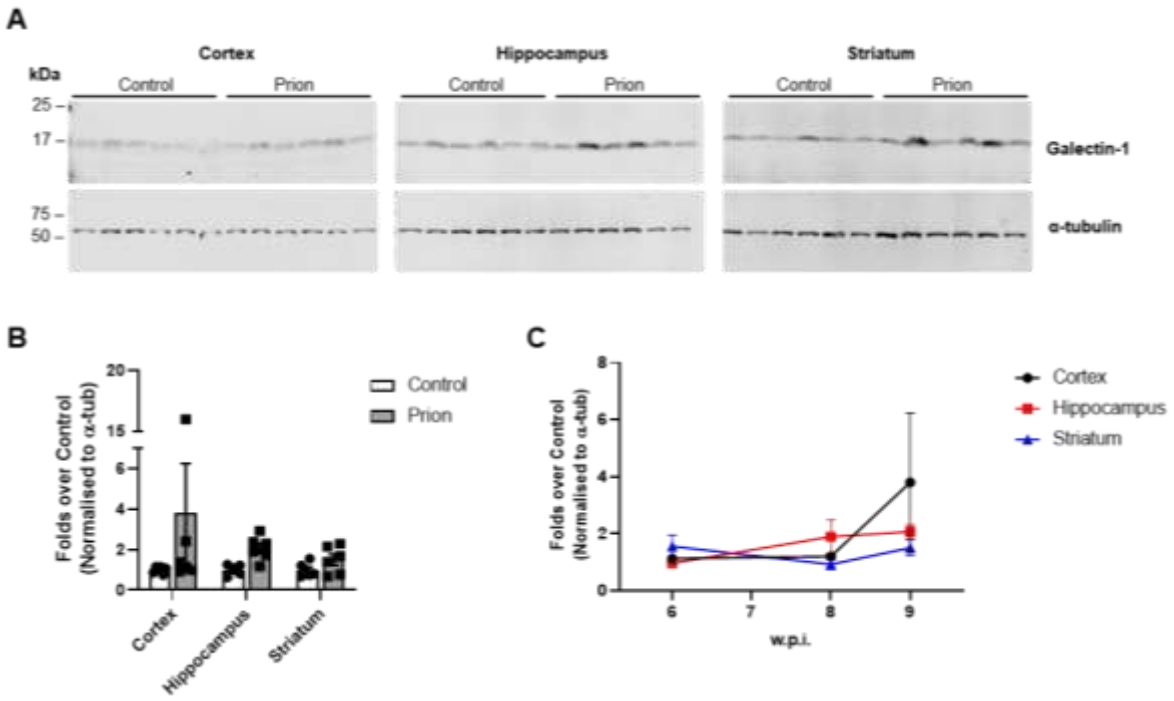

Figure 4-9 Galectin-1 expression levels in prion disease. Levels of galectin-1 protein was detected using western blot in the cortex, hippocampus, and striatum of control and prion-infected mice. Blots of samples from 9 w.p.i. mice are displayed in **(A)** and band analysis of 9 w.p.i. mice is shown in **(B)** as means ± S.E.M. of a ratio of α-tubulin expression relative to control-infected mice (N=6). **(C)** Time-course plots of band analysis of galectin-1 in prion-mice at 6, 8 and 9 w.p.i. (N=6-7) from Appendix Figure 3. Data were analysed using two-way ANOVA with Sidak's multiple comparisons test for prion vs. control, where ****P<0.0001, ***P<0.001, **P<0.01, *P<0.05.

4.2.4 Prion disease causes widespread astrogliosis

Astrogliosis is a hallmark of many conditions of the CNS including most chronic neurodegenerative disorders such as AD and PD (Sofroniew and Vinters, 2010, Liddelow and Barres, 2017). Here, astrogliosis was therefore assessed in mouse prion disease by gene expression analysis (RT-qPCR) or western blot to detect astrocyte-specific intermediate filaments such as glial fibrillary acidic protein (GFAP) and vimentin (Middeldorp and Hol, 2011, Danielsson et al., 2018) (Figure 4-10).

GFAP transcript levels are significantly upregulated in the cortex (P<0.01) and striatum (P<0.001) of prion-infected mice at 10 w.p.i. (Figure 4-10A). Interestingly, GFAP levels in the striatum of prion-infected mice are significantly higher (P<0.01) than in the hippocampus of prion infected mice. Protein levels of GFAP show an increasing trend with prion disease, reaching a significant upregulation by 2.2 to 2.6-fold compared to controls in the cortex at 9 w.p.i. (P<0.01) and in the striatum at 10 w.p.i. (P<0.0001) (Figure 4-10B). Levels of vimentin show an increasing trend from 8 w.p.i., however no significant

difference was detected between prion-infected and control mice. Both GFAP and vimentin are found to be upregulated in prion disease compared to control by 10 w.p.i. However, there is high variability in the expression level of these proteins amongst prion-diseased mice, especially in the hippocampus of prion-infected mice (Appendix Figure 4).

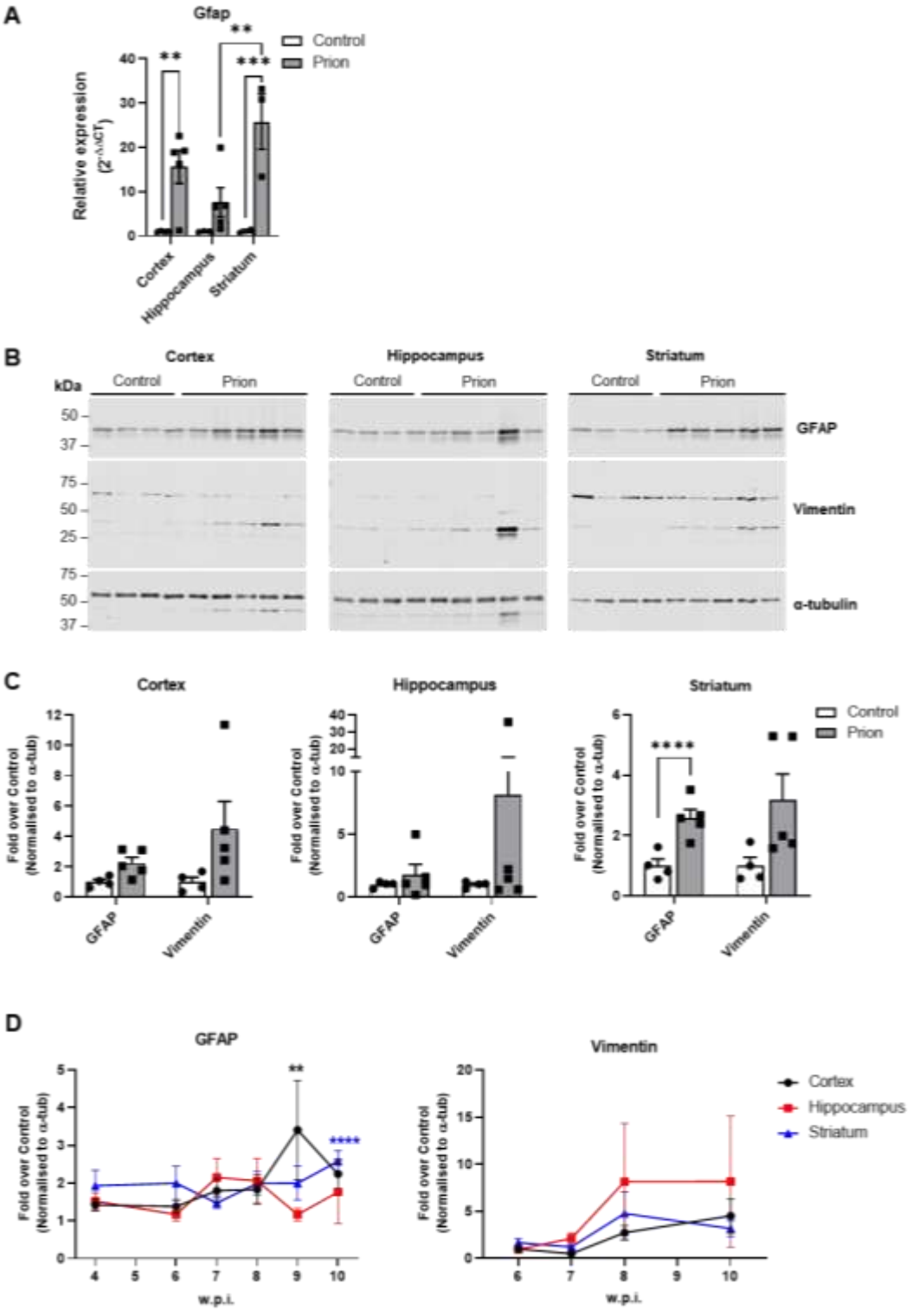

Figure 4-10 Astrogliosis is evident in prion infected mice from 8 w.p.i. (A) Quantitative RT-qPCR showing the expression of GFAP in the cortex, hippocampus or striatum of control or prion-

diseased mice at 10 w.p.i. Data are expressed as a ratio of α-tubulin RNA. Statistical analysis performed is Two-way ANOVA Tukey's multiple comparisons, where **P<0.01, ***P<0.001 (N=5 or 2-4 for striatum). **(B-D)** Astrogliosis was also assessed in the cortex, hippocampus and striatum of control or prion-infected mice by western blot using antibodies against astrocytic markers GFAP and vimentin. **(B)** Blots of lysates from cortex, hippocampus and striatum of control and prion mice at 10 w.p.i. Band analysis for (B) are shown in **(C)** as means ± S.E.M. of a ratio of α-tubulin expression relative to control-infected mice (N=4-5). **(D)** Time-course plots of band analysis of GFAP and vimentin in prion-diseased mice from 4 or 6 to 10 w.p.i. (N=4-8) from Appendix Figure 4. Data were analysed using two-way ANOVA with Sidak's multiple comparisons test for prion vs. control, where **P<0.01 and ****P<0.0001.

In addition, the distribution of astrocytes was assessed using immunohistochemical staining using antibodies specific for GFAP and vimentin on brain sections of 8- and 10 w.p.i. prion-infected or control mice (Figure 4-11 and Figure 4-12). Distinct bregma levels (bregma lateral 0.72mm (Figure 4-11A and Figure 4-12A) and 1.68mm (Figure 4-11B and Figure 4-12B) were picked, as described in 2.6.6, to allow greater regional coverage and determine differences in astrogliosis spreading. The expression of the said astrocytic markers was also quantified using Aperio software (Figure 4-13).

GFAP was found to be overall upregulated with prion disease compared to the control samples only at 10 w.p.i. In most regions – hpc, HTh, mb, Th, CPu, SNR – GFAP was increased by 4 to 5-fold compared to the control across the levels examined, suggesting a widespread upregulation of astrocytes. Medulla, Pons, and Vestibule showed a smaller upregulation by 3.2- to 3.6-fold, indicating that astrocyte reactivity might be smaller in those regions, or delayed. The cortex showed the highest level of GFAP upregulation, with 8.2- and 16.4-fold increases respectively in the bregma lateral 0.72mm and 1.68mm. The hpc displayed an overall 4.7-5.7-fold upregulation of GFAP across the levels, with the highest increase in the CA1 hippocampal region. While most hippocampal regions show a higher increase in the more lateral area, GFAP in the dentate gyrus shows the opposite behaviour. The subiculum displayed a GFAP upregulation by 6.1-fold at 10 w.p.i. compared to the control. White matter tracks such as ac and f showed a 4.4- and 3.5-fold GFAP upregulation compared to control at 10 w.p.i. Surprisingly, though most PrP_{Sc} deposition was found in the fimbria and cc, these white matter tracks only displayed a moderate upregulation in GFAP (between 1.3 and 1.7-fold across the levels).

Like GFAP, vimentin showed a significant increase in prion-diseased mice at 10 w.p.i. Moderate vimentin upregulation (2 to 3-fold over the control) was

detected across the levels in the HTh, md, Th and Ve, and no changes were detected in Mb and pn. Vimentin was found upregulated in the cortex by a 6.1- and 16.5-fold increase in bregma lateral 0.72mm and 1.68mm respectively, showing a similar trend to GFAP expression. CPu and SNR displayed an important upregulation of vimentin by 7.7 and 8.8-fold over the control, respectively. In contrast to GFAP that showed a general widespread upregulation, vimentin shows higher regional specificity, being especially upregulated in hippocampal regions and cortex. The hpc had a remarkable vimentin upregulation, by 22-fold and 56.3-fold relative to controls respectively at the bregma lateral 0.72mm and 1.68mm. The highest increase in vimentin was observed in the CA2 and DG. Like GFAP, vimentin in the DG shows the opposite trend compared to the other hippocampal regions whereby there is a 150-fold upregulation in the bregma lateral 0.72mm and 34-fold increase in the more lateral areas. This might be indicative of a pattern of spreading of astroglia activation. The ac and particularly the f show an important increase in vimentin, by 23.6 and 254-fold respectively – this is a much larger change than the one observed for GFAP in the same region, and the difference can be explained by the higher basal expression of GFAP in control animals. In contrast to GFAP, vimentin shows a significant increase at 10 w.p.i. in white matter tracks such cc and fimbria (3.5-4.4-fold over control), which is even across the levels examined.

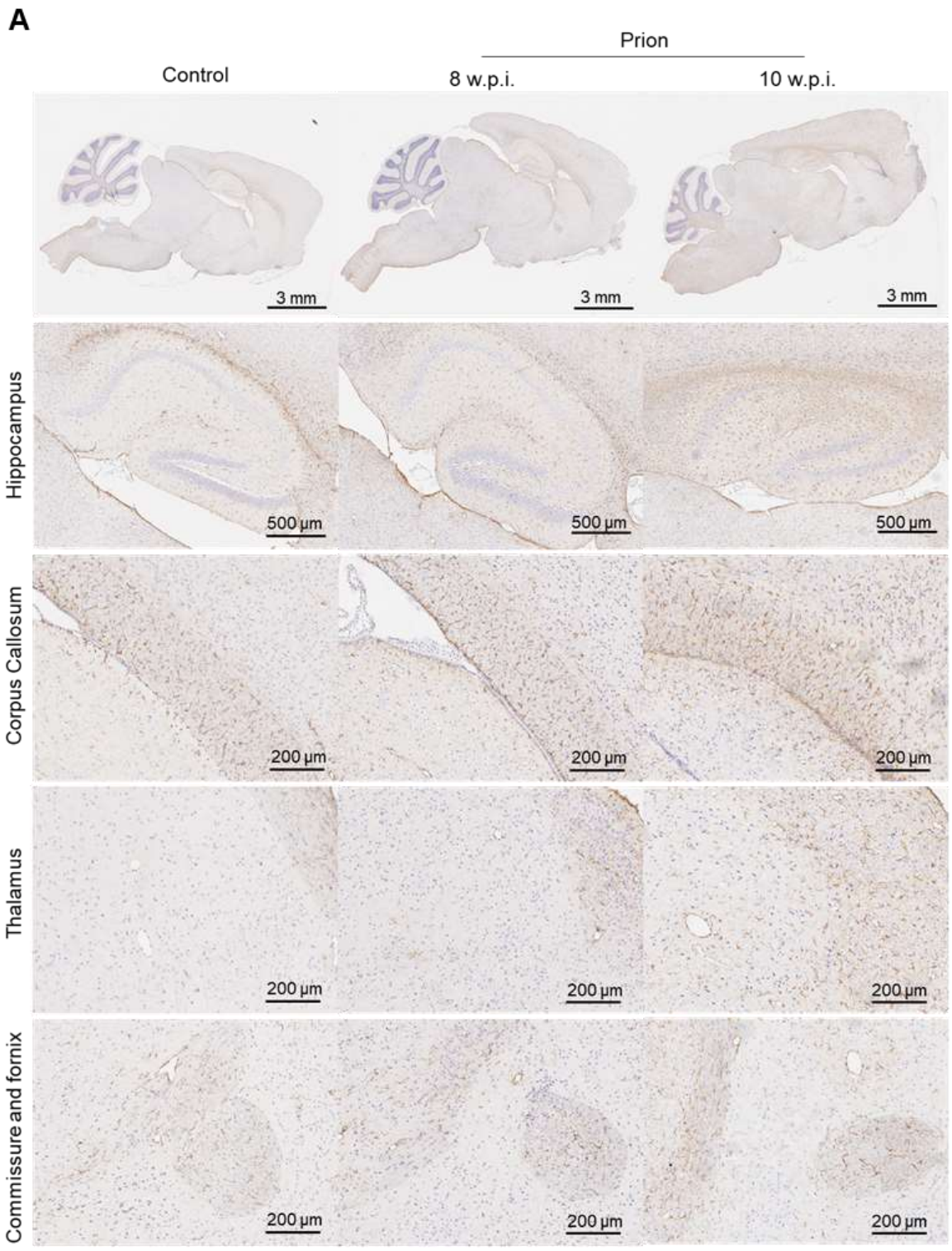
A
Prion
Control
8 w.p.i.
10 w.p.i.
3 mm
3 mm
3 mm
Hippocampus
500 µm
500 µm
500 µm
Corpus Callosum
200 µm
200 µm
200 µm
Thalamus
200 µm
200 µm
200 µm
Commissure and fornix
200 µm
200 µm
200 µm

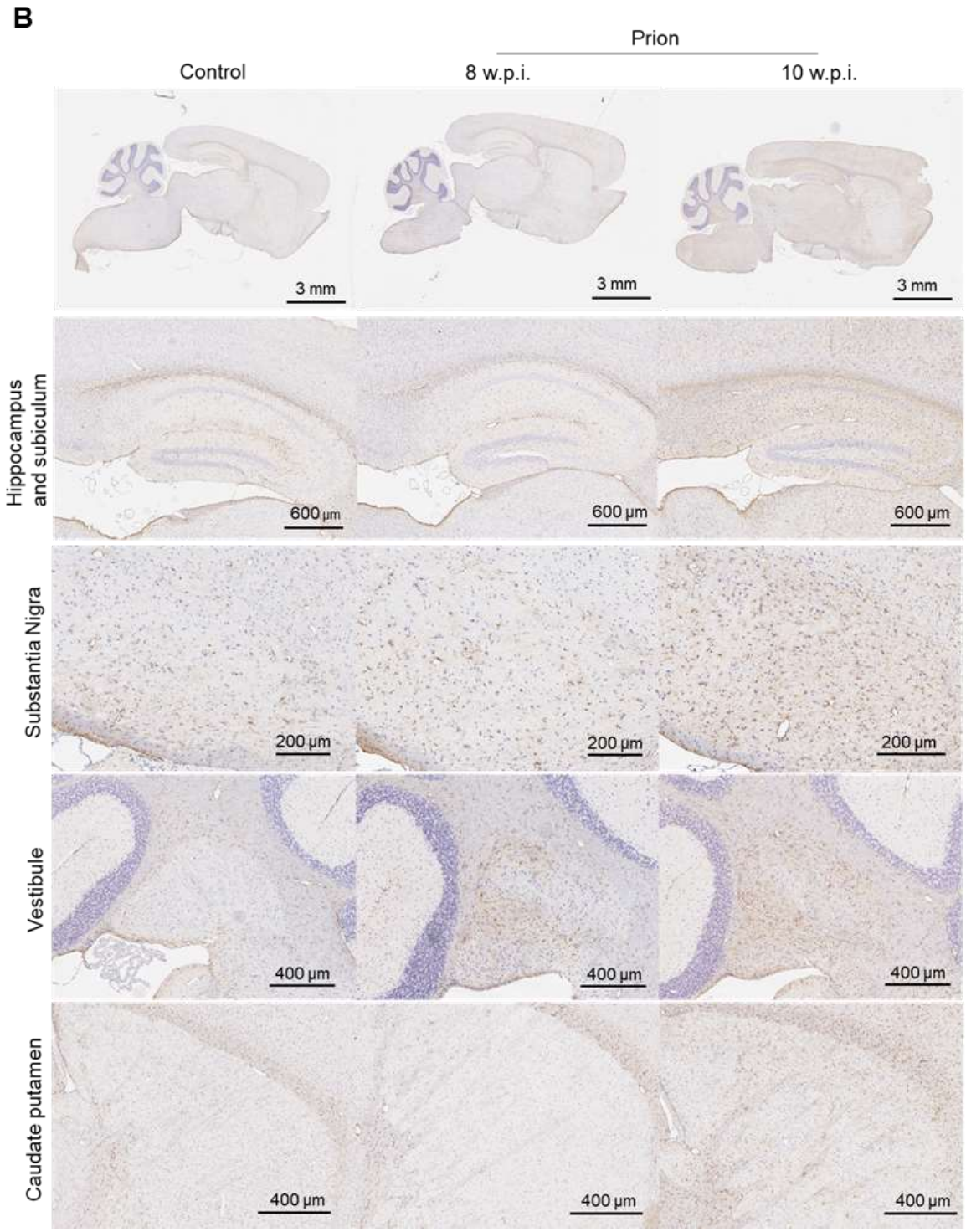

Figure 4-11 Immunohistochemical staining for astrocytic marker GFAP in mouse prion disease. Left hand side hemisphere from 8- and 10 w.p.i. control and prion-infected mice were sectioned and processed for immunohistochemistry (avidin-biotin complex method) using antibodies against GFAP. Representative images of 3-4 experiments (N=3-4) for the staining of GFAP in bregma lateral level 0.72mm **(A)** and 1.68mm **(B)** in control (10 w.p.i.) and prion-infected mice at 8- and 10 w.p.i.

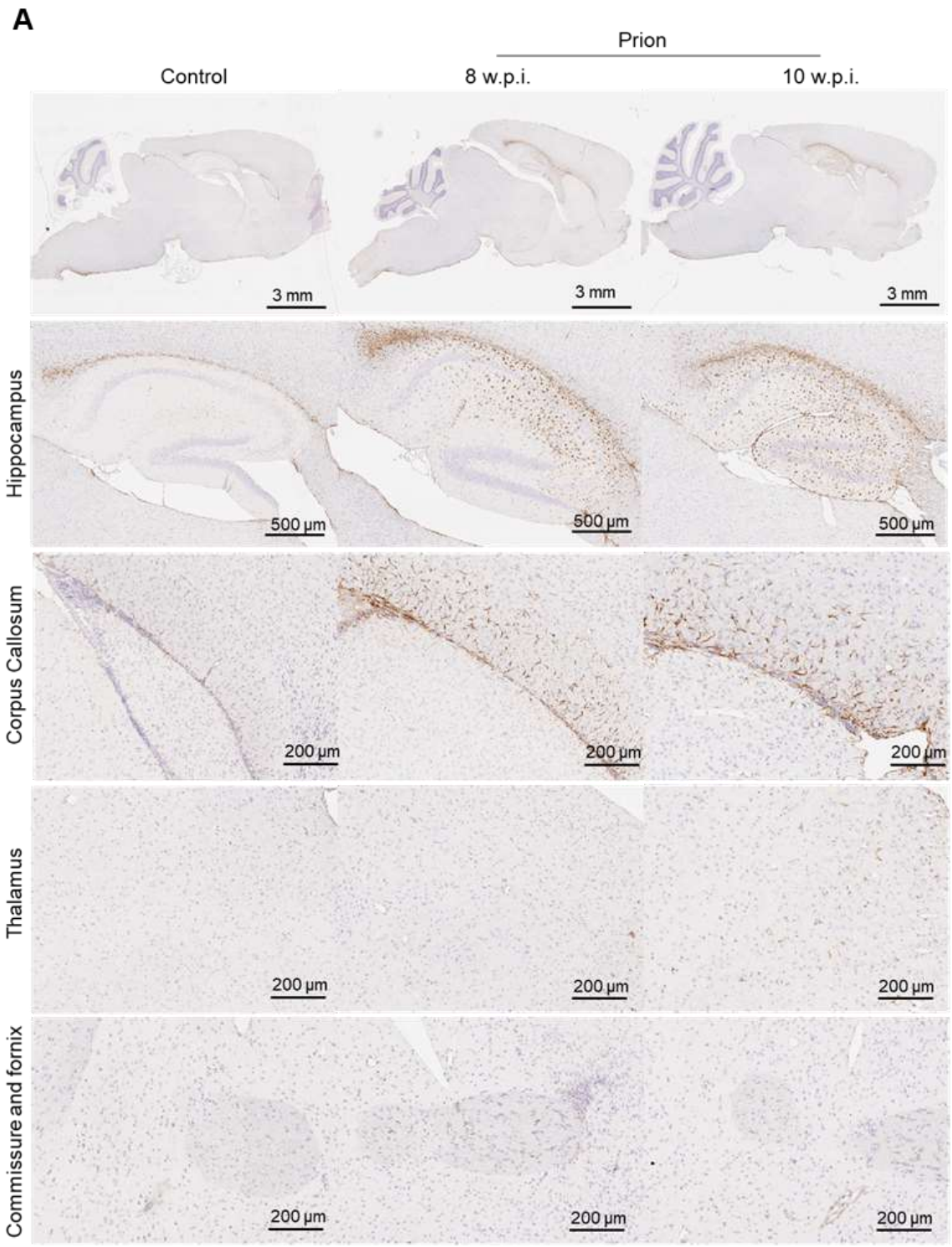
A
Prion
Control
8 w.p.i.
10 w.p.i.
3 mm
3 mm
3 mm
Hippocampus
500 µm
500 µm
500 µm
Corpus Callosum
200 µm
200 µm
200 µm
Thalamus
200 µm
200 µm
200 µm
Commissure and fornix
200 µm
200 µm
200 µm

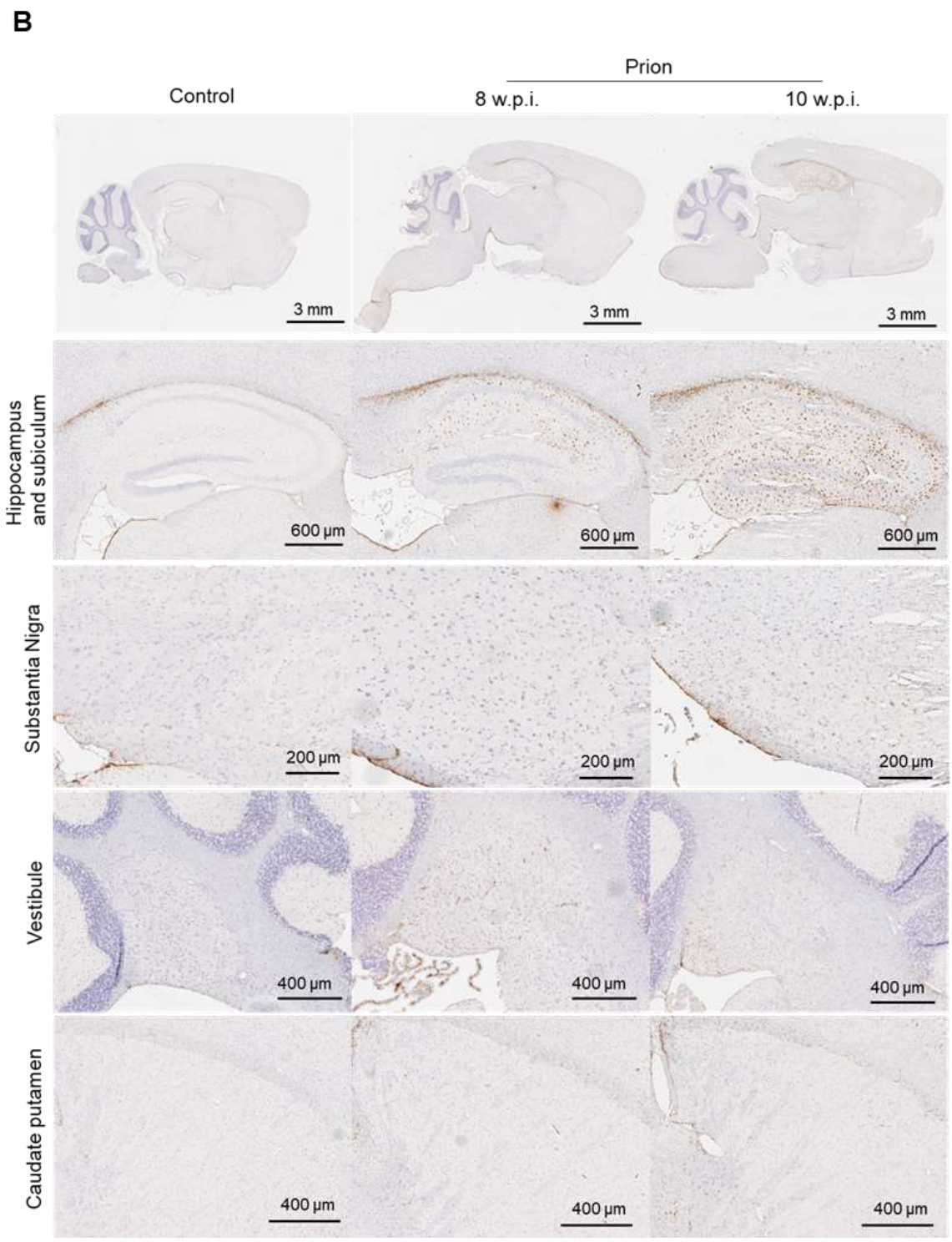

Figure 4-12 Immunohistochemical staining for astrocytic marker vimentin in the brain of prion-infected mice. Left hand side hemisphere from 8- and 10 w.p.i. control and prion-infected mice were sectioned and processed for immunohistochemistry (avidin-biotin complex method) using antibodies against vimentin. Representative images of 3-4 experiments (N=3-4) for the staining of vimentin in bregma lateral level 0.72mm **(A)** and 1.68mm **(B)** in control (10 w.p.i.) and prion-infected mice at 8- and 10 w.p.i.

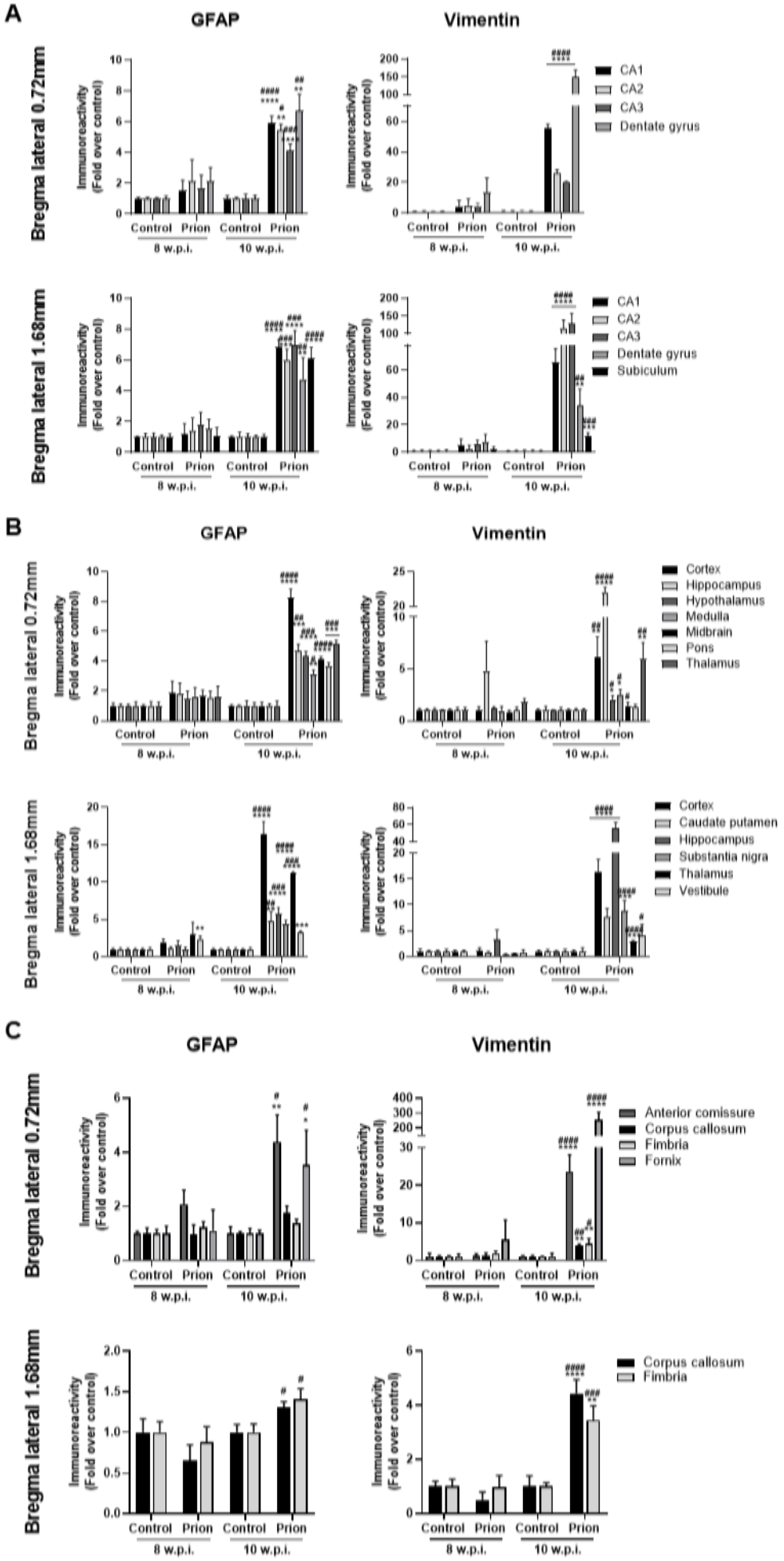
A
GFAP
Vimentin
Bregma lateral 0.72mm
Bregma lateral 1.68mm
Immunoreactivity (Fold over control)
Control Prion Control Prion
8 w.p.i.
10 w.p.i.
CA1
CA2
CA3
Dentate gyrus
Subiculum
B
GFAP
Vimentin
Bregma lateral 0.72mm
Bregma lateral 1.68mm
Cortex
Hippocampus
Hypothalamus
Medulla
Midbrain
Pons
Thalamus
Caudate putamen
Substantia nigra
Vestibule
C
GFAP
Vimentin
Bregma lateral 0.72mm
Bregma lateral 1.68mm
Anterior comissure
Corpus callosum
Fimbria
Fornix

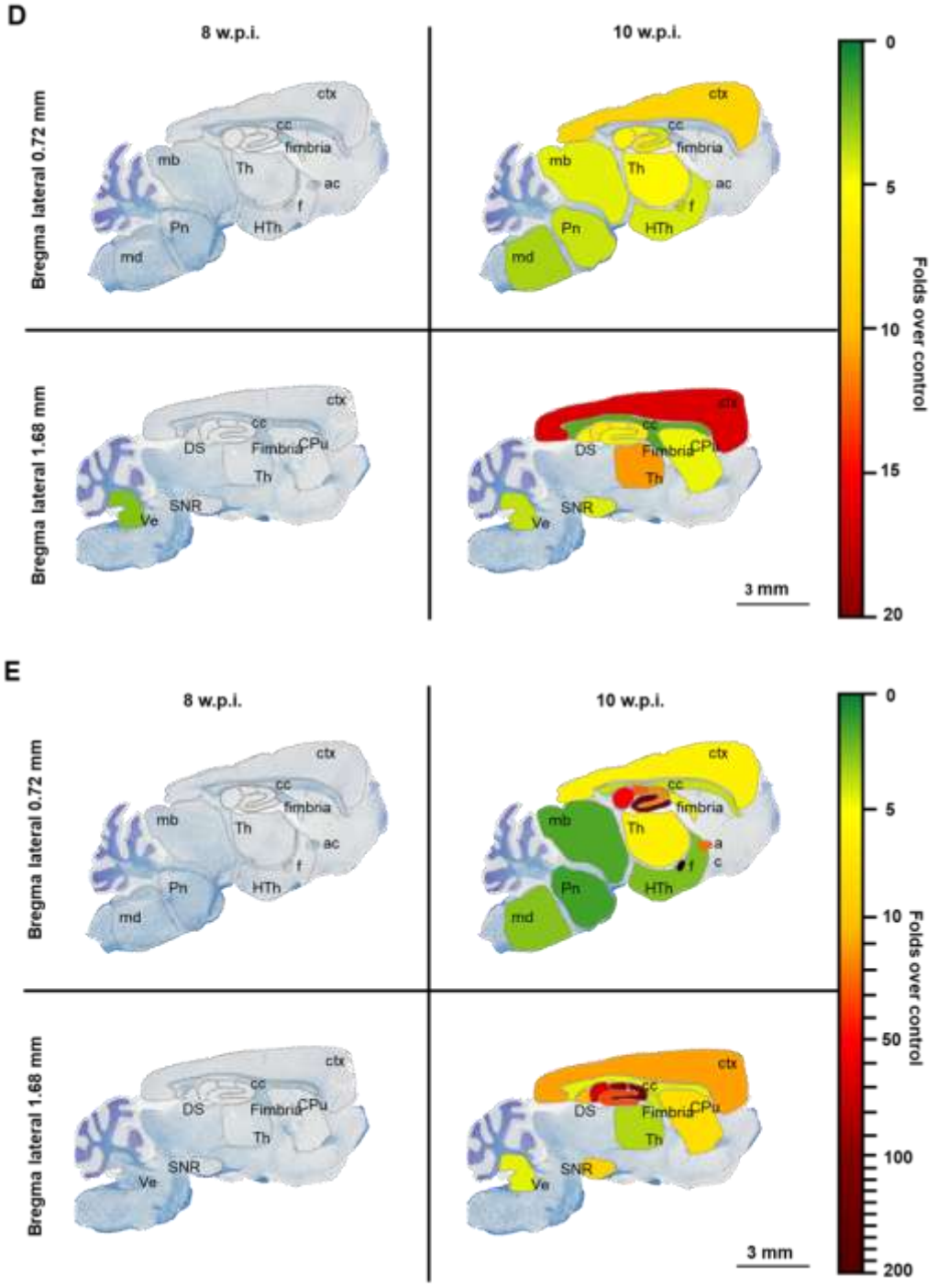

Figure 4-13 Regional changes in expression of astrocytic markers GFAP and vimentin in mouse prion disease. Analysis of immunohistochemical staining (avidin-biotin complex method) for GFAP and vimentin in control and prion-infected mice. GFAP and vimentin staining was quantified in regions of interest in sagittal sections at bregma lateral 0.72 mm and 1.68 mm, which included hippocampal regions **(A)**, other major regions **(B)**, and white matter tracks **(C)**. Images were quantified using Imagescope software (version 12.2.1.5005; Aperio) and data is displayed as mean ± S.E.M. Statistical analysis performed is Two-way ANOVA (Fisher's LSD test) where *P<0.05, **P<0.01,***P<0.001, ****P<0.0001 for prion vs control; $^{\#}$P<0.05, $^{\#\#}$P<0.01, ,$^{\#\#\#}$P<0.001, $^{\#\#\#\#}$P<0.0001 for 10 w.p.i. vs 8 w.p.i. (N=3-4). **(D-E)** Heatmap of significant changes in GFAP **(D)** and vimentin **(E)** detected at 8 and 10 w.p.i. and across the bregma levels 0.72mm and 1.68mm, and brain regions including anterior commissure (ac), caudate putamen (CPu), cortex (ctx), corpus callosum (cc), dorsal subiculum (DS), fornix (f), hippocampus (hpc), hypothalamus (HTh), midbrain (mb), medulla (md), pons (Pn), substantia nigra (SNR), thalamus (Th), and vestibule (Ve).

During astrogliosis, astrocytes undergo a morphological change that include hypertrophy, which is the increase and growth of cells (Middeldorp and Hol, 2011, Danielsson et al., 2018). I therefore decided to analyze the immunohistochemical data represented in Figure 4-11 and Figure 4-12 to help establish if the increase in astrocytic markers GFAP and vimentin is due to proliferation and/or growth of astrocytes. To do so, an algorithm was optimized in Aperio to obtain a count of GFAP- and vimentin-positive glial cells of a diverse range of sizes (Figure 4-14).

GFAP-positive astrocyte showed a robust morphological change in prion diseased mice at 10 w.p.i., whereby a shift from smaller (20-50 µm in diameter) to larger cells (ranging from 51 to 250 µm in diameter) (Figure 4-14B). Specifically, compared to the controls, prion infected hippocampi show an overall significant decrease in 20-50 µm astroglia by 6.4-12% across the bregma levels, and a robust increase in numbers of astroglia ranging from 51 to 250 µm in diameter by 18.3-19.2%, with 51-100 µm astroglia accounting for the most prominent increase. No astroglia positive for GFAP with a diameter larger than 250 µm were detected.

Similar to GFAP, most changes in vimentin-expressing astrocytes occur at 10 w.p.i. Vimentin-expressing astrocytes in the hippocampus however show a different morphological profile compared to GFAP positive cells (Figure 4-14C). There is a robust increase in total number of astrocytes of a various range of size, but not a significant decrease in smaller astrocytes as seen for GFAP-expressing cells.

Overall, these data suggests that *mouse prion disease features robust astrogliosis in the hippocampus at 10 w.p.i., whereby astrocytes undergo important hypertrophy that is characterised by a mixture of astrocytic growth and proliferation. However, whilst astrocytes expressing GFAP seem to both grow in size and number with disease, vimentin is particularly associated* with *proliferation of astrocytes.*

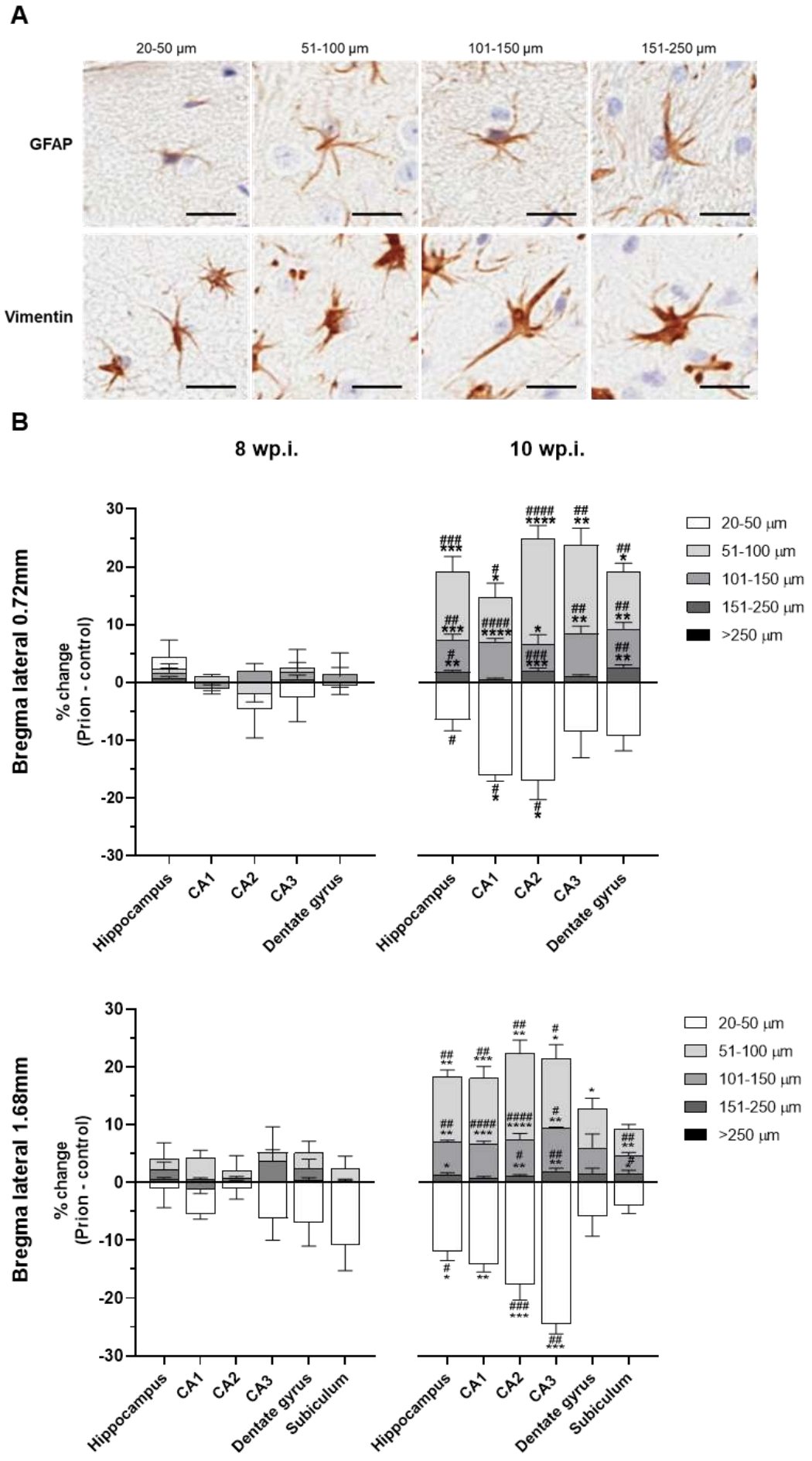
A
20-50 µm
51-100 µm
101-150 µm
151-250 µm
GFAP
Vimentin
B
8 wp.i.
10 wp.i.
Bregma lateral 0.72mm
% change (Prion - control)
20-50 µm
51-100 µm
101-150 µm
151-250 µm
>250 µm
Hippocampus
CA1
CA2
CA3
Dentate gyrus
Bregma lateral 1.68mm
Subiculum

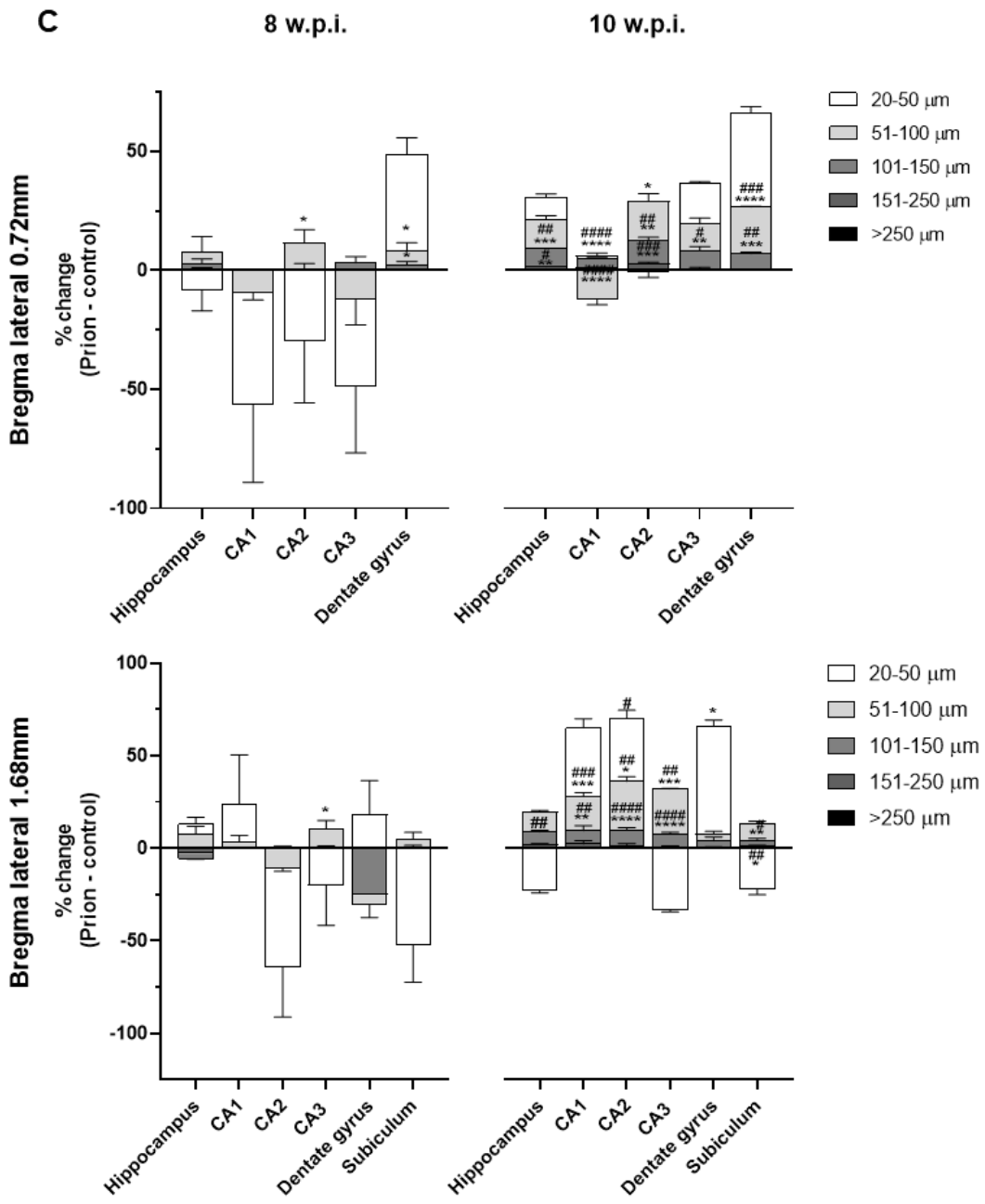

Figure 4-14 Astrocytes undergo morphological changes in prion disease.
Immunohistochemical staining (avidin-biotin complex method) using antibodies against GFAP and vimentin, astrocytic markers, was performed on brain sections from 8- and 10 w.p.i. control and prion-infected mice (see Figure 4-11 and Figure 4-12). Number of GFAP- or vimentin-stained cells were quantified using a nuclear count algorithm, tuned according to different sizes, represented in **(A)**. Scale bar 20µm. **(B-C)** Percentage change of the different populations (20-50µm, 51-100µm, 101-150µm, 151-250µm, >250µm) of GFAP-positive **(B)** or vimentin-positive **(C)** astrocytes in hippocampal regions (CA1, CA2, CA3, dentate gyrus) and subiculum was calculated and expressed as mean ± S.E.M. of prion – control. Statistical analysis performed is Two-way ANOVA (Fisher's LSD test) where *P<0.05, **P<0.01, ***P<0.001, ****P<0.0001 for prion vs control; $^{\#}$P<0.05, $^{\#\#}$P<0.01, $^{\#\#\#}$P<0.001, $^{\#\#\#\#}$P<0.0001 for 10 w.p.i. vs 8 w.p.i. (N=3-4).

4.2.5 Mouse prion disease is characterised by microgliosis

The involvement of microgliosis in prion disease has been discussed extensively in the literature (Carroll et al., 2018), and it has been demonstrated that

microglia in prion disease mainly locate at the site of and in response to PrP_{Sc} deposition (Bate et al., 2002, Williams et al., 1997, Giese et al., 1998, Van Everbroeck et al., 2004, Kercher et al., 2007, Sandberg et al., 2014, Vincenti et al., 2015, Gómez-Nicola et al., 2013). Here, activation of microglia was detected by upregulation of transcript levels of CD86, a membrane co-stimulatory receptor responsible for immune cell proliferation (Lebedeva et al., 2005). CD86 transcript levels were found to be significantly upregulated in the cortex of 10 w.p.i. prion-infected mice, and trending to increase in hippocampus and striatum (Figure 4-15).

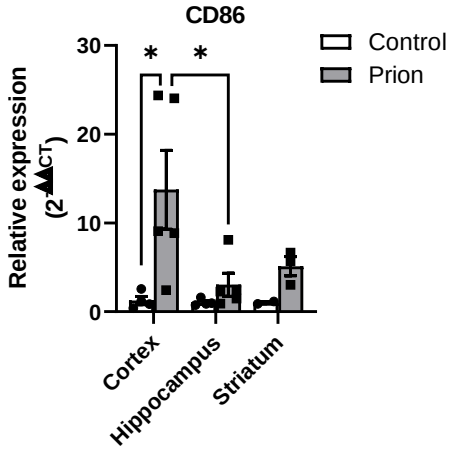

Figure 4-15 Activation of microglia was detected by upregulation of CD86 transcripts. Quantitative RT-qPCR showing the expression of CD86, marker of microglia activation, in the cortex, hippocampus or striatum of control or prion-diseased mice at 10 w.p.i. Data are expressed as a ratio of α-tubulin RNA expression. Statistical analysis performed is Two-way ANOVA Tukey's multiple comparisons, where *P<0.05, (N=5 or 2-4 for striatum).

Immunohistochemical staining using antibodies against Ionized calcium-binding adaptor molecule 1 (Iba1) was conducted on sections through bregma lateral levels 0.72mm and 1.68mm of control and prion-infected brains to assess the extent of microgliosis in multiple brain regions (Figure 4-16). Iba1 is a 17-kDa EF hand protein with actin-cross-linking and cytoskeletal organisation functions (Imai and Kohsaka, 2002, Sasaki et al., 2001) that is specifically expressed in monocytic cell lines (Imai et al., 1996), and it was shown to be upregulated in activated microglia (Ito et al., 1998).

Most changes in Iba1 expression are observed in prion-infected mice at 10 w.p.i. Larger brain regions such as *md*, *mb* and *Pn* display moderate changes in Iba1 at 10 w.p.i., between 1.5- and 1.9-fold over the control) (Figure 4-17B). Though moderate, *Th* and *Ve* show significant upregulation in Iba1 expression from 8

w.p.i. in bregma lateral 1.68mm (1.3- and 2-fold increase at 8 w.p.i., and 1.7- and 2.2-fold increase at 10 w.p.i. for Th and Ve, respectively), suggesting these regions might be affected by pathology earlier than others. Iba1 in the hpc shows an average 1.5-fold increase in both levels relative to controls at 10 w.p.i., with CA3 displaying the largest increase (Figure 4-17A).

The white matter tracks analysed display a moderate upregulation in microglia only at 10 w.p.i. (Figure 4-17C). Ac and f respectively showed 1.6 and 2.8-fold increase in Iba1 expression. The fimbria shows similar microglia upregulation across the two levels by around 2-fold, whereas the cc shows a 2.4- and 1.5-fold upregulation compared to controls in the bregma lateral 0.72mm and 1.68mm, respectively. No significant upregulation in Iba1 was observed in the ctx, CPu, HTh, SNR, in any of the levels examined.

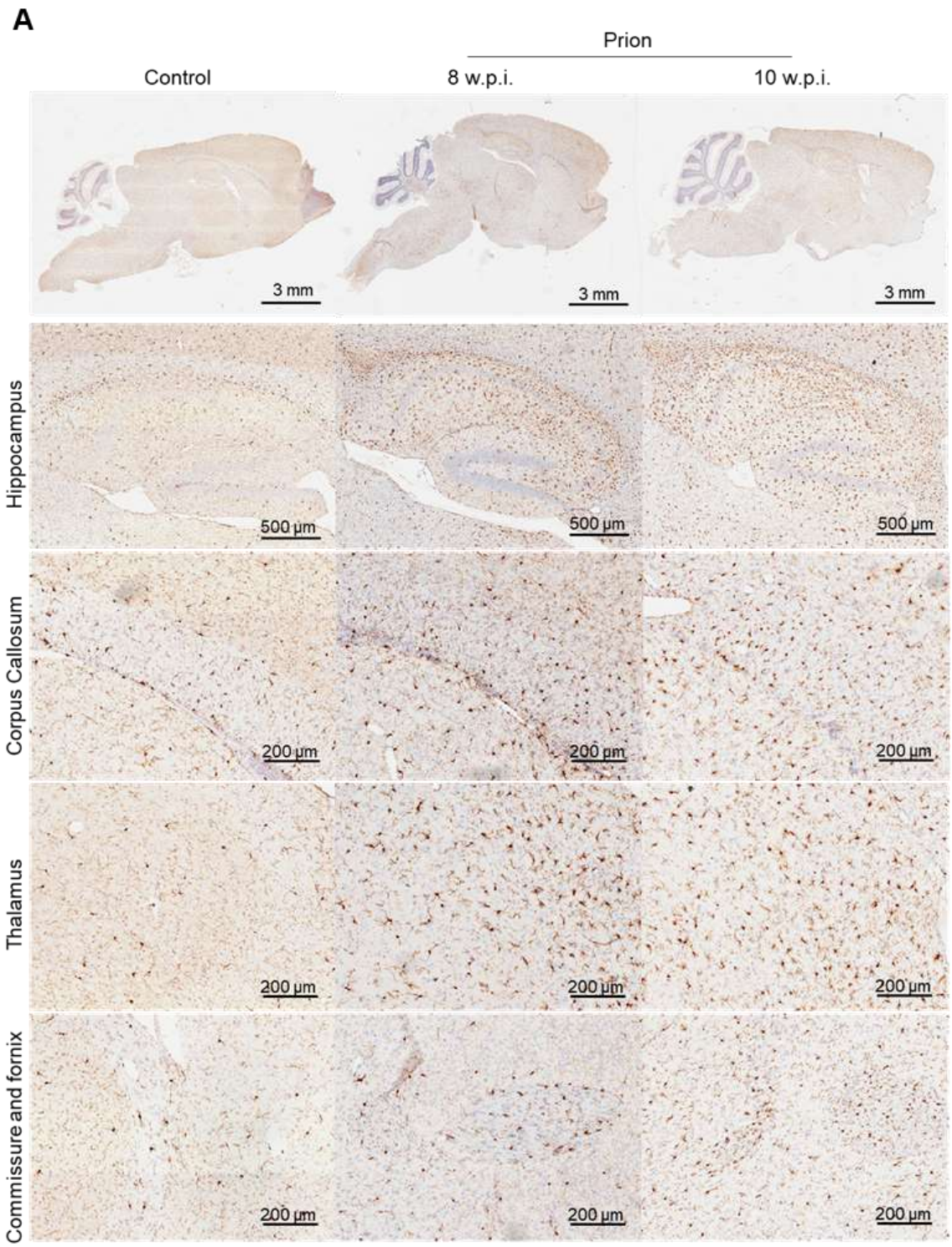
A
Prion
Control
8 w.p.i.
10 w.p.i.
3 mm
3 mm
3 mm
Hippocampus
500 µm
500 µm
500 µm
Corpus Callosum
200 µm
200 µm
200 µm
Thalamus
200 µm
200 µm
200 µm
Commissure and fornix
200 µm
200 µm
200 µm

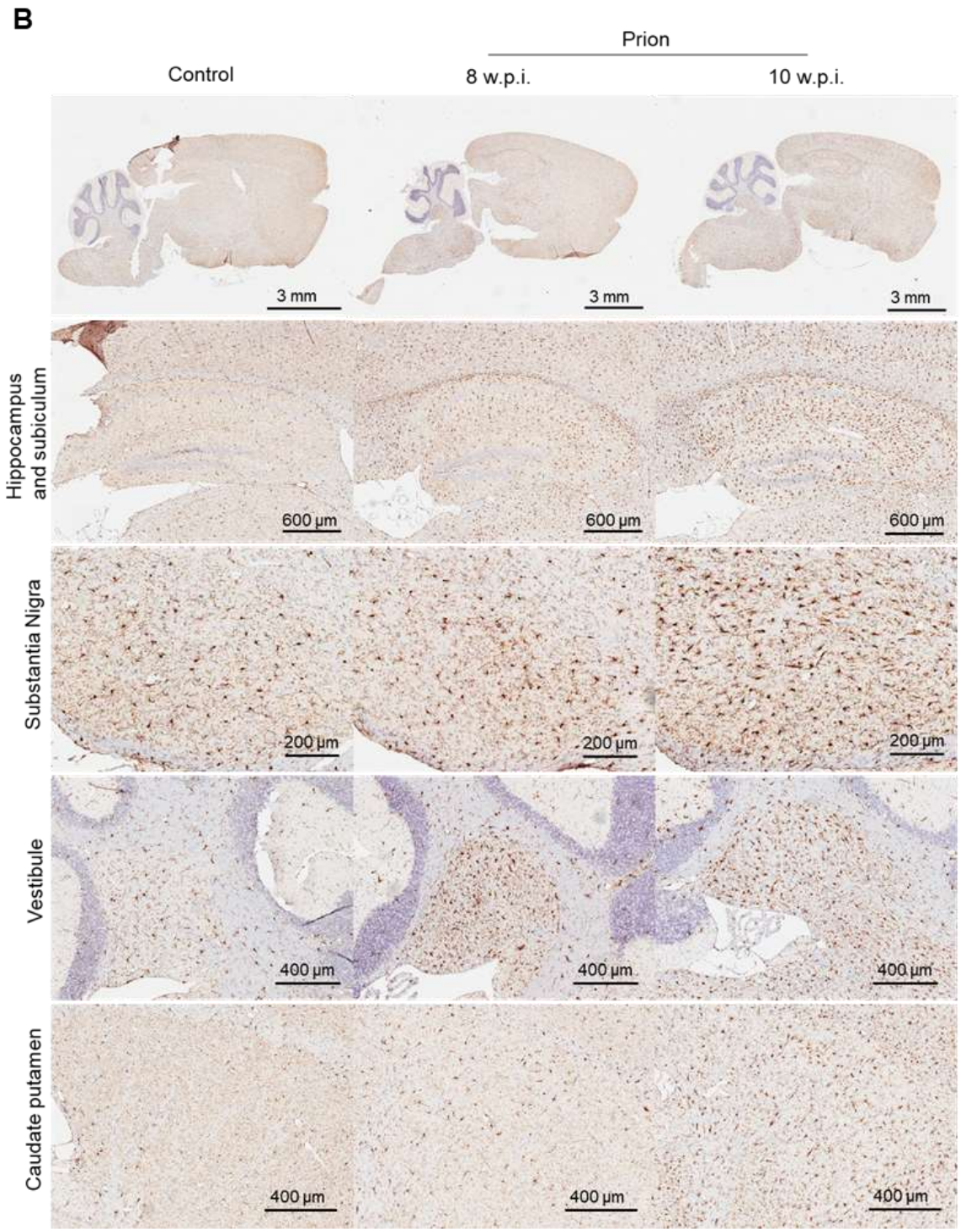

Figure 4-16 Microgliosis in the brain of prion-infected mice as visualised by immunohistochemical staining for Iba1. Left hand side hemisphere from 8- and 10 w.p.i. control and prion-infected mice were sectioned and processed for immunohistochemistry (avidin-biotin complex method) using antibodies against Iba1, a microglia/macrophage-specific calcium-binding protein. Anti-Iba1 antibody staining in bregma lateral level 0.72mm **(A)** and 1.68mm **(B)** in control and prion-infected mice at 8 and 10 w.p.i.; representative images of 3-4 mice.

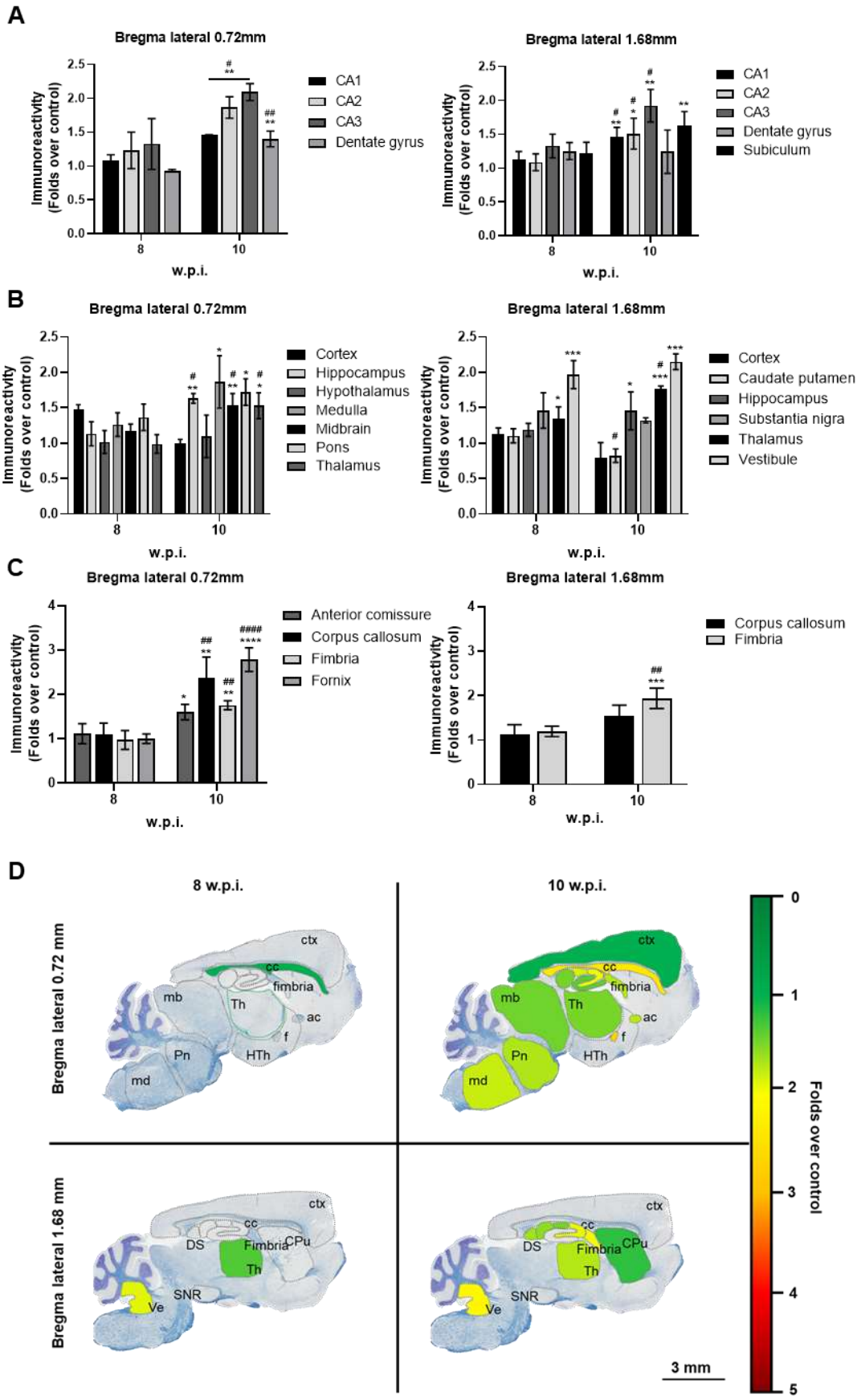

Figure 4-17 Regional distribution of microgliosis in mouse prion disease. Analysis of the immunohistochemical staining of 8- and 10 w.p.i. control and prion-infected mice using antibodies against Iba1 from Figure 4-16 . Iba1 staining was quantified in regions of interest in sagittal sections at bregma lateral 0.72 mm and 1.68 mm, which included hippocampal regions **(A),** other

major regions **(B)**, and white matter tracks **(C)**. Quantification was conducted using Imagescope software (version 12.2.1.5005; Aperio) and data is displayed as mean ± S.E.M. Statistical analysis performed is Two-way ANOVA (Fisher's LSD test) where *P<0.05, **P<0.01, ***P<0.001 for prion vs control; $^{\#}$P<0.05, $^{\#\#}$P<0.01, $^{\#\#\#\#}$P<0.0001 for 10 w.p.i. vs 8 w.p.i. (N=3-4). **(D)** Heatmap of significant changes in Iba1 detected at 8- and 10 w.p.i. and across the bregma levels 0.72mm and 1.68mm, and brain regions including anterior commissure (ac), caudate putamen (CPu), cortex (ctx), corpus callosum (cc), dorsal subiculum (DS), fornix (f), hippocampus (hpc), hypothalamus (HTh), midbrain (mb), medulla (md), pons (Pn), substantia nigra (SNR), thalamus (Th), and vestibule (Ve).

Microglia can be found as a whole spectrum of phenotypes and morphologies in healthy and neurodegenerative brains (Walker and Lue, 2015). Thus, I aimed to assess whether microglia undergo a shift in size as observed in astrocytes in mouse prion disease. Iba1-stained microglia where therefore grouped by size ranging from 20 µm to 250 µm in diameter (Figure 4-18A), and an algorithm was generated in Aperio to assess the cell count in relation to their size (Figure 4-18B).

Except for a significant increase by 4.3% in 101-150 µm microglia in the CA2 region at bregma lateral 0.72mm, no other significant changes were detected at 8 w.p.i. In 10 w.p.i. prion infected hippocampi, however, there is a robust overall increase in microglia ranging from 100 to 250 µm in size by 8.6% and 7.4% at bregma lateral 0.72 mm and 1.68 mm, respectively. A general decrease in smaller microglia ranging from 20 to 100 µm in diameter was detected, however it was only significantly different in the CA2 region at bregma lateral 0.72mm. Overall, this data indicates that *microgliosis in mouse prion disease is mostly characterised by a moderate increase in number of larger microglia ranging from 100 to 250 µm in size.*

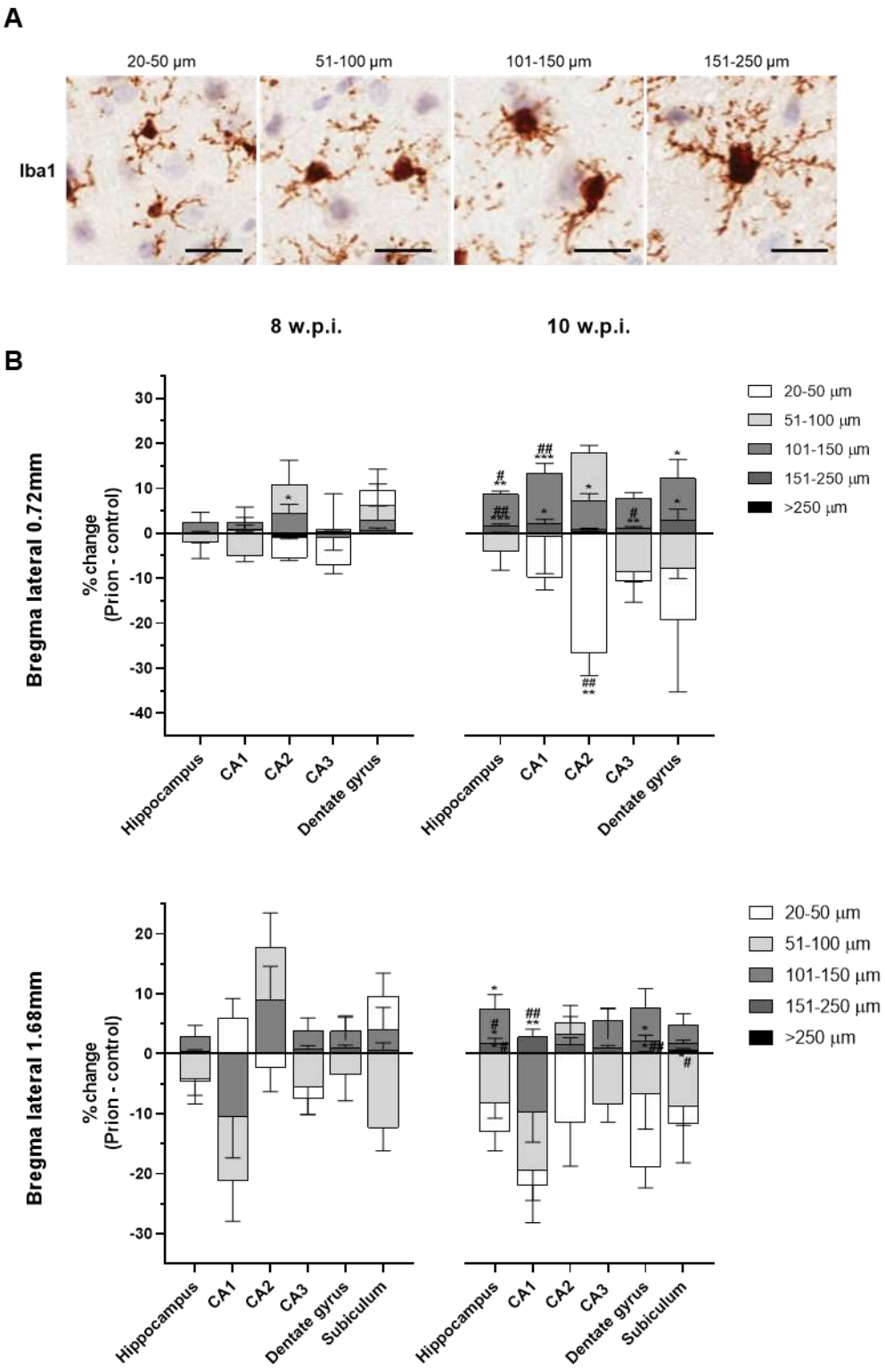

Figure 4-18 Microglia undergo morphological changes with prion disease.
Immunohistochemical staining (avidin-biotin complex method) using antibodies against Iba1 was performed on brain sections from 8- and 10 w.p.i. control and prion-infected mice (see Figure 4-16). Numbers of Iba1-stained cells were quantified using a nuclear count algorithm, tuned according to different sizes, represented in **(A).** Scalebar 20µm. **(B)** Percentage change of each population of Iba1-positive cells in hippocampal regions (CA1, CA2, CA3, dentate gyrus) and subiculum was calculated and expressed as mean ± S.E.M. of prion – control. Statistical analysis performed is Two-way ANOVA (Fisher's LSD test) where *P<0.05, **P<0.01, ***P<0.001 for prion vs control; $^{\#}$P<0.05, $^{\#\#}$P<0.01 for 10 w.p.i. vs 8 w.p.i. (N=3-4).

Activated microglia typically release pro-inflammatory cytokines during neuroinflammation, such as tumour necrosis factor α (TNF-α), interleukin-1ß (IL-1ß) and interleukin-6 (IL-6), that are capable of promoting astrogliosis *in vivo* (Ben Haim et al., 2015). Particularly, TNF-α is a major pro-inflammatory cytokine in many neurological disorders including AD (Fischer and Maier, 2015, Liddelow et al., 2017, Michaud et al., 2013, Olmos and Lladó, 2014), and it was proposed as drug target for the treatment of neurodegenerative conditions (Decourt et al., 2017, Tweedie et al., 2007). In this chapter, transcript levels of IL-1ß, IL-6 and TNF-α were analysed in the cortex, hippocampus, or striatum at 10 w.p.i. (Figure 4-19). IL-1ß, IL-6 and TNF-α transcripts show an overall upregulation in cortex, hippocampus, and striatum with prion disease at 10 w.p.i. compared to controls. IL-1ß is significantly increased in the hippocampus and cortex of prion-infected mice ($P<0.01$), while IL-6 and TNF-α show a robust upregulation in the cortex and striatum ($P<0.05$).

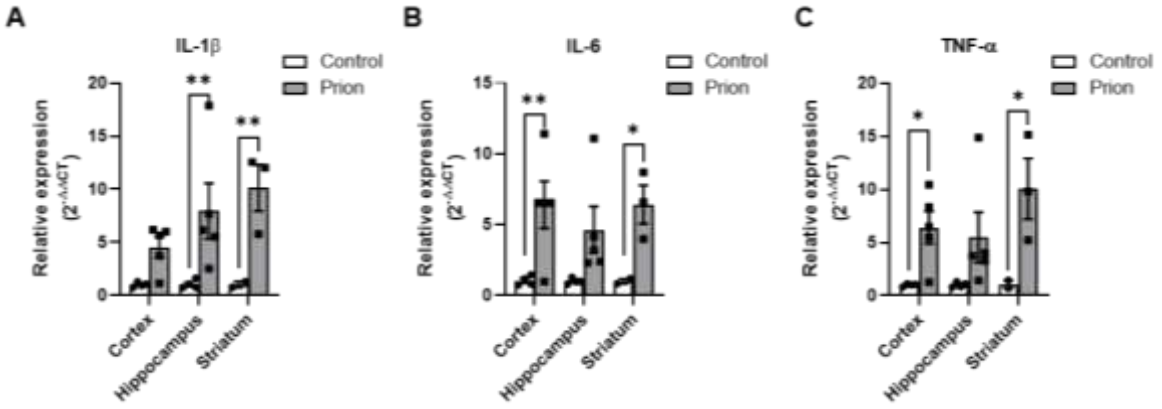

Figure 4-19 Pro-inflammatory cytokines IL-1β, IL-6 and TNF-α are upregulated with prion disease. Quantitative RT-qPCR of **(A)** IL-1β, **(B)** IL-6 and **(C)** TNF-α in the cortex, hippocampus or striatum of control or prion-diseased mice at 10 w.p.i. Data are expressed as a ratio of α-tubulin RNA expression. Statistical analysis performed is Two-way ANOVA Tukey's multiple comparisons, where *$P<0.05$, (N=5 or 2-4 for striatum).

In addition, TNF-α expression was assessed in the brain of prion-infected mice by probing TNF-α transcripts using an RNA *in situ hybridisation* (ISH) technique (RNAScope). As shown in Figure 4-20A/B, RNAScope signal is detected as punctuate dots; each dot represents a single mRNA molecule, and multiple overlapping transcripts can result in signal clusters. Both total signal and clusters were analysed in this chapter, however both measurements show similar trends, indicating that TNF-α transcripts are mostly detected as clusters.

TNF-α transcripts were only detected in the brains of 10 w.p.i. prion-infected mice, suggesting that TNF-α is not expressed prior to that disease time-point, and neither is expressed in control, healthy brains. The hippocampus showed the most robust expression of TNF-α, especially the CA2 region (Figure 4-20C). TNF-α transcripts show a robust increase in white matter tracks (anterior commissure, fornix, corpus callosum and fimbria) at 10 w.p.i. at bregma lateral 0.72mm (Figure 4-20D). Upon a closer examination of the raw data, some darker haematoxylin stain, typical of white matter tracks anatomy, was erroneously picked up as positive signal, as indicated in Figure 4-20B. Therefore, it is difficult to confidently interpret the RNAScope signal data for white matter tracks. Amongst the major brain regions examined, only the thalamus and the cortex show a significant presence of TNF-α transcripts in 10 w.p.i. prion-infected mice (Figure 4-20E).

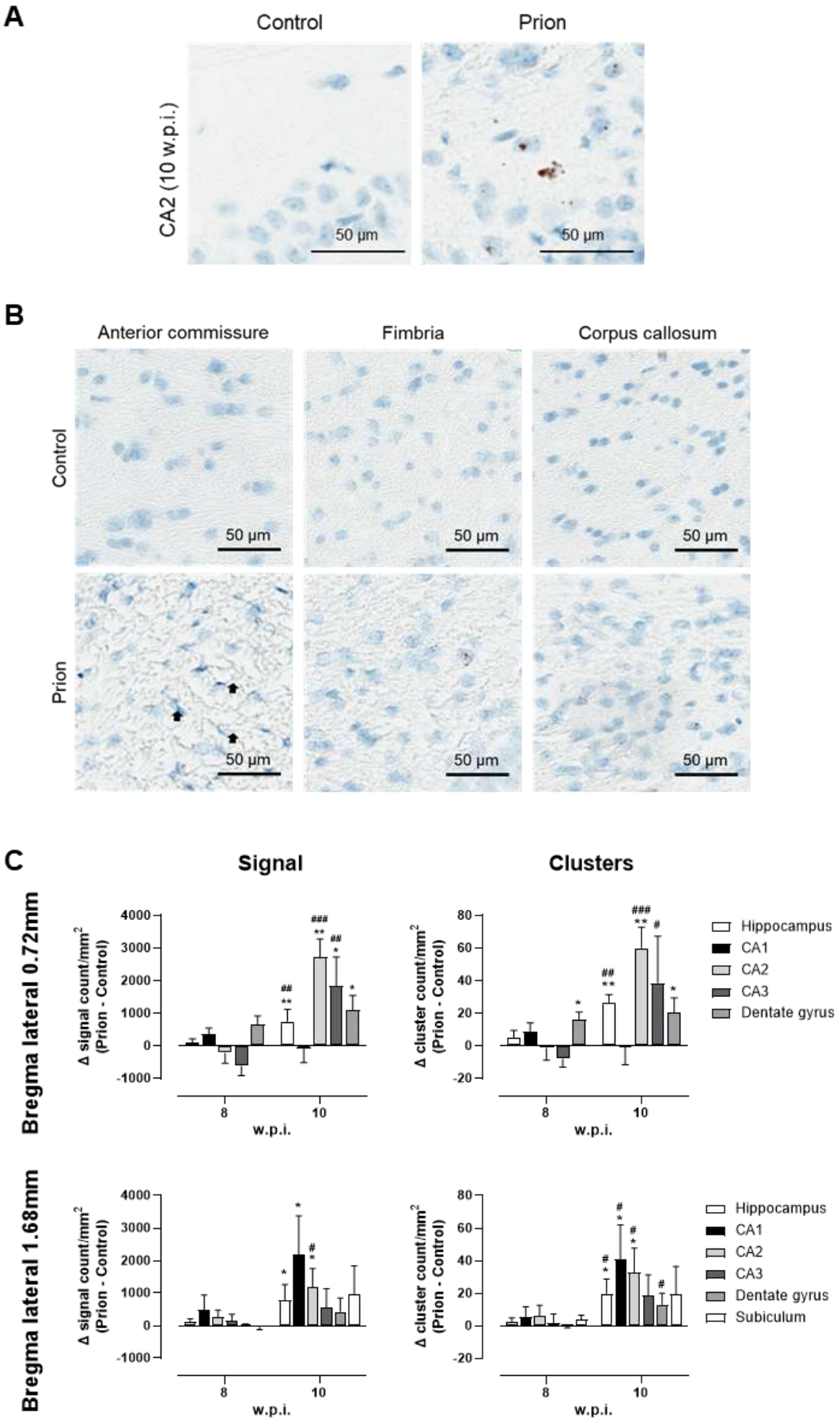
A
Control
Prion
CA2 (10 w.p.i.)
50 µm
50 µm
B
Anterior commissure
Fimbria
Corpus callosum
Control
Prion
50 µm
C
Signal
Clusters
Bregma lateral 0.72mm
Bregma lateral 1.68mm
Δ signal count/mm2 (Prion - Control)
Δ cluster count/mm2 (Prion - Control)
w.p.i.
Hippocampus
CA1
CA2
CA3
Dentate gyrus
Subiculum

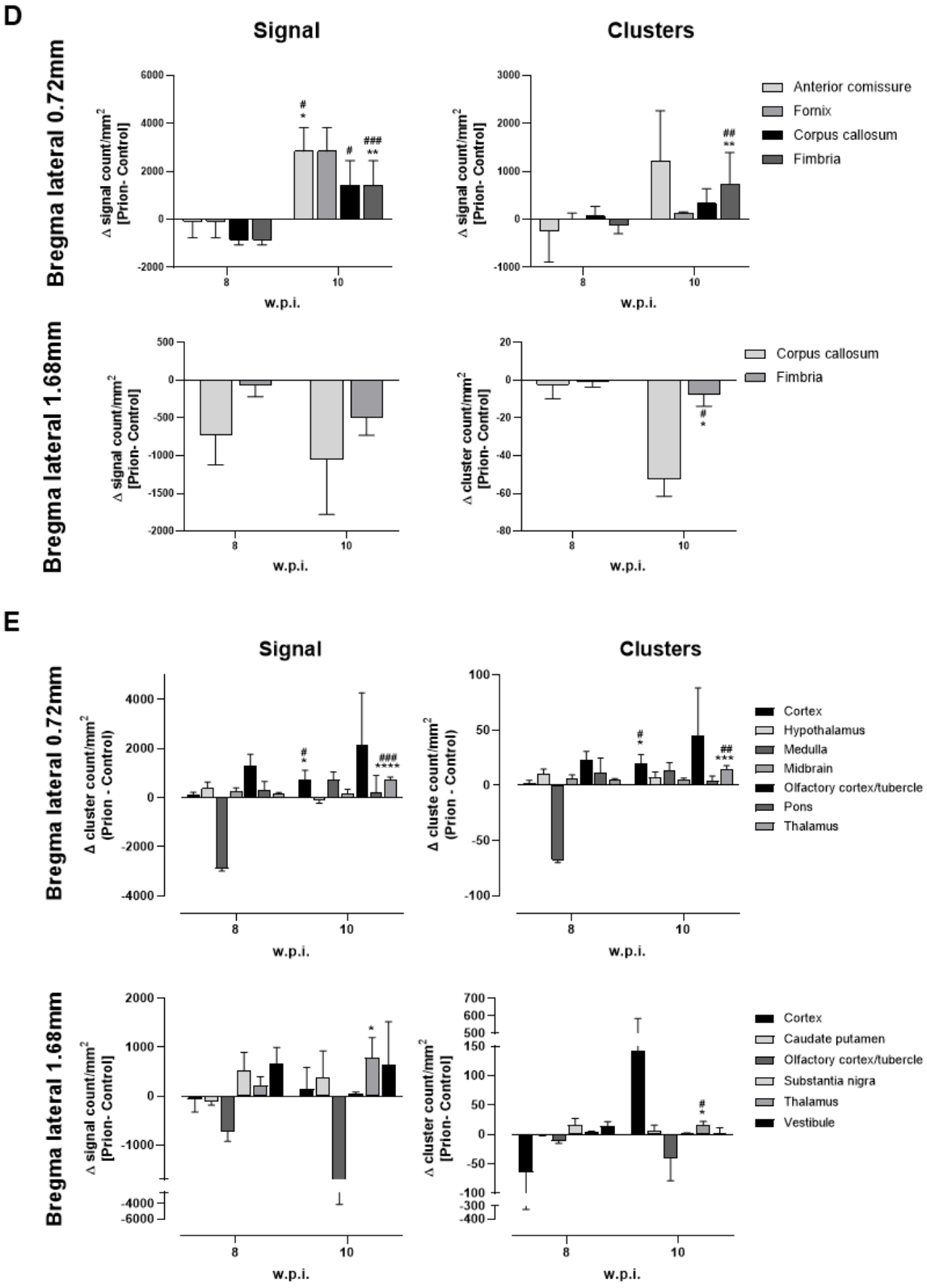

Figure 4-20 TNF-α transcript levels are increased in mouse prion disease. Left hand side hemisphere from 8- and 10 w.p.i. control and prion-infected mice were sectioned and processed for RNAScope. Sagittal brain sections at bregma lateral 0.72 mm and 1.68 mm were hybridized with probes to the mouse TNF-α (mm-TNFα cat. No. 311088). **(A-B)** Representative images of 3-4 experiments (N=3-4) of TNF-α staining showing **(A)** punctuate dots and clusters or **(B)** false positive signal detected in white matter tracks (indicated by arrows). Probe hybridisation was quantified as signal count or cluster counts in hippocampal regions **(C)**, white matter tracks **(D)** and other major regions **(E)** at bregma lateral 0.72mm and 1.68mm using Imagescope software (version 12.2.1.5005; Aperio). Data is displayed as mean ± S.E.M. and statistically analysed using Two-way ANOVA (Fisher's LSD test) where *P<0.05, **P<0.01, ***P<0.001 for prion vs control; $^{\#}$P<0.05, $^{\#\#}$P<0.01, $^{\#\#\#}$P<0.001 for 10 w.p.i. vs 8 w.p.i. (N=3-4).

Taken together, mouse prion disease displays a robust expression of TNF-α from 10 w.p.i., particularly in the hippocampus and neighboring regions such as the cortex and the thalamus, especially at bregma lateral level 0.72mm (Figure 4-21). The highest levels of TNF-α transcripts are however found in the CA1, CA2 and CA3 hippocampal regions, which are the areas where astrogliosis and microgliosis are most present in response to PrP_{Sc} deposition.

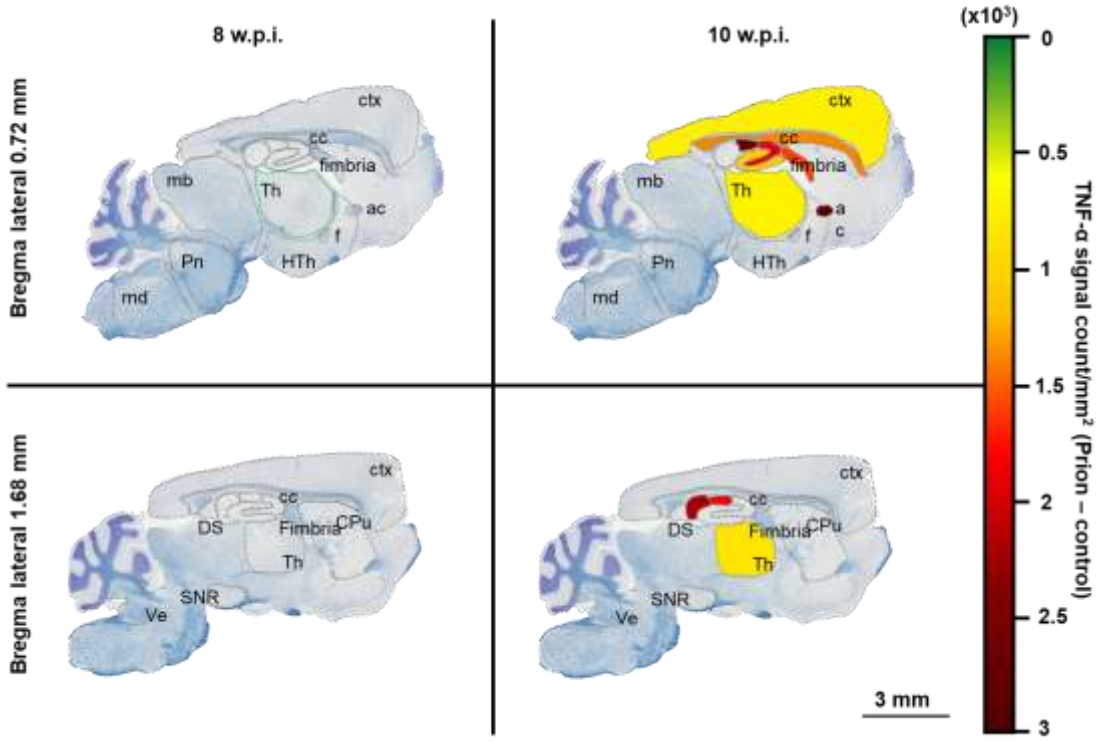

Figure 4-21 Summary heatmap of TNF-α transcript levels in mouse prion disease. Heatmap of significant changes in TNF-α detected at 8 and 10 w.p.i. and across the bregma levels 0.72mm and 1.68mm from Figure 4-20 (N=3-4). Brain regions analysed included anterior commissure (ac), caudate putamen (CPu), cortex (ctx), corpus callosum (cc), dorsal subiculum (DS), fornix (f), hippocampus (hpc), hypothalamus (HTh), midbrain (mb), medulla (md), pons (Pn), substantia nigra (SNR), thalamus (Th), and vestibule (Ve).

4.2.6 Markers of neuroinflammation positively correlate with PrP_{Sc} deposits

Immunohistochemical staining data (Figure 4-4, Figure 4-11, Figure 4-12, Figure 4-16, Figure 4-20) were used to analyse the correlations (Pearson) between PrP_{Sc} deposits and neuroinflammation markers examined above – Iba1, GFAP, vimentin and TNF-α (Figure 4-22). Unsurprisingly, most correlations identified are positive. PrP_{Sc} deposits show a robust correlation with Iba1, GFAP, vimentin and TNF-α in the CA2 region (*P<0.03), in both bregma lateral 0.72mm and 1.68mm levels. The correlation of PrP_{Sc} is high (Pearson r>0.72) with vimentin and TNF-α. PrP_{Sc} deposition also correlates with vimentin and Iba1 in the corpus callosum

(**P<0.002) in the bregma lateral 0.72mm, and with Iba1 in the fimbria (**P<0.002) in the bregma lateral 1.68mm. GFAP, vimentin and Iba1 display robust (*P<0.030), high degree (Pearson r>0.70) correlations in all the hippocampal regions i.e. CA1, CA2, CA3, dentate gyrus and subiculum. TNF-α mainly correlates with GFAP and vimentin in the hippocampus, with especially high correlation in the CA2 region (Pearson r>0.77). In addition, TNF-α significantly, strongly correlates with Iba1 in the CA2 region and fimbria.

In the absence of correlation with PrP_{Sc}, GFAP, vimentin and Iba1 show a robust (*P<0.030) correlation in the corpus callosum. In addition, Iba1 significantly (*P<0.03) correlates with GFAP and vimentin in the fimbria, with GFAP only in the anterior commissure (**P<0.002), and with vimentin in the fornix, medulla and thalamus (*P<0.03).

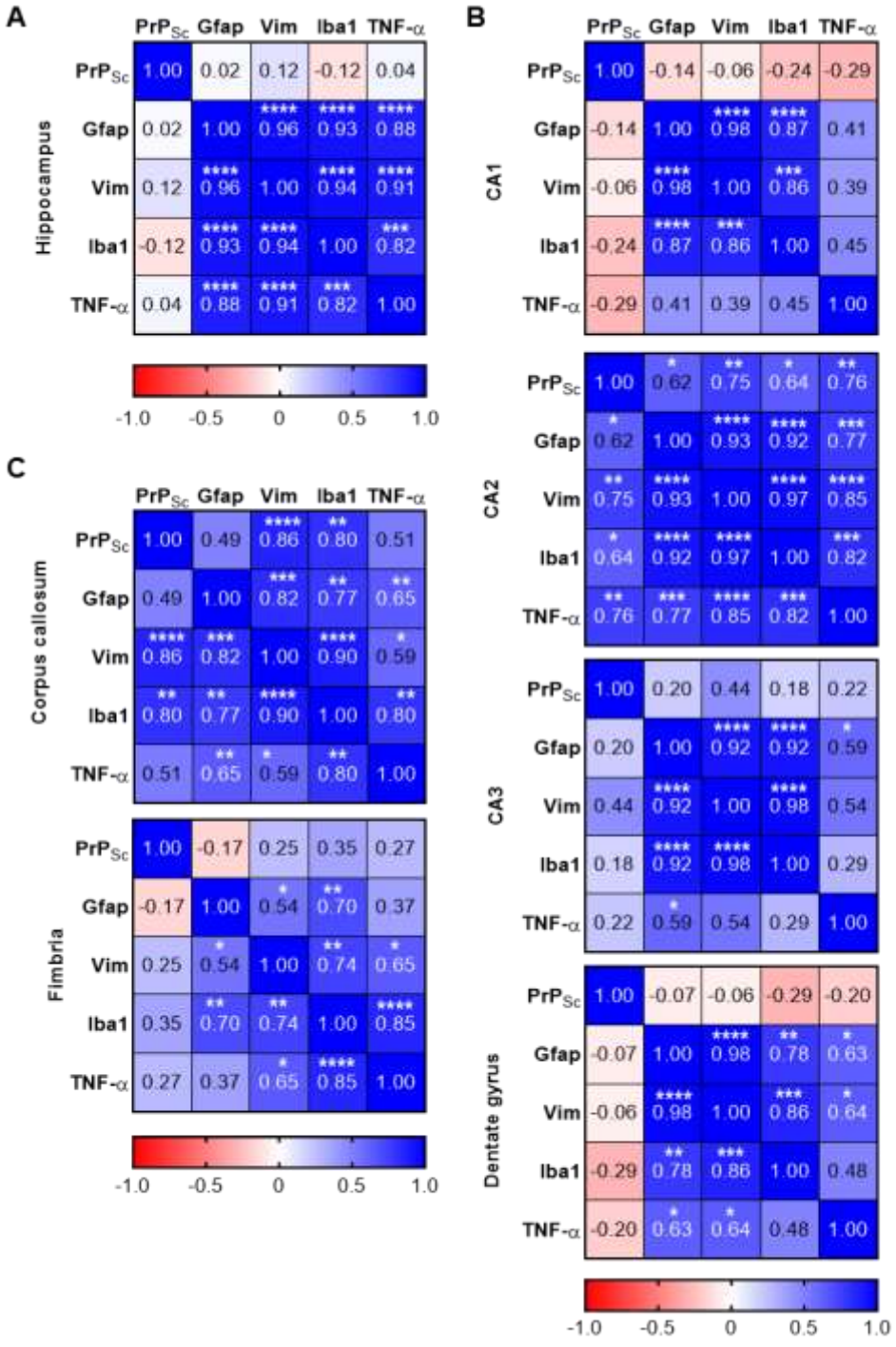
A
Hippocampus
PrPSc Gfap Vim Iba1 TNF-α
PrPSc 1.00 0.02 0.12 -0.12 0.04
Gfap 0.02 1.00 **** 0.96 **** 0.93 **** 0.88
Vim 0.12 **** 0.96 1.00 **** 0.94 **** 0.91
Iba1 -0.12 **** 0.93 **** 0.94 1.00 *** 0.82
TNF-α 0.04 **** 0.88 **** 0.91 *** 0.82 1.00
-1.0 -0.5 0 0.5 1.0
B
CA1
PrPSc Gfap Vim Iba1 TNF-α
PrPSc 1.00 -0.14 -0.06 -0.24 -0.29
Gfap -0.14 1.00 **** 0.98 **** 0.87 0.41
Vim -0.06 **** 0.98 1.00 *** 0.86 0.39
Iba1 -0.24 **** 0.87 *** 0.86 1.00 0.45
TNF-α -0.29 0.41 0.39 0.45 1.00
CA2
PrPSc 1.00 * 0.62 ** 0.75 * 0.64 ** 0.76
Gfap * 0.62 1.00 **** 0.93 **** 0.92 *** 0.77
Vim ** 0.75 **** 0.93 1.00 **** 0.97 **** 0.85
Iba1 * 0.64 **** 0.92 **** 0.97 1.00 *** 0.82
TNF-α ** 0.76 *** 0.77 **** 0.85 *** 0.82 1.00
CA3
PrPSc 1.00 0.20 0.44 0.18 0.22
Gfap 0.20 1.00 **** 0.92 **** 0.92 * 0.59
Vim 0.44 **** 0.92 1.00 **** 0.98 0.54
Iba1 0.18 **** 0.92 **** 0.98 1.00 0.29
TNF-α 0.22 * 0.59 0.54 0.29 1.00
Dentate gyrus
PrPSc 1.00 -0.07 -0.06 -0.29 -0.20
Gfap -0.07 1.00 **** 0.98 ** 0.78 * 0.63
Vim -0.06 **** 0.98 1.00 *** 0.86 * 0.64
Iba1 -0.29 ** 0.78 *** 0.86 1.00 0.48
TNF-α -0.20 * 0.63 * 0.64 0.48 1.00
-1.0 -0.5 0 0.5 1.0
C
Corpus callosum
PrPSc Gfap Vim Iba1 TNF-α
PrPSc 1.00 0.49 **** 0.86 ** 0.80 0.51
Gfap 0.49 1.00 *** 0.82 ** 0.77 ** 0.65
Vim **** 0.86 *** 0.82 1.00 **** 0.90 * 0.59
Iba1 ** 0.80 ** 0.77 **** 0.90 1.00 ** 0.80
TNF-α 0.51 ** 0.65 * 0.59 ** 0.80 1.00
Fimbria
PrPSc 1.00 -0.17 0.25 0.35 0.27
Gfap -0.17 1.00 * 0.54 ** 0.70 0.37
Vim 0.25 * 0.54 1.00 ** 0.74 * 0.65
Iba1 0.35 ** 0.70 ** 0.74 1.00 **** 0.85
TNF-α 0.27 0.37 * 0.65 **** 0.85 1.00
-1.0 -0.5 0 0.5 1.0

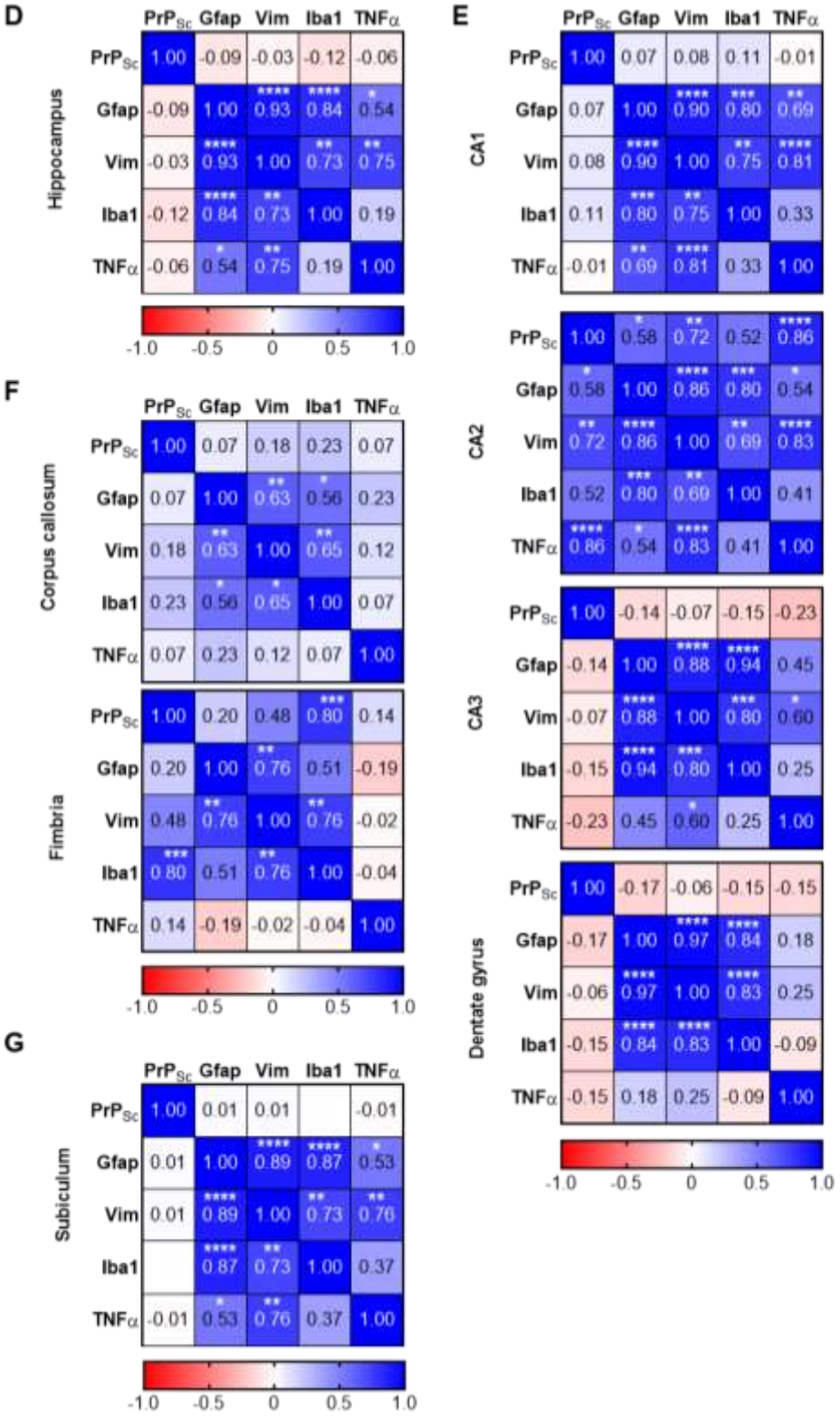

Figure 4-22 Correlations of PrP_{Sc} deposits and markers of neuroinflammation in hippocampal regions of prion-infected mice. Immunohistochemical staining using antibodies against aggregates of PrP_{Sc} (see Figure 4-3), Iba1 (see Figure 4-16), astrocytic markers GFAP and vimentin (see Figure 4-11 and Figure 4-12), and RNAScope hybridisation using probes for mouse TNF-α (see Figure 4-20), were quantified using Imagescope software (version 12.2.1.5005; Aperio). All quantification data from 8 and 10 w.p.i., control and prion-infected mice was pulled together and used to analyse the correlation between PrP_{Sc} deposition and the aforementioned neuroinflammatory markers in hippocampal regions (CA1, CA2, CA3, dentate gyrus) **(A-B, D-E)** including neighbouring white matter tracks (corpus callosum and fimbria) **(C, F)** and subiculum **(G)** at bregma lateral level 0.72mm **(A-C)** and 1.68mm **(D-G)**. Pearson correlation was applied assuming Gaussian distribution where *P<0.05, **P<0.01,***P<0.001, ****P<0.0001 (N=12-14).

In the brain regions whereby PrP_{Sc} deposits were not detected using immunohistochemical staining, the correlation between the neuroinflammatory markers amonsts themselves alone were analysed (Figure 4-23). Several of the brain regions examined showed no significant correlation among the markers of neuroinflammation, probably due to the low level of pathology present in these areas. These included hypothalamus, midbrain and pons at bregma lateral 0.72mm and cortex, caudate putamen (murine striatum), substantia nigra and vestible at bregma lateral 1.68mm.

Surprisingly, given that GFAP is typically co-expressed with vimentin, no correlation was found between GFAP and vimentin in any of the regions analysed. However, vimentin showed significant ($P<0.01$) strong (Pearson $r>0.70$) correlations with Iba1 in the anterior comissure, fornix, medulla, and thalamus, and with TNF-α in the cortex and thalamus. Iba1 and TNF-α also significantly correlated in the thalamus, especially at bregma lateral 0.68mm ($P<0.001$, Pearson $r=0.81$).

Overall, most robust correlations between PrP_{Sc}, GFAP, vimentin, Iba1 and TNF-a are found in the hippocampus, especially in the CA2 hippocampal region, cortex and thalamus.

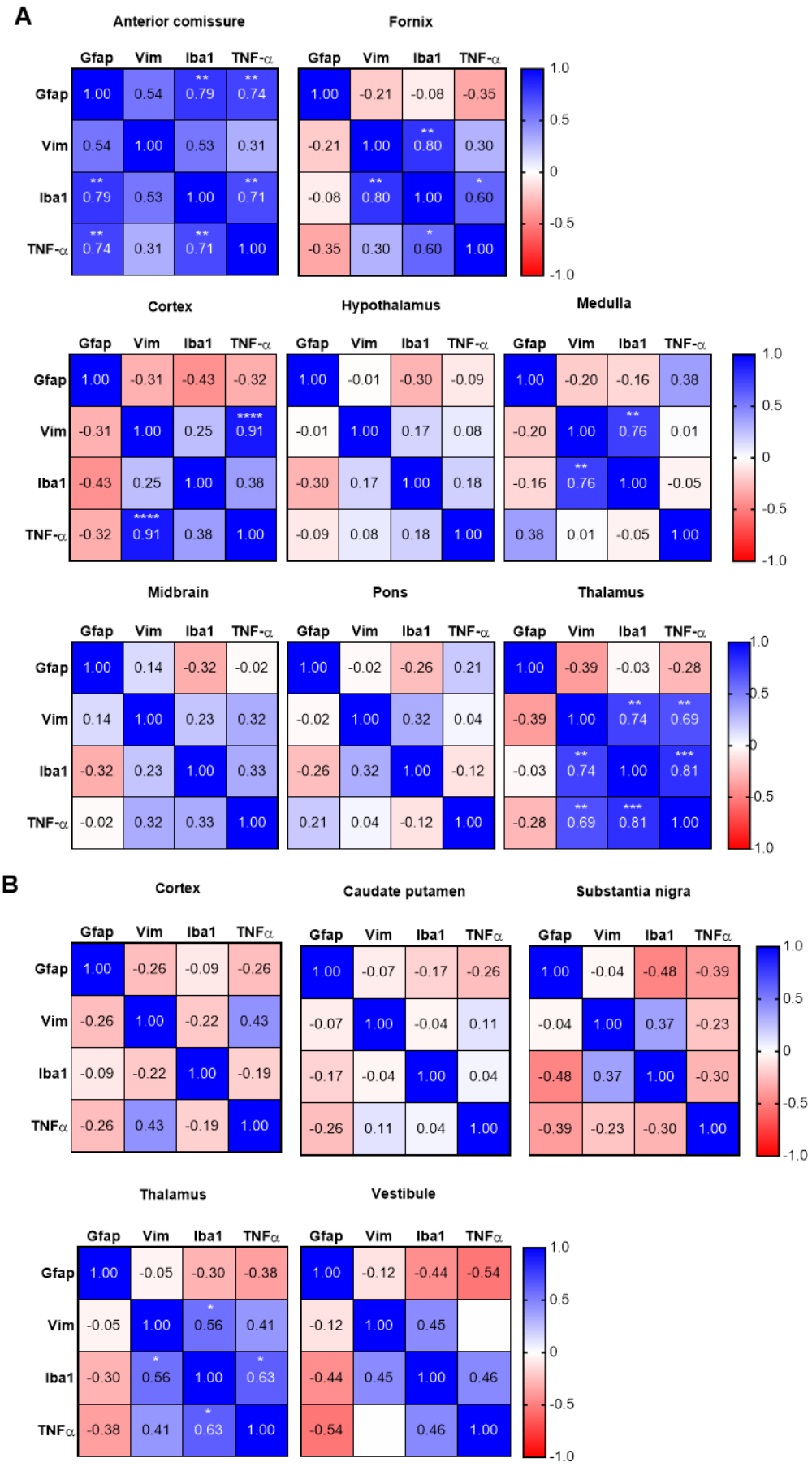
A
Anterior comissure
Fornix
Cortex
Hypothalamus
Medulla
Midbrain
Pons
Thalamus
B
Cortex
Caudate putamen
Substantia nigra
Thalamus
Vestibule
Gfap
Vim
Iba1
TNF-α
TNFα
1.0
0.5
0
-0.5
-1.0

Figure 4-23 Correlations between markers of inflammation (GFAP, vimentin, Iba1 and TNF-α) in the brain of prion infected mice. Immunohistochemical staining using antibodies against Iba1 (see Figure 4-16), astrocytic markers GFAP and vimentin (see Figure 4-11 and Figure 4-12), and RNAScope hybridisation using probes for mouse TNF-α (see Figure 4-20), were quantified using Imagescope software (version 12.2.1.5005; Aperio). All quantification data from 8 and 10 w.p.i., control and prion-infected mice was pulled together and used to analyse the correlation between GFAP, vimentin, Iba1 and TNF-α in large brain regions including cortex, hypothalamus, medulla, midbrain, pons, thalamus, Caudate putamen, substantia nigra and vestibule, and white matter tracks anterior comissure and fornix, at bregma lateral level 0.72mm **(A)** and 1.68mm **(B)**. Pearson correlation assuming Gaussian distribution where *P<0.05, **P<0.01,***P<0.001, ****P<0.0001 (N=12-14).

4.2.7 Pharmacological activation of the M1 mAChR restore memory and exert disease-modification of mouse prion disease

Since the presence of the M1 mAChR during disease is relevant for therapeutic targeting, receptor expression was assessed using western blot analysis in control- and prion diseased mice (Figure 4-24). Prion infected mice show similar M1 mAChR transcript and protein levels as control mice in cortex, hippocampus and striatum. Interestingly, the striatum showed higher expression levels of the M1 mAChR compared to the cortex. Statistical analysis however was not possible because of the low statistical power due the low sample numbers (N=2). However, previous studies also showed that M1 mAChR expression levels remain unchanged in the cortex and hippocampus of prion-diseased mice (Bradley et al., 2017).

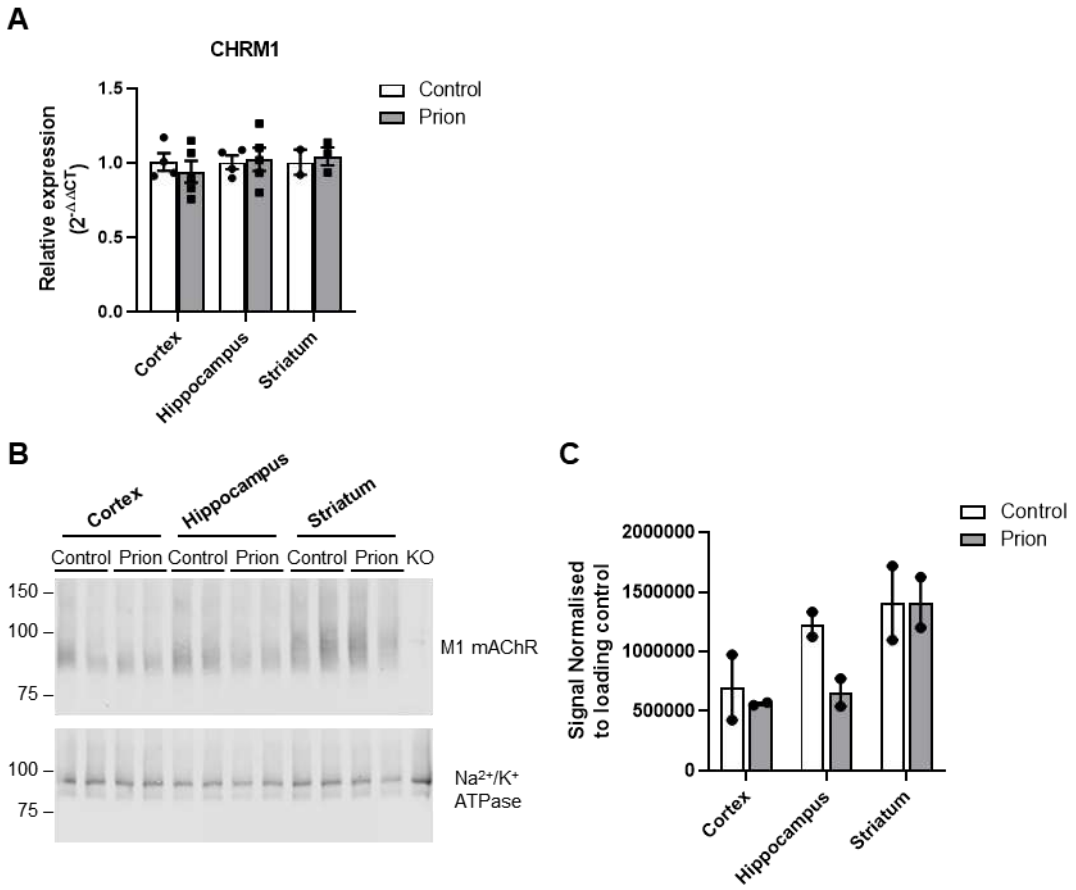

Figure 4-24 Expression of the M1 mAChR in prion infected Tg37 mice at 10 w.p.i. (A) Quantitative RT-PCR showing the expression of the M1 mAChR gene (CHRM1) mRNA in the cortex, hippocampus and striatum of control and prion-infected mice at 10 w.p.i. Data are expressed as a ratio of α-tubulin RNA expression (N=4-5 mice except 2-3 mice for striatum). **(B)** Membranes (15 µg) from cortex, hippocampus, and striatum of 10 w.p.i. control or prion-infected mice were probed in western blot using antibodies against the M1 mAChR. KO is a membrane sample from the cortex of an M1 mAChR-knock out mouse. The loading control is Sodium Potassium ATPase (Na2+/K+ ATPase) **(C)** Analysis of band intensities from (B) Receptor expression is shown as means ± S.E.M. normalised to the loading control, Na2+/K+ ATPase.

Control- and prion-infected mice (9 w.p.i.) were treated with an M1 mAChR-selective PAM VU0486846 (Rook et al., 2018, Bertron et al., 2018), to investigate the effects of M1 PAMs in a learning and memory test. Cognition in vehicle- and VU0486846- treated mice was then assessed using a fear conditioning test (Figure 4-25), that measures associative learning in which animals learn to associate the presence of a neutral stimulus i.e., tone, with a motivationally significant stimulus (the unconditioned stimulus) i.e., foot-shock. In addition, the fear conditioning protocol used allows the assessment of contextual memory in mice (Bradley et al., 2017). Hippocampal dysfunction was demonstrated to impair learning mediated by contextual cues (context retrieval), whereas lesions of the amygdala were shown to be associated to deficits in cued fear conditioning (tone retrieval) (LaBar and Disterhoft, 1998). Vehicle- and M1 PAM-

treated control mice showed appropriate contextual and cued fear conditioning responses by showing significantly higher immobility during context and tone retrieval compared to baseline conditions, indicating that their hippocampal and amygdala-based associative learning is intact. In the contrary, prion infected mice treated with vehicle show an apparent deficit in context and tone retrieval as the time spent immobile during retrieval did not significantly differ from the baseline. It should be noted that immobility levels of VU0486846-treated mice with prion disease did not differ from control mice. Nevertheless, VU0486846 treatment could restore contextual memory in prion infected mice. This was evident in the increased immobility during context retrieval of prion-infected mice treated with VU0486846 compared to baseline, at levels significantly higher than diseased mice dosed with vehicle. Tone retrieval showed no change in prion-infected mice treated with VU0486846 compared with vehicle. However, immobility levels of prion infected mice were similar to control mice, and the lack of significant difference between retrieval and baseline is likely due to increased motility of prion-infected mice during the baseline measurements. *Altogether, this data indicates that selective activation of the M1 mAChR using the VU0486846 PAM can restore hippocampal-based memory deficits in prion disease.*

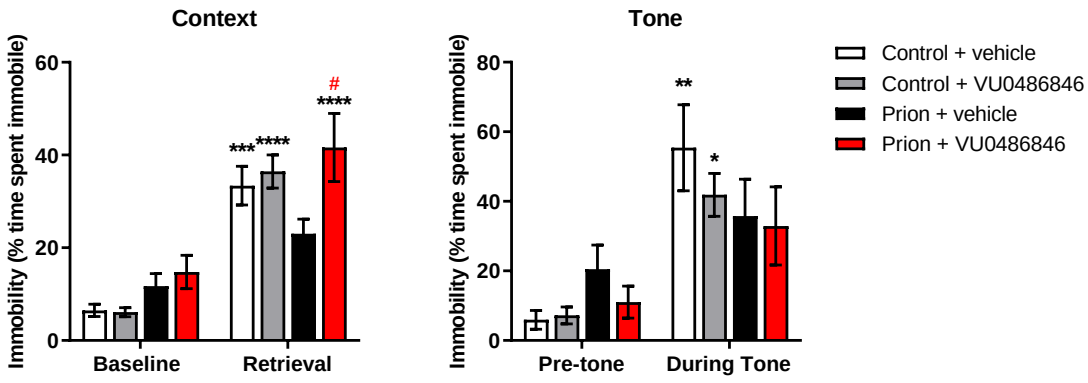

Figure 4-25 M1 PAM VU0486846 restores memory impairment in prion-infected mice. Fear-conditioning response of control and prion-infected mice following acute administration of vehicle (20% tween-80) or VU0486846 (10 mg/kg) prior to training and retrieval. Both contextual and cued (auditory tone) fear conditioning responses were tested. Data are shown as mean ± SEM. Statistical analysis performed was a two-way ANOVA with Sidak's multiple comparison test, where ****P<0.001, ***P<0.001, **P<0.01, *P<0.05 for prion versus control, and $^{\#}$P<0.05 for VU0486846 versus vehicle (N=15-17).

To investigate the impact of M1 mAChR selective activation on disease progression, prion-infected mice were dosed with VU0486846 (10 mg/kg) from 7

w.p.i., and disease severity was assessed based on symptom onset and survival of mice. Symptom onset was defined by the appearance of at least two of the early indicator signs of prion disease. Appearance of clinical signs of prion disease indicates terminal disease and the animals are culled defining their survival. Vehicle-treated prion diseased mice display a median symptom onset at 11.3 w.p.i. and their median survival is 12 w.p.i. The M1 PAM was able to significantly (P<0.01) delay symptom onset and extend the lifespan of prion ill mice by at least one week. Altogether, this shows that activation of the M1 mAChR can exert disease-modification in mouse neurodegenerative prion disease by significantly delaying symptom onset and extend the survival of terminally ill mice.

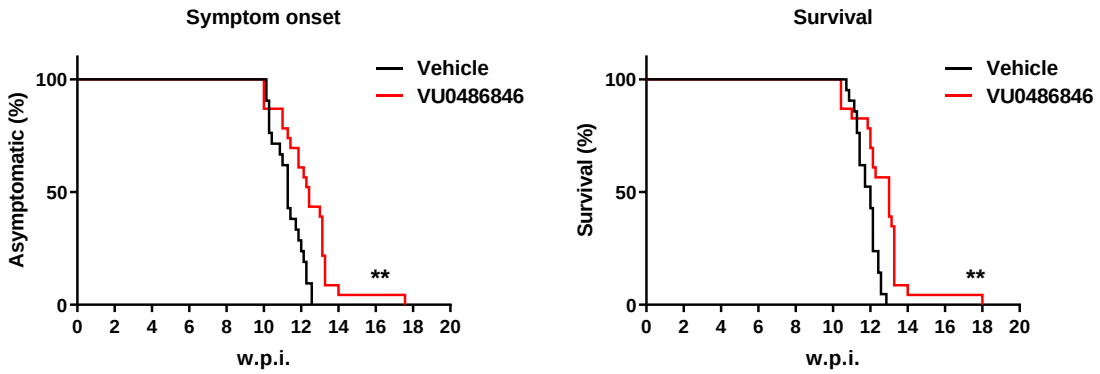

Figure 4-26 M1 PAM VU0486846 significantly delays symptom onset and extends the lifespan of prion-infected mice. Prion-infected mice were dosed with vehicle (20% tween-80) or VU0486846 (10 mg/kg) from 7 w.p.i. The appearance of at least two of the early indicators of disease (piloerection, sustained erect ears, erect penis, clasping of hind legs when lifted by tail, rigid tail, unsustained hunched posture, mild loss of coordination, and being subdued) indicated symptom onset. The additional appearance of one confirmatory sign or two confirmatory signs alone (ataxia, impairment of righting reflex, dragging of limbs, sustained hunched posture, and significant abnormal breathing) indicated clinical disease and culling of the mouse. Symptom onset and survival were analysed employing Kaplan-Meier survival plot (N=21-23) and curves were analysed with a Gehan-Breslow-Wilcoxon test, where **P<0.01.

4.3 Discussion

Insights in the pathogenesis of mouse prion disease could unravel mechanisms that are central to the development and progression of human neurodegenerations that spread through a prion-like mechanism such as AD, HD and PD (Halliday and Mallucci, 2015, Shi et al., 2015, Condello et al., 2020). In this chapter, an extensive analysis of the mouse prion disease model was conducted from 6 w.p.i. of RML prion infected Tg37 mice in several brain regions using biochemical and histology methods and to obtain a map of prion disease progression before symptom onset (Figure 4-27). This would also help the identification of early markers of prion neurodegeneration providing an important practical advantage over survival studies as such knowledge would enable the detection of disease modification earlier than at terminal stages.

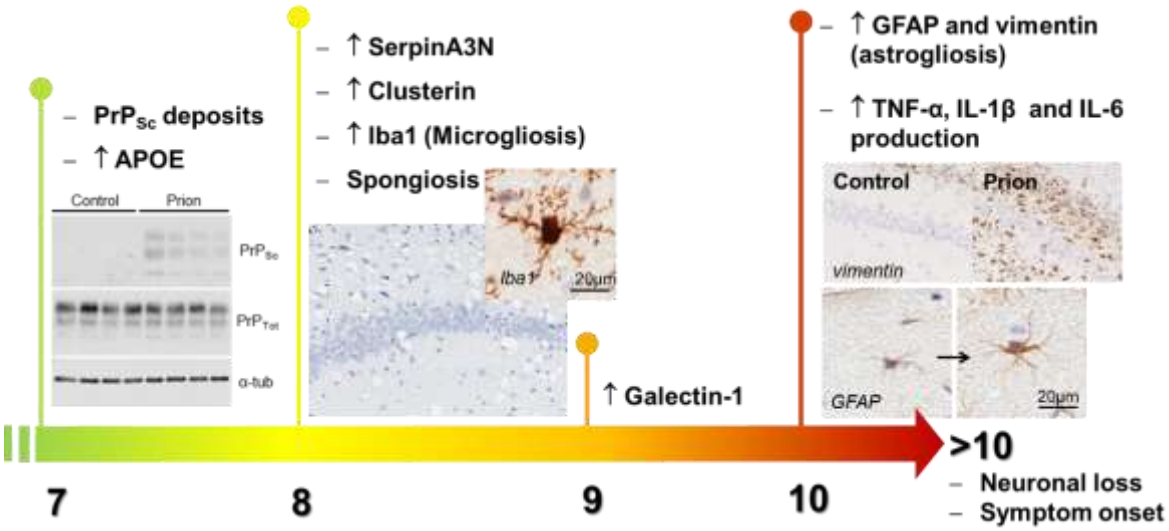

Figure 4-27 Chronological map of preclinical stages of mouse prion disease. Disease progression in RML prion infected Tg37 mice was mapped from preclinical stages of disease, prior disease onset that occurs after 10 w.p.i. The map was derived from data was obtained using a combination of biochemical analyses (RT-qPCR and western blot) and histology.

4.3.1 Accumulation of scrapie prion is the first marker of disease

Mouse prion disease progression depends on the accumulation and spreading of neurotoxic PrP_{Sc} (Mallucci, 2009). Similar to PrP_{Sc} in mouse prion disease, NFT pathology normally starts in the entorhinal cortex and hippocampus of AD patients before spreading to the associative isocortex, and its accumulation correlates with clinical features and severity of AD (Serrano-Pozo et al., 2011). Progressive accumulation of PrP_{Sc} was detected here using western blot analysis from 6 w.p.i. in the cortex, hippocampus, and striatum of RML-infected mice,

which is consistent with previous reports (Mallucci et al., 2007). This is an important finding because it establishes that prion infected Tg37 mice have already developed scrapie pathology at 7 w.p.i., when they are normally dosed for testing novel therapeutic M1 mAChR-selective ligands (Bradley et al., 2017, Dwomoh et al., 2021), when no physical symptoms are yet manifested. This establishes that the therapeutic effects exerted by activation of the M1 mAChR are not due to prevention of disease, but disease-modification.

Immunohistochemical staining using an antibody against aggregates made of 27-30 PrP_{Sc} (Abcam), however, only detected PrP_{Sc} in the hippocampus and neighbouring white matter tracks including the corpus callosum and fimbria. PrP_{Sc} staining was found particularly accumulated in the CA2 region, which was consistent with previous histological studies on hippocampal sections from prion infected Tg37 mice using a different PrP_{Sc} antibody (Mallucci et al., 2007). However, Mallucci et al. (2003) reported that PrP_{Sc} deposition in RML-infected Tg37 mice was also found in the cortex and thalamus. The antibody used for immunohistochemical staining in this chapter only recognises aggregates made of 27-30 PrP_{Sc} macromolecules and, although PrP_{Sc} peak infectivity is achieved by inoculation of 14-28 PrP aggregated molecules (Silveira et al., 2005), RML prion might form aggregates of a diverse range of sizes that might not be recognised by that specific antibody.

4.3.2 Prion disease in Tg37 mice advances rapidly between 8 and 10 w.p.i.

Similar to AD, murine prion disease is also characterised by the progressive loss of hippocampal cholinergic neuronal loss (Bradley et al., 2017, Bourgognon et al., 2018, Schliebs and Arendt, 2011). Specifically, neuronal loss in prion-infected Tg37 mice was reported to occur from 10 w.p.i. in the CA1 and CA3 regions together with the onset of the earliest symptoms (dishevelled appearance and poor grooming) (Mallucci et al., 2003), marking the onset of clinical pathology. Similarly, ME7 prion-infected mice also show conspicuous neuronal loss of hippocampal pyramidal cells during the later stages of disease (Cunningham et al., 2003, Jeffrey et al., 2000). Importantly, neuronal loss in the hippocampus of prion-infected mice was demonstrated to follow synaptic dysfunction and degeneration of presynaptic axons (Jeffrey et al., 2000).

Consistent with previous reports of neuronal loss in RML-infected Tg37 mice occurring from 10 w.p.i. (Mallucci et al., 2003), no significant neuronal loss was observed in the present study at 10 w.p.i. using immunohistochemical staining of NeuN, or western blotting using antibodies specific for presynaptic, postsynaptic, and cholinergic markers.

Spongiosis, that is the formation of intraneuronal vacuoles in cells that have not yet degenerated, was shown to proceed neuronal loss and clinical symptoms in mouse prion disease (Mallucci et al., 2003). Consistent with previous reports (Mallucci et al., 2003), I found that spongiosis is present in the hippocampus of RML-infected Tg37 mice from 8 w.p.i. and robustly increases to 10 w.p.i. This indicates that prion infected Tg37 mice at 10 w.p.i. are still at a stage of pre-clinical disease that proceed physical symptoms and neuronal loss while already manifesting the presence of PrP_{Sc} deposits in the hippocampus, cortex and striatum and hippocampal spongiosis. This is comparable to AD progression, whereby progressive depletion of pre-synaptic cholinergic neurons is in fact correlated with cognitive deficits and clinical dementia scorings (Davies and Maloney, 1976, Perry et al., 1977). Furthermore, this data demonstrates there is a dramatic, significant increase from 8 to 10 w.p.i. in all the pathological features observed, suggesting that during this two-week window the progression from subclinical to clinical pathology occurs, thereby representing a good indicator to assess the disease progression during drug studies.

4.3.3 Markers of neurodegenerative disease are detected at a pre-symptomatic stage of disease

A global unbiased transcriptomic and proteomic study conducted on RML prion and control infected Tg37 mice has found that murine prion disease displays the upregulation of proteins that are considered markers of AD. This included, for example, the upregulation of APO-E, regulator of proteolysis serpinA3N and markers of astrocytic and microglial activation galectin-1 and clusterin (Dwomoh et al., 2021). Here, APO-E, clusterin, galectin-1 and serpinA3N showed a trend to increase in prion-diseased mice from 7 or 8 w.p.i., at a pre-symptomatic phase of disease, with the most evident increases at 9 w.p.i. Both APO-E and clusterin (a.k.a. APOJ) are considered some of the highest risk factors for LOAD (Roses et al., 1995, Jiang et al., 2008, Lambert et al., 2009, Harold et al.,

2009). APO-E is the predominant apolipoprotein in the brain and plays a central role in Aß homeostasis by regulating their deposition and proteolysis (Zlokovic et al., 2005, Holtzman, 2001). The APO-E isomer E4, that displays impaired ability to promote Aß clearance, is associated to increased risk of LOAD (Roses et al., 1995, Jiang et al., 2008). Interestingly, elevation in APO-E has also been associated with human prion disease (Choe et al., 2002, Wei et al., 2011). Similar to APO-E, clusterin is also able to interact with Aß to regulate its aggregation and it was found upregulated in the cortex and hippocampus of AD patients, colocalised with Aß plaques (May et al., 1990) and also upregulated in the CSF of people with AD (Nilselid et al., 2006). However, the role of clusterin in AD has been ambiguous. Whilst some studies have demonstrated clusterin is able to promote clearance of Aß displaying neuroprotective activity (Yeh et al., 2016, Zandl-Lang et al., 2018, DeMattos et al., 2002), other reports showed that clusterin reduces Aß clearance and might instead promote Aß-mediated neurotoxicity (Killick et al., 2014, Robbins et al., 2018). Clusterin was also found to be associated with late stages in mouse ME7 prion disease (Asuni et al., 2014), and to be able to interact with protease-resistant PrP aggregates from CJD brains, suggesting that clusterin might be involved in PrP aggregation and sequestration (Freixes et al., 2004). However, this mechanism is yet to be explored. The upregulation of APO-E and clusterin in the brain of prion-infected mice further support the concept that mouse prion disease shares central disease-adaptive mechanisms with human neurodegenerations. In addition, the mouse prion disease model can be considered relevant for the investigation of AD pathogenesis, particularly for the potential modification of later stages of disease progression, as APO-E and clusterin are markers for LOAD. Strikingly, the M1 PAM VU0486846 could significantly decrease the levels of APO-E and clusterin in the hippocampus prion-ill mice, to levels similar to the healthy controls (Dwomoh et al., 2021).

SerpinA3N inhibits serine proteases that include cathepsins, chymases and elastases (Huntington et al., 2000). SerpinA3N has been associated to neurodegenerative conditions, especially AD where it has been found to be colocalised with Aß peptides, astrocytes and NFTs (Rozemuller et al., 1991, Gollin et al., 1992). Transgenic mouse models overexpressing astrocytic serpinA3N together with mutant APP were reported to have higher age-related

Aß pathology compared to mice expressing mutant APP alone (Mucke et al., 2000, Nilsson et al., 2001). Similarly, serpinA3 mRNA was found upregulated in the CNS of patients deceased from different forms of prion disease, especially striking elevation in CJD brains that showed up to about 350 fold increased compared to healthy subjects (Vanni et al., 2017). Importantly, by employing RML-infected CD1 mice, it was demonstrated that serpinA3N upregulation occurs in preclinical/pre-symptomatic stages of disease, displaying a direct correlation between this protein and prion disease progression (Vanni et al., 2017), which was consistent with previous studies in other mouse models of prion disease (Miele et al., 2008, Campbell et al., 1994, Dandoy-Dron et al., 2000). Consistent with these findings, in this chapter serpinA3N was found to be the most robustly upregulated disease marker, especially in the cortex and striatum, compared to APO-E, clusterin or the inflammatory markers investigated, thus indicating that this protein might be a marker of earlier stages of disease. Although the mechanism has not been yet understood, it is suggested that serpinA3 up-regulation might hamper the clearance of misfolded proteins over time, prions for prion diseases and Aß peptides in AD. Therefore, the upregulation of serpinA3N observed in RML prion-infected mice might be a disease-adaptive process in response to the progressing accumulation of PrP_{Sc}.

4.3.4 Neuroinflammation is exacerbated in mouse prion disease

The mouse prion disease model displays the elevation of markers of neuroinflammation that are shared with human neurodegenerations, including Iba1, GFAP and vimentin (Dwomoh et al., 2021, Heneka et al., 2015, Ransohoff, 2016). In prion disease, it has been established that microglia activation occurs in regions of PrP_{Sc} deposition and in response to PrP_{Sc} accumulation, displaying both neurotoxic and neuroprotective phenotypes during pathogenesis, corresponding to the M1 and M2 groupings of macrophages, respectively (Bate et al., 2002, Williams et al., 1997, Giese et al., 1998, Van Everbroeck et al., 2004, Kercher et al., 2007, Sandberg et al., 2014, Vincenti et al., 2015, Gómez-Nicola et al., 2013, Martinez and Gordon, 2014). Consistent with previous studies, the RML prion-infected Tg37 mice show the most significant upregulation in Iba1-stained microglia in the areas of PrP_{Sc} deposition such as the CA1 and CA2 hippocampal regions, corpus callosum and fimbria. Specifically, the increase seemed to be in the number of larger microglia ranging from 100 to 250 µm in

diameter. The relatively small increase in microglia (1.2 to 2-fold increase relative to controls) might be explained by the background presence of microglia, supposedly inactive, in the CNS of healthy control mice. Similarly, microglia were found in the brain of AD patients and in animal models of AD surrounding Aß plaques (Salter and Stevens, 2017). In AD, the inefficient clearance of Aß plaques leads to the sustained activation of microglia that can induce highly damaging neurotoxic effects by producing a variety of cytotoxic factors including superoxide, nitric oxide, and TNF-α, as well as further exacerbating inflammation by secreting pro-inflammatory cytokines such as IL-1ß (Block et al., 2007, Moss and Bates, 2001, Liu et al., 2015, Sawada et al., 1989, Lee et al., 1993). In the present study, IL-1ß, IL-6 and TNF-α transcripts were found elevated in the brain of prion-infected mice at 10 w.p.i. Interestingly, using RNAScope, TNF-α transcripts were found to be mostly produced in the CA2 hippocampal region, cortex and thalamus of RML prion infected Tg37 mice, which corresponds to the brain regions displaying most scrapie pathology (Mallucci et al., 2003).

Similar to AD, the role of microglia in the progression of prion disease remains ambiguous. Some studies showed that microglia are protective in prion disease. For instance, microglia depletion by around 98% of organotypic brain slices infected with RML prions displayed a 15-fold increase in PrP_{Sc} deposits (Falsig et al., 2008). In addition, chemical depletion of microglia using the CSF-1R tyrosine kinase inhibitor PLX5622 that prevents microglial survival (Elmore et al., 2014) significantly accelerated prion disease progression, PrP_{Sc} deposition, astrogliosis and spongiosis in mice infected with RML, ME7 or 22L prion strains (Carroll et al., 2018). In contrast, treatment of prion-diseased mice (ME7 and 22L) with the CSF-1R inhibitor GW2580 caused a 50% reduction in microglia and significantly delayed the disease progression and the onset of behavioural symptoms, and significantly extended the lifespan of terminally ill mice (Gómez-Nicola et al., 2013).

Astrogliosis is another component of neuroinflammation and is usually identified by the upregulation of GFAP and vimentin, the main proteins forming intermediate filaments in astrocytes (Middeldorp and Hol, 2011, Danielsson et al., 2018). Although GFAP and vimentin are natural partners in the formation of astrocytic intermediate filaments (Quinlan and Franke, 1983), their co-assembly

is not required and their co-expression varies in different brain regions (Middeldorp and Hol, 2011). Here, GFAP was demonstrated to undergo a widespread upregulation across the brain of prion-infected mice, whereas vimentin showed higher region specificity and more regional correlations with PrP_{Sc} deposits. Immunohistochemical staining showed here a striking upregulation of vimentin in the hippocampus, thalamus and cortex, that are brain regions that normally display most deposition of PrP_{Sc} (Mallucci et al., 2003). Further, previous studies on 22L prion-infected mice showed that astrocytes are particularly activated in the cortex, hippocampus or thalamus in response to prions (Makarava et al., 2019). Hypertrophic reactive astrocytes were also shown to accumulate near senile plaques, and are normally found in post-mortem AD brains (Medeiros and LaFerla, 2013). Astrocytes were demonstrated to be able to internalise and degrade Aß *in vivo* (Wyss-Coray et al., 2003), as well as promote Aß clearance by APO-E-mediated microglia activation and upregulating the expression of extracellular Aß-targeting proteases (Koistinaho et al., 2004, Jiang et al., 2008, Terwel et al., 2011). It is likely that activated astrocytes play a similar function in prion disease, to carry out the depletion of prion aggregates.

The differential, region-specific expression of GFAP and vimentin support the concept of astrocyte heterogeneity, whereby astrocytes assume various phenotypic profiles and exert multiple different functions in prion disease. Similar to the M1 and M2 macrophage groupings, reactive astrocytes can assume two different types in neuroinflammation, termed A1 and A2, that correspond to neurotoxic and neuroprotective phenotypes, respectively. A1 reactive astrocytes were found localised in brain regions involved in neurodegeneration in several diseases including AD, PD, HD and multiple sclerosis (Liddelow and Barres, 2017) and they have neurotoxic and pro-inflammatory activity (Stevens et al., 2007, Hong et al., 2016, Liddelow and Barres, 2017, Gilmore, 2006). In contrast, A2 astrocytes are characterised by the genetic upregulation of neurotrophic factors and genes responsible for synaptogenesis and tissue repair (Liauw et al., 2008, Zamanian et al., 2012) and carry out phagocytosis and clearance of debris and dead cells (Tasdemir-Yilmaz and Freeman, 2014, Chung et al., 2013). Here, vimentin was found especially elevated in sites of microgliosis and spongiosis, leading to the hypothesis that vimentin might be specifically linked to reactive

astrocytes with a neurotoxic phenotype. In support of this hypothesis, vimentin was previously shown to contribute to microglia activation and neurotoxicity in cerebral ischemia (Jiang et al., 2012).

Galectin-1 is a glycan-binding protein that ,together with other galectins, modulates astrocyte and microglia activation in response to insult by a specific lectin-glycan interaction, and regulates several immunological responses including apoptosis, cell activation, and cytokines release (Dhirapong et al., 2009). Here, increases in galectin-1 were detected in the hippocampus of prion diseased mice at 9 w.p.i. This is consistent with previous reports that found increases in galectin-1 in the brains of scrapie-infected rodents, as well as in the cortex of post-mortem brains from prion disease patients (Guo et al., 2017). Galectin-1 was shown to have neuroprotective effects and has been proposed as a target for the treatment of chronic neuroinflammatory and neurodegenerative diseases (Ramírez Hernández et al., 2020). Upregulation of galectin-1 was shown to hamper the proliferation of astrocytes, inhibit microglia activation while enhancing M2 microglial phenotype, and promote neurogenesis by inducing brain-derived neurotrophic factor (BDNF) to repair damaged tissue (Qu et al., 2011, Starossom et al., 2012, Sasaki et al., 2004, Ishibashi et al., 2007, Li et al., 2020). Interestingly, a preliminary study on aged PDAPPJ20 transgenic mice has shown that the administration of galectin-1 significantly enhanced cognition in a NOR test and induced a robust reduction in Aß in the hippocampus (Presa et al., 2019).

The deposition and spreading of PrP_{Sc} is closely associated with locally induced chronic neuroinflammation, that is similar to Aß plaques and NFT in AD. Given this parallel, elucidating the role of neuroinflammation in the mouse prion disease could provide insights into the modulation of the neuroinflammatory response in human neurodegenerations and might help resolve the dispute on whether neuroinflammation is beneficial or detrimental in neurodegenerative disease (Allaman et al., 2011, Ben Haim et al., 2015). Further, since the M1 PAM VU0486846 could significantly reduce the levels of galectin-1, GFAP and vimentin in prion diseased mice (Dwomoh et al., 2021), an intriguing concept is that activation of the M1 mAChR is able to modify disease progression by decreasing detrimental neuroinflammation and/or altering the ratio between neurotoxic and neuroprotective reactive astrocytes.

4.3.5 The mouse prion disease model to investigate the disease-modifying potential of the M1 mAChR

Despite significant advances in the understanding of AD pathophysiology, there are currently no treatments that can stop or slow down its disease progression (Lane et al., 2018). The M1 mAChR is a promising, validated target for the treatment of AD as selective activation of this GPCR could not only improve cognitive deficits in AD patients but was also demonstrated to exert disease-modifying effects in preclinical animal models of disease (Scarpa et al., 2021). The M1 mAChR is found highly expressed in the forebrain, including the cerebral cortex and hippocampus (Levey, 1993, Volpicelli and Levey, 2004), where it is the predominant muscarinic receptor subtype (Bradley et al., 2017) and is involved in cognitive functions, especially in short-term memory which is affected in AD (Fisher, 2008b, Ladner and Lee, 1998). The M1 mAChR was demonstrated in this chapter to also be expressed in the cortex, hippocampus and striatum of prion-diseased mice, and, similarly to observations in AD patients (Levey, 1996, Svensson et al., 1992), its expression remains relatively unaltered with disease compared to healthy mice. Importantly, since AD neurodegeneration mostly affects presynaptic neurons and the M1 mAChR is expressed postsynaptically (Levey, 1996, Svensson et al., 1992), drugs directly targeting the M1 mAChR would likely remain efficacious in late-stage AD, further validating this GPCR as a promising drug target for the treatment of dementias (Fisher, 2008a).

As opposed to other commonly used mouse models of AD, mouse prion disease is a progressive and terminal neurodegenerative condition that is advantageous to test both pro-cognitive activity and disease-modifying potential of M1 mAChR ligands. In fact, at early stages of prion disease, whilst mice show no physical signs of disease, they manifest biochemical and histopathological evidence of disease as well as behavioural changes such as a decline in burrowing behavior and a deficit in learning and memory. As the disease progresses to late stages, mice develop terminal clinical symptoms that allow the testing of the effectiveness of novel M1 mAChR ligands on survival. By using the prion disease model, Bradley et al. (2017) demonstrated that a highly selective M1 PAM, BQCA, could not only reverse memory deficits, but also significantly extend the lifespan of terminally-ill prion disease mice. In accordance with these previous

findings, a novel M1 PAM, VU0486846 (Rook et al., 2018, Bertron et al., 2018), was demonstrated here to be able to reverse cognitive deficits by restoring the contextual memory retrieval of prion diseased mice in a fear conditioning paradigm. No changes in tone retrieval were detected in prion diseased mice compared to healthy animals, but this could be since impairments in tone memory retrieval are associated with lesions of the amygdala, which are not expected be present in prion diseased mice. In contrast, impairments in contextual learning were shown to be associated to hippocampal dysfunction, which is a hallmark of mouse prion disease (Bradley et al., 2017, Mallucci et al., 2007, LaBar and Disterhoft, 1998). The pro-cognitive activity of VU0486846 was also proven in other studies. VU0486846 could significantly enhance memory in NOR and fear conditioning paradigms in rats with risperidone-induced cognitive deficits (Rook et al., 2018), as well as improve working memory in aged nonhuman primates (cynomolgus monkeys) in a touchscreen-based attention task (Norman et al., 2020).

In addition, administration of VU0486846 (10 mg/kg) from 7 w.p.i., could significantly delay symptom onset and robustly prolong the lifespan of terminally ill prion infected mice. Unbiased proteomics and transcriptomics studies on hippocampi taken from VU0486846 (10 mg/kg) or vehicle- treated, control and prion infected mice, demonstrated that mouse prion disease features AD-related neuropathology. This featured the profound upregulation of markers of neuroinflammation, markers of AD such as clusterin and APO-E, markers of synaptic loss and neuronal dysfunction as well as the elevation of proteins associated to the clearance of misfolded proteins (Dwomoh et al., 2021). Importantly, Dwomoh et al. (2021) found that VU0486846 could reduce many of the disease-associated markers to levels similar to the healthy control mice. This study indicated that the disease-modifying potential of M1 PAMs might reside in the ability of the M1 mAChR to regulate adaptive responses such as neuroinflammation that are common features of the pathology of brain diseases caused by the propagation of misfolded protein. Importantly, given the parallels between mouse prion disease and AD (Table 4-3), the therapeutic, disease-modifying potential of the M1 mAChR demonstrated here is likely relevant for the treatment of human neurodegenerative conditions.

	W.P.I.	MOST AFFECTED REGIONS	SIMILARITIES WITH AD
PrP_{Sc}	7	Hippocampus (CA2)	NFT pathology
APO-E	7	Hippocampus, striatum	A\beta proteolysis; APO-E4 isoform associated to increased risk of LOAD
Spongiosis	8	Hippocampus (CA1, CA2)	N/A
Clusterin	8	Hippocampus, cortex	Aß proteolysis; risk factor for LOAD
SerpinA3N	8	Hippocampus, cortex, striatum	unclear mechanism, potentially inhibits clearance of misfolded peptides; preclinical stages
Iba1	8	Hippocampus (CA1, CA2), cc, fimbria	activate and initiate proinflammatory mechanism upon binding to Aß
Galectin-1	9	Hippocampus	modulates neuroinflammation and prevent neurodegeneration in models of PD and AD
GFAP	10	Widespread	astrocytes accumulate near senile plaques
Vimentin	10	Hippocampus, cortex, thalamus	astrocytes accumulate near senile plaques
Neuronal Loss	>10	Hippocampus (CA1 and CA3)	Hippocampal neuronal loss of presynaptic cholinergic neurons

Table 4-3 The mouse prion disease model displays similarity with AD pathology. This table includes a summary of the similarities between the disease progression of the mouse prion disease model (RML inoculated Tg37 mice) and AD pathology, as discussed in this chapter. References are included in Discussion.

Chapter 5 Phosphorylation of the M1 muscarinic acetylcholine receptor protects from neurodegenerative disease

5.1 Introduction

The number of people living with dementia, of which AD accounts for ~70% of cases, is estimated to be ~50 million worldwide, and is predicted to more than double by 2050 to reach 139 million cases (Lane et al., 2018, World Health Organization, 2020). There is currently no treatment that can stop, prevent, or slow down disease progression, highlighting an unmet clinical need for novel treatments that not only improve cognitive symptoms but also confer disease-modification. The M1 mAChR is a validated target for the treatment of AD and other neurodegenerative diseases (Felder et al., 2018, Foster et al., 2014). Selective pharmacological activation of the M1 mAChR was demonstrated to significantly improve cognition in AD patients, and importantly to exert disease-modifying effects in animal models of neurodegenerative disease and AD (Bradley et al., 2017, Scarpa et al., 2020, Lebois et al., 2017, Bodick et al., 1997a). However, the generation of clinically effective M1 mAChR drugs has been challenging due to adverse effects associated with off-target activation of peripheral M2 and M3 mAChRs (Bymaster et al., 2003a, Melancon et al., 2013) as well as on-target activity at the M1 mAChR (Rook et al., 2017, Engers et al., 2018, Moran et al., 2018b). Like other GPCRs, the M1 mAChR can modulate multiple physiological responses by coupling to two fundamental signalling pathways: the G protein-dependent, and phosphorylation/arrestin-dependent signalling pathways. This highlights the need to investigate the physiological role of M1 mAChR-mediated signalling pathways in neurodegenerative disease and identify the pathways that lead to neuroprotective and clinically beneficial outcomes.

5.1.1 Evidence for clinical cognitive improvement by M1 mAChR ligands

Current frontline treatments for cognitive dysfunction of AD consist of AChE inhibitors, which aim to upregulate the compromised cholinergic signalling (Sanabria-Castro et al., 2017) by preventing the breakdown of ACh at the synapse (Bartus et al., 1982, Francis et al., 1999, Thompson et al., 2004). However, AChE inhibitors such as donepezil, rivastigmine, galantamine and tacrine are temporary symptomatic treatments that are only efficacious for mild to moderate AD (Neugroschl and Wang, 2011). In addition, their non-specific

nature is a drawback, causing GI and cardiovascular side effects induced by potentiation of peripheral cholinergic signalling including exocrine secretions, bradycardia, and GI distress due to contraction of cardiac and smooth muscle (Courtney, 2004, Inglis, 2002). This results in modest overall efficacy of AChE inhibitors in improving cognition and dose limitations, highlighting the need for pharmacological approaches with higher selectivity to upregulate cholinergic signalling in the brain.

Significant preclinical and clinical data suggest that selective activation of the M1 mAChR may offer an alternative strategy for improving cognitive function in AD, whilst avoiding issues that are associated with the non-selective mode of action of AChE inhibitors (Inglis, 2002, Courtney, 2004). The first attempt to offer an alternative to AChE inhibitors was led by xanomeline, a muscarinic agonist that was proposed as an M1/M4-preferring agonist. Xanomeline reached Phase II clinical trials and was shown to improve cognitive and behavioural symptoms in AD patients (Bodick et al., 1997b). The promising clinical outcomes prompted a smaller trial of xanomeline in schizophrenia, with similarly positive results (Shekhar et al., 2008).

Following the initial successful outcome of xanomeline in clinical trials (Bodick et al., 1997a), other M1 mAChR-selective orthosteric agonists have been proposed for the treatment of AD. An orthosteric M1 mAChR agonist, HTL0009936, was pursued by Sosei-Heptares in partnership with Allergan in a Phase 1b clinical trial. HTL0009936 showed robust pro-cognitive changes in brain activity even at low doses and it was well tolerated and devoid of cholinergic side effects associated with previous muscarinic orthosteric agonists (Bakker et al., 2021, Brown et al., 2021). Furthermore, HTL0018318, a selective M1 agonist, has been tested as a potential symptomatic treatment in Phase 1b and Phase 2 clinical trials for AD and other dementias, such as dementia with Lewy bodies (Bakker et al., 2020). HTL0018318 was reported to be well tolerated in humans after 28 days treatment. However, Sosei-Heptares announced the voluntary suspension of their clinical development activities with HTL0018318 due to an unexpected single animal toxicology study in non-human primates which was investigating different dosing levels over a nine-month period.

In the effort to improve the receptor subtype selectivity of muscarinic ligands, and therefore minimise peripheral side effects, drug discovery programmes have focussed on the development of M1 muscarinic ligands that target allosteric sites. BQCA, the first prototypical, highly selective M1 mAChR PAM (Ma et al., 2009), was able to significantly improve cognition in a scopolamine-induced amnesic mouse model, showing similar pro-cognitive effects to orthosteric muscarinic ligands (Ma et al., 2009). Administration of BQCA was also proven to reverse cognitive deficits in Tg2576 mice, the Aß mouse models that carry the AD-associated APP Swedish mutations (Shirey et al., 2009), and mice with prion neurodegenerative disease (Bradley et al., 2017). A structurally related PAM, PQCA, was subsequently shown to improve cognition in mice, rats and non-human primates (Uslaner et al., 2013, Lange et al., 2015) as well as in aged Tg2576 mice (Puri et al., 2015). Importantly, PQCA was shown to not only reverse memory deficits in scopolamine-treated monkeys but was also found devoid of cholinergic side effects compared to xanomeline and donepezil (Vardigan et al., 2015). These observations highlighted the potential of M1 PAMs as efficacious alternative for symptomatic treatment of AD that is safer than AChE inhibitors and muscarinic orthosteric agonists.

A selective and potent M1 ago-PAM, MK-7622, developed by Merck based on the BQCA chemical scaffold, displayed robust intrinsic activity in the absence of ACh, and was shown effective at reversing scopolamine-induced deficits in non-human primates and in humans (Uslaner et al., 2018). However, the initial clinical trial with MK-7622 was halted because the adjunctive therapy alongside AChE inhibitors failed to induce symptomatic improvements. Furthermore, 25% of the patients in the clinical trial experienced cholinergic side effects in response to MK-7622 (Voss et al., 2018). Preclinical studies in rats, dogs, and cynomolgus monkeys led by Bristol-Myers Squibb (Alt et al., 2016), and in mice and rats by Pfizer (Davoren et al., 2016) have also reported cholinergic toxic effects and behavioural convulsions following administration of highly selective M1 ligands. These observations indicated that despite encouraging preclinical data, selective M1 PAMs might still cause associated cholinergic adverse effects and lack pro-cognitive efficacy *in vivo*.

Targeting the M1 mAChR using bitopic ligands may offer more advantages compared to orthosteric ligands because they combine the pharmacology of both

orthosteric and allosteric ligands. Bitopic ligands have the potential to confer increased selectivity over the first-generation of muscarinic ligands, such as xanomeline, while maintaining the efficacy of orthosteric ligands. The bitopic ligand GSK1034702, developed by GlaxoSmithKline, entered clinical trials in 2008 (Nathan et al., 2013). GSK1034702 was initially described as a selective allosteric agonist at the M1 mAChR (Budzik et al., 2010), however it was later revealed to possess a bitopic mode of action, concomitantly interacting with the orthosteric binding pocket and allosteric site (Bradley et al., 2018). In clinical trials, GSK1034702 was shown to improve episodic memory in humans with nicotine abstinence-induced cognitive impairments. Despite being reported to be well tolerated, this compound still caused adverse GI responses in a proportion of patients (Nathan et al., 2013). This suggests that bitopic ligands can still be associated with cholinergic adverse side effects, as they are still able to interact with the highly conserved orthosteric binding pocket, and thereby activate other members of the muscarinic receptor family.

5.1.2 M1 mAChR ligands exert disease-modifying effects in preclinical animal models

Early studies *in vitro* demonstrated that activation of the M1 mAChR could reduce accumulation of AD-associated Aß pathology by interfering with APP processing *via* a PKC-dependent mechanism (Nitsch et al., 1992, Buxbaum et al., 1992) (Figure 5-1). Later, AD patients showed an overall reduction in levels of total Aß in the cerebrospinal fluid in a small trial of muscarinic agonists AF102B (Nitsch et al., 2000) or talsaclidine (Hock et al., 2000), unraveling the disease-modifying potential of targeting M1 mAChRs for the treatment of Aß pathology. Additionally, administration of the M1 muscarinic agonist AF267B on a triple transgenic mouse model of AD that exhibits both Aß and tau pathology (3xTg-AD) has been shown to not only reverse cognitive symptoms, but also to decrease the Aß and tau pathologies in these mice (Caccamo et al., 2006). In particular, reduction of Aß plaques was demonstrated to be mediated by the M1 mAChR stimulation *via* an increase in the α-secretase ADAM17/TACE *in vitro* that shifted processing of APP toward non-amyloidogenic pathways, through distinct mechanisms involving both PKC activation and ERK1/2 phosphorylation (Buxbaum et al., 1998, Haring et al., 1998, Caccamo et al., 2006) (Figure 5-1). However, acute receptor stimulation or loss of M1 mAChRs in a transgenic APP

mouse model, which carries APP with the AD-linked Swedish and Indiana mutations, did not alter ADAM expression level (Davis et al., 2010). Although these studies established that pharmacological activation of the M1 mAChR could exert disease-modifying effects by altering APP processing, the agonists used in these studies were relatively non-selective suggesting that the outcome observed might be caused by activation of both M1 and M3 subtypes, since both couple to $G\alpha_{q/11}$ pathways (Nitsch et al., 1992). However, it was later established that alterations of APP processing were mediated by the M1 mAChR specifically, as carbachol promoted the secretion of non-amyloidogenic α-secretase-cleaved APP fragments in neuronal cultures, but this effect was significantly reduced in cultures derived from M1 mAChR knockout mice (Davis et al., 2010).

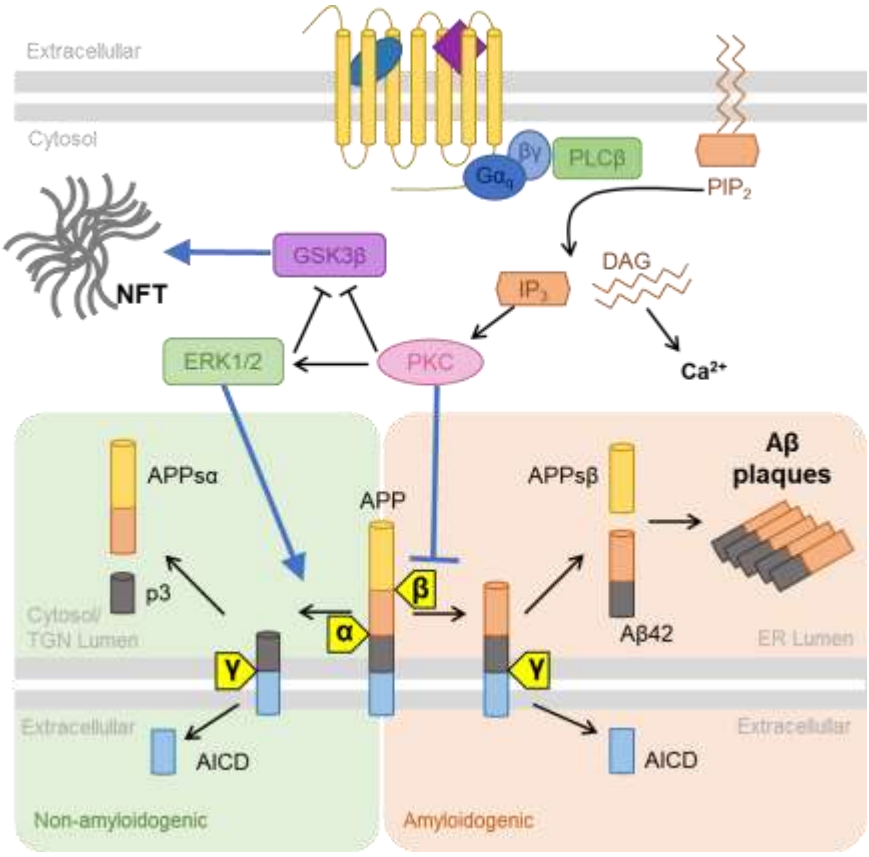

Figure 5-1 Regulation of amyloidogenic processing in AD mediated by the M1 mAChR. The proteolytic processing of APP can occur *via* a non-amyloidogenic or amyloidogenic pathways. In the non-amyloidogenic pathway, APP is initially cleaved by α-secretase within the Aβ peptide region, which prevents the formation of Aβ plaques by yielding to soluble APPα (APPsα), p3 fragment, and amyloid precursor protein intracellular domain (AICD) Stimulation of the M1 mAChR was shown to enhance non-amyloidogenic processing of APP *in vitro via* PKC- and ERK1/2-dependent mechanisms, which result in the activation of α-secretase and inhibition of β-secretase. Furthermore, M1 mAChR signalling has been shown to reduce the formation of NFTs by inhibition of GSK3β that decreases the level of hyperphosphorylated tau. In the amyloidogenic pathway, APP is cleaved by β-secretase followed by the subsequent cleavage by γ-secretase that leads to AICD, soluble APPsβ and Aβ42 fragments. APPsβ and Aβ42 fragments can aggregate resulting in Aβ plaques. Figure taken from (Scarpa et al., 2020).

Ligands with higher subtype selectivity were also reported to have disease-modifying potential *in vitro* and *in vivo*. A highly selective M1 mAChR allosteric agonist with no agonist activity at any of the other muscarinic subtypes, TBPB, was shown to promote secretion of soluble APP and reduced levels of Aß plaques *in vitro* (Jones et al., 2008). The M1 mAChR selective bitopic ligand VU0364572 was able to prevent the onset of cognitive deficits, and reduce levels of toxic Aß species and Aß pathology in the hippocampus and cortex of 5XFAD mice, that express human APP and PSEN1 transgenes with a total of five AD-linked mutations (Lebois et al., 2017). Furthermore, AF710B, a selective allosteric agonist of the M1 mAChR and sigma-1 receptor, was reported to improve cognition and reduce Aß pathology in 3xTg-AD mice (Hall et al., 2018). A study on murine prion disease, a model of terminal neurodegeneration that shares many disease features with AD and other proteinopathies (Bourgognon et al., 2018, Dwomoh et al., 2021), demonstrated that the M1 mAChR PAM BQCA could not only reverse memory deficits and improve hippocampal functions, but also significantly extend the lifespan of terminally ill mice (Bradley et al., 2017). A consequent global proteomic and transcriptomic analysis of the same mouse prion disease model demonstrated that a highly selective M1 mAChR PAMs BQCA and VU0486846, could also improve cognition and slow down disease progression in prion infected mice (Dwomoh et al., 2021). Importantly, this study demonstrated that the M1 mAChR PAM could induce disease-modification by reducing disease-associated adaptive responses such as neuroinflammation and mitochondrial/redox homeostasis while maintaining synaptic function and preventing the propagation of misfolded protein (Dwomoh et al., 2021).

5.1.3 Challenges with on-target adverse effects associated to M1 ligands

Allosteric modulators hold the promise of overcoming the challenge of cholinergic adverse responses by providing exquisite receptor subtype selectivity for the M1 mAChR (Gregory et al., 2007). However, even highly selective M1 mAChR PAMs have now been associated with adverse responses (Moran et al., 2018b, Engers et al., 2018, Rook et al., 2017).

For example, two M1 PAMs with high intrinsic activity, MK-7622 and PF-06764427, were tested for their pro-cognitive effects and adverse effect liability

in comparison with VU0453595 and VU0550164, two M1 PAMs that are devoid of intrinsic activity (Moran et al., 2018b). MK-7622 and PF-06764427 induced severe behavioural convulsions in mice, whereas VU0453595 did not. Additionally, in a NOR test, MK-7622 caused no significant cognitive improvement whereas VU0453595 showed robust efficacy in improving cognitive function (Moran et al., 2018b). A potent M1 ago-PAM, PF-06827443, also displayed cholinergic adverse effects and severe seizures in dogs (Moran et al., 2018a). These findings strongly suggested that M1 PAMs with high levels of intrinsic activity have higher adverse effect liability (i.e., behavioural convulsions), likely caused by an overstimulation of the M1 mAChR, that was previously associated to disruptions of cognitive function and induction of seizures (Cruickshank et al., 1994, Hamilton et al., 1997).

Several structurally diverse M1 PAM chemotypes have been developed by Merck, Pfizer, Vanderbilt Centre for Neuroscience Drug Discovery (VCNDD) and Monash Institute for Pharmaceutical Sciences (MIPS) that possess distinct pharmacological properties. However, the ideal pharmacological properties that are necessary for efficacious and safer M1 PAMs for AD therapeutics are still to be elucidated. For instance, PF-06764427 and VU6004256 are structurally related M1 PAMs that display similar *in vitro* intrinsic agonist activity and pharmacological profiles but can have significantly different effects *in vivo.* In mice, PF-06764427 significantly reduced spontaneous locomotor activity, reversed amphetamine-induced hyper-locomotion (AHL), lacked significant pro-cognitive activity in a NOR test and caused cholinergic toxicity and convulsions (Rook et al., 2017). In contrast, VU6004256, a slightly weaker ago-PAM than PF-06764427, induced a reduced effect on spontaneous locomotor activity and did not reverse AHL, but produced a robust improvement in the NOR task. Surprisingly, no adverse effects were reported in response to VU6004256 (Rook et al., 2017).

The molecular mechanism underpinning the ability of highly selective M1 ligands in driving such diverse physiological outcomes could be explained by signalling bias. For instance, two selective M1 PAMs that displayed similar *in vitro* effects in terms of potentiating the receptor affinity for ACh, could produce distinct effects on phosphoinositide hydrolysis and coupling to phospholipase D (Marlo et al., 2009). Additionally, further comparison of PF-06764427 and VU6004256

described above revealed distinct ability of these M1 PAMs to drive receptor internalisation, with VU6004256 failing to induce measurable internalisation (Rook et al., 2017).

5.1.4 The promise of M1-biased ligands for the treatment of AD

Important differences in *in vivo* effects of structurally related compounds such as PF-06764427 and VU6004256 (Rook et al., 2017) can be explained by ligand bias. Like many members of the GPCR superfamily, muscarinic receptors mediate signal transduction in a broadly bimodal manner, by coupling to both the canonical G protein signalling and receptor phosphorylation/arrestin-dependent signalling. Some GPCR ligands have been shown to induce biased signalling, whereby they preferentially activate some downstream pathways in preference to others (Luttrell, 2014, Kenakin and Christopoulos, 2013). When designing new M1 mAChR-selective ligands for therapeutic application, it is therefore important to define the subtle pharmacological properties of M1 compounds that drive adverse toxic effects (seizures) opposed to those that drive the beneficial therapeutic outcomes (cognitive enhancement and disease-modification). The promise of biased ligands is that ligands could be designed to drive GPCR signalling pathways that lead to clinically beneficial outcomes in preference to ones that are likely to result in adverse responses.

Whilst the molecular details of biased signalling have been extensively studied in *in vitro* transfected cell systems, understanding the physiological importance of biased signalling and further, how this might have a pathophysiological impact, has been extremely challenging. One approach to investigate this issue is by genetically engineering mice to express biased variants of receptors, to dissect the downstream signalling pathways and uncover their physiological significance. This can be achieved for example by removal of intracellular phosphorylation sites of the receptor thereby reducing coupling to arrestin but maintaining coupling to heterotrimeric G proteins. This approach has been previously successfully employed in mapping the role of the M3 mAChR signalling bias in cognition, glucose tolerance and insulin release (Bradley et al., 2016, Poulin et al., 2010, Kong et al., 2010), or in validating the role of μOR-mediated phosphorylation/arrestin-dependent signalling in inducing opioid-related adverse responses (Kliewer et al., 2020, Kliewer et al., 2019). Both these studies are

discussed in detail in Chapter 3. Our group has investigated this possibility for the M1 mAChR.

Previously, a G protein-biased M1 mAChR mouse model was generated by genetically engineering a mouse strain that expresses a variant of the M1 mAChR whereby all the recognised and putative receptor phosphorylation sites were disrupted, thereby reducing the receptor coupling to phosphorylation/arrestin-dependent signalling pathways (Bradley et al., 2020, Butcher et al., 2016). This mouse model, called M1-PD, helped to establish that phosphorylation/arrestin-dependent signalling mediated by the M1 mAChR are important in pro-cognitive activity and reducing anxiolytic behaviour, as well as protecting against peripheral and central cholinergic adverse responses such as seizures.

5.1.5 Aims

This chapter aimed to explore the role of M1 mAChR phosphorylation/arrestin-dependent signalling pathways in the disease-modifying potential of the M1 mAChR in neurodegenerative disease. This was achieved by employing knock-in mice expressing the wild-type (M1-WT) or the M1-PD receptor (described in Chapter 3) in combination with mouse prion disease, the progressive terminal neurodegenerative disease that shares many of the hallmarks of human AD (described in Chapter 4). Progression of neurodegenerative prion disease was determined in prion-infected M1-PD mice in comparison with M1-WT by assessing disease-associated behaviours, and the presence of pathological markers using biochemical and histological methods.

5.2 Results

5.2.1 M1-PD is expressed at equivalent levels to M1-WT in the transgenic knock-in mouse lines

A knock-in mouse line was generated to express the M1-PD mutant of the M1 mAChR in the natural locus of the wild-type receptor (CHRM1). Our group has previously demonstrated that receptor expression levels in the cortex and hippocampus were equivalent to that of wild-type mice (Bradley et al., 2020). Here, levels of M1 mAChR transcripts showed no significant difference in receptor transcription when comparing M1-WT and M1-PD (Figure 5-2A). Furthermore, using western blotting to detect the HA tag on the C-terminus of the receptor, it is confirmed that the protein level of mutant receptor in the cortex and hippocampus of M1-PD mice is comparable to that of the wild-type receptor (expressing a C-terminal HA tag) in M1-WT mice (Figure 5-2B-D). The expression of M1-WT was shown with the presence of a 75 kDa band whilst the M1-PD showed a slightly lower molecular weight band, which is expected due to the nature of its mutations.

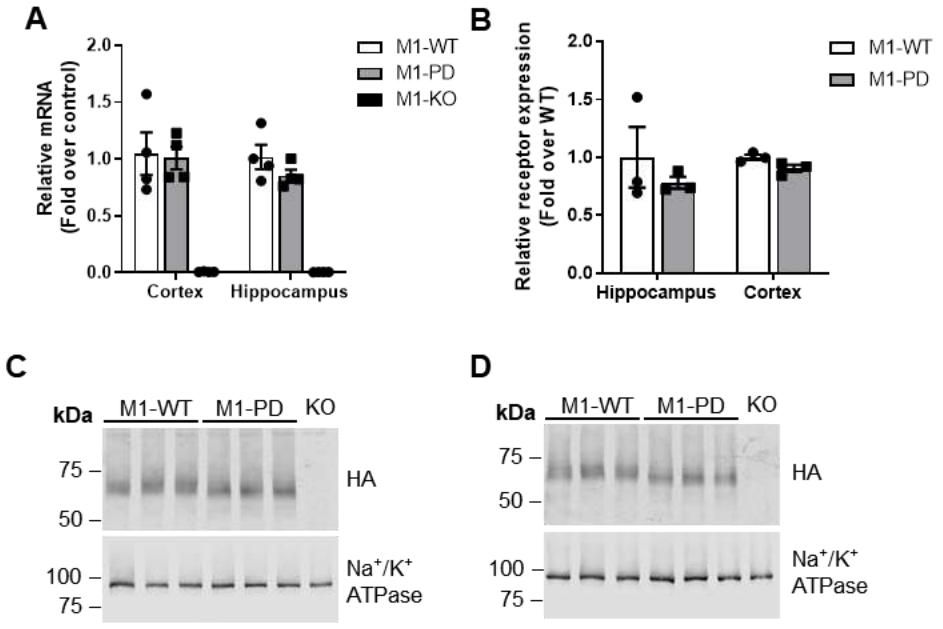

Figure 5-2 Receptor expression in M1-WT and M1-PD knock-in C57 mice. (A) Quantitative RT-PCR showing the expression of M1 mAChR mRNA in the cortex and hippocampus of M1-WT, M1-PD or M1-KO mice. Data are expressed as a ratio of α-tubulin RNA expression (N=4 mice). **(B-D)** Solubilised membranes prepared from the hippocampus **(C)** or cortex **(D)** of HA-tagged M1-WT and M1-PD knock-in mice were probed in western blot analysis for the expression of M1 mAChR using an antibody for the HA tag. Membrane prepared from M1-KO mouse (KO) was used as negative control. Data shown are three separate mice for the M1-WT and M1-PD phenotype, and one animal for the M1-KO. Na^+/K^+ ATPase expression was used as a loading control. **(B)** Quantification of (C) and (D) was conducted using a LICOR software, Image Studio Lite 5.2. n = 3. Data are shown as means ± SEM. Statistical analysis performed was multiple unpaired T-test.

Receptor expression was also analysed in prion-infected M1-WT and M1-PD knock-in mice to determine whether M1 mAChR expression was altered in disease (Figure 5-3). Transcript and protein levels of both M1-WT and M1-PD receptors were unchanged in the cortex and hippocampus of prion-infected mice compared to control mice at 16 w.p.i. This data, therefore, confirms that expression of the M1-WT and M1-PD does not change in these genotypes or during disease.

Immunohistochemical staining using an anti-HA antibody in slices taken from the hippocampus of control or prion-infected M1-WT and M1-PD mice enabled me to visualise receptor distribution (Figure 5-4). The M1-WT receptor is found diffusely localised in the CA1 region of the hippocampus, with pools of internalised receptors visible around the cell bodies of CA1 pyramidal neurons. In contrast, the M1-PD also seems diffusely expressed in the hippocampus, but the staining around the cell bodies of the CA1 pyramidal neurons is absent, suggesting there are no receptors localised around the cell bodies. Taken together with our previous data (Bradley et al., 2020), we therefore demonstrate that the M1-PD mutant receptor has reduced internalisation, since removal of phosphorylation significantly impairs receptor localisation *in vitro* and *in vivo*. Furthermore, since the expression levels of M1-WT and M1-PD are comparable, these knock-in mice can be employed to differentiate between physiological pathways that lie downstream of either G protein-dependent signalling versus ß-arrestin/phosphorylation-dependent signalling and internalisation.

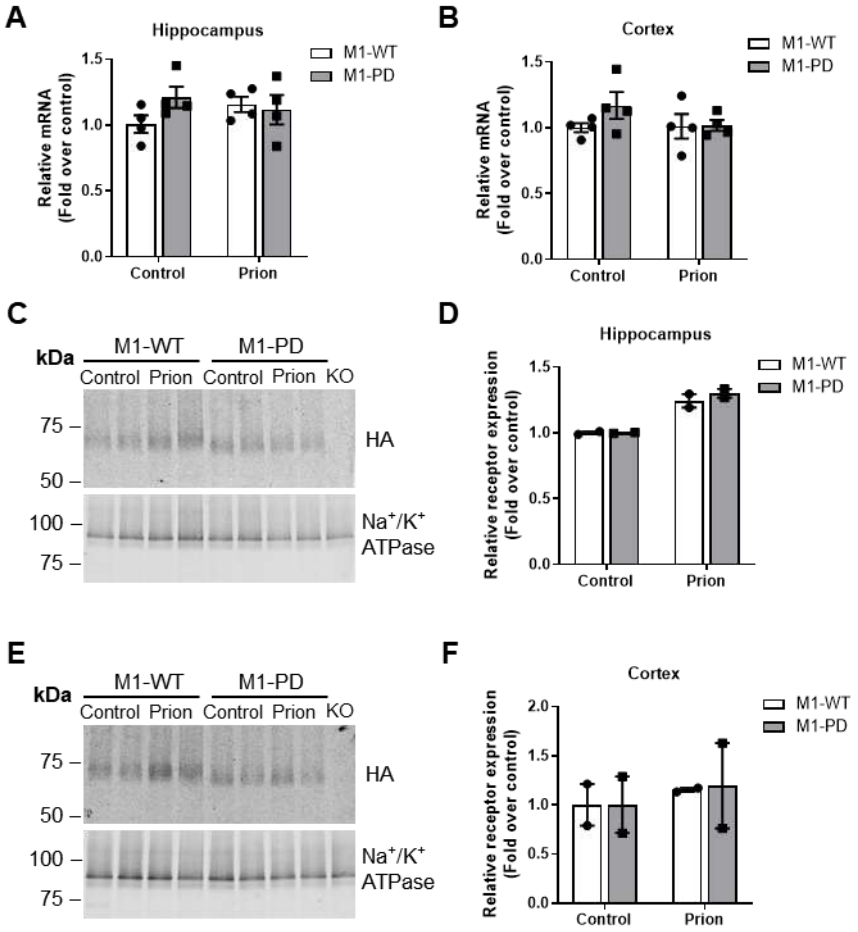

Figure 5-3 Control- and prion infected M1-PD mice show equivalent receptor expression compared to M1-WT mice. (A-B) Quantitative RT-PCR showing the expression of M1 mAChR RNA transcripts in the hippocampus **(A)** or cortex **(B)** of 16 w.p.i. control or prion-diseased, M1-WT or M1-PD mice. Data are expressed as a ratio of α-tubulin RNA expression (N=4 mice). **(C-F)** Solubilised membranes prepared from the hippocampus **(C-D)** or cortex **(E-F)** of control or prion-infected 16 w.p.i. M1-WT and M1-PD knock-in mice were probed in western blot analysis for the expression of M1 mAChR using anti-HA tag antibody. Membrane prepared from M1-KO mouse (KO) was used as negative control. Data shown are two separate mice for each genotype, with similar data being obtained on at least two further occasions. Na^+/K^+ ATPase expression was used as a loading control. **(D-F)** Quantification of (C) and (E) was conducted using a LICOR software, Image Studio Lite 5.2. n = 2. Data are shown as means ± SEM. Statistical analysis performed was multiple unpaired T-test.

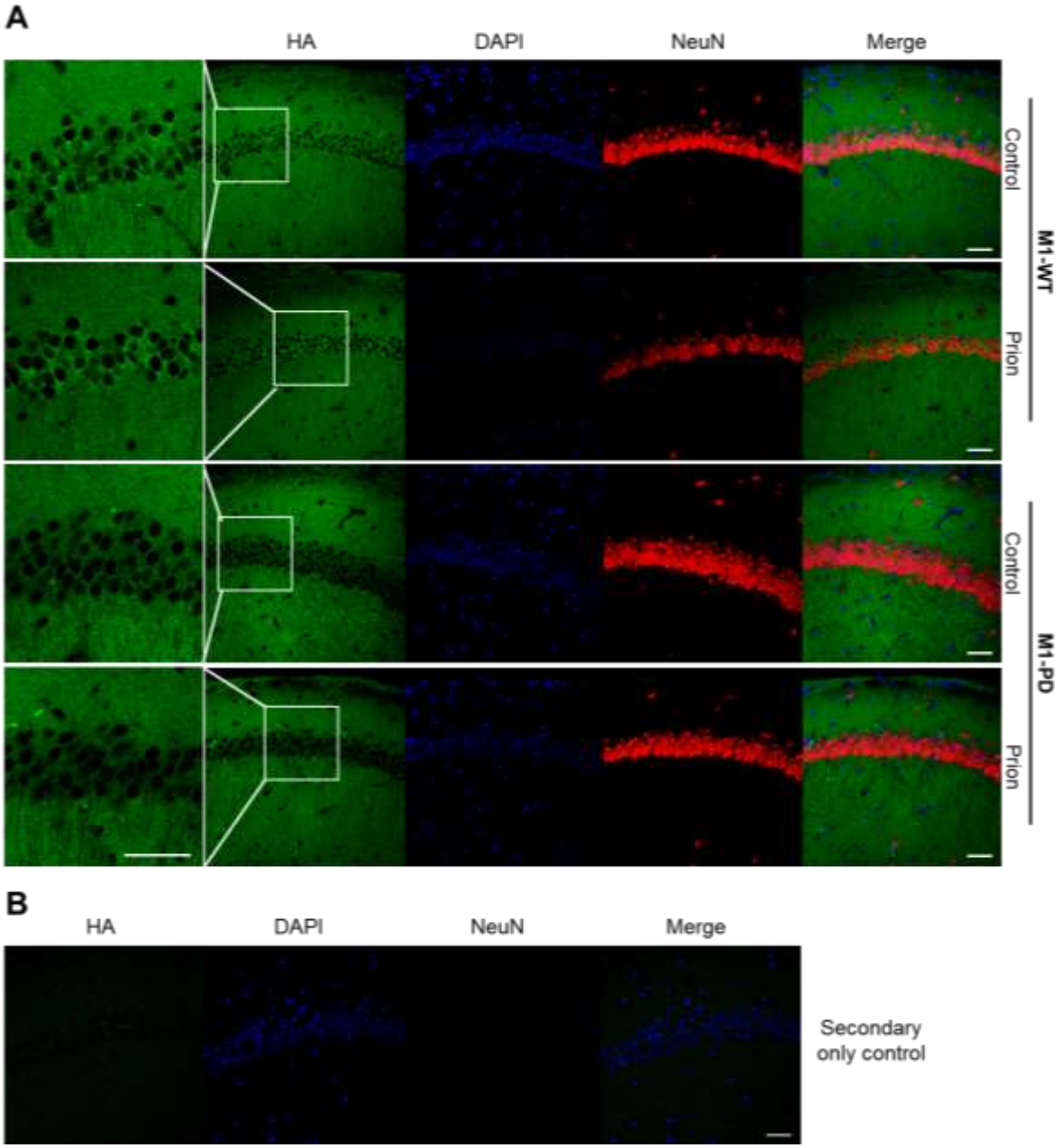

Figure 5-4 Visualisation of receptor expression in control and prion-infected M1-WT and M1-PD knock in mice. (A) Immunohistochemical staining of 18 w.p.i. control and prion-infected M1-WT and M1-PD mice. Sagittal sections through bregma lateral level 0.72mm were stained using anti-HA and anti-NeuN antibodies to visualise HA-tagged receptors and neuronal nuclei in the hippocampal CA1 region (HA, green; DAPI, blue; NeuN, red). **(B)** Secondary [antibody] only control was included to control for antibody specificity. Images are representative of 3 repeats using sections from 3 mice (N=3). Scalebar 50 µm.

5.2.2 M1-PD mice show accelerated neurodegenerative disease progression

Prion disease is characterised by the conversion of normal, cellular PrP_C into misfolded, neurotoxic scrapie PrP_{Sc}. PrP_{Sc} self-propagates, accumulates, and forms aggregates that are partially resistant to digestion by proteases (Prusiner,

1982). To determine the presence of PrP_{Sc}, lysates of cortex and hippocampus from control- or prion-infected M1-WT and M1-PD mice were incubated with Proteinase K prior western blotting using an anti-PrP antibody (Figure 5-5). No differences in total prion protein (PrP_{Tot}), which is both PrP_C and PrP_{Sc}, were detected in the cortex or hippocampus of any of the groups. Prion-infected mice, both M1-WT and M1-PD, showed the presence of PrP_{Sc} in both cortex and hippocampus at each time point, but M1-PD mice showed a higher level of PrP_{Sc} compared to the M1-WT at both disease time-points examined (16- and 18 w.p.i). Specifically, this difference was robust ($P<0.01$) in the hippocampus (Figure 5-5C, D), and non-significantly different in the cortex (Figure 5-5A, B). This suggests that removal of M1 mAChR phosphorylation either promotes accumulation of misfolded protein or causes the removal of a protective mechanism against prion misfolding and/or propagation. Since prion disease progression is dependent on the expression level of PrP_C, whereby increased PrP expression accelerates disease progression (Mallucci et al., 2003), PrP expression was analysed in M1-PD mice. Importantly, transcript levels of PrP were equivalent in M1-WT, M1-PD and M1-KO mice (Figure 5-6), indicating that the increased accumulation of PrP_{Sc} is not caused by increased expression of PrP_C.

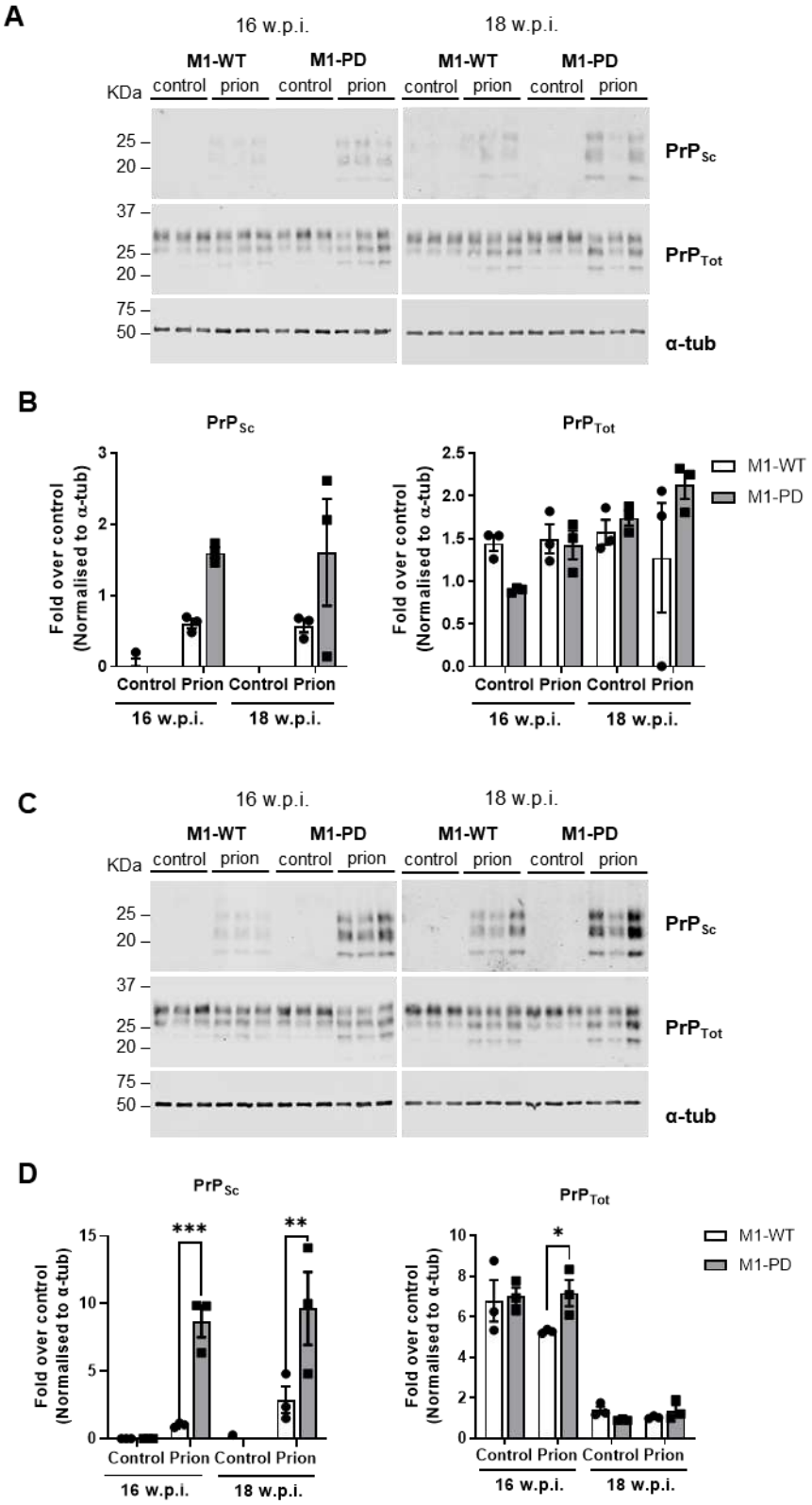

Figure 5-5 Prion-infected M1-PD mice display higher levels of PrP_{Sc} compared to prion-infected M1-WT mice. Lysates of cortex **(A-B)** and hippocampus **(C-D)** from control or prion-diseased mice at 16- and 18- w.p.i. were incubated with Proteinase K prior western blot using anti-PrP to detect PrP_{Sc}. Incubation with water was used as control to detect PrP_{Tot}. α-tubulin (α-tub) antibody was used for loading control. **(B)** and **(D)** are the band analysis of cortex (A) and hippocampus (B) respectively. Data are expressed as fold over control M1-WT, normalised to the loading control (α-tub), and each data-point represents an individual mouse. Quantification was carried using a LICOR software, Image Studio Lite 5.2. Statistical analysis performed was a two-way ANOVA Sidak multiple comparisons test where *P<0.05, **P<0.01 (N=3).

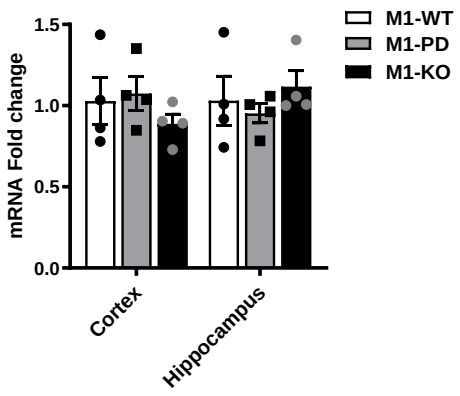

Figure 5-6 PrP expression is equivalent in M1-WT, M1-PD and M1-KO mice. Quantitative RT-PCR showing the expression of PrP mRNA in the cortex and hippocampus of M1-WT, M1-PD or M1-KO mice. Data are expressed as a ratio of α-tubulin mRNA expression (N=4 mice). Statistical analysis performed was multiple unpaired T-test.

Prion disease neurodegeneration is characterised by disruption of cholinergic innervations in the hippocampus. western blotting using antibodies specific against ChAT, the enzyme that catalyses the biosynthesis of ACh, and therefore a marker for cholinergic neurons, was performed to detect changes in population of cholinergic neurons (Figure 5-7). The only significant differences found consisted in an increase in ChAT expression in the cortex of prion-infected M1-PD mice at 18 w.p.i. compared to the respective control-infected M1-PD. However, this was caused by the presence of an outlier data-point that was identified as significant outlier using a ROUT test for outlier identification (Q=1%).

Immunohistochemical staining was conducted using antibodies against ChAT and MAP2 to visualise cholinergic innervations as well as neuronal projections (Figure 5-8). MAP2 staining did not reveal any visible differences between control or prion infected M1-WT and M1-PD, suggesting that neurons are intact. No evident differences were detected in ChAT between the two genotypes or between prion and control brains. However, whilst ChAT staining in in both hippocampal CA1 region and cortex of control M1-WT mice reveals a filamentous arrangement of this enzyme, ChAT in prion-infected M1-WT and M1-PD mice appears fragmented. This might suggest a disruption of cholinergic innervations, however more detailed analysis is required to confirm this qualitative observation.

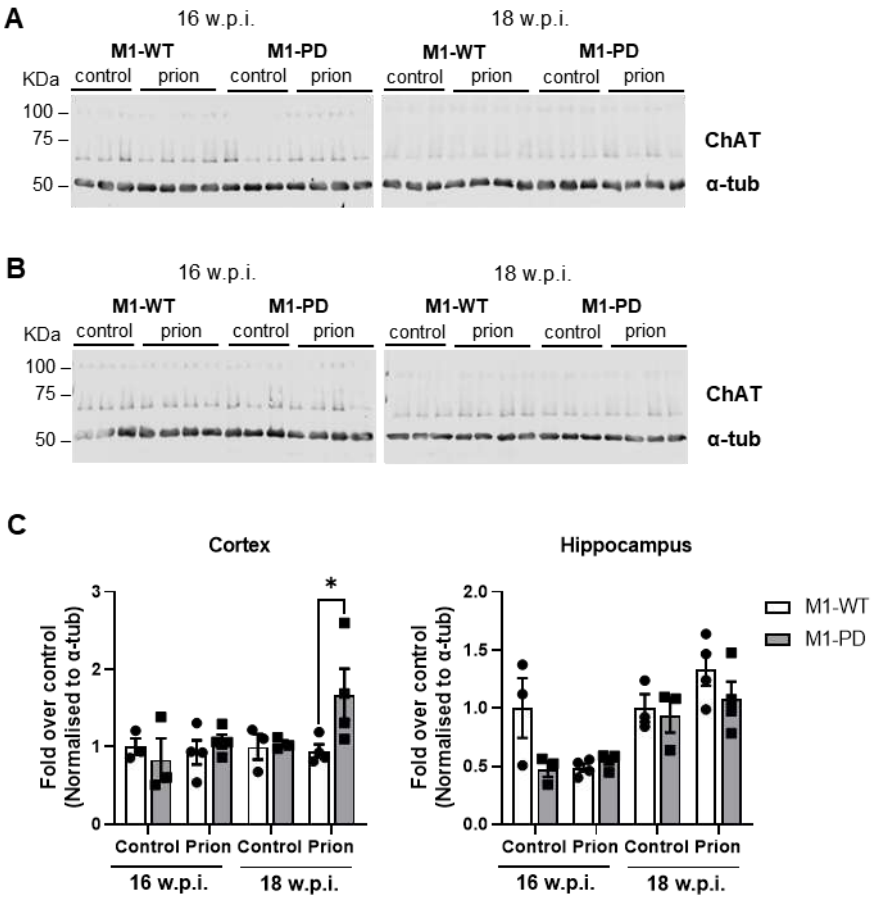

Figure 5-7 No loss of cholinergic neurons was detected in prion-infected M1-WT and M1-PD mice at 16- and 18- w.p.i. Western blots using antibodies against ChAT were conducted on lysates prepared from cortex **(A)** and hippocampus **(B)** of control or prion-infected mice at 16 and 18 w.p.i. α-tubulin antibody (α-tub) was used for loading control. **(C)** Band analysis of cortex (A) and hippocampus (B) using LICOR a software, Image Studio Lite 5.2. Data are expressed as fold over control M1-WT, normalised to the loading control (α-tub), and each point represents an individual mouse. The statistical analysis was conducted using a two-way ANOVA Sidak multiple comparisons (N=3-4) where *P>0.05. An outlier identification test was performed on panel C using ROUT method (Q=1%).

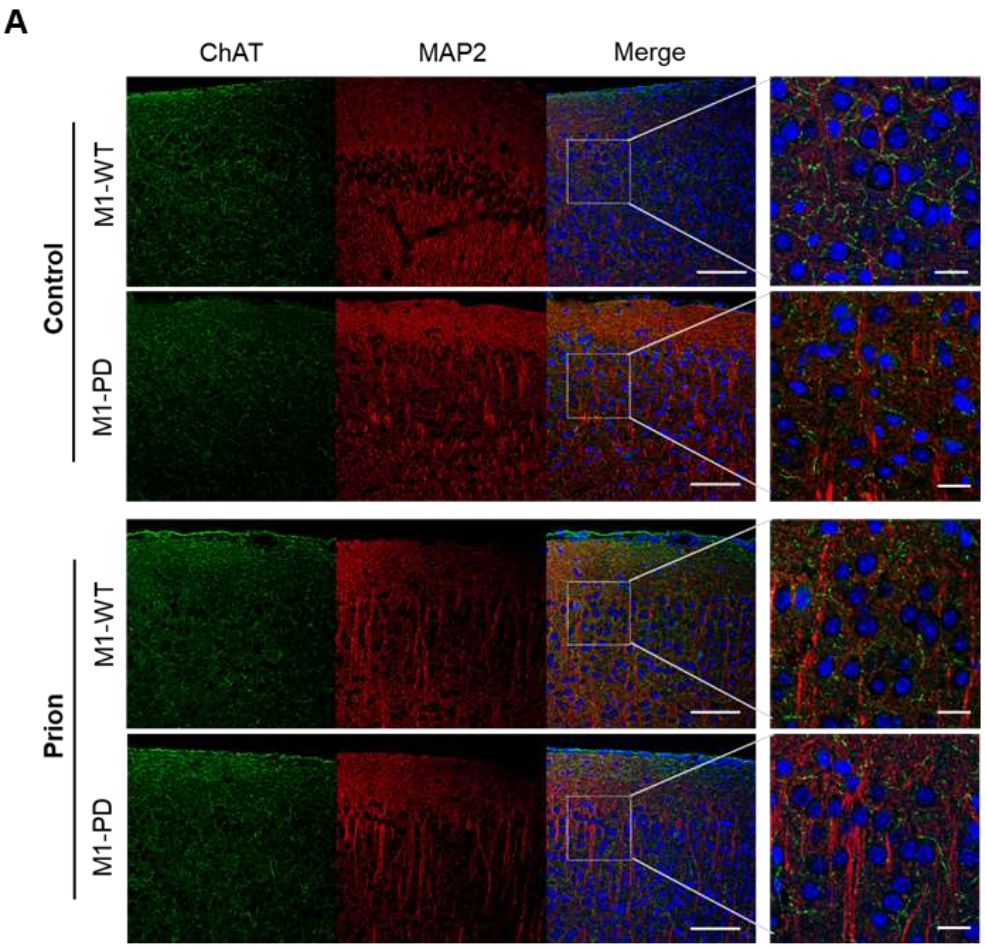
A
ChAT
MAP2
Merge
Control
M1-WT
M1-PD
Prion
M1-WT
M1-PD

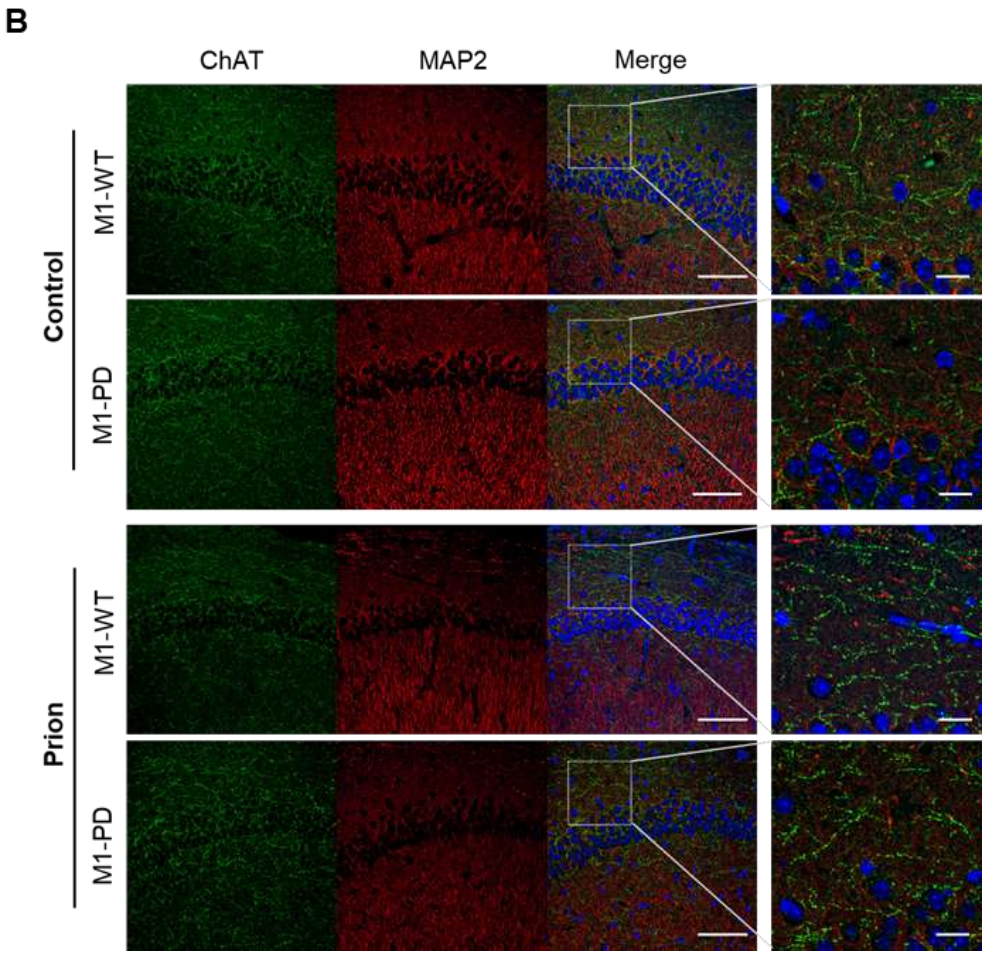
B
ChAT
MAP2
Merge
Control
M1-WT
M1-PD
Prion
M1-WT
M1-PD

Figure 5-8 Immunohistochemical staining of neurons in 18 w.p.i. control- and prion-infected M1-WT and M1-PD mice. Representative images of cortex **(A)** and hippocampal CA1 region **(B)** probed for ChAT (green), and MAP2 (red), markers for cholinergic and general neurons, respectively. The nuclei were stained blue with DAPI. Images are representative of 3 repeats using sections from 3 mice (N=3). Scale bars: 100 μm and 20 μm for the left- and right-hand side tiles respectively.

Spongiosis, which is the formation of intraneuronal vacuoles in cells that have not yet degenerated, is one of the early pathological changes that proceed neuronal loss observed in the hippocampus of prion-diseased mice (Mallucci et al., 2003). Haematoxylin and eosin (H&E) staining of control- and prion-infected M1-WT and M1-PD mice enabled observation of the microanatomy of hippocampal sections, and the severity of spongiosis was determined by using an arbitrary 4-point scoring system (see 2.9.5). As expected, no spongiosis was detected in the hippocampus from healthy mice (Figure 5-9A). Spongiosis was virtually absent in the hippocampus of prion-infected M1-WT mice at 18 w.p.i., indicating that disease hasn't yet progressed enough at this time point (Figure 5-9B). This is consistent with the observations in prion infected Tg37 mice that profound spongiosis is present just before (about one week) the onset of symptoms (Figure 4-7 and Figure 4-26). Although prion disease progression in M1-WT mice is significantly slower (~2X) than in Tg37 mice, symptom onset in prion-infected M1-WT mice is comparably at a much later time point than 18 w.p.i. (~22 w.p.i.) (Figure 5-21). In contrast, a higher number of spongiotic vesicles is observed in prion-infected M1-PD mice, which is significantly ($P<0.05$) higher in the dentate gyrus compared to prion-infected M1-WT mice (Figure 5-9C), indicating that prion disease may have progressed more rapidly in M1-PD mice.

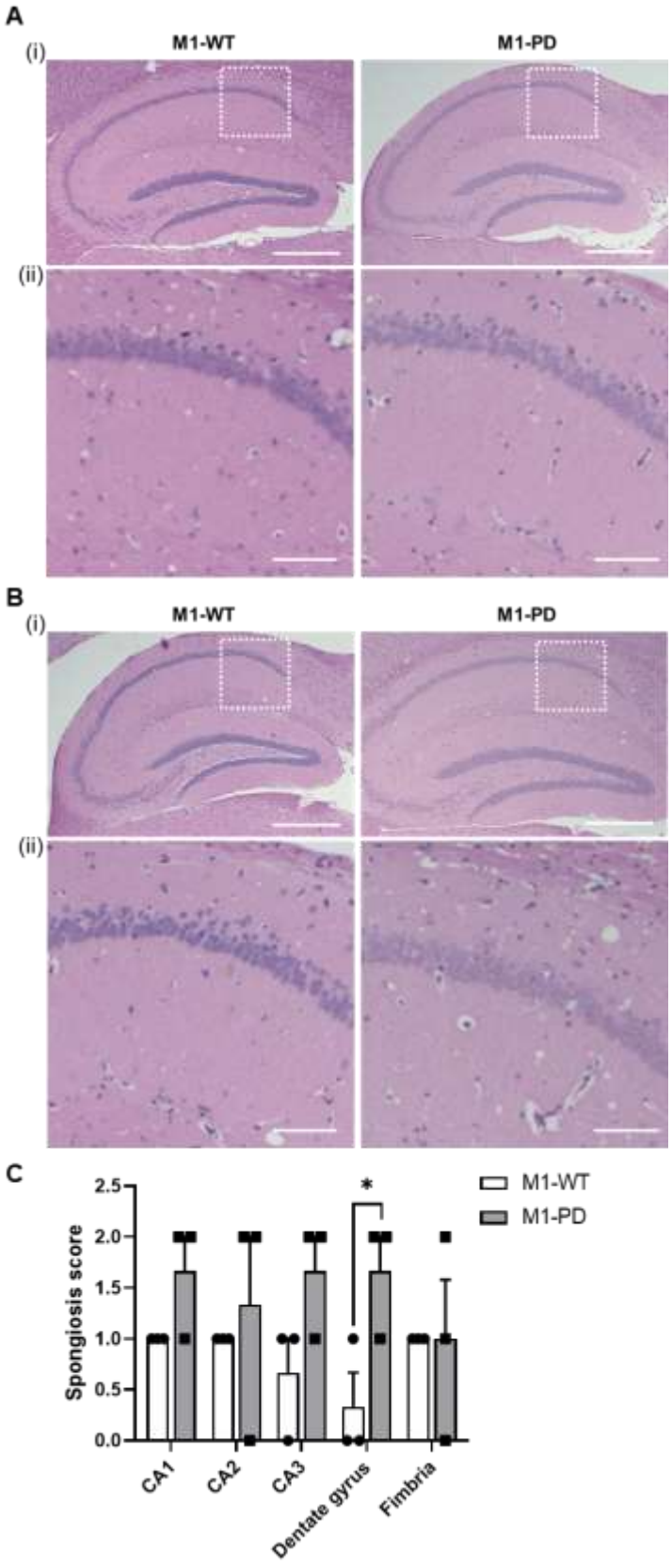

Figure 5-9 Spongiosis in the hippocampus of control or prion-infected M1-WT and M1-PD mice. Representative images of H&E staining of saline-perfused and formalin-fixed mouse brains from at least three control **(A)** or prion-infected **(B)** mice at 18 w.p.i. Images are representative of 3 repeats using sections from 3 mice (N=3). Scale bars: 500μm (i) and 100 μm (ii). **(C)** H&E staining of sagittal sections (at bregma lateral 0.72mm) from the mouse brains allowed to observe spongiotic vesicles in the hippocampus, and score spongiosis according to the 4 point-scoring system described in 2.9.5. Statistical analysis is multiple unpaired T test, where *P<0.05 (N=3).

A global transcriptomic and proteomic study on control- and prion-infected Tg37 mice (the same mouse strain characterised in Chapter 4) had revealed a panel of proteins that are significantly upregulated in prion disease, and whose expression is restored to levels similar to healthy controls following treatment with a highly selective M1 mAChR PAM, VU0486846 (Dwomoh et al., 2021). These included markers of neuroinflammation, GFAP, clusterin, vimentin and galectin-1, and markers of adaptive responses to neurodegeneration including APO-E and the protease inhibitor serpinA3N (Dwomoh et al., 2021). In this study, the upregulation of this panel of proteins was proposed to represent biomarkers of prion disease and indicators of disease severity. Here, I assessed the impact of removing the phosphorylation-dependent signalling mediated by the M1 mAChR on the regulation of disease markers APO-E, clusterin, galectin-1 and serpinA3N. To do so, western blots were conducted to probe for the said disease markers, on lysates of hippocampus and cortex from control- and prion-infected, M1-WT and M1-PD mice at 16 and 18 w.p.i. (Figure 5-10).

Strikingly, prion-diseased M1-PD mice display an evident upregulation of all the disease markers probed in the cortex and hippocampus at levels higher than observed in prion-diseased M1-WT. Specifically, clusterin expression was significantly elevated by 1.8 to 2.5 folds in the hippocampus ($P<0.0048$) and cortex ($P<0.0065$) of prion-infected M1-PD mice at 16 and 18 w.p.i. compared to prion-infected M1-WT mice. Compared to prion-diseased M1-WT, M1-PD mice showed robust upregulation of APO-E that was significantly higher in the hippocampus by 3.3 folds at 16 w.p.i. ($P=0.0003$), and in both cortex and hippocampus at 18 w.p.i by between 2.2 to 2.7 folds ($P<0.029$). However, no increases APO-E and clusterin were detected in M1-WT mice with prion disease compared to their respective controls at each of the time points tested.

Changes in galectin-1 expression were only observed in the hippocampus at 18 w.p.i. where prion disease M1-PD mice showed an upregulation in galectin-1 by 2.8-fold, which was significantly ($P=0.035$) higher than in prion-diseased M1-WT mice. Whilst no significant changes in serpinA3N were found in M1-WT mice with prion disease relative to their control, prion-diseased M1-PD mice showed a remarkable upregulation of serpinA3N in both hippocampus and cortex that was significantly ($P<0.003$) higher than in prion infected M1-WT mice in both brain regions at 18 w.p.i. In the hippocampus, serpinA3N is upregulated by 15.3- and

30.2-folds at 16 and 18 w.p.i. respectively. In the cortex, prion disease induced a 6.2-fold increase at 16 w.p.i. and a 16-fold increase at 18 w.p.i.

To summarise, the upregulation of prion disease signature proteins APO-E, clusterin, galectin-1 and serpinA3N was associated with disease progression. Prion-diseased M1-WT mice did not show evident changes in APO-E, clusterin, galectin-1 and serpinA3N at the time points tested (16 and 18 w.p.i.). However, there was a robust increase in all the probed proteins in prion-diseased M1-PD mice, indicating that these mice are at a more advanced stage of disease compared with M1-WT mice at the same disease time point.

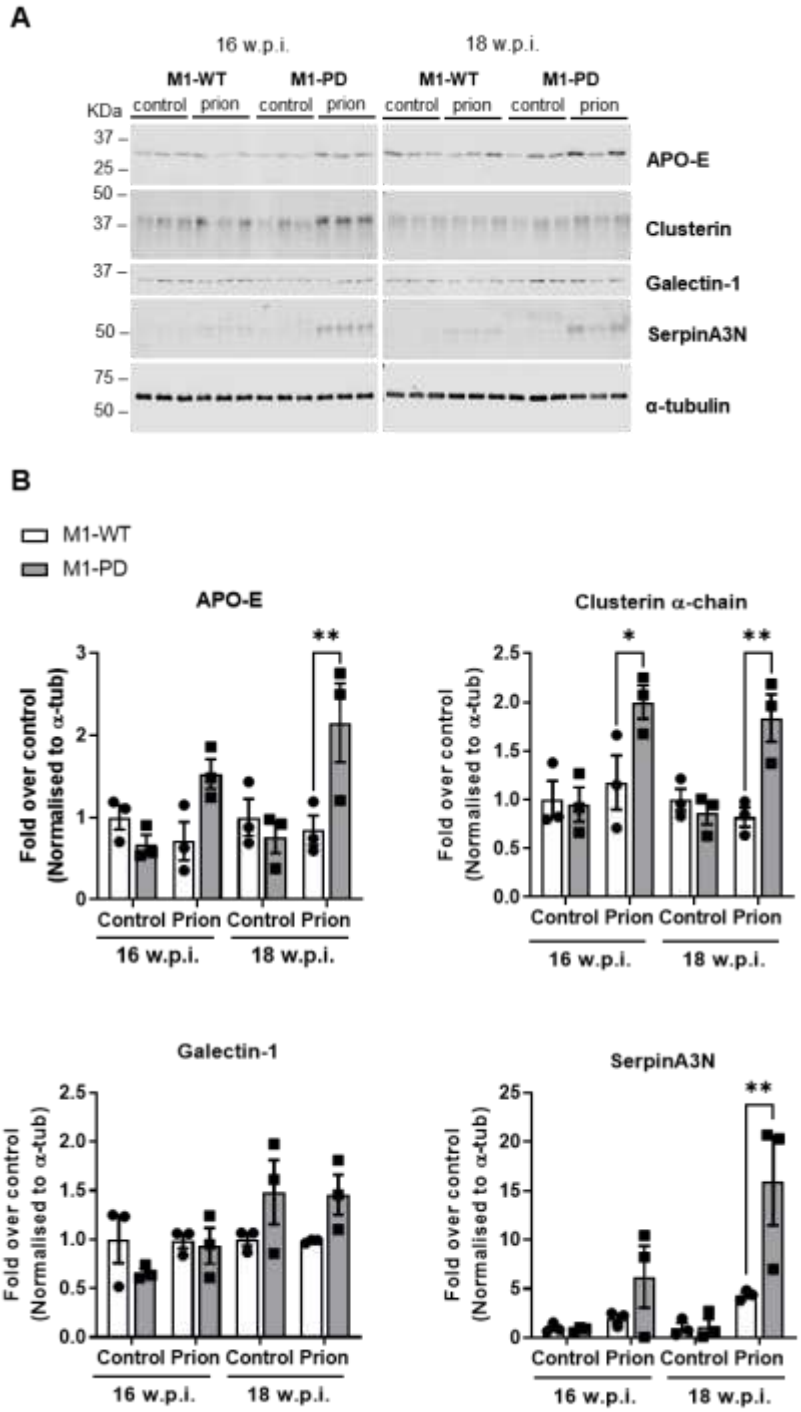
A
16 w.p.i.
18 w.p.i.
M1-WT
M1-PD
M1-WT
M1-PD
KDa
control
prion
control
prion
control
prion
control
prion
37
25
50
37
37
50
75
50
APO-E
Clusterin
Galectin-1
SerpinA3N
α-tubulin
B
M1-WT
M1-PD
APO-E
Clusterin α-chain
Galectin-1
SerpinA3N
Fold over control (Normalised to α-tub)
Control Prion Control Prion
16 w.p.i.
18 w.p.i.
*
**

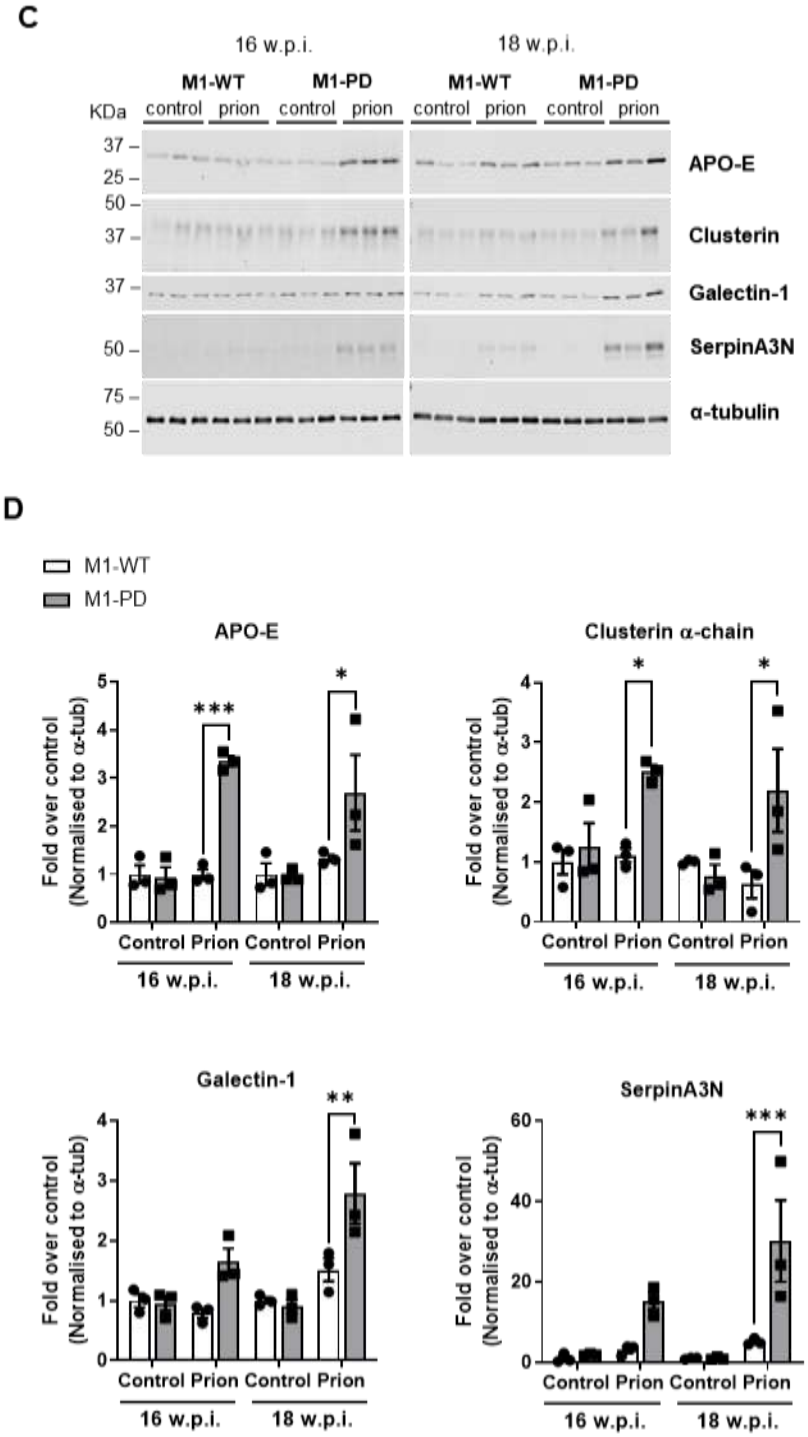

Figure 5-10 Prion-infected M1-PD show higher upregulation of markers of disease compared to prion-infected M1-WT animals. APO-E, serpinA3N, clusterin and galectin-1 were detected in the cortex **(A-B)** and hippocampus **(C-D)** by performing western blot analysis of lysates (10 µg) prepared from control- or prion infected mice at 16- and 18 w.p.i. α-tubulin antibody was used for loading control. Band analysis is shown in **(B)** and **(D)** are the band analysis of hippocampus (A) and cortex (C) respectively performed using a LICOR software, Image Studio Lite 5.2. Data are expressed as means ± S.E.M. of a ratio of α-tubulin expression relative to control-infected M1-WT (N=3 mice). Data were analysed using a two-way ANOVA with Sidak multiple comparisons where *P<0.05, **P<0.01, ***P<0.001, ****P<0.0001.

5.2.3 The M1 mAChR-mediated phosphorylation-dependent signalling pathway plays a role in neuroinflammation

As described in Chapter 4 and in the literature (Carroll and Chesebro, 2019), one of the pathological hallmarks of mouse prion disease is widespread neuroinflammation characterised by astrogliosis and microgliosis. To determine if elevated neuroinflammation is also associated with the accelerated prion disease progression observed in M1-PD mice, several markers of neuroinflammation were examined in prion-infected M1-WT versus M1-PD mice. Transcript levels of GFAP and microglial marker CD86 as well as protein levels of astrocytic markers GFAP and vimentin revealed an overall upregulation of astroglia and microglia in the hippocampus and cortex with prion disease (Figure 5-11).

In the cortex, whilst GFAP and vimentin protein levels were similar in prion infected M1-WT and M1-PD mice (Figure 5-11C-D), GFAP and CD86 transcripts were significantly higher ($P=0.017$ for CD86 and $P=0.0036$ for GFAP) in prion infected M1-PD mice at 16 w.p.i. compared to diseased M1-WT animals (Figure 5-11A).

In the hippocampus however, GFAP and vimentin were found robustly upregulated in the hippocampus of 16- and 18 w.p.i. prion-infected M1-PD mice, at levels that were significantly ($P<0.2$) higher than in prion-diseased M1-WT mice at the same disease time point (Figure 5-11CE-F). Strikingly, vimentin displayed a substantial upregulation in the hippocampus of prion-infected M1-PD mice by 38-39 folds relative to the control, which was higher ($P<0.0048$) than the increases in vimentin in the prion infected M1-WT animals by 6.4-8.7 folds. While CD86 transcripts in the hippocampus showed a robust ($P=0.012$) upregulation in prion-diseased M1-PD mice but not in prion-diseased M1-WT compared to their respective controls, no difference was detected in CD86 transcript levels in prion-infected M1-PD versus M1-WT at 16 w.p.i. GFAP transcript levels, however, showed a robust ($P=0.0011$) increase in the hippocampus of prion infected M1-PD compared to their control, at levels that are significantly ($P=0.0083$) higher than in prion infected M1-WT mice (Figure 5-11B).

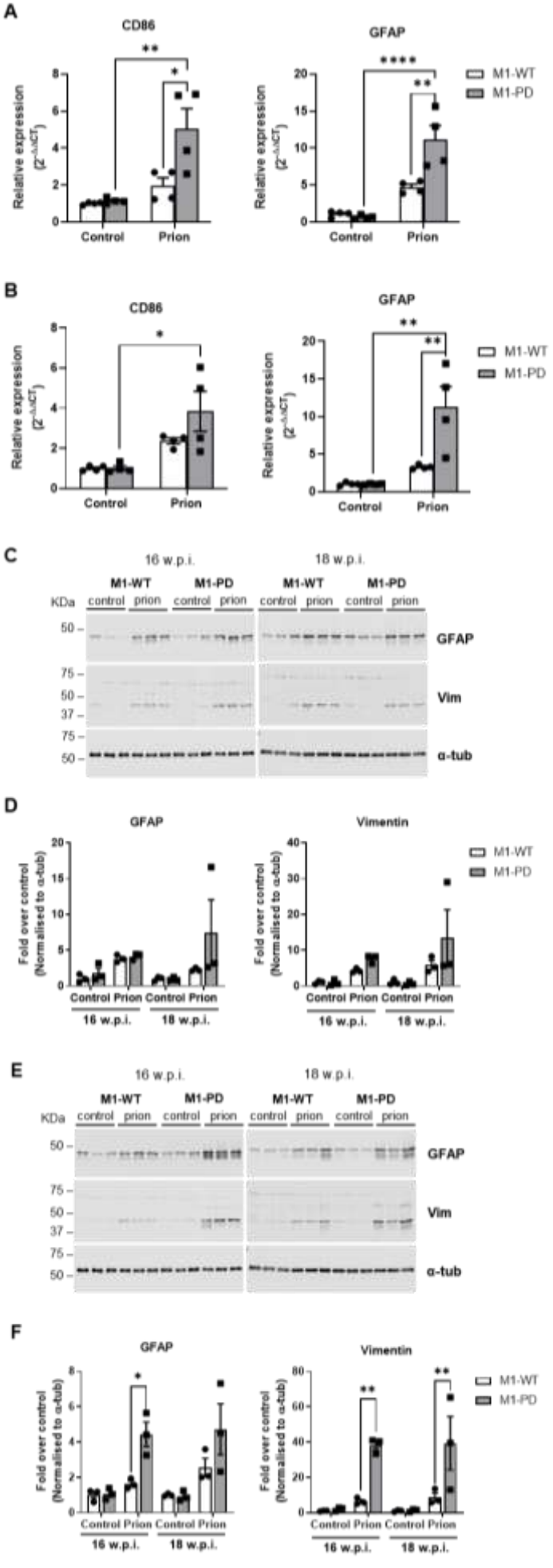
A
CD86
GFAP
Relative expression
Control
Prion
M1-WT
M1-PD
B
CD86
GFAP
C
16 w.p.i.
18 w.p.i.
M1-WT
M1-PD
KDa
control
prion
GFAP
Vim
α-tub
D
GFAP
Vimentin
Fold over control (Normalised to α-tub)
16 w.p.i.
18 w.p.i.
E
F

Figure 5-11 Neuroinflammation is exacerbated in the cortex and hippocampus of prion infected M1-PD mice compared to M1-WT. (A-B) Quantitative RT-PCR showing the expression of CD86 and GFAP, markers of microglia and astrocytes respectively, in the cortex **(A)** or hippocampus **(B)** of control or prion-diseased, M1-WT or M1-PD mice 16 w.p.i. **(C-F)** Western blots to determine astrogliosis in the cortex **(C-D)** and hippocampus **(E-F)** during prion disease used on lysates prepared from control or prion-infected mice at 16 and 18 w.p.i., and probed for GFAP and vimentin (Vim), markers for astrocytes. α-tubulin (α-tub) antibody was used for loading control. **(D)** and **(F)** are the band analysis of cortex (C) and hippocampus (E) respectively, that was carried using LICOR software, Image Studio Lite 5.2. Data are expressed as means ± S.E.M. of a ratio of α-tubulin expression relative to control-infected M1-WT, and each data point represents an individual mouse (N=3 mice). Statistical analysis performed is two-way ANOVA Sidak multiple comparisons, where *P<0.05, **P<0.01, ***P<0.001, ****P<0.0001 (N=3 for the western blots, N=4 for the RT-qPCR).

Immunohistochemical staining for GFAP and Iba-1, markers of astrocytes and microglia, respectively, also highlighted a profound increase in astrogliosis in the hippocampus and cortex of prion-diseased M1-PD, compared to prion-infected M1-WT mice (Figure 5-12). This further demonstrates that removal of phosphorylation-dependent pathways regulated by the M1 mAChR causes an acceleration in mouse prion disease progression, which is observed by an exacerbation of neuroinflammation.

Since chronic inflammation in neurodegenerative brains is characterised by the release of pro-inflammatory cytokines by microglia, that are capable of promoting astrogliosis (Ben Haim et al., 2015), the expression of pro-inflammatory cytokines were assessed in the hippocampus and cortex of 16 w.p.i. control- and prion infected mice (Figure 5-13). Transcript levels of TNF-α, IL-1β and IL-6 were found to be elevated in prion disease in both cortex and hippocampus compared to controls. TNF-α was found significantly elevated in both the hippocampus (P=0.018) and cortex (P=0.0037) of prion infected M1-PD mice compared with prion-diseased M1-WT at 16 w.p.i. However, IL-1β was significantly (P=0.031) upregulated in the cortex, but not hippocampus of prion M1-PD mice compared to prion-infected M1-WT mice. Conversely, no significant difference of IL-6 was detected in prion-infected M1-PD mice compared to the M1-WT control. This data suggests that the M1 mAChR-mediated phosphorylation-dependent signalling negatively regulates the release of pro-inflammatory cytokines TNF-α and IL-1β to decrease neuroinflammation.

There is a possibility that the M1 mAChR may modulate neuroinflammation by regulating the release of pro-inflammatory cytokines; therefore, the transcripts of anti-inflammatory cytokines IL-4, IL-10, IL-11 and IL-13, were analysed in the

cortex or hippocampus of prion-infected M1-WT or M1-PD mice at 16 w.p.i. (Figure 5-14). No differences were found between control- or prion infected M1-WT and M1-PD mice, suggesting that the M1 mAChR is not involved in the regulation of the pro-inflammatory cytokines tested, neither prion disease causes alterations in the expression of anti-inflammatory cytokines.

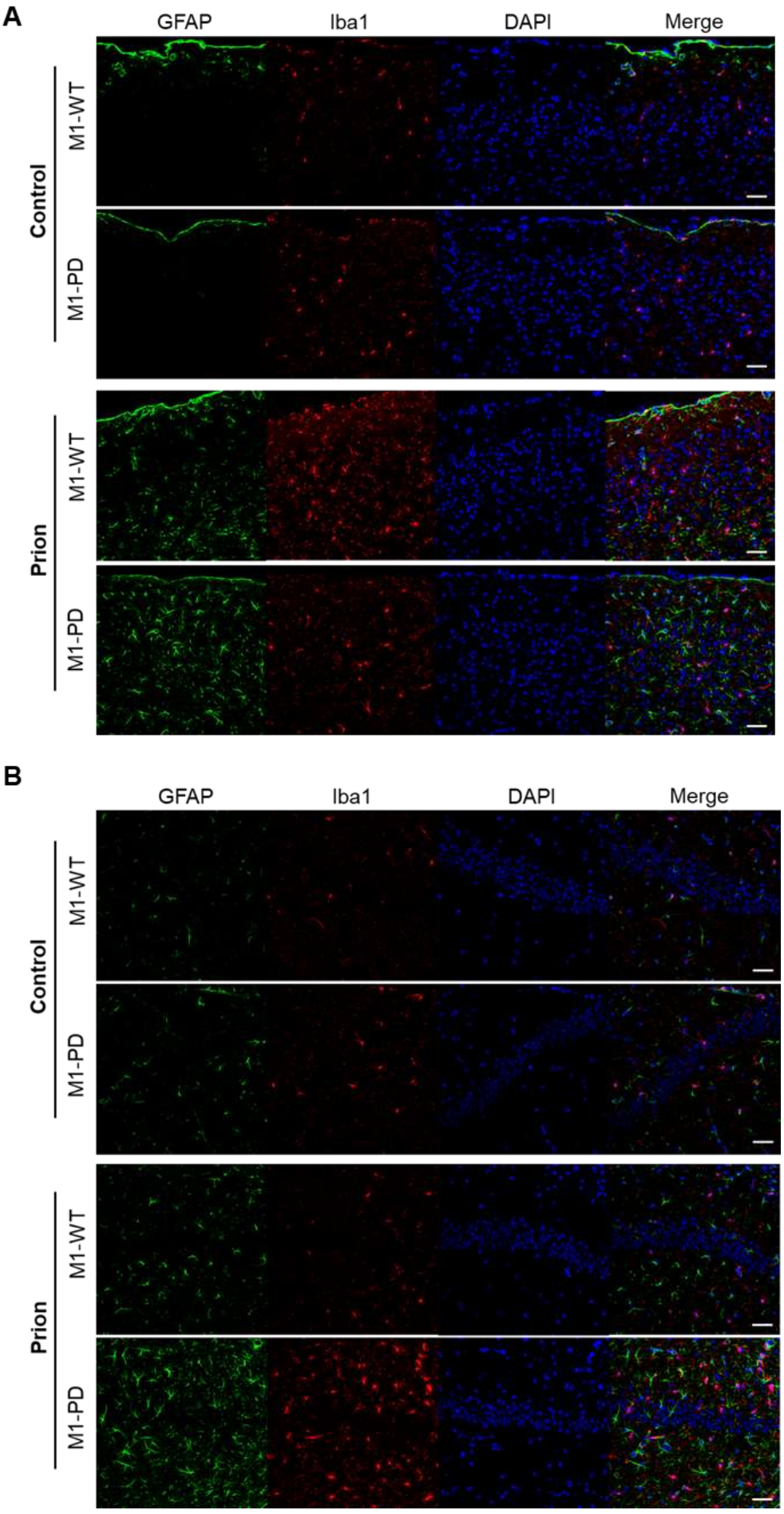
A
GFAP
Iba1
DAPI
Merge
Control
M1-WT
M1-PD
Prion
M1-WT
M1-PD
B
GFAP
Iba1
DAPI
Merge
Control
M1-WT
M1-PD
Prion
M1-WT
M1-PD

Figure 5-12 Prion infected M1-PD mice show higher level of neuroinflammation compared to M1-WT. Immunohistochemical staining of saline-perfused and formalin-fixed mouse brains from control or prion-infected mice 18 w.p.i. Cortex **(A)** and hippocampal CA1 region **(B)** of three mice, which were probed for GFAP (green), and Iba1 (red), markers for astrocytes and microglia, respectively. The nuclei were stained blue with DAPI. Scale bars: 50 µm. Data shown are representative images of three mice (N=3).

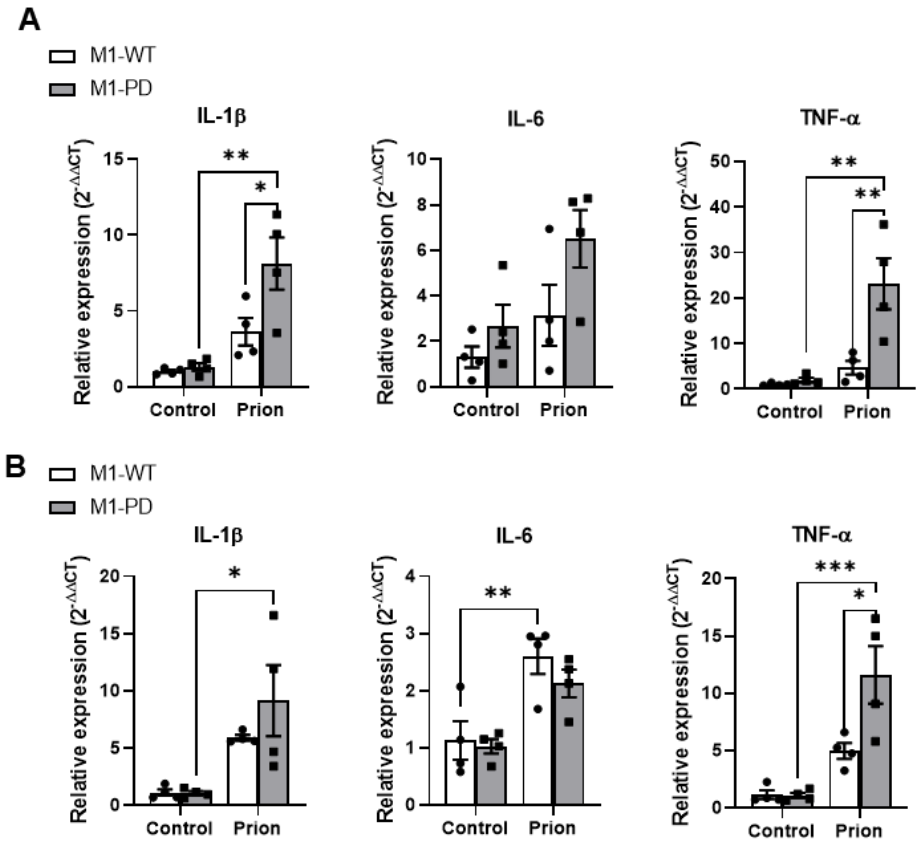

Figure 5-13 Pro-inflammatory cytokines IL-1β, IL-6 and TNF-α are significantly increased in prion-infected M1-PD mice compared to M1-WT. Quantitative RT-PCR showing the expression of pro-inflammatory cytokines (TNF-α, IL-1β, IL-6) in the cortex **(A)** and hippocampus **(B)** of control- and prion infected M1-WT and M1-PD mice at 16 w.p.i. Data are expressed as a ratio of α-tubulin RNA expression relative to control M1-WT (N=4 mice). Data were analysed using two-way ANOVA with Tukey's multiple comparisons, where *P<0.05, **P<0.01, ***P<0.001 (M1-WT vs. M1-PD).

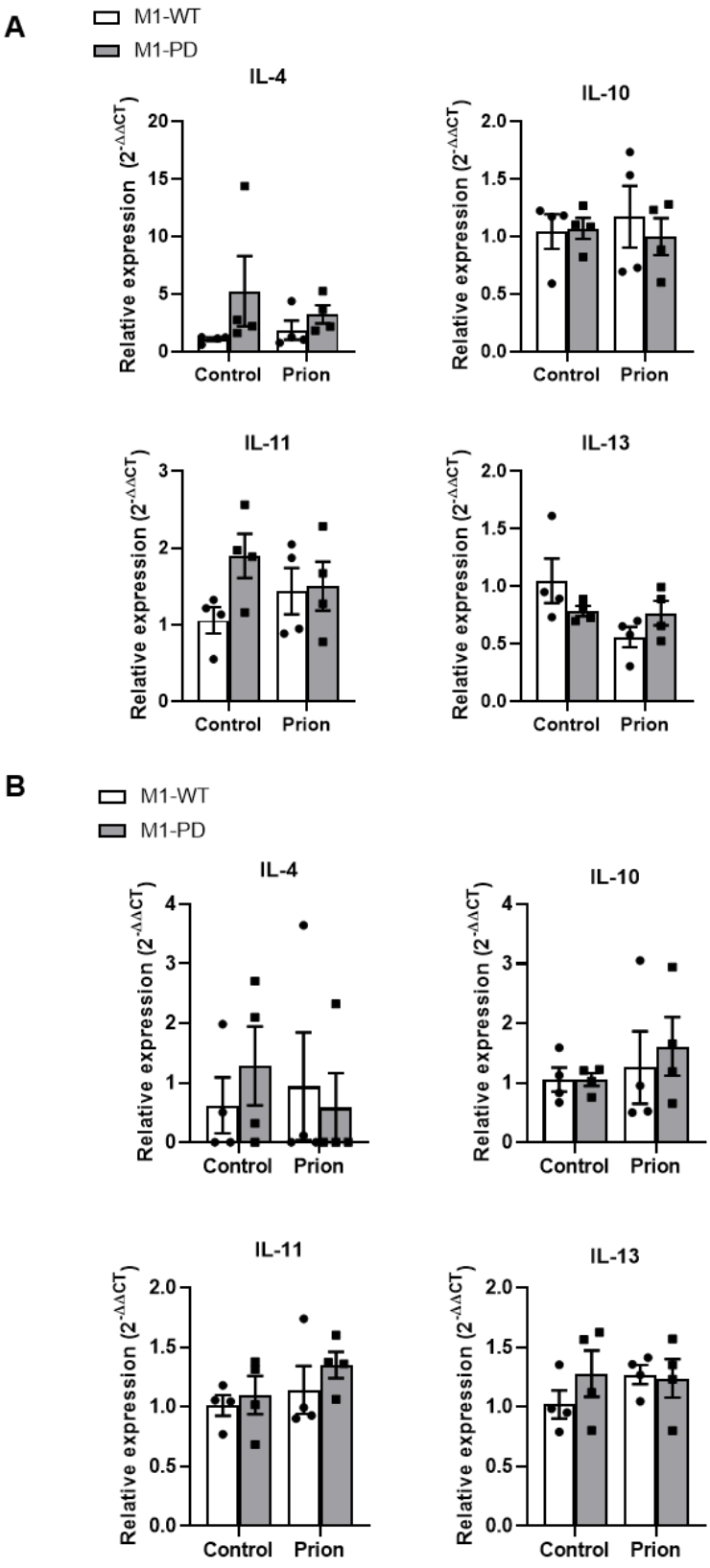

Figure 5-14 Levels of anti-inflammatory cytokines IL-4, IL-10, IL-11 and IL-13 remain unchanged with prion disease in both the M1-WT and M1-PD mice. Quantitative RT-PCR showing the expression of anti-inflammatory cytokines IL-4, IL10, IL-11 and IL-13 in the cortex **(A)** and hippocampus **(B)** of control- or prion-diseased M1-WT or M1-PD mice at 16 w.p.i. Data are expressed as a ratio of α-tubulin RNA expression (N=4 mice). Data were analysed using two-way ANOVA with Tukey's multiple comparisons.

Importantly, expression of transcripts for GFAP, CD86 and the battery of pro- and anti-inflammatory cytokines tested above, were equivalent in non-infected M1-WT and M1-PD mice (Figure 5-15), indicating that the genotypes do not alter transcription of pro-inflammatory proteins. Thus, the elevated neuroinflammation observed in prion-infected M1-PD mice compared to diseased M1-WT is not due to differences in genetic expression of inflammatory markers. *Taken together, these findings demonstrate that prion-diseased M1-PD have exacerbated neuroinflammation compared to M1-WT mice, which may underly the earlier onset of pathology described above*.

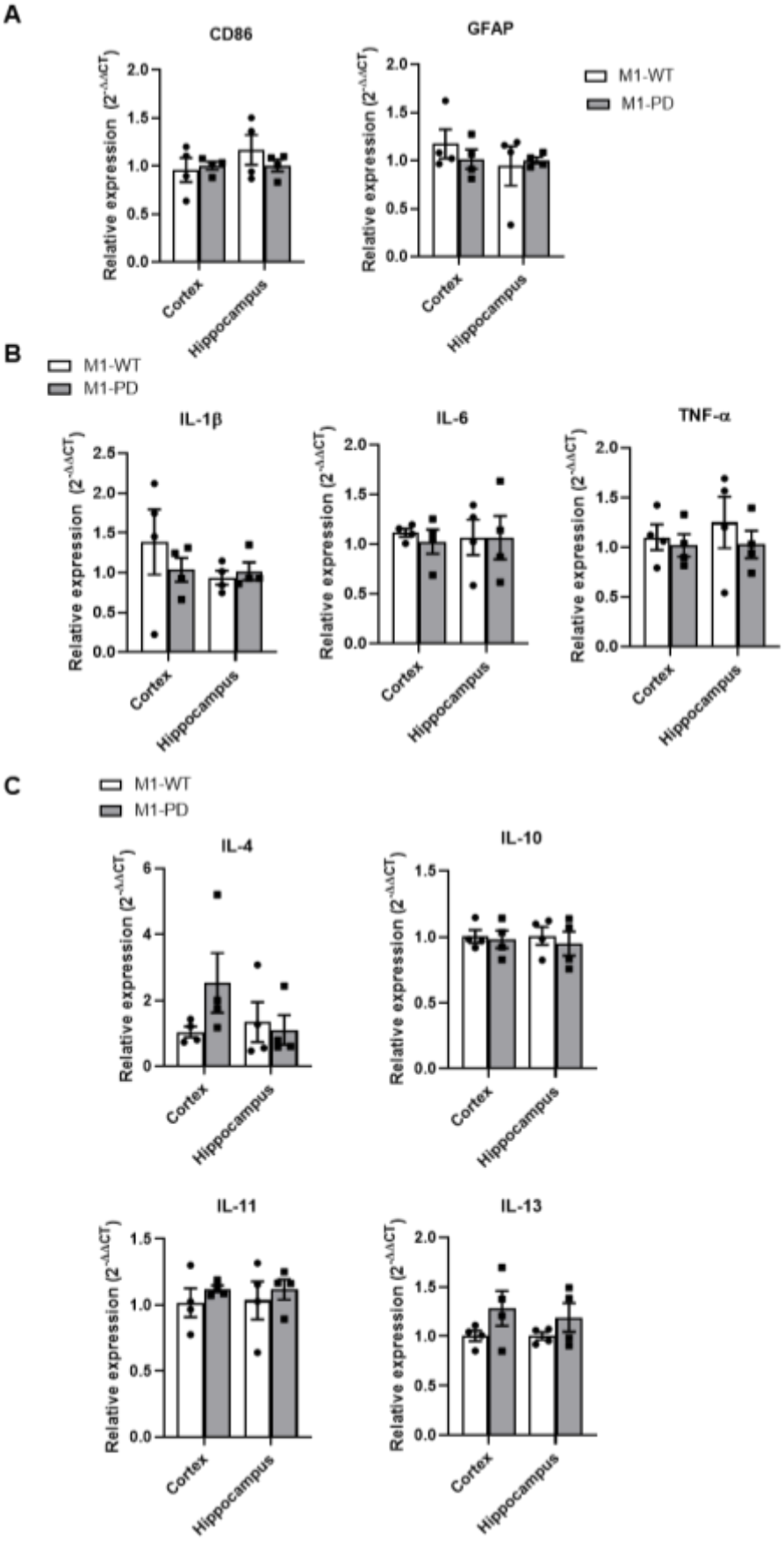

Figure 5-15 Expression of neuroinflammatory markers and cytokines in M1-WT and M1-PD mice. (A) Quantitative RT-PCR showing the expression of CD86 and GFAP, markers of microglia and astrocytes respectively, in the cortex or hippocampus of M1-WT or M1-PD mice. **(B-C)** Quantitative RT-PCR showing the expression of pro-inflammatory **(B)** TNF-α, IL-1β and IL-6, and anti-inflammatory cytokines **(C)** IL-4, IL-10, IL-11 and IL-13 in the cortex or hippocampus of M1-WT or M1-PD mice. Data are expressed as a ratio of α-tubulin RNA expression (N=4 mice).

The three major mammalian MAPKs subfamilies – ERK1/2, JNK and the p38 kinase – have been associated with the regulation of a variety of cellular functions, particularly cell survival. Specifically, JNK/SAPK and p38 MAPK have been shown to promote cell death, whereas ERK1/2 activation has been linked to both pro-death and pro-survival effects depending on the duration of the signalling and/or signalling partners (Tait and Green, 2008, Subramaniam and Unsicker, 2010). Since removal of phosphorylation from the M1 mAChR might alter the activation of MAPK pathways, I assessed the expression and activation of ERK1/2, JNK/SAPK and p38 MAPKs in control- and prion infected, M1-WT and M1-PD mice at 18 w.p.i. using western blots on hippocampal and cortical samples (Figure 5-16).

No significant difference in ERK1/2 and p38 expression or activation was found in the cortex or hippocampus of control and prion-diseased M1-WT and M1-PD mice at 18 w.p.i. suggesting that ERK1/2 signalling is not involved in the progression of mouse prion disease.

Control M1-PD mice showed a 1.3-fold increase of phosphorylated SAPK/JNK in the cortex, which was significantly ($P=0.0057$) higher than in M1-WT mice. In the hippocampus, the only significant difference detected was a 1.6-fold upregulation in total SAPK/JNK that was significantly ($P=0.029$) higher compared to prion-diseased M1-WT mice.

Further, the PI3K/AKT/mTOR signalling pathways has been shown implicated in the pathology of neurodegenerative disorders including AD, PD and HD (Xu et al., 2020, Rai et al., 2019), thus the active phosphorylated and total levels of Akt protein were also assessed in 18 w.p.i. control and prion-infected, M1-WT and M1-PD mice (Figure 5-17). No significant differences were found in either control- nor prion-diseased M1-WT and M1-PD mice at 18 w.p.i.

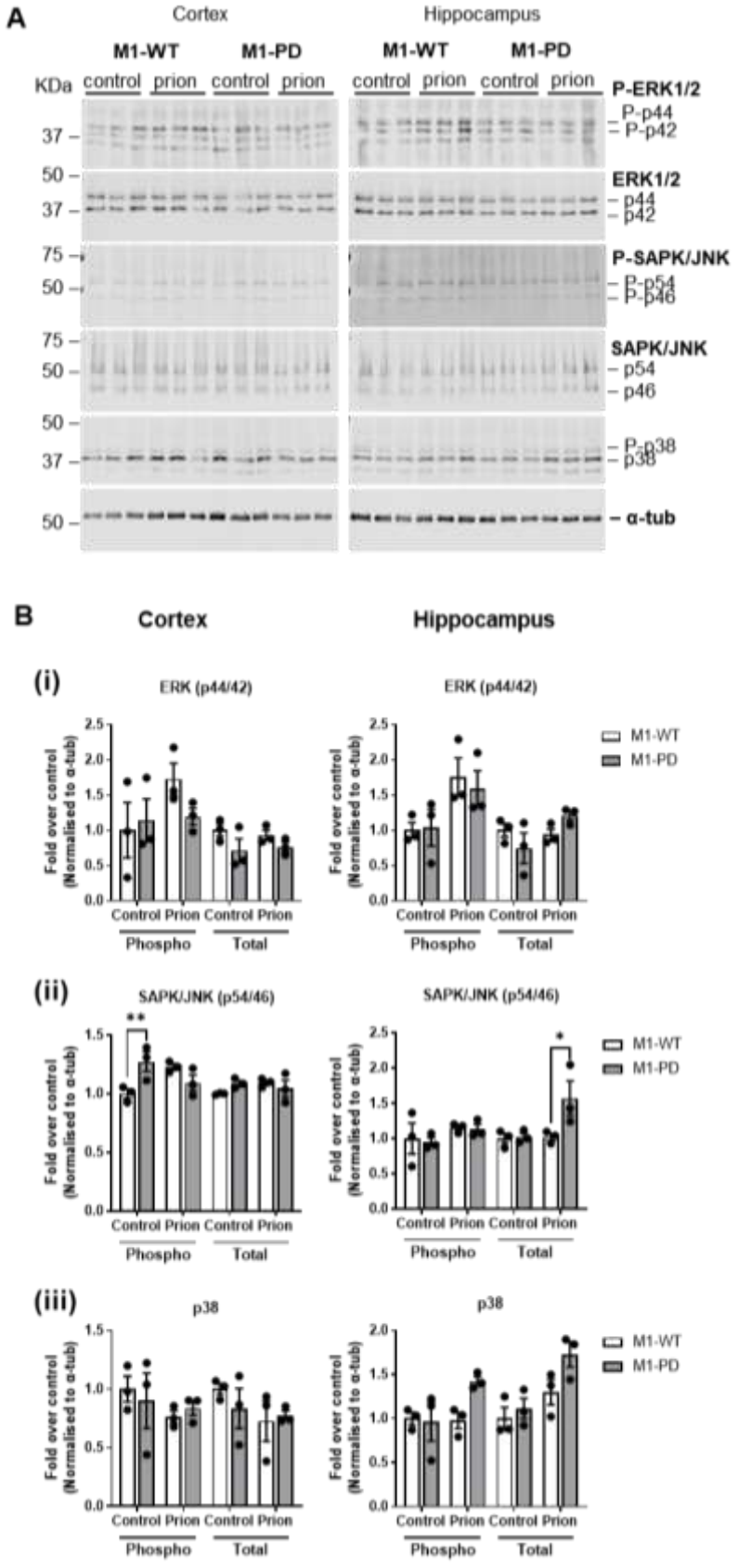

Figure 5-16 Expression of MAPKs in control- or prion-infected M1-WT and M1-PD mice. (A) Western blots to determine the expression of MAPKs in the cortex and hippocampus during prion disease were conducted on lysates prepared from control- or prion-infected, M1-WT or M1-PD mice at 18 w.p.i. α-tubulin (α-tub) antibody was used for loading control. **(B)** are the band analysis of cortex and hippocampus in (A) for **(i)** phospho- and total ERK1/2 (p44/43), **(ii)** phospho- and total SAPK/JNK (p54/46), and **(iii)** phospho- and total p38. Statistical analysis performed is two-way ANOVA with Sidak's multiple comparisons, where *P<0.05, (Fisher's LSD test), where *P<0.05 and ***P<0.001 (N=3).

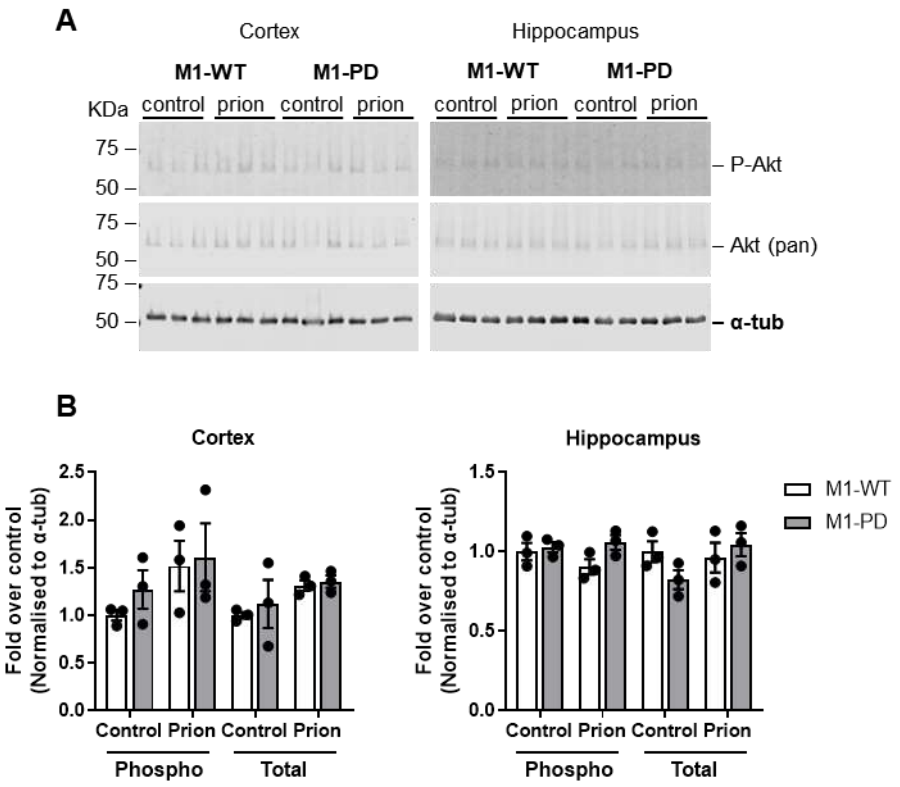

Figure 5-17 Expression of Akt in control or prion-infected M1-WT and M1-PD mice. (A) Western blots to determine the expression of phosphorylated or total Akt protein kinase in the cortex and hippocampus during prion disease was conducted on lysates prepared from control or prion-infected, M1-WT or M1-PD mice at 18 w.p.i. α-tubulin (α-tub) antibody was used for loading control. **(B)** are the band analysis of cortex and hippocampus in (A), conducted using a LICOR software, Image Studio Lite 5.2. Statistical analysis performed is two-way ANOVA with Sidak's multiple comparisons, where *P<0.05 (N=3).

5.2.4 The impact on hippocampal responses of the M1-PD mutation in prion-infected mice

Progression of mouse prion disease is characterised by behavioural abnormalities associated with decline in hippocampal functions. Burrowing behaviour in rodents gives an indication of innate hippocampal function independent from memory processes (Deacon, 2006). Prion-diseased Tg37 mice exhibit deficiencies in burrowing activity at 9 w.p.i. coincidently with a reduction in synapse number and synaptic transmission in CA1 neurons indicating a decline in hippocampal function (Moreno et al., 2012). I assessed burrowing behaviour in prion-infected M1-WT and M1-PD mice and found that M1-PD exhibited a faster decline in hippocampal activity compared to M1-WT animals since the decline in burrowing behaviour occurred earlier. Specifically, the burrowing behaviour was significantly decreased in M1-PD mice by approximately 20% compared to M1-WT at 14- (P=0.048) and 15 w.p.i. (P=0.017) (Figure 5-18). From 16 w.p.i. onwards, there were no significant differences in burrowing behaviour of prion-infected

M1-WT and M1-PD mice. Importantly, the burrowing responses of M1-WT and M1-PD mice inoculated with control brain homogenate were equivalent at through the course of the experiment, from 9- to 17 w.p.i.

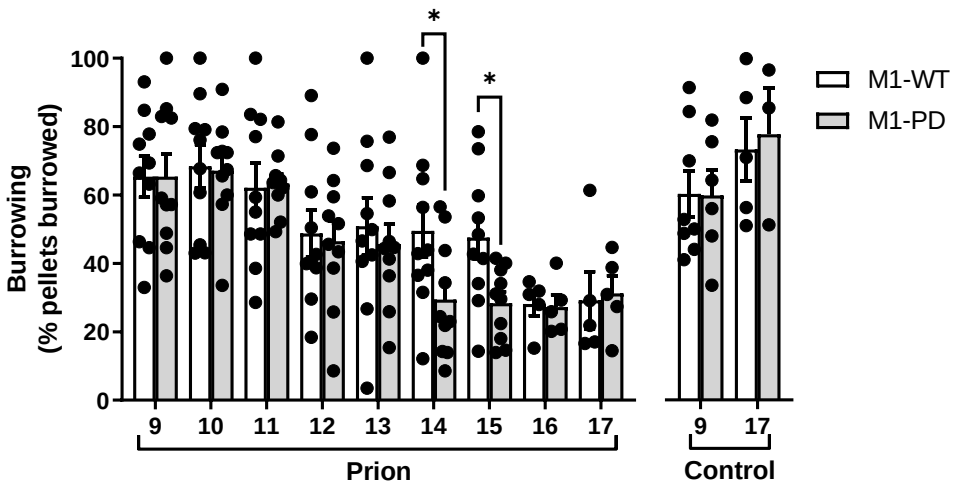

Figure 5-18 Prion-infected M1-PD mice display an earlier decline in burrowing ability than diseased M1-WT mice. Burrowing response of control and prion-infected mice was assessed following acclimatisation from 9 w.p.i. Statistical analysis was two-way ANOVA or mixed-effects model with uncorrected Fisher's LSD test; *P<0.05, N=3-10 mice.

To test whether the removal of phosphorylation would also have an impact on learning and memory processes, a contextual and cued fear conditioning test was conducted on 16 w.p.i. control- and prion-infected, M1-WT and M1-PD mice (). The contextual and cued fear conditioning paradigm is a form of Pavlovian conditioning that enables the assessment of associative learning and memory in rodents whereby an association is made between a context and/or a conditioned stimulus (tone) and an aversive stimulus (electric foot shock) (Fanselow and Poulos, 2005, LeDoux, 2000). Associative memory is assessed in the ability of mice to retrieve the context or tone and is measured in freezing behaviour, which is indicative of fearful memory. Specifically, contextual memory retrieval has been associated to hippocampal functions (Anagnostaras et al., 2001) and tone retrieval with amygdala and auditory cortex (Quirk et al., 1997). Mouse prion disease has been demonstrated to cause impairments in contextual memory retrieval that occurs at 9-10 w.p.i. in prion-infected Tg37 mice, coincidently with a decline in burrowing activity (Bradley et al., 2017). Therefore, a deficit in fear conditioning response is expected in prion-diseased mice compared to control. However, no significant difference was observed

between control and prion-infected mice, neither between M1-WT and M1-PD strains.

The baseline time spent immobile during the training phase significantly increased for all the animals following the foot-shocks, suggesting the triggering of a fear response (Figure 5-19B). A significant difference in immobility was observed between control and prion mice of both strains following the foot-shocks, whereby prion-infected mice spent less time immobile. Locomotion measurements such as total distance travelled, and speed of motility (Figure 5-19C, D) further show that prion-diseased mice (both M1-WT and M1-PD) have increased locomotion during the baseline phase. This suggests that diseased mice have overall increased locomotion compared to healthy animals, and memory acquisition or short-time memory ability might be disrupted with prion disease. In addition, overall baseline levels for both context and tone retrieval are higher compared with the levels reported in Tg37 mice (Figure 4-25). In fact, baseline of control or prion-diseased M1-WT or M1-PD mice ranged from 22% to 50% time spent immobile, while control or prion-diseased mice ranged between 6% to 20%. This however could be due to differences in locomotor behaviour between C57BL/6J (M1-WT and M1-PD) and Tg37 strains.

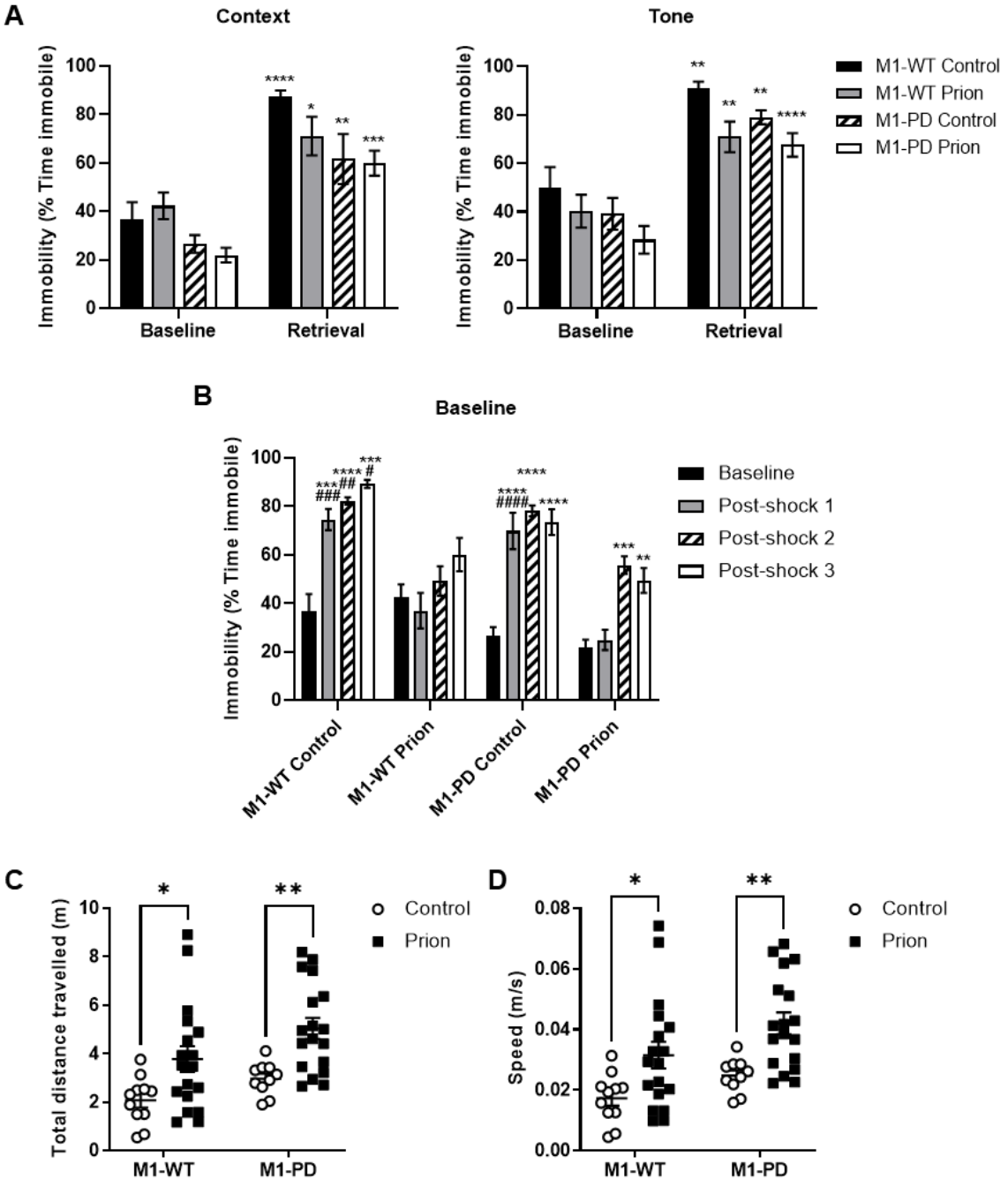

Figure 5-19 Prion-infected M1-PD mice display no differences in fear-conditioning memory responses compared with prion-infected M1-WT mice. Control or prion-infected, M1-WT and M1-PD mice (16 w.p.i.) underwent a fear conditioning test. Time immobile was measured as fear-conditioning response in **(A)** context retrieval and tone (unconditioned stimulus) retrieval, and for **(B)** the baseline on the training day. **(A)** Baseline measurements for context (in the absence of stimuli) and tone are compared to context retrieval and tone retrieval respectively to assess associative learning and memory in the mice. **(B)** Baseline immobility was recorded throughout training before and after each foot-shock. **(C)** Total distance travelled (in metres) and **(D)** speed (in meters/second) were calculated using the data acquired during the first 2 minutes of baseline to assess differences in locomotion behaviour. All data was statistically analysed using two-way ANOVA with Sidak's multiple comparison test where *P<0.05, **P<0.01, ***P<0.001, ****P < 0.0001 for control versus prion and $^{\#\#}$P<0.01, $^{\#\#\#}$P<0.001, $^{\#\#\#\#}$P<0.0001 for differences relative to baseline in (B) (N=9-14).

A previous study tested spatial working memory of M1-WT and M1-PD C57BL/6J mice using the Y-maze spontaneous alternation paradigm (Bradley et al., 2020). This paradigm is based on the innate behaviour whereby rats and mice explore previously unvisited areas. Therefore, rodents normally tend to explore a less recently visited arm of the Y-maze resulting in a spontaneous alternation of the arms entered (Dember and Fowler, 1959). Higher levels of anxiety (Bats et al., 2001), deficits in spatial memory and hippocampal lesions (Bats et al., 2001, Lalonde, 1986) were previously demonstrated to cause deficits in this innate behaviour and decrease the spontaneous alternation of arm entries. Bradley et al. (2020) found that the M1-PD mice have increased anxiolytic behaviour in an Elevated Plus Maze experiment, and a significant deficit in spontaneous alternation in the Y-maze paradigm. Whether this deficit is altered in prion disease has not been tested before. A Y-maze spontaneous alternation test was conducted on 16 w.p.i. control and prion-infected, M1-WT and M1-PD mice. No differences were observed in spontaneous alternation among any of the groups (Figure 5-20A). The lack of difference between M1-WT and M1-PD mice, which is inconsistent with the previous study (Bradley et al., 2020), might be due to the age of mice. Whilst Bradley et al. (2020) tested mice aged between 8 and 12 weeks, mice employed for this Y-maze experiment were 19-20 weeks old. Further, the lack of difference between control and prion-infected mice might indicate that either prion disease does not affect spatial working memory, or likely the disease hasn't advanced enough to see the effects on spatial working memory. Prion-infected mice, for both strains, showed an increase in number of arm entries per minute relative to their respective control (Figure 5-20B), however no significant difference was detected between M1-WT and M1-PD mice.

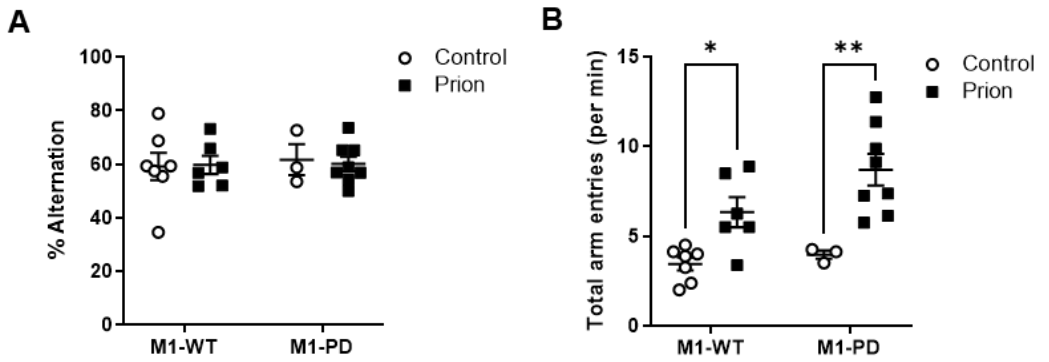

Figure 5-20 Spatial working memory response is unaltered in prion-infected M1-PD mice compared with M1-WT mice. Control and prion-infected 16 w.p.i., M1-WT or M1-PD mice were tested for 8 min in a Y maze spontaneous alternation paradigm to assess spatial working memory. **(A)** Spontaneous alternation behaviour was calculated by measuring the number of "ABC" sequences (in any order) as a proportion of the total triplet sequences made during the 8 min test. **(B)** Total distance travelled in an 8 min period by control and prion-infected, M1-WT and M1-PD. Data was statistically analysed using two-way ANOVA with a Sidak's multiple comparison test where **P=0.003, *P=0.025 (N= 3-8).

5.2.5 M1-PD show earlier disease onset and shorter survival time

Symptom onset and disease progression were assessed by the observation of the appearance of early, confirmatory, or clinical signs of disease. Mice are considered 'symptomatic' when they display at least two of the early indicators of prion disease (Mallucci et al., 2003)(Figure 5-21B,C). The appearance of at least two of the early indicators of prion disease occurred significantly earlier ($P<0.0001$) in M1-PD mice, compared to M1-WT. The median time for the onset of symptoms was 22 w.p.i. for M1-WT mice, and 20 w.p.i. for M1-PD mice. Individual early indicators of disease appeared consistently in prion-diseased M1-WT and M1-PD mice, indicating that none of the early indicators is associated to the M1-PD phenotype but it is a general feature associated to prion disease.

Mouse prion disease is a terminal neurodegenerative condition, and the animals are considered to have reached terminal disease with appearance of at least two confirmatory signs of disease or one sign of severe disease. Mice expressing the M1-PD mutant showed a significant ($P<0.0001$) acceleration of diagnosis of terminal illness (Figure 5-21A). Whilst the median survival for prion-infected M1-WT mice was 25 w.p.i., prion-infected M1-PD mice reached terminal disease at a median of 21 w.p.i.

Taken together, prion-infected M1-PD mice show accelerated disease progression that was evident in the significantly earlier symptom onset and

diagnosis of terminal illness compared to M1-WT mice. This indicates that phosphorylation/arrestin-dependent signalling pathways of the M1 mAChR physiologically contribute to a mechanism counteracting disease progression.

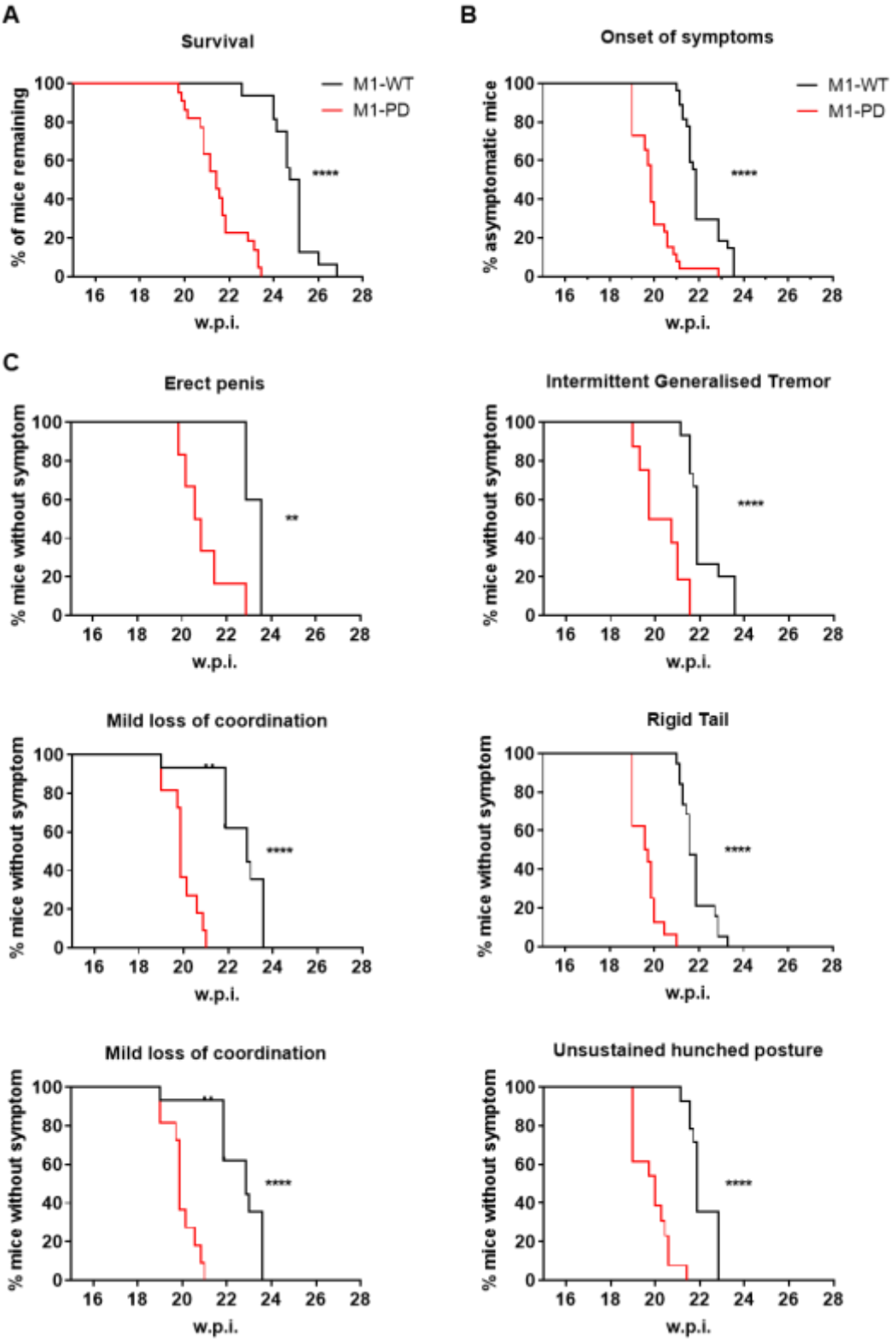

Figure 5-21 Removal of M1 mAChR phosphorylation sites accelerates prion disease and decreases survival time. (A) Kaplan-Meier survival plots (N=16-22) for prion-infected M1-WT or M1-PD knock in mice. **(B-C)** Curve comparisons (n>26-27) of onset of at least two early indicators of prion disease **(B)**, or individual symptoms **(C)**. Curves were analysed with a Gehan-Breslow-Wilcoxon test, where **P<0.01, ****P<0.0001.

5.3 Discussion

Selective activation of the M1 mAChR has been proven not only to improve cognitive symptoms in AD patients but was also demonstrated to exert disease-modifying effects in animal models of neurodegeneration and AD (Scarpa et al., 2020, Bradley et al., 2017, Lebois et al., 2017). Moreover, PAMs enable the achievement of exquisite selectivity at the M1 mAChR representing a safer therapeutic approach for the selective and safer treatment of neurodegenerative diseases (Foster et al., 2014, Gregory et al., 2007). These can engage receptor signalling resulting in beneficial physiological outcomes whilst being devoid of undesired adverse effects associated to off-target activation of peripheral cholinergic M2 and M3 mAChRs (Bymaster et al., 2003b, Conn et al., 2009). However, despite the promising evidence on the selective targeting of M1 mAChR in AD, even highly selective M1 PAMs have been associated with adverse cholinergic responses such as epileptic-like seizures (Rook et al., 2017, Moran et al., 2018a). This highlights the need to precisely define the pharmacological properties necessary in an M1 mAChR ligand to deliver therapeutically beneficial responses whilst being devoid of toxic effects that have previously been responsible for the failure of muscarinic drug discovery programmes for AD.

Previously, our group had generated a novel transgenic mouse model that was genetically engineered to express a phosphorylation-deficient variant of the M1 mAChR (M1-PD) that had all the MS-identified and other putative phosphorylation sites removed to reduce the receptor coupling to phosphorylation/arrestin-dependent pathways (Bradley et al., 2020, Butcher et al., 2016). This study established the relevance of phosphorylation/arrestin-dependent signalling pathways of the M1 mAChR in driving learning and memory, regulating anxiolytic-like behaviours and minimising central adverse cholinergic responses associated to M1 ligands (Bradley et al., 2020). Therefore, M1 mAChR compounds promoting receptor phosphorylation represent a safer approach for the symptomatic treatment of neurodegenerations compared to nonspecific muscarinic or cholinergic enhancers such as AChE inhibitors (Bodick et al., 1997b, Inglis, 2002). In support to this hypothesis, pilocarpine, a well-characterised muscarinic partial agonist that drives robust seizures (Hedlund and Bartfai, 1981), was shown to induce biased signalling toward G protein pathways

and stimulate 6-fold increases in phosphoinositide turnover over basal in the cortex when administered *in vivo* to rats (Bradley et al., 2020).

In this chapter, this study was extended to explore the role of the M1 mAChR-mediated phosphorylation/arrestin-dependent signalling in the disease-modifying potential of the M1 mAChR in neurodegenerative disease. This was achieved by employing the M1-PD mouse model (Bradley et al., 2020) in combination with mouse prion disease, a model of terminal neurodegeneration that shares key hallmarks with AD and other proteinopathies (Dwomoh et al., 2021). Removal of receptor phosphorylation in M1-PD mice caused a robust acceleration in prion disease progression compared to wild-type mice, which was evident in the earlier onset of disease-associated abnormal behaviours and hippocampal functions decline, shorter lifespan, and a robust upregulation of markers of neurodegenerative disease and neuroinflammation. This study revealed that the M1 mAChR possesses an inherent, endogenously regulated neuroprotective activity that is dependent on receptor phosphorylation-dependent signalling pathways (Figure 5-22). In addition, these findings strongly suggest that M1 mAChR-selective ligands that promote phosphorylation-dependent signalling pathways for the treatment of neurodegeneration would more likely delay neurodegenerative disease progression.

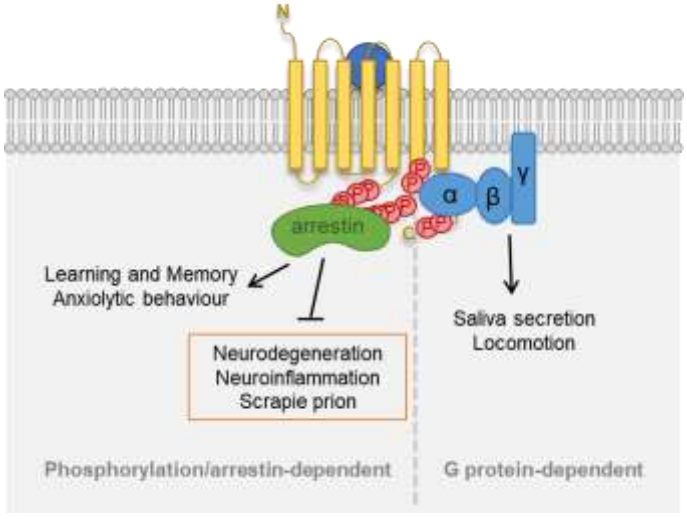

Figure 5-22 Illustration of the M1 mAChR physiological responses lying downstream of phosphorylation/arrestin-dependent versus G protein-dependent signalling. This diagram summarises the findings of this thesis and from Bradley et al. (2020). Using M1-PD mice, Bradley et al. (2020) discovered that G protein-dependent signalling pathways downstream of the M1 mAChR modulate saliva secretion and locomotory activity whereas phosphorylation/arrestin-dependent pathways are involved in learning and memory as well as anxiolytic behaviours. In this thesis, the combination of M1-PD mice with mouse prion disease let to the discovery that the phosphorylation/dependent pathways mediated by the M1 mAChR regulate an inherent neuroprotective activity that can delay neurodegenerative disease progression, counteract neuroinflammation and counteract accumulation of toxic scrapie prion.

The M1 mAChR has long been validated as a target for the symptomatic treatment of cognitive dysfunction as extensive evidence have demonstrated its involvement in learning and memory. For instance, ablation of M1 mAChRs has previously been shown to induce cognitive impairments in mice (Anagnostaras et al., 2003). For instance, in 3xTg-AD mice, while diseased mice display cognitive deficits (Billings et al., 2005), when 3xTg-AD mice and M1-KO mice are crossed, cognitive impairment is significantly worsened (Medeiros et al., 2011). Furthermore, pre-clinical and clinical studies have provided robust evidence of the cognitive improvement exerted by the pharmacological activation of the M1 mAChR (see 5.1.1). Here, by combining M1-PD mice with mouse prion disease I wished to assess the impact of removing the M1 mAChR phosphorylation-dependent pathway on neurodegeneration-induced cognitive dysfunctions. However, removal of M1 mAChR phosphorylation here showed no effects on cognitive performance of mice on cued fear-conditioning. This could be due to the disease stage at the time of testing as mice might not yet exhibit cognitive impairments. Alternatively, this data might indicate that M1 mAChR-mediated cognitive functions are not modulated by phosphorylation/arrestin-dependent pathways but instead by $G\alpha_q$ protein signalling.

The phosphorylation state of receptors plays a key regulatory role in the receptor signalling outcome, by influencing interactions with intracellular binding partners (see Chapter 3). Consequently, removal of M1 mAChR phosphorylation can significantly impact multiple downstream mechanisms and signalling pathways by influencing the interactions between the receptor and its binding and/or signalling partners and consequential active conformations of arrestins. Receptor internalisation is a recognised phosphorylation/arrestin-dependent process (Goodman et al., 1996, Laporte et al., 1999, Zhang et al., 1999). Previously, the M1 mAChR was demonstrated to preferentially localise intracellularly and associate with Golgi and ER (Yamasaki et al., 2010, Anisuzzaman et al., 2013). This characteristic localisation is not agonist-dependent and it is not affected by M1 antagonists such as atropine or pirenzepine (Butcher et al., 2016, Uwada et al., 2014), suggesting the M1 mAChR is constitutively internalised or a pool of newly synthetised receptors are retained at the Golgi and/or ER. Here, and in the previous studies (Bradley et al., 2020, Scarpa et al., 2021), removal of receptor phosphorylation was found

to cause a significant reduction in internalisation of the M1 mAChR, both *in vitro* (Chapter 3) and in *ex vivo* tissue, indicating that receptor phosphorylation is crucial for M1 mAChR localisation.

Lack of receptor phosphorylation could also cause a reduction of GPCR signalling desensitisation, resulting in excessive activation of signalling pathways (Lohse, 1993, Gurevich and Gurevich, 2019). There a possibility that the M1-PD variant might induce an overall excessive activation of G protein-signalling pathways such as ERK1/2 signalling, and sustained ERK1/2 signalling has been associated to neuronal cell death in neurodegenerative diseases such as AD, and attributed to hyperphosphorylation of tau (Guise et al., 2001, Harris et al., 2004, Pei et al., 2002), Aß toxicity (Rapoport and Ferreira, 2000, Frasca et al., 2008) and oxidative stress (Perry et al., 1999, Stanciu et al., 2000). However, it was established that whilst ACh display higher potency in $G\alpha_q$ activation at the M1-PD, the efficiency of $G\alpha_q$ activation and stimulation of $G\alpha_q$-driven pathways (inositide phosphate signalling) are comparable in the M1-PD and the M1-WT (Scarpa et al., 2021, Bradley et al., 2020). In addition, lysates from the hippocampus and cortex of control or prion-diseased M1-WT and M1-PD mice showed here similar levels of expression and activation of ERK1/2. This further indicates that the accelerated neurodegeneration observed in prion-disease M1-PD mice is not due to an overall excessive activation of the ERK1/2 pathway, but it is caused by the removal of a neuroprotective mechanism, which is dependent on M1 mAChR phosphorylation.

The activation of other MAPK signalling pathways such as the stress-activated protein kinase, JNK/SAPK, and the p38 pathways have long been established to promote neuronal cell death (Xia et al., 1995, Kummer et al., 1997, Willaime-Morawek et al., 2003) and be associated to neurodegenerative diseases including AD and PD (Pei et al., 2002, Pei et al., 2001, Wang et al., 2014, Sun et al., 2003). Given that GPCRs can regulate MAPK signalling pathways, there is a possibility that M1-PD mice exhibit a dysregulation of these pathways resulting in acceleration of neurodegeneration. No significant difference in total or activated p38 were found in the brain compared M1-PD mice compared to wild-types. However, interestingly, phosphorylated SAPK/JNK levels were significantly higher in the cortex (but not hippocampus) of control M1-PD compared to M1-WT mice, and total SAPK/JNK protein levels were upregulated

in the hippocampus of prion-diseased M1-PD mice compared to diseased wild-type animals. It would be valuable to investigate the role of the SAPK/JNK signalling pathway in more detail in prion disease and establish whether the M1 mAChR plays a regulatory role. Further, activation and expression of Akt was assessed in prion-diseased M1-PD mice compared to wild-type animals since PI3K/AKT/mTOR signalling pathways have been implicated in the pathology of neurodegenerative disorders including AD, PD and HD (Xu et al., 2020, Rai et al., 2019). However, no significant differences were found neither in disease nor control M1-WT and M1-PD mice at 18 w.p.i., indicating that the PI3K/AKT/mTOR might not be important in prion neurodegeneration.

In the context of mouse prion disease, lack of M1 mAChR phosphorylation has a significant impact on neurodegenerative disease progression. Strikingly, prion-infected M1-PD mice display higher accumulation of protease-resistant PrP_{Sc} at the disease time-points examined compared to the respective wild-type mice, suggesting that phosphorylation-dependent signalling likely accounts for the effects of M1 PAMs on PrP_{Sc} conversion. Pathogenesis of prion disease is dependent on prion proteins, as it was shown that depletion of PrP is able to reverse pathology (Mallucci et al., 2003). Pharmacological activation of the M1 mAChR using highly selective M1 PAMs, BQCA (Bradley et al., 2017) and VU0486846 (Dwomoh et al., 2021), could decrease the accumulation of PrP_{Sc} and significantly extend the lifespan of terminally ill mice with prion disease (Bradley et al., 2017, Dwomoh et al., 2021). The findings from this chapter strongly suggest that M1 mAChR-mediated signalling is able to counteract the PrP_{Sc}-driven pathogenesis, specifically through a mechanism that is dependent on receptor phosphorylation.

PrP_{Sc} self-propagate and form aggregates in a similar fashion as neurotoxic proteins typical of human proteinopathies such as AD, PD and HD (Aguzzi and Calella, 2009, Caughey et al., 1999, Mallucci et al., 2003, Sandberg et al., 2014, Prusiner, 1982, Duyckaerts et al., 2019). This raises the possibility that the neuroprotective mechanism mediated by the M1 mAChR that is able to hamper the accumulation of PrP_{Sc} in mouse prion disease might be relevant against the formation of other prion-like neurotoxic proteins such as Aß and NFT in AD, α-synuclein in PD or huntingtin in HD (Halliday and Mallucci, 2014). The UPR, particularly the ERK/elF2α branch of the UPR response, was shown to be

activated in prion disease (Moreno et al., 2012), and this is likely to be shared with human proteinopathies and it has been proposed as a potential therapeutic target (Halliday and Mallucci, 2014, Halliday and Mallucci, 2015, Moreno et al., 2012). It would be interesting to test whether the M1 mAChR has some involvement in the modulation of the UPR signalling pathway.

In addition, further supporting the neuroprotective role of the M1 mAChR in neurodegenerations caused by the misfolding of proteins, neurotoxicity and AD-like pathology was shown to be exacerbated in mouse models that resulted from the crossing the M1-KO mice with three distinct AD mouse models, APPswe/Ind, 3xTg-AD and Tg-SwDI, demonstrating that loss of M1 mAChRs could promote disease (Davis et al., 2010, Medeiros et al., 2011). Specifically, loss of M1 mAChRs in APPswe/Ind mice caused an increase in disease-associated amyloidogenic processing resulting in higher presence of Aß plaque and a significant reduction in α-secretase-cleaved APP (Davis et al., 2010). In addition, ablation of M1 mAChR in 3xTg-AD mice resulted in increased levels of hyperphosphorylated tau, by a mechanism that depends on increased $GSK3_{\beta}$ levels **(**Figure 5-1**)**, further confirming that loss of M1 receptors causes exacerbation of both Aß and tau pathologies in AD mice (Medeiros et al., 2011). In this chapter, by subtle genetic modification of the M1 mAChR, the phosphorylation/arrestin-dependent signalling mediated by the M1 mAChR was demonstrated to be specifically important for the protective mechanism against neurodegeneration caused by prion, and this could be translated to other diseases that are characterised by 'prion-like' protein aggregates.

Global proteomic and transcriptomic analyses of hippocampi from prion-infected mice identified a panel of prion disease-associated markers that are "normalised" following chronic administration of the M1 PAM VU0486846, to levels similar to the ones found in healthy mice (Dwomoh et al., 2021). These include proteins that are involved in disease-adaptive responses such as APO-E and clusterin, which are strongly associated to LOAD (Lambert et al., 2009, Harold et al., 2009, Corder et al., 1993, Strittmatter et al., 1993), inflammatory markers galectin-1, GFAP and vimentin (Starossom et al., 2012, Sundblad et al., 2017, Kamphuis et al., 2012, Kamphuis et al., 2014, Jiang et al., 2012) and serpinA3N (Dwomoh et al., 2021). Prion infected M1-PD mice were found to show significantly higher upregulation of APO-E, clusterin, galectin-1, serpinA3N,

vimentin and GFAP in prion disease, compared to their wild-type counterparts. Findings from this chapter suggest that the disease modification properties of M1 PAMs that can modulate disease-adaptive mechanisms are likely to be driven by phosphorylation/arrestin-dependent signalling pathways of the receptor. In addition, many of the protein markers that are found associated with mouse prion disease and whose levels are altered by M1 mAChR signalling pathways are shared with AD and other human neurodegenerative conditions (Dwomoh et al., 2021). This indicates that the neuroprotective activity endogenously regulated by the M1 mAChR against mouse prion disease is likely relevant in many human neurodegenerative diseases.

Disruption of cholinergic innervations is another pathological hallmark of mouse prion disease (Bradley et al., 2017, Mallucci et al., 2003), that is also shared with other neurodegenerative conditions including AD (Bartus et al., 1982, Francis et al., 1999). Cholinergic neurons are characterised by the ability of synthesising ACh from acetyl-CoA and choline by ChAT enzyme (Trifonov et al., 2009, Woolf and Butcher, 1981). No differences in levels of ChAT nor neuronal markers were detected between control and prion in M1-WT or M1-PD mice, but this is likely because animals are still at early stages of prion disease (18 w.p.i.), before onset of symptoms, clinical disease and neuronal loss. Interestingly, however, at this stage, prion disease seems to disrupt the filamentous arrangement of the enzyme as observed in immunohistochemical staining, particularly evident in the hippocampal CA1 region that is more abundant of cholinergic neurons. Nevertheless, the survival study provides sufficient evidence supporting the neuroprotective activity mediated by the phosphorylation/arrestin-dependent of the M1 mAChR against prion-induced neurodegeneration, and potentially against many other neurodegenerative conditions.

Neuroinflammation, characterised by microgliosis and astrogliosis, is another established pathological marker of mouse prion diseases that is common to many neurodegenerative disorders including AD, and it is thought to contribute to disease progression (Ransohoff, 2016, Amor et al., 2014, Bradley et al., 2017, Carroll et al., 2015). Interestingly, there has been increasing evidence in prion disease that gliosis, together with PrP_{Sc} deposition, occurs at the earliest stages of disease, preceding the onset of clinical pathology i.e. spongiosis, neuronal

damage and clinical symptoms (Baker and Manuelidis, 2003, Carroll et al., 2016, Diaz-Espinoza and Soto, 2012, Sandberg et al., 2014). Thus, suggesting that both PrP_{Sc} and gliosis might contribute to the pathogenesis of prion diseases. Recently, M1 PAMs were shown to resolve neuroinflammation in prion-diseased mice (Dwomoh et al., 2021). Here, markers of astrocytes, GFAP and vimentin, and of microglia, Iba-1 and CD86, are found upregulated with prion disease, and removal of M1 mAChR phosphorylation significantly increased the expression of these neuroinflammatory markers. Pro-inflammatory cytokines, such as TNF-α, IL-1ß and IL-6, are also found to be upregulated in the brain of prion-infected mice, and they are likely to contribute to the exacerbation of neuroinflammation. Particularly, TNF-α is a major pro-inflammatory cytokine in many neurological disorders including AD (Fischer and Maier, 2015, Liddelow et al., 2017, Michaud et al., 2013, Olmos and Lladó, 2014), and it was proposed as drug target for the treatment of neurodegenerative conditions (Decourt et al., 2017, Tweedie et al., 2007). Interestingly, TNF-α (hippocampus and cortex) and IL-1ß (cortex only) transcripts were found to be significantly increased in prion-infected M1-PD mice compared to prion-infected M1-WT mice. These data suggest that M1 mAChR phosphorylation-dependent signalling has a role in protecting against neuroinflammation, and that removal of phosphorylation-dependent signalling leads to earlier exacerbation of microgliosis and astrogliosis. However, it is to be elucidated whether the M1 mAChR is directly involved in the inflammatory mechanisms in response to neurodegeneration. Or whether the M1 mAChR modulates neuroinflammation indirectly, by regulating the upstream prion-driven neurodegeneration and/or disease-adaptive mechanisms that consequently exacerbate neuroinflammation. Intracerebral administration of the M1 mAChR-selective bitopic ligand McN-A-343 (Valant et al., 2008) was shown to cause a dose-dependent inhibition of systemic TNF-α levels in an endotoxemia (bacterial infection) rat model, demonstrating that M1 mAChRs in the CNS (but not peripheral) are key mediators of the peripheral inflammatory response through the vagus nerve (Pavlov et al., 2006). In addition, Lehner et al. (2019) recently reported that administration of the M1 PAM BQCA causes a reduction of TNF-α levels in the serum of endotoxemic mice, and selective optogenetic stimulation of cholinergic neurons in the basal forebrain demonstrated that this mechanism is mediated by neurons in this brain region, where the M1 mAChR is highly expressed. These studies propose

the possibility that the anti-inflammatory mechanism regulated by cholinergic neurons in the forebrain might be impaired in diseases associated with cholinergic dysfunction, such as AD, causing the exacerbation of neuroinflammation (Lehner et al., 2019). Furthermore, neuroinflammation was found to be significantly worsened in AD mouse models, 3xTgAD and Tg-SwDI, by the loss of M1 mAChR receptors, indicated by an increase in both astrocytes and microglia as well as an upregulation of pro-inflammatory cytokines IL-1β and TNF-α, that correlated with higher levels of Aβ and tau pathology (Medeiros et al., 2011). This provides further evidence that the M1 mAChR is a critical modulator of neuroinflammation in the context of neurodegenerative disease and strongly points towards the possibility that the M1 mAChR directly modulates immunity in the brain. Therefore, given the M1 mAChR has been shown here to have an inherent neuroprotective activity that can modify neurodegenerative disease, this activity might be associated to the regulatory role of the M1 mAChR in the immunity of the CNS.

Chapter 6 Final discussion

The M1 mAChR has been viewed for many years as a promising target for the treatment of AD and other neurodegenerative diseases (Felder et al., 2018, Foster et al., 2014). Significant preclinical and clinical data suggest that selective activation of the M1 mAChR might offer a promising alternative approach to the current treatment options, AChE inhibitors, for improving cognitive function in AD. In fact, AChE inhibitors are nonspecific and cause poorly tolerated adverse effects, including GI and cardiovascular side effects, associated to the potentiation of peripheral cholinergic signalling (Inglis, 2002, Courtney, 2004). Particularly, targeting allosteric sites at the M1 mAChR can provide exquisite receptor subtype selectivity to minimise off-target adverse responses and represent a safer alternative to AChE inhibitors and muscarinic orthosteric agonists, which normally lack of subtype selectivity (Gregory et al., 2007). Furthermore, the emergence of evidence from preclinical animal studies that the M1 mAChR can modify the underpinning neurodegenerative disease progression has generated substantial attention (Scarpa et al., 2020, Lebois et al., 2017, Bradley et al., 2017, Davis et al., 2010). Activation of the M1 mAChR was demonstrated to regulate the proteolytic processing of APP (Figure 5-1), thereby reducing the development of Aß pathology in a mouse model of Aß pathology (Davis et al., 2010). In addition, M1 mAChR-selective PAMs could slow down the progression of mouse prion disease, extending the lifespan of terminally ill animals and significantly reducing levels of proteins that are associated to disease-adaptive responses (Bradley et al., 2017, Dwomoh et al., 2021). The findings from this thesis unravel a neuroprotective activity against prion neurodegenerative disease progression that is inherently mediated by the M1 mAChR through a mechanism that is dependent on receptor phosphorylation.

Like the other members of the GPCR superfamily, the M1 mAChR transduce signalling by coupling to two fundamental signalling pathways: the G protein-dependent and the phosphorylation/arrestin-dependent signalling pathways (Costa-Neto et al., 2016). Thus, to investigate the physiological role of the M1 mAChR signalling, a phosphorylation-deficient mutant of the M1 mAChR (M1-PD) was generated, whereby all the MS-identified and putative intracellular phosphorylation sites were removed to uncouple the receptor from phosphorylation-dependent signalling (Butcher et al., 2016). *In vitro* studies in

Chapter 3 established that whilst removal of M1 mAChR receptor phosphorylation has little impact on G protein-dependent signalling (phosphoinositide accumulation), it significantly impairs agonist-induced receptor internalisation. This was consistent with other reports (Bradley et al., 2020, Scarpa et al., 2021). However, it was demonstrated that the M1-PD variant causes a reduction in arrestin recruitment by around 50% (Bradley et al., 2020, Scarpa et al., 2021). This indicated that although phosphorylation is important for arrestin recruitment to the M1 mAChR, this receptor likely interacts with arrestin in a phosphorylation-independent manner, such as through the ICL3, similarly to other muscarinic subtypes (Wu et al., 1997, Gurevich et al., 1995). To understand the physiological relevance of the M1 mAChR signalling bias, two muscarinic agonists that induce profound seizures in rodents, GSK1034702 and pilocarpine (Bradley et al., 2018, Bradley et al., 2020), were investigated *in vitro*. Both GSK1034702 and pilocarpine induce similar levels of IP1 accumulation, but significantly reduced receptor internalisation compared to the endogenous ligand ACh. The lack of signalling bias of pilocarpine calculated in Chapter 3 is not consistent with previous studies (Bradley et al., 2020), however this is likely due to limitations of the assays employed here. Bystander BRET assays are a more reliable method for the analysis of signalling mechanisms *in vitro*, as employed by Scarpa et al. (2021). Another drawback is that the M1 mAChR signalling has largely been investigated in artificial cell lines such as CHO and HEK293 cells, where the receptor is normally over-expressed (both in this thesis and in the wider literature). Although the simplicity of these *in vitro* models allows for basic GPCR signalling assays, they are not representative of the relevant signalling in the CNS. M1 mAChR-mediated signalling could be investigated in primary cell systems for example in primary hippocampal neurons, which are the most physiologically relevant for the M1 mAChR signalling (Levey, 1993). Bystander BRET assays could also be used to assess M1 mAChR signalling in primary hippocampal neuronal cultures (Scarpa et al., 2021). The stoichiometry of interacting partners e.g., GRKs, G proteins and arrestins, vary between different cell types and tissues, adding a layer of complexity to physiological signalling bias (Kenakin, 1997, Newman-Tancredi et al., 1997, Newman-Tancredi et al., 2000). Overall, data from Chapter 3 strongly indicates that the M1-PD receptor is impaired in phosphorylation/arrestin-dependent

mechanisms, drawing to the conclusion that this variant is a G protein-biased receptor, with deficits in arrestin recruitment and receptor internalisation.

A transgenic mouse model expressing the M1-PD was generated to explore the physiological role of the phosphorylation/arrestin-dependent signalling pathways mediated by the M1 mAChR (Butcher et al., 2016, Bradley et al., 2020). By employing the M1-PD mouse model, our laboratory established that phosphorylation of the M1 mAChR is important to drive cognitive processes (spatial memory), regulate anxiolytic-like behaviour, and hinder central adverse cholinergic responses such as seizures (Bradley et al., 2020). Therefore, suggesting that M1 mAChR compounds promoting receptor phosphorylation represent a safer approach for the symptomatic treatment of neurodegenerations compared to nonspecific muscarinic or cholinergic enhancers such as AChE inhibitors.

In this thesis, the M1-PD mouse model was employed in combination with the mouse prion disease model of terminal neurodegeneration to investigate the physiological relevance of the M1 mAChR signalling bias in neurodegenerative disease. Mouse prion disease was established to be a relevant model for human neurodegenerative diseases as it shares key hallmarks with those and particularly AD. As opposed to commonly used mouse models of AD, mouse prion disease is a progressive and terminal neurodegenerative condition that is advantageous to test both pro-cognitive and disease-modifying effects of M1 mAChR ligands. In fact, at early stages of prion disease, whilst mice show no physical signs of disease, they manifest biochemical and histopathological evidence of disease as well as behavioural changes such as a decline in burrowing behavior and a deficit in learning and memory (Mallucci, 2009). For instance, misfolded PrP_{Sc} was detected here through western blot analysis from 6 w.p.i. in the cortex, hippocampus and striatum of prion-infected mice, which is consistent with previous reports (Mallucci et al., 2007). This finding establishes that prion infected Tg37 mice have already developed scrapie pathology at 7 w.p.i., when dosing normally starts for therapeutic evaluation of novel M1 mAChR-selective ligands (Bradley et al., 2017, Dwomoh et al., 2021), when no physical symptoms are yet manifested. This therefore indicates that the therapeutic effects exerted by activation of the M1 mAChR are not due to prevention of disease, but disease-modification. In addition, prion-diseased mice

display the upregulation of proteins that are considered markers of AD, including APO-E, clusterin, and regulator of proteolysis serpinA3N (Dwomoh et al., 2021). In Chapter 4, APO-E, clusterin, serpinA3N and clusterin were all found to be elevated in prion-diseased mice from 7 or 8 w.p.i., at a pre-symptomatic phase of disease, with the most robust increases at 9 w.p.i. The role of serpinA3N in neurodegeneration is largely unexplored, and it might be a disease-adaptive process in response to the progressing accumulation of misfolded, toxic proteins such as PrP_{Sc}. Both APO-E and clusterin are considered some of the highest risk factors for LOAD (Roses et al., 1995, Jiang et al., 2008, Lambert et al., 2009, Harold et al., 2009). Thus, upregulation of APO-E and clusterin in the brain of prion-infected mice further support the concept that mouse prion disease shares central disease-adaptive mechanisms with human neurodegenerations and could be a relevant model for LAOD, which accounts for the majority of dementia cases. Strikingly, the M1 PAM VU0486846 could significantly decrease the levels of APO-E and clusterin in the hippocampus prion-ill mice, to levels similar to the healthy controls (Dwomoh et al., 2021). This strongly indicates that pharmacological activation of the M1 mAChR is a promising therapeutic approach for the treatment of AD.

The mouse prion disease model also displays the elevation of many inflammatory astrocytic and microglial markers that are shared with human neurodegenerations, including GFAP, vimentin and galectin-1 (Dwomoh et al., 2021, Heneka et al., 2015, Ransohoff, 2016). In Chapter 4, RML prion-infected Tg37 mice show the most significant upregulation in Iba1-stained microglia in the areas of PrP_{Sc} deposition such as the CA1 and CA2 hippocampal regions, corpus callosum and fimbria. This result is in line with previous studies showing that microglia activation occurs in response to PrP_{Sc} accumulation (Bate et al., 2002, Williams et al., 1997, Giese et al., 1998, Van Everbroeck et al., 2004, Kercher et al., 2007, Sandberg et al., 2014, Vincenti et al., 2015, Gómez-Nicola et al., 2013, Martinez and Gordon, 2014), and is comparable to observations of microglia surrounding Aß plaques in the brain of AD patients and in animal models of AD (Salter and Stevens, 2017). Overall, astrocytic markers were found upregulated with prion disease. GFAP was demonstrated to undergo a widespread upregulation across the brain of prion-infected mice, whereas vimentin showed a striking upregulation in the hippocampus, thalamus and

cortex, that are brain regions that normally display most deposition of PrP_{Sc} (Mallucci et al., 2003). In addition, vimentin was found particularly elevated in sites of microgliosis and spongiosis, leading to the hypothesis that vimentin might be specifically linked to reactive astrocytes with a neurotoxic phenotype. In support of this hypothesis, vimentin was previously shown to contribute to microglia activation and neurotoxicity in cerebral ischemia (Jiang et al., 2012). Galectin-1, a glycan-binding protein that modulates astrocyte and microglia activation and other immunological responses including apoptosis, cell activation, and cytokines release (Dhirapong et al., 2009), was found associated with mouse prion disease (Dwomoh et al., 2021). Here, increases in galectin-1 were detected in the hippocampus of prion diseased mice at 9 w.p.i. Galectin-1 was shown to have neuroprotective effects and has been proposed as a target for the treatment of chronic neuroinflammatory and neurodegenerative diseases (Ramírez Hernández et al., 2020). Interestingly, a preliminary study on aged PDAPPJ20 transgenic mice has shown that the administration of galectin-1 significantly enhanced cognition in a NOR test and induced a robust reduction in Aß in the hippocampus (Presa et al., 2019). In AD and other neurodegenerative disease, neuroinflammation is also exacerbated by the production of pro-inflammatory such as TNF-α, IL-1ß and IL-6 (Block et al., 2007, Moss and Bates, 2001, Liu et al., 2015, Sawada et al., 1989, Lee et al., 1993). In Chapter 4, TNF-α, IL-1ß and IL-6 transcript levels were found elevated in the brain of 10 w.p.i. prion-diseased mice. However, in situ hybridisation of TNF-α transcripts using RNAScope methods, established that this cytokine is mostly produced in the CA2 hippocampal region, cortex and thalamus of RML prion infected Tg37 mice, which corresponds to the brain regions displaying most scrapie pathology (Mallucci et al., 2003). Like in AD, the role of neuroinflammation in the progression of prion disease remains however ambiguous.

As the disease progresses to late stages, prion-infected mice develop terminal clinical symptoms that allow the testing of the effectiveness of novel M1 mAChR ligands on survival. Chapter 4 establishes that no significant changes in presynaptic, postsynaptic, and cholinergic markers were observed, which is consistent with previous reports that demonstrated neuronal loss in RML-infected Tg37 mice occur from 10 w.p.i. (Mallucci et al., 2003). However, spongiosis, which is the formation of intraneuronal vacuoles in cells that have

not yet degenerated, is present in the hippocampus of RML-infected Tg37 mice from 8 w.p.i. and robustly increases to 10 w.p.i. Since spongiosis was shown to proceed neuronal loss and clinical symptoms in mouse prion disease (Mallucci et al., 2003), the data from Chapter 4 indicate that prion infected Tg37 mice at 10 w.p.i. are still at a stage of pre-clinical disease that proceed physical symptoms and neuronal loss while manifesting the presence of PrP_{Sc} deposits in the hippocampus, cortex and striatum as well as hippocampal spongiosis. In addition, the dramatic, significant increase from 8 to 10 w.p.i. in all the pathological features observed, suggests that during this two-week window the progression from subclinical to clinical pathology occurs, thereby representing a good indicator to assess the disease progression during dosing studies.

Overall, Chapter 4 provides further evidence that the mouse prion disease model shares important disease hallmarks with AD and other neurodegenerative disorders, including markers of neurogenerative disease and neuroinflammation. Particularly, the spreading of PrP_{Sc} is closely associated with locally induced chronic neuroinflammation, that is similar to Aß plaques and NFT pathology in AD. Given this parallel, elucidating the role of neuroinflammation in the mouse prion disease could provide insights into the modulation of the neuroinflammatory response in human neurodegenerations and might help resolve the dispute on whether neuroinflammation is beneficial or detrimental in neurodegenerative disease (Allaman et al., 2011, Ben Haim et al., 2015). Further, since the M1 PAM VU0486846 could significantly reduce the levels of galectin-1, GFAP and vimentin in prion diseased mice (Dwomoh et al., 2021), an intriguing concept is that activation of the M1 mAChR is able to modify disease progression by decreasing detrimental neuroinflammation and/or altering the ratio between neurotoxic and neuroprotective reactive astrocytes. In addition, administration of VU0486846 (10 mg/kg) from 7 w.p.i., could significantly delay symptom onset and robustly prolong the lifespan of terminally ill prion infected mice. This was also accompanied by a significant reduction of many of the disease-associated markers – that were investigated in Chapter 4 - to levels similar to healthy control mice. This suggests that the disease-modifying potential of M1 PAMs might reside in the ability of the M1 mAChR to regulate adaptive responses such as neuroinflammation, which are common features of neurodegenerative conditions and/or diseases caused by the propagation of

'prion-like' misfolded protein. Importantly, given the parallels between mouse prion disease and AD (Dwomoh et al., 2021), the therapeutic, disease-modifying potential of the M1 mAChR demonstrated here is likely relevant for the treatment of human neurodegenerative conditions.

Chapter 4, however, revealed discrepancies between biochemical and histology data that could be associated to two reasons. Firstly, histological methods allow for analysis of the probed markers in a more accurate location in the brain (e.g., bregma lateral levels) with higher resolution of their distribution compared to biochemical techniques e.g., western blot and RT-qPCR. Secondly, histological analyses in Chapter 4 were conducted consistently on the left-hand side hemisphere of the brain, whereas the tissue analysed with biochemical methods was from either of the brain hemispheres. Since this mouse prion disease is induced by intracerebral injection in one side of the brain, it is possible that disease-associated pathology could spread differently in each of the brain hemisphere. If this hypothesis was true, the high variability observed among individual mice in the biochemical data might be since different hemispheres were being tested. This warrant further investigation to assess whether mouse prion disease spread differently accordingly to the site of injection.

When phosphorylation/arrestin-dependent signalling pathways mediated by the M1 mAChR are removed, mouse prion neurodegenerative disease was found to be significantly accelerated. This discovery in Chapter 5 reveals that the M1 mAChR has an inherent neuroprotective activity that is dependent on receptor phosphorylation/arrestin-dependent signalling. This neuroprotection can not only delay the appearance of clinical signs and disease-associated abnormal behaviours (e.g., burrowing) but also reduces scrapie pathology and markers of neurodegeneration and neuroinflammation. This included many of the proteins that were found associated with mouse prion disease (in Dwomoh et al. (2021) and Chapter 4), and that they were found 'normalised' following treatment with the M1 PAM VU0486846, such as APO-E, clusterin, serpinA3N, galectin-1, GFAP and vimentin. This strongly suggests that the disease-modifying potential of M1 mAChR-activating ligands observed in prion-diseased mice and other preclinical models of neurodegeneration and AD (Bradley et al., 2017, Lebois et al., 2017, Scarpa et al., 2020, Dwomoh et al., 2021) specifically relies on the phosphorylation/arrestin-dependent pathways mediated by the M1 mAChR. This

has important implications for drug discovery and development programmes for the treatment of neurodegenerative diseases, as this data strongly indicates that M1 mAChR ligands that maintain receptor phosphorylation will more likely deliver disease-modification while minimising associated cholinergic adverse responses (Bradley et al., 2020, Rook et al., 2017). Prion-infected M1-PD mice displayed a significant elevation in markers of neuroinflammation, GFAP, vimentin and CD86, as well as pro-inflammatory cytokines IL-1ß and TNF-α. This suggests the possibility that the M1 mAChR plays an unappreciated role in the regulation of inflammatory responses of the brain, and this might underpin the disease-modification mechanism of the M1 mAChR in neurodegeneration.

Previously, neuronal cell death in neurodegenerative diseases as well as AD-linked neuropathology such as hyperphosphorylation of tau (Guise et al., 2001, Harris et al., 2004, Pei et al., 2002), Aß toxicity (Rapoport and Ferreira, 2000, Frasca et al., 2008) and oxidative stress (Perry et al., 1999, Stanciu et al., 2000), have been associated to sustained ERK1/2 signalling. Given that lack of receptor phosphorylation could also cause a reduction of GPCR signalling desensitisation (Lohse, 1993, Gurevich and Gurevich, 2019), there a possibility that the M1-PD variant might induce an overall excessive activation of G protein-signalling pathways such as ERK1/2 signalling. However, as demonstrated in Chapter 3, stimulation of $G\alpha_q$-driven pathways (inositide phosphate signalling) are comparable in the M1-PD and the M1-WT (Scarpa et al., 2021, Bradley et al., 2020). In addition, lysates from the hippocampus and cortex of control or prion-diseased M1-WT and M1-PD mice showed here similar levels of expression and activation of ERK1/2. This further indicates that the accelerated neurodegeneration observed in prion-disease M1-PD mice is not due to an overall excessive activation of the ERK1/2 pathway, but it is caused by the removal of a neuroprotective mechanism, which is dependent on M1 mAChR phosphorylation.

Given the strong preclinical evidence demonstrating that the selective activation of the M1 mAChR induce significant disease modifying effects in different animal models of neurodegeneration and AD (Lebois et al., 2017, Caccamo et al., 2006, Fisher, 2008a, Bradley et al., 2017), it is likely that the neuroprotective activity of the M1 mAChR against mouse prion disease is also protective against other neurodegenerative conditions. In addition, prion disease is a prototypical proteinopathy that shares key diseases-associated mechanisms with AD and other

neurodegenerative disorders that are caused by neurotoxic misfolded proteins propagating in a ‘prion-like’ fashion such as AD, PD and HD (Aguzzi and Calella, 2009, Caughey et al., 1999, Mallucci et al., 2003, Sandberg et al., 2014, Prusiner, 1982, Duyckaerts et al., 2019, Dwomoh et al., 2021). This raises the possibility that the neuroprotective mechanism mediated by the M1 mAChR that is able to hamper the accumulation of PrP_{Sc} in mouse prion disease might be relevant against the formation of other prion-like neurotoxic proteins such as Aß and NFT in AD, α-synuclein in PD or huntingtin in HD (Halliday and Mallucci, 2014). In future studies, it will be interesting to discover the precise involvement of the M1 mAChR in disease mechanisms. As indicated by the findings from this thesis, these could be for example the regulation of disease-adaptive mechanisms such as neuroinflammation. This knowledge will have significant implications for M1 mAChR drug discovery programmes for the treatment of neurodegenerative disease and likely lead to novel and more targeted strategies for the disease-modifying treatment of underlying pathology.

Appendices

In order to generate representative immunoblots for PrP_{Sc} (Figure 4-2), markers of neurodegenerative disease i.e., APO-E, clusterin, and serpinA3N (Figure 4-8) and markers of neuroinflammation i.e., galectin-1, GFAP and vimentin (Figure 4-9 and Figure 4-10), western blot were first conducted using cortex, hippocampus and striatum from 4-8 separate mice. Quantification of intensity of western blot bands using Image Studio Lite (Version 5.2) allowed for identification of representative samples.

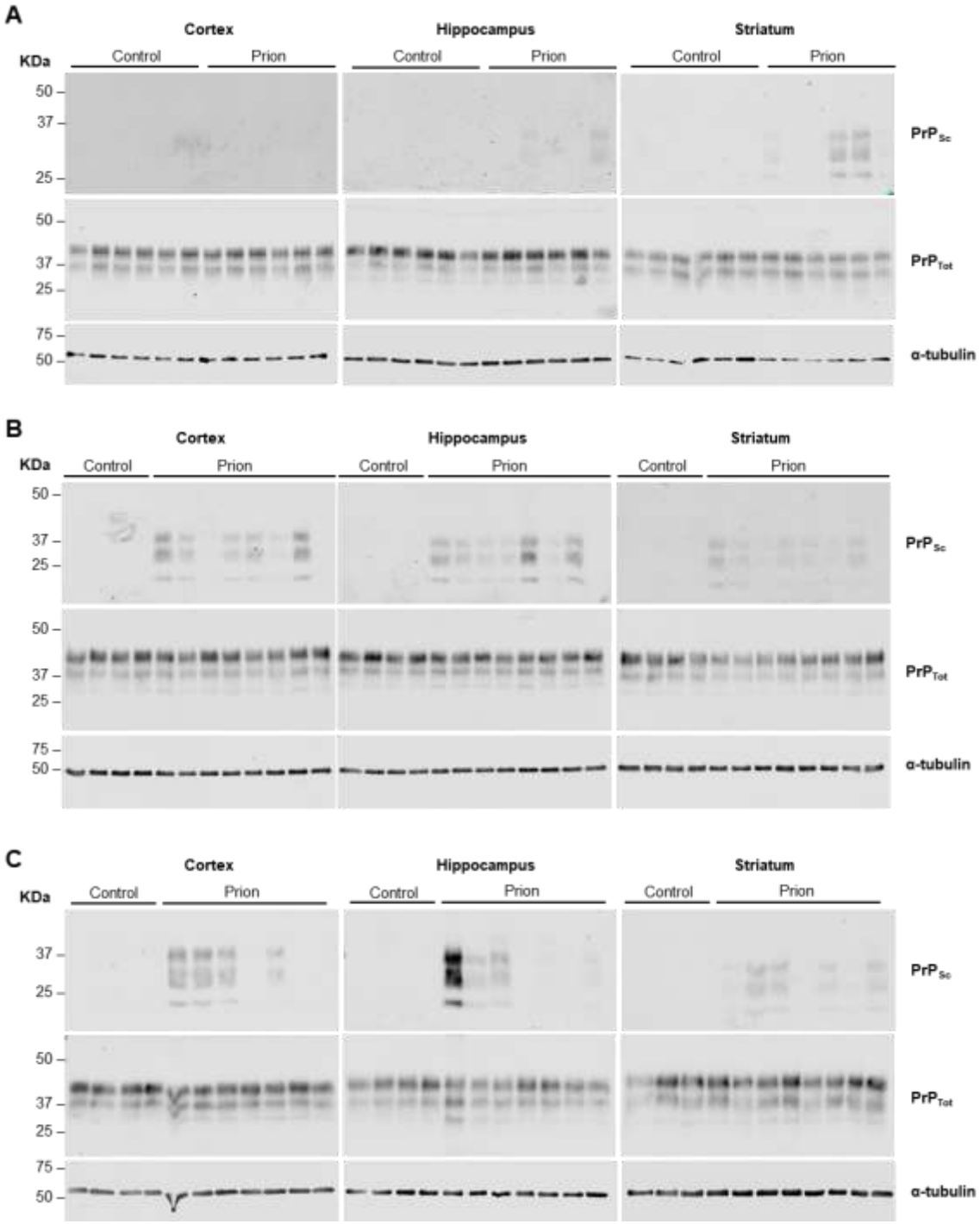

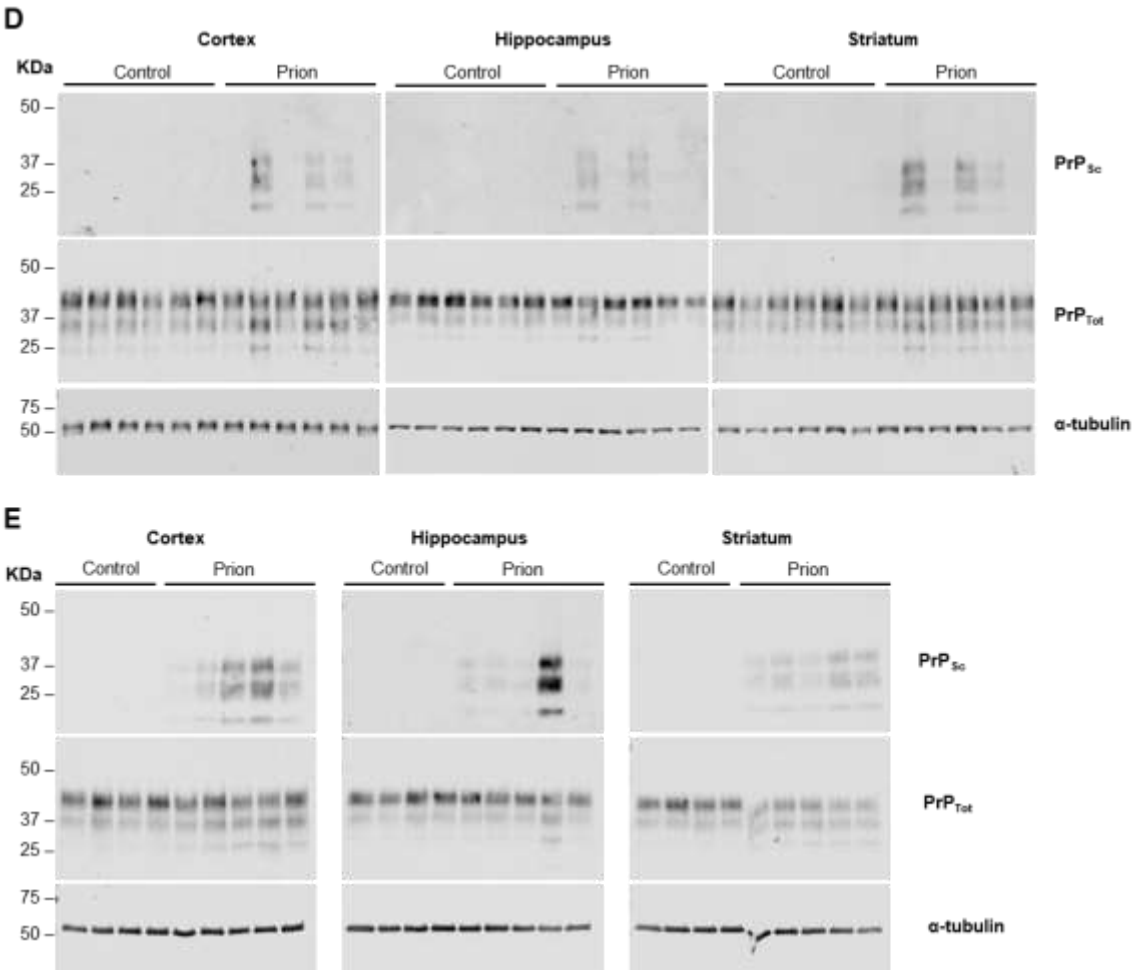

Appendix Figure 1 Western blot of protease-resistant PrP_{Sc} in control and prion-infected mice over the course of disease. Lysates of cortex, hippocampus and striatum of control or prion-infected mice at 6 **(A)**, 7 **(B)**, 8 **(C)**, 9 **(D)** and 10 w.p.i. **(E)** were incubated in the presence or absence of proteinase K prior to western blot (10 µg/mL, 37˚C for 10 minutes). to detect non-digested PrP_{Sc} and PrP_{Tot}, respectively. Digestion mixture (9 µg of samples) were loaded into 12% gels for western blot using anti-PrP antibodies.

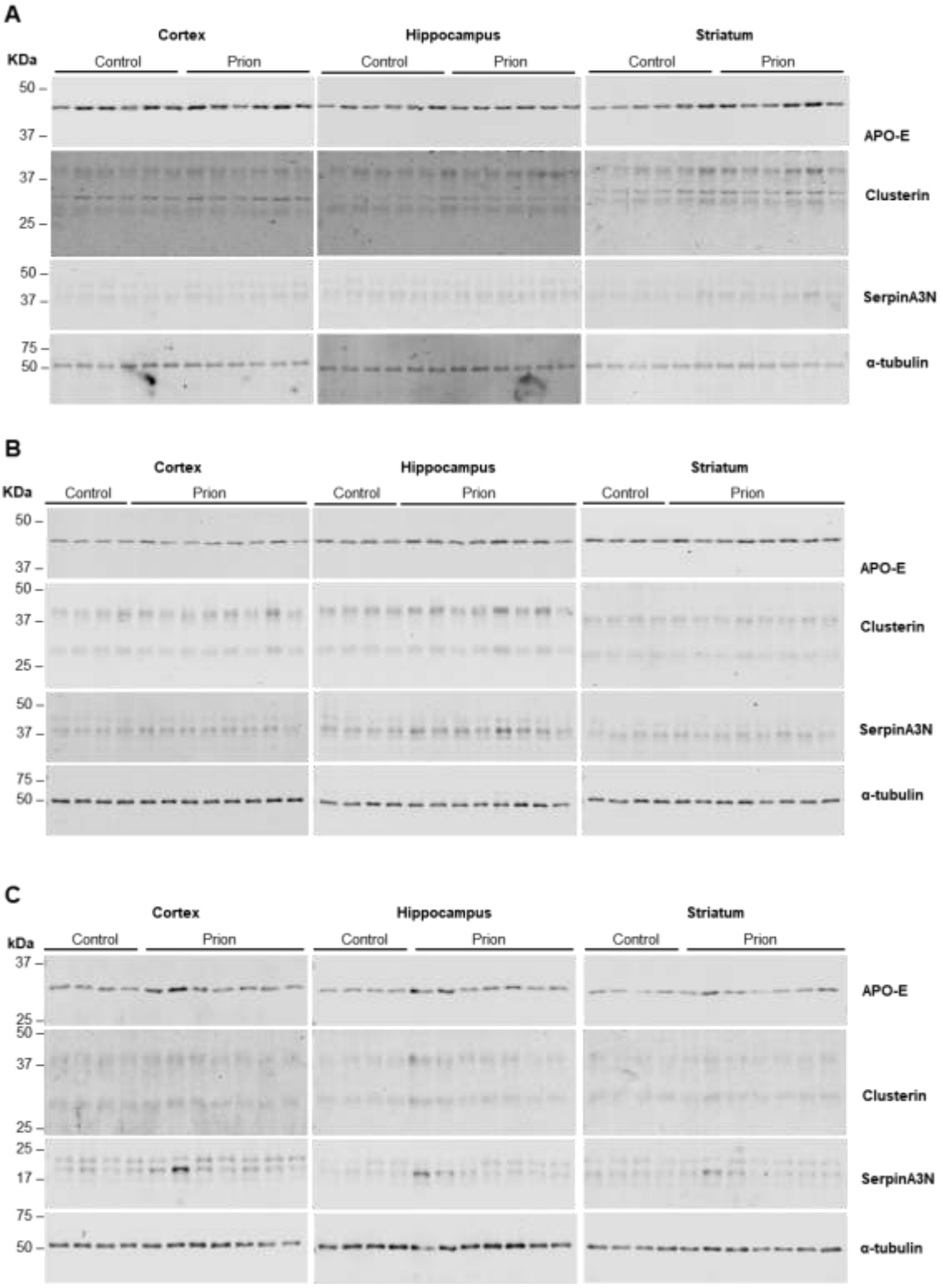
A
Cortex
Hippocampus
Striatum
KDa
Control
Prion
50 –
37 –
APO-E
37 –
25 –
Clusterin
50 –
37 –
SerpinA3N
75 –
50 –
α-tubulin
B
Cortex
Hippocampus
Striatum
KDa
Control
Prion
50 –
37 –
APO-E
50 –
37 –
25 –
Clusterin
50 –
37 –
SerpinA3N
75 –
50 –
α-tubulin
C
Cortex
Hippocampus
Striatum
kDa
Control
Prion
37 –
25 –
APO-E
50 –
37 –
25 –
Clusterin
25 –
17 –
SerpinA3N
75 –
50 –
α-tubulin

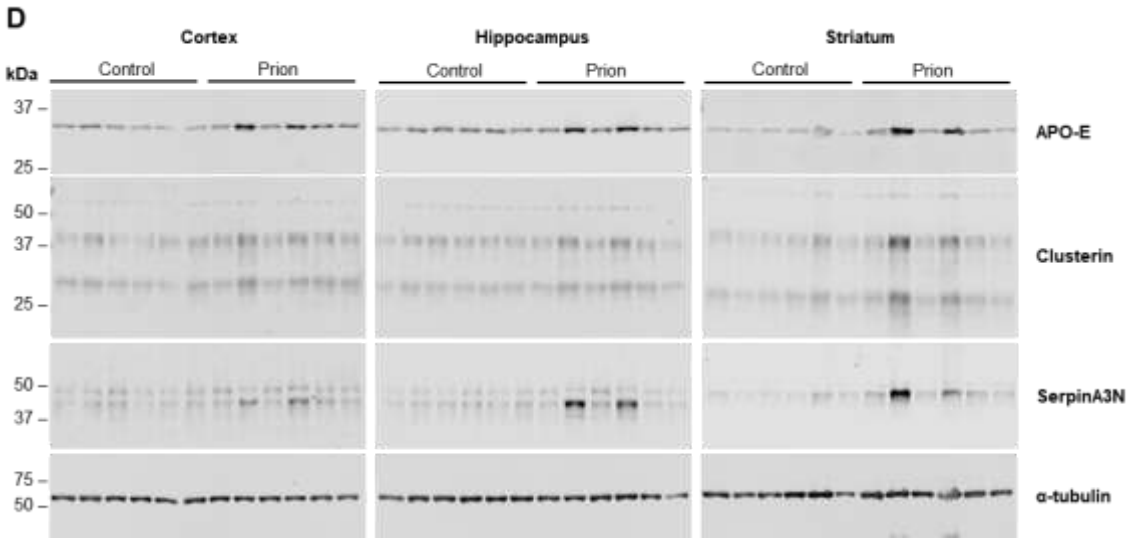

Appendix Figure 2 Western blots of markers of disease APO-E, clusterin and serpinA3N in control and prion-infected mice over the course of disease. Lysates (10 µg) of cortex, hippocampus and striatum of control or prion-infected mice at 6 **(A)**, 7 **(B)**, 8 **(C)** and 9 w.p.i. **(D)** were run in a western blot and probed with antibodies against APO-E, clusterin and serpinA3N to assess the levels of these markers of neurodegenerative disease.

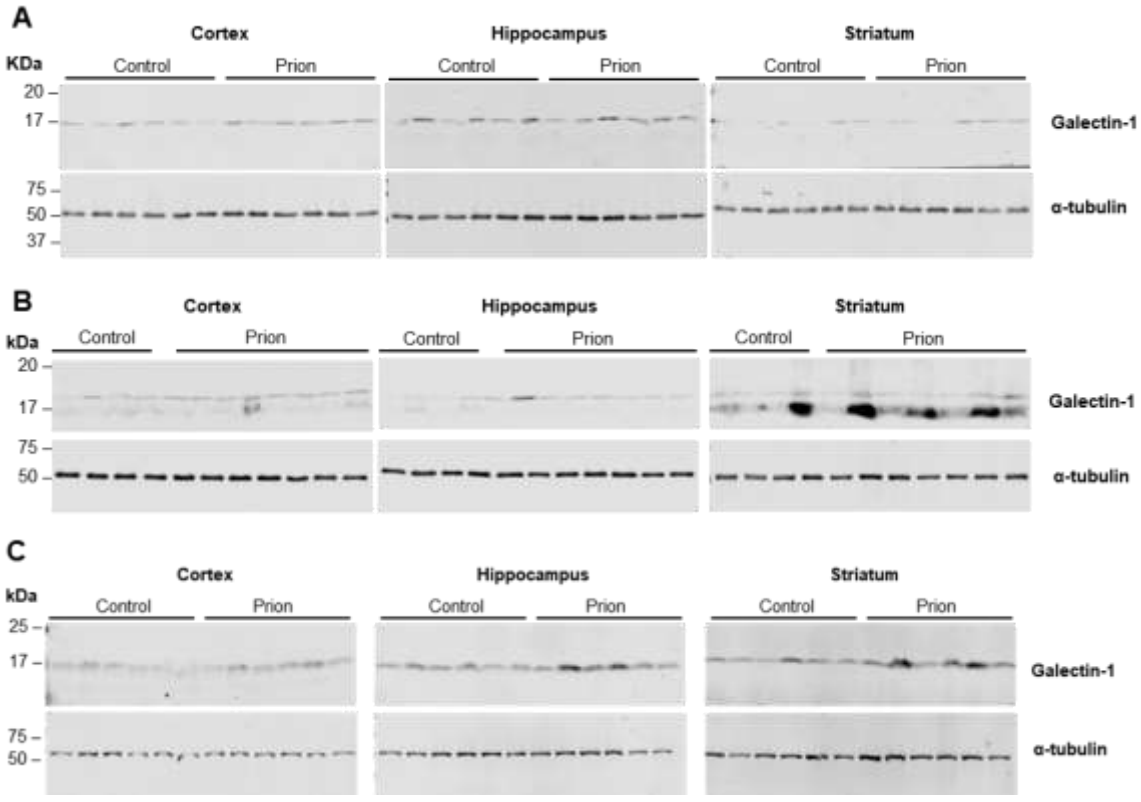

Appendix Figure 3 Western blots of markers for microglia galectin-1 in control and prion-infected mice over the course of disease. Lysates (10 µg) of cortex, hippocampus and striatum of control or prion-infected mice were probed in western blot for galectin-1 at 6 **(A)**, 8 **(B)** and 9 w.p.i. **(C)**

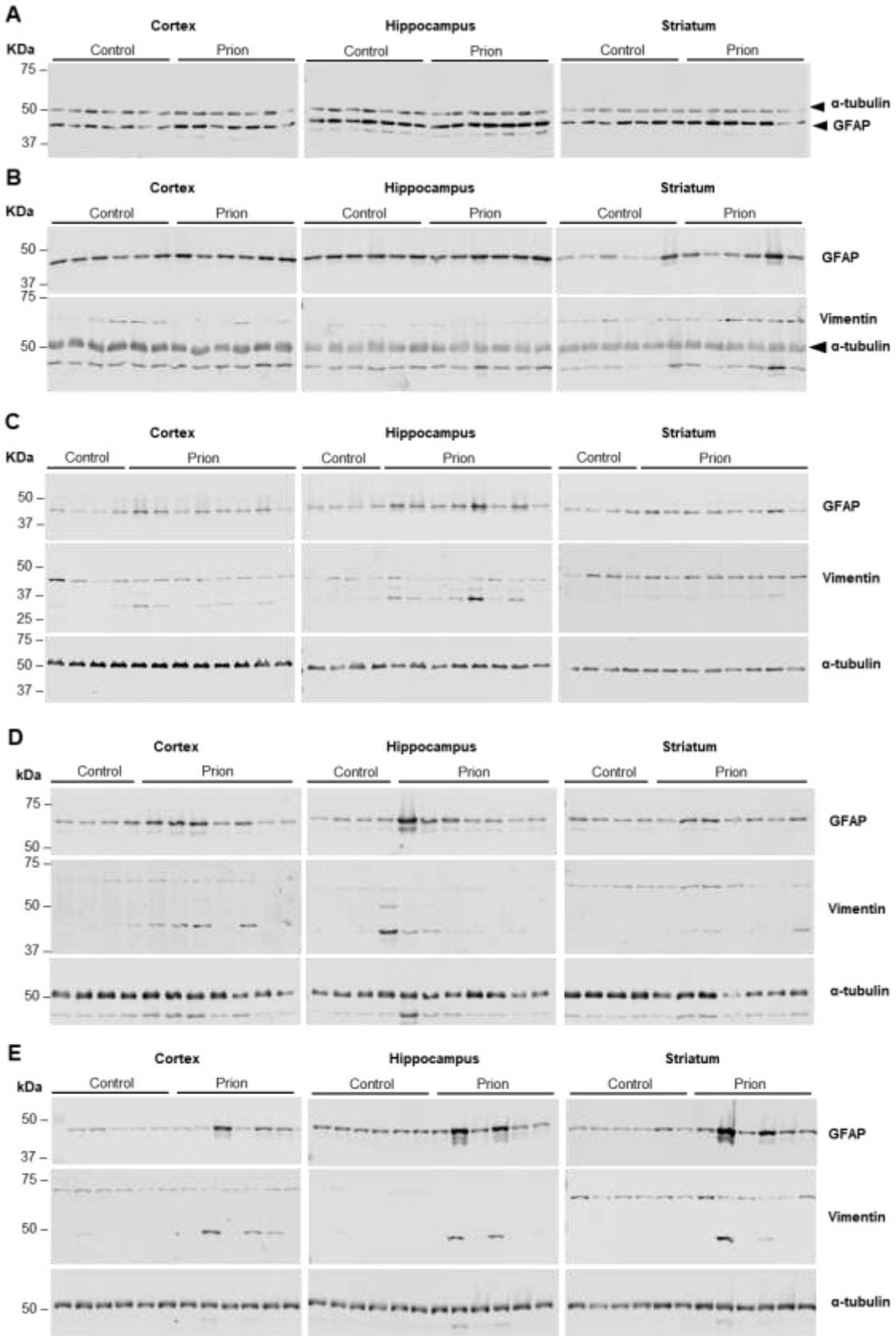

Appendix Figure 4 Western blots of astrocytic markers GFAP and vimentin in control and prion-infected mice over the course of disease. Lysates (10 µg) of cortex, hippocampus and striatum of control or prion-infected mice were probed in western blot for GFAP at 4 w.p.i. **(A)**, and for GFAP and vimentin at 6 **(B)**, 7 **(C)**, 8 **(D)** and 9 w.p.i. **(E)**.

List of References

ABOLHASSANI, N., LEON, J., SHENG, Z., OKA, S., HAMASAKI, H., IWAKI, T. & NAKABEPPU, Y. 2017. Molecular pathophysiology of impaired glucose metabolism, mitochondrial dysfunction, and oxidative DNA damage in Alzheimer's disease brain. *Mech Ageing Dev,* 161**,** 95-104.

AGUZZI, A. & CALELLA, A. M. 2009. Prions: Protein Aggregation and Infectious Diseases. *Physiological Reviews,* 89**,** 1105-1152.

AGUZZI, A. & HAASS, C. 2003. Games Played by Rogue Proteins in Prion Disorders and Alzheimer's Disease. *Science,* 302**,** 814.

AHMED, T. & GILANI, A. H. 2009. Inhibitory effect of curcuminoids on acetylcholinesterase activity and attenuation of scopolamine-induced amnesia may explain medicinal use of turmeric in Alzheimer's disease. *Pharmacol Biochem Behav,* 91**,** 554-9.

AHN, S., NELSON, C. D., GARRISON, T. R., MILLER, W. E. & LEFKOWITZ, R. J. 2003. Desensitization, internalization, and signaling functions of beta-arrestins demonstrated by RNA interference. *Proc Natl Acad Sci U S A,* 100**,** 1740-4.

AIGNER, T. G. & MISHKIN, M. 1986. The effects of physostigmine and scopolamine on recognition memory in monkeys. *Behavioral and Neural Biology,* 45**,** 81-87.

ALEXANDER, S. P. H., CHRISTOPOULOS, A., DAVENPORT, A. P., KELLY, E., MATHIE, A., PETERS, J. A., VEALE, E. L., ARMSTRONG, J. F., FACCENDA, E., HARDING, S. D., PAWSON, A. J., SOUTHAN, C., DAVIES, J. A., ABBRACCHIO, M. P., ALEXANDER, W., AL-HOSAINI, K., BÄCK, M., BARNES, N. M., BATHGATE, R., BEAULIEU, J.-M., BERNSTEIN, K. E., BETTLER, B., BIRDSALL, N. J. M., BLAHO, V., BOULAY, F., BOUSQUET, C., BRÄUNER-OSBORNE, H., BURNSTOCK, G., CALÓ, G., CASTAÑO, J. P., CATT, K. J., CERUTI, S., CHAZOT, P., CHIANG, N., CHINI, B., CHUN, J., CIANCIULLI, A., CIVELLI, O., CLAPP, L. H., COUTURE, R., CSABA, Z., DAHLGREN, C., DENT, G., SINGH, K. D., DOUGLAS, S. D., DOURNAUD, P., EGUCHI, S., ESCHER, E., FILARDO, E. J., FONG, T., FUMAGALLI, M., GAINETDINOV, R. R., GASPARO, M. D., GERARD, C., GERSHENGORN, M., GOBEIL, F., GOODFRIEND, T. L., GOUDET, C., GREGORY, K. J., GUNDLACH, A. L., HAMANN, J., HANSON, J., HAUGER, R. L., HAY, D. L., HEINEMANN, A., HOLLENBERG, M. D., HOLLIDAY, N. D., HORIUCHI, M., HOYER, D., HUNYADY, L., HUSAIN, A., IJZERMAN, A. P., INAGAMI, T., JACOBSON, K. A., JENSEN, R. T., JOCKERS, R., JONNALAGADDA, D., KARNIK, S., KAUPMANN, K., KEMP, J., KENNEDY, C., KIHARA, Y., KITAZAWA, T., KOZIELEWICZ, P., KREIENKAMP, H.-J., KUKKONEN, J. P., LANGENHAN, T., LEACH, K., LECCA, D., LEE, J. D., LEEMAN, S. E., LEPRINCE, J., LI, X. X., WILLIAMS, T. L., LOLAIT, S. J., LUPP, A., MACRAE, R., MAGUIRE, J., MAZELLA, J., MCARDLE, C. A., et al. 2021. THE CONCISE GUIDE TO

PHARMACOLOGY 2021/22: G protein-coupled receptors. *British Journal of Pharmacology,* 178**,** S27-S156.

ALLAMAN, I., BELANGER, M. & MAGISTRETTI, P. J. 2011. Astrocyte-neuron metabolic relationships: for better and for worse. *Trends Neurosci,* 34**,** 76-87.

ALLEN, J. A., YOST, J. M., SETOLA, V., CHEN, X., SASSANO, M. F., CHEN, M., PETERSON, S., YADAV, P. N., HUANG, X. P., FENG, B., JENSEN, N. H., CHE, X., BAI, X., FRYE, S. V., WETSEL, W. C., CARON, M. G., JAVITCH, J. A., ROTH, B. L. & JIN, J. 2011. Discovery of ß-arrestin-biased dopamine D2 ligands for probing signal transduction pathways essential for antipsychotic efficacy. *Proc Natl Acad Sci U S A,* 108**,** 18488-93.

ALT, A., PENDRI, A., BERTEKAP, R. L., LI, G., BENITEX, Y., NOPHSKER, M., ROCKWELL, K. L., BURFORD, N. T., SUM, C. S., CHEN, J., HERBST, J. J., FERRANTE, M., HENDRICSON, A., CVIJIC, M. E., WESTPHAL, R. S., O'CONNELL, J., BANKS, M., ZHANG, L., GENTLES, R. G., JENKINS, S., LOY, J. & MACOR, J. E. 2016. Evidence for Classical Cholinergic Toxicity Associated with Selective Activation of Muscarinic Receptors. *Journal of Pharmacology and Experimental Therapeutics,* 356**,** 293.

ALVAREZ-CURTO, E., INOUE, A., JENKINS, L., RAIHAN, S. Z., PRIHANDOKO, R., TOBIN, A. B. & MILLIGAN, G. 2016. Targeted Elimination of G Proteins and Arrestins Defines Their Specific Contributions to Both Intensity and Duration of G Protein-coupled Receptor Signaling *. *Journal of Biological Chemistry,* 291**,** 27147-27159.

ALZFORUM. 2021. *Alzheimer's Mouse Models* [Online]. Available: https://www.alzforum.org/research-models/alzheimers-disease/commonly-used [Accessed 8 December 2021].

ALZHEIMER'S ASSOCIATION. 2021. *2021 Alzheimer's Disease facts and figures* [Online]. Available: https://www.alz.org/media/Documents/alzheimers-facts-and-figures.pdf [Accessed 8 December 2021].

ALZHEIMER, A. 1907. Über eine eigenartige Erkrankung der Hirnrinde. Vortrag in der Versammlung Südwestdeutscher Irrenärzte in Tübingen am 3. November 1906. *Allg Z Psychiatr Psych Gerichtl Med,* 1907**,** 146-148.

AMOR, S., PEFEROEN, L. A., VOGEL, D. Y., BREUR, M., VAN DER VALK, P., BAKER, D. & VAN NOORT, J. M. 2014. Inflammation in neurodegenerative diseases--an update. *Immunology,* 142**,** 151-66.

ANAGNOSTARAS, S. G., GALE, G. D. & FANSELOW, M. S. 2001. Hippocampus and contextual fear conditioning: recent controversies and advances. *Hippocampus,* 11**,** 8-17.

ANAGNOSTARAS, S. G., MURPHY, G. G., HAMILTON, S. E., MITCHELL, S. L., RAHNAMA, N. P., NATHANSON, N. M. & SILVA, A. J. 2003. Selective

cognitive dysfunction in acetylcholine M1 muscarinic receptor mutant mice. *Nat Neurosci,* 6**,** 51-8.

ANAND, R., GILL, K. D. & MAHDI, A. A. 2014. Therapeutics of Alzheimer's disease: Past, present and future. *Neuropharmacology,* 76 Pt A**,** 27-50.

ANISUZZAMAN, A. S. M., UWADA, J., MASUOKA, T., YOSHIKI, H., NISHIO, M., IKEGAYA, Y., TAKAHASHI, N., MATSUKI, N., FUJIBAYASHI, Y., YONEKURA, Y., MOMIYAMA, T. & MURAMATSU, I. 2013. Novel contribution of cell surface and intracellular M1-muscarinic acetylcholine receptors to synaptic plasticity in hippocampus. *Journal of Neurochemistry,* 126**,** 360-371.

APPLETON, K. M., LEE, M. H., ALELE, C., LUTTRELL, D. K., PETERSON, Y. K., MORINELLI, T. A. & LUTTRELL, L. M. 2013. Biasing the parathyroid hormone receptor: relating in vitro ligand efficacy to in vivo biological activity. *Methods Enzymol,* 522**,** 229-62.

ARMBRUSTER, B. N., LI, X., PAUSCH, M. H., HERLITZE, S. & ROTH, B. L. 2007. Evolving the lock to fit the key to create a family of G protein-coupled receptors potently activated by an inert ligand. *Proceedings of the National Academy of Sciences of the United States of America,* 104**,** 5163-5168.

ARSHAVSKY, V. Y., DIZHOOR, A. M., SHESTAKOVA, I. K. & PHILIPPOV, P. 1985. The effect of rhodopsin phosphorylation on the light-dependent activation of phosphodiesterase from bovine rod outer segments. *FEBS Lett,* 181**,** 264-6.

ASUNI, A. A., GRAY, B., BAILEY, J., SKIPP, P., PERRY, V. H. & O'CONNOR, V. 2014. Analysis of the hippocampal proteome in ME7 prion disease reveals a predominant astrocytic signature and highlights the brain-restricted production of clusterin in chronic neurodegeneration. *J Biol Chem,* 289**,** 4532-45.

ATTRAMADAL, H., ARRIZA, J. L., AOKI, C., DAWSON, T. M., CODINA, J., KWATRA, M. M., SNYDER, S. H., CARON, M. G. & LEFKOWITZ, R. J. 1992. Beta-arrestin2, a novel member of the arrestin/beta-arrestin gene family. *Journal of Biological Chemistry,* 267**,** 17882-17890.

BAAMEUR, F., MORGAN, D. H., YAO, H., TRAN, T. M., HAMMITT, R. A., SABUI, S., MCMURRAY, J. S., LICHTARGE, O. & CLARK, R. B. 2010. Role for the regulator of G-protein signaling homology domain of G protein-coupled receptor kinases 5 and 6 in beta 2-adrenergic receptor and rhodopsin phosphorylation. *Mol Pharmacol,* 77**,** 405-15.

BAKER, C. A. & MANUELIDIS, L. 2003. Unique inflammatory RNA profiles of microglia in Creutzfeldt-Jakob disease. *Proc Natl Acad Sci U S A,* 100**,** 675-9.

BAKKER, C., PRINS, S., LIPTROT, J., HART, E. P., KLAASSEN, E. S., BROWN, G. A., BROWN, A., CONGREVE, M., WEIR, M., MARSHALL, F. H., STEVENS, J., CROSS, D. M., TASKER, T., NATHAN, P. J. & GROENEVELD, G. J. 2021. Safety, pharmacokinetics and pharmacodynamics of HTL0009936, a selective muscarinic M1-acetylcholine receptor agonist: A randomized cross-over trial. *British Journal of Clinical Pharmacology,* n/a.

BAKKER, C., TASKER, T., LIPTROT, J., HART, E. P., KLAASSEN, E. S., PRINS, S., VAN DER DOEF, T. F., BROWN, G. A., BROWN, A., CONGREVE, M., WEIR, M., MARSHALL, F. H., CROSS, D. M., GROENEVELD, G. J. & NATHAN, P. J. 2020. First-in-man study to investigate safety, pharmacokinetics and exploratory pharmacodynamics of HTL0018318, a novel M(1) -receptor partial agonist for the treatment of dementias. *Br J Clin Pharmacol*.

BALDWIN, J. M. 1993. The probable arrangement of the helices in G protein-coupled receptors. *Embo j,* 12**,** 1693-703.

BARAK, L. S., TIBERI, M., FREEDMAN, N. J., KWATRA, M. M., LEFKOWITZ, R. J. & CARON, M. G. 1994. A highly conserved tyrosine residue in G protein-coupled receptors is required for agonist-mediated beta 2-adrenergic receptor sequestration. *J Biol Chem,* 269**,** 2790-5.

BARTELT-HUNT, S. L. & BARTZ, J. C. 2013. Behavior of Prions in the Environment: Implications for Prion Biology. *PLOS Pathogens,* 9**,** e1003113.

BARTUS, R. T., DEAN, R. L., BEER, B. & LIPPA, A. S. 1982. The cholinergic hypothesis of geriatric memory dysfunction. *Science,* 217**,** 408.

BASAK, I., PATIL, K. S., ALVES, G., LARSEN, J. P. & MØLLER, S. G. 2016. microRNAs as neuroregulators, biomarkers and therapeutic agents in neurodegenerative diseases. *Cellular and Molecular Life Sciences,* 73**,** 811-827.

BASILE, A. S., FEDOROVA, I., ZAPATA, A., LIU, X., SHIPPENBERG, T., DUTTAROY, A., YAMADA, M. & WESS, J. 2002. Deletion of the M5 muscarinic acetylcholine receptor attenuates morphine reinforcement and withdrawal but not morphine analgesia. *Proc Natl Acad Sci U S A,* 99**,** 11452-7.

BATE, C., BOSHUIZEN, R. S., LANGEVELD, J. P. & WILLIAMS, A. 2002. Temporal and spatial relationship between the death of PrP-damaged neurones and microglial activation. *Neuroreport,* 13**,** 1695-700.

BATEMAN, R. J., AISEN, P. S., DE STROOPER, B., FOX, N. C., LEMERE, C. A., RINGMAN, J. M., SALLOWAY, S., SPERLING, R. A., WINDISCH, M. & XIONG, C. 2011. Autosomal-dominant Alzheimer's disease: a review and proposal for the prevention of Alzheimer's disease. *Alzheimers Res Ther,* 3**,** 1.

BATS, S., THOUMAS, J. L., LORDI, B., TONON, M. C., LALONDE, R. & CASTON, J. 2001. The effects of a mild stressor on spontaneous alternation in mice. *Behavioural Brain Research,* 118**,** 11-15.

BAZARSUREN, A., GRAUSCHOPF, U., WOZNY, M., REUSCH, D., HOFFMANN, E., SCHAEFER, W., PANZNER, S. & RUDOLPH, R. 2002. In vitro folding, functional characterization, and disulfide pattern of the extracellular domain of human GLP-1 receptor. *Biophys Chem,* 96**,** 305-18.

BEN HAIM, L., CARRILLO-DE SAUVAGE, M. A., CEYZÉRIAT, K. & ESCARTIN, C. 2015. Elusive roles for reactive astrocytes in neurodegenerative diseases. *Front Cell Neurosci,* 9**,** 278.

BENOVIC, J. L., DEBLASI, A., STONE, W. C., CARON, M. G. & LEFKOWITZ, R. J. 1989. Beta-adrenergic receptor kinase: primary structure delineates a multigene family. *Science,* 246**,** 235-40.

BENOVIC, J. L., KÜHN, H., WEYAND, I., CODINA, J., CARON, M. G. & LEFKOWITZ, R. J. 1987. Functional desensitization of the isolated beta-adrenergic receptor by the beta-adrenergic receptor kinase: potential role of an analog of the retinal protein arrestin (48-kDa protein). *Proceedings of the National Academy of Sciences of the United States of America,* 84**,** 8879-8882.

BERIZZI, A. E., PERRY, C. J., SHACKLEFORD, D. M., LINDSLEY, C. W., JONES, C. K., CHEN, N. A., SEXTON, P. M., CHRISTOPOULOS, A., LANGMEAD, C. J. & LAWRENCE, A. J. 2018. Muscarinic M(5) receptors modulate ethanol seeking in rats. *Neuropsychopharmacology : official publication of the American College of Neuropsychopharmacology,* 43**,** 1510-1517.

BERTRON, J. L., CHO, H. P., GARCIA-BARRANTES, P. M., PANARESE, J. D., SALOVICH, J. M., NANCE, K. D., ENGERS, D. W., ROOK, J. M., BLOBAUM, A. L., NISWENDER, C. M., STAUFFER, S. R., CONN, P. J. & LINDSLEY, C. W. 2018. The discovery of VU0486846: steep SAR from a series of M1 PAMs based on a novel benzomorpholine core. *Bioorganic & Medicinal Chemistry Letters,* 28**,** 2175-2179.

BILLINGS, L. M., ODDO, S., GREEN, K. N., MCGAUGH, J. L. & LAFERLA, F. M. 2005. Intraneuronal Abeta causes the onset of early Alzheimer's disease-related cognitive deficits in transgenic mice. *Neuron,* 45**,** 675-88.

BIRDSALL, N. J., BURGEN, A. S., HULME, E. C., STOCKTON, J. M. & ZIGMOND, M. J. 1983. The effect of McN-A-343 on muscarinic receptors in the cerebral cortex and heart. *Br J Pharmacol,* 78**,** 257-9.

BIRDSALL, N. J. & LAZARENO, S. 2005. Allosterism at muscarinic receptors: ligands and mechanisms. *Mini Rev Med Chem,* 5**,** 523-43.

BIRDSALL, N. J. M., BRADLEY, S., BROWN, D. A., BUCKLEY, N. J., CHALLISS, R. A. J., CHRISTOPOULOS, A., EGLEN, R. M., EHLERT, F., FELDER, C. C.,

HAMMER, R., KILBINGER, H. J., LAMBRECHT, G., LANGMEAD, C., MITCHELSON, F., MUTSCHLER, E., NATHANSON, N. M., SCHWARZ, R. D., THAL, D., TOBIN, A. B., VALANT, C. & WESS, J. 2021. Acetylcholine receptors (muscarinic) in GtoPdb v.2021.2. *IUPHAR/BPS Guide to Pharmacology CITE,* 2021.

BIRKS, R. & MACINTOSH, F. C. 1961. ACETYLCHOLINE METABOLISM OF A SYMPATHETIC GANGLION. *Canadian Journal of Biochemistry and Physiology,* 39**,** 787-827.

BLOCK, M. L., ZECCA, L. & HONG, J. S. 2007. Microglia-mediated neurotoxicity: uncovering the molecular mechanisms. *Nat Rev Neurosci,* 8**,** 57-69.

BODICK, N., W OFFEN, W., SHANNON, H., SATTERWHITE, J., LUCAS, R., VAN LIER, R. & PAUL, S. 1997a. *The selective muscarinic agonist xanomeline improves both the cognitive deficits and behavioral symptoms of Alzheimer disease*.

BODICK, N. C., OFFEN, W. W., LEVEY, A. I. & ET AL. 1997b. Effects of xanomeline, a selective muscarinic receptor agonist, on cognitive function and behavioral symptoms in alzheimer disease. *Archives of Neurology,* 54**,** 465-473.

BOESE, A. S., SABA, R., CAMPBELL, K., MAJER, A., MEDINA, S., BURTON, L., BOOTH, T. F., CHONG, P., WESTMACOTT, G., DUTTA, S. M., SABA, J. A. & BOOTH, S. A. 2016. MicroRNA abundance is altered in synaptoneurosomes during prion disease. *Molecular and Cellular Neuroscience,* 71**,** 13-24.

BOHN, L. M., LEFKOWITZ, R. J., GAINETDINOV, R. R., PEPPEL, K., CARON, M. G. & LIN, F. T. 1999. Enhanced morphine analgesia in mice lacking beta-arrestin 2. *Science,* 286**,** 2495-8.

BONNER, T. I., BUCKLEY, N. J., YOUNG, A. C. & BRANN, M. R. 1987. Identification of a family of muscarinic acetylcholine receptor genes. *Science,* 237**,** 527-32.

BONNER, T. I., YOUNG, A. C., BRANN, M. R. & BUCKLEY, N. J. 1988. Cloning and expression of the human and rat m5 muscarinic acetylcholine receptor genes. *Neuron,* 1**,** 403-10.

BOURGOGNON, J.-M., SPIERS, J. G., SCHEIBLICH, H., ANTONOV, A., BRADLEY, S. J., TOBIN, A. B. & STEINERT, J. R. 2018. Alterations in neuronal metabolism contribute to the pathogenesis of prion disease. *Cell Death & Differentiation,* 25**,** 1408.

BRADLEY, S. J., BOURGOGNON, J.-M., SANGER, H. E., VERITY, N., MOGG, A. J., WHITE, D. J., BUTCHER, A. J., MORENO, J. A., MOLLOY, C., MACEDO-HATCH, T., EDWARDS, J. M., WESS, J., PAWLAK, R., READ, D. J., SEXTON, P. M., BROAD, L. M., STEINERT, J. R., MALLUCCI, G. R., CHRISTOPOULOS, A., FELDER, C. C. & TOBIN, A. B. 2017. M1 muscarinic allosteric

modulators slow prion neurodegeneration and restore memory loss. *J Clin Invest.,* 127**,** 487-499.

BRADLEY, S. J., MOLLOY, C., BUNDGAARD, C., MOGG, A. J., THOMPSON, K. J., DWOMOH, L., SANGER, H. E., CRABTREE, M. D., BROOKE, S. M., SEXTON, P. M., FELDER, C. C., CHRISTOPOULOS, A., BROAD, L. M., TOBIN, A. B. & LANGMEAD, C. J. 2018. Bitopic Binding Mode of an M1 Muscarinic Acetylcholine Receptor Agonist Associated with Adverse Clinical Trial Outcomes. *Molecular Pharmacology,* 93**,** 645.

BRADLEY, S. J., MOLLOY, C., VALUSKOVA, P., DWOMOH, L., SCARPA, M., ROSSI, M., FINLAYSON, L., SVENSSON, K. A., CHERNET, E., BARTH, V. N., GHERBI, K., SYKES, D. A., WILSON, C. A., MISTRY, R., SEXTON, P. M., CHRISTOPOULOS, A., MOGG, A. J., ROSETHORNE, E. M., SAKATA, S., JOHN CHALLISS, R. A., BROAD, L. M. & TOBIN, A. B. 2020. Biased M1-muscarinic-receptor-mutant mice inform the design of next-generation drugs. *Nat Chem Biol,* 16**,** 240-249.

BRADLEY, S. J., WIEGMAN, C. H., IGLESIAS, M. M., KONG, K. C., BUTCHER, A. J., PLOUFFE, B., GOUPIL, E., BOURGOGNON, J. M., MACEDO-HATCH, T., LEGOUILL, C., RUSSELL, K., LAPORTE, S. A., KÖNIG, G. M., KOSTENIS, E., BOUVIER, M., CHUNG, K. F., AMRANI, Y. & TOBIN, A. B. 2016. Mapping physiological G protein-coupled receptor signaling pathways reveals a role for receptor phosphorylation in airway contraction. *Proc Natl Acad Sci U S A,* 113**,** 4524-9.

BRIAND, L. A., GRITTON, H., HOWE, W. M., YOUNG, D. A. & SARTER, M. 2007. Modulators in concert for cognition: Modulator interactions in the prefrontal cortex. *Progress in Neurobiology,* 83**,** 69-91.

BRIDGES, T. M. & LINDSLEY, C. W. 2008. G-Protein-Coupled Receptors: From Classical Modes of Modulation to Allosteric Mechanisms. *ACS Chemical Biology,* 3**,** 530-541.

BROWN, A. J. H., BRADLEY, S. J., MARSHALL, F. H., BROWN, G. A., BENNETT, K. A., BROWN, J., CANSFIELD, J. E., CROSS, D. M., DE GRAAF, C., HUDSON, B. D., DWOMOH, L., DIAS, J. M., ERREY, J. C., HURRELL, E., LIPTROT, J., MATTEDI, G., MOLLOY, C., NATHAN, P. J., OKRASA, K., OSBORNE, G., PATEL, J. C., PICKWORTH, M., ROBERTSON, N., SHAHABI, S., BUNDGAARD, C., PHILLIPS, K., BROAD, L. M., GOONAWARDENA, A. V., MORAIRTY, S. R., BROWNING, M., PERINI, F., DAWSON, G. R., DEAKIN, J. F. W., SMITH, R. T., SEXTON, P. M., WARNECK, J., VINSON, M., TASKER, T., TEHAN, B. G., TEOBALD, B., CHRISTOPOULOS, A., LANGMEAD, C. J., JAZAYERI, A., COOKE, R. M., RUCKTOOA, P., CONGREVE, M. S., WEIR, M. & TOBIN, A. B. 2021. From structure to clinic: Design of a muscarinic M1 receptor agonist with potential to treatment of Alzheimer's disease. *Cell,* 184**,** 5886-5901.e22.

BROWN, D. R., SCHULZ-SCHAEFFER, W. J., SCHMIDT, B. & KRETZSCHMAR, H. A. 1997. Prion protein-deficient cells show altered response to oxidative stress due to decreased SOD-1 activity. *Exp Neurol,* 146**,** 104-12.

BUDZIK, B., GARZYA, V., SHI, D., WALKER, G., WOOLLEY-ROBERTS, M., PARDOE, J., LUCAS, A., TEHAN, B., RIVERO, R. A., LANGMEAD, C. J., WATSON, J., WU, Z., FORBES, I. T. & JIN, J. 2010. Novel N-Substituted Benzimidazolones as Potent, Selective, CNS-Penetrant, and Orally Active M1 mAChR Agonists. *ACS medicinal chemistry letters,* 1**,** 244-248.

BÜELER, H., AGUZZI, A., SAILER, A., GREINER, R. A., AUTENRIED, P., AGUET, M. & WEISSMANN, C. 1993. Mice devoid of PrP are resistant to scrapie. *Cell,* 73**,** 1339-1347.

BÜELER, H., FISCHER, M., LANG, Y., BLUETHMANN, H., LIPP, H.-P., DEARMOND, S. J., PRUSINER, S. B., AGUET, M. & WEISSMANN, C. 1992. Normal development and behaviour of mice lacking the neuronal cell-surface PrP protein. *Nature,* 356**,** 577-582.

BUELS, K. S. & FRYER, A. D. 2012. Muscarinic receptor antagonists: effects on pulmonary function. *Handb Exp Pharmacol***,** 317-41.

BURSTEIN, A. H., SABBAGH, M., ANDREWS, R., VALCARCE, C., DUNN, I. & ALTSTIEL, L. 2018. Development of Azeliragon, an Oral Small Molecule Antagonist of the Receptor for Advanced Glycation Endproducts, for the Potential Slowing of Loss of Cognition in Mild Alzheimer's Disease. *J Prev Alzheimers Dis,* 5**,** 149-154.

BUSCHE, M. A. & HYMAN, B. T. 2020. Synergy between amyloid-β and tau in Alzheimer’s disease. *Nature Neuroscience,* 23**,** 1183-1193.

BUTCHER, A. J., BRADLEY, S. J., PRIHANDOKO, R., BROOKE, S. M., MOGG, A., BOURGOGNON, J.-M., MACEDO-HATCH, T., EDWARDS, J. M., BOTTRILL, A. R., CHALLISS, R. A. J., BROAD, L. M., FELDER, C. C. & TOBIN, A. B. 2016. An Antibody Biosensor Establishes the Activation of the M1 Muscarinic Acetylcholine Receptor during Learning and Memory. *The Journal of Biological Chemistry,* 291**,** 8862-8875.

BUTCHER, A. J., PRIHANDOKO, R., KONG, K. C., MCWILLIAMS, P., EDWARDS, J. M., BOTTRILL, A., MISTRY, S. & TOBIN, A. B. 2011. Differential G-protein-coupled receptor phosphorylation provides evidence for a signaling bar code. *J Biol Chem,* 286**,** 11506-18.

BUXBAUM, J. D., LIU, K. N., LUO, Y., SLACK, J. L., STOCKING, K. L., PESCHON, J. J., JOHNSON, R. S., CASTNER, B. J., CERRETTI, D. P. & BLACK, R. A. 1998. Evidence that tumor necrosis factor alpha converting enzyme is involved in regulated alpha-secretase cleavage of the Alzheimer amyloid protein precursor. *J Biol Chem,* 273**,** 27765-7.

BUXBAUM, J. D., OISHI, M., CHEN, H. I., PINKAS-KRAMARSKI, R., JAFFE, E. A., GANDY, S. E. & GREENGARD, P. 1992. Cholinergic agonists and interleukin 1 regulate processing and secretion of the Alzheimer beta/A4 amyloid protein precursor. *Proc Natl Acad Sci U S A,* 89**,** 10075-8.

BYMASTER, F. P., CARTER, P. A., YAMADA, M., GOMEZA, J., WESS, J., HAMILTON, S. E., NATHANSON, N. M., MCKINZIE, D. L. & FELDER, C. C. 2003a. Role of specific muscarinic receptor subtypes in cholinergic parasympathomimetic responses, in vivo phosphoinositide hydrolysis, and pilocarpine-induced seizure activity. *European Journal of Neuroscience,* 17**,** 1403-1410.

BYMASTER, F. P., MCKINZIE, D. L., FELDER, C. C. & WESS, J. 2003b. Use of M1–M5 Muscarinic Receptor Knockout Mice as Novel Tools to Delineate the Physiological Roles of the Muscarinic Cholinergic System. *Neurochemical Research,* 28**,** 437-442.

CACCAMO, A., ODDO, S., BILLINGS, L. M., GREEN, K. N., MARTINEZ-CORIA, H., FISHER, A. & LAFERLA, F. M. 2006. M1 receptors play a central role in modulating AD-like pathology in transgenic mice. *Neuron,* 49**,** 671-82.

CALEBIRO, D., NIKOLAEV, V. O., GAGLIANI, M. C., DE FILIPPIS, T., DEES, C., TACCHETTI, C., PERSANI, L. & LOHSE, M. J. 2009. Persistent cAMP-signals triggered by internalized G-protein-coupled receptors. *PLoS Biol,* 7**,** e1000172.

CALZOLAI, L., LYSEK, D. A., PÉREZ, D. R., GÜNTERT, P. & WÜTHRICH, K. 2005. Prion protein NMR structures of chickens, turtles, and frogs. *Proceedings of the National Academy of Sciences of the United States of America,* 102**,** 651.

CAMPBELL, I. L., EDDLESTON, M., KEMPER, P., OLDSTONE, M. B. & HOBBS, M. V. 1994. Activation of cerebral cytokine gene expression and its correlation with onset of reactive astrocyte and acute-phase response gene expression in scrapie. *J Virol,* 68**,** 2383-7.

CARMAN, C. V. & BENOVIC, J. L. 1998. G-protein-coupled receptors: turn-ons and turn-offs. *Curr Opin Neurobiol,* 8**,** 335-44.

CARPENTER, B., NEHMÉ, R., WARNE, T., LESLIE, A. G. & TATE, C. G. 2016. Structure of the adenosine A(2A) receptor bound to an engineered G protein. *Nature,* 536**,** 104-7.

CARROLL, J. A. & CHESEBRO, B. 2019. Neuroinflammation, Microglia, and Cell-Association during Prion Disease. *Viruses,* 11.

CARROLL, J. A., RACE, B., WILLIAMS, K., STRIEBEL, J. & CHESEBRO, B. 2018. Microglia Are Critical in Host Defense against Prion Disease. *J Virol,* 92.

CARROLL, J. A., STRIEBEL, J. F., RACE, B., PHILLIPS, K. & CHESEBRO, B. 2015. Prion infection of mouse brain reveals multiple new upregulated genes involved in neuroinflammation or signal transduction. *J Virol,* 89**,** 2388-404.

CARROLL, J. A., STRIEBEL, J. F., RANGEL, A., WOODS, T., PHILLIPS, K., PETERSON, K. E., RACE, B. & CHESEBRO, B. 2016. Prion Strain Differences in Accumulation of PrPSc on Neurons and Glia Are Associated with Similar Expression Profiles of Neuroinflammatory Genes: Comparison of Three Prion Strains. *PLoS Pathog,* 12**,** e1005551.

CASTELLANI, R. J., PERRY, G. & SMITH, M. A. 2004. Prion disease and Alzheimer's disease: pathogenic overlap. *Acta Neurobiol Exp (Wars),* 64**,** 11-7.

CAUGHEY, B., HORIUCHI, M., DEMAIMAY, R. & RAYMOND, G. J. 1999. Assays of protease-resistant prion protein and its formation. *Methods Enzymol,* 309**,** 122-33.

CAULFIELD, M. P. & BIRDSALL, N. J. 1998. International Union of Pharmacology. XVII. Classification of muscarinic acetylcholine receptors. *Pharmacol Rev,* 50**,** 279-90.

CEN, B., XIONG, Y., MA, L. & PEI, G. 2001. Direct and differential interaction of beta-arrestins with the intracellular domains of different opioid receptors. *Mol Pharmacol,* 59**,** 758-64.

CHANDLER, R. L. 1961. ENCEPHALOPATHY IN MICE PRODUCED BY INOCULATION WITH SCRAPIE BRAIN MATERIAL. *The Lancet,* 277**,** 1378-1379.

CHATURVEDI, M., MAHARANA, J. & SHUKLA, A. K. 2020. Terminating G-Protein Coupling: Structural Snapshots of GPCR-β-Arrestin Complexes. *Cell,* 180**,** 1041-1043.

CHE, T., DWIVEDI-AGNIHOTRI, H., SHUKLA, A. K. & ROTH, B. L. 2021. Biased ligands at opioid receptors: Current status and future directions. *Science Signaling,* 14**,** eaav0320.

CHEN, C. Y., DION, S. B., KIM, C. M. & BENOVIC, J. L. 1993. Beta-adrenergic receptor kinase. Agonist-dependent receptor binding promotes kinase activation. *J Biol Chem,* 268**,** 7825-31.

CHEN, Q., PERRY, N. A., VISHNIVETSKIY, S. A., BERNDT, S., GILBERT, N. C., ZHUO, Y., SINGH, P. K., THOLEN, J., OHI, M. D., GUREVICH, E. V., BRAUTIGAM, C. A., KLUG, C. S., GUREVICH, V. V. & IVERSON, T. M. 2017. Structural basis of arrestin-3 activation and signaling. *Nat Commun,* 8**,** 1427.

CHEN, Y. & STRUHL, G. 1996. Dual roles for patched in sequestering and transducing Hedgehog. *Cell,* 87**,** 553-63.

CHOE, L. H., GREEN, A., KNIGHT, R. S., THOMPSON, E. J. & LEE, K. H. 2002. Apolipoprotein E and other cerebrospinal fluid proteins differentiate ante mortem variant Creutzfeldt-Jakob disease from ante mortem sporadic Creutzfeldt-Jakob disease. *Electrophoresis,* 23**,** 2242-6.

CHRISTOPOULOS, A., CHANGEUX, J.-P., CATTERALL, W. A., FABBRO, D., BURRIS, T. P., CIDLOWSKI, J. A., OLSEN, R. W., PETERS, J. A., NEUBIG, R. R., PIN, J.-P., SEXTON, P. M., KENAKIN, T. P., EHLERT, F. J., SPEDDING, M. & LANGMEAD, C. J. 2014. International Union of Basic and Clinical Pharmacology. XC. Multisite Pharmacology: Recommendations for the Nomenclature of Receptor Allosterism and Allosteric Ligands.

CHUNG, W.-S., CLARKE, L. E., WANG, G. X., STAFFORD, B. K., SHER, A., CHAKRABORTY, C., JOUNG, J., FOO, L. C., THOMPSON, A., CHEN, C., SMITH, S. J. & BARRES, B. A. 2013. Astrocytes mediate synapse elimination through MEGF10 and MERTK pathways. *Nature,* 504**,** 394-400.

CLAING, A., PERRY, S. J., ACHIRILOAIE, M., WALKER, J. K. L., ALBANESI, J. P., LEFKOWITZ, R. J. & PREMONT, R. T. 2000. Multiple endocytic pathways of G protein-coupled receptors delineated by GIT1 sensitivity. *Proceedings of the National Academy of Sciences,* 97**,** 1119.

COHEN, R. M., REZAI-ZADEH, K., WEITZ, T. M., RENTSENDORJ, A., GATE, D., SPIVAK, I., BHOLAT, Y., VASILEVKO, V., GLABE, C. G., BREUNIG, J. J., RAKIC, P., DAVTYAN, H., AGADJANYAN, M. G., KEPE, V., BARRIO, J. R., BANNYKH, S., SZEKELY, C. A., PECHNICK, R. N. & TOWN, T. 2013. A transgenic Alzheimer rat with plaques, tau pathology, behavioral impairment, oligomeric aß, and frank neuronal loss. *J Neurosci,* 33**,** 6245-56.

COLLINGE, J., WHITTINGTON, M. A., SIDLE, K. C., SMITH, C. J., PALMER, M. S., CLARKE, A. R. & JEFFERYS, J. G. 1994. Prion protein is necessary for normal synaptic function. *Nature,* 370**,** 295-7.

CONDELLO, C., DEGRADO, W. F. & PRUSINER, S. B. 2020. Prion biology: implications for Alzheimer's disease therapeutics. *Lancet Neurol,* 19**,** 802-803.

CONGDON, E. E. & SIGURDSSON, E. M. 2018. Tau-targeting therapies for Alzheimer disease. *Nat Rev Neurol,* 14**,** 399-415.

CONN, P. J., JONES, C. K. & LINDSLEY, C. W. 2009. Subtype-selective allosteric modulators of muscarinic receptors for the treatment of CNS disorders. *Trends in Pharmacological Sciences,* 30**,** 148-155.

CORDER, E. H., SAUNDERS, A. M., STRITTMATTER, W. J., SCHMECHEL, D. E., GASKELL, P. C., SMALL, G. W., ROSES, A. D., HAINES, J. L. & PERICAK-VANCE, M. A. 1993. Gene dose of apolipoprotein E type 4 allele and the risk of Alzheimer's disease in late onset families. *Science,* 261**,** 921-3.

COSTA-NETO, C. M., PARREIRAS, E. S. L. T. & BOUVIER, M. 2016. A Pluridimensional View of Biased Agonism. *Mol Pharmacol,* 90**,** 587-595.

COURTNEY, C., FARRELL, D., GRAY, R., HILLS, R., LYNCH, L., SELLWOOD, E., EDWARDS, S., HARDYMAN, W., RAFTERY, J., CROME, P., LENDON, C.,

SHAW, H., BENTHAM, P. & GROUP, A. D. C. 2004. Long-term donepezil treatment in 565 patients with Alzheimer's disease (AD2000): randomised double-blind trial. *Lancet,* 363**,** 2105-15.

COURTNEY, C. E. A. 2004. Long-term donepezil treatment in 565 patients with Alzheimer's disease (AD2000): randomised double-blind trial. *The Lancet,* 363**,** 2105-2115.

CROOK, J. M., TOMASKOVIC-CROOK, E., COPOLOV, D. L. & DEAN, B. 2000. Decreased muscarinic receptor binding in subjects with schizophrenia: a study of the human hippocampal formation. *Biological Psychiatry,* 48**,** 381-388.

CRUICKSHANK, J. W., BRUDZYNSKI, S. M. & MCLACHLAN, R. S. 1994. Involvement of M1 muscarinic receptors in the initiation of cholinergically induced epileptic seizures in the rat brain. *Brain Research,* 643**,** 125-129.

CUMMINGS, B. J., HEAD, E., RUEHL, W., MILGRAM, N. W. & COTMAN, C. W. 1996. The canine as an animal model of human aging and dementia. *Neurobiol Aging,* 17**,** 259-68.

CUNNINGHAM, C., DEACON, R., WELLS, H., BOCHE, D., WATERS, S., DINIZ, C. P., SCOTT, H., RAWLINS, J. N. & PERRY, V. H. 2003. Synaptic changes characterize early behavioural signs in the ME7 model of murine prion disease. *Eur J Neurosci,* 17**,** 2147-55.

DANDOY-DRON, F., BENBOUDJEMA, L., GUILLO, F., JAEGLY, A., JASMIN, C., DORMONT, D., TOVEY, M. G. & DRON, M. 2000. Enhanced levels of scrapie responsive gene mRNA in BSE-infected mouse brain. *Brain Res Mol Brain Res,* 76**,** 173-9.

DANIELSSON, F., PETERSON, M. K., CALDEIRA ARAÚJO, H., LAUTENSCHLÄGER, F. & GAD, A. K. B. 2018. Vimentin Diversity in Health and Disease. *Cells,* 7.

DANN, C. E., HSIEH, J.-C., RATTNER, A., SHARMA, D., NATHANS, J. & LEAHY, D. J. 2001. Insights into Wnt binding and signalling from the structures of two Frizzled cysteine-rich domains. *Nature,* 412**,** 86-90.

DAVENPORT, A. P., ALEXANDER, S. P., SHARMAN, J. L., PAWSON, A. J., BENSON, H. E., MONAGHAN, A. E., LIEW, W. C., MPAMHANGA, C. P., BONNER, T. I., NEUBIG, R. R., PIN, J. P., SPEDDING, M. & HARMAR, A. J. 2013. International Union of Basic and Clinical Pharmacology. LXXXVIII. G protein-coupled receptor list: recommendations for new pairings with cognate ligands. *Pharmacol Rev,* 65**,** 967-86.

DAVIES, P. & MALONEY, A. J. 1976. Selective loss of central cholinergic neurons in Alzheimer's disease. *Lancet,* 2**,** 1403.

DAVIS, A. A., FRITZ, J. J., WESS, J., LAH, J. J. & LEVEY, A. I. 2010. Deletion of M1 muscarinic acetylcholine receptors increases amyloid pathology in vitro and in vivo. *J Neurosci,* 30**,** 4190-6.

DAVOREN, J. E., LEE, C.-W., GARNSEY, M., BRODNEY, M. A., CORDES, J., DLUGOLENSKI, K., EDGERTON, J. R., HARRIS, A. R., HELAL, C. J., JENKINSON, S., KAUFFMAN, G. W., KENAKIN, T. P., LAZZARO, J. T., LOTARSKI, S. M., MAO, Y., NASON, D. M., NORTHCOTT, C., NOTTEBAUM, L., O'NEIL, S. V., PETTERSEN, B., POPIOLEK, M., REINHART, V., SALOMON-FERRER, R., STEYN, S. J., WEBB, D., ZHANG, L. & GRIMWOOD, S. 2016. Discovery of the Potent and Selective M1 PAM-Agonist N-[(3R,4S)-3-Hydroxytetrahydro-2H-pyran-4-yl]-5-methyl-4-[4-(1,3-thiazol-4-yl)benzyl]pyridine-2-carboxamide (PF-06767832): Evaluation of Efficacy and Cholinergic Side Effects. *Journal of Medicinal Chemistry,* 59**,** 6313-6328.

DE LEAN, A., STADEL, J. M. & LEFKOWITZ, R. J. 1980. A ternary complex model explains the agonist-specific binding properties of the adenylate cyclase-coupled beta-adrenergic receptor. *Journal of Biological Chemistry,* 255**,** 7108-7117.

DEACON, R. M. J. 2006. Burrowing in rodents: a sensitive method for detecting behavioral dysfunction. *Nature Protocols,* 1**,** 118-121.

DEAN, B., CROOK, J. M., OPESKIN, K., HILL, C., KEKS, N. & COPOLOV, D. L. 1996. The density of muscarinic M1 receptors is decreased in the caudate-putamen of subjects with schizophrenia. *Mol Psychiatry,* 1**,** 54-8.

DEAN, B., MCLEOD, M., KERIAKOUS, D., MCKENZIE, J. & SCARR, E. 2002. Decreased muscarinic1 receptors in the dorsolateral prefrontal cortex of subjects with schizophrenia. *Molecular Psychiatry,* 7**,** 1083-1091.

DECOURT, B., LAHIRI, D. K. & SABBAGH, M. N. 2017. Targeting Tumor Necrosis Factor Alpha for Alzheimer's Disease. *Curr Alzheimer Res,* 14**,** 412-425.

DEGRAFF, J. L., GUREVICH, V. V. & BENOVIC, J. L. 2002. The third intracellular loop of alpha 2-adrenergic receptors determines subtype specificity of arrestin interaction. *J Biol Chem,* 277**,** 43247-52.

DELEAULT, N. R., GEOGHEGAN, J. C., NISHINA, K., KASCSAK, R., WILLIAMSON, R. A. & SUPATTAPONE, S. 2005. Protease-resistant prion protein amplification reconstituted with partially purified substrates and synthetic polyanions. *J Biol Chem,* 280**,** 26873-9.

DELEZ, A. L., GUSTAFSON, D. P. & LUTTRELL, C. N. 1957. Some clinical and histological observations on scrapie in sheep. *J Am Vet Med Assoc,* 131**,** 439-46.

DEMATTOS, R. B., DELL, M. A., PARSADANIAN, M., TAYLOR, J. W., HARMONY, J. A. K., BALES, K. R., PAUL, S. M., ARONOW, B. J. & HOLTZMAN, D. M.

2002. Clusterin promotes amyloid plaque formation and is critical for neuritic toxicity in a mouse model of Alzheimer's disease. *Proceedings of the National Academy of Sciences,* 99**,** 10843.

DEMBER, W. N. & FOWLER, H. 1959. Spontaneous alternation after free and forced trials. *Canadian Journal of Psychology/Revue canadienne de psychologie,* 13**,** 151-154.

DEWIRE, S. M., AHN, S., LEFKOWITZ, R. J. & SHENOY, S. K. 2007. Beta-arrestins and cell signaling. *Annu Rev Physiol,* 69**,** 483-510.

DHIRAPONG, A., LLEO, A., LEUNG, P., GERSHWIN, M. E. & LIU, F. T. 2009. The immunological potential of galectin-1 and -3. *Autoimmun Rev,* 8**,** 360-3.

DI CHIARA, G., MORELLI, M. & CONSOLO, S. 1994. Modulatory functions of neurotransmitters in the striatum: ACh/dopamine/NMDA interactions. *Trends Neurosci,* 17**,** 228-33.

DIAZ-ESPINOZA, R. & SOTO, C. 2012. High-resolution structure of infectious prion protein: the final frontier. *Nat Struct Mol Biol,* 19**,** 370-7.

DICKINSON, A. G., STAMP, J. T. & RENWICK, C. C. 1974. Maternal and lateral transmission of scrapie in sheep. *Journal of Comparative Pathology,* 84**,** 19-25.

DIGBY, G. J., NOETZEL, M. J., BUBSER, M., UTLEY, T. J., WALKER, A. G., BYUN, N. E., LEBOIS, E. P., XIANG, Z., SHEFFLER, D. J., CHO, H. P., DAVIS, A. A., NEMIROVSKY, N. E., MENNENGA, S. E., CAMP, B. W., BIMONTE-NELSON, H. A., BODE, J., ITALIANO, K., MORRISON, R., DANIELS, J. S., NISWENDER, C. M., OLIVE, M. F., LINDSLEY, C. W., JONES, C. K. & CONN, P. J. 2012. Novel allosteric agonists of M1 muscarinic acetylcholine receptors induce brain region-specific responses that correspond with behavioral effects in animal models. *J Neurosci,* 32**,** 8532-44.

DRAGIC, T., TRKOLA, A., THOMPSON, D. A., CORMIER, E. G., KAJUMO, F. A., MAXWELL, E., LIN, S. W., YING, W., SMITH, S. O., SAKMAR, T. P. & MOORE, J. P. 2000. A binding pocket for a small molecule inhibitor of HIV-1 entry within the transmembrane helices of CCR5. *Proc Natl Acad Sci U S A,* 97**,** 5639-44.

DROR, R. O., MILDORF, T. J., HILGER, D., MANGLIK, A., BORHANI, D. W., ARLOW, D. H., PHILIPPSEN, A., VILLANUEVA, N., YANG, Z., LERCH, M. T., HUBBELL, W. L., KOBILKA, B. K., SUNAHARA, R. K. & SHAW, D. E. 2015. SIGNAL TRANSDUCTION. Structural basis for nucleotide exchange in heterotrimeric G proteins. *Science (New York, N.Y.),* 348**,** 1361-1365.

DROR, R. O., PAN, A. C., ARLOW, D. H., BORHANI, D. W., MARAGAKIS, P., SHAN, Y., XU, H. & SHAW, D. E. 2011. Pathway and mechanism of drug binding to G-protein-coupled receptors. *Proceedings of the National Academy of Sciences,* 108**,** 13118.

DRUBE, J., HAIDER, R. S., MATTHEES, E. S. F., REICHEL, M., ZEINER, J., FRITZWANKER, S., ZIEGLER, C., BARZ, S., KLEMENT, L., FILOR, J., WEITZEL, V., KLIEWER, A., MIESS, E., KOSTENIS, E., SCHULZ, S. & HOFFMANN, C. 2022. GPCR kinase knockout cells reveal the impact of individual GRKs on arrestin binding and GPCR regulation. *Nat Commun,* 13**,** 540.

DUFFY, P., WOLF, J., COLLINS, G., DEVOE, A. G., STREETEN, B. & COWEN, D. 1974. Letter: Possible person-to-person transmission of Creutzfeldt-Jakob disease. *N Engl J Med,* 290**,** 692-3.

DUYCKAERTS, C., CLAVAGUERA, F. & POTIER, M. C. 2019. The prion-like propagation hypothesis in Alzheimer's and Parkinson's disease. *Curr Opin Neurol,* 32**,** 266-271.

DWOMOH, L., ROSSI, M., SCARPA, M., KHAJEHALI, E., MOLLOY, C., HERZYK, P., MISTRY, S. N., BOTTRILL, A. R., SEXTON, P. M., CHRISTOPOULOS, A., CONN, P. J., LINDSLEY, C. W., BRADLEY, S. J. & TOBIN, A. B. 2021. Activation of M1 muscarinic receptors reduce pathology and slow progression of neurodegenerative disease. *bioRxiv***,** 2021.07.30.454298.

EBERT, U. & KIRCH, W. 1998. Scopolamine model of dementia: electroencephalogram findings and cognitive performance. *Eur J Clin Invest,* 28**,** 944-9.

ELMORE, M. R., NAJAFI, A. R., KOIKE, M. A., DAGHER, N. N., SPANGENBERG, E. E., RICE, R. A., KITAZAWA, M., MATUSOW, B., NGUYEN, H., WEST, B. L. & GREEN, K. N. 2014. Colony-stimulating factor 1 receptor signaling is necessary for microglia viability, unmasking a microglia progenitor cell in the adult brain. *Neuron,* 82**,** 380-97.

ENGERS, J. L., CHILDRESS, E. S., LONG, M. F., CAPSTICK, R. A., LUSCOMBE, V. B., CHO, H. P., DICKERSON, J. W., ROOK, J. M., BLOBAUM, A. L., NISWENDER, C. M., ENGERS, D. W., CONN, P. J. & LINDSLEY, C. W. 2018. VU6007477, a Novel M1 PAM Based on a Pyrrolo[2,3-b]pyridine Carboxamide Core Devoid of Cholinergic Adverse Events. *ACS Medicinal Chemistry Letters,* 9**,** 917-922.

FALSIG, J., JULIUS, C., MARGALITH, I., SCHWARZ, P., HEPPNER, F. L. & AGUZZI, A. 2008. A versatile prion replication assay in organotypic brain slices. *Nature Neuroscience,* 11**,** 109-117.

FANSELOW, M. S. & POULOS, A. M. 2005. The neuroscience of mammalian associative learning. *Annu Rev Psychol,* 56**,** 207-34.

FEINSTEIN, T. N., YUI, N., WEBBER, M. J., WEHBI, V. L., STEVENSON, H. P., KING, J. D., JR., HALLOWS, K. R., BROWN, D., BOULEY, R. & VILARDAGA, J. P. 2013. Noncanonical control of vasopressin receptor type 2 signaling by retromer and arrestin. *J Biol Chem,* 288**,** 27849-60.

FELDER, C. C. 1995. Muscarinic acetylcholine receptors: signal transduction through multiple effectors. *Faseb j,* 9**,** 619-25.

FELDER, C. C. 2019. GPCR drug discovery-moving beyond the orthosteric to the allosteric domain. *Adv Pharmacol,* 86**,** 1-20.

FELDER, C. C., BYMASTER, F. P., WARD, J. & DELAPP, N. 2000. Therapeutic Opportunities for Muscarinic Receptors in the Central Nervous System. *Journal of Medicinal Chemistry,* 43**,** 4333-4353.

FELDER, C. C., GOLDSMITH, P. J., JACKSON, K., SANGER, H. E., EVANS, D. A., MOGG, A. J. & BROAD, L. M. 2018. Current status of muscarinic M1 and M4 receptors as drug targets for neurodegenerative diseases. *Neuropharmacology,* 136**,** 449-458.

FELKER, G. M., BUTLER, J., COLLINS, S. P., COTTER, G., DAVISON, B. A., EZEKOWITZ, J. A., FILIPPATOS, G., LEVY, P. D., METRA, M., PONIKOWSKI, P., SOERGEL, D. G., TEERLINK, J. R., VIOLIN, J. D., VOORS, A. A. & PANG, P. S. 2015. Heart failure therapeutics on the basis of a biased ligand of the angiotensin-2 type 1 receptor. Rationale and design of the BLAST-AHF study (Biased Ligand of the Angiotensin Receptor Study in Acute Heart Failure). *JACC Heart Fail,* 3**,** 193-201.

FERGUSON, S. S., DOWNEY, W. E., 3RD, COLAPIETRO, A. M., BARAK, L. S., MÉNARD, L. & CARON, M. G. 1996. Role of beta-arrestin in mediating agonist-promoted G protein-coupled receptor internalization. *Science,* 271**,** 363-6.

FERRANDON, S., FEINSTEIN, T. N., CASTRO, M., WANG, B., BOULEY, R., POTTS, J. T., GARDELLA, T. J. & VILARDAGA, J. P. 2009. Sustained cyclic AMP production by parathyroid hormone receptor endocytosis. *Nat Chem Biol,* 5**,** 734-42.

FINK-JENSEN, A., SCHMIDT, L. S., DENCKER, D., SCHÜLEIN, C., WESS, J., WÖRTWEIN, G. & WOLDBYE, D. P. 2011. Antipsychotic-induced catalepsy is attenuated in mice lacking the M4 muscarinic acetylcholine receptor. *Eur J Pharmacol,* 656**,** 39-44.

FISCHER, R. & MAIER, O. 2015. Interrelation of oxidative stress and inflammation in neurodegenerative disease: role of TNF. *Oxid Med Cell Longev,* 2015**,** 610813.

FISHER, A. 2008a. Cholinergic treatments with emphasis on M1 muscarinic agonists as potential disease-modifying agents for Alzheimer's disease. *Neurotherapeutics,* 5**,** 433-442.

FISHER, A. 2008b. M1 Muscarinic Agonists Target Major Hallmarks of Alzheimer's Disease – The Pivotal Role of Brain M1 Receptors. 237–240.

FLICKER, C., SERBY, M. & FERRIS, S. H. 1990. Scopolamine effects on memory, language, visuospatial praxis and psychomotor speed. *Psychopharmacology,* 100**,** 243-250.

FOOD AND DRUG ADMINISTRATION 2021. FDA Grants Accelerated Approval for Alzheimer's Drug.

FOORD, S. M., BONNER, T. I., NEUBIG, R. R., ROSSER, E. M., PIN, J.-P., DAVENPORT, A. P., SPEDDING, M. & HARMAR, A. J. 2005. International Union of Pharmacology. XLVI. G Protein-Coupled Receptor List. *Pharmacological Reviews,* 57**,** 279.

FOSTER, D. J., CHOI, D. L., CONN, P. J. & ROOK, J. M. 2014. Activation of M1 and M4 muscarinic receptors as potential treatments for Alzheimer's disease and schizophrenia. *Neuropsychiatr Dis Treat,* 10**,** 183-91.

FRANCIS, P. T., PALMER, A. M., SNAPE, M. & WILCOCK, G. K. 1999. The cholinergic hypothesis of Alzheimer's disease: a review of progress. *Journal of neurology, neurosurgery, and psychiatry,* 66**,** 137-147.

FRASCA, G., CARBONARO, V., MERLO, S., COPANI, A. & SORTINO, M. A. 2008. Integrins mediate beta-amyloid-induced cell-cycle activation and neuronal death. *J Neurosci Res,* 86**,** 350-5.

FREDRIKSSON, R., LAGERSTRÖM, M. C., LUNDIN, L.-G. & SCHIÖTH, H. B. 2003. The G-Protein-Coupled Receptors in the Human Genome Form Five Main Families. Phylogenetic Analysis, Paralogon Groups, and Fingerprints. *Molecular Pharmacology,* 63**,** 1256.

FREIXES, M., PUIG, B., RODRÍGUEZ, A., TORREJÓN-ESCRIBANO, B., BLANCO, R. & FERRER, I. 2004. Clusterin solubility and aggregation in Creutzfeldt-Jakob disease. *Acta Neuropathol,* 108**,** 295-301.

GAJDUSEK, D. C. & ZIGAS, V. 1957. Degenerative disease of the central nervous system in New Guinea; the endemic occurrence of kuru in the native population. *N Engl J Med,* 257**,** 974-8.

GALANDRIN, S., OLIGNY-LONGPRÉ, G. & BOUVIER, M. 2007. The evasive nature of drug efficacy: implications for drug discovery. *Trends in Pharmacological Sciences,* 28**,** 423-430.

GAMES, D., ADAMS, D., ALESSANDRINI, R., BARBOUR, R., BERTHELETTE, P., BLACKWELL, C., CARR, T., CLEMENS, J., DONALDSON, T., GILLESPIE, F. & ET AL. 1995. Alzheimer-type neuropathology in transgenic mice overexpressing V717F beta-amyloid precursor protein. *Nature,* 373**,** 523-7.

GAN, L., COOKSON, M. R., PETRUCELLI, L. & LA SPADA, A. R. 2018. Converging pathways in neurodegeneration, from genetics to mechanisms. *Nat Neurosci,* 21**,** 1300-1309.

GAUTAM, N., DOWNES, G. B., YAN, K. & KISSELEV, O. 1998. The G-protein betagamma complex. *Cell Signal,* 10**,** 447-55.

GELBER, E. I., KROEZE, W. K., WILLINS, D. L., GRAY, J. A., SINAR, C. A., HYDE, E. G., GUREVICH, V., BENOVIC, J. & ROTH, B. L. 1999. Structure and function of the third intracellular loop of the 5-hydroxytryptamine2A receptor: the third intracellular loop is alpha-helical and binds purified arrestins. *J Neurochem,* 72**,** 2206-14.

GERSHENGORN, M. C., GERAS-RAAKA, E., VARMA, A. & CLARK-LEWIS, I. 1998. Chemokines activate Kaposi's sarcoma-associated herpesvirus G protein-coupled receptor in mammalian cells in culture. *The Journal of clinical investigation,* 102**,** 1469-1472.

GERSTMANN, J., STRÄUSSLER, E. & SCHEINKER, I. 1935. Über eine eigenartige hereditär- familiäre Erkrankung des Zentralnervensystems. *Zeitschrift für die gesamte Neurologie und Psychiatrie,* 154**,** 736-762.

GHOSH, E., KUMARI, P., JAIMAN, D. & SHUKLA, A. K. 2015. Methodological advances: the unsung heroes of the GPCR structural revolution. *Nature Reviews Molecular Cell Biology,* 16**,** 69-81.

GHOSHAL, A., ROOK, J. M., DICKERSON, J. W., ROOP, G. N., MORRISON, R. D., JALAN-SAKRIKAR, N., LAMSAL, A., NOETZEL, M. J., POSLUSNEY, M. S., WOOD, M. R., MELANCON, B. J., STAUFFER, S. R., XIANG, Z., DANIELS, J. S., NISWENDER, C. M., JONES, C. K., LINDSLEY, C. W. & CONN, P. J. 2016. Potentiation of M1 Muscarinic Receptor Reverses Plasticity Deficits and Negative and Cognitive Symptoms in a Schizophrenia Mouse Model. *Neuropsychopharmacology : official publication of the American College of Neuropsychopharmacology,* 41**,** 598-610.

GIESE, A., BROWN, D. R., GROSCHUP, M. H., FELDMANN, C., HAIST, I. & KRETZSCHMAR, H. A. 1998. Role of microglia in neuronal cell death in prion disease. *Brain Pathol,* 8**,** 449-57.

GILMAN, S., KOLLER, M., BLACK, R. S., JENKINS, L., GRIFFITH, S. G., FOX, N. C., EISNER, L., KIRBY, L., ROVIRA, M. B., FORETTE, F. & ORGOGOZO, J. M. 2005. Clinical effects of Abeta immunization (AN1792) in patients with AD in an interrupted trial. *Neurology,* 64**,** 1553-62.

GILMORE, T. D. 2006. Introduction to NF-kappaB: players, pathways, perspectives. *Oncogene,* 25**,** 6680-4.

GLASSE, R. 1967. Cannibalism in the Kuru region of New Guinea. *Trans N Y Acad Sci,* 29**,** 748-54.

GLENN, M. J., NESBITT, C. & MUMBY, D. G. 2003. Perirhinal cortex lesions produce variable patterns of retrograde amnesia in rats. *Behav Brain Res,* 141**,** 183-93.

GOLDGABER, D., GOLDFARB, L. G., BROWN, P., ASHER, D. M., BROWN, W. T., LIN, S., TEENER, J. W., FEINSTONE, S. M., RUBENSTEIN, R., KASCSAK, R. J. & ET AL. 1989. Mutations in familial Creutzfeldt-Jakob disease and Gerstmann-Sträussler-Scheinker's syndrome. *Exp Neurol,* 106**,** 204-6.

GOLLIN, P. A., KALARIA, R. N., EIKELENBOOM, P., ROZEMULLER, A. & PERRY, G. 1992. Alpha 1-antitrypsin and alpha 1-antichymotrypsin are in the lesions of Alzheimer's disease. *Neuroreport,* 3**,** 201-3.

GÓMEZ-NICOLA, D., FRANSEN, N. L., SUZZI, S. & PERRY, V. H. 2013. Regulation of microglial proliferation during chronic neurodegeneration. *J Neurosci,* 33**,** 2481-93.

GOMEZA, J., ZHANG, L., KOSTENIS, E., FELDER, C., BYMASTER, F., BRODKIN, J., SHANNON, H., XIA, B., DENG, C. & WESS, J. 1999. Enhancement of D1 dopamine receptor-mediated locomotor stimulation in M(4) muscarinic acetylcholine receptor knockout mice. *Proceedings of the National Academy of Sciences of the United States of America,* 96**,** 10483-10488.

GOMEZA, J., ZHANG, L., KOSTENIS, E., FELDER, C. C., BYMASTER, F. P., BRODKIN, J., SHANNON, H., XIA, B., DUTTAROY, A., DENG, C. X. & WESS, J. 2001. Generation and pharmacological analysis of M2 and M4 muscarinic receptor knockout mice. *Life Sci,* 68**,** 2457-66.

GONZÁLEZ-MAESO, J., WEISSTAUB, N. V., ZHOU, M., CHAN, P., IVIC, L., ANG, R., LIRA, A., BRADLEY-MOORE, M., GE, Y., ZHOU, Q., SEALFON, S. C. & GINGRICH, J. A. 2007. Hallucinogens recruit specific cortical 5-HT(2A) receptor-mediated signaling pathways to affect behavior. *Neuron,* 53**,** 439-52.

GONZÁLEZ, A., PEREZ-ACLE, T., PARDO, L. & DEUPI, X. 2011. Molecular basis of ligand dissociation in β-adrenergic receptors. *PloS one,* 6**,** e23815-e23815.

GOODMAN, O. B., KRUPNICK, J. G., SANTINI, F., GUREVICH, V. V., PENN, R. B., GAGNON, A. W., KEEN, J. H. & BENOVIC, J. L. 1996. β-Arrestin acts as a clathrin adaptor in endocytosis of the β2-adrenergic receptor. *Nature,* 383**,** 447-450.

GOSENS, R. & GROSS, N. 2018. The mode of action of anticholinergics in asthma. *Eur Respir J,* 52.

GOSENS, R., ZAAGSMA, J., MEURS, H. & HALAYKO, A. J. 2006. Muscarinic receptor signaling in the pathophysiology of asthma and COPD. *Respir Res,* 7**,** 73.

GÖTZ, J., SCHILD, A., HOERNDLI, F. & PENNANEN, L. 2004. Amyloid-induced neurofibrillary tangle formation in Alzheimer's disease: insight from transgenic mouse and tissue-culture models. *Int J Dev Neurosci,* 22**,** 453-65.

GRAY, J. A. & MCNAUGHTON, N. 1983. Comparison between the behavioural effects of septal and hippocampal lesions: A review. *Neuroscience & Biobehavioral Reviews,* 7**,** 119-188.

GREGORY, K. J., SEXTON, P. M. & CHRISTOPOULOS, A. 2007. Allosteric modulation of muscarinic acetylcholine receptors. *Current neuropharmacology,* 5**,** 157-167.

GRUNDMANN, M., MERTEN, N., MALFACINI, D., INOUE, A., PREIS, P., SIMON, K., RÜTTIGER, N., ZIEGLER, N., BENKEL, T., SCHMITT, N. K., ISHIDA, S., MÜLLER, I., REHER, R., KAWAKAMI, K., INOUE, A., RICK, U., KÜHL, T., IMHOF, D., AOKI, J., KÖNIG, G. M., HOFFMANN, C., GOMEZA, J., WESS, J. & KOSTENIS, E. 2018. Lack of beta-arrestin signaling in the absence of active G proteins. *Nature Communications,* 9**,** 341.

GUISE, S., BRAGUER, D., CARLES, G., DELACOURTE, A. & BRIAND, C. 2001. Hyperphosphorylation of tau is mediated by ERK activation during anticancer drug-induced apoptosis in neuroblastoma cells. *J Neurosci Res,* 63**,** 257-67.

GUNN-MOORE, D. A., MCVEE, J., BRADSHAW, J. M., PEARSON, G. R., HEAD, E. & GUNN-MOORE, F. J. 2006. Ageing changes in cat brains demonstrated by beta-amyloid and AT8-immunoreactive phosphorylated tau deposits. *J Feline Med Surg,* 8**,** 234-42.

GUO, Y.-J., SHI, Q., YANG, X.-D., LI, J.-L., MA, Y., XIAO, K., CHEN, C., HAN, J. & DONG, X.-P. 2017. Increases of Galectin-1 and its S-nitrosylated form in the Brain Tissues of Scrapie-Infected Rodent Models and Human Prion Diseases. *Molecular Neurobiology,* 54**,** 3707-3716.

GUREVICH, E. V., TESMER, J. J., MUSHEGIAN, A. & GUREVICH, V. V. 2012. G protein-coupled receptor kinases: more than just kinases and not only for GPCRs. *Pharmacol Ther,* 133**,** 40-69.

GUREVICH, V. V., DION, S. B., ONORATO, J. J., PTASIENSKI, J., KIM, C. M., STERNE-MARR, R., HOSEY, M. M. & BENOVIC, J. L. 1995. Arrestin interactions with G protein-coupled receptors. Direct binding studies of wild type and mutant arrestins with rhodopsin, beta 2-adrenergic, and m2 muscarinic cholinergic receptors. *J Biol Chem,* 270**,** 720-31.

GUREVICH, V. V. & GUREVICH, E. V. 2004. The molecular acrobatics of arrestin activation. *Trends in Pharmacological Sciences,* 25**,** 105-111.

GUREVICH, V. V. & GUREVICH, E. V. 2006. The structural basis of arrestin-mediated regulation of G-protein-coupled receptors. *Pharmacol Ther,* 110**,** 465-502.

GUREVICH, V. V. & GUREVICH, E. V. 2019. GPCR Signaling Regulation: The Role of GRKs and Arrestins. *Frontiers in Pharmacology,* 10**,** 125.

HAASS, C., LEMERE, C. A., CAPELL, A., CITRON, M., SEUBERT, P., SCHENK, D., LANNFELT, L. & SELKOE, D. J. 1995. The Swedish mutation causes early-onset Alzheimer's disease by beta-secretase cleavage within the secretory pathway. *Nat Med,* 1**,** 1291-6.

HAGA, K. & HAGA, T. 1992. Activation by G protein beta gamma subunits of agonist- or light-dependent phosphorylation of muscarinic acetylcholine receptors and rhodopsin. *Journal of Biological Chemistry,* 267**,** 2222-2227.

HAGA, K., KRUSE, A. C., ASADA, H., YURUGI-KOBAYASHI, T., SHIROISHI, M., ZHANG, C., WEIS, W. I., OKADA, T., KOBILKA, B. K., HAGA, T. & KOBAYASHI, T. 2012. Structure of the human M2 muscarinic acetylcholine receptor bound to an antagonist. *Nature,* 482**,** 547-51.

HALL, H., IULITA, M. F., GUBERT, P., FLORES AGUILAR, L., DUCATENZEILER, A., FISHER, A. & CUELLO, A. C. 2018. AF710B, an M1/sigma-1 receptor agonist with long-lasting disease-modifying properties in a transgenic rat model of Alzheimer's disease. *Alzheimers Dement,* 14**,** 811-823.

HALLIDAY, M. & MALLUCCI, G. R. 2014. Targeting the unfolded protein response in neurodegeneration: A new approach to therapy. *Neuropharmacology,* 76**,** 169-174.

HALLIDAY, M. & MALLUCCI, G. R. 2015. Review: Modulating the unfolded protein response to prevent neurodegeneration and enhance memory. *Neuropathol Appl Neurobiol,* 41**,** 414-27.

HAMELMANN, E. 2018. Long-acting muscarinic antagonists for the treatment of asthma in children—a new kid in town. *Allergo Journal International,* 27**,** 220-227.

HAMILTON, S. E., LOOSE, M. D., QI, M., LEVEY, A. I., HILLE, B., MCKNIGHT, G. S., IDZERDA, R. L. & NATHANSON, N. M. 1997. Disruption of the M1 receptor gene ablates muscarinic receptor-dependent M current regulation and seizure activity in mice. *Proceedings of the National Academy of Sciences of the United States of America,* 94**,** 13311-13316.

HAMILTON, S. E. & NATHANSON, N. M. 2001. The M1 Receptor Is Required for Muscarinic Activation of Mitogen-activated Protein (MAP) Kinase in Murine Cerebral Cortical Neurons *. *Journal of Biological Chemistry,* 276**,** 15850-15853.

HAN, M., GUREVICH, V. V., VISHNIVETSKIY, S. A., SIGLER, P. B. & SCHUBERT, C. 2001. Crystal structure of beta-arrestin at 1.9 A: possible mechanism of receptor binding and membrane Translocation. *Structure,* 9**,** 869-80.

HANSEEUW, B. J., BETENSKY, R. A., SCHULTZ, A. P., PAPP, K. V., MORMINO, E. C., SEPULCRE, J., BARK, J. S., COSIO, D. M., LAPOINT, M., CHHATWAL, J. P., RENTZ, D. M., SPERLING, R. A. & JOHNSON, K. A. 2017.

Fluorodeoxyglucose metabolism associated with tau-amyloid interaction predicts memory decline. *Ann Neurol,* 81**,** 583-596.

HARAGUCHI, T., FISHER, S., OLOFSSON, S., ENDO, T., GROTH, D., TARENTINO, A., BORCHELT, D. R., TEPLOW, D., HOOD, L., BURLINGAME, A., LYCKE, E., KOBATA, A. & PRUSINER, S. B. 1989. Asparagine-linked glycosylation of the scrapie and cellular prion proteins. *Archives of Biochemistry and Biophysics,* 274**,** 1-13.

HARING, R., FISHER, A., MARCIANO, D., PITTEL, Z., KLOOG, Y., ZUCKERMAN, A., ESHHAR, N. & HELDMAN, E. 1998. Mitogen-activated protein kinase-dependent and protein kinase C-dependent pathways link the m1 muscarinic receptor to beta-amyloid precursor protein secretion. *J Neurochem,* 71**,** 2094-103.

HARKANY, T., ABRAHÁM, I., TIMMERMAN, W., LASKAY, G., TÓTH, B., SASVÁRI, M., KÓNYA, C., SEBENS, J. B., KORF, J., NYAKAS, C., ZARÁNDI, M., SOÓS, K., PENKE, B. & LUITEN, P. G. 2000. beta-amyloid neurotoxicity is mediated by a glutamate-triggered excitotoxic cascade in rat nucleus basalis. *Eur J Neurosci,* 12**,** 2735-45.

HARKANY, T., O'MAHONY, S., KELLY, J. P., SOÓS, K., TÖRÕ, I., PENKE, B., LUITEN, P. G., NYAKAS, C., GULYA, K. & LEONARD, B. E. 1998. Beta-amyloid(Phe(SO3H)24)25-35 in rat nucleus basalis induces behavioral dysfunctions, impairs learning and memory and disrupts cortical cholinergic innervation. *Behav Brain Res,* 90**,** 133-45.

HARMAR, A. J. 2001. Family-B G-protein-coupled receptors. *Genome Biol,* 2**,** Reviews3013.

HAROLD, D., ABRAHAM, R., HOLLINGWORTH, P., SIMS, R., GERRISH, A., HAMSHERE, M. L., PAHWA, J. S., MOSKVINA, V., DOWZELL, K., WILLIAMS, A., JONES, N., THOMAS, C., STRETTON, A., MORGAN, A. R., LOVESTONE, S., POWELL, J., PROITSI, P., LUPTON, M. K., BRAYNE, C., RUBINSZTEIN, D. C., GILL, M., LAWLOR, B., LYNCH, A., MORGAN, K., BROWN, K. S., PASSMORE, P. A., CRAIG, D., MCGUINNESS, B., TODD, S., HOLMES, C., MANN, D., SMITH, A. D., LOVE, S., KEHOE, P. G., HARDY, J., MEAD, S., FOX, N., ROSSOR, M., COLLINGE, J., MAIER, W., JESSEN, F., SCHÜRMANN, B., HEUN, R., VAN DEN BUSSCHE, H., HEUSER, I., KORNHUBER, J., WILTFANG, J., DICHGANS, M., FRÖLICH, L., HAMPEL, H., HÜLL, M., RUJESCU, D., GOATE, A. M., KAUWE, J. S. K., CRUCHAGA, C., NOWOTNY, P., MORRIS, J. C., MAYO, K., SLEEGERS, K., BETTENS, K., ENGELBORGHS, S., DE DEYN, P. P., VAN BROECKHOVEN, C., LIVINGSTON, G., BASS, N. J., GURLING, H., MCQUILLIN, A., GWILLIAM, R., DELOUKAS, P., AL-CHALABI, A., SHAW, C. E., TSOLAKI, M., SINGLETON, A. B., GUERREIRO, R., MÜHLEISEN, T. W., NÖTHEN, M. M., MOEBUS, S., JÖCKEL, K.-H., KLOPP, N., WICHMANN, H. E., CARRASQUILLO, M. M., PANKRATZ, V. S., YOUNKIN, S. G., HOLMANS, P. A., O'DONOVAN, M., OWEN, M. J. & WILLIAMS, J. 2009. Genome-wide association study identifies variants at CLU and PICALM associated with Alzheimer's disease. *Nature Genetics,* 41**,** 1088-1093.

HARRIS, F. M., BRECHT, W. J., XU, Q., MAHLEY, R. W. & HUANG, Y. 2004. Increased tau phosphorylation in apolipoprotein E4 transgenic mice is associated with activation of extracellular signal-regulated kinase: modulation by zinc. *J Biol Chem,* 279**,** 44795-801.

HÄRTIG, W., KLEIN, C., BRAUER, K., SCHÜPPEL, K. F., ARENDT, T., BRÜCKNER, G. & BIGL, V. 2000. Abnormally phosphorylated protein tau in the cortex of aged individuals of various mammalian orders. *Acta Neuropathol,* 100**,** 305-12.

HAUSER, A. S., ATTWOOD, M. M., RASK-ANDERSEN, M., SCHIÖTH, H. B. & GLORIAM, D. E. 2017. Trends in GPCR drug discovery: new agents, targets and indications. *Nature Reviews Drug Discovery,* 16**,** 829.

HEDLUND, B. & BARTFAI, T. 1981. Binding of [3H]-pilocarpine to membranes from rat cerebral cortex. *Naunyn Schmiedebergs Arch Pharmacol,* 317**,** 126-30.

HEITZ, F., HOLZWARTH, J. A., GIES, J.-P., PRUSS, R. M., TRUMPP-KALLMEYER, S., HIBERT, M. F. & GUENET, C. 1999. Site-directed mutagenesis of the putative human muscarinic M2 receptor binding site. *European Journal of Pharmacology,* 380**,** 183-195.

HENEKA, M. T., CARSON, M. J., KHOURY, J. E., LANDRETH, G. E., BROSSERON, F., FEINSTEIN, D. L., JACOBS, A. H., WYSS-CORAY, T., VITORICA, J., RANSOHOFF, R. M., HERRUP, K., FRAUTSCHY, S. A., FINSEN, B., BROWN, G. C., VERKHRATSKY, A., YAMANAKA, K., KOISTINAHO, J., LATZ, E., HALLE, A., PETZOLD, G. C., TOWN, T., MORGAN, D., SHINOHARA, M. L., PERRY, V. H., HOLMES, C., BAZAN, N. G., BROOKS, D. J., HUNOT, S., JOSEPH, B., DEIGENDESCH, N., GARASCHUK, O., BODDEKE, E., DINARELLO, C. A., BREITNER, J. C., COLE, G. M., GOLENBOCK, D. T. & KUMMER, M. P. 2015. Neuroinflammation in Alzheimer's disease. *The Lancet Neurology,* 14**,** 388-405.

HERMANS, E. 2003. Biochemical and pharmacological control of the multiplicity of coupling at G-protein-coupled receptors. *Pharmacol Ther,* 99**,** 25-44.

HEUER, E., ROSEN, R. F., CINTRON, A. & WALKER, L. C. 2012. Nonhuman Primate Models of Alzheimer-Like Cerebral Proteopathy. *Current Pharmaceutical Design,* 18**,** 1159-1169.

HILL, J. M. & LUKIW, W. J. 2016. microRNA (miRNA)-Mediated Pathogenetic Signaling in Alzheimer’s Disease (AD). *Neurochemical Research,* 41**,** 96-100.

HIRSCH, J. A., SCHUBERT, C., GUREVICH, V. V. & SIGLER, P. B. 1999. The 2.8 A crystal structure of visual arrestin: a model for arrestin's regulation. *Cell,* 97**,** 257-69.

HOCK, C., MADDALENA, A., HEUSER, I., NABER, D., OERTEL, W., VON DER KAMMER, H., WIENRICH, M., RASCHIG, A., DENG, M., GROWDON, J. H. & NITSCH, R. M. 2000. Treatment with the selective muscarinic agonist talsaclidine decreases cerebrospinal fluid levels of total amyloid beta-peptide in patients with Alzheimer's disease. *Ann N Y Acad Sci,* 920**,** 285-91.

HOLTZMAN, D. M. 2001. Role of apoe/Abeta interactions in the pathogenesis of Alzheimer's disease and cerebral amyloid angiopathy. *J Mol Neurosci,* 17**,** 147-55.

HONG, C. S., GOINS, W. F., GOSS, J. R., BURTON, E. A. & GLORIOSO, J. C. 2006. Herpes simplex virus RNAi and neprilysin gene transfer vectors reduce accumulation of Alzheimer's disease-related amyloid-beta peptide in vivo. *Gene Ther,* 13**,** 1068-79.

HONG, S., BEJA-GLASSER, V. F., NFONOYIM, B. M., FROUIN, A., LI, S., RAMAKRISHNAN, S., MERRY, K. M., SHI, Q., ROSENTHAL, A., BARRES, B. A., LEMERE, C. A., SELKOE, D. J. & STEVENS, B. 2016. Complement and microglia mediate early synapse loss in Alzheimer mouse models. *Science,* 352**,** 712-716.

HOOZEMANS, J. J., VAN HAASTERT, E. S., NIJHOLT, D. A., ROZEMULLER, A. J., EIKELENBOOM, P. & SCHEPER, W. 2009. The unfolded protein response is activated in pretangle neurons in Alzheimer's disease hippocampus. *Am J Pathol,* 174**,** 1241-51.

HOOZEMANS, J. J., VEERHUIS, R., VAN HAASTERT, E. S., ROZEMULLER, J. M., BAAS, F., EIKELENBOOM, P. & SCHEPER, W. 2005. The unfolded protein response is activated in Alzheimer's disease. *Acta Neuropathol,* 110**,** 165-72.

HOU, Y., DAN, X., BABBAR, M., WEI, Y., HASSELBALCH, S. G., CROTEAU, D. L. & BOHR, V. A. 2019. Ageing as a risk factor for neurodegenerative disease. *Nature Reviews Neurology,* 15**,** 565-581.

HOUSLAY, M. D. & BAILLIE, G. S. 2005. Beta-arrestin-recruited phosphodiesterase-4 desensitizes the AKAP79/PKA-mediated switching of beta2-adrenoceptor signalling to activation of ERK. *Biochem Soc Trans,* 33**,** 1333-6.

HSIAO, K., CHAPMAN, P., NILSEN, S., ECKMAN, C., HARIGAYA, Y., YOUNKIN, S., YANG, F. & COLE, G. 1996. Correlative memory deficits, Abeta elevation, and amyloid plaques in transgenic mice. *Science,* 274**,** 99-102.

HU, J., STERN, M., GIMENEZ, L. E., WANKA, L., ZHU, L., ROSSI, M., MEISTER, J., INOUE, A., BECK-SICKINGER, A. G., GUREVICH, V. V. & WESS, J. 2016. A G Protein-biased Designer G Protein-coupled Receptor Useful for Studying the Physiological Relevance of Gq/11-dependent Signaling Pathways. *J Biol Chem,* 291**,** 7809-20.

HUANG, L.-K., CHAO, S.-P. & HU, C.-J. 2020a. Clinical trials of new drugs for Alzheimer disease. *Journal of Biomedical Science,* 27**,** 18.

HUANG, W., MASUREEL, M., QU, Q., JANETZKO, J., INOUE, A., KATO, H. E., ROBERTSON, M. J., NGUYEN, K. C., GLENN, J. S., SKINIOTIS, G. & KOBILKA, B. K. 2020b. Structure of the neurotensin receptor 1 in complex with β-arrestin 1. *Nature,* 579**,** 303-308.

HULME, E. C., BIRDSALL, N. J. M. & BUCKLEY, N. J. 1990. Muscarinic Receptor Subtypes. *Annual Review of Pharmacology and Toxicology,* 30**,** 633-673.

HULME, E. C., LU, Z. L., SALDANHA, J. W. & BEE, M. S. 2003. Structure and activation of muscarinic acetylcholine receptors. *Biochemical Society Transactions,* 31**,** 29.

HUNTINGTON, J. A., READ, R. J. & CARRELL, R. W. 2000. Structure of a serpin-protease complex shows inhibition by deformation. *Nature,* 407**,** 923-6.

IMAI, Y., IBATA, I., ITO, D., OHSAWA, K. & KOHSAKA, S. 1996. A Novel Geneiba1in the Major Histocompatibility Complex Class III Region Encoding an EF Hand Protein Expressed in a Monocytic Lineage. *Biochemical and Biophysical Research Communications,* 224**,** 855-862.

IMAI, Y. & KOHSAKA, S. 2002. Intracellular signaling in M-CSF-induced microglia activation: Role of Iba1. *Glia,* 40**,** 164-174.

INGELSSON, M., FUKUMOTO, H., NEWELL, K. L., GROWDON, J. H., HEDLEY-WHYTE, E. T., FROSCH, M. P., ALBERT, M. S., HYMAN, B. T. & IRIZARRY, M. C. 2004. Early Abeta accumulation and progressive synaptic loss, gliosis, and tangle formation in AD brain. *Neurology,* 62**,** 925-31.

INGLIS, F. 2002. The tolerability and safety of cholinesterase inhibitors in the treatment of dementia. *Int J Clin Pract Suppl***,** 45-63.

INSEL, P. A., WILDERMAN, A., ZAMBON, A. C., SNEAD, A. N., MURRAY, F., AROONSAKOOL, N., MCDONALD, D. S., ZHOU, S., MCCANN, T., ZHANG, L., SRIRAM, K., CHINN, A. M., MICHKOV, A. V., LYNCH, R. M., OVERLAND, A. C. & CORRIDEN, R. 2015. G Protein-Coupled Receptor (GPCR) Expression in Native Cells: "Novel" endoGPCRs as Physiologic Regulators and Therapeutic Targets. *Molecular pharmacology,* 88**,** 181-187.

IRANNEJAD, R., TOMSHINE, J. C., TOMSHINE, J. R., CHEVALIER, M., MAHONEY, J. P., STEYAERT, J., RASMUSSEN, S. G. F., SUNAHARA, R. K., EL-SAMAD, H., HUANG, B. & VON ZASTROW, M. 2013. Conformational biosensors reveal GPCR signalling from endosomes. *Nature,* 495**,** 534-538.

ISHIBASHI, S., KUROIWA, T., SAKAGUCHI, M., SUN, L., KADOYA, T., OKANO, H. & MIZUSAWA, H. 2007. Galectin-1 regulates neurogenesis in the

subventricular zone and promotes functional recovery after stroke. *Experimental Neurology,* 207**,** 302-313.

ITO, D., IMAI, Y., OHSAWA, K., NAKAJIMA, K., FUKUUCHI, Y. & KOHSAKA, S. 1998. Microglia-specific localisation of a novel calcium binding protein, Iba1. *Molecular Brain Research,* 57**,** 1-9.

JACK, C. R., JR., KNOPMAN, D. S., WEIGAND, S. D., WISTE, H. J., VEMURI, P., LOWE, V., KANTARCI, K., GUNTER, J. L., SENJEM, M. L., IVNIK, R. J., ROBERTS, R. O., ROCCA, W. A., BOEVE, B. F. & PETERSEN, R. C. 2012. An operational approach to National Institute on Aging-Alzheimer's Association criteria for preclinical Alzheimer disease. *Ann Neurol,* 71**,** 765-75.

JACOB, H., PYRKOSCH, W. & STRUBE, H. 1950. Die erbliche Form der Creutzfeldt-Jakobschen Krankheit. *Archiv für Psychiatrie und Nervenkrankheiten,* 184**,** 653-674.

JANETOPOULOS, C., JIN, T. & DEVREOTES, P. 2001. Receptor-mediated activation of heterotrimeric G-proteins in living cells. *Science,* 291**,** 2408-11.

JEFFREY, M., HALLIDAY, W. G., BELL, J., JOHNSTON, A. R., MACLEOD, N. K., INGHAM, C., SAYERS, A. R., BROWN, D. A. & FRASER, J. R. 2000. Synapse loss associated with abnormal PrP precedes neuronal degeneration in the scrapie-infected murine hippocampus. *Neuropathol Appl Neurobiol,* 26**,** 41-54.

JIANG, Q., LEE, C. Y. D., MANDREKAR, S., WILKINSON, B., CRAMER, P., ZELCER, N., MANN, K., LAMB, B., WILLSON, T. M., COLLINS, J. L., RICHARDSON, J. C., SMITH, J. D., COMERY, T. A., RIDDELL, D., HOLTZMAN, D. M., TONTONOZ, P. & LANDRETH, G. E. 2008. ApoE Promotes the Proteolytic Degradation of Aβ. *Neuron,* 58**,** 681-693.

JIANG, S. X., SLINN, J., AYLSWORTH, A. & HOU, S. T. 2012. Vimentin participates in microglia activation and neurotoxicity in cerebral ischemia. *J Neurochem,* 122**,** 764-74.

JONES, C. K., BRADY, A. E., DAVIS, A. A., XIANG, Z., BUBSER, M., TANTAWY, M. N., KANE, A. S., BRIDGES, T. M., KENNEDY, J. P., BRADLEY, S. R., PETERSON, T. E., ANSARI, M. S., BALDWIN, R. M., KESSLER, R. M., DEUTCH, A. Y., LAH, J. J., LEVEY, A. I., LINDSLEY, C. W. & CONN, P. J. 2008. Novel selective allosteric activator of the M1 muscarinic acetylcholine receptor regulates amyloid processing and produces antipsychotic-like activity in rats. *J Neurosci,* 28**,** 10422-33.

JUST, S., ILLING, S., TRESTER-ZEDLITZ, M., LAU, E. K., KOTOWSKI, S. J., MIESS, E., MANN, A., DOLL, C., TRINIDAD, J. C., BURLINGAME, A. L., VON ZASTROW, M. & SCHULZ, S. 2013. Differentiation of opioid drug effects by hierarchical multi-site phosphorylation. *Mol Pharmacol,* 83**,** 633-9.

KAMPHUIS, W., MAMBER, C., MOETON, M., KOOIJMAN, L., SLUIJS, J. A., JANSEN, A. H., VERVEER, M., DE GROOT, L. R., SMITH, V. D., RANGARAJAN, S., RODRÍGUEZ, J. J., ORRE, M. & HOL, E. M. 2012. GFAP isoforms in adult mouse brain with a focus on neurogenic astrocytes and reactive astrogliosis in mouse models of Alzheimer disease. *PLoS One,* 7**,** e42823.

KAMPHUIS, W., MIDDELDORP, J., KOOIJMAN, L., SLUIJS, J. A., KOOI, E. J., MOETON, M., FRERIKS, M., MIZEE, M. R. & HOL, E. M. 2014. Glial fibrillary acidic protein isoform expression in plaque related astrogliosis in Alzheimer's disease. *Neurobiol Aging,* 35**,** 492-510.

KANG, Y., ZHOU, X. E., GAO, X., HE, Y., LIU, W., ISHCHENKO, A., BARTY, A., WHITE, T. A., YEFANOV, O., HAN, G. W., XU, Q., DE WAAL, P. W., KE, J., TAN, M. H. E., ZHANG, C., MOELLER, A., WEST, G. M., PASCAL, B. D., VAN EPS, N., CARO, L. N., VISHNIVETSKIY, S. A., LEE, R. J., SUINO-POWELL, K. M., GU, X., PAL, K., MA, J., ZHI, X., BOUTET, S., WILLIAMS, G. J., MESSERSCHMIDT, M., GATI, C., ZATSEPIN, N. A., WANG, D., JAMES, D., BASU, S., ROY-CHOWDHURY, S., CONRAD, C. E., COE, J., LIU, H., LISOVA, S., KUPITZ, C., GROTJOHANN, I., FROMME, R., JIANG, Y., TAN, M., YANG, H., LI, J., WANG, M., ZHENG, Z., LI, D., HOWE, N., ZHAO, Y., STANDFUSS, J., DIEDERICHS, K., DONG, Y., POTTER, C. S., CARRAGHER, B., CAFFREY, M., JIANG, H., CHAPMAN, H. N., SPENCE, J. C. H., FROMME, P., WEIERSTALL, U., ERNST, O. P., KATRITCH, V., GUREVICH, V. V., GRIFFIN, P. R., HUBBELL, W. L., STEVENS, R. C., CHEREZOV, V., MELCHER, K. & XU, H. E. 2015. Crystal structure of rhodopsin bound to arrestin by femtosecond X-ray laser. *Nature,* 523**,** 561-567.

KARASAWA, H., TAKETO, M. M. & MATSUI, M. 2003. Loss of anti-cataleptic effect of scopolamine in mice lacking muscarinic acetylcholine receptor subtype 4. *Eur J Pharmacol,* 468**,** 15-9.

KARCH, C. M. & GOATE, A. M. 2015. Alzheimer's Disease Risk Genes and Mechanisms of Disease Pathogenesis. *Biological Psychiatry,* 77**,** 43-51.

KAUPMANN, K., MALITSCHEK, B., SCHULER, V., HEID, J., FROESTL, W., BECK, P., MOSBACHER, J., BISCHOFF, S., KULIK, A., SHIGEMOTO, R., KARSCHIN, A. & BETTLER, B. 1998. GABAB-receptor subtypes assemble into functional heteromeric complexes. *Nature,* 396**,** 683-687.

KENAKIN, T. 1997. Differences between natural and recombinant G protein-coupled receptor systems with varying receptor/G protein stoichiometry. *Trends Pharmacol Sci,* 18**,** 456-64.

KENAKIN, T. 2001. Inverse, protean, and ligand-selective agonism: matters of receptor conformation. *Faseb j,* 15**,** 598-611.

KENAKIN, T. 2002. Efficacy at g-protein-coupled receptors. *Nature Reviews Drug Discovery,* 1**,** 103-110.

KENAKIN, T. 2019. Biased Receptor Signaling in Drug Discovery. *Pharmacological Reviews,* 71**,** 267.

KENAKIN, T. & CHRISTOPOULOS, A. 2013. Signalling bias in new drug discovery: detection, quantification and therapeutic impact. *Nature Reviews Drug Discovery,* 12**,** 205-216.

KERCHER, L., FAVARA, C., STRIEBEL, J. F., LACASSE, R. & CHESEBRO, B. 2007. Prion protein expression differences in microglia and astroglia influence scrapie-induced neurodegeneration in the retina and brain of transgenic mice. *J Virol,* 81**,** 10340-51.

KESHET, G. I., OVADIA, H., TARABOULOS, A. & GABIZON, R. 1999. Scrapie-infected mice and PrP knockout mice share abnormal localization and activity of neuronal nitric oxide synthase. *J Neurochem,* 72**,** 1224-31.

KHAN, S. M., SUNG, J. Y. & HÉBERT, T. E. 2016. Gβγ subunits-Different spaces, different faces. *Pharmacol Res,* 111**,** 434-441.

KIERNAN, J. A. 1984. Chromoxane cyanine R. I. Physical and chemical properties of the dye and of some of its iron complexes. *J Microsc,* 134**,** 13-23.

KIERNAN, J. A. 2007. Histochemistry of Staining Methods for Normal and Degenerating Myelin in the Central and Peripheral Nervous Systems. *Journal of Histotechnology,* 30**,** 87-106.

KILLICK, R., RIBE, E. M., AL-SHAWI, R., MALIK, B., HOOPER, C., FERNANDES, C., DOBSON, R., NOLAN, P. M., LOURDUSAMY, A., FURNEY, S., LIN, K., BREEN, G., WROE, R., TO, A. W. M., LEROY, K., CAUSEVIC, M., USARDI, A., ROBINSON, M., NOBLE, W., WILLIAMSON, R., LUNNON, K., KELLIE, S., REYNOLDS, C. H., BAZENET, C., HODGES, A., BRION, J. P., STEPHENSON, J., PAUL SIMONS, J. & LOVESTONE, S. 2014. Clusterin regulates ß-amyloid toxicity via Dickkopf-1-driven induction of the wnt–PCP–JNK pathway. *Molecular Psychiatry,* 19**,** 88-98.

KIM, M., VISHNIVETSKIY, S. A., VAN EPS, N., ALEXANDER, N. S., CLEGHORN, W. M., ZHAN, X., HANSON, S. M., MORIZUMI, T., ERNST, O. P., MEILER, J., GUREVICH, V. V. & HUBBELL, W. L. 2012. Conformation of receptor-bound visual arrestin. *Proc Natl Acad Sci U S A,* 109**,** 18407-12.

KIM, Y. M. & BENOVIC, J. L. 2002. Differential roles of arrestin-2 interaction with clathrin and adaptor protein 2 in G protein-coupled receptor trafficking. *J Biol Chem,* 277**,** 30760-8.

KIMBERLIN, R. H. & WALKER, C. A. 1978. Evidence that the Transmission of One Source of Scrapie Agent to Hamsters Involves Separation of Agent Strains from a Mixture. *Journal of General Virology,* 39**,** 487-496.

KINOSHITA, A., FUKUMOTO, H., SHAH, T., WHELAN, C. M., IRIZARRY, M. C. & HYMAN, B. T. 2003. Demonstration by FRET of BACE interaction with the amyloid precursor protein at the cell surface and in early endosomes. *J Cell Sci,* 116**,** 3339-46.

KISTEMAKER, L. E. & GOSENS, R. 2015. Acetylcholine beyond bronchoconstriction: roles in inflammation and remodeling. *Trends Pharmacol Sci,* 36**,** 164-71.

KISTNER, A., GOSSEN, M., ZIMMERMANN, F., JERECIC, J., ULLMER, C., LÜBBERT, H. & BUJARD, H. 1996. Doxycycline-mediated quantitative and tissue-specific control of gene expression in transgenic mice. *Proceedings of the National Academy of Sciences,* 93**,** 10933.

KLIEWER, A., GILLIS, A., HILL, R., SCHMIEDEL, F., BAILEY, C., KELLY, E., HENDERSON, G., CHRISTIE, M. J. & SCHULZ, S. 2020. Morphine-induced respiratory depression is independent of β-arrestin2 signalling. *British Journal of Pharmacology,* 177**,** 2923-2931.

KLIEWER, A., SCHMIEDEL, F., SIANATI, S., BAILEY, A., BATEMAN, J. T., LEVITT, E. S., WILLIAMS, J. T., CHRISTIE, M. J. & SCHULZ, S. 2019. Phosphorylation-deficient G-protein-biased μ-opioid receptors improve analgesia and diminish tolerance but worsen opioid side effects. *Nature Communications,* 10**,** 367.

KNAUS, K. J., MORILLAS, M., SWIETNICKI, W., MALONE, M., SUREWICZ, W. K. & YEE, V. C. 2001. Crystal structure of the human prion protein reveals a mechanism for oligomerization. *Nat Struct Biol,* 8**,** 770-4.

KOBILKA, B. K. 2002. Agonist-induced conformational changes in the beta2 adrenergic receptor. *J Pept Res,* 60**,** 317-21.

KOHOUT, T. A., LIN, F. S., PERRY, S. J., CONNER, D. A. & LEFKOWITZ, R. J. 2001. beta-Arrestin 1 and 2 differentially regulate heptahelical receptor signaling and trafficking. *Proc Natl Acad Sci U S A,* 98**,** 1601-6.

KOHOUT, T. A., NICHOLAS, S. L., PERRY, S. J., REINHART, G., JUNGER, S. & STRUTHERS, R. S. 2004. Differential desensitization, receptor phosphorylation, beta-arrestin recruitment, and ERK1/2 activation by the two endogenous ligands for the CC chemokine receptor 7. *J Biol Chem,* 279**,** 23214-22.

KOISTINAHO, M., LIN, S., WU, X., ESTERMAN, M., KOGER, D., HANSON, J., HIGGS, R., LIU, F., MALKANI, S., BALES, K. R. & PAUL, S. M. 2004. Apolipoprotein E promotes astrocyte colocalization and degradation of deposited amyloid-beta peptides. *Nat Med,* 10**,** 719-26.

KOLAHIAN, S. & GOSENS, R. 2012. Cholinergic regulation of airway inflammation and remodelling. *J Allergy (Cairo),* 2012**,** 681258.

KOLAKOWSKI, L. F., JR. 1994. GCRDb: a G-protein-coupled receptor database. *Recept Channels,* 2**,** 1-7.

KONG, K. C., BUTCHER, A. J., MCWILLIAMS, P., JONES, D., WESS, J., HAMDAN, F. F., WERRY, T., ROSETHORNE, E. M., CHARLTON, S. J., MUNSON, S. E., CRAGG, H. A., SMART, A. D. & TOBIN, A. B. 2010. M3 muscarinic receptor promotes insulin release via receptor phosphorylation/arrestin-dependent activation of protein kinase D1. *Proceedings of the National Academy of Sciences,* 107**,** 21181.

KRASEL, C., BÜNEMANN, M., LORENZ, K. & LOHSE, M. J. 2005. Beta-arrestin binding to the beta2-adrenergic receptor requires both receptor phosphorylation and receptor activation. *J Biol Chem,* 280**,** 9528-35.

KRASEL, C., ZABEL, U., LORENZ, K., REINER, S., AL-SABAH, S. & LOHSE, M. J. 2008. Dual Role of the ß₂-Adrenergic Receptor C Terminus for the Binding of ß-Arrestin and Receptor Internalization *. *Journal of Biological Chemistry,* 283**,** 31840-31848.

KRUSE, A. C., HU, J., PAN, A. C., ARLOW, D. H., ROSENBAUM, D. M., ROSEMOND, E., GREEN, H. F., LIU, T., CHAE, P. S., DROR, R. O., SHAW, D. E., WEIS, W. I., WESS, J. & KOBILKA, B. 2012. Structure and Dynamics of the M3 Muscarinic Acetylcholine Receptor. *Nature,* 482**,** 552-556.

KÜHN, H. 1974. Light-dependent phosphorylation of rhodopsin in living frogs. *Nature,* 250**,** 588-590.

KÜHN, H. & DREYER, W. J. 1972. Light dependent phosphorylation of rhodopsin by ATP. *FEBS Lett,* 20**,** 1-6.

KUMMER, J. L., RAO, P. K. & HEIDENREICH, K. A. 1997. Apoptosis Induced by Withdrawal of Trophic Factors Is Mediated by p38 Mitogen-activated Protein Kinase*. *Journal of Biological Chemistry,* 272**,** 20490-20494.

KUNISHIMA, N., SHIMADA, Y., TSUJI, Y., SATO, T., YAMAMOTO, M., KUMASAKA, T., NAKANISHI, S., JINGAMI, H. & MORIKAWA, K. 2000. Structural basis of glutamate recognition by a dimeric metabotropic glutamate receptor. *Nature,* 407**,** 971-977.

LABAR, K. S. & DISTERHOFT, J. F. 1998. Conditioning, awareness, and the hippocampus. *Hippocampus,* 8**,** 620-626.

LADNER, C. J. & LEE, J. M. 1998. Pharmacological Drug Treatment of Alzheimer Disease: The Cholinergic Hypothesis Revisited. *Journal of Neuropathology & Experimental Neurology,* 57**,** 719-731.

LAFERLA, F. M. & GREEN, K. N. 2012. Animal models of Alzheimer disease. *Cold Spring Harb Perspect Med,* 2.

LAGERSTRÖM, M. C. & SCHIÖTH, H. B. 2008. Structural diversity of G protein-coupled receptors and significance for drug discovery. *Nature Reviews Drug Discovery,* 7**,** 339-357.

LALONDE, R. 1986. Delayed spontaneous alternation in weaver mutant mice. *Brain Research,* 398**,** 178-180.

LAMBERT, J.-C., HEATH, S., EVEN, G., CAMPION, D., SLEEGERS, K., HILTUNEN, M., COMBARROS, O., ZELENIKA, D., BULLIDO, M. J., TAVERNIER, B., LETENNEUR, L., BETTENS, K., BERR, C., PASQUIER, F., FIÉVET, N., BARBERGER-GATEAU, P., ENGELBORGHS, S., DE DEYN, P., MATEO, I., FRANCK, A., HELISALMI, S., PORCELLINI, E., HANON, O., DE PANCORBO, M. M., LENDON, C., DUFOUIL, C., JAILLARD, C., LEVEILLARD, T., ALVAREZ, V., BOSCO, P., MANCUSO, M., PANZA, F., NACMIAS, B., BOSSÙ, P., PICCARDI, P., ANNONI, G., SERIPA, D., GALIMBERTI, D., HANNEQUIN, D., LICASTRO, F., SOININEN, H., RITCHIE, K., BLANCHÉ, H., DARTIGUES, J.-F., TZOURIO, C., GUT, I., VAN BROECKHOVEN, C., ALPÉROVITCH, A., LATHROP, M., AMOUYEL, P. & THE EUROPEAN ALZHEIMER'S DISEASE INITIATIVE, I. 2009. Genome-wide association study identifies variants at CLU and CR1 associated with Alzheimer's disease. *Nature Genetics,* 41**,** 1094-1099.

LAMBRIGHT, D. G., SONDEK, J., BOHM, A., SKIBA, N. P., HAMM, H. E. & SIGLER, P. B. 1996. The 2.0 A crystal structure of a heterotrimeric G protein. *Nature,* 379**,** 311-9.

LAMMICH, S., KOJRO, E., POSTINA, R., GILBERT, S., PFEIFFER, R., JASIONOWSKI, M., HAASS, C. & FAHRENHOLZ, F. 1999. Constitutive and regulated alpha-secretase cleavage of Alzheimer's amyloid precursor protein by a disintegrin metalloprotease. *Proc Natl Acad Sci U S A,* 96**,** 3922-7.

LANE, C. A., HARDY, J. & SCHOTT, J. M. 2018. Alzheimer's disease. *Eur J Neurol,* 25**,** 59-70.

LANE, J. R., SEXTON, P. M. & CHRISTOPOULOS, A. 2013. Bridging the gap: bitopic ligands of G-protein-coupled receptors. *Trends in Pharmacological Sciences,* 34**,** 59-66.

LANGE, H. S., CANNON, C. E., DROTT, J. T., KUDUK, S. D. & USLANER, J. M. 2015. The M1 Muscarinic Positive Allosteric Modulator PQCA Improves Performance on Translatable Tests of Memory and Attention in Rhesus Monkeys. *J Pharmacol Exp Ther,* 355**,** 442-50.

LANGMEAD, C. J., FRY, V. A. H., FORBES, I. T., BRANCH, C. L., CHRISTOPOULOS, A., WOOD, M. D. & HERDON, H. J. 2006. Probing the Molecular Mechanism of Interaction between 4- *n* -Butyl-1-[4-(2-methylphenyl)-4-oxo-1-butyl]-piperidine (AC-42) and the Muscarinic M_1 Receptor: Direct Pharmacological Evidence That AC-42 Is an Allosteric Agonist. *Molecular Pharmacology,* 69**,** 236.

LANGMEAD, C. J., WATSON, J. & REAVILL, C. 2008. Muscarinic acetylcholine receptors as CNS drug targets. *Pharmacology & Therapeutics,* 117, 232-243.

LAPORTE, S. A., OAKLEY, R. H., ZHANG, J., HOLT, J. A., FERGUSON, S. S., CARON, M. G. & BARAK, L. S. 1999. The beta2-adrenergic receptor/betaarrestin complex recruits the clathrin adaptor AP-2 during endocytosis. *Proc Natl Acad Sci U S A,* 96, 3712-7.

LAWLER, C. P., PRIOLEAU, C., LEWIS, M. M., MAK, C., JIANG, D., SCHETZ, J. A., GONZALEZ, A. M., SIBLEY, D. R. & MAILMAN, R. B. 1999. Interactions of the Novel Antipsychotic Aripiprazole (OPC-14597) with Dopamine and Serotonin Receptor Subtypes. *Neuropsychopharmacology,* 20, 612-627.

LAWLOR, P. A., BLAND, R. J., DAS, P., PRICE, R. W., HOLLOWAY, V., SMITHSON, L., DICKER, B. L., DURING, M. J., YOUNG, D. & GOLDE, T. E. 2007. Novel rat Alzheimer's disease models based on AAV-mediated gene transfer to selectively increase hippocampal Abeta levels. *Mol Neurodegener,* 2, 11.

LEBEDEVA, T., DUSTIN, M. L. & SYKULEV, Y. 2005. ICAM-1 co-stimulates target cells to facilitate antigen presentation. *Curr Opin Immunol,* 17, 251-8.

LEBOIS, E. P., BRIDGES, T. M., LEWIS, L. M., DAWSON, E. S., KANE, A. S., XIANG, Z., JADHAV, S. B., YIN, H., KENNEDY, J. P., MEILER, J., NISWENDER, C. M., JONES, C. K., CONN, P. J., WEAVER, C. D. & LINDSLEY, C. W. 2010. Discovery and characterization of novel subtype-selective allosteric agonists for the investigation of M(1) receptor function in the central nervous system. *ACS Chem Neurosci,* 1, 104-121.

LEBOIS, E. P., DIGBY, G. J., SHEFFLER, D. J., MELANCON, B. J., TARR, J. C., CHO, H. P., MILLER, N. R., MORRISON, R., BRIDGES, T. M., XIANG, Z., DANIELS, J. S., WOOD, M. R., CONN, P. J. & LINDSLEY, C. W. 2011. Development of a highly selective, orally bioavailable and CNS penetrant M1 agonist derived from the MLPCN probe ML071. *Bioorg Med Chem Lett,* 21, 6451-5.

LEBOIS, E. P., SCHROEDER, J. P., ESPARZA, T. J., BRIDGES, T. M., LINDSLEY, C. W., CONN, P. J., BRODY, D. L., DANIELS, J. S. & LEVEY, A. I. 2017. Disease-Modifying Effects of M1 Muscarinic Acetylcholine Receptor Activation in an Alzheimer's Disease Mouse Model. *ACS Chemical Neuroscience,* 8, 1177-1187.

LEDOUX, J. E. 2000. Emotion circuits in the brain. *Annu Rev Neurosci,* 23, 155-84.

LEE, K. B., PALS-RYLAARSDAM, R., BENOVIC, J. L. & HOSEY, M. M. 1998. Arrestin-independent internalization of the m1, m3, and m4 subtypes of muscarinic cholinergic receptors. *J Biol Chem,* 273, 12967-72.

LEE, S., LIU, W., BROSNAN, C. & BERMAN, J. 1993. Cytokine production by human fetal microglia and astrocytes. Differential induction by lipopolysaccharide and IL-1 beta. *Journal of immunology (Baltimore, Md. : 1950),* 150**,** 2659-67.

LEHNER, K. R., SILVERMAN, H. A., ADDORISIO, M. E., ROY, A., AL-ONAIZI, M. A., LEVINE, Y., OLOFSSON, P. S., CHAVAN, S. S., GROS, R., NATHANSON, N. M., AL-ABED, Y., METZ, C. N., PRADO, V. F., PRADO, M. A. M., TRACEY, K. J. & PAVLOV, V. A. 2019. Forebrain Cholinergic Signaling Regulates Innate Immune Responses and Inflammation. *Frontiers in Immunology,* 10**,** 585.

LESTER, D. B., ROGERS, T. D. & BLAHA, C. D. 2010. Acetylcholine-dopamine interactions in the pathophysiology and treatment of CNS disorders. *CNS Neurosci Ther,* 16**,** 137-62.

LEVEY, A. I. 1993. Immunological localization of m1-m5 muscarinic acetylcholine receptors in peripheral tissues and brain. *Life Sci,* 52**,** 441-8.

LEVEY, A. I. 1996. Muscarinic acetylcholine receptor expression in memory circuits: Implications for treatment of Alzheimer disease. *Proceedings of the National Academy of Sciences,* 93**,** 13541.

LEVEY, A. I., KITT, C. A., SIMONDS, W. F., PRICE, D. L. & BRANN, M. R. 1991. Identification and localization of muscarinic acetylcholine receptor proteins in brain with subtype-specific antibodies. *J Neurosci,* 11**,** 3218-26.

LI, J., XIANG, B., SU, W., ZHANG, X., HUANG, Y. & MA, L. 2003. Agonist-induced formation of opioid receptor-G protein-coupled receptor kinase (GRK)-G beta gamma complex on membrane is required for GRK2 function in vivo. *J Biol Chem,* 278**,** 30219-26.

LI, L., HOMAN, K. T., VISHNIVETSKIY, S. A., MANGLIK, A., TESMER, J. J. G., GUREVICH, V. V. & GUREVICH, E. V. 2015. G Protein-coupled Receptor Kinases of the GRK4 Protein Subfamily Phosphorylate Inactive G Protein-coupled Receptors (GPCRs). *The Journal of biological chemistry,* 290**,** 10775-10790.

LI, Y., CHEN, N., WU, C., LU, Y., GAO, G., DUAN, C., YANG, H. & LU, L. 2020. Galectin-1 attenuates neurodegeneration in Parkinson's disease model by modulating microglial MAPK/IκB/NFκB axis through its carbohydrate-recognition domain. *Brain, Behavior, and Immunity,* 83**,** 214-225.

LIANG, Y.-L., KHOSHOUEI, M., RADJAINIA, M., ZHANG, Y., GLUKHOVA, A., TARRASCH, J., THAL, D. M., FURNESS, S. G. B., CHRISTOPOULOS, G., COUDRAT, T., DANEV, R., BAUMEISTER, W., MILLER, L. J., CHRISTOPOULOS, A., KOBILKA, B. K., WOOTTEN, D., SKINIOTIS, G. & SEXTON, P. M. 2017. Phase-plate cryo-EM structure of a class B GPCR–G-protein complex. *Nature,* 546**,** 118-123.

LIAUW, J., HOANG, S., CHOI, M., EROGLU, C., CHOI, M., SUN, G.-H., PERCY, M., WILDMAN-TOBRINER, B., BLISS, T., GUZMAN, R. G., BARRES, B. A. & STEINBERG, G. K. 2008. Thrombospondins 1 and 2 are necessary for synaptic plasticity and functional recovery after stroke. *Journal of cerebral blood flow and metabolism : official journal of the International Society of Cerebral Blood Flow and Metabolism,* 28**,** 1722-1732.

LIDDELOW, S. A. & BARRES, B. A. 2017. Reactive Astrocytes: Production, Function, and Therapeutic Potential. *Immunity,* 46**,** 957-967.

LIDDELOW, S. A., GUTTENPLAN, K. A., CLARKE, L. E., BENNETT, F. C., BOHLEN, C. J., SCHIRMER, L., BENNETT, M. L., MÜNCH, A. E., CHUNG, W.-S., PETERSON, T. C., WILTON, D. K., FROUIN, A., NAPIER, B. A., PANICKER, N., KUMAR, M., BUCKWALTER, M. S., ROWITCH, D. H., DAWSON, V. L., DAWSON, T. M., STEVENS, B. & BARRES, B. A. 2017. Neurotoxic reactive astrocytes are induced by activated microglia. *Nature,* 541**,** 481-487.

LIEBERMAN-BLUM, S. S., FUNG, H. B. & BANDRES, J. C. 2008. Maraviroc: A CCR5-receptor antagonist for the treatment of HIV-1 infection. *Clinical Therapeutics,* 30**,** 1228-1250.

LIN, M. T. & BEAL, M. F. 2006. Mitochondrial dysfunction and oxidative stress in neurodegenerative diseases. *Nature,* 443**,** 787-795.

LIU, J. J., HORST, R., KATRITCH, V., STEVENS, R. C. & WÜTHRICH, K. 2012. Biased signaling pathways in β2-adrenergic receptor characterized by 19F-NMR. *Science,* 335**,** 1106-10.

LIU, Z., LI, T., LI, P., WEI, N., ZHAO, Z., LIANG, H., JI, X., CHEN, W., XUE, M. & WEI, J. 2015. The Ambiguous Relationship of Oxidative Stress, Tau Hyperphosphorylation, and Autophagy Dysfunction in Alzheimer's Disease. *Oxid Med Cell Longev,* 2015.

LODOWSKI, D. T., PITCHER, J. A., CAPEL, W. D., LEFKOWITZ, R. J. & TESMER, J. J. 2003. Keeping G proteins at bay: a complex between G protein-coupled receptor kinase 2 and Gbetagamma. *Science,* 300**,** 1256-62.

LOHSE, M. J. 1993. Molecular mechanisms of membrane receptor desensitization. *Biochim Biophys Acta,* 1179**,** 171-88.

LOHSE, M. J., ANDEXINGER, S., PITCHER, J., TRUKAWINSKI, S., CODINA, J., FAURE, J. P., CARON, M. G. & LEFKOWITZ, R. J. 1992. Receptor-specific desensitization with purified proteins. Kinase dependence and receptor specificity of beta-arrestin and arrestin in the beta 2-adrenergic receptor and rhodopsin systems. *J Biol Chem,* 267**,** 8558-64.

LOHSE, M. J., BENOVIC, J. L., CODINA, J., CARON, M. G. & LEFKOWITZ, R. J. 1990. beta-Arrestin: a protein that regulates beta-adrenergic receptor function. *Science,* 248**,** 1547-50.

LUKIW, W. J., DUA, P., POGUE, A. I., EICKEN, C. & HILL, J. M. 2011. Upregulation of Micro RNA-146a (miRNA-146a), A Marker for Inflammatory Neurodegeneration, in Sporadic Creutzfeldt–Jakob Disease (sCJD) and Gerstmann–Straussler–Scheinker (GSS) Syndrome. *Journal of Toxicology and Environmental Health, Part A,* 74**,** 1460-1468.

LUTTRELL, L. M. 2008. Reviews in molecular biology and biotechnology: transmembrane signaling by G protein-coupled receptors. *Mol Biotechnol,* 39**,** 239-64.

LUTTRELL, L. M. 2014. Minireview: More than just a hammer: ligand "bias" and pharmaceutical discovery. *Mol Endocrinol,* 28**,** 281-94.

LUTTRELL, L. M., FERGUSON, S. S., DAAKA, Y., MILLER, W. E., MAUDSLEY, S., DELLA ROCCA, G. J., LIN, F., KAWAKATSU, H., OWADA, K., LUTTRELL, D. K., CARON, M. G. & LEFKOWITZ, R. J. 1999. Beta-arrestin-dependent formation of beta2 adrenergic receptor-Src protein kinase complexes. *Science,* 283**,** 655-61.

LUTTRELL, L. M. & KENAKIN, T. P. 2011. Refining efficacy: allosterism and bias in G protein-coupled receptor signaling. *Methods Mol Biol,* 756**,** 3-35.

LUTTRELL, L. M. & LEFKOWITZ, R. J. 2002. The role of beta-arrestins in the termination and transduction of G-protein-coupled receptor signals. *J Cell Sci,* 115**,** 455-65.

LUTTRELL, L. M., MAUDSLEY, S. & GESTY-PALMER, D. 2018. Translating in vitro ligand bias into in vivo efficacy. *Cell Signal,* 41**,** 46-55.

LYSEK, D. A., SCHORN, C., NIVON, L. G., ESTEVE-MOYA, V., CHRISTEN, B., CALZOLAI, L., VON SCHROETTER, C., FIORITO, F., HERRMANN, T., GUNTERT, P. & WUTHRICH, K. 2005. Prion protein NMR structures of cats, dogs, pigs, and sheep. *Proc Natl Acad Sci U S A,* 102**,** 640-5.

MA, L., SEAGER, M. A., WITTMANN, M., JACOBSON, M., BICKEL, D., BURNO, M., JONES, K., GRAUFELDS, V. K., XU, G., PEARSON, M., MCCAMPBELL, A., GASPAR, R., SHUGHRUE, P., DANZIGER, A., REGAN, C., FLICK, R., PASCARELLA, D., GARSON, S., DORAN, S., KREATSOULAS, C., VENG, L., LINDSLEY, C. W., SHIPE, W., KUDUK, S., SUR, C., KINNEY, G., SEABROOK, G. R. & RAY, W. J. 2009. Selective activation of the M1 muscarinic acetylcholine receptor achieved by allosteric potentiation. *Proceedings of the National Academy of Sciences,* 106**,** 15950.

MAEDA, S., QU, Q., ROBERTSON, M. J., SKINIOTIS, G. & KOBILKA, B. K. 2019. Structures of the M1 and M2 muscarinic acetylcholine receptor/G-protein complexes. *Science,* 364**,** 552.

MAHLEY, R. W. & RALL, S. C., JR. 2000. Apolipoprotein E: far more than a lipid transport protein. *Annu Rev Genomics Hum Genet,* 1**,** 507-37.

MAKARAVA, N., CHANG, J. C., KUSHWAHA, R. & BASKAKOV, I. V. 2019. Region-Specific Response of Astrocytes to Prion Infection. *Front Neurosci,* 13**,** 1048.

MALLUCCI, G., DICKINSON, A., LINEHAN, J., KLÖHN, P.-C., BRANDNER, S. & COLLINGE, J. 2003. Depleting Neuronal PrP in Prion Infection Prevents Disease and Reverses Spongiosis. *Science,* 302**,** 871.

MALLUCCI, G., RATTÉ, S., ASANTE, E., LINEHAN, J., GOWLAND, I., JEFFERYS, J. & COLLINGE, J. 2002. Post-natal knockout of prion protein alters hippocampal CA1 properties, but does not result in neurodegeneration. *The EMBO journal,* 21**,** 202-10.

MALLUCCI, G. R. 2009. Prion neurodegeneration: starts and stops at the synapse. *Prion,* 3**,** 195-201.

MALLUCCI, G. R., WHITE, M. D., FARMER, M., DICKINSON, A., KHATUN, H., POWELL, A. D., BRANDNER, S., JEFFERYS, J. G. & COLLINGE, J. 2007. Targeting cellular prion protein reverses early cognitive deficits and neurophysiological dysfunction in prion-infected mice. *Neuron,* 53**,** 325-35.

MALVIYA, M., KUMAR, Y. C., ASHA, D., CHANDRA, J. N., SUBHASH, M. N. & RANGAPPA, K. S. 2008. Muscarinic receptor 1 agonist activity of novel N-arylthioureas substituted 3-morpholino arecoline derivatives in Alzheimer's presenile dementia models. *Bioorg Med Chem,* 16**,** 7095-101.

MANDERS, E. M. M., VERBEEK, F. J. & ATEN, J. A. 1993. Measurement of co-localization of objects in dual-colour confocal images. *Journal of Microscopy,* 169**,** 375-382.

MANGLIK, A., KRUSE, A. C., KOBILKA, T. S., THIAN, F. S., MATHIESEN, J. M., SUNAHARA, R. K., PARDO, L., WEIS, W. I., KOBILKA, B. K. & GRANIER, S. 2012. Crystal structure of the μ-opioid receptor bound to a morphinan antagonist. *Nature,* 485**,** 321-326.

MANN, D., TEUBER, C., TENNIGKEIT, S. A., SCHRÖTER, G., GERWERT, K. & KÖTTING, C. 2016. Mechanism of the intrinsic arginine finger in heterotrimeric G proteins. *Proc Natl Acad Sci U S A,* 113**,** E8041-e8050.

MANSON, J., WEST, J. D., THOMSON, V., MCBRIDE, P., KAUFMAN, M. H. & HOPE, J. 1992. The prion protein gene: a role in mouse embryogenesis? *Development,* 115**,** 117.

MANSON, J. C., CLARKE, A. R., HOOPER, M. L., AITCHISON, L., MCCONNELL, I. & HOPE, J. 1994. 129/Ola mice carrying a null mutation in PrP that abolishes mRNA production are developmentally normal. *Mol Neurobiol,* 8**,** 121-7.

MARCHESE, A. & TREJO, J. 2013. Ubiquitin-dependent regulation of G protein-coupled receptor trafficking and signaling. *Cell Signal,* 25**,** 707-16.

MARION, S., OAKLEY, R. H., KIM, K. M., CARON, M. G. & BARAK, L. S. 2006. A beta-arrestin binding determinant common to the second intracellular loops of rhodopsin family G protein-coupled receptors. *J Biol Chem,* 281**,** 2932-8.

MARLO, J. E., NISWENDER, C. M., DAYS, E. L., BRIDGES, T. M., XIANG, Y., RODRIGUEZ, A. L., SHIREY, J. K., BRADY, A. E., NALYWAJKO, T., LUO, Q., AUSTIN, C. A., WILLIAMS, M. B., KIM, K., WILLIAMS, R., ORTON, D., BROWN, H. A., LINDSLEY, C. W., WEAVER, C. D. & CONN, P. J. 2009. Discovery and characterization of novel allosteric potentiators of M1 muscarinic receptors reveals multiple modes of activity. *Molecular pharmacology,* 75**,** 577-588.

MARTINEZ, F. O. & GORDON, S. 2014. The M1 and M2 paradigm of macrophage activation: time for reassessment. *F1000Prime Rep,* 6**,** 13.

MASH, D. C., FLYNN, D. D. & POTTER, L. T. 1985. Loss of M2 muscarine receptors in the cerebral cortex in Alzheimer's disease and experimental cholinergic denervation. *Science,* 228**,** 1115-7.

MATHEWS, J., GLASSE, R. & LINDENBAUM, S. 1968. KURU AND CANNIBALISM. *The Lancet,* 292**,** 449-452.

MATSUI, M., MOTOMURA, D., KARASAWA, H., FUJIKAWA, T., JIANG, J., KOMIYA, Y., TAKAHASHI, S. & TAKETO, M. M. 2000. Multiple functional defects in peripheral autonomic organs in mice lacking muscarinic acetylcholine receptor gene for the M3 subtype. *Proc Natl Acad Sci U S A,* 97**,** 9579-84.

MAY, P. C., LAMPERT-ETCHELLS, M., JOHNSON, S. A., POIRIER, J., MASTERS, J. N. & FINCH, C. E. 1990. Dynamics of gene expression for a hippocampal glycoprotein elevated in Alzheimer's disease and in response to experimental lesions in rat. *Neuron,* 5**,** 831-839.

MCDONALD, P. H., CHOW, C. W., MILLER, W. E., LAPORTE, S. A., FIELD, M. E., LIN, F. T., DAVIS, R. J. & LEFKOWITZ, R. J. 2000. Beta-arrestin 2: a receptor-regulated MAPK scaffold for the activation of JNK3. *Science,* 290**,** 1574-7.

MEAD, S., STUMPF, M. P., WHITFIELD, J., BECK, J. A., POULTER, M., CAMPBELL, T., UPHILL, J. B., GOLDSTEIN, D., ALPERS, M., FISHER, E. M. & COLLINGE, J. 2003. Balancing selection at the prion protein gene consistent with prehistoric kurulike epidemics. *Science,* 300**,** 640-3.

MEDEIROS, R., KITAZAWA, M., CACCAMO, A., BAGLIETTO-VARGAS, D., ESTRADA-HERNANDEZ, T., CRIBBS, D. H., FISHER, A. & LAFERLA, F. M. 2011. Loss of muscarinic M1 receptor exacerbates Alzheimer's disease-like pathology and cognitive decline. *Am J Pathol,* 179**,** 980-91.

MEDEIROS, R. & LAFERLA, F. M. 2013. Astrocytes: conductors of the Alzheimer disease neuroinflammatory symphony. *Exp Neurol,* 239**,** 133-8.

MEDORI, R., MONTAGNA, P., TRITSCHLER, H. J., LEBLANC, A., CORTELLI, P., TINUPER, P., LUGARESI, E. & GAMBETTI, P. 1992. Fatal familial insomnia: a second kindred with mutation of prion protein gene at codon 178. *Neurology,* 42**,** 669-70.

MELANCON, B. J., TARR, J. C., PANARESE, J. D., WOOD, M. R. & LINDSLEY, C. W. 2013. Allosteric modulation of the M1 muscarinic acetylcholine receptor: improving cognition and a potential treatment for schizophrenia and Alzheimer's disease. *Drug Discov Today,* 18**,** 1185-99.

MEYER-LUEHMANN, M., COOMARASWAMY, J., BOLMONT, T., KAESER, S., SCHAEFER, C., KILGER, E., NEUENSCHWANDER, A., ABRAMOWSKI, D., FREY, P., JATON, A. L., VIGOURET, J. M., PAGANETTI, P., WALSH, D. M., MATHEWS, P. M., GHISO, J., STAUFENBIEL, M., WALKER, L. C. & JUCKER, M. 2006. Exogenous induction of cerebral beta-amyloidogenesis is governed by agent and host. *Science,* 313**,** 1781-4.

MICHAUD, M., BALARDY, L., MOULIS, G., GAUDIN, C., PEYROT, C., VELLAS, B., CESARI, M. & NOURHASHEMI, F. 2013. Proinflammatory cytokines, aging, and age-related diseases. *J Am Med Dir Assoc,* 14**,** 877-82.

MIDDELDORP, J. & HOL, E. M. 2011. GFAP in health and disease. *Progress in Neurobiology,* 93**,** 421-443.

MIELE, G., SEEGER, H., MARINO, D., EBERHARD, R., HEIKENWALDER, M., STOECK, K., BASAGNI, M., KNIGHT, R., GREEN, A., CHIANINI, F., WÜTHRICH, R. P., HOCK, C., ZERR, I. & AGUZZI, A. 2008. Urinary alpha1-antichymotrypsin: a biomarker of prion infection. *PLoS One,* 3**,** e3870.

MILLIGAN, G. 2018. G protein-coupled receptors not currently in the spotlight: free fatty acid receptor 2 and GPR35. *Br J Pharmacol,* 175**,** 2543-2553.

MILLIGAN, G., SHIMPUKADE, B., ULVEN, T. & HUDSON, B. D. 2017. Complex Pharmacology of Free Fatty Acid Receptors. *Chem Rev,* 117**,** 67-110.

MINETTI GIULIA, C., FEIGE JEROME, N., BOMBARD, F., HEIER, A., MORVAN, F., NÜRNBERG, B., LEISS, V., BIRNBAUMER, L., GLASS DAVID, J. & FORNARO, M. 2014. Gαi2 Signaling Is Required for Skeletal Muscle Growth, Regeneration, and Satellite Cell Proliferation and Differentiation. *Molecular and Cellular Biology,* 34**,** 619-630.

MÖLLER, D., BANERJEE, A., UZUNESER, T. C., SKULTETY, M., HUTH, T., PLOUFFE, B., HÜBNER, H., ALZHEIMER, C., FRIEDLAND, K., MÜLLER, C. P., BOUVIER, M. & GMEINER, P. 2017. Discovery of G Protein-Biased Dopaminergics with a Pyrazolo[1,5-a]pyridine Substructure. *J Med Chem,* 60**,** 2908-2929.

MOMBAERTS, P. 2004. Genes and ligands for odorant, vomeronasal and taste receptors. *Nat Rev Neurosci,* 5**,** 263-78.

MONASKY, M. M., TAGLIERI, D. M., HENZE, M., WARREN, C. M., UTTER, M. S., SOERGEL, D. G., VIOLIN, J. D. & SOLARO, R. J. 2013. The ß-arrestin-biased ligand TRV120023 inhibits angiotensin II-induced cardiac hypertrophy while preserving enhanced myofilament response to calcium. *Am J Physiol Heart Circ Physiol,* 305**,** H856-66.

MORAN, P. M. 1993. Differential effects of scopolamine and mecamylamine on working and reference memory in the rat. *Pharmacology Biochemistry and Behavior,* 45**,** 533-538.

MORAN, S. P., CHO, H. P., MAKSYMETZ, J., REMKE, D. H., HANSON, R. M., NISWENDER, C. M., LINDSLEY, C. W., ROOK, J. M. & CONN, P. J. 2018a. PF-06827443 Displays Robust Allosteric Agonist and Positive Allosteric Modulator Activity in High Receptor Reserve and Native Systems. *ACS Chem Neurosci,* 9**,** 2218-2224.

MORAN, S. P., DICKERSON, J. W., CHO, H. P., XIANG, Z., MAKSYMETZ, J., REMKE, D. H., LV, X., DOYLE, C. A., RAJAN, D. H., NISWENDER, C. M., ENGERS, D. W., LINDSLEY, C. W., ROOK, J. M. & CONN, P. J. 2018b. M1-positive allosteric modulators lacking agonist activity provide the optimal profile for enhancing cognition. *Neuropsychopharmacology,* 43**,** 1763-1771.

MORENO, J. A., RADFORD, H., PERETTI, D., STEINERT, J. R., VERITY, N., MARTIN, M. G., HALLIDAY, M., MORGAN, J., DINSDALE, D., ORTORI, C. A., BARRETT, D. A., TSAYTLER, P., BERTOLOTTI, A., WILLIS, A. E., BUSHELL, M. & MALLUCCI, G. R. 2012. Sustained translational repression by eIF2alpha-P mediates prion neurodegeneration. *Nature,* 485**,** 507-11.

MOSS, D. W. & BATES, T. E. 2001. Activation of murine microglial cell lines by lipopolysaccharide and interferon-gamma causes NO-mediated decreases in mitochondrial and cellular function. *Eur J Neurosci,* 13**,** 529-38.

MOU, L., GATES, A., MOSSER, V. A., TOBIN, A. & JACKSON, D. A. 2006. Transient hypoxia induces sequestration of M1 and M2 muscarinic acetylcholine receptors. *J Neurochem,* 96**,** 510-9.

MUCKE, L., YU, G. Q., MCCONLOGUE, L., ROCKENSTEIN, E. M., ABRAHAM, C. R. & MASLIAH, E. 2000. Astroglial expression of human alpha(1)-antichymotrypsin enhances alzheimer-like pathology in amyloid protein precursor transgenic mice. *Am J Pathol,* 157**,** 2003-10.

MULLARD, A. 2021. Controversial Alzheimer's drug approval could impact other diseases. *Nature*.

MULLERSHAUSEN, F., ZECRI, F., CETIN, C., BILLICH, A., GUERINI, D. & SEUWEN, K. 2009. Persistent signaling induced by FTY720-phosphate is mediated by internalized S1P1 receptors. *Nat Chem Biol,* 5**,** 428-34.

MULUGETA, E., KARLSSON, E., ISLAM, A., KALARIA, R., MANGAT, H., WINBLAD, B. & ADEM, A. 2003. Loss of muscarinic M4 receptors in hippocampus of Alzheimer patients. *Brain Research,* 960**,** 259-262.

MURRELL, J., FARLOW, M., GHETTI, B. & BENSON MERRILL, D. 1991. A mutation in the Amyloid Precursor Protein Associated with Hereditary Alzheimer's Disease. *Science,* 254**,** 97-99.

NACHMANSOHN, D. & MACHADO, A. L. 1943. THE FORMATION OF ACETYLCHOLINE. A NEW ENZYME: "CHOLINE ACETYLASE". *Journal of Neurophysiology,* 6**,** 397-403.

NASLAVSKY, N., STEIN, R., YANAI, A., FRIEDLANDER, G. & TARABOULOS, A. 1997. Characterization of Detergent-insoluble Complexes Containing the Cellular Prion Protein and Its Scrapie Isoform. *Journal of Biological Chemistry,* 272**,** 6324-6331.

NÄSLUND, J., HAROUTUNIAN, V., MOHS, R., DAVIS, K. L., DAVIES, P., GREENGARD, P. & BUXBAUM, J. D. 2000. Correlation Between Elevated Levels of Amyloid ß-Peptide in the Brain and Cognitive Decline. *JAMA,* 283**,** 1571-1577.

NATHAN, P. J., WATSON, J., LUND, J., DAVIES, C. H., PETERS, G., DODDS, C. M., SWIRSKI, B., LAWRENCE, P., BENTLEY, G. D., O'NEILL, B. V., ROBERTSON, J., WATSON, S., JONES, G. A., MARUFF, P., CROFT, R. J., LARUELLE, M. & BULLMORE, E. T. 2013. The potent M1 receptor allosteric agonist GSK1034702 improves episodic memory in humans in the nicotine abstinence model of cognitive dysfunction. *International Journal of Neuropsychopharmacology,* 16**,** 721-731.

NATHANSON, N., WILESMITH, J. & GRIOT, C. 1997. Bovine Spongiform Encephalopathy (BSE): Causes and Consequences of a Common Source Epidemic. *American Journal of Epidemiology,* 145**,** 959-969.

NATHANSON, N. M. 1987. Molecular Properties of the Muscarinic Acetylcholine Receptor. *Annual Review of Neuroscience,* 10**,** 195-236.

NATHANSON, N. M. 2000. A multiplicity of muscarinic mechanisms: Enough signaling pathways to take your breath away. *Proceedings of the National Academy of Sciences,* 97**,** 6245-6247.

NEER, E. J. 1995. Heterotrimeric G proteins: organizers of transmembrane signals. *Cell,* 80**,** 249-57.

NEER, E. J. & CLAPHAM, D. E. 1988. Roles of G protein subunits in transmembrane signalling. *Nature,* 333**,** 129-134.

NELSON, C. D., PERRY, S. J., REGIER, D. S., PRESCOTT, S. M., TOPHAM, M. K. & LEFKOWITZ, R. J. 2007. Targeting of diacylglycerol degradation to M1 muscarinic receptors by beta-arrestins. *Science,* 315**,** 663-6.

NEUGROSCHL, J. & WANG, S. 2011. Alzheimer's Disease: Diagnosis and Treatment Across the Spectrum of Disease Severity. *The Mount Sinai Journal of Medicine, New York,* 78**,** 596-612.

NEVES, S. R., RAM, P. T. & IYENGAR, R. 2002. G Protein Pathways. *Science,* 296**,** 1636.

NEWMAN-TANCREDI, A., AUDINOT, V., MOREIRA, C., VERRIÈLE, L. & MILLAN, M. J. 2000. Inverse agonism and constitutive activity as functional correlates of serotonin h5-HT(1B) receptor/G-protein stoichiometry. *Mol Pharmacol,* 58**,** 1042-9.

NEWMAN-TANCREDI, A., CONTE, C., CHAPUT, C., VERRIÈLE, L. & MILLAN, M. J. 1997. Agonist and inverse agonist efficacy at human recombinant serotonin 5-HT1A receptors as a function of receptor:G-protein stoichiometry. *Neuropharmacology,* 36**,** 451-9.

NILSELID, A. M., DAVIDSSON, P., NÄGGA, K., ANDREASEN, N., FREDMAN, P. & BLENNOW, K. 2006. Clusterin in cerebrospinal fluid: Analysis of carbohydrates and quantification of native and glycosylated forms. *Neurochemistry International,* 48**,** 718-728.

NILSSON, L. N., BALES, K. R., DICARLO, G., GORDON, M. N., MORGAN, D., PAUL, S. M. & POTTER, H. 2001. Alpha-1-antichymotrypsin promotes beta-sheet amyloid plaque deposition in a transgenic mouse model of Alzheimer's disease. *J Neurosci,* 21**,** 1444-51.

NITSCH, R. M., DENG, M., TENNIS, M., SCHOENFELD, D. & GROWDON, J. H. 2000. The selective muscarinic M1 agonist AF102B decreases levels of total Abeta in cerebrospinal fluid of patients with Alzheimer's disease. *Ann Neurol,* 48**,** 913-8.

NITSCH, R. M., SLACK, B. E., WURTMAN, R. J. & GROWDON, J. H. 1992. Release of Alzheimer amyloid precursor derivatives stimulated by activation of muscarinic acetylcholine receptors. *Science,* 258**,** 304-7.

NOBLES, K. N., XIAO, K., AHN, S., SHUKLA, A. K., LAM, C. M., RAJAGOPAL, S., STRACHAN, R. T., HUANG, T. Y., BRESSLER, E. A., HARA, M. R., SHENOY, S. K., GYGI, S. P. & LEFKOWITZ, R. J. 2011. Distinct phosphorylation sites on the ß(2)-adrenergic receptor establish a barcode that encodes differential functions of ß-arrestin. *Sci Signal,* 4**,** ra51.

NORMAN, C. L., GOULD, R. W., BRAGG, C., LINDSLEY, C. W., JONES, C. K. & NADER, M. A. 2020. The Effects of the M1 Muscarinic Acetylcholine Receptor Positive Allosteric Modulator VU0486846 on Cognitive Performance in Aged Nonhuman Primates. *The FASEB Journal,* 34**,** 1-1.

NORMAN, J. L. & ANDERSON, S. L. 2016. Novel class of medications, orexin receptor antagonists, in the treatment of insomnia - critical appraisal of suvorexant. *Nat Sci Sleep,* 8**,** 239-47.

NYGAARD, R., ZOU, Y., DROR, R. O., MILDORF, T. J., ARLOW, D. H., MANGLIK, A., PAN, A. C., LIU, C. W., FUNG, J. J., BOKOCH, M. P., THIAN, F. S., KOBILKA, T. S., SHAW, D. E., MUELLER, L., PROSSER, R. S. & KOBILKA, B. K. 2013. The dynamic process of ß(2)-adrenergic receptor activation. *Cell,* 152**,** 532-542.

O'HAYRE, M., EICHEL, K., AVINO, S., ZHAO, X., STEFFEN, D. J., FENG, X., KAWAKAMI, K., AOKI, J., MESSER, K., SUNAHARA, R., INOUE, A., VON ZASTROW, M. & GUTKIND, J. S. 2017. Genetic evidence that ß-arrestins are dispensable for the initiation of ß(2)-adrenergic receptor signaling to ERK. *Sci Signal,* 10.

OAKLEY, R. H., LAPORTE, S. A., HOLT, J. A., BARAK, L. S. & CARON, M. G. 1999. Association of beta-arrestin with G protein-coupled receptors during clathrin-mediated endocytosis dictates the profile of receptor resensitization. *J Biol Chem,* 274**,** 32248-57.

OAKLEY, R. H., LAPORTE, S. A., HOLT, J. A., CARON, M. G. & BARAK, L. S. 2000. Differential Affinities of Visual Arrestin, ßArrestin1, and ßArrestin2 for G Protein-coupled Receptors Delineate Two Major Classes of Receptors*. *Journal of Biological Chemistry,* 275**,** 17201-17210.

OBLAK, A. L., FORNER, S., TERRITO, P. R., SASNER, M., CARTER, G. W., HOWELL, G. R., SUKOFF-RIZZO, S. J., LOGSDON, B. A., MANGRAVITE, L. M., MORTAZAVI, A., BAGLIETTO-VARGAS, D., GREEN, K. N., MACGREGOR, G. R., WOOD, M. A., TENNER, A. J., LAFERLA, F. M. & LAMB, B. T. 2020. Model organism development and evaluation for late-onset Alzheimer's disease: MODEL-AD. *Alzheimers Dement (N Y),* 6**,** e12110.

ODDO, S., CACCAMO, A., KITAZAWA, M., TSENG, B. P. & LAFERLA, F. M. 2003a. Amyloid deposition precedes tangle formation in a triple transgenic model of Alzheimer's disease. *Neurobiol Aging,* 24**,** 1063-70.

ODDO, S., CACCAMO, A., SHEPHERD, J. D., MURPHY, M. P., GOLDE, T. E., KAYED, R., METHERATE, R., MATTSON, M. P., AKBARI, Y. & LAFERLA, F. M. 2003b. Triple-transgenic model of Alzheimer's disease with plaques and tangles: intracellular Abeta and synaptic dysfunction. *Neuron,* 39**,** 409-21.

OESCH, B., WESTAWAY, D., WÄLCHLI, M., MCKINLEY, M. P., KENT, S. B. H., AEBERSOLD, R., BARRY, R. A., TEMPST, P., TEPLOW, D. B., HOOD, L. E., PRUSINER, S. B. & WEISSMANN, C. 1985. A cellular gene encodes scrapie PrP 27-30 protein. *Cell,* 40**,** 735-746.

OIKAWA, N., KIMURA, N. & YANAGISAWA, K. 2010. Alzheimer-type tau pathology in advanced aged nonhuman primate brains harboring substantial amyloid deposition. *Brain Res,* 1315**,** 137-49.

OKAE, H. & IWAKURA, Y. 2010. Neural tube defects and impaired neural progenitor cell proliferation in Gß1-deficient mice. *Developmental Dynamics,* 239**,** 1089-1101.

OLDHAM, W. M. & HAMM, H. E. 2008. Heterotrimeric G protein activation by G-protein-coupled receptors. *Nature Reviews Molecular Cell Biology,* 9**,** 60-71.

OLMOS, G. & LLADÓ, J. 2014. Tumor necrosis factor alpha: a link between neuroinflammation and excitotoxicity. *Mediators Inflamm,* 2014**,** 861231.

OVERK, C. R., FELDER, C. C., TU, Y., SCHOBER, D. A., BALES, K. R., WUU, J. & MUFSON, E. J. 2010. Cortical M1 receptor concentration increases without a concomitant change in function in Alzheimer's disease. *J Chem Neuroanat,* 40**,** 63-70.

OWEN, F., LOFTHOUSE, R., CROW, T. J., BAKER, H. F., POULTER, M., COLLINGE, J., RISBY, D., RIDLEY, R. M., HSIAO, K. & PRUSINER, S. B. 1989. INSERTION IN PRION PROTEIN GENE IN FAMILIAL CREUTZFELDT-IAKOB DISEASE. *The Lancet,* 333**,** 51-52.

PALCZEWSKI, K., BUCZYŁKO, J., KAPLAN, M. W., POLANS, A. S. & CRABB, J. W. 1991. Mechanism of rhodopsin kinase activation. *J Biol Chem,* 266**,** 12949-55.

PAN, K. M., BALDWIN, M., NGUYEN, J., GASSET, M., SERBAN, A., GROTH, D., MEHLHORN, I., HUANG, Z., FLETTERICK, R. J., COHEN, F. E. & ET AL. 1993. Conversion of alpha-helices into beta-sheets features in the formation of the scrapie prion proteins. *Proc Natl Acad Sci U S A,* 90**,** 10962-6.

PANDEY, R. S., KOTREDES, K. P., PREUSS, C., OBLAK, A. L., LAMB, B. T., HOWELL, G., SASNER, M., CARTER, G. W. & CENTER, M.-A. 2020. Transcriptomic profiling of APOE4/Trem2*R47H mouse models for late-onset Alzheimer's disease. *Alzheimer's & Dementia,* 16**,** e045390.

PARCHI, P., GIESE, A., CAPELLARI, S., BROWN, P., SCHULZ-SCHAEFFER, W., WINDL, O., ZERR, I., BUDKA, H., KOPP, N., PICCARDO, P., POSER, S., ROJIANI, A., STREICHEMBERGER, N., JULIEN, J., VITAL, C., GHETTI, B., GAMBETTI, P. & KRETZSCHMAR, H. 1999. Classification of sporadic Creutzfeldt-Jakob disease based on molecular and phenotypic analysis of 300 subjects. *Ann Neurol,* 46**,** 224-33.

PARK, J. Y., LEE, S. Y., KIM, H. R., SEO, M. D. & CHUNG, K. Y. 2016. Structural mechanism of GPCR-arrestin interaction: recent breakthroughs. *Arch Pharm Res,* 39**,** 293-301.

PAVLOV, V. A., OCHANI, M., GALLOWITSCH-PUERTA, M., OCHANI, K., HUSTON, J. M., CZURA, C. J., AL-ABED, Y. & TRACEY, K. J. 2006. Central muscarinic cholinergic regulation of the systemic inflammatory response during

endotoxemia. *Proceedings of the National Academy of Sciences of the United States of America,* 103, 5219.

PEI, J. J., BRAAK, E., BRAAK, H., GRUNDKE-IQBAL, I., IQBAL, K., WINBLAD, B. & COWBURN, R. F. 2001. Localization of active forms of C-jun kinase (JNK) and p38 kinase in Alzheimer's disease brains at different stages of neurofibrillary degeneration. *J Alzheimers Dis,* 3, 41-48.

PEI, J. J., BRAAK, H., AN, W. L., WINBLAD, B., COWBURN, R. F., IQBAL, K. & GRUNDKE-IQBAL, I. 2002. Up-regulation of mitogen-activated protein kinases ERK1/2 and MEK1/2 is associated with the progression of neurofibrillary degeneration in Alzheimer's disease. *Brain Res Mol Brain Res,* 109, 45-55.

PERRY, E. K., PERRY, R. H., BLESSED, G. & TOMLINSON, B. E. 1977. Necropsy evidence of central cholinergic deficits in senile dementia. *Lancet,* 1, 189.

PERRY, G., RODER, H., NUNOMURA, A., TAKEDA, A., FRIEDLICH, A. L., ZHU, X., RAINA, A. K., HOLBROOK, N., SIEDLAK, S. L., HARRIS, P. L. & SMITH, M. A. 1999. Activation of neuronal extracellular receptor kinase (ERK) in Alzheimer disease links oxidative stress to abnormal phosphorylation. *Neuroreport,* 10, 2411-5.

PERRY, S. J., BAILLIE, G. S., KOHOUT, T. A., MCPHEE, I., MAGIERA, M. M., ANG, K. L., MILLER, W. E., MCLEAN, A. J., CONTI, M., HOUSLAY, M. D. & LEFKOWITZ, R. J. 2002. Targeting of cyclic AMP degradation to beta 2-adrenergic receptors by beta-arrestins. *Science,* 298, 834-6.

PITCHER, J. A., INGLESE, J., HIGGINS, J. B., ARRIZA, J. L., CASEY, P. J., KIM, C., BENOVIC, J. L., KWATRA, M. M., CARON, M. G. & LEFKOWITZ, R. J. 1992. Role of beta gamma subunits of G proteins in targeting the beta-adrenergic receptor kinase to membrane-bound receptors. *Science,* 257, 1264.

POLLOK-KOPP, B., HÜTTENRAUCH, F., RETHORN, S. & OPPERMANN, M. 2007. Dynamics of protein kinase C-mediated phosphorylation of the complement C5a receptor on serine 334. *J Biol Chem,* 282, 4345-4353.

POULIN, B., BUTCHER, A., MCWILLIAMS, P., BOURGOGNON, J.-M., PAWLAK, R., KONG, K. C., BOTTRILL, A., MISTRY, S., WESS, J., ROSETHORNE, E. M., CHARLTON, S. J. & TOBIN, A. B. 2010. The M3 muscarinic receptor regulates learning and memory in a receptor phosphorylation/arrestin-dependent manner. *Proceedings of the National Academy of Sciences,* 107, 9440.

PREMONT, R. T., MACRAE, A. D., STOFFEL, R. H., CHUNG, N., PITCHER, J. A., AMBROSE, C., INGLESE, J., MACDONALD, M. E. & LEFKOWITZ, R. J. 1996. Characterization of the G Protein-coupled Receptor Kinase GRK4:

IDENTIFICATION OF FOUR SPLICE VARIANTS (∗). *Journal of Biological Chemistry,* 271**,** 6403-6410.

PRESA, J. L., POMILIO, C., VINUESA, A., BENTIVEGNA, M., ALAIMO, A., GREGOSA, A., KIM, K. S., BEAUQUIS, J., RABINOVICH, G. & SARAVIA, F. 2019. Galectin-1 improves cognition and reduces amyloid-ß deposits in an animal model of Alzheimer's disease possibly by modulating microglia phenotype and increasing Aß clearance. *IBRO Reports,* 6**,** S477.

PRESLAND, J. 2005. Identifying novel modulators of G protein-coupled receptors via interaction at allosteric sites. *Curr Opin Drug Discov Devel,* 8**,** 567-76.

PRICE, D. L. & SISODIA, S. S. 1998. MUTANT GENES IN FAMILIAL ALZHEIMER'S DISEASE AND TRANSGENIC MODELS. *Annual Review of Neuroscience,* 21**,** 479-505.

PRÖMEL, S., LANGENHAN, T. & ARAÇ, D. 2013. Matching structure with function: the GAIN domain of adhesion-GPCR and PKD1-like proteins. *Trends Pharmacol Sci,* 34**,** 470-8.

PRUSINER, S. B. 1982. Novel proteinaceous infectious particles cause scrapie. *Science,* 216**,** 136-44.

PRUSINER, S. B., MCKINLEY, M. P., BOWMAN, K. A., BOLTON, D. C., BENDHEIM, P. E., GROTH, D. F. & GLENNER, G. G. 1983. Scrapie prions aggregate to form amyloid-like birefringent rods. *Cell,* 35**,** 349-358.

PURI, V., WANG, X., VARDIGAN, J. D., KUDUK, S. D. & USLANER, J. M. 2015. The selective positive allosteric M1 muscarinic receptor modulator PQCA attenuates learning and memory deficits in the Tg2576 Alzheimer's disease mouse model. *Behav Brain Res,* 287**,** 96-9.

QU, W. S., WANG, Y. H., MA, J. F., TIAN, D. S., ZHANG, Q., PAN, D. J., YU, Z. Y., XIE, M. J., WANG, J. P. & WANG, W. 2011. Galectin-1 attenuates astrogliosis-associated injuries and improves recovery of rats following focal cerebral ischemia. *J Neurochem,* 116**,** 217-26.

QUINLAN, R. A. & FRANKE, W. W. 1983. Molecular interactions in intermediate-sized filaments revealed by chemical cross-linking. Heteropolymers of vimentin and glial filament protein in cultured human glioma cells. *Eur J Biochem,* 132**,** 477-84.

QUIRK, G. J., ARMONY, J. L. & LEDOUX, J. E. 1997. Fear conditioning enhances different temporal components of tone-evoked spike trains in auditory cortex and lateral amygdala. *Neuron,* 19**,** 613-24.

RAEHAL, K. M., WALKER, J. K. & BOHN, L. M. 2005. Morphine side effects in beta-arrestin 2 knockout mice. *J Pharmacol Exp Ther,* 314**,** 1195-201.

RAFFA, R. B. 2009. The M5 muscarinic receptor as possible target for treatment of drug abuse. *Journal of Clinical Pharmacy and Therapeutics,* 34**,** 623-629.

RAI, S. N., DILNASHIN, H., BIRLA, H., SINGH, S. S., ZAHRA, W., RATHORE, A. S., SINGH, B. K. & SINGH, S. P. 2019. The Role of PI3K/Akt and ERK in Neurodegenerative Disorders. *Neurotox Res,* 35**,** 775-795.

RAJAGOPAL, S., AHN, S., ROMINGER, D. H., GOWEN-MACDONALD, W., LAM, C. M., DEWIRE, S. M., VIOLIN, J. D. & LEFKOWITZ, R. J. 2011. Quantifying ligand bias at seven-transmembrane receptors. *Mol Pharmacol,* 80**,** 367-77.

RAMÍREZ HERNÁNDEZ, E., SÁNCHEZ-MALDONADO, C., MAYORAL CHÁVEZ, M. A., HERNÁNDEZ-ZIMBRÓN, L. F., PATRICIO MARTÍNEZ, A., ZENTENO, E. & LIMÓN PÉREZ DE LEÓN, I. D. 2020. The therapeutic potential of galectin-1 and galectin-3 in the treatment of neurodegenerative diseases. *Expert Review of Neurotherapeutics,* 20**,** 439-448.

RANKIN, M. L., MARINEC, P. S., CABRERA, D. M., WANG, Z., JOSE, P. A. & SIBLEY, D. R. 2006. The D1 dopamine receptor is constitutively phosphorylated by G protein-coupled receptor kinase 4. *Mol Pharmacol,* 69**,** 759-69.

RANSOHOFF, R. M. 2016. How neuroinflammation contributes to neurodegeneration. *Science,* 353**,** 777.

RAPOPORT, M. & FERREIRA, A. 2000. PD98059 prevents neurite degeneration induced by fibrillar beta-amyloid in mature hippocampal neurons. *J Neurochem,* 74**,** 125-33.

RASMUSSEN, S. G. F., DEVREE, B. T., ZOU, Y., KRUSE, A. C., CHUNG, K. Y., KOBILKA, T. S., THIAN, F. S., CHAE, P. S., PARDON, E., CALINSKI, D., MATHIESEN, J. M., SHAH, S. T. A., LYONS, J. A., CAFFREY, M., GELLMAN, S. H., STEYAERT, J., SKINIOTIS, G., WEIS, W. I., SUNAHARA, R. K. & KOBILKA, B. K. 2011. Crystal structure of the ß2 adrenergic receptor–Gs protein complex. *Nature,* 477**,** 549-555.

REARDON, S. 2018. Frustrated Alzheimer's researchers seek better lab mice. *Nature*. England.

REITER, E., AHN, S., SHUKLA, A. K. & LEFKOWITZ, R. J. 2012. Molecular Mechanism of ß-Arrestin-Biased Agonism at Seven-Transmembrane Receptors. *Annual Review of Pharmacology and Toxicology,* 52**,** 179-197.

RIBÉ, E. M., PÉREZ, M., PUIG, B., GICH, I., LIM, F., CUADRADO, M., SESMA, T., CATENA, S., SÁNCHEZ, B., NIETO, M., GÓMEZ-RAMOS, P., MORÁN, M. A., CABODEVILLA, F., SAMARANCH, L., ORTIZ, L., PÉREZ, A., FERRER, I., AVILA, J. & GÓMEZ-ISLA, T. 2005. Accelerated amyloid deposition,

neurofibrillary degeneration and neuronal loss in double mutant APP/tau transgenic mice. *Neurobiol Dis,* 20**,** 814-22.

RICHARDS, R. I., ROBERTSON, S. A. & KASTNER, D. L. 2018. Neurodegenerative diseases have genetic hallmarks of autoinflammatory disease. *Human molecular genetics,* 27**,** R108-R118.

RIEK, R., HORNEMANN, S., WIDER, G., BILLETER, M., GLOCKSHUBER, R. & WUTHRICH, K. 1996. NMR structure of the mouse prion protein domain PrP(121-231). *Nature,* 382**,** 180-2.

RIEK, R., HORNEMANN, S., WIDER, G., GLOCKSHUBER, R. & WUTHRICH, K. 1997. NMR characterization of the full-length recombinant murine prion protein, mPrP(23-231). *FEBS Lett,* 413**,** 282-8.

RITCHIE, D. L., BOYLE, A., MCCONNELL, I., HEAD, M. W., IRONSIDE, J. W. & BRUCE, M. E. 2009. Transmissions of variant Creutzfeldt-Jakob disease from brain and lymphoreticular tissue show uniform and conserved bovine spongiform encephalopathy-related phenotypic properties on primary and secondary passage in wild-type mice. *J Gen Virol,* 90**,** 3075-3082.

RIVERA-MILLA, E., STUERMER, C. A. O. & MÁLAGA-TRILLO, E. 2003. An evolutionary basis for scrapie disease: identification of a fish prion mRNA. *Trends in Genetics,* 19**,** 72-75.

ROBBINS, J. P., PERFECT, L., RIBE, E. M., MARESCA, M., DANGLA-VALLS, A., FOSTER, E. M., KILLICK, R., NOWOSIAD, P., REID, M. J., POLIT, L. D., NEVADO, A. J., EBNER, D., BOHLOOLY-Y, M., BUCKLEY, N., PANGALOS, M. N., PRICE, J. & LOVESTONE, S. 2018. Clusterin Is Required for ß-Amyloid Toxicity in Human iPSC-Derived Neurons. *Frontiers in Neuroscience,* 12**,** 504.

ROED, S. N., WISMANN, P., UNDERWOOD, C. R., KULAHIN, N., IVERSEN, H., CAPPELEN, K. A., SCHÄFFER, L., LEHTONEN, J., HECKSHER-SOERENSEN, J., SECHER, A., MATHIESEN, J. M., BRÄUNER-OSBORNE, H., WHISTLER, J. L., KNUDSEN, S. M. & WALDHOER, M. 2014. Real-time trafficking and signaling of the glucagon-like peptide-1 receptor. *Mol Cell Endocrinol,* 382**,** 938-49.

ROFINA, J. E., VAN EDEREN, A. M., TOUSSAINT, M. J., SECRÈVE, M., VAN DER SPEK, A., VAN DER MEER, I., VAN EERDENBURG, F. J. & GRUYS, E. 2006. Cognitive disturbances in old dogs suffering from the canine counterpart of Alzheimer's disease. *Brain Res,* 1069**,** 216-26.

RON, D. & WALTER, P. 2007. Signal integration in the endoplasmic reticulum unfolded protein response. *Nature Reviews Molecular Cell Biology,* 8**,** 519-529.

ROOK, J. M., ABE, M., CHO, H. P., NANCE, K. D., LUSCOMBE, V. B., ADAMS, J. J., DICKERSON, J. W., REMKE, D. H., GARCIA-BARRANTES, P. M., ENGERS, D.

W., ENGERS, J. L., CHANG, S., FOSTER, J. J., BLOBAUM, A. L., NISWENDER, C. M., JONES, C. K., CONN, P. J. & LINDSLEY, C. W. 2017. Diverse Effects on M1 Signaling and Adverse Effect Liability within a Series of M1 Ago-PAMs. *ACS Chem Neurosci,* 8**,** 866-883.

ROOK, J. M., BERTRON, J. L., CHO, H. P., GARCIA-BARRANTES, P. M., MORAN, S. P., MAKSYMETZ, J. T., NANCE, K. D., DICKERSON, J. W., REMKE, D. H., CHANG, S., HARP, J. M., BLOBAUM, A. L., NISWENDER, C. M., JONES, C. K., STAUFFER, S. R., CONN, P. J. & LINDSLEY, C. W. 2018. A Novel M1 PAM VU0486846 Exerts Efficacy in Cognition Models without Displaying Agonist Activity or Cholinergic Toxicity. *ACS Chem Neurosci,* 9**,** 2274-2285.

ROSENBAUM, D. M., RASMUSSEN, S. G. F. & KOBILKA, B. K. 2009. The structure and function of G-protein-coupled receptors. *Nature,* 459**,** 356-363.

ROSENKILDE, M. M. & SCHWARTZ, T. W. 2000. Potency of ligands correlates with affinity measured against agonist and inverse agonists but not against neutral ligand in constitutively active chemokine receptor. *Mol Pharmacol,* 57**,** 602-9.

ROSES, A. D., SAUNDERS, A. M., CORDER, E. H., PERICAK-VANCE, M. A., HAN, S. H., EINSTEIN, G., HULETTE, C., SCHMECHEL, D. E., HOLSTI, M., HUANG, D. & ET AL. 1995. Influence of the susceptibility genes apolipoprotein E-epsilon 4 and apolipoprotein E-epsilon 2 on the rate of disease expressivity of late-onset Alzheimer's disease. *Arzneimittelforschung,* 45**,** 413-7.

ROSZKOWSKI, A. P. 1961. An unusual type of sympathetic ganglionic stimulant. *J Pharmacol Exp Ther,* 132**,** 156-70.

ROTH, B. L. & CHUANG, D. M. 1987. Multiple mechanisms of serotonergic signal transduction. *Life Sci,* 41**,** 1051-64.

ROZEMULLER, J. M., ABBINK, J. J., KAMP, A. M., STAM, F. C., HACK, C. E. & EIKELENBOOM, P. 1991. Distribution pattern and functional state of alpha 1-antichymotrypsin in plaques and vascular amyloid in Alzheimer's disease. A immunohistochemical study with monoclonal antibodies against native and inactivated alpha 1-antichymotrypsin. *Acta Neuropathol,* 82**,** 200-7.

RUBINSZTEIN, D. C. 2006. The roles of intracellular protein-degradation pathways in neurodegeneration. *Nature,* 443**,** 780-786.

RUPNIAK, N. M. J., SAMSON, N. A., TYE, S. J., FIELD, M. J. & IVERSEN, S. D. 1991. Evidence against a specific effect of cholinergic drugs on spatial memory in primates. *Behavioural Brain Research,* 43**,** 1-6.

RUSH, D. K. 1988. Scopolamine amnesia of passive avoidance: A deficit of information acquisition. *Behavioral and Neural Biology,* 50**,** 255-274.

RUSTED, J. M. & WARBURTON, D. M. 1988. The effects of scopolamine on working memory in healthy young volunteers. *Psychopharmacology,* 96**,** 145-152.

SAFAR, J., ROLLER, P. P., GAJDUSEK, D. C. & GIBBS, C. J., JR. 1993. Thermal stability and conformational transitions of scrapie amyloid (prion) protein correlate with infectivity. *Protein Sci,* 2**,** 2206-16.

SAIDAK, Z., BLAKE-PALMER, K., HAY, D. L., NORTHUP, J. K. & GLASS, M. 2006. Differential activation of G-proteins by μ-opioid receptor agonists. *British Journal of Pharmacology,* 147**,** 671-680.

SAITO, T., MATSUBA, Y., MIHIRA, N., TAKANO, J., NILSSON, P., ITOHARA, S., IWATA, N. & SAIDO, T. C. 2014. Single App knock-in mouse models of Alzheimer's disease. *Nat Neurosci,* 17**,** 661-3.

SAITO, T., MATSUBA, Y., YAMAZAKI, N., HASHIMOTO, S. & SAIDO, T. C. 2016. Calpain Activation in Alzheimer's Model Mice Is an Artifact of APP and Presenilin Overexpression. *J Neurosci,* 36**,** 9933-6.

SAKAMOTO, A., CHEN, M., KOBAYASHI, T., KRONENBERG, H. M. & WEINSTEIN, L. S. 2005. Chondrocyte-Specific Knockout of the G Protein Gsα Leads to Epiphyseal and Growth Plate Abnormalities and Ectopic Chondrocyte Formation. *Journal of Bone and Mineral Research,* 20**,** 663-671.

SALTER, M. W. & STEVENS, B. 2017. Microglia emerge as central players in brain disease. *Nat Med,* 23**,** 1018-1027.

SANABRIA-CASTRO, A., ALVARADO-ECHEVERRÍA, I. & MONGE-BONILLA, C. 2017. Molecular Pathogenesis of Alzheimer's Disease: An Update. *Ann Neurosci.* Allschwilerstrasse 10, P.O. Box · Postfach · Case postale, CH–4009, Basel, Switzerland · Schweiz · Suisse, Phone: +41 61 306 11 11, Fax: +41 61 306 12 34, karger@karger.ch.

SANDBERG, M. K., AL-DOUJAILY, H., SHARPS, B., DE OLIVEIRA, M. W., SCHMIDT, C., RICHARD-LONDT, A., LYALL, S., LINEHAN, J. M., BRANDNER, S., WADSWORTH, J. D. F., CLARKE, A. R. & COLLINGE, J. 2014. Prion neuropathology follows the accumulation of alternate prion protein isoforms after infective titre has peaked. *Nature Communications,* 5**,** 4347.

SANTOS, R., URSU, O., GAULTON, A., BENTO, A. P., DONADI, R. S., BOLOGA, C. G., KARLSSON, A., AL-LAZIKANI, B., HERSEY, A., OPREA, T. I. & OVERINGTON, J. P. 2017. A comprehensive map of molecular drug targets. *Nature reviews. Drug discovery,* 16**,** 19-34.

SARTER, M., LUSTIG, C. & TAYLOR, S. F. 2012. Cholinergic contributions to the cognitive symptoms of schizophrenia and the viability of cholinergic treatments. *Neuropharmacology,* 62**,** 1544-53.

SASAGURI, H., NILSSON, P., HASHIMOTO, S., NAGATA, K., SAITO, T., DE STROOPER, B., HARDY, J., VASSAR, R., WINBLAD, B. & SAIDO, T. C. 2017. APP mouse models for Alzheimer's disease preclinical studies. *Embo j,* 36**,** 2473-2487.

SASAKI, T., HIRABAYASHI, J., MANYA, H., KASAI, K. & ENDO, T. 2004. Galectin-1 induces astrocyte differentiation, which leads to production of brain-derived neurotrophic factor. *Glycobiology,* 14**,** 357-63.

SASAKI, Y., OHSAWA, K., KANAZAWA, H., KOHSAKA, S. & IMAI, Y. 2001. Iba1 Is an Actin-Cross-Linking Protein in Macrophages/Microglia. *Biochemical and Biophysical Research Communications,* 286**,** 292-297.

SAULIÈRE, A., BELLOT, M., PARIS, H., DENIS, C., FINANA, F., HANSEN, J. T., ALTIÉ, M.-F., SEGUELAS, M.-H., PATHAK, A., HANSEN, J. L., SÉNARD, J.-M. & GALÉS, C. 2012. Deciphering biased-agonism complexity reveals a new active AT1 receptor entity. *Nature Chemical Biology,* 8**,** 622-630.

SAWADA, M., KONDO, N., SUZUMURA, A. & MARUNOUCHI, T. 1989. Production of tumor necrosis factor-alpha by microglia and astrocytes in culture. *Brain research,* 491**,** 394-397.

SCARPA, M., HESSE, S. & BRADLEY, S. J. 2020. M1 muscarinic acetylcholine receptors: A therapeutic strategy for symptomatic and disease-modifying effects in Alzheimer's disease? *Adv Pharmacol,* 88**,** 277-310.

SCARPA, M., MOLLOY, C., JENKINS, L., STRELLIS, B., BUDGETT, R. F., HESSE, S., DWOMOH, L., MARSANGO, S., TEJEDA, G. S., ROSSI, M., AHMED, Z., MILLIGAN, G., HUDSON, B. D., TOBIN, A. B. & BRADLEY, S. J. 2021. Biased M1 muscarinic receptor mutant mice show accelerated progression of prion neurodegenerative disease. *Proc Natl Acad Sci U S A,* 118**,** e2107389118.

SCHIÖTH, H. B. & FREDRIKSSON, R. 2005. The GRAFS classification system of G-protein coupled receptors in comparative perspective. *Gen Comp Endocrinol,* 142**,** 94-101.

SCHLIEBS, R. & ARENDT, T. 2006. The significance of the cholinergic system in the brain during aging and in Alzheimer's disease. *J Neural Transm (Vienna),* 113**,** 1625-44.

SCHLIEBS, R. & ARENDT, T. 2011. The cholinergic system in aging and neuronal degeneration. *Behavioural Brain Research,* 221**,** 555-563.

SCHULTE, G. 2010. International Union of Basic and Clinical Pharmacology. LXXX. The Class Frizzled Receptors. *Pharmacological Reviews,* 62**,** 632.

SEEGER, T., FEDOROVA, I., ZHENG, F., MIYAKAWA, T., KOUSTOVA, E., GOMEZA, J., BASILE, A. S., ALZHEIMER, C. & WESS, J. 2004. M2 muscarinic

acetylcholine receptor knock-out mice show deficits in behavioral flexibility, working memory, and hippocampal plasticity. *The Journal of neuroscience : the official journal of the Society for Neuroscience,* 24, 10117-10127.

SEEMAN, P. & SEEMAN, N. 2011. Alzheimer's disease: ß-amyloid plaque formation in human brain. *Synapse,* 65, 1289-1297.

SELKOE, D. J. 2011. Resolving controversies on the path to Alzheimer's therapeutics. *Nat Med,* 17, 1060-5.

SERRANO-POZO, A., FROSCH, M. P., MASLIAH, E. & HYMAN, B. T. 2011. Neuropathological alterations in Alzheimer disease. *Cold Spring Harb Perspect Med,* 1, a006189.

SEVIGNY, J., CHIAO, P., BUSSIÈRE, T., WEINREB, P. H., WILLIAMS, L., MAIER, M., DUNSTAN, R., SALLOWAY, S., CHEN, T., LING, Y., O'GORMAN, J., QIAN, F., ARASTU, M., LI, M., CHOLLATE, S., BRENNAN, M. S., QUINTERO-MONZON, O., SCANNEVIN, R. H., ARNOLD, H. M., ENGBER, T., RHODES, K., FERRERO, J., HANG, Y., MIKULSKIS, A., GRIMM, J., HOCK, C., NITSCH, R. M. & SANDROCK, A. 2016. The antibody aducanumab reduces Aß plaques in Alzheimer's disease. *Nature,* 537, 50-6.

SHEKHAR, A., POTTER, W. Z., LIGHTFOOT, J., LIENEMANN, J., DUBÉ, S., MALLINCKRODT, C., BYMASTER, F. P., MCKINZIE, D. L. & FELDER, C. C. 2008. Selective Muscarinic Receptor Agonist Xanomeline as a Novel Treatment Approach for Schizophrenia. *American Journal of Psychiatry,* 165, 1033-1039.

SHELTON, R. C. 2019. Serotonin and Norepinephrine Reuptake Inhibitors. *Handb Exp Pharmacol,* 250, 145-180.

SHENOY, S. K., DRAKE, M. T., NELSON, C. D., HOUTZ, D. A., XIAO, K., MADABUSHI, S., REITER, E., PREMONT, R. T., LICHTARGE, O. & LEFKOWITZ, R. J. 2006. beta-arrestin-dependent, G protein-independent ERK1/2 activation by the beta2 adrenergic receptor. *J Biol Chem,* 281, 1261-73.

SHENOY, S. K. & LEFKOWITZ, R. J. 2011. ß-Arrestin-mediated receptor trafficking and signal transduction. *Trends Pharmacol Sci,* 32, 521-33.

SHENOY, S. K., MCDONALD, P. H., KOHOUT, T. A. & LEFKOWITZ, R. J. 2001. Regulation of receptor fate by ubiquitination of activated beta 2-adrenergic receptor and beta-arrestin. *Science,* 294, 1307-13.

SHENOY, S. K., MODI, A. S., SHUKLA, A. K., XIAO, K., BERTHOUZE, M., AHN, S., WILKINSON, K. D., MILLER, W. E. & LEFKOWITZ, R. J. 2009. Beta-arrestin-dependent signaling and trafficking of 7-transmembrane receptors is reciprocally regulated by the deubiquitinase USP33 and the E3 ligase Mdm2. *Proc Natl Acad Sci U S A,* 106, 6650-5.

SHI, Q., CHEN, L. N., ZHANG, B. Y., XIAO, K., ZHOU, W., CHEN, C., ZHANG, X. M., TIAN, C., GAO, C., WANG, J., HAN, J. & DONG, X. P. 2015. Proteomics analyses for the global proteins in the brain tissues of different human prion diseases. *Mol Cell Proteomics,* 14**,** 854-69.

SHIRAISHI, Y., KOFUKU, Y., UEDA, T., PANDEY, S., DWIVEDI-AGNIHOTRI, H., SHUKLA, A. K. & SHIMADA, I. 2021. Biphasic activation of ß-arrestin 1 upon interaction with a GPCR revealed by methyl-TROSY NMR. *Nature Communications,* 12**,** 7158.

SHIREY, J. K., BRADY, A. E., JONES, P. J., DAVIS, A. A., BRIDGES, T. M., KENNEDY, J. P., JADHAV, S. B., MENON, U. N., XIANG, Z., WATSON, M. L., CHRISTIAN, E. P., DOHERTY, J. J., QUIRK, M. C., SNYDER, D. H., LAH, J. J., LEVEY, A. I., NICOLLE, M. M., LINDSLEY, C. W. & CONN, P. J. 2009. A selective allosteric potentiator of the M(1) muscarinic acetylcholine receptor increases activity of medial prefrontal cortical neurons and restores impairments in reversal learning. *The Journal of neuroscience : the official journal of the Society for Neuroscience,* 29**,** 14271-14286.

SHMERLING, D., HEGYI, I., FISCHER, M., BLATTLER, T., BRANDNER, S., GOTZ, J., RULICKE, T., FLECHSIG, E., COZZIO, A., VON MERING, C., HANGARTNER, C., AGUZZI, A. & WEISSMANN, C. 1998. Expression of amino-terminally truncated PrP in the mouse leading to ataxia and specific cerebellar lesions. *Cell,* 93**,** 203-14.

SHUKLA, A. K., MANGLIK, A., KRUSE, A. C., XIAO, K., REIS, R. I., TSENG, W.-C., STAUS, D. P., HILGER, D., UYSAL, S., HUANG, L.-Y., PADUCH, M., TRIPATHI-SHUKLA, P., KOIDE, A., KOIDE, S., WEIS, W. I., KOSSIAKOFF, A. A., KOBILKA, B. K. & LEFKOWITZ, R. J. 2013. Structure of active ß-arrestin-1 bound to a G-protein-coupled receptor phosphopeptide. *Nature,* 497**,** 137-141.

SHUKLA, A. K., WESTFIELD, G. H., XIAO, K., REIS, R. I., HUANG, L.-Y., TRIPATHI-SHUKLA, P., QIAN, J., LI, S., BLANC, A., OLESKIE, A. N., DOSEY, A. M., SU, M., LIANG, C.-R., GU, L.-L., SHAN, J.-M., CHEN, X., HANNA, R., CHOI, M., YAO, X. J., KLINK, B. U., KAHSAI, A. W., SIDHU, S. S., KOIDE, S., PENCZEK, P. A., KOSSIAKOFF, A. A., WOODS JR, V. L., KOBILKA, B. K., SKINIOTIS, G. & LEFKOWITZ, R. J. 2014. Visualization of arrestin recruitment by a G-protein-coupled receptor. *Nature,* 512**,** 218-222.

SIBLEY, D. R., STRASSER, R. H., BENOVIC, J. L., DANIEL, K. & LEFKOWITZ, R. J. 1986. Phosphorylation/Dephosphorylation of the ß -adrenergic Receptor Regulates Its Functional Coupling to Adenylate Cyclase and Subcellular Distribution. *Proceedings of the National Academy of Sciences of the United States of America,* 83**,** 9408-9412.

SICHERER, S. H. & SIMONS, F. E. R. 2017. Epinephrine for First-aid Management of Anaphylaxis. *Pediatrics,* 139.

SIDEROVSKI, D. P., HESSEL, A., CHUNG, S., MAK, T. W. & TYERS, M. 1996. A new family of regulators of G-protein-coupled receptors? *Current Biology,* 6**,** 211-212.

SILVEIRA, J. R., RAYMOND, G. J., HUGHSON, A. G., RACE, R. E., SIM, V. L., HAYES, S. F. & CAUGHEY, B. 2005. The most infectious prion protein particles. *Nature,* 437**,** 257-61.

SIPOS, E., KURUNCZI, A., KASZA, A., HORVÁTH, J., FELSZEGHY, K., LAROCHE, S., TOLDI, J., PÁRDUCZ, A., PENKE, B. & PENKE, Z. 2007. Beta-amyloid pathology in the entorhinal cortex of rats induces memory deficits: implications for Alzheimer's disease. *Neuroscience,* 147**,** 28-36.

SLOAN, H. L., GOOD, M. & DUNNETT, S. B. 2006. Double dissociation between hippocampal and prefrontal lesions on an operant delayed matching task and a water maze reference memory task. *Behav Brain Res,* 171**,** 116-26.

SMRCKA, A. V. 2008. G protein βγ subunits: central mediators of G protein-coupled receptor signaling. *Cell Mol Life Sci,* 65**,** 2191-214.

SOERGEL, D. G., SUBACH, R. A., BURNHAM, N., LARK, M. W., JAMES, I. E., SADLER, B. M., SKOBIERANDA, F., VIOLIN, J. D. & WEBSTER, L. R. 2014. Biased agonism of the μ-opioid receptor by TRV130 increases analgesia and reduces on-target adverse effects versus morphine: A randomized, double-blind, placebo-controlled, crossover study in healthy volunteers. *Pain,* 155**,** 1829-1835.

SOFRONIEW, M. V. & VINTERS, H. V. 2010. Astrocytes: biology and pathology. *Acta Neuropathol,* 119**,** 7-35.

SOMMER, M. E., ELGETI, M., HILDEBRAND, P. W., SZCZEPEK, M., HOFMANN, K. P. & SCHEERER, P. 2015. Chapter Twenty-Six - Structure-Based Biophysical Analysis of the Interaction of Rhodopsin with G Protein and Arrestin. *In:* SHUKLA, A. K. (ed.) *Methods in Enzymology*. Academic Press.

SONG, X., COFFA, S., FU, H. & GUREVICH, V. V. 2009. How does arrestin assemble MAPKs into a signaling complex? *J Biol Chem,* 284**,** 685-95.

SPALDING, T. A., MA, J. N., OTT, T. R., FRIBERG, M., BAJPAI, A., BRADLEY, S. R., DAVIS, R. E., BRANN, M. R. & BURSTEIN, E. S. 2006. Structural requirements of transmembrane domain 3 for activation by the M1 muscarinic receptor agonists AC-42, AC-260584, clozapine, and N-desmethylclozapine: evidence for three distinct modes of receptor activation. *Mol Pharmacol,* 70**,** 1974-83.

SPALDING, T. A., TROTTER, C., SKJAERBAEK, N., MESSIER, T. L., CURRIER, E. A., BURSTEIN, E. S., LI, D., HACKSELL, U. & BRANN, M. R. 2002. Discovery of an ectopic activation site on the M(1) muscarinic receptor. *Mol Pharmacol,* 61**,** 1297-302.

SPARKES, R. S., SIMON, M., COHN, V. H., FOURNIER, R. E., LEM, J., KLISAK, I., HEINZMANN, C., BLATT, C., LUCERO, M., MOHANDAS, T. & ET AL. 1986. Assignment of the human and mouse prion protein genes to homologous chromosomes. *Proceedings of the National Academy of Sciences of the United States of America,* 83**,** 7358-7362.

SPERLING, R. A., MORMINO, E. C., SCHULTZ, A. P., BETENSKY, R. A., PAPP, K. V., AMARIGLIO, R. E., HANSEEUW, B. J., BUCKLEY, R., CHHATWAL, J., HEDDEN, T., MARSHALL, G. A., QUIROZ, Y. T., DONOVAN, N. J., JACKSON, J., GATCHEL, J. R., RABIN, J. S., JACOBS, H., YANG, H. S., PROPERZI, M., KIRN, D. R., RENTZ, D. M. & JOHNSON, K. A. 2019. The impact of amyloid-beta and tau on prospective cognitive decline in older individuals. *Ann Neurol,* 85**,** 181-193.

SRIRAM, K. & INSEL, P. A. 2018. G Protein-Coupled Receptors as Targets for Approved Drugs: How Many Targets and How Many Drugs? *Mol Pharmacol,* 93**,** 251-258.

STAHL, N., BORCHELT, D. R., HSIAO, K. & PRUSINER, S. B. 1987. Scrapie prion protein contains a phosphatidylinositol glycolipid. *Cell,* 51**,** 229-240.

STALLAERT, W., CHRISTOPOULOS, A. & BOUVIER, M. 2011. Ligand functional selectivity and quantitative pharmacology at G protein-coupled receptors. *Expert Opinion on Drug Discovery,* 6**,** 811-825.

STANCIU, M., WANG, Y., KENTOR, R., BURKE, N., WATKINS, S., KRESS, G., REYNOLDS, I., KLANN, E., ANGIOLIERI, M. R., JOHNSON, J. W. & DEFRANCO, D. B. 2000. Persistent activation of ERK contributes to glutamate-induced oxidative toxicity in a neuronal cell line and primary cortical neuron cultures. *J Biol Chem,* 275**,** 12200-6.

STAROSSOM, S. C., MASCANFRONI, I. D., IMITOLA, J., CAO, L., RADDASSI, K., HERNANDEZ, S. F., BASSIL, R., CROCI, D. O., CERLIANI, J. P., DELACOUR, D., WANG, Y., ELYAMAN, W., KHOURY, S. J. & RABINOVICH, G. A. 2012. Galectin-1 deactivates classically activated microglia and protects from inflammation-induced neurodegeneration. *Immunity,* 37**,** 249-63.

STAUS, D. P., HU, H., ROBERTSON, M. J., KLEINHENZ, A. L. W., WINGLER, L. M., CAPEL, W. D., LATORRACA, N. R., LEFKOWITZ, R. J. & SKINIOTIS, G. 2020. Structure of the M2 muscarinic receptor–β-arrestin complex in a lipid nanodisc. *Nature,* 579**,** 297-302.

STENGEL, P. W., GOMEZA, J., WESS, J. & COHEN, M. L. 2000. M2 and M4 Receptor Knockout Mice: Muscarinic Receptor Function in Cardiac and Smooth Muscle In Vitro. *Journal of Pharmacology and Experimental Therapeutics,* 292**,** 877.

STERNE-MARR, R., GUREVICH, V. V., GOLDSMITH, P., BODINE, R. C., SANDERS, C., DONOSO, L. A. & BENOVIC, J. L. 1993. Polypeptide variants of beta-arrestin and arrestin3. *Journal of Biological Chemistry,* 268**,** 15640-15648.

STEVENS, B., ALLEN, N. J., VAZQUEZ, L. E., HOWELL, G. R., CHRISTOPHERSON, K. S., NOURI, N., MICHEVA, K. D., MEHALOW, A. K., HUBERMAN, A. D., STAFFORD, B., SHER, A., LITKE, ALAN M., LAMBRIS, J. D., SMITH, S. J., JOHN, S. W. M. & BARRES, B. A. 2007. The Classical Complement Cascade Mediates CNS Synapse Elimination. *Cell,* 131**,** 1164-1178.

STOFFEL, R. H., RANDALL, R. R., PREMONT, R. T., LEFKOWITZ, R. J. & INGLESE, J. 1994. Palmitoylation of G protein-coupled receptor kinase, GRK6. Lipid modification diversity in the GRK family. *Journal of Biological Chemistry,* 269**,** 27791-27794.

STRADA, O., VYAS, S., HIRSCH, E. C., RUBERG, M., BRICE, A., AGID, Y. & JAVOY-AGID, F. 1992. Decreased choline acetyltransferase mRNA expression in the nucleus basalis of Meynert in Alzheimer disease: an in situ hybridization study. *Proc Natl Acad Sci U S A,* 89**,** 9549-53.

STRITTMATTER, W. J., SAUNDERS, A. M., SCHMECHEL, D., PERICAK-VANCE, M., ENGHILD, J., SALVESEN, G. S. & ROSES, A. D. 1993. Apolipoprotein E: high-avidity binding to beta-amyloid and increased frequency of type 4 allele in late-onset familial Alzheimer disease. *Proc Natl Acad Sci U S A,* 90**,** 1977-81.

STRUMBO, B., RONCHI, S., BOLIS, L. C. & SIMONIC, T. 2001. Molecular cloning of the cDNA coding for Xenopus laevis prion protein. *FEBS Letters,* 508**,** 170-174.

STURCHLER-PIERRAT, C., ABRAMOWSKI, D., DUKE, M., WIEDERHOLD, K. H., MISTL, C., ROTHACHER, S., LEDERMANN, B., BÜRKI, K., FREY, P., PAGANETTI, P. A., WARIDEL, C., CALHOUN, M. E., JUCKER, M., PROBST, A., STAUFENBIEL, M. & SOMMER, B. 1997. Two amyloid precursor protein transgenic mouse models with Alzheimer disease-like pathology. *Proc Natl Acad Sci U S A,* 94**,** 13287-92.

SUBRAMANIAM, S. & UNSICKER, K. 2010. ERK and cell death: ERK1/2 in neuronal death. *The FEBS Journal,* 277**,** 22-29.

SUN, A., LIU, M., NGUYEN, X. V. & BING, G. 2003. P38 MAP kinase is activated at early stages in Alzheimer's disease brain. *Exp Neurol,* 183**,** 394-405.

SUNDBLAD, V., MOROSI, L. G., GEFFNER, J. R. & RABINOVICH, G. A. 2017. Galectin-1: A Jack-of-All-Trades in the Resolution of Acute and Chronic Inflammation. *The Journal of Immunology,* 199**,** 3721.

SUNDERLAND, T., TARIOT, P. N., WEINGARTNER, H., MURPHY, D. L., NEWHOUSE, P. A., MUELLER, E. A. & COHEN, R. M. 1986. Pharmacologic modelling of Alzheimer's disease. *Progress in Neuro-Psychopharmacology and Biological Psychiatry,* 10**,** 599-610.

SUTTON, R. B., VISHNIVETSKIY, S. A., ROBERT, J., HANSON, S. M., RAMAN, D., KNOX, B. E., KONO, M., NAVARRO, J. & GUREVICH, V. V. 2005. Crystal

structure of cone arrestin at 2.3A: evolution of receptor specificity. *J Mol Biol,* 354, 1069-80.

SVENSSON, A.-L., ALAFUZOFF, I. & NORDBERG, A. 1992. Characterization of muscarinic receptor subtypes in Alzheimer and control brain cortices by selective muscarinic antagonists. *Brain Research,* 596, 142-148.

SZCZEPEK, M., BEYRIÈRE, F., HOFMANN, K. P., ELGETI, M., KAZMIN, R., ROSE, A., BARTL, F. J., VON STETTEN, D., HECK, M., SOMMER, M. E., HILDEBRAND, P. W. & SCHEERER, P. 2014. Crystal structure of a common GPCR-binding interface for G protein and arrestin. *Nature Communications,* 5, 4801.

TAIT, S. W. G. & GREEN, D. R. 2008. Caspase-independent cell death: leaving the set without the final cut. *Oncogene,* 27, 6452-6461.

TASDEMIR-YILMAZ, O. E. & FREEMAN, M. R. 2014. Astrocytes engage unique molecular programs to engulf pruned neuronal debris from distinct subsets of neurons. *Genes Dev,* 28, 20-33.

TERWEL, D., STEFFENSEN, K. R., VERGHESE, P. B., KUMMER, M. P., GUSTAFSSON, J., HOLTZMAN, D. M. & HENEKA, M. T. 2011. Critical role of astroglial apolipoprotein E and liver X receptor-α expression for microglial Aβ phagocytosis. *J Neurosci,* 31, 7049-59.

THAL, D. M., SUN, B., FENG, D., NAWARATNE, V., LEACH, K., FELDER, C. C., BURES, M. G., EVANS, D. A., WEIS, W. I., BACHHAWAT, P., KOBILKA, T. S., SEXTON, P. M., KOBILKA, B. K. & CHRISTOPOULOS, A. 2016. Crystal structures of the M1 and M4 muscarinic acetylcholine receptors. *Nature,* 531, 335-340.

THATHIAH, A. & DE STROOPER, B. 2011. The role of G protein-coupled receptors in the pathology of Alzheimer's disease. *Nature Reviews Neuroscience,* 12, 73.

THIYAGARAJAN, M. M., STRACQUATANIO, R. P., PRONIN, A. N., EVANKO, D. S., BENOVIC, J. L. & WEDEGAERTNER, P. B. 2004. A Predicted Amphipathic Helix Mediates Plasma Membrane Localization of GRK5*. *Journal of Biological Chemistry,* 279, 17989-17995.

THOMAS, R. L., LANGMEAD, C. J., WOOD, M. D. & CHALLISS, R. A. J. 2009. Contrasting Effects of Allosteric and Orthosteric Agonists on M(1) Muscarinic Acetylcholine Receptor Internalization and Down-regulation. *The Journal of Pharmacology and Experimental Therapeutics,* 331, 1086-1095.

THOMPSON, K. J., KHAJEHALI, E., BRADLEY, S. J., NAVARRETE, J. S., HUANG, X. P., SLOCUM, S., JIN, J., LIU, J., XIONG, Y., OLSEN, R. H. J., DIBERTO, J. F., BOYT, K. M., PINA, M. M., PATI, D., MOLLOY, C., BUNDGAARD, C., SEXTON, P. M., KASH, T. L., KRASHES, M. J., CHRISTOPOULOS, A., ROTH, B. L. & TOBIN, A. B. 2018. DREADD Agonist 21 Is an Effective Agonist for

Muscarinic-Based DREADDs in Vitro and in Vivo. *ACS Pharmacology & Translational Science,* 1**,** 61-72.

THOMPSON, S., LANCTOT KL FAU - HERRMANN, N. & HERRMANN, N. 2004. The benefits and risks associated with cholinesterase inhibitor therapy in Alzheimer's disease.

THOMSEN, A. R. B., PLOUFFE, B., CAHILL, T. J., 3RD, SHUKLA, A. K., TARRASCH, J. T., DOSEY, A. M., KAHSAI, A. W., STRACHAN, R. T., PANI, B., MAHONEY, J. P., HUANG, L., BRETON, B., HEYDENREICH, F. M., SUNAHARA, R. K., SKINIOTIS, G., BOUVIER, M. & LEFKOWITZ, R. J. 2016. GPCR-G Protein-β-Arrestin Super-Complex Mediates Sustained G Protein Signaling. *Cell,* 166**,** 907-919.

THOMSEN, M., LINDSLEY, C. W., CONN, P. J., WESSELL, J. E., FULTON, B. S., WESS, J. & CAINE, S. B. 2012. Contribution of both M1 and M4 receptors to muscarinic agonist-mediated attenuation of the cocaine discriminative stimulus in mice. *Psychopharmacology (Berl),* 220**,** 673-85.

TIMMERS, M., TESSEUR, I., BOGERT, J., ZETTERBERG, H., BLENNOW, K., BÖRJESSON-HANSON, A., BAQUERO, M., BOADA, M., RANDOLPH, C., TRITSMANS, L., VAN NUETEN, L., ENGELBORGHS, S. & STREFFER, J. R. 2019. Relevance of the interplay between amyloid and tau for cognitive impairment in early Alzheimer's disease. *Neurobiol Aging,* 79**,** 131-141.

TOBIN, A. B. 2008. G-protein-coupled receptor phosphorylation: where, when and by whom. *British journal of pharmacology,* 153 Suppl 1**,** S167-S176.

TOBIN, A. B., BUTCHER, A. J. & KONG, K. C. 2008. Location, location, location...site-specific GPCR phosphorylation offers a mechanism for cell-type-specific signalling. *Trends Pharmacol Sci,* 29**,** 413-20.

TORRECILLA, I., SPRAGG, E. J., POULIN, B., MCWILLIAMS, P. J., MISTRY, S. C., BLAUKAT, A. & TOBIN, A. B. 2007. Phosphorylation and regulation of a G protein-coupled receptor by protein kinase CK2. *J Cell Biol,* 177**,** 127-37.

TOUHARA, K., INGLESE, J., PITCHER, J. A., SHAW, G. & LEFKOWITZ, R. J. 1994. Binding of G protein beta gamma-subunits to pleckstrin homology domains. *Journal of Biological Chemistry,* 269**,** 10217-10220.

TRIFONOV, S., HOUTANI, T., HAMADA, S., KASE, M., MARUYAMA, M. & SUGIMOTO, T. 2009. In situ hybridization study of the distribution of choline acetyltransferase mRNA and its splice variants in the mouse brain and spinal cord. *Neuroscience,* 159**,** 344-357.

TWEEDIE, D., SAMBAMURTI, K. & GREIG, N. H. 2007. TNF-alpha inhibition as a treatment strategy for neurodegenerative disorders: new drug candidates and targets. *Curr Alzheimer Res,* 4**,** 378-85.

UNAL, H. & KARNIK, S. S. 2012. Domain coupling in GPCRs: the engine for induced conformational changes. *Trends Pharmacol Sci,* 33**,** 79-88.

UNTERBERGER, U., HÖFTBERGER, R., GELPI, E., FLICKER, H., BUDKA, H. & VOIGTLÄNDER, T. 2006. Endoplasmic reticulum stress features are prominent in Alzheimer disease but not in prion diseases in vivo. *J Neuropathol Exp Neurol,* 65**,** 348-57.

USLANER, J. M., EDDINS, D., PURI, V., CANNON, C. E., SUTCLIFFE, J., CHEW, C. S., PEARSON, M., VIVIAN, J. A., CHANG, R. K., RAY, W. J., KUDUK, S. D. & WITTMANN, M. 2013. The muscarinic M1 receptor positive allosteric modulator PQCA improves cognitive measures in rat, cynomolgus macaque, and rhesus macaque. *Psychopharmacology (Berl),* 225**,** 21-30.

USLANER, J. M., KUDUK, S. D., WITTMANN, M., LANGE, H. S., FOX, S. V., MIN, C., PAJKOVIC, N., HARRIS, D., CILISSEN, C., MAHON, C., MOSTOLLER, K., WARRINGTON, S. & BESHORE, D. C. 2018. Preclinical to Human Translational Pharmacology of the Novel M1 Positive Allosteric Modulator MK-7622. *J Pharmacol Exp Ther,* 365**,** 556-566.

UTTLEY, L., CARROLL, C., WONG, R., HILTON, D. A. & STEVENSON, M. 2020. Creutzfeldt-Jakob disease: a systematic review of global incidence, prevalence, infectivity, and incubation. *The Lancet Infectious Diseases,* 20**,** e2-e10.

UWADA, J., YOSHIKI, H., MASUOKA, T., NISHIO, M. & MURAMATSU, I. 2014. Intracellular localization of the M1 muscarinic acetylcholine receptor through clathrin-dependent constitutive internalization is mediated by a C-terminal tryptophan-based motif. *Journal of Cell Science,* 127**,** 3131.

VALANT, C., GREGORY, K. J., HALL, N. E., SCAMMELLS, P. J., LEW, M. J., SEXTON, P. M. & CHRISTOPOULOS, A. 2008. A novel mechanism of G protein-coupled receptor functional selectivity. Muscarinic partial agonist McN-A-343 as a bitopic orthosteric/allosteric ligand. *J Biol Chem,* 283**,** 29312-21.

VALANT, C., ROBERT LANE, J., SEXTON, P. M. & CHRISTOPOULOS, A. 2012. The best of both worlds? Bitopic orthosteric/allosteric ligands of g protein-coupled receptors. *Annu Rev Pharmacol Toxicol,* 52**,** 153-78.

VAN DAM, D. & DE DEYN, P. P. 2011. Animal models in the drug discovery pipeline for Alzheimer's disease. *Br J Pharmacol,* 164**,** 1285-300.

VAN DEN BOS, E., AMBROSY, B., HORSTHEMKE, M., WALBAUM, S., BACHG, A. C., WETTSCHURECK, N., INNAMORATI, G., WILKIE, T. M. & HANLEY, P. J. 2020. Knockout mouse models reveal the contributions of G protein subunits to complement C5a receptor-mediated chemotaxis. *The Journal of biological chemistry,* 295**,** 7726-7742.

VAN DER KANT, R. & GOLDSTEIN, L. S. 2015. Cellular functions of the amyloid precursor protein from development to dementia. *Dev Cell,* 32**,** 502-15.

VAN DER WESTHUIZEN, E. T., CHOY, K. H. C., VALANT, C., MCKENZIE-NICKSON, S., BRADLEY, S. J., TOBIN, A. B., SEXTON, P. M. & CHRISTOPOULOS, A. 2020. Fine Tuning Muscarinic Acetylcholine Receptor Signaling Through Allostery and Bias. *Front Pharmacol,* 11**,** 606656.

VAN DER WESTHUIZEN, E. T., SPATHIS, A., KHAJEHALI, E., JORG, M., MISTRY, S. N., CAPUANO, B., TOBIN, A. B., SEXTON, P. M., SCAMMELLS, P. J., VALANT, C. & CHRISTOPOULOS, A. 2018. Assessment of the Molecular Mechanisms of Action of Novel 4-Phenylpyridine-2-One and 6-Phenylpyrimidin-4-One Allosteric Modulators at the M1 Muscarinic Acetylcholine Receptors. *Mol Pharmacol,* 94**,** 770-783.

VAN EVERBROECK, B., DOBBELEIR, I., DE WAELE, M., DE LEENHEIR, E., LÜBKE, U., MARTIN, J. J. & CRAS, P. 2004. Extracellular protein deposition correlates with glial activation and oxidative stress in Creutzfeldt-Jakob and Alzheimer's disease. *Acta Neuropathol,* 108**,** 194-200.

VANNI, S., MODA, F., ZATTONI, M., BISTAFFA, E., DE CECCO, E., ROSSI, M., GIACCONE, G., TAGLIAVINI, F., HAÏK, S., DESLYS, J. P., ZANUSSO, G., IRONSIDE, J. W., FERRER, I., KOVACS, G. G. & LEGNAME, G. 2017. Differential overexpression of SERPINA3 in human prion diseases. *Scientific Reports,* 7**,** 15637.

VARDIGAN, J. D., CANNON, C. E., PURI, V., DANCHO, M., KOSER, A., WITTMANN, M., KUDUK, S. D., RENGER, J. J. & USLANER, J. M. 2015. Improved cognition without adverse effects: novel M1 muscarinic potentiator compares favorably to donepezil and xanomeline in rhesus monkey. *Psychopharmacology (Berl),* 232**,** 1859-66.

VASSAR, R. 2002. Beta-secretase (BACE) as a drug target for Alzheimer's disease. *Adv Drug Deliv Rev,* 54**,** 1589-602.

VENKATAKRISHNAN, A. J., DEUPI, X., LEBON, G., TATE, C. G., SCHERTLER, G. F. & BABU, M. M. 2013. Molecular signatures of G-protein-coupled receptors. *Nature,* 494**,** 185.

VERGHESE, P. B., CASTELLANO, J. M. & HOLTZMAN, D. M. 2011. Apolipoprotein E in Alzheimer's disease and other neurological disorders. *Lancet Neurol,* 10**,** 241-52.

VEY, M., PILKUHN, S., WILLE, H., NIXON, R., DEARMOND, S. J., SMART, E. J., ANDERSON, R. G., TARABOULOS, A. & PRUSINER, S. B. 1996. Subcellular colocalization of the cellular and scrapie prion proteins in caveolae-like membranous domains. *Proceedings of the National Academy of Sciences of the United States of America,* 93**,** 14945-14949.

VINCENTI, J. E., MURPHY, L., GRABERT, K., MCCOLL, B. W., CANCELLOTTI, E., FREEMAN, T. C. & MANSON, J. C. 2015. Defining the Microglia Response during the Time Course of Chronic Neurodegeneration. *J Virol,* 90**,** 3003-17.

VINSON, C. R. & ADLER, P. N. 1987. Directional non-cell autonomy and the transmission of polarity information by the frizzled gene of Drosophila. *Nature,* 329**,** 549-51.

VINSON, C. R., CONOVER, S. & ADLER, P. N. 1989. A Drosophila tissue polarity locus encodes a protein containing seven potential transmembrane domains. *Nature,* 338**,** 263-4.

VIOLIN, J. D., DEWIRE, S. M., YAMASHITA, D., ROMINGER, D. H., NGUYEN, L., SCHILLER, K., WHALEN, E. J., GOWEN, M. & LARK, M. W. 2010. Selectively engaging ß-arrestins at the angiotensin II type 1 receptor reduces blood pressure and increases cardiac performance. *J Pharmacol Exp Ther,* 335**,** 572-9.

VISCUSI, E. R., WEBSTER, L., KUSS, M., DANIELS, S., BOLOGNESE, J. A., ZUCKERMAN, S., SOERGEL, D. G., SUBACH, R. A., COOK, E. & SKOBIERANDA, F. 2016. A randomized, phase 2 study investigating TRV130, a biased ligand of the μ-opioid receptor, for the intravenous treatment of acute pain. *Pain,* 157**,** 264-272.

VISHNIVETSKIY, S. A., GIMENEZ, L. E., FRANCIS, D. J., HANSON, S. M., HUBBELL, W. L., KLUG, C. S. & GUREVICH, V. V. 2011. Few residues within an extensive binding interface drive receptor interaction and determine the specificity of arrestin proteins. *J Biol Chem,* 286**,** 24288-99.

VISHNIVETSKIY, S. A., HOSEY, M. M., BENOVIC, J. L. & GUREVICH, V. V. 2004. Mapping the Arrestin-Receptor Interface: STRUCTURAL ELEMENTS RESPONSIBLE FOR RECEPTOR SPECIFICITY OF ARRESTIN PROTEINS *. *Journal of Biological Chemistry,* 279**,** 1262-1268.

VÖGLER, O., BOGATKEWITSCH, G. S., WRISKE, C., KRUMMENERL, P., JAKOBS, K. H. & VAN KOPPEN, C. J. 1998. Receptor subtype-specific regulation of muscarinic acetylcholine receptor sequestration by dynamin. Distinct sequestration of m2 receptors. *J Biol Chem,* 273**,** 12155-60.

VOLPICELLI, L. A. & LEVEY, A. I. 2004. Muscarinic acetylcholine receptor subtypes in cerebral cortex and hippocampus. *Progress in Brain Research*. Elsevier.

VOSS, T., LI, J., CUMMINGS, J., FARLOW, M., ASSAID, C., FROMAN, S., LEIBENSPERGER, H., SNOW-ADAMI, L., MCMAHON, K. B., EGAN, M. & MICHELSON, D. 2018. Randomized, controlled, proof-of-concept trial of MK-7622 in Alzheimer's disease. *Alzheimers Dement (N Y),* 4**,** 173-181.

VOYTKO, M. L. & TINKLER, G. P. 2004. Cognitive function and its neural mechanisms in nonhuman primate models of aging, Alzheimer disease, and menopause. *Front Biosci,* 9**,** 1899-914.

VU, T. K., HUNG, D. T., WHEATON, V. I. & COUGHLIN, S. R. 1991. Molecular cloning of a functional thrombin receptor reveals a novel proteolytic mechanism of receptor activation. *Cell,* 64**,** 1057-68.

VUCKOVIC, Z., GENTRY, P. R., BERIZZI, A. E., HIRATA, K., VARGHESE, S., THOMPSON, G., VAN DER WESTHUIZEN, E. T., BURGER, W. A. C., RAHMANI, R., VALANT, C., LANGMEAD, C. J., LINDSLEY, C. W., BAELL, J., TOBIN, A. B., SEXTON, P. M., CHRISTOPOULOS, A. & THAL, D. M. 2019. Crystal structure of the M5 muscarinic acetylcholine receptor. *bioRxiv***,** 730622.

WALKER, D. G. & LUE, L.-F. 2015. Immune phenotypes of microglia in human neurodegenerative disease: challenges to detecting microglial polarization in human brains. *Alzheimer's research & therapy,* 7**,** 56-56.

WALKER, L. C., HUCKSTEP, K. L., CHEN, N. A., HAND, L. J., LINDSLEY, C. W., LANGMEAD, C. J. & LAWRENCE, A. J. 2021. Muscarinic M4 and M5 receptors in the ventral subiculum differentially modulate alcohol seeking versus consumption in male alcohol-preferring rats. *British Journal of Pharmacology,* 178**,** 3730-3746.

WANG, F., WANG, X., YUAN, C. G. & MA, J. 2010. Generating a prion with bacterially expressed recombinant prion protein. *Science,* 327**,** 1132-5.

WANG, L., BENZINGER, T. L., SU, Y., CHRISTENSEN, J., FRIEDRICHSEN, K., ALDEA, P., MCCONATHY, J., CAIRNS, N. J., FAGAN, A. M., MORRIS, J. C. & ANCES, B. M. 2016. Evaluation of Tau Imaging in Staging Alzheimer Disease and Revealing Interactions Between β-Amyloid and Tauopathy. *JAMA Neurol,* 73**,** 1070-7.

WANG, Q. & LIMBIRD, L. E. 2002. Regulated interactions of the alpha 2A adrenergic receptor with spinophilin, 14-3-3zeta, and arrestin 3. *J Biol Chem,* 277**,** 50589-96.

WANG, R. & REDDY, P. H. 2017. Role of Glutamate and NMDA Receptors in Alzheimer's Disease. *J Alzheimers Dis,* 57**,** 1041-1048.

WANG, S., ZHANG, C., SHENG, X., ZHANG, X., WANG, B. & ZHANG, G. 2014. Peripheral expression of MAPK pathways in Alzheimer's and Parkinson's diseases. *J Clin Neurosci,* 21**,** 810-4.

WANG, W., ZHAO, F., MA, X., PERRY, G. & ZHU, X. 2020. Mitochondria dysfunction in the pathogenesis of Alzheimer’s disease: recent advances. *Molecular Neurodegeneration,* 15**,** 30.

WATT, M. L., SCHOBER, D. A., HITCHCOCK, S., LIU, B., CHESTERFIELD, A. K., MCKINZIE, D. & FELDER, C. C. 2011. Pharmacological characterization of LY593093, an M1 muscarinic acetylcholine receptor-selective partial orthosteric agonist. *J Pharmacol Exp Ther,* 338**,** 622-32.

WAUGH, M. G., CHALLISS, R. A., BERSTEIN, G., NAHORSKI, S. R. & TOBIN, A. B. 1999. Agonist-induced desensitization and phosphorylation of m1-muscarinic receptors. *Biochemical Journal,* 338**,** 175-183.

WEI, H., AHN, S., SHENOY, S. K., KARNIK, S. S., HUNYADY, L., LUTTRELL, L. M. & LEFKOWITZ, R. J. 2003. Independent beta-arrestin 2 and G protein-mediated pathways for angiotensin II activation of extracellular signal-regulated kinases 1 and 2. *Proc Natl Acad Sci U S A,* 100**,** 10782-7.

WEI, X., HERBST, A., MA, D., AIKEN, J. & LI, L. 2011. A Quantitative Proteomic Approach to Prion Disease Biomarker Research: Delving into the Glycoproteome. *Journal of Proteome Research,* 10**,** 2687-2702.

WELDON, D. T., ROGERS, S. D., GHILARDI, J. R., FINKE, M. P., CLEARY, J. P., O'HARE, E., ESLER, W. P., MAGGIO, J. E. & MANTYH, P. W. 1998. Fibrillar beta-amyloid induces microglial phagocytosis, expression of inducible nitric oxide synthase, and loss of a select population of neurons in the rat CNS in vivo. *The Journal of neuroscience : the official journal of the Society for Neuroscience,* 18**,** 2161-2173.

WESS, J. 1993. Molecular basis of muscarinic receptor function. *Trends in Pharmacological Sciences,* 14**,** 308-313.

WESS, J. 2005. Allosteric binding sites on muscarinic acetylcholine receptors. *Mol Pharmacol,* 68**,** 1506-9.

WESS, J., EGLEN, R. M. & GAUTAM, D. 2007. Muscarinic acetylcholine receptors: mutant mice provide new insights for drug development. *Nat Rev Drug Discov,* 6**,** 721-33.

WETTSCHURECK, N. & OFFERMANNS, S. 2005. Mammalian G proteins and their cell type specific functions. *Physiol Rev,* 85**,** 1159-204.

WHITE, K. L., ROBINSON, J. E., ZHU, H., DIBERTO, J. F., POLEPALLY, P. R., ZJAWIONY, J. K., NICHOLS, D. E., MALANGA, C. J. & ROTH, B. L. 2015. The G protein-biased κ-opioid receptor agonist RB-64 is analgesic with a unique spectrum of activities in vivo. *J Pharmacol Exp Ther,* 352**,** 98-109.

WHITEHOUSE, P. J., PRICE, D. L., CLARK, A. W., COYLE, J. T. & DELONG, M. R. 1981. Alzheimer disease: evidence for selective loss of cholinergic neurons in the nucleus basalis. *Ann Neurol,* 10**,** 122-6.

WHITEHOUSE, P. J., PRICE, D. L., STRUBLE, R. G., CLARK, A. W., COYLE, J. T. & DELON, M. R. 1982. Alzheimer's disease and senile dementia: loss of neurons in the basal forebrain. *Science,* 215**,** 1237-9.

WIESSNER, C., WIEDERHOLD, K. H., TISSOT, A. C., FREY, P., DANNER, S., JACOBSON, L. H., JENNINGS, G. T., LÜÖND, R., ORTMANN, R., REICHWALD, J., ZURINI, M., MIR, A., BACHMANN, M. F. & STAUFENBIEL, M. 2011. The second-generation active Aß immunotherapy CAD106 reduces amyloid accumulation in APP transgenic mice while minimizing potential side effects. *J Neurosci,* 31**,** 9323-31.

WILCOCK, G. K., ESIRI, M. M., BOWEN, D. M. & SMITH, C. C. 1982. Alzheimer's disease. Correlation of cortical choline acetyltransferase activity with the severity of dementia and histological abnormalities. *J Neurol Sci,* 57**,** 407-17.

WILCOCK, G. K., GAUTHIER, S., FRISONI, G. B., JIA, J., HARDLUND, J. H., MOEBIUS, H. J., BENTHAM, P., KOOK, K. A., SCHELTER, B. O., WISCHIK, D. J., DAVIS, C. S., STAFF, R. T., VUKSANOVIC, V., AHEARN, T., BRACOUD, L., SHAMSI, K., MAREK, K., SEIBYL, J., RIEDEL, G., STOREY, J. M. D., HARRINGTON, C. R. & WISCHIK, C. M. 2018. Potential of Low Dose Leuco-Methylthioninium Bis(Hydromethanesulphonate) (LMTM) Monotherapy for Treatment of Mild Alzheimer's Disease: Cohort Analysis as Modified Primary Outcome in a Phase III Clinical Trial. *J Alzheimers Dis,* 61**,** 435-457.

WILDEN, U., HALL, S. W. & KÜHN, H. 1986. Phosphodiesterase activation by photoexcited rhodopsin is quenched when rhodopsin is phosphorylated and binds the intrinsic 48-kDa protein of rod outer segments. *Proc Natl Acad Sci U S A,* 83**,** 1174-8.

WILL, R. G., IRONSIDE, J. W., ZEIDLER, M., ESTIBEIRO, K., COUSENS, S. N., SMITH, P. G., ALPEROVITCH, A., POSER, S., POCCHIARI, M. & HOFMAN, A. 1996. A new variant of Creutzfeldt-Jakob disease in the UK. *The Lancet,* 347**,** 921-925.

WILLAIME-MORAWEK, S., BRAMI-CHERRIER, K., MARIANI, J., CABOCHE, J. & BRUGG, B. 2003. C-jun N-terminal kinases/c-Jun and p38 pathways cooperate in ceramide-induced neuronal apoptosis. *Neuroscience,* 119**,** 387-397.

WILLIAMS, A., LUCASSEN, P. J., RITCHIE, D. & BRUCE, M. 1997. PrP deposition, microglial activation, and neuronal apoptosis in murine scrapie. *Exp Neurol,* 144**,** 433-8.

WONG, B. S., BROWN, D. R., PAN, T., WHITEMAN, M., LIU, T., BU, X., LI, R., GAMBETTI, P., OLESIK, J., RUBENSTEIN, R. & SY, M. S. 2001. Oxidative impairment in scrapie-infected mice is associated with brain metals perturbations and altered antioxidant activities. *J Neurochem,* 79**,** 689-98.

WOOLF, N. J. & BUTCHER, L. L. 1981. Cholinergic neurons in the caudate-putamen complex proper are intrinsically organized: A combined evans blue and acetylcholinesterase analysis. *Brain Research Bulletin,* 7**,** 487-507.

WOOLLEY, M. L., CARTER, H. J., GARTLON, J. E., WATSON, J. M. & DAWSON, L. A. 2009. Attenuation of amphetamine-induced activity by the non-selective muscarinic receptor agonist, xanomeline, is absent in muscarinic M4 receptor knockout mice and attenuated in muscarinic M1 receptor knockout mice. *Eur J Pharmacol,* 603**,** 147-9.

WOOTTEN, D., CHRISTOPOULOS, A., MARTI-SOLANO, M., BABU, M. M. & SEXTON, P. M. 2018. Mechanisms of signalling and biased agonism in G protein-coupled receptors. *Nature Reviews Molecular Cell Biology,* 19**,** 638-653.

WORLD HEALTH ORGANIZATION. 2020. *Dementia* [Online]. Available: https://www.who.int/news-room/fact-sheets/detail/dementia [Accessed].

WORLD HEALTH ORGANIZATION. 2021. *Dementia* [Online]. Available: https://www.who.int/news-room/fact-sheets/detail/dementia [Accessed 8 December 2021].

WU, G., KRUPNICK, J. G., BENOVIC, J. L. & LANIER, S. M. 1997. Interaction of arrestins with intracellular domains of muscarinic and alpha2-adrenergic receptors. *J Biol Chem,* 272**,** 17836-42.

WU, N., MACION-DAZARD, R., NITHIANANTHAM, S., XU, Z., HANSON, S. M., VISHNIVETSKIY, S. A., GUREVICH, V. V., THIBONNIER, M. & SHOHAM, M. 2006. Soluble mimics of the cytoplasmic face of the human V1-vascular vasopressin receptor bind arrestin2 and calmodulin. *Mol Pharmacol,* 70**,** 249-58.

WYATT, D., MALIK, R., VESECKY, A. C. & MARCHESE, A. 2011. Small ubiquitin-like modifier modification of arrestin-3 regulates receptor trafficking. *J Biol Chem,* 286**,** 3884-93.

WYSS-CORAY, T., LOIKE, J. D., BRIONNE, T. C., LU, E., ANANKOV, R., YAN, F., SILVERSTEIN, S. C. & HUSEMANN, J. 2003. Adult mouse astrocytes degrade amyloid-beta in vitro and in situ. *Nat Med,* 9**,** 453-7.

XIA, Z., DICKENS, M., RAINGEAUD, J., DAVIS, R. J. & GREENBERG, M. E. 1995. Opposing effects of ERK and JNK-p38 MAP kinases on apoptosis. *Science,* 270**,** 1326-1331.

XU, F., NA, L., LI, Y. & CHEN, L. 2020. Roles of the PI3K/AKT/mTOR signalling pathways in neurodegenerative diseases and tumours. *Cell & Bioscience,* 10**,** 54.

XU, W., TAN, L., WANG, H. F., JIANG, T., TAN, M. S., ZHAO, Q. F., LI, J. Q., WANG, J. & YU, J. T. 2015. Meta-analysis of modifiable risk factors for Alzheimer's disease. *J Neurol Neurosurg Psychiatry,* 86**,** 1299-306.

YAMADA, M., BASILE, A. S., FEDOROVA, I., ZHANG, W., DUTTAROY, A., CUI, Y., LAMPING, K. G., FARACI, F. M., DENG, C. X. & WESS, J. 2003. Novel insights into M5 muscarinic acetylcholine receptor function by the use of gene targeting technology. *Life Sci,* 74**,** 345-53.

YAMADA, M., CHIBA, T., SASABE, J., NAWA, M., TAJIMA, H., NIIKURA, T., TERASHITA, K., AISO, S., KITA, Y., MATSUOKA, M. & NISHIMOTO, I. 2005. Implanted cannula-mediated repetitive administration of Abeta25-35 into the mouse cerebral ventricle effectively impairs spatial working memory. *Behav Brain Res,* 164**,** 139-46.

YAMADA, M., LAMPING, K. G., DUTTAROY, A., ZHANG, W., CUI, Y., BYMASTER, F. P., MCKINZIE, D. L., FELDER, C. C., DENG, C.-X., FARACI, F. M. & WESS, J. 2001a. Cholinergic dilation of cerebral blood vessels is abolished in M5 muscarinic acetylcholine receptor knockout mice. *Proceedings of the National Academy of Sciences,* 98**,** 14096.

YAMADA, M., MIYAKAWA, T., DUTTAROY, A., YAMANAKA, A., MORIGUCHI, T., MAKITA, R., OGAWA, M., CHOU, C. J., XIA, B., CRAWLEY, J. N., FELDER, C. C., DENG, C. X. & WESS, J. 2001b. Mice lacking the M3 muscarinic acetylcholine receptor are hypophagic and lean. *Nature,* 410**,** 207-12.

YAMASAKI, M., MATSUI, M. & WATANABE, M. 2010. Preferential localization of muscarinic M1 receptor on dendritic shaft and spine of cortical pyramidal cells and its anatomical evidence for volume transmission. *J Neurosci,* 30**,** 4408-18.

YEATMAN, H. R., LANE, J. R., CHOY, K. H., LAMBERT, N. A., SEXTON, P. M., CHRISTOPOULOS, A. & CANALS, M. 2014. Allosteric modulation of M1 muscarinic acetylcholine receptor internalization and subcellular trafficking. *J Biol Chem,* 289**,** 15856-66.

YEH, F. L., WANG, Y., TOM, I., GONZALEZ, L. C. & SHENG, M. 2016. TREM2 Binds to Apolipoproteins, Including APOE and CLU/APOJ, and Thereby Facilitates Uptake of Amyloid-Beta by Microglia. *Neuron,* 91**,** 328-340.

ZAHN, R., LIU, A., LÜHRS, T., RIEK, R., VON SCHROETTER, C., LÓPEZ GARCÍA, F., BILLETER, M., CALZOLAI, L., WIDER, G. & WÜTHRICH, K. 2000. NMR solution structure of the human prion protein. *Proceedings of the National Academy of Sciences,* 97**,** 145.

ZAMANIAN, J. L., XU, L., FOO, L. C., NOURI, N., ZHOU, L., GIFFARD, R. G. & BARRES, B. A. 2012. Genomic analysis of reactive astrogliosis. *J Neurosci,* 32**,** 6391-410.

ZANDL-LANG, M., FANAEE-DANESH, E., SUN, Y., ALBRECHER, N. M., GALI, C. C., ČANČAR, I., KOBER, A., TAM-AMERSDORFER, C., STRACKE, A., STORCK, S. M., SAEED, A., STEFULJ, J., PIETRZIK, C. U., WILSON, M. R., BJÖRKHEM, I. & PANZENBOECK, U. 2018. Regulatory effects of simvastatin and apoJ on APP processing and amyloid-β clearance in blood-brain barrier endothelial cells. *Biochimica et Biophysica Acta (BBA) - Molecular and Cell Biology of Lipids,* 1863**,** 40-60.

ZEMPEL, H. & MANDELKOW, E. 2014. Lost after translation: missorting of Tau protein and consequences for Alzheimer disease. *Trends Neurosci,* 37**,** 721-32.

ZENKO, D. & HISLOP, J. N. 2017. Regulation and trafficking of muscarinic acetylcholine receptors. *Neuropharmacology*.

ZERR, I. & PARCHI, P. 2018. Chapter 9 - Sporadic Creutzfeldt–Jakob disease. *In:* POCCHIARI, M. & MANSON, J. (eds.) *Handbook of Clinical Neurology*. Elsevier.

ZHAN, X., GIMENEZ, L. E., GUREVICH, V. V. & SPILLER, B. W. 2011. Crystal structure of arrestin-3 reveals the basis of the difference in receptor binding between two non-visual subtypes. *J Mol Biol,* 406**,** 467-78.

ZHANG, J., BARAK, L. S., ANBORGH, P. H., LAPORTE, S. A., CARON, M. G. & FERGUSON, S. S. 1999. Cellular trafficking of G protein-coupled receptor/beta-arrestin endocytic complexes. *J Biol Chem,* 274**,** 10999-1006.

ZHANG, J., FERGUSON, S. S., BARAK, L. S., MÉNARD, L. & CARON, M. G. 1996. Dynamin and beta-arrestin reveal distinct mechanisms for G protein-coupled receptor internalization. *J Biol Chem,* 271**,** 18302-5.

ZHANG, J. H., PANDEY, M., SEIGNEUR, E. M., PANICKER, L. M., KOO, L., SCHWARTZ, O. M., CHEN, W., CHEN, C. K. & SIMONDS, W. F. 2011. Knockout of G protein β5 impairs brain development and causes multiple neurologic abnormalities in mice. *J Neurochem,* 119**,** 544-54.

ZHANG, W., BASILE, A. S., GOMEZA, J., VOLPICELLI, L. A., LEVEY, A. I. & WESS, J. 2002. Characterization of central inhibitory muscarinic autoreceptors by the use of muscarinic acetylcholine receptor knock-out mice. *J Neurosci,* 22**,** 1709-17.

ZHANG, Y., SUN, B., FENG, D., HU, H., CHU, M., QU, Q., TARRASCH, J. T., LI, S., SUN KOBILKA, T., KOBILKA, B. K. & SKINIOTIS, G. 2017. Cryo-EM structure of the activated GLP-1 receptor in complex with a G protein. *Nature,* 546**,** 248-253.

ZHAO, Y., JABER, V. & LUKIW, W. J. 2016. Over-Expressed Pathogenic miRNAs in Alzheimer's Disease (AD) and Prion Disease (PrD) Drive Deficits in TREM2-

Mediated Aß42 Peptide Clearance. *Frontiers in Aging Neuroscience,* 8**,** 140.

ZHOU, X. E., HE, Y., DE WAAL, P. W., GAO, X., KANG, Y., VAN EPS, N., YIN, Y., PAL, K., GOSWAMI, D., WHITE, T. A., BARTY, A., LATORRACA, N. R., CHAPMAN, H. N., HUBBELL, W. L., DROR, R. O., STEVENS, R. C., CHEREZOV, V., GUREVICH, V. V., GRIFFIN, P. R., ERNST, O. P., MELCHER, K. & XU, H. E. 2017. Identification of Phosphorylation Codes for Arrestin Recruitment by G Protein-Coupled Receptors. *Cell,* 170**,** 457-469.e13.

ZHUO, Y., VISHNIVETSKIY, S. A., ZHAN, X., GUREVICH, V. V. & KLUG, C. S. 2014. Identification of receptor binding-induced conformational changes in non-visual arrestins. *The Journal of biological chemistry,* 289**,** 20991-21002.

ZIDAR, D. A., VIOLIN, J. D., WHALEN, E. J. & LEFKOWITZ, R. J. 2009. Selective engagement of G protein coupled receptor kinases (GRKs) encodes distinct functions of biased ligands. *Proc Natl Acad Sci U S A,* 106**,** 9649-54.

ZLOKOVIC, B. V., DEANE, R., SALLSTROM, J., CHOW, N. & MIANO, J. M. 2005. Neurovascular pathways and Alzheimer amyloid beta-peptide. *Brain Pathol,* 15**,** 78-83.